Flooding induced changes in the mobility, bioaccessibility and solid phase distribution of potentially harmful elements

Diana Elizabeth Katherine McLaren

January 2019

A thesis submitted for the degree of

Doctor of Philosophy,

Biological and Environmental Sciences,

Faculty of Natural Sciences,

University of Stirling

DECLARATION OF AUTHORSHIP

I, Diana Elizabeth Katherine McLaren, declare that this thesis has been composed by me and it embodies the results of my own research. Where appropriate I have acknowledged the nature and extent of work carried out in collaboration with others.

..... Diana E K McLaren

27th January 2019

ABSTRACT

The Intergovernmental Panel on Climate Change (IPCC) predicts that the number of extreme precipitation events will increase considerably by the end of the century for mid-latitude land masses such as the UK. Potentially harmful elements (PHEs) such as arsenic, cadmium, copper, lead and zinc can be chemically mobilised during flood events, potentially increasing their availability to receptors. The development of floodplains for residential and industrial uses increases the risk of a source - pathway - receptor linkage occurring for PHEs. This thesis aims to characterise changes in the solid phase distribution and bioaccessibility of PHEs before, during and after drying to provide new knowledge of PHE mobility in catchments.

Soils were collected from a UK catchment with a history of lead and zinc mining and characterised in terms of pseudo-total PHE content, the bioaccessible content of PHEs and their solid phase distribution. Laboratory inundation studies using microcosms were conducted to understand PHE behaviour during controlled wetting and drying episodes. The results demonstrated that flooding resulted in the mobilisation of the PHEs into porewaters. However, the pattern of mobility was shown to vary for different PHEs. Bioaccessibility testing after each wet and dry cycle determined the changes in PHE availability to humans and highlighted an increase in the bioaccessible fraction of PHEs in this study in the region of 5-10 %. The solid phase distribution of PHEs during wetting and drying cycles was then determined using sequential extractions and a self-modelling mixture resolution algorithm to help explain the earlier findings on PHE availability. Broad scale changes in the solid phase distribution of PHEs varied between soils. For arsenic, generally the greatest change was observed in the iron oxide components. Other PHEs exhibited redistribution between soil components, often to those that were more labile.

The spatial prediction of, and the influence of flooding on PHE bioaccessibility in the Tyne catchment was investigated. Microcosm experiments were conducted to quantity the flooding induced changes in bioaccessibility. This was followed by a combination of geospatial, regression and machine learning methods to map PHE bioaccessibility at a catchment scale. A key output was the production of maps highlighting bioaccessible content of PHEs in flood prone areas of the Tyne catchment. Furthermore, flooding induced changes in bioaccessibility were mapped at a catchment scale, which highlighted areas where there was a greater potential for flooding induced increases in bioaccessibility and consequently human exposure.

ACKNOWLEDGEMENTS

I would firstly like to thank my two main supervisors Prof. David Copplestone and Dr Joanna Wragg, for without them, this thesis would not have been possible. I am incredibly grateful for their guidance and support throughout the whole process. I am even thankful for Jo's asking of "why?" and David's frequent (and probably needed) kicks up the backside (metaphorically speaking, of course). I really couldn't have asked for a better lead supervisory team.

I'd also like to extend thanks to my other supervisors, Dr Karen Johnson and Dr Clare Wilson for their input, guidance and comments.

There are many other people at the University of Stirling I'd like to thank. Firstly, a big thank you to Ian Washbourne for running my samples through the ICP-OES and for subsequently teaching me how use it when he realised how many samples I actually had! I am also grateful to Lorna English for her analytical help in the instrument lab and for always being so cheery. A huge thanks goes to Chris Sneddon for meticulously constructing the work of art that was my end over end rotator for the UBM method. I'd like to thank those who helped me conduct fieldwork: Magdalena Fleischmann and Angela Davie - thank you both for braving the cold and putting up with my marching! Finally for Stirling University, I'd like to thank Katherine Raines for being a good friend throughout my undergraduate and PhD and for sharing rants, laughs, frustration and coffee.

I'd like to thank those at the BGS Keyworth that helped me. Firstly I'd like to thank Dr Mark Cave for being helpful and so very patient when teaching me the ways of the CISED SMMR. Thank you to Simon Kemp for conducting the XRD analysis on my samples and to Bob Lister for providing spatial datasets.

Thank you to my family for being there (putting up with me) throughout the entirety of my PhD. Finally, thank you to Kenneth Porter for supporting me through my PhD whilst completing his own.

To anyone I've forgotten, I sincerely apologise. It's late and my thesis is due tomorrow, therefore my brain is tired!

CONTENTS

LIST OF TABLES

LIST OF FIGURES

LIST OF ACRONYMS

BARGE	Bioaccessibility Research Group of Europe
BAC	Bioaccessible concentration
BAF	Bioaccessible fraction
BGS	British Geological Survey
C4SL	Category 4 screening levels
CISED	Chemometric identification of substrates and element distributions
DEFRA	Department for Food and Rural Affairs
DI	Deionised water
EQS	Environmental quality standard
GAC	Generic assessment criteria
GBASE	Geochemical baseline survey of the environment
HCl	Hydrochloric acid
HDPE	High density polyethylene
HNO_3	Nitric acid
ICP-OES	Inductively coupled plasma optical emission spectroscopy
IDW	Inverse distance weight
IPPC	Intergovernmental Panel on Climate Change
ISC	Intrinsic soil constituent
LOAEL	Lowest observable adverse effects level
LOD	Limit of detection
LOI	Loss on ignition
MLR	Multiple linear regression
ORP	Oxidation reduction potential
PBET	Physiologically based extraction test
PCA	Principle component analysis
PHE	Potentially harmful element
QC	Quality control
RF	Random forest
RIVM	Rijksinstituut voor Volksgezondheid en Milieu (National Institute for Public Health and the Environment)

S4UL	Suitable 4 use levels
SGV	Soil guideline value
SOM	Soil organic matter
TOC	Total organic carbon
SMMR	Self-modelling mixture resolution algorithm
UBM	Universal bioaccessibility method
UKSHS	UK Soil and Herbage Survey
WFD	Water framework directive
XRFS	X-ray fluorescence spectrometry
XRD	X-Ray diffraction

GLOSSARY

Bioaccessibility	The fraction of a PHE that is soluble in the gastrointestinal fluids and available for uptake across the gastrointestinal wall.
Bioavailability	The fraction of a bioaccessible element that crosses the gastrointestinal wall into the blood stream.
Brownfield	Land that has previously been used for industrial purposes.
Component	An output of the SMMR. A component is a fraction of the soil with a distinct chemical signature/composition.
Cross Validation	A technique to evaluate predictive models by partitioning the original sample into a training set to train the model, and a test set to evaluate the model.
Chemometrics	The use of mathematical and statistical methods to improve the understanding of chemical information and to correlate quality parameters or physical properties to analytical instrument data.
Clustering	A technique for classifying objects into groups based on their properties.
Hazard	A source of potential damage, harm or adverse health effects on something or someone.
Intrinsic Soil Constituent	An assemblage of soil particles from a common biogenic, geogenic or anthropogenic input, with a consistent chemical composition present at varying concentrations in a number of similarly developed soils.
Phytoavailable	The availability of a PHE for uptake by plants.
Reference Material	A material with properties that are sufficiently homogenised and well established to be able to be used for the evaluation of method performance of laboratory and field instruments.
Risk	The likelihood that a person, organism or entity may be harmed or suffers adverse health effects if exposed to a hazard.
Solid phase distribution	The partitioning of soil components and potentially harmful elements within soil as a whole.
Stomatal conductance	The measure of the rate of passage of carbon dioxide (CO_2) entering, or water vapour exiting through the stomata of a leaf.
Total Digest	An acid extraction to digest a solid sample into solution prior to analysis.

1. INTRODUCTION

1.1 Background

The Intergovernmental Panel on Climate Change (IPCC) predicts that the number of extreme precipitation events will increase considerably by the end of the century for mid-latitude land masses such as the UK (Intergovernmental Panel on Climate Change, 2018). Periods of summer droughts have also been predicted to increase. Analysis of UK weather patterns over the last 40 years has shown a change from short to longer duration summer rain events, increasing the risk of flood events (Jones *et al.,* 2013). Additionally, the intensity and number of extreme spring and autumn rainfall events has increased (Jones *et al.,* 2013). These changes are likely to have considerable economic, social and environmental consequences for catchment management, especially in flood sensitive areas (Pimentel *et al.,* 1995; Haines, *et al.,* 2006; Ciscar *et al.,* 2011).

Predicting future climate change scenarios and, in the case of this thesis, the impact of extended flooding events is therefore important for adaptation purposes and climate change resilience. The Adaptation Sub-Committee of the Committee on Climate Change's report (Adaptation Sub-Committee, 2011) assessed the UK's vulnerability to climate change and concluded that it was increasing. The reasons given include development on floodplains; this has increased considerably in the last 10 years. Floodplain development for residential and industrial uses increases the probability of a source - pathway - receptor linkage for potentially harmful elements (PHEs) due to increasing human interaction with unsealed soils in these floodplain areas. It has been estimated that there are 62,000 hectares of brownfield sites within England alone. Increased morbidity in people living in close proximity to brownfield sites has been shown to occur due to the presence of elevated levels of metals, inorganic compounds, organic chemicals and occasionally radionuclides (Bambra *et al.,* 2014).

Human interaction with soils can occur regularly and consequently exposure to PHEs could occur. This could lead to health impacts depending upon the concentrations of PHEs that people are exposed to especially if these concentrations exceed guideline values for soils (section 1.4). The main pathways of exposure are through dermal contact, inhalation or ingestion of PHE enriched material. Ingestion can arise both from direct consumption of material or from the consumption of vegetables and other plant material with soil attached, or from PHE enriched foodstuffs. Additionally, hand to mouth transport is particularly prevalent in children as they are likely to directly eat soil when playing. Inhalation and

ingestion of dust particles and associated PHEs can provide additional transport pathways and are more likely to occur when bare patches of ground are present (Breshears *et al.,* 2012). The predicted increases in drought periods during summer months could lead to an increase in dust particles from dry ground with consequent increased exposure to PHEs associated with dust particles.

Evidence suggests that the availability of PHEs to human receptors can increase when some soils are subjected to flooding (Florido *et al.,* 2011). Research into the detailed environmental processes controlling the movement and availability of PHEs associated with flood events within a catchment (Figure 1.1) will strengthen our understanding of the consequences of climate change induced flooding events. This is particularly important as temperature and moisture regimes may significantly alter the availability of contaminants to humans, livestock and food crops.

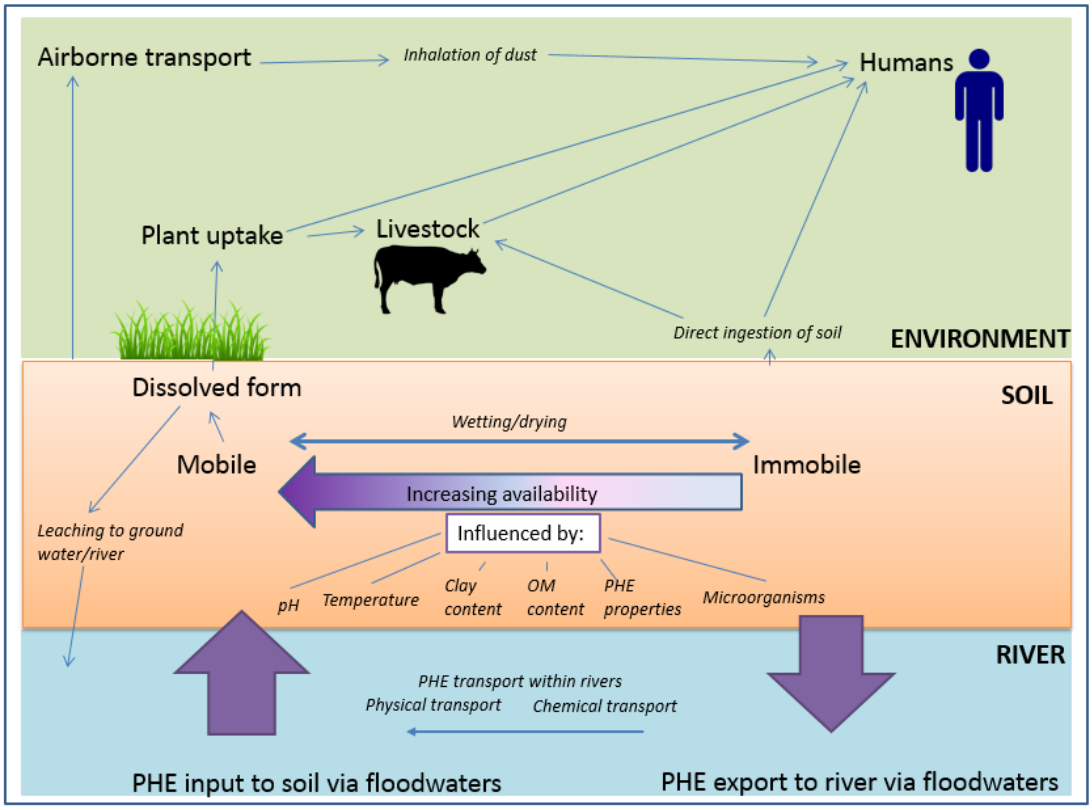

Figure 1.1: simple overview of the movement and fate of PHEs within soil, with respect to flooding.

This chapter will firstly outline the physical movement of soil bound PHEs to show the potential for floodplains to provide both a sink for, and subsequent source of, contamination. Secondly the physico-chemical changes induced by flooding that promote the chemical

mobilisation of PHEs will be explored with reference to metal and metalloid enrichment. Finally, PHE availability to human and plant receptors will be addressed.

The aim of this chapter is to explore the potential for PHE mobilisation to occur as a result of climate induced flooding conditions and will be constrained to the key PHEs: arsenic (As), lead (Pb), cadmium (Cd), copper (Cu) and zinc (Zn) because of their ubiquity as soil contaminants, and their toxicity to humans and the wildlife when present in elevated concentrations.

1.2 UK future climate change scenarios and hydrological regimes

The UK Climate Projections 2009 (UKCP09) are probabilistic model outputs based on thousands of different input scenarios (Kay and Jones, 2012). Charlton and Anwell (2014) summarise the UKCP09 predictions in a briefing report stating that summer and winter maximum temperatures in the UK will, on the whole, rise based on medium carbon dioxide (CO_2) emission scenarios (Figure 1.2). Annual precipitation will show little change; however, winter precipitation levels are likely to increase up to 56 % in England for the wettest days (Jenkins *et al.,* 2009). Southern England is predicted to experience prolonged periods of drought with summer precipitation reducing by 65 % in some areas. Although annual precipitation levels show little change, the predicted increase in extreme precipitation events is likely to lead to increases in surface water flooding (Charlton and Anwell, 2009). This may have implications for PHE mobilisation, as outlined in section 1.5. The recently published UKCP18 projections show similar results to the UKCP09 report as winter precipitation events are predicted to increase on average by up to 35 % (Lowe *et al.,* 2018). Average rainfall has increased 4 % over the past decade (2008 – 2017) when compared to the 1981 -2010 period (Lowe *et al.,* 2018).

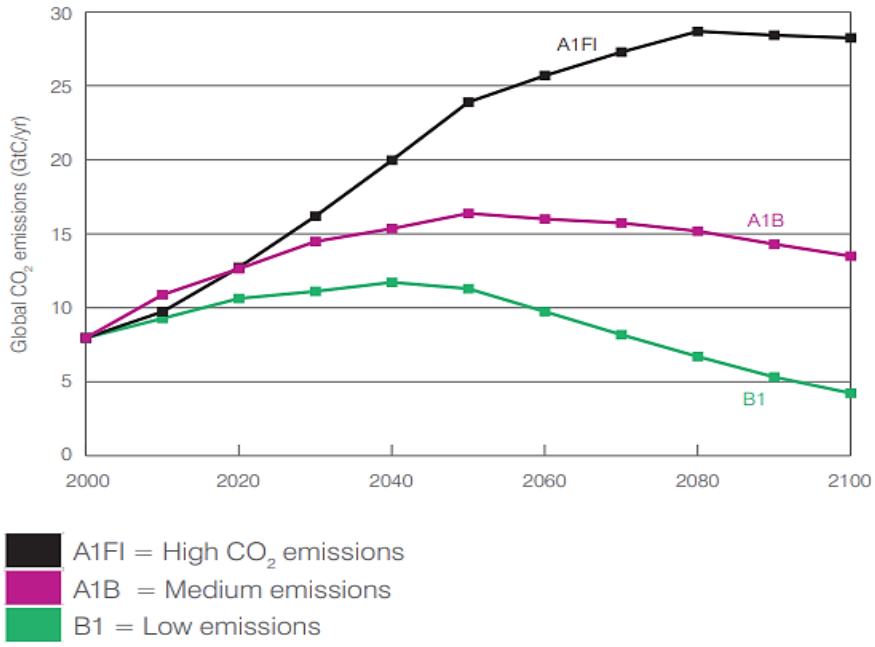

Figure 1.2: emissions scenarios for UKCP09. Sourced from: https://arcc.ouce.ox.ac.uk/wp-content/D4FC/06-appendix1-Bill-Gething-CCreport-0510.pdf . A1F1, A1B and B1 refer to emissions scenarios. A1F1 refers to a scenario characterized a population growth of 9 billion in 2050 and a reliance on fossil fuels. A1B refers to a scenario with similar population growth, but a balanced use of all energy sources. B1 refers to a more ecologically friendly scenario, with a reduction in material intensity and declining population after 2050.

Climate change resulting from anthropogenic emissions of CO_2 is likely to have considerable effects on the hydrological regimes found in UK catchments. Fast reacting catchments, or 'flashy' rivers, are more responsive to intense rainfall events due to their higher base flow index. Modelling of changes in flood frequency for the next 30 years in the Thames river basin show that chalk areas will likely experience a 10 % increase in peak flow rates and a 30 to 50 % increase for clay areas of the catchment (Bell *et al.,* 2012). The difference in peak flow rates is related to infiltration rates through chalk and clay based soils; with chalk based soils having higher infiltration rates than clays (Bell *et al.,* 2012). Although different modelling approaches yield different results, the Bell *et al.,* (2012) study is in line with estimated changes suggested by the Environment Agency (Environment Agency, 2011). In addition to underlying geology and soil types, reduced stomatal conductance as a result of increased atmospheric CO_2 levels could also affect potential evaporation leading to increased river flow rates (Bell *et al.,* 2012).

Fluctuations in river stage are likely to influence redox transitional zones by reducing redox potential, and therefore altering the biogeochemical factors that control PHE fate and

behaviour in riparian and floodplain soils and sediments. The impacts of climatic change on flow rates will also in turn affect erosion and deposition rates in UK catchments (Coulthard *et al.,* 2012). Modelling of sediment transport in the River Swale, using the Cellular Automaton Evolutionary Slope and River (CAESAR) model under a high CO_2 emissions scenario reported increased river sediment yields of 100 % (Coulthard *et al.,* 2012). Increased sediment yield may result in higher loads of contaminated sediment being transported and deposited on floodplain soils. However, an increased sediment load may also result in the dilution of contaminated sediment with 'clean' sediments.

1.3 Overview of PHE behaviour in soil

PHEs such as metals, metalloids and radioactive isotopes can be transported within a river system dissolved in the water column or associated with its suspended material. Major sources of PHEs into UK soils include atmospheric deposition, runoff from sewage sludge application, livestock manures, inorganic fertilisers, industrial wastes and mining wastes (Nicholson *et al.,* 2003). Geological sources can also provide elevated concentrations of metals and radionuclides in soils (Lieser, 1995; Garret, 2000; Khan *et al.,* 2010), for example, ironstones have been shown to be a source of As enrichment in soils (Palumboe-Roe *et al.,* 2005). Less than 1 % of PHEs remain dissolved within the water column, whereas over 99 % are stored within river sediments (Filgueiras *et al.,* 2004). Therefore, the fate and behaviour of PHEs within these sediments is of interest regarding exposure to receptors such as freshwater flora and fauna within the river. Potential receptors are extended to humans and if PHE enriched sediments are deposited onto floodplains. This thesis mainly considers human receptors; however some comparisons are made to water quality values that are of relevance to biota.

Flood events can physically move large quantities of sediment within the water column through a catchment (Dennis *et al.,* 2003) so PHEs can be deposited and consequently accumulate within floodplain soils and sediments when flow rates are reduced (Frohne *et al.,* 2011). As a result, floodplains themselves can become a secondary source of contaminants as well as a sink (Zhao and Marriott, 2013). Subsequent chemical mobilisation of PHEs induced by changes in pH and redox potential (E_h) may provide a pathway to receptors through the increased availability for uptake into plant and animal tissues. Additionally, PHEs can be released chemically into overlying water columns during flooding, resulting in implications for water quality standards such as those set by the Water

Framework Directive (Lynch *et al.,* 2014). Both the physical and chemical movement of PHEs is discussed below.

1.3.1 Arsenic

Arsenic (As) is a metalloid with chemistry similar to that of phosphorous (Smith *et al.,* 1998; Environment Agency, 2009) and is found in soils naturally, mainly originating from sedimentary rocks such as mud stones and shales. Anthropogenic inputs include atmospheric deposition from the burning of fossils fuels, the use of pesticides such as Pb-arsenates (Smith *et al.,* 1998; Wilson *et al*, 2010), the previous widespread use of Cu-Cr-arsenates as wood preservers and anthropogenic mining activities. Mean concentrations of As in rural soils are 10.9 mg kg^{-1} as reported by the UK Soil and Herbage Survey (UKSHS) (Environment Agency, 2007). The Normal Background Concentrations (NBC) report gives As concentrations as 32 mg kg^{-1} in non-mineralised areas and 290 mg kg^{-1} in mineralised areas (Ander *et al.,* 2013). Geological sources such as ironstones can greatly increase soil concentrations of As, which is seen in the areas around Northampton and Lincoln (Palumbo-Roe, 2005). Arsenic is usually present in soil as the more mobile and toxic (inorganic) arsenite (As(III)) at lower pH or as arsenate (As(V)) during oxidising conditions (Wilson *et al.,* 2010). Both species will bind to Iron (Fe) and Manganese (Mn) oxides, soil organic matter (SOM) and clays. During reducing conditions microbes utilise As, reducing As(V) to the more mobile As(III) after Fe reduction, but before sulphate reduction (Mitsunobu *et al.,* 2006; Wilson *et al.,* 2010). Organic As usually makes up approximately <5 % of total As in soils and is less toxic than As(III) or As(V); therefore its environmental impact is considered to be low (Huang *et al.,* 2010).

The toxicity of As is related to its speciation, for example As(III) is more toxic than As(V) as As(III) is highly reactive with living tissue (Vahter and Concha, 2001). Change in redox potential is the main driver for As speciation during flooding, therefore influencing As toxicity (Masscheleyn *et al.,* 1991). Lethal ranges of total inorganic As are reported to be in the region of 1-3 mg kg^{-1} with chronic exposure resulting in skin lesions and damage to nervous, renal, endocrine and hepatic systems (Hughes, 2002). As is a recognised carcinogen with chronic exposure leading to increased risk of organ, skin and lung cancer (Kapaj *et al.,* 2006). The majority of As is absorbed through the intestine via the ingestion pathway (Ratnaike, 2003), although inhalation of dust can also be a prominent pathway, especially in arid environments (Hysong *et al.,* 2003). Dermal exposure also occurs but provides a much less significant uptake pathway (Ratnaike, 2003).

Plant sensitivity to As is highly variable and is dependent on plant species and As speciation. Mycorrhizal fungi can play an important role in As uptake into plants (Meharg and Hartley-Whitaker, 2002). This is because mycorrhizal fungi aid phosphorous (P) transfer into plant tissue and As is chemically similarly to P (Environment Agency, 2009). Speciation of As is known to vary in plant tissue, suggesting that As transformation occurs within the plant itself (Meharg and Harley-Whitaker, 2002). Additionally, flooding of paddy fields has reportedly increased bioavailability of As(III) to rice plants due to the reducing conditions present during inundation (Zhao *et al.,* 2008).

1.3.2 Cadmium

Cadmium occurs naturally in soils as a result of geological weathering, mainly from sedimentary rocks. It is often associated with zinc (Zn) bearing ores (Environment Agency, 2009). Its ubiquity within the environment arises from anthropogenic sources, particularly phosphate fertilisers which on average contain around 79 mg kg^{-1} of Cd (Alloway, 1995; Environment Agency, 2009). Other sources include: metalliferous mining, zinc ore smelting and application of sewage sludge to agricultural areas (Thomson and Bannigan, 2008).

Cadmium (Cd) mobility is greater at lower pH and will form insoluble sulphides during prolonged anaerobic conditions. SOM content is also influential on Cd mobility by reducing its availability as Cd binds to organic ligands (Pinto *et al.,* 2004). Typical values of Cd in UK soils are around 0.39 mg kg^{-1} as reported in the UKSHS (Environment Agency, 2007). The NBC report gives values of Cd concentrations as 1.0 mg kg^{-1} in non-mineralised areas and 17 mg kg^{-1} in mineralised areas (Ander *et al.,* 2013).

Uptake of Cd is governed by plant species as well as soil charcterisitics. For example, some garden vegetables such as lettuces, spinach and cabbages can bio-accumulate higher concentrations of Cd than potatoes and peas (Alloway, 1995). Cd is not an essential element and is therefore toxic in low concentrations to plants and animals. In plants, phytotoxicity is induced at concentrations between 5-20 mg kg^{-1} and is often expressed by chlorosis and stunted growth (Environment Agency, 2007; Samantaray and Rout, 1997).

Cadmium uptake in humans can result in deleterious effects on the kidneys, liver and vascular systems as well as on reproductive endpoints (Thompson and Bannigan, 2008). Chronic effects of Cd can also lead to osteoporosis like symptoms known as itai-itai disease (Pan *et al.,* 2009). The lowest observable adverse effects level (LOAEL) for Cd in small wild mammals is reported to be 3.5–7.5 mg kg^{-1} body weight day^{-1} (Shore and Douben, 1994). In humans, the no effects level is around 500 µg $week^{-1}$ and biological half-life has been shown

to be up to 16 years for humans, highlighting the potential for retention within the body (Jarup *et al.,* 1983).

1.3.3. Copper

Copper (Cu) is usually present in a divalent state (Cu^{2+}) in the soil environment and has an affinity for binding with organic matter (Alloway, 2013). Sources of Cu enrichment in floodplain soils and sediments can originate from geological sources such as the weathering of Cu enriched parent material, or from a variety of anthropogenic sources such as copper containing pesticides, sewage sludge, vehicle emissions and industrial releases (Sharma *et al.,* 2009). The NBC report gives values for Cu concentrations as 62 mg kg^{-1} in non-mineralised areas and 340 mg kg^{-1} in mineralised areas (Ander *et al.,* 2013). Copper in soil typically binds to soil constituents in the order of Mn-oxides> SOM> Fe-oxides > clay minerals (Alloway, 2013). Porewater Cu tends to be bound to dissolved organic carbon (DOC) in the form of humic and fulvic acids.

Copper is an essential element required for biological functions within the body. However, exceeding daily requirements of 0.9 mg day^{-1} (Goldhaber, 2003) for humans can result in a range of health effects from nausea and irritation of nasal passages to damage of the liver and kidneys should enough be consumed (Sharma *et al.,* 2009). Information on the concentrations of Cu required by the ingestion exposure route to induce adverse health effects is scarce; although Muller-Hocker *et al.,* (1993) reported that infants consuming water containing 2-3mg L^{-1} experienced liver damage.

Copper is an essential micronutrient for plants and used in various processes such as photosynthesis and respiration. However, concentrations of > 5 mg kg^{-1} of plant tissue (dry weight) can result in loss of yield in plants (Alloway, 2013).

1.3.4 Lead

Lead (Pb) is a naturally occurring non-essential metal present as thirteen isotopes (Zimdahl and Skogerboe, 1977) and most commonly found in the mineral galena (PbS) (Hettiarachchi and Pierzynski, 2004). It has radiogenic isotopes which originate from the Uranium-235, -238 and Thorium-232 decay series (Komarek *et al.,* 2008). Additional environmental inputs of Pb from anthropogenic activities include: combustion of leaded petrol, fertiliser application, sewage sludge application, Pb piping, paint particles and manufacture, mining and industrial activities (Komarek *et al.,* 2008; Tangahu *et al.,* 2011). Median soil background concentrations within England are 47 mg kg^{-1} although this does increase a thousand-fold in

enriched areas (Ander *et al.,* 2011). The NBC report gives Pb concentrations as 180 mg kg^{-1} in non-mineralised areas and 2,400 mg kg^{-1} in mineralised areas (Ander *et al.,* 2013).

The solubility and mobility of Pb greatly depends upon its chemical form in the soil. For example, compounds such as Pb acetates and Pb chlorides are relatively soluble whereas metallic Pb and Pb phosphate are insoluble in soils (Canadian Council of Ministers of the Environment, 1999). Anaerobic conditions such as prolonged waterlogging or inundation can lead to the formation of insoluble and unreactive PbS. pH is a dominant factor affecting Pb mobility in soils (Sauve *et al.,* 1998) as some Pb compounds, inlcuding $Pb(OH)_2$ are significantly more soluble at lower pH such as pH 4.0 as opposed to pH 7.0 (Canadian Council of Ministers of the Environment, 1999). This is reflected in plant uptake of Pb being higher in low pH soils (Allinson and Dzialo, 1981).

Lead is toxic to humans and reported to affect every organ within the body. Children are the most susceptible to Pb poisoning due to the accidental ingestion of soil (Hettiarachchi and Pierzynski, 2004). Furthermore, children are at a higher risk from Pb exposure as they generally have a higher sensitivity to Pb than adults (Entwistle *et al.,* 2019). Levels of 50-80 µg dL^{-1} will induce symptoms such as joint pain, tiredness and gastrointestinal symptoms in adults (Canadian Council of Ministers of the Environment, 1999). Lead exposure is also known to negatively impact cognitive functions, particularly in children. Studies have shown that performance at school was reduced at blood lead concentrations of ≤ 50 µg dL^{-1} (Skerfving *et al.,* 2015).

1.3.5 Zinc

Zinc (Zn) is a transition metal with 5 stable isotopes and approximately 30 short lived radioisotopes (Broadley *et al.,* 2007) and it is essential for human and animal life. It commonly exists in a 2+ oxidation state, is classed as redox- stable and can form numerous soluble salts and compounds. It enters the soil mainly through geological weathering of parent material and is abundant in the lithosphere, particularly in sedimentary rocks. Anthropogenic inputs occur though mining and smelting activities, phosphate fertiliser inputs and sewage sludge application, as well as industrial emissions from galvanising plants (Alloway, 1995; Newhook *et al.,* 2003; Broadley *et al.,* 2007).

Behaviour in soils is mainly influenced by pH and solubility. Desorption can occur at lower pH so calcareous soils have the potential to limit crop growth due to the reduced availability of Zn. Toxic effects can be observed at levels of 300 mg kg^{-1} dry weight in leaf tissue (Chaney, 1993) often displayed as reduced growth and chlorosis (Nagajyoti *et al.,* 2010). .

Zinc is an essential element used for biological functions such as enzyme activity. Deficiency in Zn in humans can lead to impaired growth and Pneumonia (Hambidge, 2000), while elevated concentrations can prove to be toxic (Fraga, 2005) resulting in vomiting and anaemia (Fosmire, 1990). Recommended daily allowances of Zn are 15 mg day^{-1} with toxic effects observed in humans when intakes are in the region of 100-300 mg day^{-1}.

1.4 Generic Assessment Criteria for Soil PHEs

Generic assessment criteria (GAC) are risk based assessment criteria used for screening soils and determining whether there is potential for risk to human health (Lijzen *et al.,* 2001). GACs have many different names such as 'soil screening values' and 'intervention values', but will be referred to as GACs within this thesis. The different GAC values referred to in this thesis are outlined in Table 1.1.

Table 1.1. Generic Assessment Criteria (GAC) for Soil PHEs.

GAC	Developed by:	Contaminants	Year	Notes:
ICRCL Trigger Values	ICRCL	11 PHEs 5 organic substances	1976	Superseded by SGVs
Soil Guideline Values (SGVs)	Environment Agency	Arsenic, cadmium, chromium, lead, nickel, mercury, selenium, benzo[a]pyrene, inorganic cyanide and phenol.	2002	Superseded by C4SLs and S4ULs
Category 4 Screening Levels (C4SLs)	DEFRA	Arsenic, cadmium, chromium (VI), lead, benzo(a)pyrene and benzene	2014	Less conservative than SGVs
Suitable 4 Use Levels (S4Uls)	Land Quality Management (LQM) /Charted Institute of Environmental Health (CIEH)	89 substances including metals, BTEX, PAHS, phenols, VOCs and pesticides	2015	Uses revised human health exposure assumptions
Dutch Target and Intervention Levels	National Institute for Public Health and the Environment (RIVM)	12 inorganics and 83 organic substances	2000	Dutch criteria

1.5 Physical contaminant (re)-mobilisation and deposition

One method for large scale translocation of PHEs from source to floodplain is through the physical (re-)mobilisation of contaminant containing sediments and soils by floodwaters. The complex nature of floodwater velocities and currents results in a large variation in

suspension and deposition energies. Sediment loading in the water column, shear bed stress and flow velocity also determine deposition rates of sediment bound PHEs onto floodplains. In general, flow velocities are low on large floodplains and therefore such areas are more susceptible to sediment deposition (Forstner *et al.,* 2004).

A source of soil contamination is historically mined ore fields which are common in the UK and Europe. Floodplains within ore field catchments can contain metal rich alluvium originating from spoil tips and contain elements such as Pb, Zn, Cd and Cu (Foulds *et al.,* 2014) at levels that can often exceed soil GACs (Gozzard *et al.,* 2011, Section 1.4). Elevated PHE concentrations may cause negative health effects for receptors exposed to such sediments as well as implications for meeting European Union (EU) wide targets such as the Water Framework Directive's (WFD) chemical and ecological parameters, as enriched sediment can influence PHE concentrations of overlying waters. Mine spoil material can have a high potential for physical movement of PHEs within a catchment because of its nature and often close proximity to water courses.

Foulds *et al.,* (2014) investigated the physical remobilisation and consequent deposition of mining alluvium in Welsh catchments affected by the 2012 floods. The study quantified elemental sediment contamination throughout a series of Welsh catchments and found a large proportion of sampled sites exceeded industrial soil guideline values (SGVs), by up to a factor of 71. Industrial guideline values are the most generous with respect to the SGVs. The wider implications of the contaminated sediment mobilisation were explored by sampling from previously inundated allotments and floodplain grown silage bales (Foulds *et al.,* 2014). In this study the Dutch soil guideline values (Table 1.1) were exceeded in allotments and homogenous contamination profiles showed mixing of flood sediments into the soil profile as a result of cultivation. Silage bales also exceeded Pb benchmark criteria for animal feeds (EC Directive 2002/32/EC) and the introduction of these contaminated foodstuffs to cattle resulted in Pb blood poisoning and mortality of young livestock.

The study by Foulds *et al.,* (2014) conveys the wider implications for physical PHE remobilisation in relation to PHE exposure and highlights a river's effectiveness at dispersing contaminants. It also reinforces the view that a geomorphological approach is needed to identify sensitive sedimentation zones in a catchment, as physical movement can establish a link between source and receptor. For example, large scale bank erosion was responsible for the deposition of mining waste contaminated sediments on the River Swale floodplain during autumn flooding events in 2000 (Dennis *et al.,* 2003). In light of the predicted increases in

the magnitude and intensity of flooding events the identification of contaminant sources, such as mining spoil heaps, which may be susceptible to large scale remobilisation downstream, could act as a driver for the remediation of such sites.

Flooding induced contaminant movement has been investigated using paired farms within the UK. Paired farms can provide useful comparisons for assessing the effects of flooding on contaminant levels in grazing land in industrial catchments (Lake *et al.,* 2014; Lake *et al.,* 2015). Lake *et al.,* (2015) used paired farms to assess soil, grass and animal product levels of dioxins and polychlorinated biphenyls (PCBs) and found concentrations to be significantly higher in industrial catchment floodplain farms, as opposed to those situated in non-industrial catchments. Samples were also collected from flooded and non-flooded areas of one field, with the flooded sections having PCB concentrations that were at least four times higher.

When determining the fate of (re-)mobilised contaminants it is important to understand floodplain sediment dynamics. Greenwood *et al.,* (2013) investigated sediment remobilisation over a series of inundation events using labelling techniques with artificial radioisotopes: caesium-134 ($t_{½}$ = 2.06 years) and cobalt-60 ($t_{½}$ = 5.26 years). Three consecutive inundation events were studied, and significant amounts of sediment were removed during the first two flooding events: 63.8 % and 11.9 % respectively. No significant sediment (re-)mobilisation occurred during the third event because of the amount of sediment removal which occurred during the first two events. Furthermore, topography was found to have affected spatial differences in remobilisation. The large-scale sediment loss observed during the first two flooding episodes highlights the ability of flood waters to act as an effective disperser of PHEs from source to floodplain.

Sediment transport models have also been used for predicting the fate of remobilised PHE enriched sediment (e.g. Coulthard and Macklin, 2003; Singer *et al.,* 2013; Kinouchi *et al.,* 2015). It has been reported that up to 90 % of PHEs are transported from a source in a sediment bound form, conveying the usefulness of such sediment dynamic tools as predictors of PHE fate (Coulthard and Macklin, 2003). The output of one particular model called TRACER showed that 70 % of PHEs were retained within the River Swale's floodplain sediments 200 years on from mine closure (Coulthard and Macklin, 2003). Interestingly, the model's outputs from the River Swale show that the increased flood magnitudes predicted by climate models will result in the dilution of PHE enriched floodplain sediments with 'clean' sediments originating from 'clean' areas within the catchment. This result is very catchment

specific and reliant on the geomorphology of the area and the extent of PHE enriched soils and sediments.

Rivers can physically remobilise and redistribute PHEs within a catchment but it is the ability of flood events to change the chemical behaviour and characteristics of PHEs that dictates their potential availability to receptors and ability to chemically mobilise into overlying and porewaters. It is therefore important to understand how PHEs behave under changes during wetting and drying to determine their risk to human and ecological health.

1.6 Physico-chemical changes

Changes in climate, particularly prolonged wetting cycles or periods of drought can act as drivers for changes in soil components. This can in turn affect chemical PHE mobility. PHEs exist in soil and sediments in different fractions, which dictate their ecotoxicity, availability, solubility and mobilisation potential. The fractions within soil and sediments have mainly been defined as water soluble, exchangeable, carbonate-associated, Fe-Mn oxides associated, organic/sulphide associated and residual, as shown in Figure 1.3 (Li *et al.,* 2001; Luo *et al.,* 2011; Park *et al.,* 2011). PHEs associated with the residual fraction are in general less available to plants, animals and microorganisms, whereas those present in the water soluble and exchangeable fractions etc. may be available, depending on the surrounding physico-chemical environment.

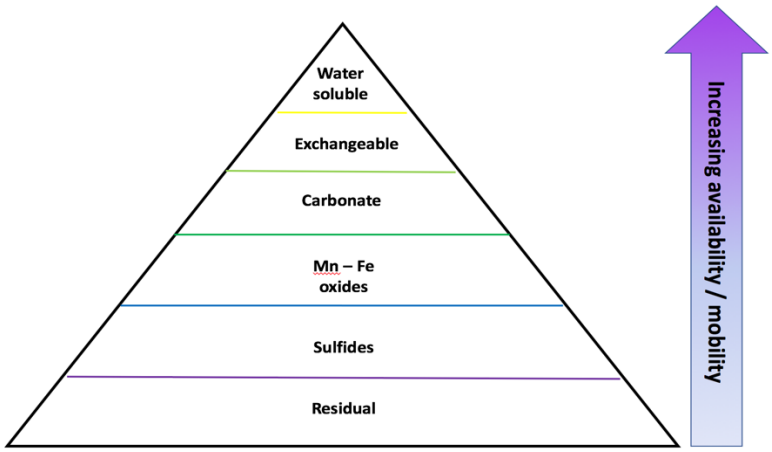

Figure 1.3: common solid phase fractions of soil and their potential for mobility/availability.

PHE mobilisation during inundation can result in the disassociation with one fraction before associating with another, potentially resulting in changes in mobility/availability. Influential controlling factors of PHE mobility processes include pH, temperature, redox potential, SOM content and microbial activity. These processes can be summarised as:

- Dissolution of carbonates and metal oxides during reducing periods
- Dissolution of sulphates during oxidising periods
- Precipitation of metal sulphide complexes during strong reducing conditions
- Adsorption onto Fe-Mn (hydr)oxides during oxidising conditions or prolonged reducing conditions
- Decomposition or association with organic compounds

A rise in river stage generally results in the inundation of river bank sediments and floodplain soils, causing reductions in pH and oxidisation reduction potential (ORP) (Frohne *et al.,* 2011). A high ORP results in oxidising conditions and low ORP promotes reducing conditions. Changes in pH and redox potential can significantly alter the speciation and solubility of metals, therefore affecting their potential availability and mobility (Charlatchka and Cambier, 2000). During periods of inundation, aerobic microbes consume any remaining oxygen over a period of hours to days. Once oxygen levels have depleted, facultative and strict anaerobes utilise electron acceptors in the order of: nitrates, manganese oxides, iron oxides and sulphate (Lynch *et al.,* 2014). The latter three are displayed in equations 1 to 3 and Figure 1.4. The reduction of sulphate produces sulphides, which can precipitate with metals to form insoluble metal sulphide complexes. This reaction occurs at low redox potentials of around -150 mV (Du Laing *et al.,* 2009).

(1) $MnO_2 + 2e^- + 4H^+ \leftrightarrow Mn_2^+ + 2H_2O$

(2) $Fe_2O_3 + 2e^- + 6H^+ \leftrightarrow 2Fe_2^+ + 3H_2O$

(3) $SO^{-2}_4 + 8e^- + 8H^+ \leftrightarrow S_2- + 4H_2O$

Fe-Mn (hydr)oxides, shown in equations 1 and 2, are amorphous or microcrystalline substances with a high affinity for metal sorption. Dry soils that are then subjected to sudden rewetting demonstrate high levels of metal release into overlying and porewater. For example, under reducing conditions, Fe(III) is reduced to Fe(II) and Mn(III/V) to Mn(II) resulting in the mobilisation of associated PHEs. This process happens at about +200 mV in acidic and neutral soils but considerably lower ORP values for alkaline soils (Bissen and Frimmel, 2003). The release of PHEs from Fe-Mn (hydr)oxides and consequential rise in

porewater and overlying water PHE concentrations is dependent on the duration of inundation, as prolonged flooding can result in the immobilisation of metals because of the formation of metal sulphide complexes, as shown in Figure 1.4 (Lynch *et al.,* 2014). This arises from the reduction of sulphates, shown in equation 3. Metals such as Cu, Cd and Zn often form direct precipitates with sulphides (CuS, CdS and ZnS), or PHEs can co-precipitate with FeS minerals (Du Laing *et al.,* 2007). The formation of such insoluble compounds can result in a decline in porewater and overlying water PHE concentrations.

Relationships between organic matter and PHEs are complicated and depend on the form of the SOM and individual PHEs. SOM can act as both a source and sink for PHEs within soils during inundation. Complexation of PHEs with dissolved organic matter (DOM) resulting from SOM degradation can result in increased PHE mobilisation and availability for uptake by plants (Grybos *et al.,* 2007; McCauley *et al.,* 2009; Zheng *et al.,* 2011). For example, SOM can also influence As mobility by facilitating reduction and oxidation reactions in soil (Redman *et al.,* 2002; Dobran *et al.,* 2006). SOM is reported to be competitive with both As(V) and As(III) with binding sites on Fe-oxides such as hematite (Redman *et al.,* 2002), and increases in DOC are known to coincide with increases in As mobilisation, particularly for As(III) (Dobran *et al.,* 2006). Increases in soil pH can weaken positive surface charges on SOM, resulting in As release from soil particles (Grybos *et al.,* 2007). Flooding induced desorption can happen at higher redox potential for OM than Fe(II) (Grybos *et al.,* 2007), suggesting that SOM could play a greater role in As mobilisation than Fe for some soils (Williams *et al.,* 2011).

A return to oxidising conditions seen during receding flood waters promotes the oxidation of sulphides and the release of associated PHEs. This spike in PHE concentrations can be attenuated by the reformation of poorly crystalline or amorphous Fe/Mn minerals (Du Laing *et al.,* 2007). Contrastingly, in some cases slow oxidation kinetics of many metal sulphides result in a large portion of metals being retained within the sediments themselves (Chapman, *et al*., 1998). Stable conditions of ORP over time can promote mineral aging and the immobilisation of metals and metalloids but repeated wetting and drying of sediments may prevent this, resulting in the increased availability within floodplain soils and sediments. Understanding the effects of these redox-transitional zones that form on river floodplains as a result of inundation is therefore important for predicting the behaviour of metals and metalloids. A summary of PHE behaviour as a consequence of flooding is shown in Table 1.2.

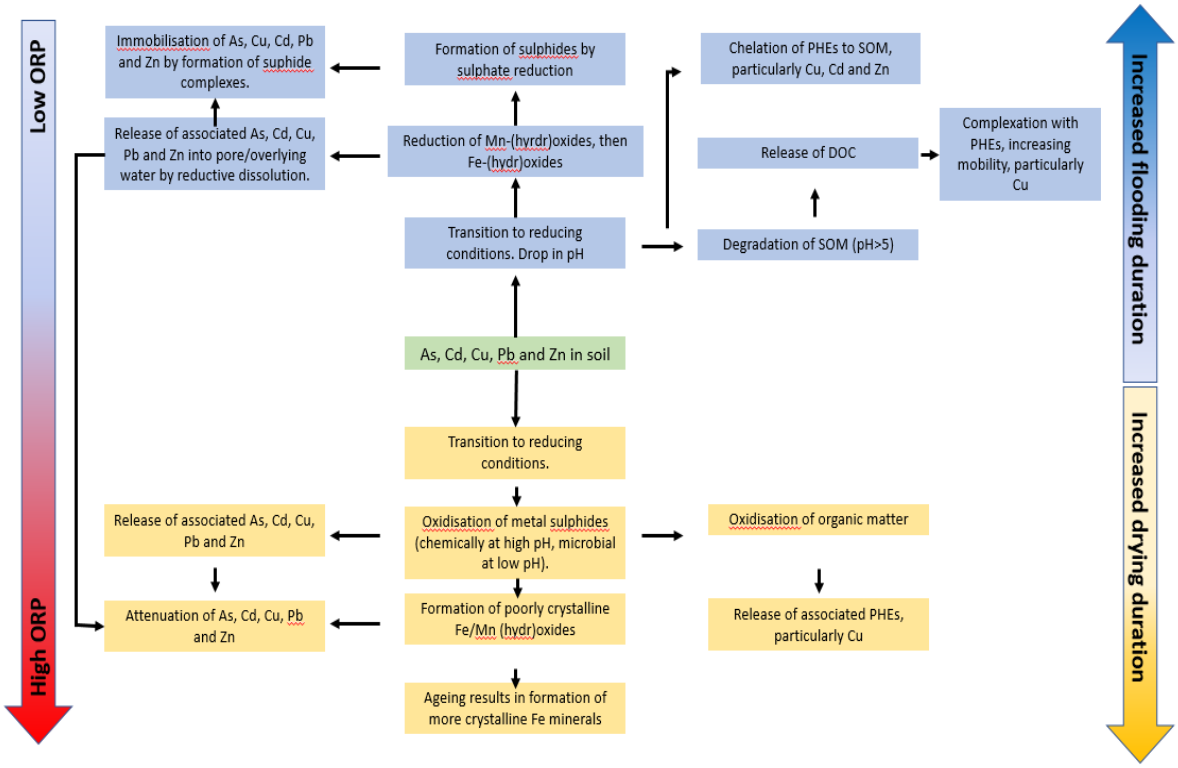

Figure 1.4: conceptual model of the main physico-chemical changes during flooding.

Table 1.2: Summary of PHE behaviour under flooding.

PHE	Mainly associated with:	Main drivers of mobilisation	Immobilised by:	References
Arsenic	Iron (hydr)oxides	Redox potential Reactivity of Iron hydr(oxides)	Sulphides	Alloway (2013) Roberts *et al.*, (2010) Huang (2014)
Cadmium	Zinc bearing minerals Fe (hydr)oxides	Redox potential pH Reduction of Fe/Mn oxides	Sulphides	Alloway (2013) Robson *et al.*, (2014) Kashem and Singh (2001) Honma *et al.*, (2016)
Copper	Organic matter	Complexion with DOC	Sulphides	Du Laing *et al.*, (2009) Liu *et al.*, (2013)
Lead	Fe/Mn hydr(oxides) Organic matter	pH Reduction of Fe oxides Complexion with DOC	Sulphides Phosphates	Alloway (2013) Du Laing *et al.*, (2009)
Zinc	Zinc bearing minerals Fe (hydr)oxides	Redox potential pH Reduction of Fe/Mn oxides Complexion with DOC	Sulphides	Alloway (2013) Du Laing *et al.*, (2009) Kashem and Singh (2001)

1.6.1 Evidence of flooding induced PHE mobility from the literature

Studies on how temperature, gas phase composition, pH and microbial activity can affect As and Zn release (Joubert *et al.,* 2007) have shown temperature to have a clear and significant relationship with As release. The effects of microbial activity on PHE mobility were less clear as half of the samples displayed positive relationships and half displayed a negative relationship between microbial activity and PHE mobility. Experimental design was expected to account for the negative relationships observed because microbial activity itself is affected by the physical and chemical status of soils; highlighting the intricate and complex nature of chemical mobilisation. Additionally, flood waters can increase the levels of DOC; which in turn can promote microbial activity (Lynch *et al.,* 2014). Given that climate change is predicted to affect microbial activity through changes in temperature and precipitation (Joubert, *et al.,* 2007) this may result in changes to the distribution of PHEs in soils and sediments.

A study by Tack *et al.,* (2006) examined the effects of soil moisture content and hydrological regimes on soil solution content of Cu, Cd and Zn. Soils were either kept dry, at field capacity or inundated with water for 14 days before being returned to field moisture capacity and sampled. Concentrations were highest in porewaters of dried soils and lowest in those of inundated soils. This is likely to be due to a surge of microbial activity within the re-moistened dried soils causing temporary anaerobiosis, highlighting the importance of sudden rewetting of dried soils (Tack *et al.,* 2006). Changes in redox potential are also known to be driven by factors such as temperature and SOM content. For example, small changes in water content combined with optimal temperature and SOM will result in a lowering of E_h promoting reducing conditions; whereas, low temperatures combined with flooding conditions can result in E_h remaining positive (Schulz-Zunkel and Keuger, 2009).

In laboratory experiments conducted by Du Laing *et al.,* (2007), contaminated floodplain soils were subjected to different durations of wetting and drying cycles to determine the effects on porewater PHE content. PHE content was found to vary significantly with moisture regime. Mn and Fe concentrations increased in porewater during periods of inundation; which highlights reductive dissolution of these oxides with Mn oxides in particular reflecting the hydrological regimes. Cd concentrations rise initially and then decrease steadily over time with permanent inundation. This is likely to be attributed to its combination with sulphides, resulting in the immobilisation of Cd. Cyclic wetting episodes followed by drying showed a peak in Cd concentrations during dry episodes and a low during inundation,

potentially because of dilution effect during soil flooding. Zn tends to peak during mid drying periods and porewater concentrations were found to be lowest during inundation periods. This release during drying periods may be attributed to the oxidisation of sulphides and subsequent release of PHEs. With respect to Cr and Zn, short periods of inundation (around 2 days) followed by longer periods of drying are likely to result in increases in their mobility. Our current understanding of the factors controlling the behaviour of PHEs highlight the importance of potential climatic changes as intense periods of rainfall followed by prolonged periods of drying could result in an increased availability of PHEs, potentially increasing the risk to receptors.

1.7 Availability to plants and wildlife

Flooding induced PHE (re-)mobilisation has been reported to pose toxicological risks to aquatic organisms occupying the water column when they are taken up in to the body (Wolz *et al.,* 2009). Bioavailability is the proportion of any particular PHE that crosses the gastrointestinal wall and is available for uptake by a receptor (Naidu *et al.,* 2008). The bioavailable fraction of PHEs can be between 0 % and 100 % depending on the source and receptor characteristics (Vig *et al.,* 2003).

Phytoavailability, defined as availability to plants, is greatly dependent and influenced by a variety of factors, including pH, cation exchange capacity, organic matter content, Fe and Mn oxides and redox potential (Wong, 2003). pH is deemed to be the most important factor controlling metal availability to plants and has a negative correlation with availability, as PHEs are usually more available at a lower pH (Zeng *et al.,* 2011). For example, reduction in soil pH induced desorption and dissolution from soil constituents for Cd, Zn and Pb (Zeng *et al.,* 2011). Metals can be maintained in an available form by organic matter, which can also supply chelating agents to the soil, further increasing metal availability to plants (McCauley et al., 2009). For example, the addition of chelating agents to soils has been shown to increase the uptake of Pb by plants (Blaylock *et al.,* 1997). Phytoavailability is also element specific, for example, Zn being essential for life is readily taken up by plants, because it is relatively labile and less strongly bound to soil than other elements, such as Cu (Smith, 2009).

The thin film diffusive gradient technique (DGT) is an effective technique for measuring the availability of PHEs by providing in situ measurements of labile PHE concentrations. DGT was first applied to soils in 1998 and has proven an effective mimic of plant uptake mechanisms as local concentrations are reduced (Zhang et al., 1998). As a result, DGT can account for rates of supply and release. In an assessment into the inundation of floodplain soils

containing elevated levels of Cu, use of DGT showed that Cu availability was considerably higher in the first week after inundation but then immobilised for the remaining study period (van der Geest *et al.,* 2008). Available Cu was predicted to be lost into the overlying water column or utilised by Mn and Fe hydroxides at the sediment water interface (van der Geest *et al.,* 2008). However, other studies suggest that the reduction of Mn and Fe oxides result in the release of PHEs such as Cd and Zn (Teuchies *et al.,* 2013), highlighting the implications of short term flooding events as previously unavailable PHEs may become available and be released into the overlying water column. However, prolonged periods of flooding over several weeks reduced the availability of certain PHEs due to reducing conditions. This work did not consider the subsequent periods of drying that will follow inundation which has been shown to increase the availability of some inorganic elements such as phosphorous (Schönbrunner *et al.,* 2012). DGT was not used in this project as the receptors of interest were humans, so bioaccessibility testing was a more appropriate method of determining availability of PHEs.

Floodplains containing enriched levels of PHEs can also have implications for grazing animals, especially those destined for human consumption. The movement and subsequent deposition of alluvium results in fertile floodplains, which are often used for agricultural purposes. Smith *et al.,* (2009) examined Pb partitioning in Welsh mining catchment floodplains and potential availability to sheep. The highest Pb concentrations were found in vegetation in winter months (January to March) and the study stated that Pb concentrations often exceeded the Inter Departmental Committee for the Redevelopment of Contaminated Land (ICRCL) (1990) trigger levels. There is a potential risk to grazing livestock of bioaccumulation of Pb as sheep are exposed to both soil particles and vegetation when grazing., The study by Smith et al., (2009) looks at the potential availability of Pb to grazing animals using pseudo-total Pb concentrations and suggests that animals are at risk of toxicological effects calculated from soil ingestion rates for the year. However, these calculations do not consider the available mass of ingested Pb to the sheep as the study did not chemically simulate the sheep stomach. Consequently, there may be an over or under estimation of the potential risks of animals grazing on this specific floodplain.

1.8 Human Bioaccessibility

Human risk assessments of contaminated soils assume that the total amount of contaminant present within a soil is available for uptake within the human body. This is now considered to be conservative as only a proportion of a contaminant generally dissolves within the

digestive system (Pelfrêne *et al.,* 2012). Human bioaccessibility is therefore defined as the proportion of a contaminant that is released into solution by digestive fluids (Wragg *et al.,* 2011). Once a PHE crosses the intestinal wall then it can enter the blood stream, potentially resulting in detrimental health effects.

Measurements of bioaccessibility are intended to provide a better estimate of the maximum amount of PHEs available for uptake across the intestinal wall and are particularly useful inputs into the types of decision making tools typically used for human risk assessments. Such measurements are usually carried out *in vitro* using simulated gastrointestinal fluids, as *in vivo* studies are often costly and subject to ethical approval (Wragg *et al.,* 2011).

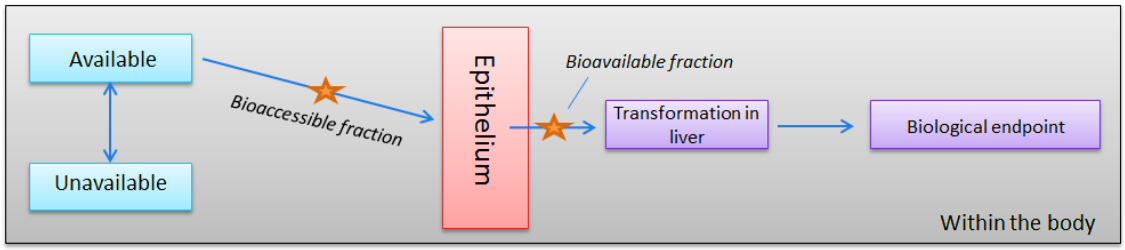

Figure 1.5: overview of PHE movement inside the body.

Quantification of soil ingestion has been estimated by the US Environmental Protection Agency at around 200 mg day^{-1} (US EPA, 2002). However, some pica affected children can ingest up to 20 g day^{-1} (Van der Wiele, 2007). Pathways include hand to mouth transfer often by children engaging in outdoor activities, ingestion of soil present on vegetables or other garden produce or inhalation of airborne particulate material (e.g. as a dust). Ingestion and inhalation of soil tends to be confined to smaller soil particles (<250 µm) as they are more likely to be ingested and adhere to hands (Ruby and Lowney, 2012; Cave *et al.,* 2013). The <10 µm fraction represents airborne particulate matter that can be inhaled and has been used in studies that mimic epithelial lung fluid, including studies by Dean *et al.,* (2017). The larger surface to volume ratio results in higher concentrations of PHEs being present in these fractions (Madrid *et al.,* 2008; Dennis *et al.,* 2003). Once PHE enriched material has been ingested and digested in the gastrointestinal environment, the bioaccessible fraction has the potential to cross the intestinal epithelium and enter the blood stream (Figure 1.5). Once in the circulatory system the fraction of contaminant is referred to as the bioavailable fraction and is transported for biotransformation within the liver (Van der Wiele, 2007). The definition of the terms bioaccessibility and bioavailability here refer to those associated with human risk assessment.

Pelfrêne *et al.,* (2012) used a statistical modelling approach to predict bioaccessibility in agricultural soils contaminated by a nearby Pb smelter. Strong relationships were found between predicted and measured Pb bioaccessibility for gastric and gastrointestinal phases (R_2 > 0.84). It was found that total carbonate, organic matter, sand, phosphate, free Fe-Mn oxide, pseudo-total Al and trace element content appeared as the main variables governing bioaccessibility. Following on from this, Pelfrêne *et al.,* (2013) applied the modelling approach to forest and urban soils to investigate the effects of land use on bioaccessibility. Both studies highlight that there are an influential set of variables on contaminant bioaccessibility. However, the work focused solely on a small number of soil types and PHEs so there is scope to investigate the relationships between the solid phase distributions of PHEs and consequently predict bioaccessibility in other soil types.

Additional routes for PHE exposure to humans can arise through the ingestion of contaminated animal products, as animals grazing on PHE enriched soils can accumulate PHEs in their tissues (Abrahams and Blackwell, 2013; Foulds *et al.,* 2014). Ruminants are a prominent dietary component for many human beings. Because of their physiology, bioaccessibility tests representing the human GI environment, such as the BARGE (BioAccessibility Research Group of Europe) Unified BARGE Method (UBM), are not applicable for estimation of animal uptake. Furthermore, the bioaccessibility of polycyclic aromatic hydrocarbons (PAHs) in different digestive compartments in cows has been studied showing that bioaccessibility varied between the different compartments and that monogastric models may not be suitable (Jurjanz & Rychen, 2007). Instead, four compartments need to be simulated: the rumen, abomasum, intestinal colloids and intestinal liquids. Using this model, Jurjanz & Rychen (2007) showed that bioaccessible phenanthrene was elevated in the rumen compartment (17 to 24 %) but remained relatively unaffected in the remaining compartments, with intestinal fluid solubilisation rates remaining at about 25 % regardless of the compound.

The bioaccessibility of PAHs to humans has been reviewed by Harris *et al.,* (2013) who highlighted that PAH bioaccessibility testing needs further research. Currently, the majority of bioaccessible tests are based around the ingestion of soil, whereas PAHs are often ingested in foodstuffs and do not consider dietary fats that are known to be influential towards PAH bioaccessibility.

There are few studies investigating the effect of flooding and hydrological regimes on the bioaccessibility of PHEs. One study by Florido *et al.,* (2011) demonstrated that

bioaccessibility is not consistently affected by flooding and that it is likely other factors such as the solid phase distribution of PHEs that will impact flooding induced change in bioaccessibility. For example, one soil from a mining affected catchment in south west Spain demonstrated an increase in bioaccessible Pb of 200 % whereas Zn showed a reduction in bioaccessibility. Reducing conditions were induced for 15 days by flushing with N_2. Samples and soil samples were dried prior to bioaccessibility testing using the Simple Bioaccessibility Extraction Test (SBET) glycine method. Consequently, the results obtained from this study may not be representative of the effects of flooding on PHE bioaccessibility in the environment during and post flooding events, as reductions in ORP may happen quicker in artificial systems flushed with N_2. Drying of soils is also known to affect PHE bioaccessibility prior to bioaccessibility testing which may result in an under or over estimation of flooding induced changes in PHE bioaccessibility (Furman et al., 2007).

Inundation of soil under anoxic conditions has shown increased bioaccessibility of Cu and Pb to humans. (Florido *et al.,* 2011). Soils were kept under reducing conditions before drying. It is possible that the increase in the bioaccessibility of Cu and Pb could be attributed to the sudden oxidisation of the soils post reduction phase. There is evidence that some PHEs peak in availability during drying phases after inundation (Du Laing, 2007) which may explain the observed increases in bioaccessibility. This increase upon drying was demonstrated in a study by Furman *et al.,* (2007) where wetland soils were either dried, freeze dried or, as wet soils, before subjected to bioaccessibility testing. The results demonstrated that bioaccessible Pb was on average 15 % lower in wet soils as opposed to dried soils (corrected for water content), indicating that standard sample preparation methods which involve the oven drying of soil may result in over estimation of Pb bioaccessibility. The authors concluded that this was because of oxygenation of soils during drying and an increase in Mn extractability. Taking this into account, there is scope to examine the effects of wetting and drying cycles on PHE bioaccessibility. Combining this with knowledge on changes in the solid phase distribution of PHEs would give insight into the fractions of soil that are most bioaccessible.

1.9 Project Rationale

Developing a greater understanding of the behaviour and fate of PHEs within catchments is important for predicting the potential risk of exposure to humans and biota as well as water quality parameters such as those outlined by the water framework directive. Climate change is likely to influence the hydrological cycle and potentially result in more frequent and extreme flood events. As floodwaters have the ability to physically redistribute sediment

contaminated with PHEs within a catchment, there is potential for their relocation to areas where humans are present and may interact with the soil such as allotments or farmland. Inundation of floodplain catchments that have PHE enrichment may provide a link between source and human receptors via flooding induced increases in the availability and bioaccessibility of PHEs.

A review of the literature showed that there has been considerable interest, and studies into, the remobilisation of PHEs because of inundation. PHE behaviour and fate in floodplain soils has been shown to be complex, dependent on soil properties and to be element specific. Wetting and drying cycles have been shown to result in changes in availability, bioaccessibility and solid phase distribution of PHEs. Specifically, work has looked at the effects of altered wetting and drying regimes on PHE concentrations in porewater indicating that prolonged periods of drying followed by inundation promote the greatest release of PHEs into solution.

Most studies have been confined to the laboratory. Therefore, mesocosm studies simulating repeated wetting and drying cycles of floodplain soils using whole soil blocks could provide greater insight in more realistic scenarios. The relationships between soil characteristics and PHE mobility have been studied fairly intensively, but not with respect to wetting and drying cycles and how this can influence the mechanisms of PHE release. A detailed understanding of the effects of the magnitude and intensity of wetting and drying cycles on PHE mobility is lacking in the literature, meaning there is scope for new studies to explore this further.

Consequently, the following recommendations for the assessment of flooding induced PHE mobility on human and environmental health that will be used for this study are:

- Detailed laboratory studies involving wetting and drying cycles to geochemically characterise the flooding induced changes in bioavailability and bioaccessibility of PHEs.
- Avoiding the use of intrusive sample preparation techniques such as drying prior to bioaccessibility testing to gain a more realistic insight into PHE bioaccessibility during and post flooding.
- To determine any relationships between soil characteristics, land use, flooding and temperature regimes and bioaccessibility allowing for the prediction of human health risk indices of PHE enriched catchments.

1.10 Project aims

The primary aim of this project was to determine the effects of wetting and drying cycles on the mobilisation and bioaccessibility of PHEs in a UK catchment. This was achieved by:

- Assessing the mobility of PHEs from a range of soils within a UK catchment under wetting and drying cycles.

Soils vary greatly in their characteristics, and therefore PHE mobilisation into pore and overlying waters is unlikely to follow the same trend for each individual soil, resulting in heterogeneous mobilisation of PHE in a catchment. The underlying mechanisms driving such mobility can be examined by:

- Geochemically characterising changes in the solid phase distribution and the human accessibility of PHEs before, during and after drying and wetting – a novel approach not previously investigated in detail.

Assessing these changes could provide useful information for the effective management and remediation of PHE enriched soils utilised by human receptors. To assess the spatial extent of PHE mobilisation, the final project objective was to:

- Predict and map changes in PHE bioaccessibility in select catchments under flooding.
- These predictions could be used to locate areas within a catchment where there is a greater propensity for changes in PHE availability and those areas where the greatest risk of mobilisation may occur under inundation. The outcomes from this project are catchment specific and a proof of concept that geochemical tools such as sequential extractions, chemometric modelling and bioaccessibility testing can be used to spatially predict bioaccessibility and subsequent flooding induced change in the bioaccessibility of PHEs.

The objectives and project as a whole are displayed pictorially in Figure 1.6. More specific aims and objectives are outlined in each of the data chapters.

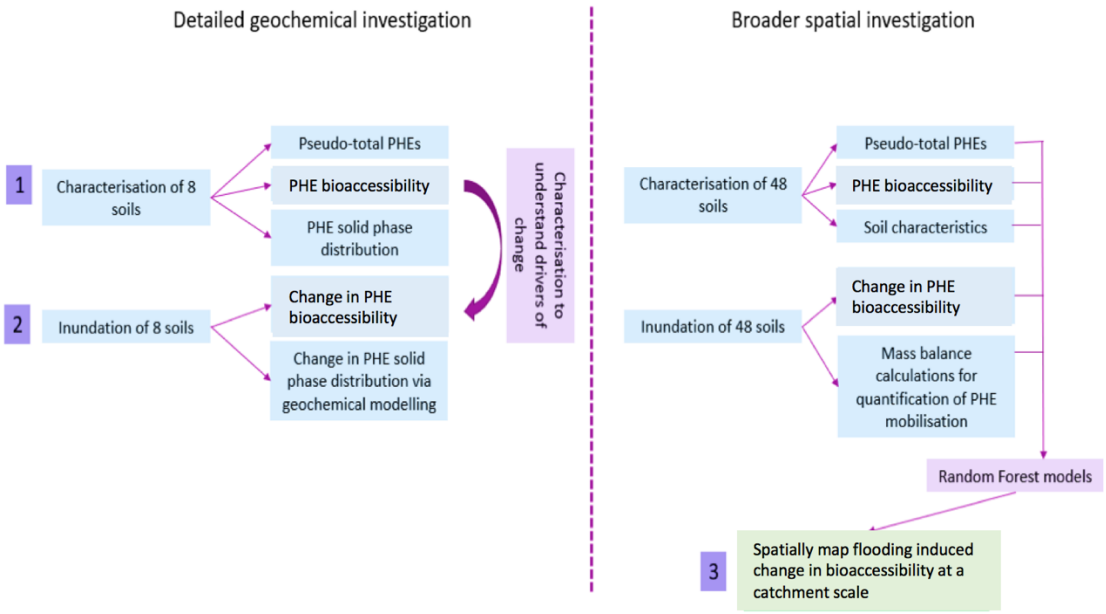

Figure 1.6: Project overview.

2. SITE DESCRIPTION AND METHODOLOGY

2.1 Introduction

This chapter describes the study site and sample collection methodologies and the experimental methodologies used in multiple chapters along with associated instrumentation and quality control procedures. Some methodologies only used in specific experiments applicable to one chapter are described in the associated chapter.

2.2 Site description

2.2.1 Catchment overview

The Tyne catchment in North East England covers an area of approximately 2,300 km^2 and includes the rivers Allen, Derwent, Rede, South and North Tyne. The catchment has several reservoirs supplying water regionally and which are used to regulate river flow in the Tyne, Wear and Tees river systems via water transfer infrastructure. Upper areas of the catchment are remote and composed of narrow valleys. The middle catchment is mainly comprised of alluvial floodplain soils and used for agriculture. The lower reaches of the river are heavily urbanised and contain the majority of the catchment's 1 million people (Tyne Catchment Flood Management Plan, 2009).

2.2.2 Flooding in the Tyne catchment

The steep sided upland valleys of the Tyne catchment can result in a flood wave which travels down through the catchment, increasing in size (Figure 2.1). Flash floods tend to occur in the summer months from localised cells of extreme rainfall occurring in short and intense bursts. For example, 26.2mm of rainfall was recorded to fall in 15 minutes in Alston (Archer and Fowler, 2015). The sudden increases in discharge (Q) seen in Figure 2.1 shows the responsiveness of the upper Tyne catchment to such rainfall events.

Recent large flood events have been recorded in 2005, 2012 and 2015/2016. Intense rainfall (50 mm) was recorded over a two-hour period in 2012, resulting in the flooding of homes, landslides and damage to highways. Flood depths were estimated to be between 0.1 - > 1.1 m (Smith *et al.,* 2017). The more recent floods in 2015/2016 were considered to be the highest on record since the 1771 (Barker *et al.,* 2016).

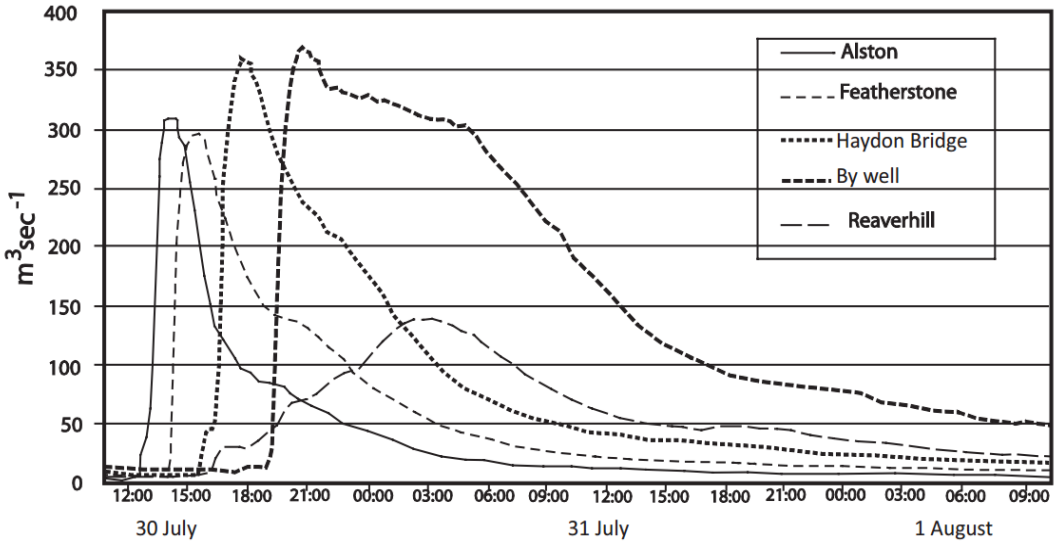

Figure 2.1: Progress of the flood wave through the Tyne catchment. Sourced from Archer and Fowler, 2015.

2.2.3 Underlying geology

The North and South Tyne catchments are mainly underlain with sedimentary rocks such as sandstones, mudstones and shales from the Carboniferous period. Small igneous outcrops of andesite in the North Tyne and dolerite in the South Tyne are also present. Areas of mineralisation are confined to the headlands of the South Tyne, and in small areas near the North/South Tyne confluence (Figure 2.2).

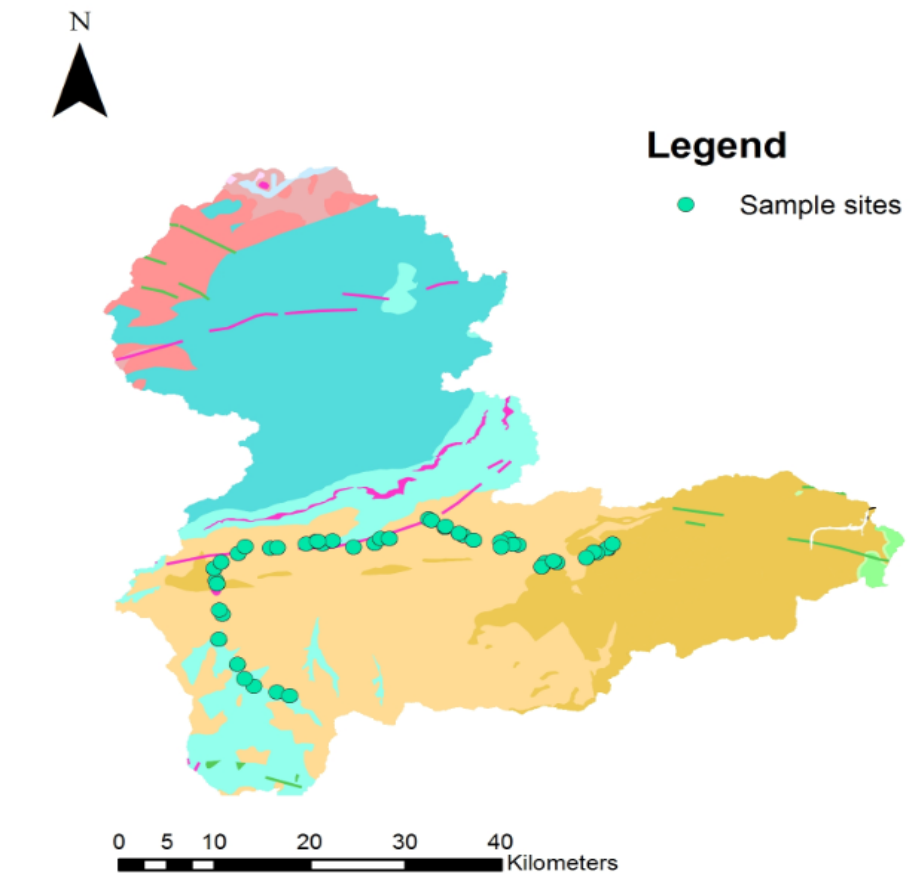

DOLERITE AND THOLEIITIC BASALT
DOLOMITISED LIMESTONE AND DOLOMITE
DOLOSTONE

LAVA, TUFF, VOLCANICLASTIC ROCK AND SEDIMENTARY ROCK
LIMESTONE
LIMESTONE AND CALCAREOUS SANDSTONE
LIMESTONE AND MUDSTONE, INTERBEDDED
LIMESTONE WITH SUBORDINATE SANDSTONE AND ARGILLACEOUS ROCKS
LIMESTONE, ARGILLACEOUS ROCKS AND SUBORDINATE SANDSTONE, INTERBEDDED
LIMESTONE, MUDSTONE AND CALCAREOUS MUDSTONE
LIMESTONE, MUDSTONE, SANDSTONE AND SILTSTONE, WITH SUBORDINATE CHERT, COAL AND CONGLOMERATE
LIMESTONE, SANDSTONE, SILTSTONE AND MUDSTONE

METALIMESTONE
METASEDIMENTARY ROCK
METAVOLCANICLASTIC IGNEOUS-ROCK AND METAVOLCANICLASTIC SEDIMENTARY-ROCK
MICA SCHIST
MIGMATITIC ROCK
MUDSTONE, CHERT AND SMECTITE-CLAYSTONE
MUDSTONE, SANDSTONE AND CONGLOMERATE
MUDSTONE, SANDSTONE AND LIMESTONE
MUDSTONE, SILTSTONE AND SANDSTONE
MUDSTONE, SILTSTONE, LIMESTONE AND SANDSTONE
MUDSTONE, SILTSTONE, SANDSTONE, COAL, IRONSTONE AND FERRICRETE

SANDSTONE, SILTSTONE AND MUDSTONE

Figure 2.2: Bedrock geology found in the Tyne catchment. Sample locations added for reference. Data sourced from: https://map.bgs.ac.uk/arcgis/services/BGS_Detailed_Geology/MapServer/WMSServer?

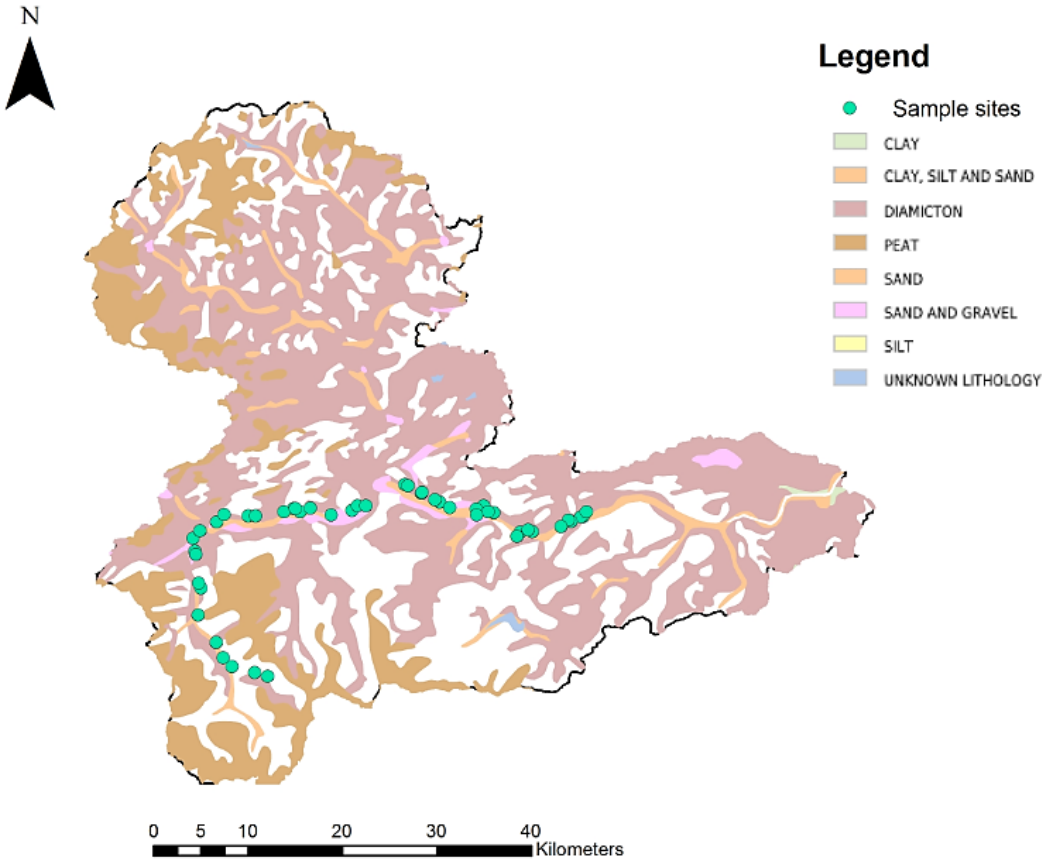

Figure 2.3: Superficial deposits or geology found in the Tyne catchment. Sample locations added for reference. Data sourced from: https://map.bgs.ac.uk/arcgis/services/BGS_Detailed_Geology/MapServer/WMSServer?

2.2.4 Industrial history

The Tyne catchment has a rich industrial history, which still results in the introduction of a suite of geogenic and anthropogenic contaminants such as metals and organic substances into the river system despite the decline in heavy industry. Currently, a significant source of PHEs into the Tyne system is from the many abandoned metal mines found in the catchment, particularly in the rivers Nent, East Allen and West Allen (Table 2.1). The Northern Pennine ore fields cover an area of 4,000 km^2 and are believed to have affected 12,000 km^2 of river basin, including the Tyne valley resulting in sediment PHE concentrations such as Pb, As and Zn exceeding SGV values (Macklin *et al.,* 1997). Inputs from abandoned metal mines occur through both point and diffuse sources. Mine adits can drain metal rich water from the mines

directly into watercourses. More diffuse sources occur though the erosion and transportation of PHE rich mining spoil which are found frequently in the upper catchments (Figure 2.4) through both physical and chemical pathways, as outlined in Sections chapter 1.5 and 1.6.

Table 2.1: Ranges of sediment PHE concentrations in mg kg^{-1}. nr = not recorded.

River	As	Cd	Cu	Pb	Zn	Source
West Allen	nr	5-33	22-40	98-3166	74-1131	Aspinall and Macklin, 1985
Nent	nr	nr	nr	224-15,800	4,360-38,000	Macklin, 1986
South Tyne	nr	nr	nr	15-10,490	130-15,270	Macklin and Lewin 1989
South Tyne	nr	2.3-116.9	8-384	410-9,798	590-16,520	Macklin and Smith, 1990
South Tyne	nr	1.8-160	16.8-228	2,770-13,000	791-38,200	Hudson-Edwards et al.,, 1998
South Tyne	nr	2.6-8.0	11.1-42.5	615-2,340	722-2,340	Macklin et al.,, 1992; Hudson Edwards et al.,, 1998

2.3 Sampling locations

2.3.1 Sample sites

Samples for the inundation work in Chapters 3, 4 and 5 were collected from the locations shown in Figure 2.4. These sites were chosen as they represent different soil types found within the Tyne catchment. The land uses that were investigated include urban, rough grassland, improved grassland and arable, as these had the largest percentage land cover at a distance of 25 m from the Tyne catchment watercourses (Figures 2.5 and 2.6). The study sites are focused within the south Tyne catchment as this is where most of the mining activity was located (Macklin and Hudson-Edwards, 1997) and where elevated levels of PHEs are found in floodplain soils.

Sample locations (n=48) for Chapter 6 (Figure 2.4) were randomly selected from the EA flood outline layer in ArcMap 10 using the 'generate random points' tool. 48 points were selected to be generated at random within the constraints of the flood outline layer. Sampling locations were generated at random to avoid bias in the selection of sample sites.

The sampling locations were generated throughout the South Tyne catchment until Prudhoe, as the river becomes tidal after then and this work does not consider the implications of tidal flooding.

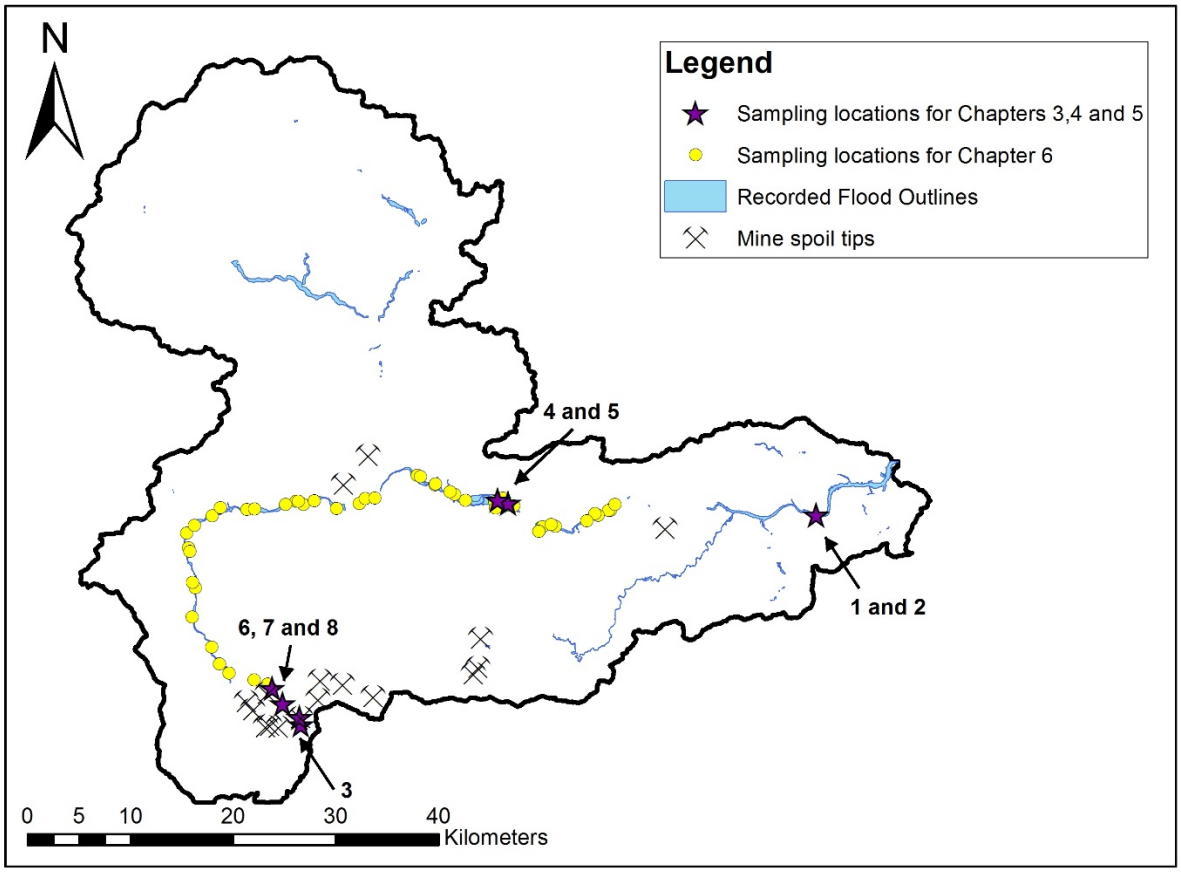

Figure 2.4: Sampling locations in the Tyne catchment.

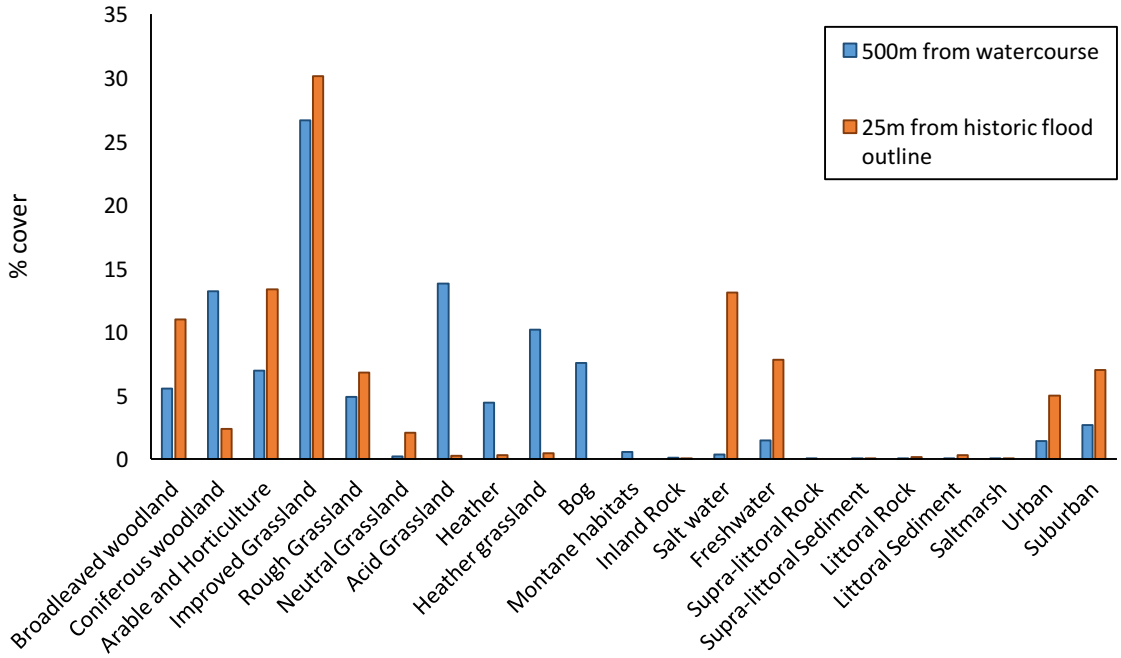

Figure 2.5: bar plot showing the % cover of each land use classification 500 m and 25 m from water courses within the Tyne catchment. Summary data calculated from the 25 m raster dataset from Rowland *et al.,* (2017).

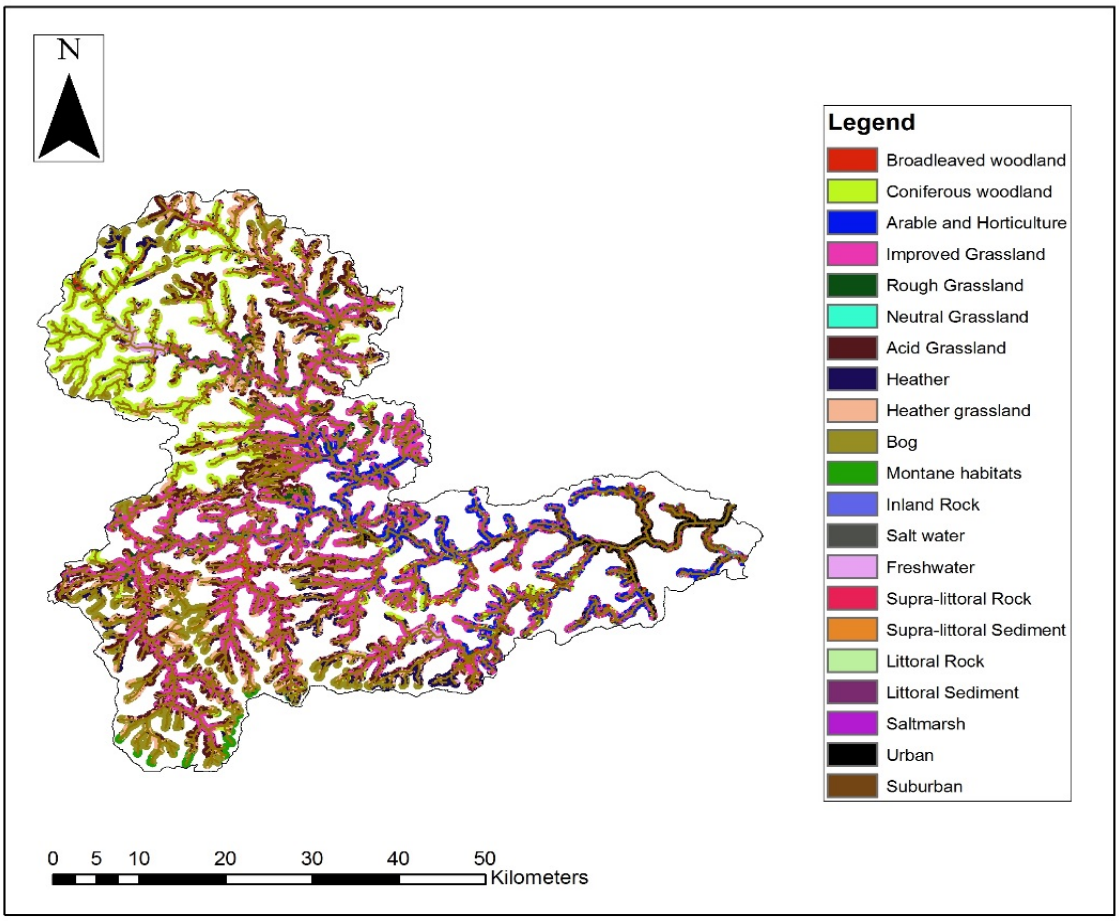

Figure 2.6: land use clipped to a 500 m buffer zone of water courses within the Tyne catchment. 25 m raster dataset from Rowland *et al.,* (2017).

Soils 1 and 2 (Figure 2.4) were selected on the basis that they were post-industrial technosols and were situated in an urban park area. The soils are situated on a former Lead Arsenate works and known to be enriched in PHEs such as Pb, As and Zn (Okorie *et al.,* 2010; Okorie *et al.,* 2011; McCann *et al.,* 2015). Soil 3 was collected from an upland peat soil. Whilst this particular soil was not actually within a floodplain area, its high organic content made it of interest.

Soils 4 and 5 (Figure 2.4) were collected from the mid reaches of the Tyne catchment and were situated on agricultural soils, in areas that have recently witnessed extensive flooding, the last of which was during the storms of December 2016. These soils were chosen as they are used for the production of food and livestock, therefore PHE mobilisation from these soils could create a pathway from source to human receptors. Soil 6 was in the upper reaches

of the Tyne catchment, on the River Nent floodplain, downstream from mine spoil tips and represented an upland grass area used for livestock. The Nent is known for having poor ecological and chemical status for a series of parameters used in the WFD, arising from PHE concentrations within the river (Armitage *et al.,* 2007; Mayes *et al.,* 2009).

The final two soils, 7 and 8, were mine spoil tip material and are therefore loosely classed as a soil in this thesis (Figures 2.4, 2.7 and 2.8). They represent sources of PHEs within the whole of the River Tyne catchment and deemed important for understanding how PHEs behave and can be a source to human receptors.

Figure 2.7: spoil tip material sampled for sample location 7

Figure 2.8: spoil tip material sampled for sample location 8

2.4 Field sampling techniques

2.4.1 Soil collection

All the soil samples (Figure 2.4) were collected using a soil auger to a depth of 15 cm. This depth was considered the most appropriate for the purposes of human exposure and interaction with flood waters, as food is generally grown within the upper layer of soil. A 1 m^2 sampling area was used, with 5 samples being taken (Figure 2.9) and bulked together to form one composite sample to average out small scale sampling heterogeneity. Samples were packed into pre-labelled bags and returned to the laboratory for processing.

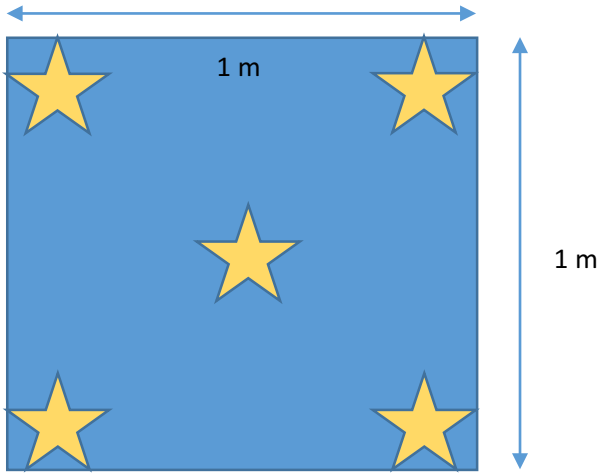

Figure 2.9: diagram of sample individual sampling locations. Each auger location is denoted by a star. The five samples were bulked together into one composite sample.

2.4.2 Bulk soil preparation

The soils for chapters 3, 4, 5 and 6 were processed in the following manner.

Each soil (approx. 2 kg) had any vegetation removed and was gently broken up by hand using a pestle and mortar, prior to placement into foil trays and left to air dry in the laboratory. The soils were turned over by hand to aid the drying process. Once soils were dry in appearance and to the touch, they were passed through a 6.3 mm sieve with the intention of preserving most of the natural aggregates and allow some homogenisation to take place. The <6.3mm fraction was removed for use in the microcosms and for further characterisation work. The >6.3 mm fraction mainly consisted of stones and plant material and was discarded.

A sub sample of the <6.3 mm fraction was removed as a grab sample (approx. 100 g) for further characterisation work. This subsample was oven dried at 105 °C for at least 48 hours until a constant weight was achieved. Once dry, the samples were ground to <250 μm in a rotary ball mill before being placed in zip lock bags ready for further analytical procedures such as loss on ignition (LOI)(Section 2.8) and digests for pseudo-total element content (Section 2.11).

2.5 Microcosm set up

2.5.1 Microcosms used in Chapters 3 and 4

Microcosms were used in Chapters 4 and 5 to determine any flooding induced changes on the solid phase distribution, mobility and bioaccessibility of PHEs in the eight soils shown in Figure 2.4.

1 L HDPE bottles sourced from Azlon were used for the microcosm experiment. Rhizons (5 cm flex from Rhizosphere) were placed into the bottom of the bottles at a 45 degree angle. The microcosms were then filled with 250 g of the < 6.3 mm fraction of soil – three replicates were produced for each of the eight soils, resulting in 24 microcosms in total. The plastic tubing from the Rhizons was taped to the top of the plastic bottle to prevent the Rhizon from moving within the soil column.

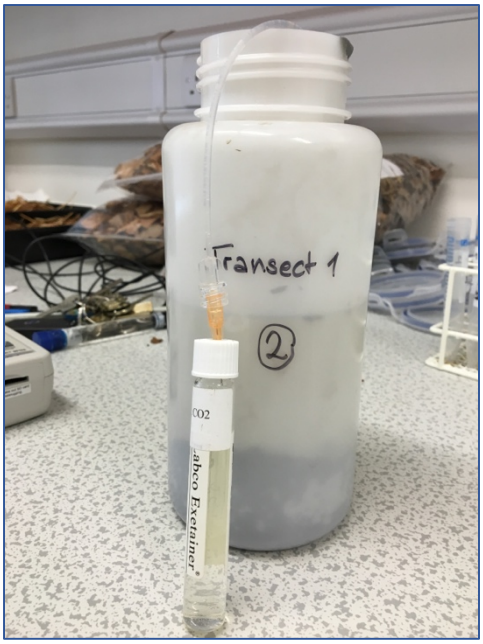

Figure 2.10: photograph of the microcosm set up showing the plastic tubing from the Rhizons connected to an exetainer for porewater extraction

The microcosms were carefully filled with 500 ml of Tyne river water (pH 7.7), trying not to disturb the underlying soils. The elemental concentrations of the river water are provided in Table A.2.1. The bottles were left with their tops off to observe changes in ORP in an environment where the overlying water is in contact with oxygen, as it would be in the natural environment. The flooding and drying regimes for inundation work conducted in Chapters 4 and 5 are outlined in Figure 2.11.

2.5.2.1 Microcosm sample collection

Samples were collected every two days (Figure 2.11) to observe the patterns of PHE mobility in sufficient detail, similar to the study by Du Laing *et al.,* (2007) and the first sample was collected after 24 hours, similar to Frohne *et al.,* (2011). Both studies examined the effects of changing inundation regimes on metal mobilisation so were influential in the setup of this study.

Porewater samples were collected, according to the regime outlined in Figure 2.11. 12 ml exetainers were attached to a vacuum pump to create a vacuum. The collection of porewater was achieved by the insertion of the exetainers onto the needles attached to the Rhizons (Figure 2.10). Exetainers were left in place for two days, although most would fill in minutes. Pore waters were acidified to 2 % HNO_3 and stored in plastic 15 ml falcon tubes at 4 °C prior to analysis by inductively coupled optical emission spectroscopy (ICP-OES).

Overlying water samples were collected with a 5 ml pipette. The tip was placed as close to the sediment surface as possible without disturbing the soil surface. 15 ml was collected and filtered through a Whatman No 2 filter paper into a 15 ml falcon tube. Filtration was carried out to remove any sediment that was also collected. Samples were acidified to 2 % HNO_3 acid and stored at 4 °C prior to analysis by ICP-OES.

Soil samples were collected at the end of each wetting and drying cycle to determine redox induced changes in the solid phase distribution and bioaccessibility of PHEs. A spatula was used to take a surface scrape of soil after the removal of the inundation water at the end of each wetting stage. Water was carefully removed using a large pipette and discarded as overlying water sub samples had already been taken. Approximately 3 g of material was collected by surface scrapes for the UBM (Section 2.12) and the Chemometric Identification of Substrates and Element Distributions (CISED) methodologies (Section 2.13). Scrapes were placed into 50 ml falcon tubes and centrifuged at 3500 rpm for 5 minutes to remove any further water from the sample. The samples were then immediately subjected to the UBM and CISED methodologies (Sections 2.12 and 2.13). Samples were not dried as the aim of this work was to quantify the availability and solid phase distribution of PHEs during soil wetting and drying cycles. An additional surface scrape was taken and weighed prior to oven drying at 105 °C to constant dry weight. This was used to determine the moisture content of each sample for moisture correction (Section 2.6).

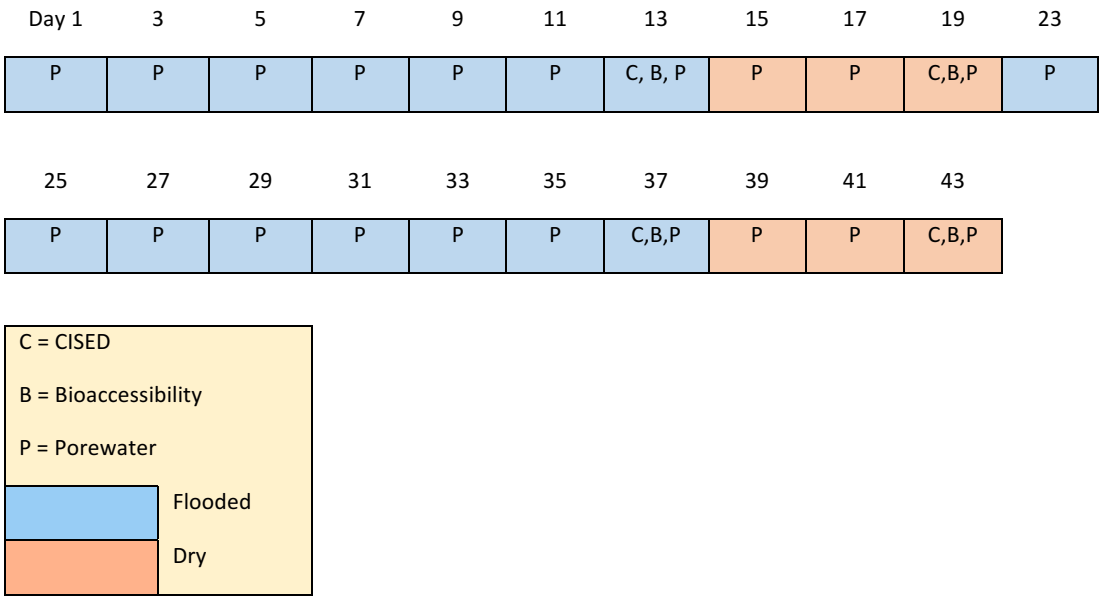

Figure 2.11: diagram showing the time steps at which CISED, bioaccessibility and porewater samples were taken. Overlying water samples were only collected when soils where inundated and are discussed in Chapter 4. CISED and bioaccessibility data are discussed in Chapter 5.

2.5.2 Catchment scale inundation experiment in Chapter 6

The 48 floodplain samples collected throughout the Tyne catchment floodplain (Figure 2.4) were inundated for a period of one week to provide data on flooding induced changes in bioaccessibility over a sufficient number of samples for spatial mapping.

10 g of ground homogenised sample (section 2.4.2) was placed into a 50 ml plastic bottle and then inundated with 30 ml of Tyne river water to form a 1:3 solid:liquid ratio. The samples were left for a period of one week in an incubator set to 11 °C. This temperature was selected as it isthe average winter temperature in the UK. After one week, the water was pipetted off and the volume recorded. Water samples were filtered through a Whatman No 2 filter paper into 15 ml falcon centrifuge tubes. The water samples were made up to a 2 % HNO_3 concentration for preservation and refrigerated at 4 °C until analysis by ICP-OES. The volume of overlying water was subtracted from the initial volume, to determine the volume of pore water. This information was used for mass balance concentrations to determine PHE content in the solid and liquid phases during inundation. The partitioning of PHEs into overlying water was determined using the following:

$$\%\ \text{PHE mobilised into overlying water} = (\text{PHE}_{\text{total (mg/kg)}} / 100) * (\text{PHE}_{\text{water (mg/ml)}} * \text{Overlying water vol}_{\text{(ml)}})$$

Once the overlying water was removed, a surface scrape of the remaining 10 g of soils in each microcosm was collected. The surface scrapes (approximately 1 g) from each microcosm were subjected to the UBM method (Section 2.12), to determine flooding induced changes in the bioaccessibility of the 48 samples. The remaining sample was dried to determine the moisture content of the soil to allow for moisture correction (Section 2.6.2).

2.6 Soil moisture content

2.6.1 In the field

Soil moisture content was determined using an Eilkelkamp soil moisture meter connected to a Thetaprobe. The probe was inserted into the soil so that the prongs were entirely in the soil. Five measurements at each auger location (Figure 2.9) were taken and averaged.

2.6.2 In the lab

The moisture content of each sample was determined by measuring the weight loss that occurs when a soil is heated to 105 °C for at least 48 hrs until a constant weight was achieved. Each soil was weighed prior to and after drying, the decrease in weight was calculated as a proportion of the initial weight and expressed as a percentage weight loss. Moisture content values quoted in this thesis have been calculated using the following equation:

$$MC = \frac{M_w - M_d}{M_w} \cdot 100$$

Where: MC is the moisture content (%)

M_w is the mass of wet sample (g) and

M_d is the mass of dry sample (g)

The bioaccessible PHE data for the wet samples in Chapter 5 and 6 was corrected for moisture content using the following equation:

$$C1 = C \cdot \frac{MC + 100}{100}$$

Where: C1 is moisture content corrected bioaccessible PHE concentration (mg kg^{-1})

C is measured bioaccessible PHE concentration (mg kg^{-1})

MC is the moisture content (%)

All bioaccessible data for the wet test soils were corrected for moisture content in subsequent data interpretations in this thesis. The same equation was used to correct the CISED data from wet soil samples in Chapters 5 and 6.

2.7 Soil pH

The pH of each soil was measured using a glass slurry electrode and Orion 720A meter. The pH meter was calibrated to 4, 7 and 9. To 10.0 g (± 0.01 g) of the <2mm dry sub-sample size fractions of each sample 25 ml of 0.01 M $CaCl_2$ was added. The samples were magnetically stirred for one minute and then left to settle for 10 minutes. Prior to analysis the samples were stirred to reform the suspension. Buffer check solutions were analysed before and after every ten soil suspensions.

2.8 Loss on ignition (LOI) and particle size analysis

2.8.1 LOI

Organic matter may be estimated rapidly by Loss on Ignition, which determines the organic matter content of soil by the loss in weight of a dry soil sample after ignition at a high temperature. Most of the weight loss is due to oxidation of organic carbon but some additional weight loss is due to decomposition of free carbonates and to loss of structural water from clays.

10 g of the <250μm subsamples of each soil was oven dried at 105 °C for at least 48 hours and placed in a desiccator to cool. Crucibles were weighed (±0.01 g) and filled with approximately 5 g of sample and reweighed (±0.01 g). The crucibles were placed in a muffle furnace for 4.5 hrs at 450 °C. Once the required time period had elapsed, crucibles were placed in a desiccator to cool before being reweighed (±0.01 g). LOI is calculated using the following equation:

$$LOI = \frac{W2 - W3}{W2 - W1} * 100$$

Where: *W1* was the weight of the dry empty crucible

W2 was the weight of the crucible and oven dry sample

W3 was the weight of the crucible and sample after the muffle furnace

2.8.2 Particle size analysis

Soil samples from the < 6.3 mm sevied fraction were added to 50 ml plastic sample bottles to a depth of approximately 0.5cm and topped up to 1.5cm with distilled water. 2 ml of dispersant sodium hexametaphosphate, $(NaPO_3)_6$, was added to aid deflocculation and samples were agitated mechanically for 30 minutes.

A Coulter LS 230 laser granulometer was used to determine particle sizes from 2 to 2,000 μm within each sample. A magnetic stirrer was used to create a vortex ensuring a representative sample was obtained. Five measurements were made of each sample and the mean used. Particle sizes were classified according to the Udden – Wentworth classification scheme (Wentworth, 1922) for grain size and are given as a percentage volume frequency.

2.9 Oxidation-reduction potential (ORP)

ORP probes containing a platinum (Pt) electrode were placed within the soils under experimentation. The probes were placed 2 cm from the bottom of the soil column in the

microcosm experiments and connected to a pCE-PHD 1 data logger. An AgCl 3M KCl reference electrode was also connected to the data logger and placed in contact with the soil surface to provide a fixed chemical reference potential. The difference between the two potentials was displayed by the data logger in mV. The reference electrode has a potential of +210 mV versus the Standard Hydrogen Electrode, so ORP was calculated as the value displayed on the data logger + 210 mV.

2.10 X-Ray Diffraction analysis

X-Ray diffraction (XRD) is a non-destructive technique used to identify and quantify the mineralogy of rocks, soils and sediments. XRD analysis for this work was conducted at the British Geological Survey (BGS) in Keyworth.

2.10.1 Sample prep

15 g of the <250 μm fraction was wet micronised with acetone for 10 minutes and then dried at 55 °C, disaggregated and back loaded into standard aluminium sample holders.

2.10.2 Instrumentation

A Phillips PW1700 series diffractometer with cobalt target tube operating at 45kV and 40mA was used for the XRD analysis. The soil samples were scanned from 3-75°2 theta at 0.70°2 theta per minute. The data were analysed using PANalytical X'pert software that was coupled to an International Centre for Diffraction Data (ICDD) database running on a dedicated PC system, for interpretation purposes.

2.11 Pseudo-totals metal content by microwave digestion

0.250 g (±0.002 g) of <250 μm of soil was weighed out into Teflon tubes prior to the addition of 2 ml of concentrated HNO_3. The Teflon tubes were then loaded into a MARS microwave (CEM Corporation). A pre-set programme was selected that is suitable for the digestion of soils. Once the programme was completed, the soils were filtered through a Whatman No 2 filter paper with the addition of deionised water. Samples were made up to 100 ml with deionised water resulting in a matrix of 2 % HNO_3. Samples were then stored in a refrigerator prior to analysis by ICP-OES.

2.12 Unified BARGE method

2.12.1 Background

The Bioaccessibility Research Group of Europe (BARGE) developed the Unified BARGE Method (UBM) to harmonise the use of bioaccessibility testing. The Dutch Rijksinstituut voor

Volksgezondheid en Milieu (RIVM) methodology was determined to be the most representative of the human gastrointestinal tract and was adapted by BARGE for the purposes of repeatability and reproducibility. An inter-laboratory comparison exercise was undertaken to test the new methodology and ensure consistent results, which are published in Wragg *et al.,* (2011). The UBM was selected for this work because there are published studies validating the UBM against *in vivo* studies (Denys *et al.,* 2012). Additionally, there are published studies that provide reference data using the BGS 102 reference soil for quality control purposes.

2.12.2 Soil preparation

The UBM was used to determine the bioaccessibility of metals within each of the soils and sediments sampled. Many studies use the <250 µm fraction of the soil to perform bioaccessibility tests because, as described in chapter 1, it poses the largest threat to human health through adherence to hands, ingestion and inhalation. In this thesis, the samples used were <650 µm and when collected wet from the inundation experiments it was not possible to separate out the <250 µm fraction. However, larger particles will still adhere to hands when wet, therefore this adaptation to the method was considered appropriate work conducted in this thesis. A subsample of each soil at each time step was dried to determine and correct for the moisture content of each soil (Section 2.6). This allowed for a comparison between bioaccessibility at different points drying the wetting and drying regime.

2.12.3 Preparation of digestive fluids

Four digestive solutions are used in the UBM: saliva, gastric fluid, duodenal fluid and bile which are each made by the combination of an organic and inorganic solution. 37% HCl or 1M NaOH were used to amend the pH if necessary. The fluids were kept in a 37 °C water bath for an hour prior to starting the UBM procedure to allow them to thoroughly heat through.

2.12.4 Analytical method

The procedure was carried out according to the schematic in Figure 2.12 and has been described in full in other publications (Wragg *et al.,* 2009 and Roussel *et al.,* 2010). The UBM was conducted at a temperature of 37 °C over three stages (the mouth, stomach and intestinal tract) to mimic conditions in the human body. The mouth, stomach and small intestinal cavity stages were kept at pH 1.2 and intestinal tract stage at pH 6.3. The test is meant to be representative of the body in a fasting condition which should provide more conservative results. Two test extracts were produced at the end: the gastric phase which

consists of the mouth and stomach compartments, and the intestinal phase, consisting of the small and large intestinal phases.

0.3 g (± 0.001 g) of soil was accurately weighed out and placed into a labelled 50 ml Beckman polycarbonate tube with a screw on cap. 4.5 ml of saliva was added by pipette and inverted by hand for approximately 10 seconds before the addition of 6.75 ml of gastric fluid. The target pH is 1.20 (±0.05) and was adjusted by the addition of 37 % HCL or 1M NaOH as required. Samples were inverted again by hand for 10 seconds before rechecking the pH. This process was repeated until the pH remained stable. Once a stable pH was reached, the tubes were then placed into a rotator water bath at 37 °C for 1 hour. Once the tubes were removed, the pH was checked and if pH <1.50 then the procedure was repeated from the beginning. If pH was >1.50 then the gastric only samples were centrifuged at 4500 g and supernatant removed. The supernatant was acidified to 2 % HNO_3 with 500 µL of concentrated HNO_3 and kept refrigerated prior to analysis by ICP-OES.

The gastro intestinal samples received 13.5 ml of duodenal fluid and 4.5 ml of bile by pipette before inversion for 10 seconds by hand. The pH should be pH 6.5 (±0.05) and was adjusted by addition of 37 % HCL or 1M NaOH as required. The tubes were then placed into a rotator at 37 °C for 4 hours. Once removed, the final pH was noted and samples were centrifuged for 15 minutes at 4500 g. the supernatant was removed by pipette and samples acidified with 1 ml of HNO_3 before refrigeration.

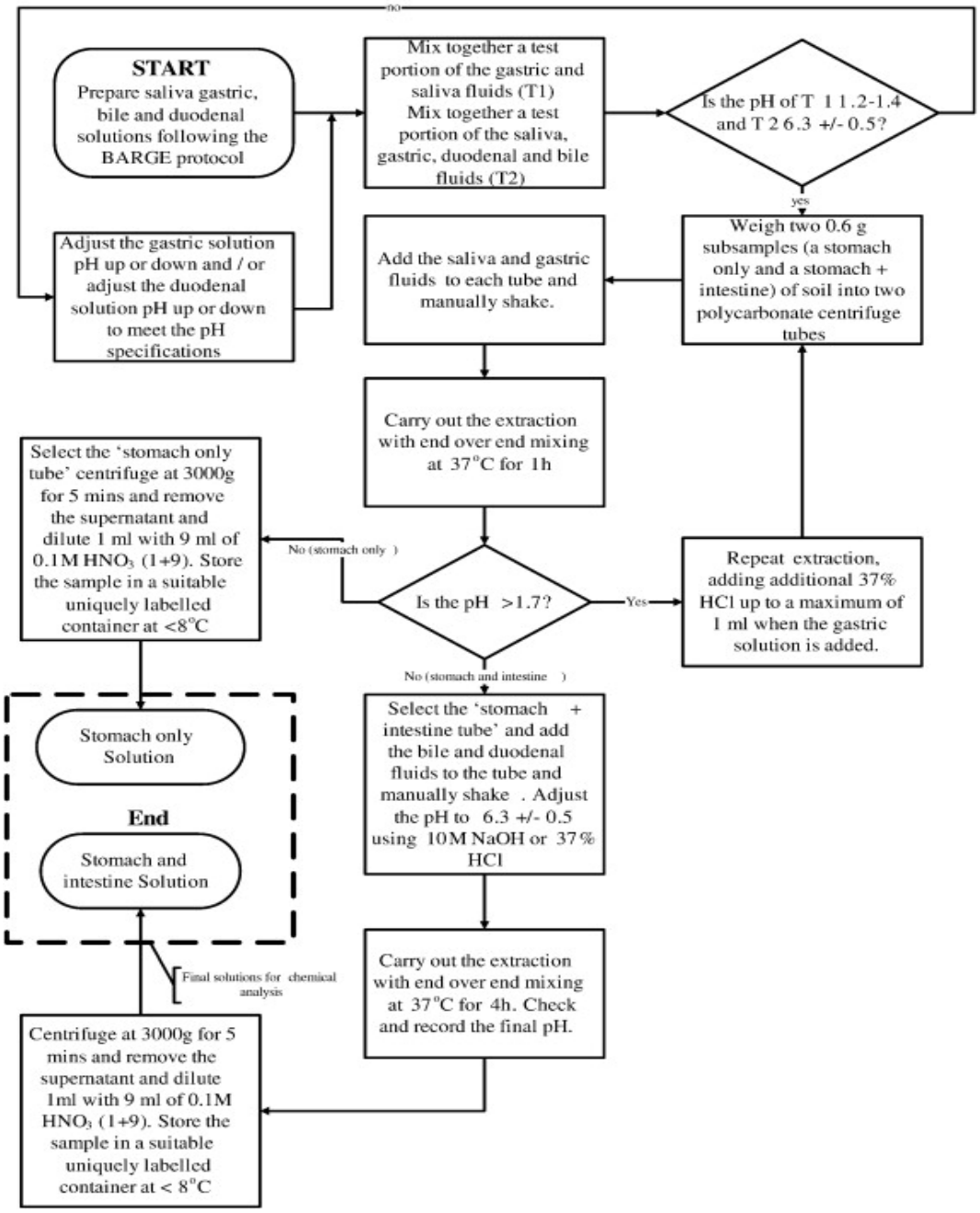

Figure 2.12: schematic of the UBM method, after Wragg et al., (2011).

2.12.5 Data analysis

Data from the ICP-OES analysis were corrected for moisture content using the formula in Section 2.6. Bioaccessibility was expressed in mg of bioaccessible content per kg of solid matrix. A bioaccessible % of an element was also expressed using the following equation:

$$Bioaccessible\ \% = \frac{Concentration\ of\ bioaccesible\ metal\ (mg\ kg{-}1)}{Concentration\ of\ total\ metal\ in\ sample\ (mg\ kg{-}1)} * 100$$

2.13 The Chemometric Identification of Substrates and Element Distributions (CISED)

2.13.1 Introduction

The CISED method is a non-specific sequential extraction procedure that used a range of extractants ranging from de-ionised water to 5 M aqua regia. The elemental data from each extractant are then subjected to a chemometric mixture resolution algorithm to determine the number and composition of physio-chemical components in soil (Section 2.15).

This method was chosen because it addressed some issues that arise with other sequential extraction techniques. Firstly, the method can be completed in 8 hours, which was advantageous for the inundation work carried out in this study, as samples had to be subjected to the CISED method immediately after being collected. Many techniques also have a high salt content in the reagents, which can be problematic when analysing extracts by ICP-OES, as they can block the nebulizer(Cave *et al*., 2004). The simple acid extractants used in the CISED method means this does not occur.

2.13.2 Analytical method

Aqua regia was made to the following concentrations using analytical grade reagents, as shown in Table 2.2. Deionised water was sourced from a Duo™ water purification system.

2 g (±0.02 g) of soil was weighed out into 50 ml plastic falcon centrifuge tubes. 10 ml of extractant was added (step 1) before the tubes were rotated for 10 minutes at approximately 30 rpm. The tubes were then centrifuged for 10 minutes at 4500 G. Upon completion, the extracts were carefully removed by a pipette and stored in 15 ml plastic falcon centrifuge tubes prior to analysis by ICP-OES. Volumes of each extract were recorded. The process was repeated for the remaining steps in Table 2.2, producing 14 extracts for each sample. Extracts were stored at 4 °C.

Table 2.2: Concentration and volume of aqua regia and H_20_2 at each step

Step	Extractant concentration (Aqua Regia)	Volume (ml) Added	Volume of H_2O_2 (ml) Added
1 and 2	DI	10	-
3 and 4	0.01 M	10	-
5 and 6	0.05 M	10	-
7 and 8	0.1 M	9.75	0.25
9 and 10	0.5 M	9.50	0.50
11 and 12	1.0 M	9.25	0.75
13 and 14	5.0 M	9.00	1.00

2.14 Elemental quantification of total digest, UBM and CISED solutions using ICP-OES

2.14.1 Instrumentation

Major and trace elemental concentrations were determined using an Thermo Scientific iCAP 6300 series ICP spectrometer coupled to a 240 sample autochanger. The equipment contained a high energy Echelle cross dispersion optical system with a wavelength coverage of 166 to 847 nm and a high performance solid state Charge Injection Device (CID) camera system. iTEVA operating software provides full control of the instrument.

2.14.2 Analytical method

Approximately 5 ml of sample was used by the instrument for analysis. The CISED extractions were collated by matrix type, for example, all 0.01 M samples were used in one run. Respective standards were made for each matrix. Standards contained Al, As, Ba, Ca, Cd, Co, Cr, Cu, Fe, K, Li, Mg, Mn, Na, Ni, P, Pb, S, Si, Sr, V and Zn ranging from 50 to 10,000 $\mu g\ L^{-1}$. The standards were made within 24 hours of use and kept refrigerated until needed. The full range of standards were analysed at the start and end of each run to check for drift. Random standards and blanks, subsampled from the standards, were analysed at intervals of every 10 samples during the run for the purposes of quality control. Outputs were converted to mg kg^{-1} using the following equation:

$$M = C\ (\frac{V}{m})$$

Where:

M is the element concertation in mg kg-1

C is the element concentration in the extract (mg L-1)

V is the sample volume in ml

m is the mass of the sample (g)

2.15 Data manipulation

2.15.1 Self-modelling mixture resolution algorithm (SMMR)

Soils are made up from a mixture of components originating from the underlying geology, biogenic inputs, river and wind deposited material and anthropogenic inputs (Rowell, 1994). To understand the fate and behaviour of PHEs, it is first important to understand which components are present in soil and the distribution of PHEs within each of the components. Components are made up of various elements, and as a result, they have unique chemical signatures. For example, a Fe-oxide component will mainly consist of Fe.

The application of a mixture resolution algorithm, described by Cave et al., (2004), can determine the number and composition of components present within each soil studied using multivariate techniques. The SMMR essentially unmixes a mixture of elemental data, to determine the soil components present. The multi element data were entered into a matrix that had the extractable solids for 23 elements over the 14 extracts. Where data were below the reporting limit, the value was replaced by that of half the reporting limit. Elements were removed from the input when 75 % of their values were below the reporting limit.

The algorithm is programmed into MATLAB™ and can be run in a complied version of the software as described by Cave *et al.,* (2004). The algorithm generates characterization proportion and composition matrices, as shown in Figure 2.13. Matrix A is the concentration data for the elements of interest in each of the 14 extracts from the CISED method (Section 2.13). Once these data are subjected to the algorithm, the proportion of each component leached (matrix B) and the concentration of each component (matrix C) are derived.

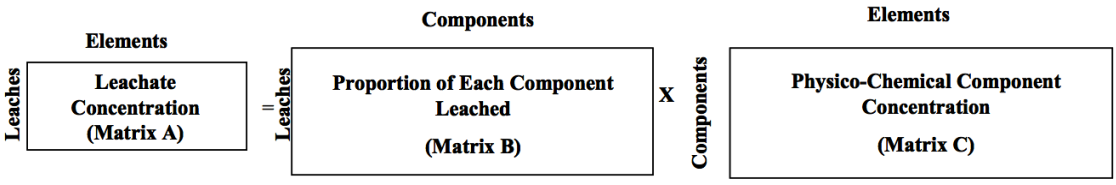

Figure 2.13: A simplified schematic of the CISED algorithm

Matrix B is plotted as a series of extractograms (Figure 2.16) showing the extracted solids for each component over the 14 steps shown in Table 2.2. Matrix C shows the percentage of each element associated with each component. For example, a Fe-oxide component will likely have a high (>50 %) percentage of Fe. Wragg (2005) summarised the algorithm steps from the work done by Cave *et al.,* 2004. The summarised steps by Wragg (2005) are reported below:

1. The extraction matrix A is scaled to its maximum and subjected to principal component analysis (PCA) to estimate the number of components present. This is implemented within the MATLAB™ programme.
2. Varimax rotation (within MATLAB™) of the scores from the PCA (0-1) gives the first approximation of the shape of each of the extraction profiles of each component.
3. To estimate the relative proportion of each of the leached components needed to make up the leachate concentration data (matrix A), a multiple linear regression (MLR) is carried out within MATLAB™. The dependant variable is the sum of each row in the leachate concentration matrix (scaled to 1) and the independent variable is the scaled score matrix from the PCA in stage 2. The columns of the scaled score matrix are multiplied by their corresponding MLR coefficients, creating a new matrix that has its rows scaled to 1. This new matrix is a first approximation of the proportion of the extraction profiles (scaled matrix B).
4. The composition of each component (matrix C) can be calculated as a first approximation, once both scaled data matrix A and B are known, using the equation $A = BC$, or in its pseudoinverse form $C = AB'[B'B]^{-1}$, where B' is the transpose of B.
5. Because in the first approximation of matrix C some values are negative values they are corrected to 0 and a second approximation of matrix B is required within MATLAB™ using the equation $B = [C'C^{-1}]\ C'A$. This second approximation and subsequent iterations are used to refine the approximation of the proportions and

compositions of each of the components until no further significant changes to the proportions or compositions information for each component is made

6. At this stage an input from the operator, to interpret the number of components determined by the CISED algorithm to enable completion of the mixture resolution process, is required. The algorithm provides a graphical plot (an iteration and average fit plot), an example of which is shown in Figure 2.14. This shows, the modelled number of components present in the extracted soil sample and how many iterations of the data set were carried out to achieve a close fit between the actual and modelled data. The modelled number of components generally ranges from 2-15, with differing degrees of closeness of fit.
7. The iteration and average fit plot (Figure 2.14) is split into two halves. The upper half identifies the number of iterations completed by the algorithm to determine the number of components present and the fit of the modelled data compared to the actual input data for that number of components. The lowest point on the fit line gives the first indication of the number of acid extractable components present in the test soil that gives a good fit between the actual and modelled data.
8. The lower half of the iteration and average fit plot (Figure 2.14) summarises the average difference between the actual extraction and the modelled extraction data using Bayesian information criterion (BIC) and Akaike information criterion (AICc). The lowest point on this plot tells the operator how many components are present in the test soil. This value is then required as an input into the mixture resolution algorithm implemented by MATLAB™.
9. Once the number of components, as determined using the iteration and average fit plot, is inputted into the mixture resolution algorithm, the final component composition, the concentration of each component in each stage of the CISED extraction (profile concentration data) and information on the distribution of each of the input elements are calculated and provided as graphical or tabular outputs resulting in completion of the mixture resolution algorithm.

The application of the CISED algorithm generates several outputs that report the amounts of extractable solids in each component at each extraction point, the proportion of major and trace elements associated with each component (%) and the distribution of each element within each component (mg kg^{-1}). Modelled and actual data are displayed in plots to give an indication of model fit.

The number of components to be used is decided using AICc scores. The lowest score is chosen. For example, the most parsimonious model for Figure 2.14 would use 10 components.

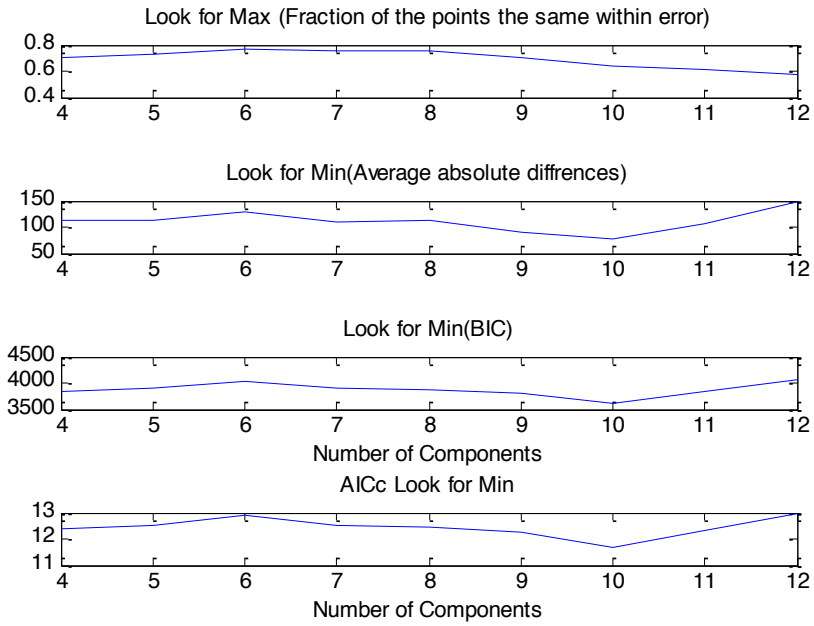

Figure 2.14: AICc to determine the number of components used within the model

The model performance is assessed using the model fit plots, as shown below in Figure 2.15.

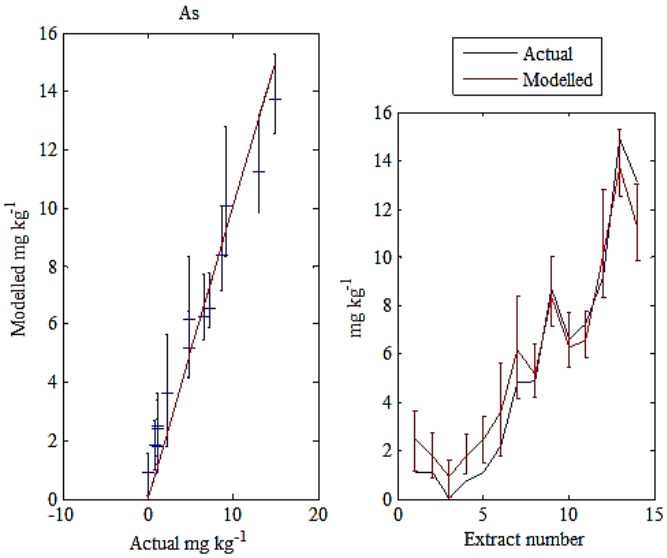

Figure 2.15: plots showing the actual data plotted against the modelled data, to assess model performance and fit.

The component extraction profile and distribution plots are used for aiding the identification of each component. Component identification is done using the plots in Figure 2.16, in conjunction with information on land use, mineralogy (from XRD data in this study) and underlying geology. The extraction profile and distribution plots can portray information about each component. For example, a component that is mainly composed of Al and Fe, such as that below, and has a late extraction profile where the majority of solids are extracted over the higher acid concentrations, can be identified as an Al-Fe oxide. Extraction profiles can be indicative of the reactivity and availability of a component, as more labile components will be extracted over lower acid strengths then less available components.

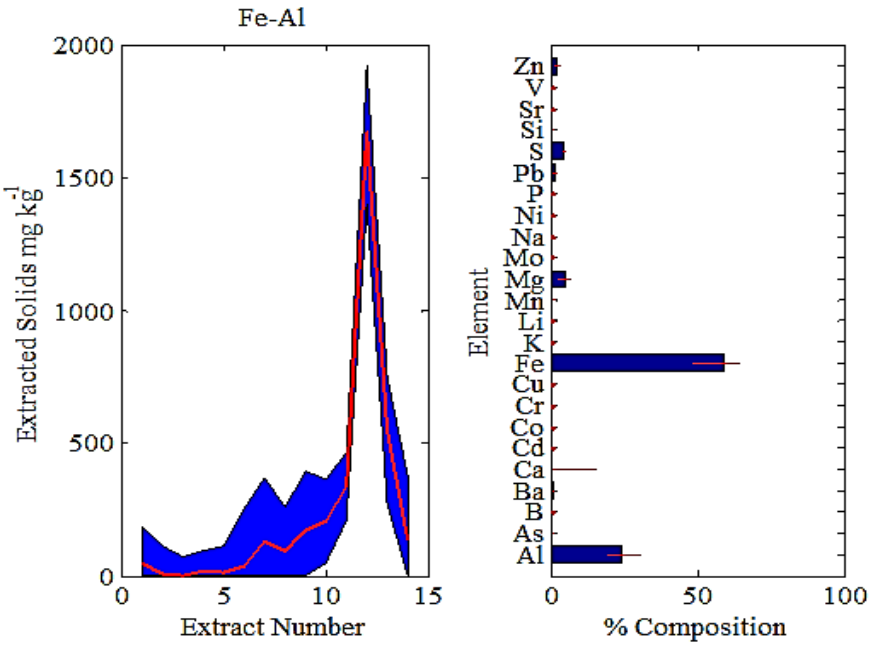

Figure 2.16: extraction profile (left) and composition plot (right)

Finally, the distribution plots give an indication of the elemental association with each component. For example, Figure 2.17 below shows the distribution of As in each of the modelled components. Elements that have an error bar intersecting the y axis have uncertainty associated with the component that element originates from.

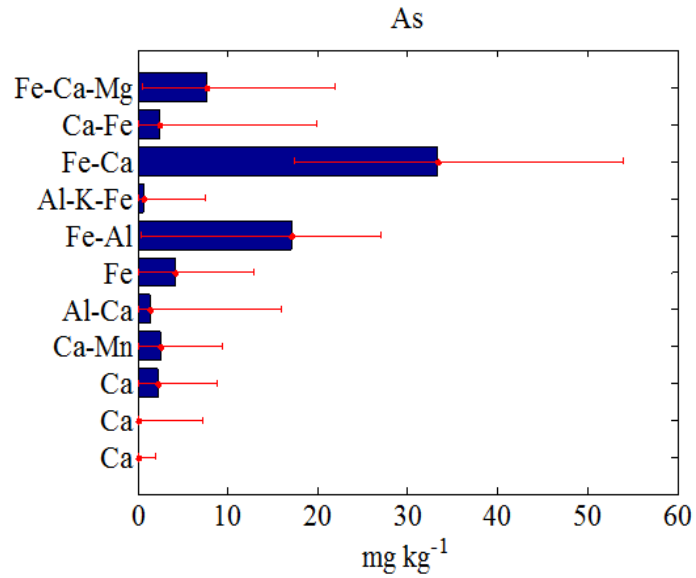

Figure 2.17 Arsenic distribution plot generated using the CISED SMMR

2.16 Quality Control

2.19.1 Sample analysis

A set of 8 standards ranging from 50 to 10,000 μg L^{-1} were run at the start and end of each set of samples. This was done to determine if any drift in the measurements by the ICP-OES were present during sample analysis. Standards and blanks were also placed after every 10 samples in the auto-changer.

2.19.2 Blanks

Blanks samples were used in the total digest, UBM and CISED procedures to assess for any contamination of equipment. Samples analysed in this study were all within 2 times the LOD values shown within Table 2.3.

LOD values were determined by analysing eight replicates of a standard of known concentration. The LOD values is defined as the minimum concentration of a substance that can be measured and reported with 99% confidence that the analyte concentration is greater than zero and is determined from analysis of a sample in a given matrix. LOD values were calculated using the following equation:

$$LOD = (STDEV(A:B)*2.998)$$

A:B refers to the range of concentrations from the ICP-OES and 2.998 refers to the t statistic for the number of standards run.

Table 2.3: University of Stirling ICP-OES limits of detection (μg l^{-1})

Sample ID	Al	As	B	Ba	Ca	Cd	Co	Cr	Cu	Fe	K	Li
LOD (μg l^{-1})	3.52	3.40	0.33	0.12	13.69	0.19	0.28	0.70	0.71	2.63	9.83	13.63

Sample ID	Mg	Mn	Mo	Na	Ni	P	Pb	S	Si	Sr	V	Zn
LOD (μg l^{-1})	1.46	0.67	0.58	5.23	5.39	2.58	2.98	18.73	7.17	0.70	0.93	2.43

2.19.3 Reference materials

The certified reference material 'Reference Material No. 142 R' from the Community Bureau of Reference was used during the pseudo-total digest procedures. The reference material provides reproducible pseudo-total concentrations for eight elements to verify the digestion procedure performance. All values in this study were within the tolerated limits of the CRM.

To determine the accuracy of the UBM results, a guidance material (BGS 102) was used. BGS 102 is a homogenised ferritic brown earth soil and is described as "naturally contaminated", with elevated PHEs such as Pb and As originating from local geology (Wragg, 2009).

BGS 102 has been well documented by Hamilton *et al.,* (2015) which provides reproducible concentrations for 55 elements. Currently there are no certified reference soils for use in bioaccessibility studies, only guidance materials, most of which only provide the bioaccessible fractions for a small number of PHEs. BGS 102 was selected because it had the widest range of reproducible values for both the gastric and gastrointestinal phases used by the UBM. The total elemental concentrations of BGS 102 are documented in its certificate of analysis. The data below in Figures 2.18 and 2.19 show the BGS 102 concentrations for As and Pb, and compare them to the guidance concentrations found in the BGS 102 certificate of analysis (Wragg, 2009). Arsenic data were within the threshold limits. One value of Pb was out with the tolerable limit. As it was not possible to repeat the UBM on these samples, the Pb data were treated with caution.

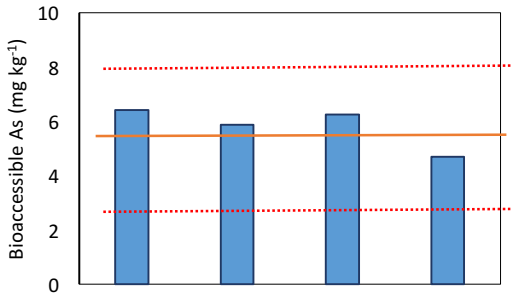

Figure 2.18: BGS 102 UBM data (gastrointestinal) for As from this work (n=4). The orange line indicates the guidance concentration for Arsenic as per the BGS certificate of analysis. The dotted red lines indicate the confidence intervals (1 S.D).

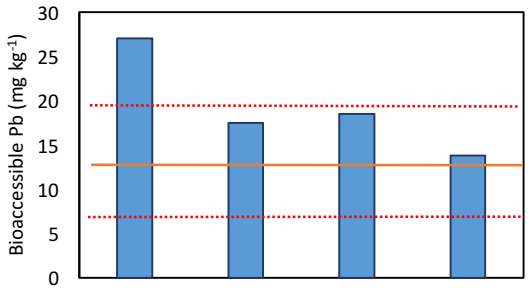

Figure 2.19: BGS 102 UBM data (gastric) for Pb from this work (n=4). The orange line indicates the guidance concentration for Pb as per the BGS certificate of analysis. The dotted red lines indicate the confidence intervals (1 S.D).

3. CHARACTERISATION OF POTENTIALLY HARMFUL ELEMENTS FROM A SELECTION OF SOILS WITHIN THE TYNE CATCHMENT WITH REFERENCE TO HUMAN HEALTH

3.1 Introduction

Soils can act as a sink and source for environmental contaminants originating from both geogenic and anthropogenic sources such as industrial wastes, agriculture, power generation from coal combustion, vehicle emissions and metal ore mining (Caboche *et al.,* 2010; Reis *et al.,* 2014; Wragg *et al.,* 2012; Cox *et al.,* 2013). The UK's history of metal mining has resulted in areas of disused mine workings enriched with metals and metalloids, which can be mobilised chemically and physically throughout a catchment via flooding (Alloway and Davies, 1971; Geeson *et al.,* 1998; Smith *et al.,* 2009; Foulds *et al.,* 2014). These materials can be introduced into river systems by processes such as erosion and surface run off (Dennis *et al.,* 2003; Foulds *et al.,* 2014). As rivers are effective dispersers of eroded material, they can therefore move significant quantities of potentially harmful elements (PHEs) throughout the catchment, introducing them to floodplain soils via deposition during periods of high flow (Dennis *et al.,* 2003; Macklin *et al.,* 2006; Foulds *et al.,* 2014). The presence of PHE enriched sediment on floodplain soils can have ecotoxicological consequences for crops, livestock and ultimately humans through acute or chronic poisoning if concentrations are high enough or through long exposure times. Direct source-receptor pathways through the ingestion and inhalation of PHE enriched soils and sediments can occur as a result of our interactions with soil for recreation, work and the production of foodstuffs (Albering *et al.,* 1999; Wijnhoven *et al.,* 2006; Roy and McDonald. 2015). For example, evidence has shown that livestock receiving foodstuffs grown on a PHE contaminated floodplain resulted in lead (Pb) blood poisoning and livestock mortality (Foulds *et al.,* 2014).

When considering source-receptor pathways, characterising the solid phase distribution of PHEs is important for understanding their availability, as only the bioavailable fraction of a soil is taken up by a receptor following solubilisation after ingestion, inhalation and dermal contact (Cox *et al.,* 2013). Bioaccessibility is defined in Section 1.8 as the fraction of a PHE that is dissolved into gastrointestinal fluid. This measure of PHE availability may be a more appropriate way of assessing the health risks associated with ingestion of PHE enriched material compared to the use of the pseudototal concentration of a PHE (Wragg *et al.,* 2011). This is because bioaccessibility testing provides a more realistic estimate of PHE content that is potentially available for uptake across the cell wall, as opposed to using pseudo-total

concentrations. Understanding the relationships between the pseudo-total content, solid phase distribution and bioaccessibility of PHEs can provide the essential knowledge needed to underpin decision-making processes involved with contaminated land remediation and development, as well as determining the risks associated with PHE enriched material in flood prone areas.

Exposure to soils and sediments exceeding Generic Assessment Criteria (GACs) such as those outlined in Table 1.1, may pose a risk to human health. Category 4 Screening Levels (C4SLs) or Suitable 4 Use Levels (S4ULs) are health based generic assessment criteria (GACs) developed for the Department for Environment, Food and Rural Affairs (Defra) by CL:AIRE and Land Quality Management LTD respectively. GACs are screening criteria that have been created using the Contaminated Land Exposure Assessment (CLEA) tool (v1.06) and can be used to determine whether long-term risks to humans from soil PHEs may occur, and whether further site investigations need to be conducted with respect to human health risk assessment (CL:AIRE, 2010). They are calculated using total concentrations, with the assumption that a PHE is 100 % bioaccessible, except for lead, with is assumed to be 60 % bioaccessible.

The aim of this chapter is to assess the role that the solid phase distribution of PHEs has on their bioaccessibility in a range of soil types from the Tyne catchment with reference to human exposure, and thus providing new knowledge of geochemical controls on PHEs within certain soils within the Tyne catchment. This chapter also provides pre-inundation data for the soils referred to in Chapters 4 and 5, to aid interpretation of flood induced changes on PHE bioaccessibility and mobility. The aim is broken down into the following objectives:

- To characterise the bioaccessibility and solid phase distribution of a selection of PHEs: Arsenic (As), Cadmium (Cd), Copper (Cu), Lead (Pb) and Zinc (Zn) using the BARGE UBM gastro-intestinal extraction and a non-specific sequential extraction process to determine the geochemical fractionation of PHEs for the soils under investigation
- To compare PHE concentrations with GACs to determine their hazard to human health
- To determine which solid phases are the source of the bioaccessible PHEs in soils

3.2 Methods

A full site description and justification for sample site locations along with the analytical methods applied to the soils are given in Section 2.2. Table 3.1 provides a brief overview of the soils used within this chapter, with their spatial distribution shown in Figure 2.4. Soil

samples were collected within the Tyne catchment using the methods described in section 2.4 and analysed for pseudo-totals metal content, LOI, pH, XRD and LOI (Sections 2.7, 2.8, 2.10, 2.11).

Table 3.1: Test soil description and sampling location.

Sample number	Location	Geology	Description	Land use
Soil 1	St Anthony's Head	Sandstone	Technosol from a former Pb works site	Recreational parkland
Soil 2	St Anthony's Head	Sandstone	Technosol from a former Pb works site. Fragments of pure Pb present	Recreational parkland
Soil 3	Nenthead	Sandstone, mudstone and limestone	Histosol. Peat soil in upper catchment	Rough grazing
Soil 4	Corbridge	Sandstone with alluvium superficial deposits	Cambisol soil from mid catchment	Agricultural
Soil 5	Corbridge	Sandstone, mudstone and limestone	Cambisol from mid catchment. Sourced from river bank	Rough grazing
Soil 6	Nent Valley	Limestone, sandstone, siltstone and mudstone with alluvium superficial deposits	Stagnosol from upper catchment	Rough grazing
Soil 7	Nenthead	Sandstone, mudstone and limestone	Spoil tip material	Rough grazing
Soil 8	Nenthead	Limestone	Spoil tip material	Rough grazing. Tourist attraction

3.2.1. Bioaccessibility

The BARGE Unified Bioaccessibility Method (UBM) was used to determine the bioaccessibility of PHEs of interest in the soils under investigation. A full description of the method is found in Section 2.12.

3.2.2 Chemometric Identification of Substrates and Element Distributions (CISED)

A sequential extraction procedure was applied to the test soils to identify the presence of soil components (and the association of PHE therein) such as carbonates, iron oxides, sulphides etc. The CISED methodology used (Section 2.13) was that described by Cave *et al.,* 2004; Wragg, 2005; Marinho *et al.,* 2016; Reis *et al.,* 2014).

3.2.3. Self-modelling mixture resolution algorithm for CISED data (SMMR)

A chemometric self-modelling mixture algorithm outlined in Cave *et al.,* 2004 was applied to the chemical composition data and used to identify the number, chemical composition and amount of each component in each sample. Components are defined by using multivariate

techniques to the chemical composition data from the CISED extraction process for each soil. The SMMR process is described fully in Section 2.15

3.2.4 Statistical analysis

The soils in this study were collected from geochemically similar locations within the Tyne catchment. As a result, the CISED identified components were categorised into a common set of physico-chemical groupings, referred to in this work as clusters. This allows the clusters which are the hosts of PHEs and those which contribute towards the bioaccessibility to be identified. Clustering provides a broader overview of the soils and the PHE distributions within them than the individual components associated with each soil.

The use of this approach can provide a greater insight into PHE potential availability to humans and ecological receptors, however when applied to multiple samples the amount of data (variability of number and composition of each component) and resulting interpretation become cumbersome. For example, components that are all dominated with Ca are likely to be grouped together into a carbonate cluster. This can allow for easier comparison of the distribution of PHEs across different soils as a common set of clusters is generated from all the components from each soil under investigation. The grouping of components into cluster is outlined in Figure 3.1.

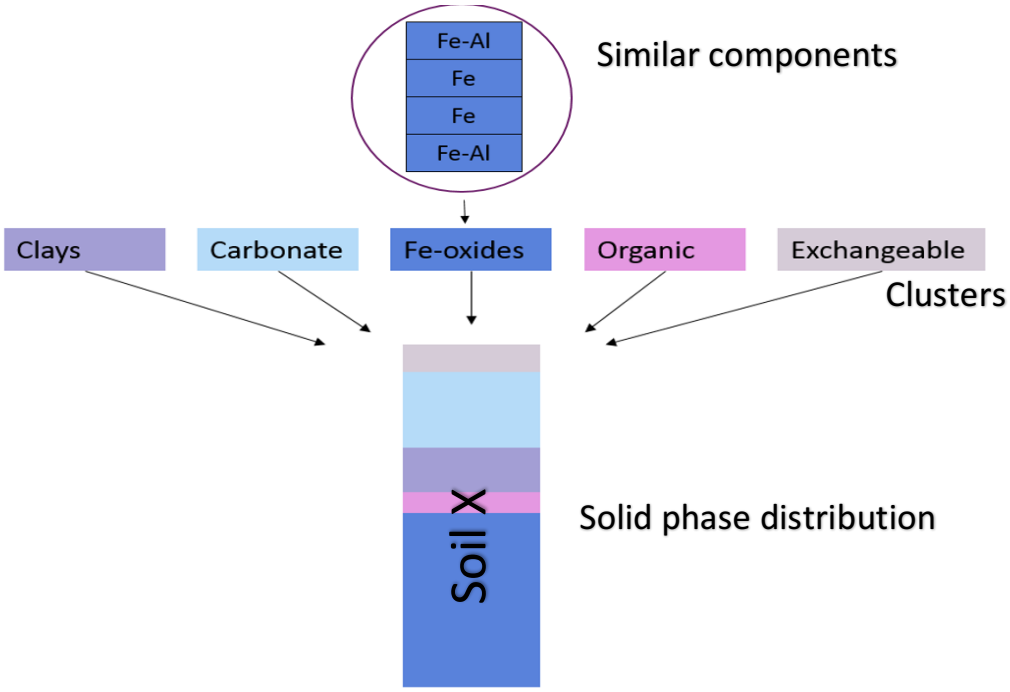

Figure 3.1: Schematic showing the grouping of similar components to form clusters, and the combination of common clusters to make up the solid phase distribution of soil.

A clustering methodology described in detail by Wragg (2005) was used to group soil components from the CISED into more general 'clusters' such as an Iron-Oxide cluster and subsequently determine PHE distribution within each cluster. This involved creating a matrix of 15 element columns (after removal of elements with >75 % of values <LOD) and 70 extraction rows containing the total extracted solids (mg kg^{-1}) for each extraction step for each soil and percentage major and trace element composition (Aluminium (Al), Arsenic (As), Calcium (Ca), Cadmium (Cd), Chromium (Cr), Copper (Cu), Iron (Fe), Potassium (K), Magnesium (Mg), Manganese (Mn), Sodium (Na), Phosphorus (P), Lead (Pb), Sulphur (S), Silicon (Si), Zinc (Zn)). The matrix was laid out as follows:

1. the data were arranged in to columns in the following order (left to right) - the sample name, the acid extractant, the component name, the major elements that contribute to the naming of all of the components, and the total extracted solids in each of the 14 extracts (1-14)

2. the columns were populated with the major contributing elements as a percentage ranging from 0-100 % from the CISED mixture resolution algorithm and the total extracted solids as the original CISED extraction data prior to mixture resolution analysis.

The matrix was mean centered, scaled and then subjected to hierarchal cluster analysis using Euclidean distance as a distance metric and Ward's method to determine the combination of clusters. The resulting colour map (Figure 3.2) displays the distribution of elements and their extraction points. These data were used to determine the point at which the dendrogram should be split (denoted by a black line in Figure 3.2) to determine the number of clusters present within the eight soils under investigation. The splitting was done using information from the extractograms produced by the SMMR and the composition and the elemental data in the colour map. For example, a visual inspection of the colour map (Figure 3.2) acts as a starting point for cluster determination as obvious clusters can be seen from the colours in the extraction number and element composition sides of the colour map.

Analyses were performed in R 3.2.4 (R Core Team, 2016) using the gplots package (Warnes *et al.,* 2015) heatmap() function for hierarchal cluster analysis and production of the colour map.

3.2.5 Comparison to environmental quality standards

Pseudo-total metal concentrations were compared to threshold criteria listed in Table 3.2 below to determine any potential human health risk associated with the soils under

investigation. A combination of Category 4 Screening Levels (C4SLs) and Suitable 4 Use Levels (S4ULs) were used, covering the suite of PHEs used in this study. These values were chosen as they are the most up to date values available in the UK (Table 1.1). The C4SLs and S4ULs are calculated with the assumption that the PHEs in soil are 100 % bioavailable, except for lead, which is calculated under the assumption that it is 60 % bioavailable. Bioavailability in this work is defined as the proportion of a PHE that is available for uptake by the body. Bioaccessibility is described in Section 1.7 and can be used as a proxy for bioavailability (Brandon *et al.,* 2006; Hillwalker and Anderson, 2014).

Table 3.2: Contaminated land assessment values – C4SLs and S4ULs. All values are expressed in mg kg^{-1} dry weight.

	Arsenic [1]	Cadmium [1]	Copper [1]	Lead [2]	Zinc [1]
Residential – home grown produce	37	11	2400	200	3700
Residential – no home grown produce	40	85	7100	330	40000
Allotments	43	1.9	520	84	620
Commercial	640	190	68000	2700	730000
Residential Open Space	79	120	12000	760	81000
Parkland Open Space	170	560	44000	1400	170000

1. S4ULs – Land Quality Management ltd (2015)
2. C4SLs – DEFRA (2014)

The values selected for the purposes of this study were the Parkland Open Space values as the sampling locations were all open countryside space where humans may spend time recreationally.

3.3 Results and Discussion

3.3.1 Pseudo-total metals content, soil characteristics and mineralogy

The pseudo-total PHE content, pH and organic carbon content (Table 3.3) were analysed to chemically characterise the soils and determine the variation in soil characteristics across the catchment and identify areas where PHE enrichment is present. Soil 3 had the highest organic carbon content as it was a peat soil, located in the upper Tyne catchment (Figure 2.4). Soil 3 was also more acidic than the remaining soils in the Tyne catchment, again because it was a peat soil. Soil 8 had the lowest organic carbon content, likely to be because it is considered only loosely a soil and was composed of mine spoil material. The remaining soils in the Tyne catchment are close to neutral and show little variation in pH. This is likely to be related to their common underlying geology (Figure 2.2). The small variation in pH is likely to be a result of soil type and land use. For example, soils 1 and 2 have organic carbon

content ranging from 14.9 % to 20.6 %. Both soils are in a residential park area with trees, which are likely to influence the organic matter content.

Table 3.3: Characterisation of the soils used. Values in bold italics exceed GACs. All element data are in mg kg^{-1}.

Soil	As	Cu	Cd	Pb	Zn	Soil organic carbon (%)	pH
1	136	6.32	0.284	744	466	14.9	6.89
2	***572***	528	13.7	***19200***	8580	20.6	6.54
3	1.16	5.01	0.41	172	44.4	90.6	2.95
4	6.59	20.7	1.60	157	143	6.73	6.81
5	1.06	4.10	2.40	319	540	2.89	6.99
6	25.6	68.3	21.4	***3750***	7710	18.3	6.22
7	33.0	168	53.4	***29400***	17000	7.18	6.87
8	21.3	1520	1.54	***25300***	53400	1.00	6.47

Comparing the PHE concentrations to GACs identified any soils that may pose a risk to human health via the ingestion or inhalation exposure pathways. Only soil 2 exceeded GACs for As and soils 2, 6, 7 and 8 for Pb. The average PHE concentration (across the 8 test soils) was ranked as follows: Cd<As<Cu<Pb<Zn. Pseudo-total PHE content appears to be related to location in the catchment and land use. For example, high Pb concentrations were observed in soils 7 and 8, which are mine spoil tip material in the Pb and Zn mining areas of the upper catchment (Table 3.1, Figure 2.4). Elevated Pb concentrations were also observed in soil 2 (Table 3.3), which was collected from a former lead-arsenate works (where elevated concentrations of As are also observed). Elevated Pb concentrations were also reported for soil 6 (Table 3.3), which was located downstream from the Pb and Zn mine spoilt tips. It is hypothesised that flood transported Pb enriched material has been deposited there.

A qualitative analysis of the mineralogy of the eight soils is reported below in Table 3.4. These data were used to aid identification of each component / cluster in the SMMR and hierarchal clustering outputs. Lead and Zn bearing minerals such as cerussite, galena and sphalerite were present in soils 7 and 8, the mine spoil material and are likely to be the sources of the elevated concentrations of Pb and Zn in these soils.

Table 3.4: XRD results showing mineralogy of the 8 soils under investigation. ? refers to a tentative identification. * refers to Pb bearing minerals and + to Zn bearing minerals L = low mass, M = medium mass and H = high mass for broad quantification.

	Silicates						Phyllosilicates/ clay minerals				Carbonates		
	quartz	cristobalite	albite	microcline	pyroxene	mullite	muscovite	clinochore	kaolinite	calcite	siderite	dolomite	cerussite*
1	H		L	L			L	L	L	L			
2	H	L	L	L		L	L		L	L-M			
3	H	L	L						L				
4	H		L	L			L	L	L	L			
5	H		L				L	L	L	L			
6	H		L				L	L	L			L	
7	H		L	L		L	L		L	L	L		L-M
8	L-M												

	Sulphides/sulphate				Oxides/hydroxides				phosphate	Metal
	pyrite	galena*	sphalerite+	barite	hematite	goethite	lepidocrocite	?pyrochroite	fluorapatite	lead*
1	L				L			?L		
2					L					M
3	L									
4					L			?L		
5					L			?L		
6	L							?L		
7		L				L				
8		L-M	L	?L	L		L		?L	M-H

3.3.2 Bioaccessibility of PHEs

Table 3.5 provides a summary of the As, Cd, Cu, Pb and Zn bioaccessibility for each of the eight test soils. The bioaccessible fraction for As ranged from 5-35 % (<LOD to 152 mg kg^{-1}) in the gastric phase, and unlike pseudo-total concentrations, did not exceed some GACs. This highlights that the use of pseudo-total PHE concentrations for human health risk assessment may lead to unnecessary and more costly, detailed site investigations as the bioaccessible content of a PHE may be considerably lower than assuming the pseudo-total concentration. The bioaccessible fraction (BAF) is defined in Section 1.8 as a percentage of the bioaccessible content and differs from the bioaccessible content, which is given in mg kg^{-1}.

Gastrointestinal values given in Table 3.5 were generally lower for the gastric values ranging from 0.2-19 % (<LOD to 133 mg kg^{-1}), indicating that whilst PHEs are mobilised into solution in the gastric phase, the increase in pH and addition of enzymes/bile salts during the gastrointestinal phase can result in lower measured bioaccessibility. This could be a result of different processes occurring in the gastrointestinal fluids, for example, through re-association of soluble metal with the soil matrix, increased pH resulting in PHE precipitation (Pb and Zn) or complexion by pepsin (Roussel *et al.,* 2009). Bioaccessible As was higher in the gastrointestinal phase for soil 6, however the difference was 6 mg kg^{-1} between the two phases.

Table 3.5: bioaccessible fraction of PHEs expressed as a % of the pseudo-total content. <LOD denotes samples that were below the limits of detection. Bioaccessible content are the actual values in mg kg^{-1} are expressed in () below the % values. Values in bold exceed GACs.

	Gastric (bioaccessible %)					**Gastrointestinal (bioaccessible %)**				
Soil No.	**As**	**Cu**	**Cd**	**Pb**	**Zn**	**As**	**Cu**	**Cd**	**Pb**	**Zn**
1	34	35	48	41	28	0.2	0.2	0.3	0.3	0.2
	(46.8)	(18.5)	(1.9)	(302)	(132)	(0.3)	(0.1)	(0.01)	(2.0)	(0.9)
2	26	23	59	40	23	19	26	35	16	9
	(**152**)	(123)	(8.1)	(**7,805**)	(1,970)	(**113**)	(137)	(0.7)	(**3,160**)	(801)
3	<LOD	72	50	48	53	0.0	0.0	0.0	0.0	0.0
		(12.9)	(0.2)	(83.9)	(23.6)					
4	<LOD	36	22	47	26	<LOD	58	22	5	5
		(7.7)	(0.3)	(73.8)	(37.7)		(12.2)	(0.1)	(8.7)	(7.2)
5	<LOD	55	>LOD	62	50	<LOD	15	6	5	5
		(5.0)		(198)	(268)		(1.4)	(0.1)	(18.3)	(9.5)
6	8	50	52	65	30	14	58	24	27	11
	(2.1)	(33.9)	(11.2)	(**2,450**)	(2,360)	(3.6)	(39.7)	(5.3)	(1,017)	(892)
7	5	31	49	36	56	3	40	76	5	37
	(1.71)	(52.8)	(26.1)	(**10,800**)	(9,580)	(1.2)	(68.1)	(40.6)	(**1,417**)	(6,388)
8	35	0.6	49	17	16	17	4	57	3	10
	(7.5)	(9.7)	(0.77)	(**4,350**)	(8,600)	(3.8)	(61.0)	(0.9)	(779)	(5,431)

Bioaccessible Cu and Cd was highly variable for the soils under investigation, ranging from 0.6-72 % (5.0 to 123 mg kg^{-1} and <LOD to 26.1 mg kg^{-1} respectively). Bioaccessibility for Pb and Zn in the remaining soils was also considerable, ranging from 16-65 % in the gastric phase. Large masses of Pb (10,811 and 4,344 mg kg^{-1}) and Zn (9,578 and 8,597 mg kg^{-1}) were available in soils 7 and 8 respectively, with the Pb values exceeding GACs (Table 3.3).

3.3.3 Comparison of Bioaccessible PHEs to General Assessment Criteria

Bioaccessibility data were compared to lowest observed effect levels from the literature and GACs to contextualise the results of this study (Table 3.5). The GACs are generated using generic exposure parameters, therefore site-specific uses and exposure pathways such as ingestion of contaminated foodstuffs are not considered. The only route of exposure considered in this work is through direct ingestion of soil, as no methods were used for the determination of uptake via dermal contact. Inhalation was not considered as no methods for determining the uptake of PHEs through the lungs were used in this thesis.

The maximum As bioaccessibility for this study was 152 mg kg^{-1} (ranging between 1.71 and 152 mg kg^{-1}), which exceeded allotment GACs and was in a similar range to the open parkland GAC of 172 mg kg^{-1}. Based on an accidental soil ingestion rate of 100 mg day^{-1} acute exposure, As poisoning is unlikely unless large quantities of soil (e.g. kilograms) were to be consumed at the concentrations observed in this study (Hogan *et al.,* 1998). Lethal doses of As are seen at an individual dose of 100-300 mg and effects such as vomiting are induced at doses of about 5 mg (Ratnaike, 2003). Children can exhibit pica behaviour, which is defined for this work as an ingestion rate of soil that far exceeds the 200 mg day^{-1} seen in an average child, resulting in soil ingestion rates of up to 5,000 mg day^{-1} (Calabrese *et al.,* 1991). As a result, regular use of some of the higher enriched locations (sites 1 and 2) by children could result in chronic As poisoning by ingestion of soil through playing. Soil 2 exceeds residential open space GACs, indicating that young individuals could be at risk of As exposure through repeated playing activities.

Minimal risk levels for chronic doses of Cd have been proposed at 0.1 mg kg day^{-1} for periods equal to or greater than 1 year (ATSDR, 2012). Some sites in this study have a bioaccessible Cd concentration of 26 mg kg^{-1}, however, chronic effects may be seen only if considerable quantities of soil were to be regularly ingested, especially by infants. GACs for Cd are not exceeded for Parkland open space but are for allotment values for some sites (Table 3.3) suggesting that a risk to human health may be present through the production of food stuffs, but not for the other generic exposure pathways used for parkland open spaces.

For this study GACs were not exceeded for total Cu at any of the study sites so it is unlikely that the bioaccessible levels of Cu will be detrimental to human health. Copper, as outline in Section 1.3.3 is an essential element, where deficiencies as well as exceedances can lead to adverse health effects.

Bioaccessibility of the Pb in soils in this study that exceed GACs ranged from 14 and 10,800 mg kg^{-1} (BAF 17-68 %). A study by Mielke *et al.,* (1998) which modelled blood Pb levels of soil suggested that soil Pb levels exceeding 80 mg kg^{-1} could result in chronic poisoning of children exhibiting pica behaviour. However, Mielke *et al.,* (1998) also report that blood Pb levels in children increase above background at soil concentrations of 500-1,000 mg kg^{-1}. The results from the Mielke et al., (1998) study suggest that exposure to the soils that exceed GACS for bioaccessible Pb in this study (Table 3.5) would likely result in Pb blood levels above background levels. Background levels for people living in rural areas in the Northern hemisphere are 3.2 μg dl^{-1} (Tong *et al.,* 2000).

The solid phase distribution of Pb is known to affect mobility and mine spoil tip 'soils' have been reported to have a lower bioaccessible fraction than other soil because of the presence of the more insoluble forms of Pb (Ruby *et al.,* 1993; Gasser *et al.,* 1996; Roussel *et al.,* 2009). However, because of the high pseudo-total metal concentrations associated with the spoil tip samples in this study (samples 7 (29,400 mg kg^{-1}) and 8 (25,300 mg kg^{-1})), the bioaccessible content (10,811 and 4,344 mg kg^{-1} respectively) exceeded the GAC of 1,400 mg kg^{-1} so may result in significant exposure if sufficient quantities of material were to be ingested. Bioaccessible concentrations also exceeded GACs for Pb in soil 6, a floodplain soil with 2,450 mg kg^{-1}. Soil 6 is located downstream from the mine spoil tips, therefore the elevated Pb concentrations may occur from remobilisation of Pb from the mining areas.

Although an essential element, a Zn intake of 100-300 mg day^{-1} is reported to result in adverse health effects such as induced Cu deficiency, impaired immune system function and anaemia (Fosmire, 1990). 10 g of material from the soil with the highest bioaccessible Zn content (9,578 mg kg^{-1}) would have to be consumed daily to result in adverse health effects, providing there were no other oral sources of Zn. GACs were not exceeded for Zn for open parkland spaces for the two mining spoil tip soils which had the highest Zn bioaccessible concentrations (Table 3.5). Despite the highest bioaccessible concentrations, the mining spoil tips had the lowest percentage bioaccessible fraction.

3.3.4 Identification and interpretation of soil clusters from the CISED extractions

A chemometric self-modelling mixture algorithm outlined in Cave *et al.,* 2004 and used by other researchers (e.g. Wragg, 2005; Marinho *et al.,* 2016; Reis *et al.,* 2014) was applied to the extraction data and used to identify the number, chemical composition and amount of each component in each sample.

The colour map (Figure 3.2) shows that 10 clusters were associated with the 8 soils used within this study. These have been identified as described by Wragg and Cave (2012) using a combination of the CISED outputs (extractograms, composition plots etc), the colour map and data from XRD analysis. Individual component extractograms, are shown in Figure 3.3 as patterns in extract steps 8-14 (shown on the right-hand side of the colour map) were obscured in the colour map by the large extractable mass of cluster 9.

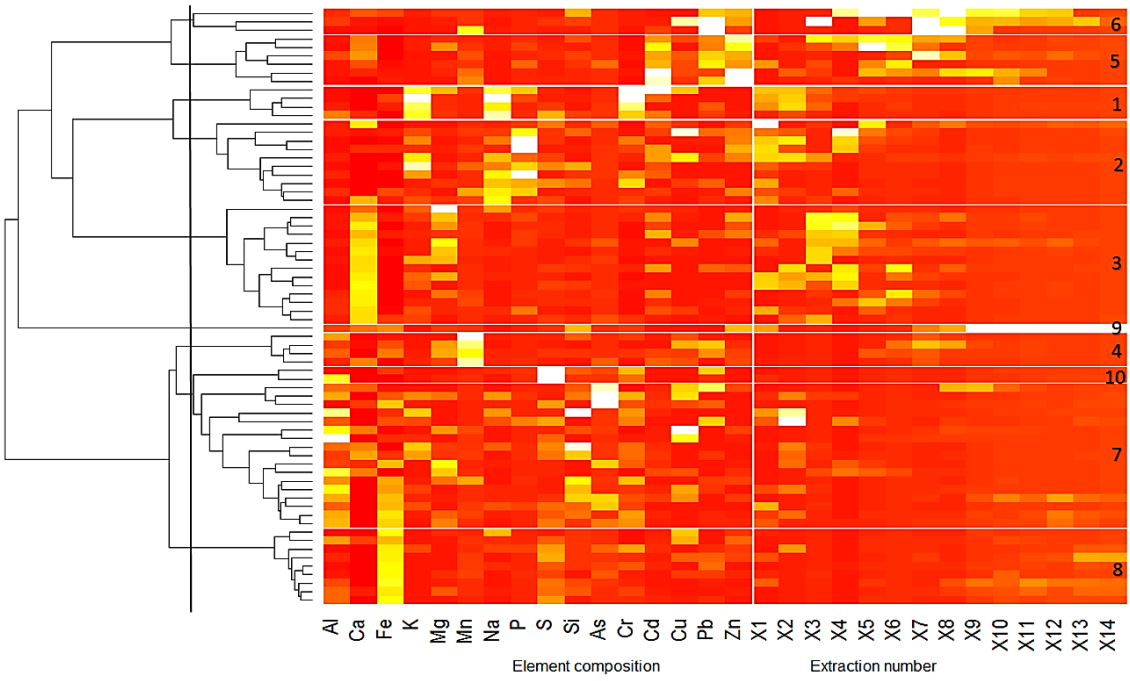

Figure 3.2: colour map and associated clustergram for the 8 soils. The dendrogram on the left-hand side shows the relationship between the individual components. The horizontal lines divide the colour map into soil clusters shown by splitting the dendrogram with the vertical black line in the left-hand side. High concentrations are shown in yellow/white with low concentrations in red. The white vertical line on the colour map divides the elemental data for each contributing component on the left from its extraction position on the right. Extraction data ranges from deionised water at X1 to 5 M Aqua Regia at X14. Clusters are numbered on the right hand side of the figure, according to their ease of extractability. NB: Data used in the hierarchal cluster analysis have been mean centred and scaled.

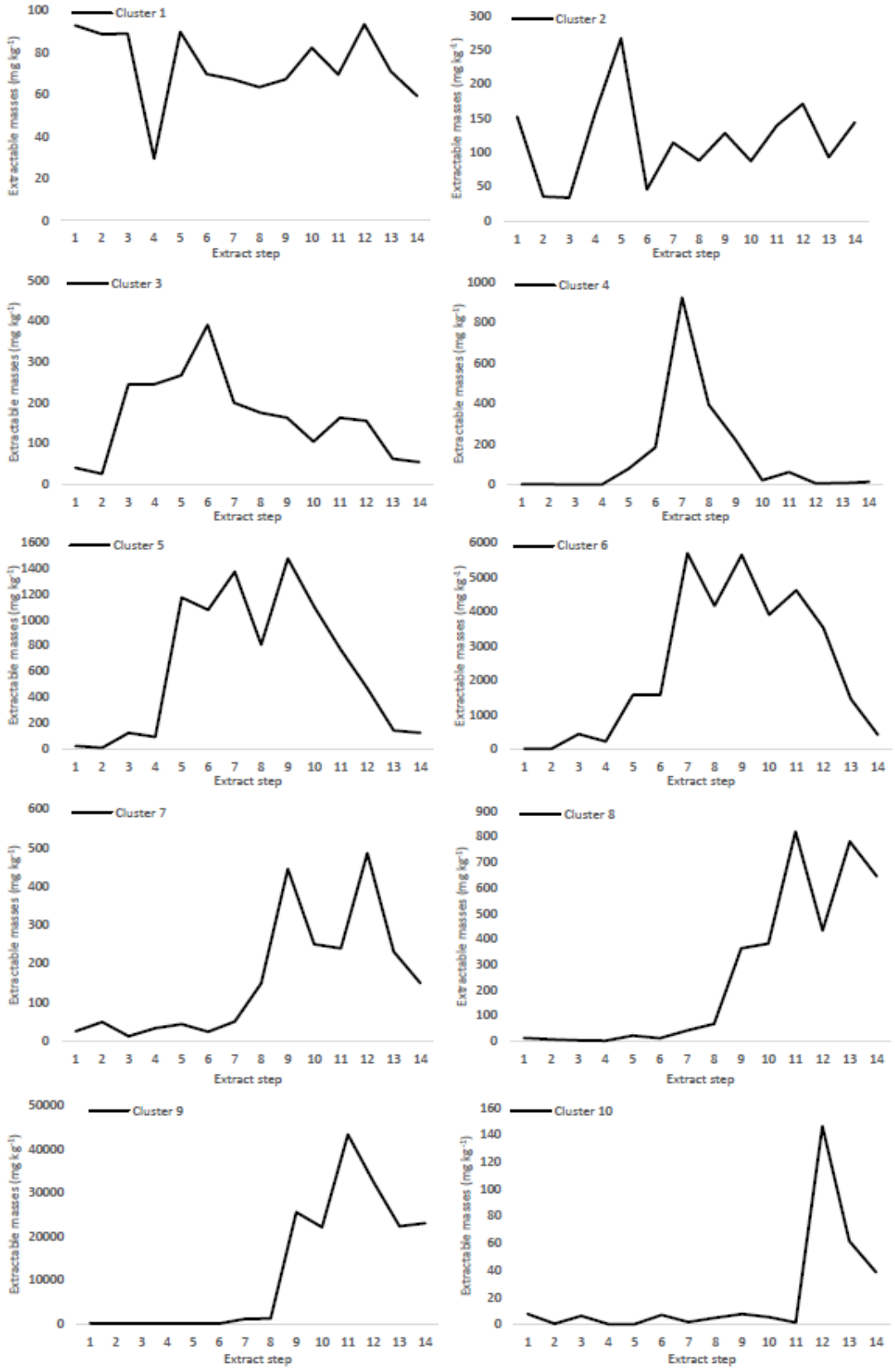

Figure 3.3: Extractograms for clusters 1 – 10.

Cluster 1: Residual pore salts and organics: The presence of Na and K, combined with an early extraction window in the colour map indicates that this cluster is likely to be residual pore water salts (Cox *et al.,* 2013). A low mass of material was extracted at each stage of the CISED approach (89 approx. 50 mg kg^{-1}). However, as masses were low in the second half of extraction profile in comparison to other clusters, this pattern is not clear in Figure 3.2. The lack of a clear extraction window is shown in Figure 3.3. The presence of S was similar to the findings of Wragg and Cave (2012) suggesting that this cluster could have originated from organic material.

Cluster 2: Exchangeable: most samples associated with this cluster showed a peak in the extracted solids between DI and 0.05 M, with a saw-tooth pattern across the extraction profile. The dominant elements in this cluster were P, Na, K and Zn and are considered to be associated with the exchangeable material based on a similar extraction profile seen by Wragg and Cave (2012) with elemental composition as described by Whitehead (2000). Extractable masses peaked at about 250 mg kg^{-1} with the addition of weak acid but were continually extracted throughout the profile in lower quantities.

Cluster 3: Carbonate cluster: The XRD analysis identified the presence of calcite, siderite and dolomite in the test soils that contain this extractable component, which is represented in the colour map by the presence of Ca and Mg. Most of this component was extracted on the first addition of acid, over a narrow range of acid concentrations (0.01 – 0.05 M), peaking at about 400 mg kg^{-1}. In a similar way to Cox *et al.,* (2013), this cluster has been identified as a carbonate fraction. Zn was also identified as being present in this cluster in small amounts and could be associated with calcite (Anju and Banerjee, 2011).

Cluster 4: Mn oxides: This cluster was dominated by Mn and has a clear extraction window peaking at about 0.1 M, after the addition of H_2O_2 which is known to dissolve Mn oxides (Manning and Golberg, 1996). Similar extraction profiles are seen in the literature (Cave *et al.,* 2004; Palumbo-Roe *et al.,* 2005; Wragg *et al.,* 2014).

Cluster 5: Zinc minerals: Zn dominates this cluster and is therefore likely to be derived from Zn bearing minerals. The main extraction windows occurred between acid concentrations 0.05 and 1 M with peaks occurring at 0.05 or 0.5 M. Peak extractable masses were 5,500 mg kg^{-1}. Smithsonite ($ZnC0_3$) is common within the Nent valley of the upper Tyne catchment and could be a source of the components within this cluster (Nuttal and Younger, 2002), however, smithsonite was not identified by XRD making this unlikely. The dominance of Ca in the samples is also suggestive of secondary Zn bearing minerals, such as carbonate

minerals, being the source of the extractable Zn. Calcite (confirmed by XRD) can sequester Zn (Chaterjee, 2009) and has been shown to be present in mine workings and on spoil tips in the Nent valley (Nuttal and Younger, 2002).

Cluster 6: Pb dominated cluster: this cluster contained Pb, Fe, Ca and Zn with peaks in extracted solids seen between 0.05 and 5 M aqua regia, with a similar profile to cluster 5. Extractable masses were lower, peaking at 1,000 mg kg^{-1}. The dominance of Pb (approx. 50 %) and Zn (approx. 20 %) led to this cluster being defined as a Pb mineral cluster. Cerussite was identified by XRD and is likely to be a source of the Ca and Pb in this cluster. A later extraction window, likely to be from the presence of Pb, differentiated cerussite from the carbonate cluster. The presence of manganese (25 %) from one of the samples is likely to arise from association of Pb with manganese Mn-oxides (O'Reilly and Hochella, 2003).

Cluster 7: Al and Fe oxides: Al and Fe were, for most samples, the most prevalent in the components found in this cluster. The varying extraction windows and association with other elements such as As, Cu, Pb and Si suggest that they are relatively impure Al-Fe oxides. The presence of Si can indicate an association with clay materials (Wragg, 2005). The majority of mass was extracted after the addition of 0.1 M aqua regia, peaking at 500 mg kg^{-1} after the addition of 1 M aqua regia.

Cluster 8: Fe oxides: The presence of Fe (and S) and late extraction windows have defined this fraction as a Fe-oxide fraction, consisting of both pure and impure Fe oxides, indicated by the presence or absence of associated elements and possibly sulphides. Clear extraction windows were seen with the majority of solids being extracted by 0.5 – 5 M Aqua Regia. XRD analysis of the soils identified hematite and goethite as mineral sources of Fe oxides, which are crystalline Fe-oxides and difficult to dissolve, hence the late extraction window shown in Figure 3.3. The slight variation in extraction profiles for each of the components in this cluster is likely to be related to the pureness and degree of crystallinity of the Fe oxides.

Cluster 9: Sphalerite: This cluster consisted of a single component from soil 8 which was from spoil tip material and was mainly composed from Fe (35 %), Ca (30 %), Zn (20 %) and Al (10 %). Magnesium, S and Si are also present (2-4 %). The window of extraction was clear and occurred at acid concentrations of 0.5-5 M. The presence of Fe, Zn and S indicates that this cluster is likely to be derived from impure sphalerite minerals (ZnS) and associated with calcite or some other calcium dominated minerals. XRD analysis confirmed the presence of sphalerite within this sample which is known to have been mined in the Nent Valley, from where this spoil pit sample was taken (Nuttall and Younger, 2002).

Cluster 10: Galena: this cluster has been defined as galena (PbS) because the dominant components were Pb and S, and the masses extracted with the addition of 1 M and 5 M Aqua Regia. It is well documented that galena was mined within the area (Macklin et al., 1994; Nuttall and Younger, 1999; Nuttall and Younger, 2002). Extractable masses were low, peaking at 140 mg kg^{-1} and hence this extraction window was not clear in the colourmap (Figure 3.2). Galena was confirmed by XRD analysis in the spoil tip samples (7 and 8) but not in sample 3 from which this component originates, suggesting quantities were around the LOD.

3.3.5 Solid phase distribution of PHEs

The distribution of the PHEs of interest is summarised in Figure 3.4 and Table 3.6. Figure 3.4a shows the majority of As was associated with the Al-Fe-oxide, Fe-oxide and Sphalerite phases (clusters 7 and 8), which is well documented in the literature (Wragg, 2005; Pedersen et al., 2006; Wragg et al., 2007; Wragg and Cave, 2012; Smedley and Kinniburgh, 2013; Palumbo-Roe *et al.,* 2015). Another clear source of As was the carbonate cluster, an association that is also documented in the literature (Magalhaes, 2002). The association of As with the easily extractable carbonate phases (cluster 3) suggests that this source could potentially influence the amount of As mobilised from soil because of the greater solubility of carbonates compared to Fe oxides.

The majority of Cd (Figure 3.4b) was associated with the Zn minerals and sphalerite clusters in the soils used in this study. Cadmium is reported to have a geochemical association with Zn, particularly in Zn mining impacted soils (Anju and Banerjee, 2010). Cadmium is also known to be associated with Fe and Mn oxides, because of their strong affinity for metals (Lion *et al*, 1982; Dong *et al.,* 2007), but concentrations were low in these clusters compared to others. This is likely to be because the Zn minerals and sphalerite clusters are associated with the mining impacted soils, and therefore geochemical enrichment results in higher concentrations of Cd (Table 3.3). Copper was mainly associated with the Al-Fe-oxide, Mn-oxide Pb and Zn mineral phases (Figure 3.4c), with outlier values in the exchangeable phase (cluster 2).

Table 3.6 Clusters associated with each soil and their PHE content in mg kg^{-1}.

Soil No.	Cluster	As	Cd	Cu	Pb	Zn
1	Carbonate	20	0.9	6.2	71	71
	Mn-oxide	9.4	0.6	8.3	18	80
	Al-Fe oxide	140	2.1	49	355	285
2	Porewater/organic	.	3.7	12	.	.
	Exchangeable	24	6.9	9.7	570	795
	Carbonate	19	3.9	38	570	450
	Zn mineral	13	10	42	4200	2500
	Al-Fe oxide	400	2.7	165	3600	900
3	Exchangeable	0.05	0.01	.	.	.
	Carbonate	0.4	0.02	0.2	1.25	1.05
	Al-Fe oxide	0.35	0.27	14	18	43
	Fe-oxide	0.9	0.35	1.56	100	64
	Galena	0.47	.	.	58	1.29
4	Exchangeable	0.12	0.07	.	.	0.87
	Carbonate	0.45	0.40	1.51	34	32
	Mn-oxide	.	0.03	2.02	7.35	.
	Al-Fe oxide	0.61	0.47	5.55	115	24
	Fe-oxide	.	0.05	5.1	.	60
5	Exchangeable	0.04	0.01	.	6.9	2.74
	Carbonate	1.21	0.27	0.58	33	70
	Mn-oxide	0.08	0.34	2.69	227	80
	Al-Fe oxide	0.42	0.1	.	22	.
	Fe-oxide	1.21	0.27	0.58	33	70
6	Porewater/organic	.	0.38	.	.	.
	Exchangeable	0.35	0.61	.	.	175
	Carbonate	.	2	1.51	.	600
	Mn-oxide	.	.	35	1100	125
	Zn minerals	.	11	1.87	1000	2800
	Fe-oxide	14	0.21	5.77	210	80
7	Porewater/organic	0.48	.	0.29	88	.
	Exchangeable	0.29	.	0.43	9.2	143
	Carbonate	0.11	1.18	0.75	106	170
	Zn minerals	1.11	65	74	3000	18000
	Pb minerals	0.17	3.32	5.52	9000	710
	Fe-oxide	4.67	0.34	25	675	385
8	Exchangeable	0.39	2.15	80	300	485
	Pb minerals	6.55	2.98	610	32000	15000
	Al-Fe oxide	0.84	.	0.23	360	.
	Sphalerite	30	3.62	.	65	30000

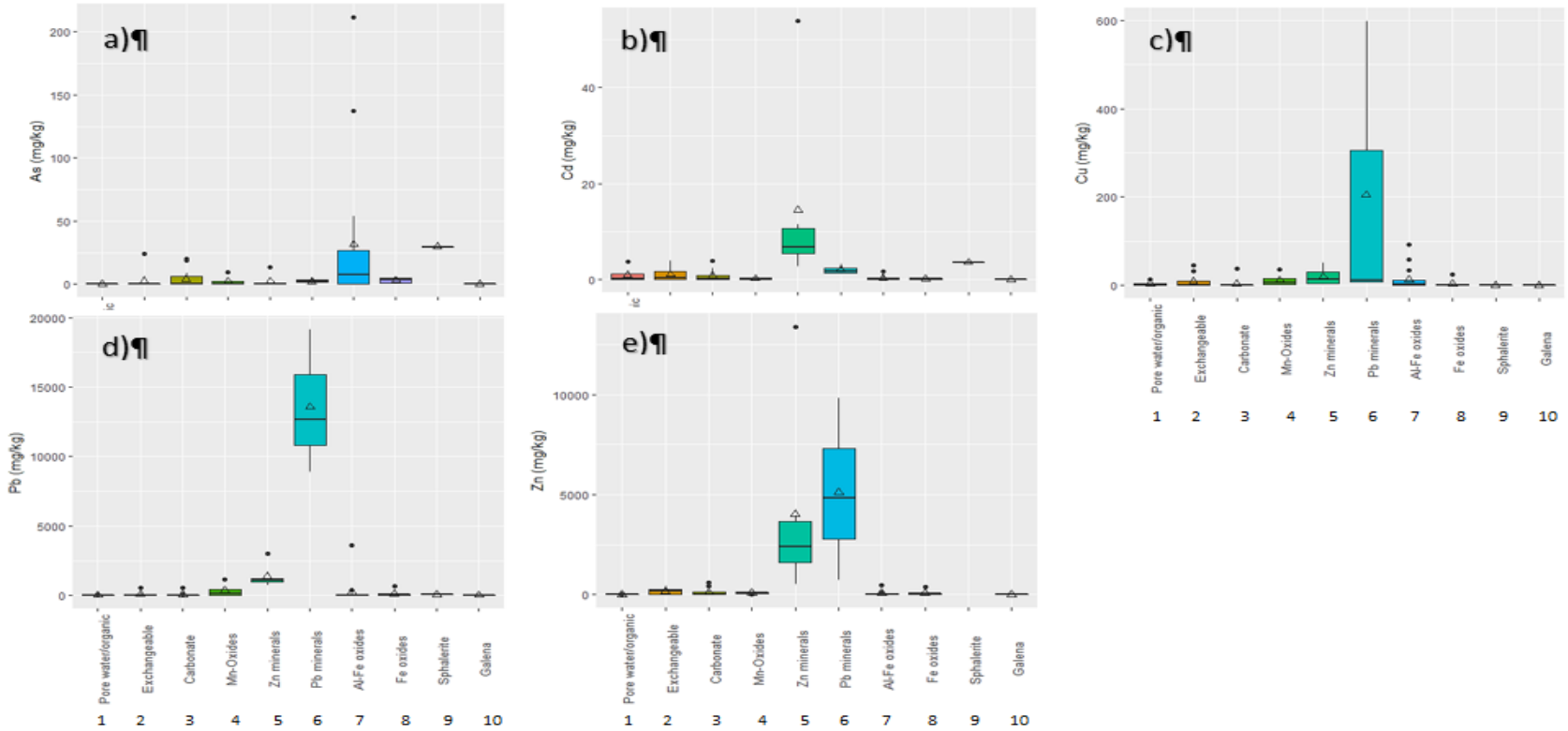

Figures 3.4a-e: boxplots showing the distribution of extractable PHEs in each cluster for the 8 combined soils. Clusters are ordered from the most easily extractable to the least easily extractable. Triangles represent the mean for each cluster. The sphalerite phase is omitted for the Zn plot as it contains a single component with a value of 30605 mg kg^{-1}. Circles represent outliers, which are defined as 1.5 times the interquartile range above the upper quartile and below the lower quartile.

The majority of Pb was associated with the more easily extractable Pb mineral phases (cluster 6) suggesting the presence of more soluble mineral forms of Pb, as opposed to those associated with galena (Figure 3.4d). Lead was also found to be associated with the Mn-oxides cluster, which is well documented in the literature because their affinity to bind with PHEs, particularly Pb and Cd, even at low concentrations (Degs *et al.,* 2001; Hettiarachchi and Pierzynski, 2002; Dong *et al.,* 2007). Zinc and Pb mineral phases provide the highest source of Zn (Figure 3.4e).

3.3.6 Relationship between CISED clusters and bioaccessibility

The CISED extraction process identified the most mobile/potentially available sources of PHEs within the study soils and, in conjunction with the bioaccessibility testing, provided an insight into the sources of bioaccessible PHEs. The solid phase distribution of PHEs and their ease of extractability within soil components is known to affect the bioaccessibility of a PHE (Cox *et al.,* 2013; Wragg *et al.,* 2014). For example, As and its association with different minerals has been reported to result in significant variations in bioaccessibility (Meunier *et al.,* 2010). Some studies such as Pelfrêne *et al.,* (2012) report that physico-chemical parameters such as free Fe-Mn oxide, organic matter and pseudo-total Mn significantly contribute to PHE bioaccessibility. Therefore, CISED information can be used to determine the underlying mechanisms that change the behaviour/mobility of PHEs in soil as a result of environmental changes such as flooding or drought. These are examined further in Chapters 4 and 5.

The contribution of each cluster to the bioaccessible content of PHEs is shown in Figure 3.5 by cumulative mass curves, also used by Cox *et al* (2013) and Wragg *et al.,* (2014). Clusters are ordered by ease of extraction, with the most easily extractable clusters on the left. The data for each PHE are visualised using two plots (high and low) because of the large variation in concentration.

Figure 3.5 suggests that the majority of bioaccessible As in soils 1 and 2 originated from the carbonate and Mn oxide clusters. The Al-Fe oxide cluster partly contributed to the bioaccessible fraction of As in soil 2 and not soil 1, indicating a weaker association of As with these clusters and resulting in greater dissolution of As in gastric fluid. The exchangeable, Mn-oxide and Zn mineral clusters contributed to the bioaccessible As content of soils 6-8. Lead minerals provide a significant contribution of the bioaccessible content for soil 8. Arsenic associated with the Fe-oxide and sphalerite cluster was mostly inaccessible for soils 6-8.

Soils 6-8 showed a similar pattern to soil 2 as the second Fe oxide cluster did not contribute towards the bioaccessible fraction of As, indicating that As associated with Fe oxides tends to remain inaccessible if ingested in these soils. Arsenic bioaccessibility has been shown to decrease with increased crystallinity of Fe oxides (Palumboe-Roe *et al.,* 2015), therefore it is hypothesised that the Fe-oxides in the Fe-oxide cluster are more crystalline and therefore less easily dissolved in the gastric solution. This is further corroborated by the results on the XRD analysis, which showed the presence of goethite and hematite. Additionally, the CISED extraction profile in Figure 3.3 showed this cluster was extracted over more concentrated acids and therefore less available than the amorphous Al-Fe oxide cluster.

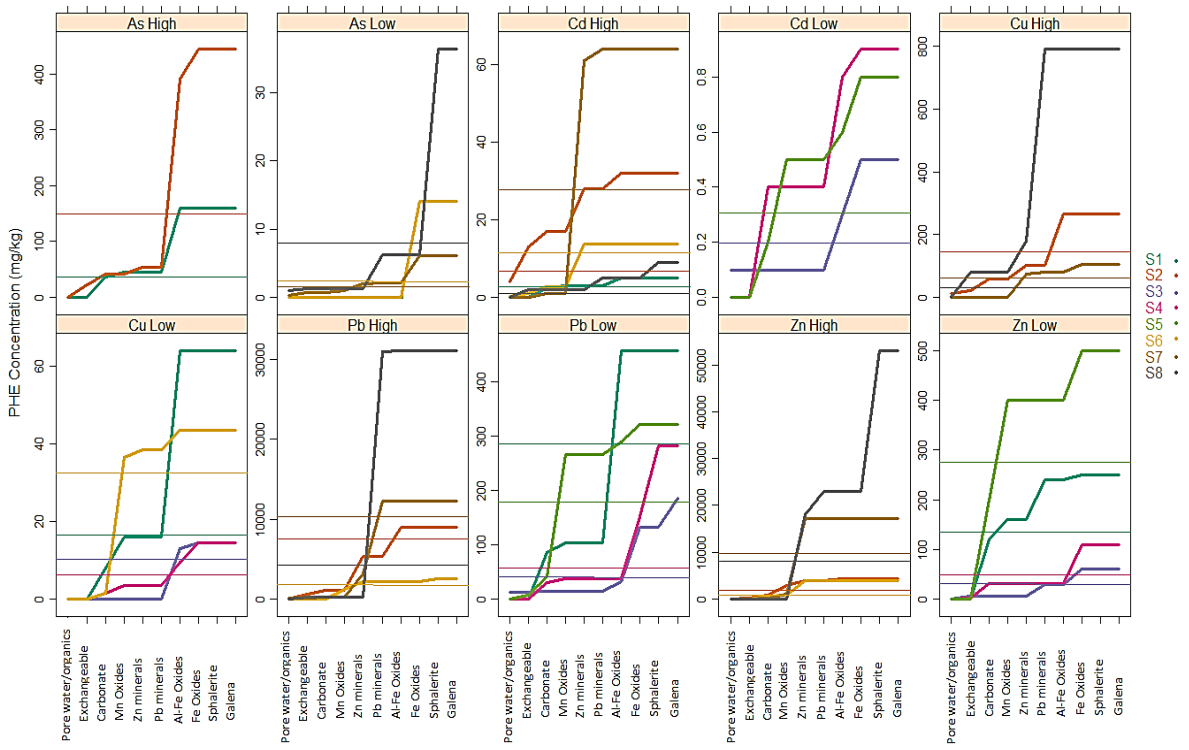

Figure 3.5: Cumulative mass extracted in the CISED components and its relationship to bioaccessible fractions. The thick solid line represents the cumulative mass extracted and the corresponding thin line refers to the bioaccessible amount extracted (mg kg^{-1}). Values below the thin line are interpreted as contributing towards the bioaccessible content.

Cadmium (Figure 3.5) is present within all the clusters except sphalerite and galena. The Mn-oxide, exchangeable and pore water clusters have the greatest contribution to bioaccessible Cd. In most of the soils used in this study, the carbonate cluster only partly contributed to bioaccessibility as organic and clay bound Cd was much more likely to be accessible (ATSDR, 2012). Soils 6 and 7 were different from the others as both the Mn-oxide and Zn mineral clusters had the greatest contribution of bioaccessible Cd. Soil 5 appeared to

be entirely bioaccessible, but this is likely to be because the Cd concentrations in the second plot were close to the LOD. It has been reported that Cd bound to Al-oxides or alumina-silicates was found to increase bioaccessibility (Pelfrêne *et al.,* 2013). The Al-Fe oxide phase was only found to contribute to the bioaccessible content of Cd in only one out of the eight soils under investigation in this work. This may well be because the Al-oxides were impure, associated with Fe and therefore less soluble.

The results shown in Figure 3.5 suggest that bioaccessible Cu originated from the pore water cluster to the Zn minerals clusters for soils 1-6, with the Fe-oxide bound Cu remaining inaccessible. Soils 7 and 8, spoil tip material, had fewer contributing fractions, as the PHEs shown in Table 3.6 tended to be associated with fewer clusters than the other soils in this study.

Partial dissolution of Al-Fe-oxides contributed to some of the Pb bioaccessible fraction, but the majority comes from the more easily accessible clusters e.g. Mn-oxides and Pb bearing minerals. Carbonate, Mn-oxide and Al-Fe oxide clusters had the greatest contributions for soils 4 and 5 (>50 %). The degree of Al-Fe oxide crystallinity in soils 1 and 2 was considered to be the reason for the partial contribution from the Al-Fe oxide phase in soil 2 but not in soil 1 (Palumbo-Roe and Klinck, 2007). However, Fe-oxides in soils 1 and 2 were present as haematite (Table 3.4) which is reported to be the most stable Fe-oxide (Bonneville *et al.,* 2004), therefore the contribution to Pb accessibility was likely to be through a desorption process rather than dissolution of haematite.

The Pb mineral cluster provided a significant source of bioaccessible Pb (>60 %) for the mine spoil soils (7 and 8) through partial dissolution. Lead bearing minerals have been reported to dissolve slowly and incompletely in the digestive tract, often resulting in a low bioaccessible fraction (Ruby *et al.,* 1993). This was seen in Table 3.4, where the two mine spoil tip soils had the lowest gastric bioaccessible fraction for Pb and is also likely to account for the partial contribution of the Pb minerals cluster to the bioaccessible fraction of Pb seen in Figure 3.5. The presence of Pb bearing minerals in the sample was linked to the intensive Pb and Zn mining that occurred within the Tyne catchment (Figure 2.4; Section 2.4).

Fewer clusters contributed towards the bioaccessible content of Zn than other PHEs. Contribution to the bioaccessible Zn originated from the exchangeable to Mn-oxide clusters, which were extracted at lower acid concentrations and therefore deemed to be more available in gastric fluid with a pH of roughly 1.2. Soils 3 and 4 were an exception to this as partial dissolution of the Pb minerals cluster occurred (Figure 3.5). For all soils, except soil 8,

most of the Zn was found in more easily extractable clusters and less was associated with the Al-Fe-oxide phases. Soil 8 was mostly composed of sphalerite and approximately 50 % of the pseudo-total Zn was associated with this phase. Studies looking at bioaccessibility of sphalerite associated PHEs using *in vivo* rat models have shown bioaccessible concentrations to be low (Bergmann *et al.,* 2000). Similar results were seen here where the sphalerite cluster in soil did not contribute to the bioaccessible fraction of Zn.

PHEs such as Zn, Pb and Cd associated with carbonates and Mn-oxides are more labile than other clusters such as Fe-oxides, because of their relative solubility (Schaider *et al.,* 2007; Roussel *et al.,* 2010). For example, Reis *et al.,* (2014) showed that Pb bioaccessibility could be as high as 90 % when the majority of Pb was associated with highly soluble carbonate phases, as opposed to much less soluble Fe-oxide phases. Therefore, soils with high proportions of PHEs associated with the carbonate fraction and other more easily extracted phases such as Mn-oxides are likely to be more bioaccessible. For example, soil 5 has its largest proportion of Zn associated with the carbonate and Mn-oxide fractions and has a bioaccessible fraction of 50 %, whereas soil 8 has the majority of Zn associated with sphalerite and a corresponding bioaccessible fraction of 16 %. Knowledge of the main hosts of bioaccessible PHEs can provide useful information for the prediction of bioaccessibility at a catchment scale. For example, if the solid phases of soils are known, then it will be possible to use these in models to predict bioaccessibility.

While it has been reported that the exchangeable and carbonate fractions of soils can be used to predict PHE bioaccessibility (Schaider *et al.,* 2007), the results of this study show that other fractions such as Zn minerals and Mn-oxides can also be important contributors. It is therefore recommended that they should be included when predicting the PHE bioaccessibility of floodplain soils in different catchments based on their similar characteristics and underlying geology. This could a) reduce the need for extensive sampling and costly extraction tests b) be used to produce maps of the spatial distribution of PHE bioaccessibility in catchments c) allow better targeting of remediation strategies of PHE enriched soils in catchments. Ultimately using the approach outlined here will provide an input into decision-making on how best to manage PHE enriched floodplain soils and potentially reduce the risk to humans from PHEs.

3.4 Conclusions

There was considerable variation in the total and bioaccessible PHE concentrations for a suite of PHEs from eight soils within the Tyne catchment, with four out of the eight sites exceeding

human health GACs for one or more PHEs. For example, the mining waste soils may have had the lowest bioaccessible fractions for Pb and Zn, but their bioaccessible content still exceeded GACs, presenting a potential hazard to human receptors. Mine spoil tips are variable in their composition, but this work highlights the importance of containing material within these spoil tips and preventing their mobilisation into the environment. Whilst the PHE bioaccessible concentrations of these spoil tips were too low to result in acute poisoning (Section 3.3.3), chronic poisoning could occur if human receptors were in regular contact with some of the affected sites.

The CISED identified components and their subsequent comparison to bioaccessibility values showed the potential relationships between the solid phase distribution of PHEs and their availability to human receptors. This study showed that not all soil components contributed to PHE bioaccessibility for the soils under investigation, as the bioaccessible content was related to the solubility of the different PHE containing components present. For example, results from the determination of the solid phase distribution of PHEs highlighted the Fe oxides as hosts of PHEs such as As and Pb. The degree of crystallinity (and resulting solubility) of the Fe oxide phases could be a significant factor in the release of the bioaccessible fraction of various PHEs assessed in this study. Knowledge on the solid phase distribution can indicate the likely fate and behaviour of PHEs during flooding conditions. For example, the majority of As was associated with the Fe-Al oxides and the literature reports that reductive dissolution of these crystalline structures can result in the release of associated PHEs under reducing conditions (section 1.5). Other PHE bearing phases were the Mn-oxide phase and the Pb and Zn dominated phases, all of which could undergo reductive dissolution if reducing conditions occur and pH drops during flooding. The presence of pyrite in samples may result in the formation if metal sulphide complexes during the inundation periods used, potentially reducing PHE bioaccessibility.

Bioaccessibility testing on soils from the Tyne catchment has shown that available (via oral ingestion) PHE concentrations were lower than those measured using a pseudo-total digestion, thereby providing a more realistic estimation of the hazard present. Combining bioaccessibility with results obtained from the CISED extraction (and associated data manipulations) gave an insight into why certain PHEs were (more) bioaccessible compared to other PHEs and why between-soil differences occurred regardless of the pseudo-total concentration. The approach also provided underpinning lines of evidence to support decision-making processes. The soils in this study showed variability, likely from differing

underlying geology and land uses, resulting in the variations in PHE bioaccessibility and solid phase distribution seen between samples. The PHEs in the soils used in this study originated from both geogenic and anthropogenic inputs, as shown in the site description in Section 2.2. Similar results were also seen in other studies using different soil types and contamination sources (e.g. Reis *et al.,* 2014; Pelfrêne *et al.,* 2012), highlighting the variability that can occur between soils within a single catchment. Such knowledge is important for conducting site-specific risk assessments for human receptors utilising PHE enriched soils within a catchment. The approach used within this study can be applied to other catchments to gain a greater understanding of the effects of the sold phase distribution of PHEs on their overall bioaccessibility.

Chapter 4 will examine the fate and behaviour of PHEs under wetting and drying regimes for the eight soils used in this chapter through laboratory microcosm experiments.

4. FLOODING INDUCED CHANGES IN THE MOBILITY OF POTENTIALLY HARMFUL ELEMENTS (PHES) IN SOILS FROM A HISTORIC UK MINING CATCHMENT

4.1 Introduction

Many UK catchments experience continuing freshwater inputs of potentially harmful elements (PHEs) from both point and diffuse sources associated with past mining activities, despite the cessation of metal mining (Lynch *et al.,* 2017). These materials can be introduced into river systems by processes such as erosion and surface run off (Dennis *et al.,* 2003; Foulds *et al.,* 2014), or through point sources such as discharge from adits and shafts (Younger, 2000). As discussed in Chapter 1, rivers are effective dispersers of eroded material, having the ability to move significant quantities of potentially contaminated material throughout a catchment, introducing them to floodplain soils via deposition during periods of high flow (Dennis *et al.,* 2003; Macklin *et al.,* 2006; Foulds *et al.,* 2014). The presence of PHE enriched sediment onto floodplain soils can have ecotoxicological consequences for receptors such as crops, livestock and ultimately humans through acute or chronic poisoning if concentrations are high enough through floodplain/river linkages.

Flooding, through fluctuations in oxidation reduction potential (ORP), can alter the physico-chemical properties of PHE enriched soils and sediments by changing their mobilisation potential and availability (Lynch *et al.,* 2017; Shaheen *et al.,* 2017; El-Naggar *et al.,* 2018). Processes such as desorption and dissolution, which can affect mobilisation and availability of PHEs, are complex and dependent on numerous factors such as soil type, major element composition, inundation duration, mineralogy, temperature and overlying water composition (Du Laing *et al.,* 2009). For example, hydrous oxides of manganese, aluminium and iron are known to be influential on the binding and release of PHEs because of their large capacity for sorption (Tack *et al.,* 2006).

The association of PHEs and solid phases is shown in Table 3.6 and Figure 3.4 displays that PHEs were associated with the Mn, Al and Fe oxides in the eight Tyne soil samples used in this study. Flooding is known to cause the reduction of these oxides through oxidation of organic matter, resulting in the release of associated PHEs (Lynch *et al.,* 2014; Pan *et al.,* 2016). PHEs can also be immobilized during prolonged flooding conditions following the formation of metal sulphide complexes as SO_4^{2-} is reduced to HS^- (Vink *et al.,* 2010; Pan *et al.,* 2016). Post flooding conditions generally return to an oxidising environment where Fe and Mn oxides precipitate with PHEs, reducing their mobility (Du Laing *et al.,* 2009; Ciszewski

and Grygar, 2016). Over time, dehydration can age Mn and Fe (hydr)oxides to a more crystalline state, immobilising PHEs through association (Figure 1.1) (Zheung and Zhang, 2010).

To understand the significance of PHE mobilisation and subsequent risk to receptors such as humans, livestock and foodstuffs, it is important to first understand the factors which are most important for controlling the mobilisation and availability of PHEs in sediments and floodplain soils. Figure 1.4 predicts that PHEs will be initially released into porewaters from the dissolution of Mn/Fe (hydr)oxides and association with dissolved organic carbon (DOC) before possible association with other solid phases such as sulphides and organic compounds. In this chapter, these associations are tested by:

- Examining PHE mobilisation into porewater during wetting and drying cycles in a laboratory microcosm.

Following on from this, multiple linear regression was used to:

- Identify the main factors that influence PHE mobilisation into the porewater of the soils used in this study.

Finally, the potential risk to ecological receptors was assessed by

- Comparing porewater PHE concentrations to the relevant Environmental Quality Standards (EQSs).

Potential risk to humans is determined in Chapter 5 where flooding induced changes in PHE bioaccessibility are investigated.

4.2 Methods

A full description of the methods used is given in Chapter 2. A brief description of each method is reported below.

4.2.1 Sample collection and characterisation

A full site description, along with justification for selection of the sample site locations, is given in Section 2.2. Table 4.1 provides a brief overview of the soils used within this study. The colours show how soils were grouped by their characteristics, underlying geology, land uses and concentrations of PHEs present (shown in Table 3.2). For example, soils 1 and 2 are both technosols from a former Pb works which are now used as recreational parkland. This grouping was used in regression analysis, outlined in section 4.2.6. Soil samples were collected from the Tyne catchment using the methods described in section 2.3.

Table 4.1: Description and location of each of the soils used within this study. Colours indicate grouping of soils for multiple linear regression.

Sample number	Location	Geology	Description	Land use
Soil 1	St Anthony's Head	Sandstone	Technosol from a former Pb works site	Recreational parkland
Soil 2	St Anthony's Head	Sandstone	Technosol from a former Pb works site. Fragments of pure Pb present	Recreational parkland
Soil 3	Nenthead	Sandstone, mudstone and limestone	Histosol. Peat soil in upper catchment	Rough grazing
Soil 4	Corbridge	Sandstone with alluvium superficial deposits	Cambisol soil from mid catchment	Agricultural
Soil 5	Corbridge	Sandstone, mudstone and limestone	Cambisol from mid catchment. Sourced from river bank	Rough grazing
Soil 6	Nent Valley	Limestone, sandstone, siltstone and mudstone with alluvium superficial deposits	Stagnosol from upper catchment	Rough grazing
Soil 7	Nenthead	Sandstone, mudstone and limestone	Spoil tip material	Rough grazing
Soil 8	Nenthead	Limestone	Spoil tip material	Rough grazing. Tourist attraction

4.2.2 Microcosm set up and inundation regime

Microcosms were used to simulate inundation and drying events in a controlled manner. The setup of the microcosms is described in detail in Section 2.5. Figure 2.11 displays the inundation regime used throughout the experiment and the frequency of sampling.

Oxidation reduction potential (ORP) was measured daily, using the method outlined in section 2.9. Only 6 probes were available, so these were used in soils 2-7, as soils 2 and 7 were similar to soils 1 and 8 respectively (Table 4.1). Porewater was extracted every second day using Rhizons™, as described in Section 2.4. Extracted porewater was acidified to 2 % HNO_3 acid and stored in a refrigerator (~4 °C) until analysis by ICP-OES.

4.2.3 Statistical analysis

Multiple linear regression (MLR) was used to establish the significant variables influencing PHE mobility into porewater. Log transformations were made where necessary to meet the requirements of MLR, using the log command in R. For example, exploratory plots were made prior to MLR and log transformations made where the relationship between predictor and response variable were not linear.

Model simplification, for the purposes of parsimony, was carried out on a step by step basis where the highest order terms were removed until only the significant variables remained. Soils were grouped by their characteristics shown in Table 4.1. This was done because grouping the soils by their characteristics made it easier to fit MLR models to the elemental porewater data.

4.2.4 Comparison of porewater concentrations with Environmental Quality Standards (EQS) for water bodies

Porewater PHE concentrations were compared to EQS values to determine their potential risk to ground and surface waters. EQSs have been defined by the UK Technical Advisory Group (UKTAG) to meet the requirements of the Water Framework Directive (WFD). Where EQSs are exceeded, this indicates that the exposure to a particular PHE could cause a potential risk to receptors. Some EQSs have a proposed total value in $\mu g\ l^{-1}$ and others, such as Cu and Zn, are determined based on a bioavailable concentration. The required bioavailable calculation for Cu and Zn was determined using the UKTAG Bioavailability Assessment Tool (WFD-UKTAG 2012a; WFD-UKTAG 2013). The required inputs are the pH, $CaCO_3$ content and DOC content of the water to derive a bioavailable concentration for the selected PHEs. The calculation of a Zn value by the tool also required the natural background concentration within in the river, defined in the Tyne as 1.30 $\mu g\ l^{-1}$ of Zn (WFD-UKTAG, 2012b).

4.3 Results and discussion

4.3.1. Oxidation Reduction Potential during wetting and drying

Oxidation reduction potential (Figure 4.1) values generally follow the pattern of the wetting and drying sequences, declining during inundation and rising during dry periods, as might be expected from the literature (Du Laing *et al.,* 2007; Frohne *et al.,* 2016; Shaheen *et al.,* 2017). Generally, as outlined in Section 1.5, inundation resulted in the consumption of O_2 by microbial respiration, leading to reducing conditions. pH was observed to increase during a move to reducing conditions as reduction reactions consumed H^+ (Kashem and Singh, 2001).

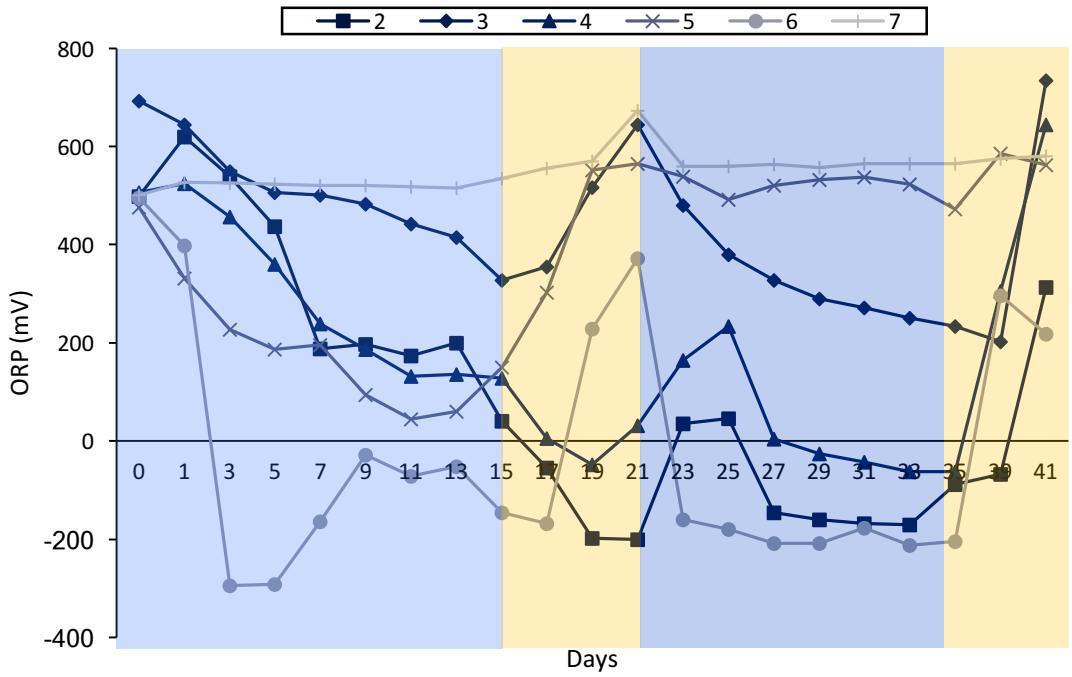

Figure 4.1: Oxidation reduction potential (ORP) in mV for soils 2-7 over the duration of the experiment. Data are not available for soils 1 and 8 because of lack of probes. The blue depicts periods of inundation and yellow periods of drying.

Sample 7 was the exception to the general trend of declining ORP during inundation as the ORP measurements remained mostly constant throughout the experiment at around 550 mV. This is likely to be because soil 7 was spoil tip material with elevated Zn and Pb concentrations (17,000 and 294,000 mg kg^{-1} respectively). Given these Zn and Pb concentrations, microbial communities are likely to be limited (Aceves *et al.,* 1999) which may explain the lack of fluctuation in ORP. Similar results were observed by Lynch *et al.,* (2017) on Zn enriched mine impacted river bank sediments leading these authors to conclude that desorption rather than microbial induced reductive dissolution was the main driver of Zn mobilisation in spoil tip material under short term inundation (weeks).

Soil 5, a sandy river bank soil with low SOM content (<2 %), initially decreased from approximately 500 mV to 50 mV during inundation before rising again to 500 mV during soil drying. The initial drop in ORP suggests microbial consumption of O_2 through reduction of the low amounts of SOM in soil 5 was occurring (Du Laing *et al.,* 2009). ORP then fluctuated around 500 mV during the following inundation and drying sequence which may be a result of reduced microbial activity as the available biological resources were consumed during the first inundation period, with no opportunity for these to be replenished.

ORP for soils 2, 3 and 4 remained low (<200 mV) during the second period of inundation than the first. This is likely to be a result of continued microbial activity from favourable wet conditions in the soils from the first wetting cycle (Jenne, 1968). Soils 2, 3 and 4 have a higher SOM content than soil 5 (Table 3.3), which may explain the difference in ORP behaviour. Additionally, the higher organic matter (OM) content of these soils (Table 3.3) retained water so the soils did not dry out to the low moisture conditions seen prior to the first inundation.

The ORP for soil 6 decreased to -300 mV during inundation and rose to 400 mV during drying periods. The observed variation in ORP suggests that the drivers and patterns of PHE mobilisation were different between the eight soils, highlighting the need to fully understand the mechanisms controlling PHE mobilisation.

4.3.2 Influence of wetting and drying periods on porewater PHE mobilisation

4.3.2.1 Arsenic

Measurement of porewater PHE concentrations for soils 1 to 5 showed an increasing trend of As mobilisation during both wetting periods, which coincided with the decreasing trends observed for ORP (Figures 4.2 and 4.3) (Weber *et al.,* 2009). Mobilisation of As into porewaters can occur when As(V) is reduced to the more mobile and toxic As(III) (Roberts *et al.,* 2010; Vink *et al.,* 2010; Frohne *et al.,* 2011; Simmler *et al.,* 2017). The CISED data for soils 1 to 5 showed that As was mainly associated with Fe oxides (Chapter 3 and Table 4.5). Reducing conditions of about 300 to -100 mV (at pH 6-7) are known to result in the release of co-precipitated As via the reductive dissolution of Fe(III)(hydr)oxides (Charlatchka and Cambier, 2000), which is well documented in the literature (Joubert *et al.,* 2007; Burton *et al.,* 2008; Cheng *et al.,* 2009; Xu *et al.,* 2017).

Suitable conditions for the reduction of Fe(III)(hydr)oxides were observed for all the soils used in this study, except for soils 3 and 7. This was further supported by the positive relationship between As and Fe observed in porewaters (Table 4.2), and is consistent with results from other studies (Roberts *et al.,* 2010; Weber *et al.,* 2009). Therefore, it is likely that the reductive dissolution of Fe-oxides can occur over short term wetting events, such as those used in this study. Short term flooding events may result in mobilisation of PHEs from these sources into pore waters, as Fe oxides are known to have an affinity for PHEs (Palumbo-Roe *et al.,* 2015). The environmental implications of PHE mobilisation from short term flooding events are discussed in Section 4.3.2.

Soils 1 and 2 displayed the same pattern of As mobilisation into porewater which is likely to be a result of their similar land use and soil properties (Table 4.1). The majority of As in soils

7 and 8 was associated with more crystalline Fe-oxides and sphalerite (Table 4.5) and little mobilisation of As was observed for these soils. This was likely to be a consequence of the small changes seen in ORP meaning sufficient reducing conditions were not achieved for the dissolution of Fe (Figure 4.3). Soils 7 and 8 were spoil tip material situated in the upper mining area of the catchment (Figure 2.6), hence the presence of sphalerite. The low rates of mobilisation observed for these soils suggest that As associated with sphalerite and crystalline Fe-oxides, which are less likely to be released via reductive dissolution during short term flooding events (<14 days), as sufficiently low reducing conditions were not reached for these soils (Figure 4.1). The CISED data in Chapter 3 also highlighted the stability of this soil component as it was the least easily extracted (Figure 3.3). The mobilisation of As from soils 7 and 8 (Figure 4.3) is therefore more likely to be explained by desorption processes.

Little to no mobilisation of As was observed for soil 3 (Figures 4.2 and 4.3) which was a highly organic soil (>90 % SOM). Some studies have shown that the addition of SOM to soils can promote the mobilisation of As under flooding conditions through increased As volatilization (Huang *et al.,* 2012), competition for binding sites or through the formation of aqueous DOC complexes (Wang and Mulligan, 2006). However, soil 3 contained a low concentration of As (1.16 mg kg^{-1}) that was mostly associated with Fe-oxides. Sufficient reducing conditions were not achieved in soil 3 for the reductive dissolution of Fe-oxides, potentially accounting for the lack of As mobilisation seen in Figure 4.2.

Soil 6 also demonstrated little As mobility into porewaters (Figure 4.3). Soil 6 reached the lowest ORP (-300 mV) and had the majority of As associated with Fe-oxides. Therefore it was expected that As would behave in a similar manner as in soils 1 to 5, being mobilised by reductive dissolution of Fe(III)(hydr)oxides. However, the mechanisms resulting in the low mobility of As into porewaters in this soil are unclear with the available data.

The sharp decline in pore water concentrations observed for soils 1 and 2 during the second drying episode was assumed to be from the oxidation of As(III) to the less mobile As(V) and the subsequent sorption of As(V) onto metal oxides, as a consequence of the rise in ORP (Parsons *et al.,* 2013; Shaheen *et al.,* 2014). It is well documented that the mineralogy and oxidation status of Fe minerals influences the rate of As sorption (Dixit and Hering, 2003). A return to oxic conditions can result in the reformation of reactive Fe(III)-oxyhydroxides such as ferrihydrite at the soil-water interface, as this has a high sorption capacity and is known to become enriched with As (Mandaliev *et al.,* 2014; Simmler *et al.,* 2017). The second

inundation period could have resulted in the reduction of these poorly crystalline fractions and induced the observed second release of As into overlying waters, as seen also in soils 1 and 2 (Figure 4.3). This result highlights the importance of multiple inundation events in promoting As mobility in comparison to long duration events where As can become immobilised by sulphates if sufficient reducing conditions are reached (< - 100 mV). The predicted increases in the frequency of winter precipitation events (Section 1.2) are likely to result in an increase in flooding. Therefore, As mobility may increase through repeated flood events as a build-up of As associated with poorly crystalline or amorphous Fe (hydr)oxides could occur.

No significant relationship was observed between S and As for all soils in the MLR output (and it is therefore not included in Table 4.2), suggesting that As immobilisation did not arise from sulphate reduction and the consequent formation of AsS complexes. Sulphide complexes are relatively stable compared to other PHE enriched minerals and PHE concentrations should decline towards zero in a sulphide-controlled environment (Vink *et al.,* 2010). However, this was not observed in Figures 4.2 and 4.3 for the eight soils analysed here. Little mobilisation of As was seen from soil 8, where the As was mostly associated with sphalerite (ZnS). Sufficient reducing conditions were not reached in soils 7 and 8 for the reduction of ZnS and consequent release of associated As.

Table 4.2: output from multiple linear regression models for porewater As mobilisation. Soils were split according to their characteristics and geographic locations (see Table 4.1). NS = not significant.

Soils	r^2	Element	Coefficient	p-value
1, 2	0.81	Fe	0.62	p<0.001
		Si	1.13	p<0.001
3-6	0.79	Ca	-0.40	p<0.001
		Fe	0.12	p<0.001
		Si	1.02	p<0.001
7, 8	NS	NS	NS	NS

The results from Figures 4.2 and 4.3 show that whilst prolonged flooding has been reported in the literature to result in the immobilisation of As through the formation of sulphide complexes, repeated short term flooding events may result in the reductive dissolution of Fe-(hydr)oxides during flooding and re-association with more reactive Fe minerals during drying oxidising periods. This has the potential to result in an increase in the mobility of As

during soil flooding, therefore potentially becoming more available to receptors such as plants through As mobilisation into porewater.

4.3.2.2 Copper

Copper mobility generally follows the same pattern for all the soils used within this study with porewater concentrations decreasing during inundation periods (~90 %) and then increasing during drying episodes (Figures 4.3 and 4.4). This behaviour of Cu has been reported in other studies (e.g. Hofacker *et al.,* 2013; Shaheen *et al.,* 2017) and can be a result of the re-association of Cu with sulphides during prolonged reducing conditions at <-100 mV (Du Laing *et al.,* 2007). Copper is known to preferentially bind to sulphides over other PHEs, therefore, Cu will bind first to any available sulphides present during flooding, forming stable metal-sulphide complexes (Vink *et al.,* 2010). Sulphate reduction has been shown to occur after about five days in a laboratory microcosm inundation experiment by Hofacker *et al.,* (2013) and therefore sulphate reduction was expected in this study at ORP < -100 mV (Kashem and Singh, 2001). However, only soils 2 and 6 reached this condition (Figure 4.1). Consequently, the decline in Cu concentrations seen in the soils in this study is hypothesised to be due to the reduction of Cu^{2+} to Cu^{1+} as seen in Shaheen et al., (2017). This mechanism could result in low Cu mobilisation during the inundation periods, facilitated by electron donors such as Fe^{2+} and bacteria (Weber *et al.,* 2009b; Shaheen *et al.,* 2016; Shaheen *et al.,* 2017).

Copper displayed a negative relationship with Fe, Mn and Ca in soils 1 and 2 (Table 4.3), suggesting there were other sources such as SOM providing binding sites during reducing conditions (Balint *et al.,* 2015). Similar results were found by Shaheen *et al.,* (2017) who concluded that SOM was a preferential binding site over Fe/Mn (hydr)oxides for Cu under reducing conditions. The binding of Cu(II) to SOM during inundation could result in the formation of colloidal particles in pore and overlying waters, thereby reducing Cu mobility as seen by Hofacker *et al.* (2013).

Mobilisation of Cu into porewater was <LOD for soil 3, which has a SOM content of >90 %, suggesting that the Cu remained fully bound to SOM during inundation of this soil. Soil 5, with <2 % SOM and soil 8 with <1 % showed the smallest decreases in porewater Cu concentrations (<60 %) in comparison to other soils. Therefore, soils with low SOM may have reduced ability to immobilise Cu during flooding events.

A significant positive relationship was observed between Cu and Al for soils 3-6 (Table 4.3), however MLR outputs reported that this relationship only explains about 20 % of the

variation in Cu. Consequently, there are likely to be other factors influencing Cu mobilisation, such as dissolved organic matter (DOM) and S. It is hypothesised that the addition of other variables such as DOM and sulphates (not measured) would improve the model output in Table 4.3.

Other studies into Cu mobility have also shown increases in soluble and available Cu during a rise in ORP, highlighting the ecotoxicological implications during soil drying periods (Frohne 2011; Shaheen *et al.,* 2014). Inundation after prolonged drying periods can result in higher concentrations of Cu in solution originating from the oxidation of SOM (Balint *et al.,* 2015) or the oxidation of sulphates and release of associated Cu (Shaheen *et al.,* 2017; Naggar *et al.,* 2018). This may result in an increase in available Cu to plant and animal receptors in porewaters and may be a mechanism driving the increase in porewater Cu concentrations in this study that coincide with a rise in ORP. Section 1.2 highlights that climate change predictions show increased drought periods during summer, which may promote the mobility of Cu as previously flooded soils dry out.

113 4.3: Multiple linear regression analysis for porewater Cu. Response variables were log transformed and predictors log transformed where mentioned below.

Soils	r^2	Element	Coefficient	p-value
1, 2	0.79	Log(Ca) Log(Fe) Log(Mn) Log(Si)	-3.44 -0.77 -0.24 6.6	p<0.001 p<0.001 p=0.01 p<0.001
3-6	0.21	Al	0.02	p<0.001
7-8	0.43	Si	0.05	p<0.001

4.3.2.3 Zinc

Porewater patterns of Zn mobilisation are inconsistent between the soils in this study. This is similar to the findings of Indraratne and Kumaragamage (2017), who looked at Zn mobilisation from uncontaminated agricultural floodplain soils. Porewater concentrations of Zn in soils 1 and 2 showed little change with wetting and drying (Figure 4.2). The pattern of Zn concentrations in porewater for soil 3 (Figure 4.2) is unclear because of variation in the replicate microcosm results. In soil 4, Zn porewater concentrations showed a pulsed pattern of mobilisation (Figure 4.3 and 4.4), which has been reported in Lynch *et al.,* (2017) where it was suggested to represent a shift in the mechanisms controlling Zn release from soils during

periods of inundation. These mechanisms may include the reductive dissolution of various metal oxides such as Mn and Al in response to changing ORP values. Soils 6 and 7 showed a rise in Zn concentrations over the first 7 days of inundation, followed by a gradual decline over the second inundation period. Declines in porewater Zn concentrations were also observed during the drying periods for soils 6 and 7. The initial rise in porewater concentrations may come from disassociation of Zn from soil particles during the first inundation, followed by re-association over the remaining duration of the experiment. Soil 8 showed little mobilisation for Zn after the first day and porewater concentrations declined throughout the experiment.

Fe and Mn (hydr)oxides are reported as influencing the mobilisation dynamics of Zn under changing redox conditions (Lynch *et al.,* 2014; Lynch *et al.,* 2017; Shaheen *et al.,* 2017). The conventional release/retention pattern generally reported in the literature is that Fe/Mn oxides are reduced, and any co-precipitated Zn released, under reducing conditions (Lynch *et al.,* 2014) and a return to oxic conditions sees the precipitation of Fe/Mn (hydr)oxides and Zn (Lynch *et al.,* 2017). However, soils 3-5 did not show a significant relationship between Zn and Fe, but with Mn instead (Table 4.4). Similar results have been reported in Shaheen *et al.,* (2017), suggesting that the chemistry and form of Mn/Fe is important for the binding of PHEs such as Zn and that Zn behaviour will vary depending on these soil characteristics. Mn (hydr)oxides have also been shown to be preferentially reduced during microbial respiration over Fe at higher redox potentials which may explain the lack of a relationship between porewater Fe and Zn in soils 3-5 (Maria-Cervantes *et al.,* 2010). Additionally, the lower pH of soil 3 may have prevented Zn from associating with Fe oxides (Shaheen *et al.,* 2017). Soils 6, 7 and 8 showed a continued decline in soluble Zn during oxidising periods, which is thought to be a result of the formation of persistent ZnS (Hong *et al.,* 2011; Bunquin *et al.,* 2017).

A negative relationship between Zn and Fe in soils 1-2 (Table 4.4) suggests that Fe may not be the preferential binding site for Zn in these soils. Similar findings were reported by Frohne *et al.,* (2011). The negative relationship with Zn and Ca seen in soils 1 and 2 may be a result of Ca buffering pH changes (Nedrich and Burton Jr, 2017). For example, in calcareous soils, release of Ca may prevent acidification that can drive PHE release, (Hudson-Edwards *et al.,* 2006) as the presence of high $CaCO_3$ levels in waters may buffer pH levels and therefore hinder the release of Zn from secondary minerals such as Zn carbonate minerals.

Soil 6 (Figure 4.3) shows a declining trend in Zn porewater concentrations over the inundation and drying periods and showed no significant trends with any other major

elements. Consequently, the mechanisms driving the porewater Zn concentrations are unclear from the data available in this thesis.

Soils 7 and 8 had a significant positive relationship between Zn and Si. This may be a result of the mobilisation of Zn from more reactive mineral forms containing Si, such as hemimorphite which has been reported to form quartz grains on mine spoil tip material in the Tyne Valley (Hudson-Edwards *et al.,* 2006). The majority of Zn was mainly in the form of ZnS (see Table 4.5) in soil 8, so it is hypothesised that this was stable for the duration of the experiment as result of the consistent redox potential (Figure 4.1).

Table 4.4: Multiple linear regression analysis for porewater Zn. Response variables were log transformed and predictors log transformed where mentioned below.

Soils	**r^2**	**Element**	**Coefficient**	**p-value**
1-2	0.91	Log(Ca)	-7.69	p<0.001
		Log(Fe)	-0.77	p<0.001
		Log(Si)	12.24	p<0.001
3-5	0.74	Log(Al)	0.33	p<0.001
		Log(Mn)	0.15	p<0.001
		Log(Si)	-1.72	p<0.001
6	NS	NS	NS	NS
7-8	0.42	Log(Si)	1.78	p<0.001

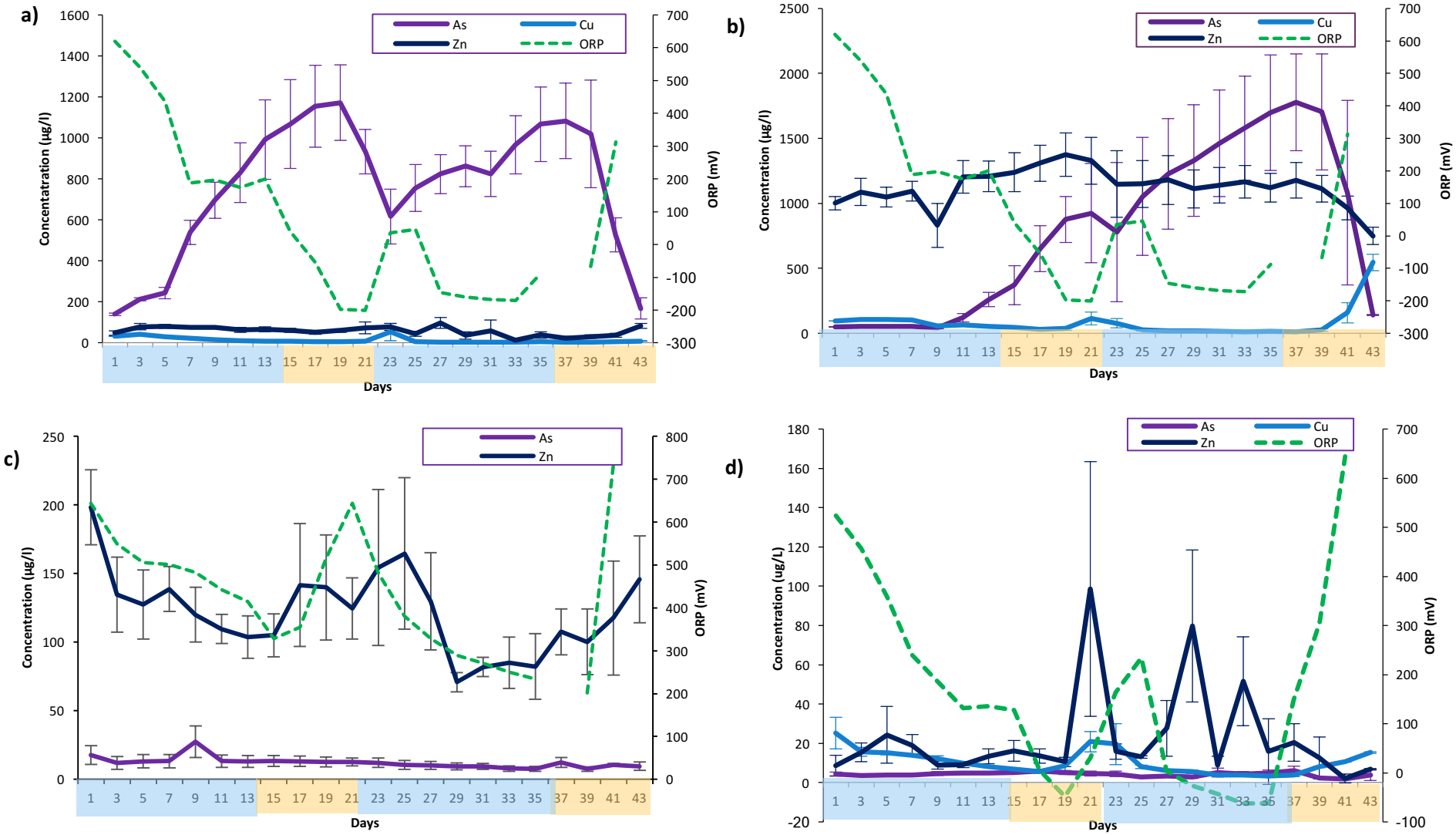

Figure 4.2: a) porewater concentrations for soil 1, b) porewater concentrations for soil 2, c) porewater concentrations for soil 3, d) porewater concentrations for soil 4. Error bars denote the standard error (n=3). Blue area depicts inundation periods and orange drying period. ORP for day 37 is missing.

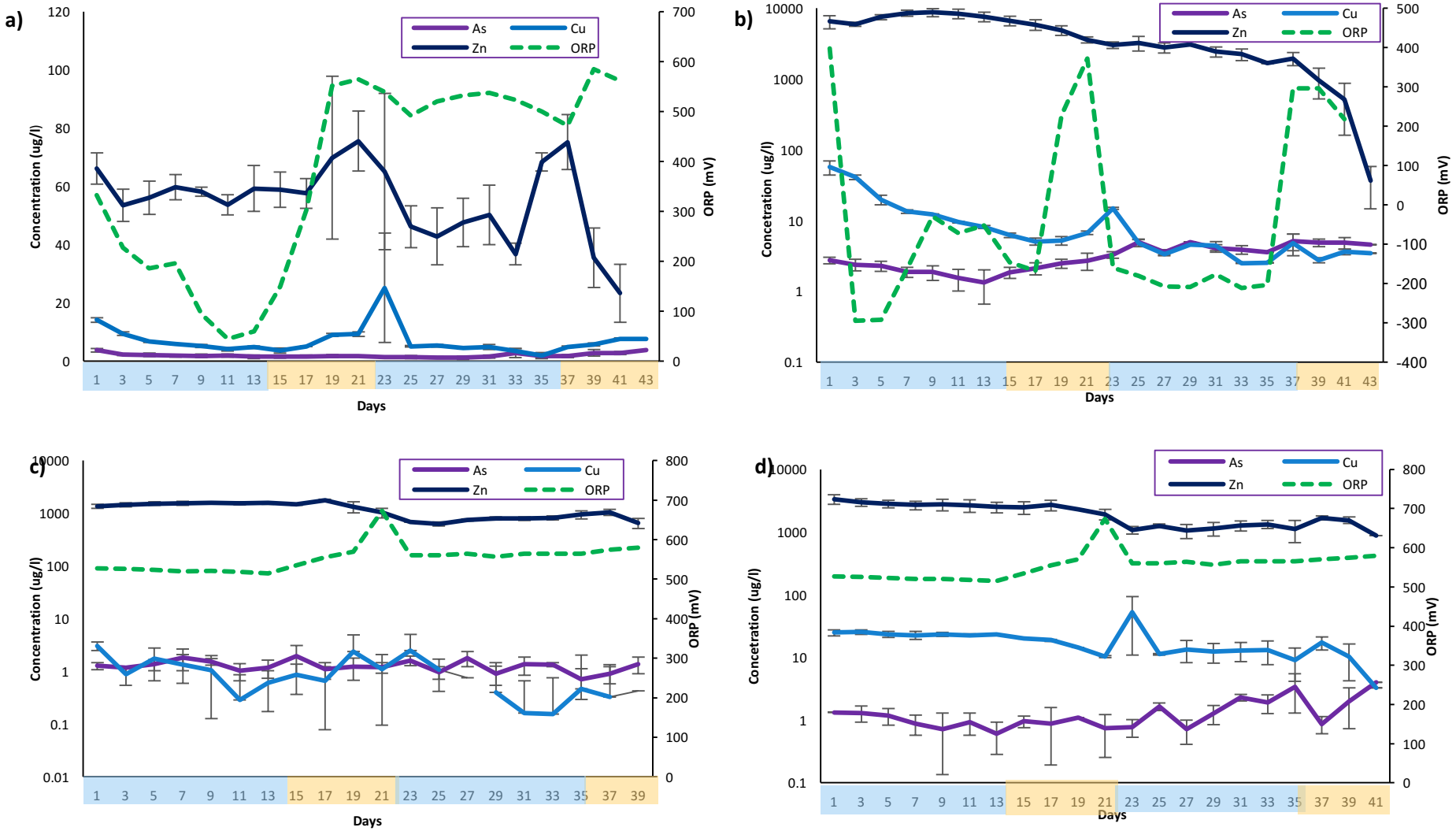

Figure 4.3: a) porewater concentrations for soil 5, b) porewater concentrations for soil 6, c) porewater concentrations for soil 7, d) porewater concentrations for soil 8. Error bars denote the standard error (n=3). Blue area depicts inundation periods and orange drying periods. ORP for day 37 is missing.

4.4.1 Comparison of PHE porewater concentrations to Environmental Quality Standards

Porewater PHE concentrations were compared to environmental quality standards (EQS) to contextualise the results from Figures 4.2 and 4.3 and determine if they pose a potential risk to environmental receptors (Table 4.5). Arsenic EQS values were exceeded by porewater concentrations for soils 1 and 2, with the highest concentration being 1,120 μg l^{-1}, suggesting a potential risk to aquatic environments from inundation of these soils. The potential mobilisation of As from soils 1 and 2 via surface run off may also provide a secondary source of As into receiving waters under a changing climate. This is because increases in precipitation are likely to increase surface run off, leaching and flooding (Wijngaard *et al.,* 2017). Soils 1, 2 and 8 had porewater bioavailable Cu concentrations which exceeded the EQS values.

Table 4.5: Comparison of porewater concentrations to water quality standards. Bioavailable fractions were calculated using the UKTAG Bioavailability Tool

PHE	Water quality standard (μg l^{-1})	Exceeded?	Soils which exceed standard
Arsenic	50	**Yes**	1,2
Copper	1 (bioavailable)	**Yes**	1,2,8
Zinc	10.9 (bioavailable + background concentration*)	**Yes**	All

*Background Zn concentration for the Tyne is 1.30 μg l^{-1} (WFD-UKTAG, 2012b)

All porewater concentrations from the eight soils exceeded the EQS value for Zn. Soils 4-8 were all in close proximity to river channels in the Tyne catchment so likely to experience fluctuations in river stage resulting in periodic soil inundation, therefore providing a pathway from source to river channel for the mobilisation of trace metals. Soils 6-8 were collected from the River Nent floodplain of the upper Tyne catchment and were found to have porewater concentrations reaching 8,820 μg/l. Poor ecological status has been recorded for freshwater invertebrates in the river Nent resulting from trace metal concentrations (Environment Agency, 2017) such as those observed for Zn in this study. Negative effects on benthic organisms have been reported from exposure to Zn concentrations in streams following Zn release from sediments (Nedrich and Burton Jr., 2017). The study by Nedrich and Burton Jr (2017) showed that individual growth rates of the freshwater amphipod *Hyalella azteca* were negatively correlated with dissolved pore water concentrations of Zn.

Despite there not being a single identifiable mechanism responsible for Zn mobilisation, all soils displayed considerable increases of Zn into porewaters immediately after inundation. The results in Figures 4.2 and 4.3, and comparison of pore water concentrations to EQS values (Table 4.5) indicate that there may be an increased risk from Zn exposure. Generally, lower concentrations are released into overlying waters because of the dilution effect of channel currents and freshwater water entering water channels. However, PHE mobilisation into ground water and porewaters can enter river channels via the hyporheic zone and has been shown to increase stream concentrations in the absence of any point sources, highlighting the importance of secondary diffuse sources (Palumboe-Roe *et al.,* 2012). Therefore, understanding the characteristics and mobilisation potential of PHEs in soils is important for the effective management of mining impacted catchments and achieving good ecological status. For example, understanding the fate and behaviour of PHEs in a range of soil types can help identify areas within a catchment that have the greatest propensity for PHE mobilisation under inundation. Highlighting such areas may be useful in targeting areas for site specific remediation, depended on soil type and the PHE present.

Studies in the Tyne have sources of PHEs listed as both diffuse and point sources, highlighting the issues with floodplain soils and sediments being both a sink (Hudson-Edwards *et al.,* 1996) and source (Macklin *et al.,* 1997) of PHEs. For example, porewater concentrations of As exceeded its respective EQS values for soils 1 and 2, where As was expected to originate from the former lead arsenate works where the soils were sampled. The elevated Zn porewater concentrations that exceeded the Zn EQS value were likely to have originated from geogenic sources and diffuse inputs from the Pb and Zn mine spoil tips in the upper reaches of the catchment. Copper was likely to have originated from mining activities in soil 8 and industrial processes for soils 1 and 2.

4.5 Conclusions

The results from this laboratory experiment showed that floodplain soils can act as a source of PHEs into waterbodies in the Tyne catchment through chemical mobilisation into porewaters. This potential release from bank sediments and floodplain soils could have implications for water quality targets in the Tyne such as those of the WFD. For example, the River Nent in the upper South Tyne catchment has failed WFD targets for stream concentrations of Cd, Pb and Zn that originate from both point and diffuse sources (Environment Agency, 2017).

This study showed the potential for PHE mobilisation from a range of soils in the Tyne catchment through mechanisms such as changes in mineralogy, reductive dissolution and desorption. Mobilisation of soil/bank sediment PHEs into ground water, overlying water and changes in PHE availability can result in the exceedance of EQS values and consequently an increased risk to human and ecological receptors. Experimental inundation increased some PHEs close to or above their respective EQS values, highlighting the need for more detailed work into understanding the effects of changes in environmental conditions such as flooding on PHE bioaccessibility for a wider range of soil types. This will be explored further in Chapter 5 where determining changes in the solid phase distribution of PHEs can be used to identify the sources and drivers of PHE mobility.

5. FLOODING INDUCED CHANGES IN THE SOLID PHASE DISTRIBUTION AND BIOACCESSIBILITY OF POTENTIALLY HARMFUL ELEMENTS (PHES)

5.1 Introduction

The solid phase distribution of a PHE can dictate its availability, toxicity and potential for mobilisation (Lin *et al.,* 2018). Flooding of soil has the potential to result in changes in the microbial activity, pH, temperature and redox potential of soils, thereby inducing the redistribution of PHEs amongst the solid phases, as outlined in Section 1.5 (Antic-Mladenovic *et al.,* 2017; Du Laing *et al.,* 2007). The changes in the solid phase distribution of PHEs can also potentially influence PHE bioaccessibility. For example, inundation of soil under anoxic conditions has shown increased bioaccessibility of Cu and Pb to humans (Florido *et al.,* 2011). However, the current state of knowledge on the effects of inundation on PHE bioaccessibility is still limited and more research is needed on how PHE behaviour in different soil types could affect human health. As bioaccessibility is now considered a more appropriate method for human risk assessment of soils and sediments (Pelfrêne *et al.,* 2012), understanding the potential effects of flooding on PHE bioaccessibility is important for the assessment of risk associated with exposure to PHEs in floodplains. Additionally, an understanding of how PHEs can be redistributed amongst the solid phase components of soils can provide insights into why changes in bioaccessibility and mobility occur.

Sequential extractions, such as the Tessier method (Tessier et al., 1979), are often conducted to determine the changes in pre-defined solid phases of PHEs as a consequence of inundation. An alternative technique is the non-specific Chemometric Identification of Substrates and Element Distributions (CISED) method (Cave, 2004), combined with chemometric modelling to determine the fate and behaviour of PHEs in the solid phases before, during and after flood events. The CISED method is a useful tool for ascertaining the underlying mechanisms driving PHE mobilisation and changes in availability as it can be used to determine the masses of PHEs associated with each soil component. Extraction profiles provide information on the potential availability of a component as solids that are extracted over distilled water and weak acid additions will be more mobile and available than those extracted at high acid additions. An increase in extractable masses, or a shift in the extraction profile (described in Section 2.15.1) where the greatest mass of solids is extracted earlier in the profile can show that inundation may increase the potential availability and mobility of a component and associated PHEs. A decrease in the extractable masses of metal oxides

suggests that reductive dissolution of these oxides may be occurring under the reducing conditions experienced during inundation. This has implications for metal mobility as associated PHEs will be mobilised either into porewaters or associated with other components within the soil, therefore determining PHE availability. For example, association with more labile components such as carbonates or with porewater can result in increased availability to receptors (Pelfrêne *et al.,* 2013).

The aim of this work is to explore whether flooding results in detectable changes in the solid phase distribution of PHEs in eight soils from the Tyne catchment. Secondly, changes in the bioaccessibility of PHEs will be determined using the UBM method.

5.2 Methods

A full description of the methods used is given in Chapter 2. A brief description is given below.

5.2.1 Sample collection and preparation

A full site description, along with justification for selection of the sample site locations, is given in Section 2.2. Table 4.1 provides a brief overview of the soils and their characteristics used within this study.

5.2.2 Microcosm set up and inundation regime

Microcosms were used to simulate inundation and drying events in a controlled manner. The setup of the microcosms is described in detail in Section 2.5. Samples were collected as surface scrapes for the CISED and UBM procedures at the end of every wetting and drying sequence, as described in Section 2.5.2. Chapter 2 displays the inundation regime used throughout the experiment. Time steps are outlined below:

- T0 = Pre first inundation period
- T1 = First inundation period (14 days)
- T2 = First drying period (7 days)
- T3 = Second inundation period (14 days)
- T4 = Second drying period (7 days)

5.2.3 Data manipulation

A chemometric self-modelling mixture algorithm outlined in Cave *et al.,* 2004 and Section 2.15 was applied to the chemical composition data and used to identify the number, chemical composition and amount of each component in each sample, as was done in

Chapter 3. However, the five time steps (pre flooding, first inundation, first drying, second inundation and second drying) for all soils were analysed by the self-modelling mixture resolution algorithm (SMMR) together, as opposed to separately as occurred in Chapter 3. This was done to create a uniform set of components across the soils for ease of comparison between soils and time steps. Consequently, the modelled components are slightly different to those presented in Chapter 3, which only included CISED data from the dry eight soils. The CISED determined components (Section 2.15.1) in this chapter were also not subjected to hierarchal cluster analysis. However, the components can be linked to the clusters in Chapter 3, as both datasets originate from the same soils.

Components were defined by applying multivariate techniques to the chemical composition data from the CISED extraction process for each soil. The SMMR process is described fully in Section 2.13.

Analyses were performed in R 3.2.4 (R Core Team, 2016) using the Lattice package (Sarakar, 2008) for the generation of the extraction profiles. Microsoft excel was used for the generation of stacked bar plots.

5.3. Results and Discussion

5.3.1 Flooding induced changes in the CISED extraction profiles

Generally, inundation either increased the amount of extractable solids, or resulted in an earlier peak of extractable solids in the soils used in this study. However, these patterns were variable depending on soil type. This shows that the variation in component behaviour in each individual soil can have consequences for the mobility and availability of associated PHEs. Extraction profiles display the mass of solids at each extraction step for every component and can give an insight into the potential availability and mobility of the elements associated with that component (Cave *et al.,* 2015).

Figure 5.1 showed the flooding induced changes in the extraction profiles for each component for soil 1. The remaining plots for soils 2-8 are in Appendix 2. The effects of wetting and drying cycles on the CISED extraction profiles for each component are summarised in Table 5.1, providing an outline of the change in each component's extractogram.

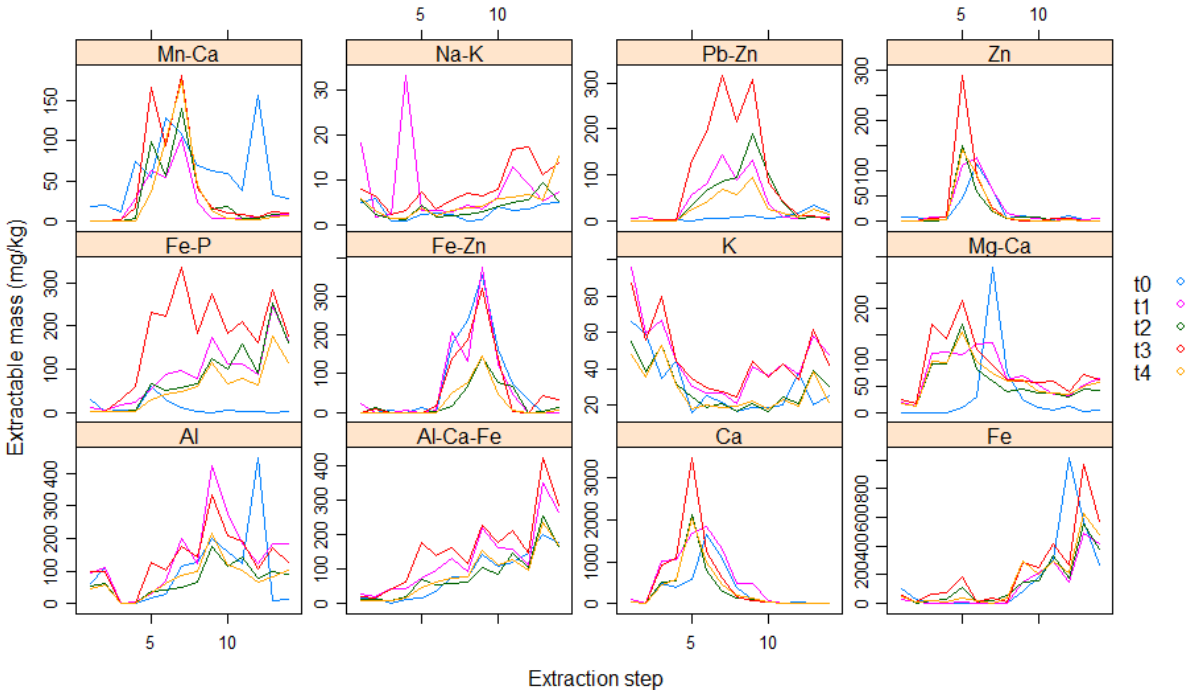

Figure 5.1: Extraction profiles showing CISED extractable solids in mg/kg for soil 1 at time steps 0-4. T0 = pre-flooding, T1= flooded, T2=drying, T3= flooded, T4=drying.

Table 5.1: Summary of the main changes in the extractograms for each component for all soils.

Mn-Ca	**Na-K**	**Pb-Zn**	**Zn**
• Solids extracted earlier after first flood for soils 1, 5, 6, 7 • Greatest solids extracted at T0 for soils 2, 3, 4, 8.	• More extractable solids after flooding: soils 1, 2, and 4,6,7,8. • Soils 3 and 5 have greatest total extractable solids during T0.	• Little to no extractable solids during T0 for soils 1, 2, 5,6,7,8. • Greatest extractable solids during T0. Solids are extracted earlier post flooding. Soils 3 and 4.	• Greatest solids extracted after flooding for soils 1, 2, 6. • Lower extractable mass after flooding for soils 3,4,5,7 and 8.
Fe-P	**Fe-Zn**	**K**	**Mg-Ca**
• Increases in extractable solids after flooding for all soils. Peak extraction is later in profile after flooding.	• Decrease in extractable solids during drying only. Soils 1, 2. • Greatest extracted solids at T0. Soils 3, 4. • Soils 5, 6,7 show no clear patterns or trends. • Little change. Soil 8.	• Increase in extractable solids during wetting periods. Soils 1, 2,6,7,8. • Little change. Soils 4, 5. • Solids only really extracted during T0. Soil 3.	• Earlier extraction profile of solids after wetting. Soils 1, 2, 3,4,5,6. • Reduction is extractable solids after flooding. Soil 7. • Increase in extractable solids after flooding. Soil 8.
Al	**Al-Ca-Fe**	**Ca**	**Fe**
• Earlier peak extraction of solids. Soil 1, 6,7. • Greatest extractable mass at T0. Soils 2,3,4,5. • Little change. Soil 8.	• Increase in extractable solids after flooding. Soils 1, 2,4,6,7. • Little change. Soil 8. • Earlier peak extractable solids. Soil 5. Greatest extracted solids at T0. Soil 3.	• Earlier peak in extractable solids. Soils 1, 2, 6. • Little change. Soils 4, 7. • Increase in extractable solids after drying. Soils 5. • T0 has greatest extractable solids. Soils 3, 8.	• Slightly later extraction profile after flooding. Soil 1, 5,6. • T0 has greatest extractable solids. Soil 3, 4. • Little change, Soils 2, 7,8.

Wetting/drying cycles appeared to affect the CISED extraction profiles for the manganese oxide component in two ways (Table 5.1). Firstly, a shift in peak extraction to earlier in the extraction profile was seen for soils 1, 5, 6 and 7 during the wetting and drying cycles compared to the T0 samples. Secondly, a reduction in the peak extractable solids during wetting and drying was observed for the remaining soils. The reduction in extractable solids of the Mn-Ca component after the initial flooding stage suggests the dissolution of Mn-oxides during wetting, which may result in the release of any associated PHEs. This interpretation is corroborated by the porewater data in Chapter 4 as significant positive relationships were observed between porewater concentrations of Mn and Zn (Table 4.4).

Inundation appeared to affect the Pb-Zn dominated component in two different ways for the soils used in this study (Table 5.1). Firstly, little to no solids were extracted for this component during the T0 step, with an increase in the extractable mass seen for the remainder of the experiment after the first inundation. This suggests that flooding has increased the extractable solids in these soils, indicating the formation of more reactive forms of Pb and Zn bearing minerals during the wetting and drying phases. Secondly, for soils 3 and 4 only, the greatest extractable masses were observed at T0. The peak extractable solids were less after inundation and extracted earlier in the profile, again suggesting a change in the reactivity of Pb and Zn minerals.

The extraction profiles for the Zn component showed two main patterns after inundation (Table 5.1). Soils 1, 2 and 6 displayed an increase in extractable solids after the first inundation step. The remaining soils showed the opposite pattern, with extractable solids being highest during the T0 period. No change in the ease of extraction was observed. For example, no time step was extracted under less or more acidic conditions.

The extraction profile pattern for the Fe and P dominated cluster was similar for all soils. The T0 extraction profile had an early peak around 0.05 M aqua regia addition. The wetting and drying samples all demonstrated peak solids being extracted later than the T0 stage, at 0.05-5 M aqua regia. It is hypothesised for these soils that Fe was changed into more soluble forms at the first wetting stage, making it more easily dissolved and therefore increasing the CISED extractable mass of the Fe-P component. This result suggests that Fe and any associated PHEs may be becoming more available and mobile after wetting and drying cycles, increasing the potential for PHE mobilisation. Phosphorus may be turned into an insoluble form after the first flooding period, hence the shift in extraction profile patterns to one that is characteristic of Fe oxides in other studies (Wragg and Cave, 2012; Cox *et al.,* 2013).

The extraction profiles for the Fe-Zn component showed mixed responses to wetting and drying for the soils in this chapter (Table 5.1). A decrease in extractable solids was served for soils 1 and 2 during soil drying. Soils 3 and 4 demonstrated a greater extractable mass for T0 compared to the wetting and drying stages, indicating that flooding may reduce the extractability of this component for soils 3 and 4. Little change in the extraction profiles or no clear patterns were observed in soils 5, 6, 7 and 8.

The extraction profiles for the K (exchangeable) component remained the same shape for all the soils except soil 3. For soil 3 there was a peak extraction at around 0.01 M for T0. However, this profile was weakly defined, so could be an outlier in the dataset. The extractable masses were higher for the wetting and drying stages for the majority of soils, compared to the T0 samples (Table 5.1).

An earlier extraction profile was seen for the wetting and drying cycles than the T0 samples for the Mg and Ca dominated component for soils 1-6, suggesting wetting and drying has increased the reactivity and extractability of this component. Soil 7 showed a reduction in the extractable solids of this component after wetting and drying whilst soil 8 showed an increase.

Wetting and drying cycles resulted in earlier extraction profiles for soils 1, 2, 6 and 7 for the Al component. Lower extractable masses were observed for soils 3, 4, and 5, suggesting reductive dissolution of Al oxides after the inundation periods. This result is supported by the porewater data in Chapter 4 for soils 3, 4 and 5, where Al displayed positive relationships with PHEs in porewater during soil flooding (Table 4.3). Little change was observed in the extraction profiles for soil 8, suggesting that the mineral forms in this component are likely to be less reactive than those found in the other soils used in this study.

Soils 1, 2, 4, 6 and 7 all had higher extractable solids for the Al-Fe component for the wetting and drying samples, as opposed to those collected at the T0 period. This component was weakly defined for soil 3 as solids were <8 mg kg^{-1} but the extraction profile suggests the greatest extractable masses occurred at the T0 period. Extraction profiles were similar for soil 5 except for a second extraction peak for the second drying period. This component was also weakly defined with extractable peak solids being <5 mg kg^{-1}. Little change was seen in the extraction profile for soil 8.

Wetting and drying cycles affected the carbonate component in several ways. Firstly, soils 1 and 2 showed similar extraction patterns where the peak amount of extractable component

occurred slightly earlier in the profile (about 0.01 M as opposed to 0.05 M) and the peak amount of extractable solids was higher for the wetting and drying cycles, compared to the T0 step. Extraction profile shape remained the same for soil 6 but greater masses of solids were extracted during wetting and drying cycles. Soil 3 showed the opposite pattern to soil 6, suggesting the amount of carbonate phase was reduced in this soil during wetting and drying. Extraction profiles for 4, 5 and 8 were similar. Soil 7 extraction profiles indicated a reduction in the mass of extractable solids during inundation.

The Fe component was the most difficult component to extract. Little change was seen in the profile shapes for soils 2, 7 and 8. In soils, 1, 5 and 6 the Fe component was extracted later in the CISED method after wetting and drying. The extraction profiles for soils 3 and 4 showed reduced extractable solids after wetting and drying.

The effects of wetting and drying on the solid phase components of the eight soils in this study was complex, highlighting that changes in redox potential affects soil components in different ways, having varied consequences for the mobility and availability of PHEs. Studying the changes in the solid phase distribution of PHEs can provide more insight into the potential drivers of changes in PHE mobilisation and availability.

5.3.2 Flooding induced changes in the solid phase distribution of PHEs

The wetting and drying of soils, through changes in ORP and pH, can change the solid phase distribution of PHEs, thereby affecting their mobility and availability (Lin *et al.,* 2018). The following section discusses these changes but does not discuss the original solid phase distribution of PHEs in the soils used in this study, as this is outlined in detail in Chapter 3. Broad patterns of change observed in the solid phase distribution of PHEs are reported and discussed below, rather than deterministic changes. This is because the use of sequential extractions and subsequent chemometric modelling can result in uncertainty around the data. This uncertainty is shown in the distribution plots when error bars go through the y-axis (e.g. Figure 5.7).

The aim of the following work was not to be able to quantify the changes in the association of each PHE with each soil component during the wetting and drying regime, but to examine the trends and changes therein with regard to availability to human and ecological receptors.

5.3.2.1 Arsenic

The majority of As was associated with the Al-Fe oxides component (Figure 5.2). Approximately <2 % of As was associated with the more crystalline Fe oxides in soils 1 and 2,

compared to >20 % for the remaining soils. Little change was seen in the solid phase distribution of As in soils 1 and 2 during wetting and drying (Figure 5.3). Prolonged reducing conditions greater than 14 days may result in reductions of As concentrations in the Al-Fe oxide components as a result of reductive dissolution and more observable changes in the solid phase distribution of As in soils 1 and 2 through potential re-association with other components such as porewaters.

The bioaccessible fraction (BAF) of As (Figure 5.4) for soils 1 and 2 was about 10 - 15 % higher in the wetting periods than the drying periods. The sources of this change are assumed to be partial dissolution of the Al-Fe oxides, as this component was shown to partially contribute to bioaccessibility in Chapter 3, Figure 3.4. Changes in the As associated with the Al-Fe component were not reflected in the solid phase distribution of As (Figure 5.3) because As was reported as a % of the total CISED extractable As for each time step. An increase in CISED extractable As during wetting (approximately 200 mg kg^{-1}) may explain the increases in bioaccessibility that are not reflected in the solid phase distribution in Figure 5.3, suggesting desorption of As from soil particles during soil flooding.

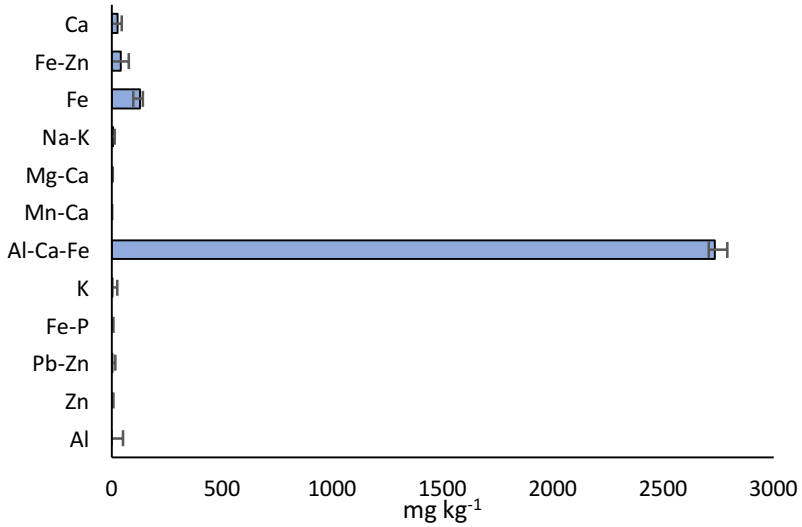

Figure 5.2: Distribution of As in CISED extractable components.

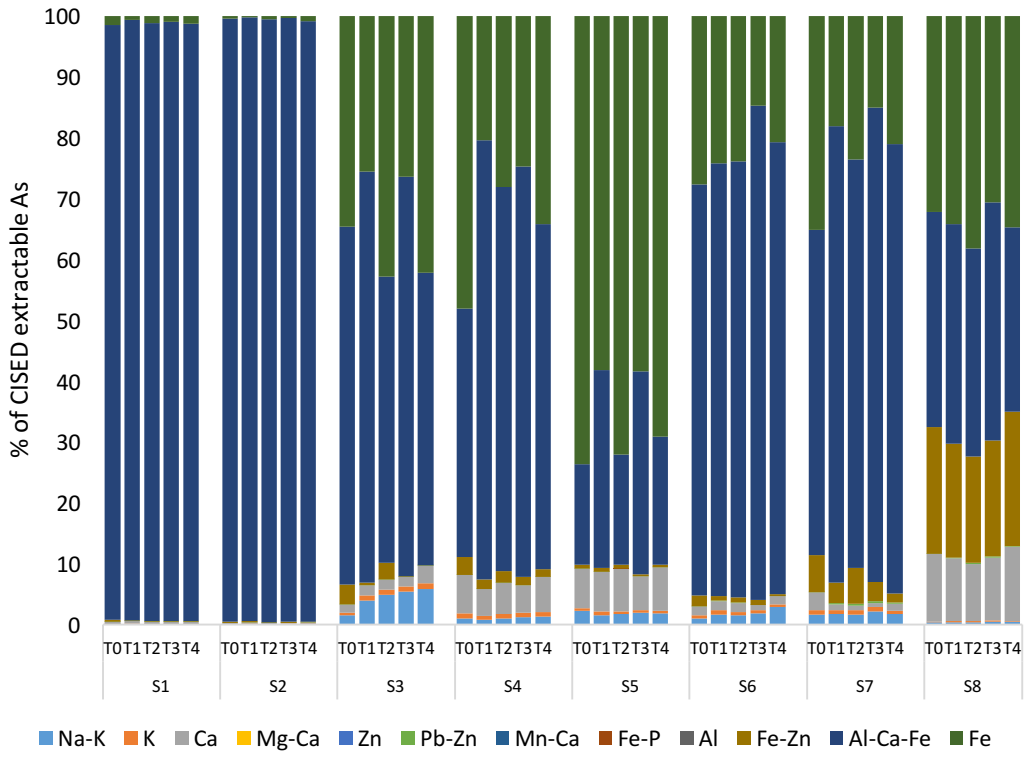

Figure 5.3: CISED stacked bar chart shows the solid phase distribution of Arsenic as a % of the total CISED extractable Arsenic for each soil at each time step.

Arsenic concentrations in the Fe component varied between approximately 20-70 % for soils 3-8 (Figure 5.3). Concentrations in this component were generally higher in the drying phases than the wetting phases, indicating that As concentrations may associate with less crystalline Fe-Al oxides during flooding, rather than the more crystalline Fe oxides. These results are similar to those found by Martin *et al.,* (2007). Increases were seen in As concentrations associated with the Na-K (porewater/organics) component and Ca (carbonate) component in soil 3 during the wetting and drying periods. The reduction in Fe-oxide associated As and increase in carbonate and porewater/organics associated As suggests potential redistribution of As to these components. The results of Chapter 4 show little mobility for As into porewater suggesting As remained associated with Fe-oxides as a result of ORP remaining too high for reductive dissolution of Fe oxides (Section 4.3.2.1). Figure 5.3 suggests As may remain associated in the solid phases of the soils by being redistributed to Al-Fe component.

The solid phase distribution of As was different in soils 1 and 2, compared to the other soils (Figure 5.3). This is likely to be because As originated from anthropogenic sources in this soil,

as opposed to being of geogenic origin like soils 3-8. PHEs of geogenic origin are generally more associated with more stable crystalline fractions of the soil compared to 'fresher' anthropogenically introduced PHEs (Jenne, 1977; Martin *et al*., 1987).

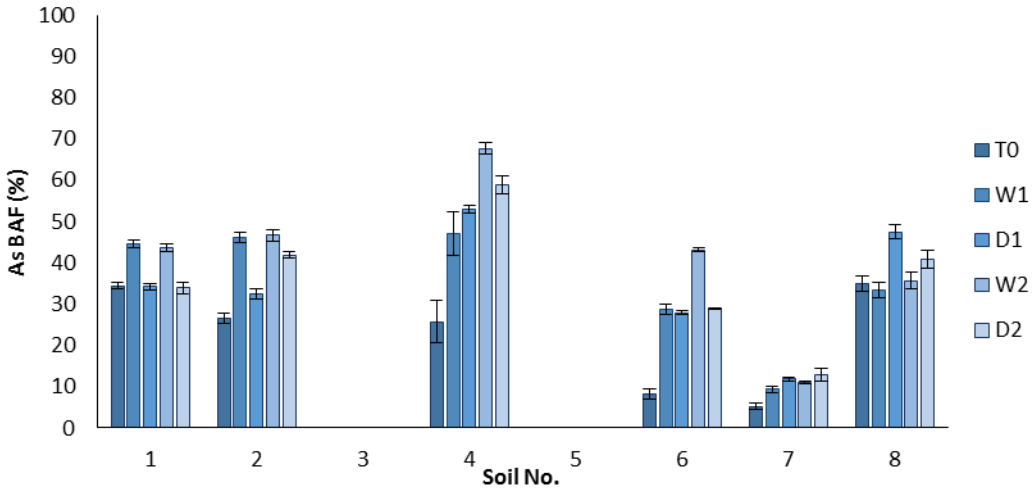

Figure 5.4: The bioaccessible fraction of As (%) at each time step. Error bars represent the standard error (n=3). No values are given for soils 3 and 5 as bioaccessible As was <LOD. T0 = pre-inundation, W1 = first inundation, D1 = first dying period, W2 = second inundation period and D2 = second drying period

Bioaccessibility (Figure 5.4) for soils 3 and 5 is not shown as As concentrations were around the LOD which resulted in a BAF of 100 %. Soils 4 and 6 showed an increase in As bioaccessibility during wetting, which suggests partial dissolution of the Al-Fe oxides (Figure 3.4) as the majority of the As was associated with this component (Figure 5.2). Arsenic is well known to associate with Al-Fe oxides (Bissen and Frimmel, 2003; Palumbo-Roe *et al.,* 2015), as shown in Figure 3.3a. Increases in As bioaccessibility may also arise from desorption of As from the more labile components such as carbonates.

Bioaccessible arsenic concentrations for the drying periods were higher than the initial T0 phase (Figure 5.4). This was likely to be because the soils were still moist and at field capacity between inundation periods and therefore hydrous oxides would be unlikely to return to a dehydrated and more crystalline state (Jenne, 1969). This suggests that the As associated with the Al-Fe oxides during and after inundation was more reactive than in a dried soil. This pattern was also reflected in the increasing porewater concentrations seen in Chapter 4 (Figures 4.3 and 4.4) where increasing As was released into porewaters during inundation.

The results from this chapter showed that the bioaccessible fractions for As were broadly comparable across the 8 soils, with soil 4 having the highest BAF, as opposed to soils 1 and 2 (Figure 5.4). Generally, the BAF of the remaining PHEs for soils 1 and 2 were either comparable to, or lower than those of the remaining soils. Therefore, in terms of potential flooding induced increases in bioaccessibility, the brownfield sites were not of high importance for human receptor exposure. However, there may be an argument that these soils could have higher rates of human interaction than rural soils, therefore increasing the chance of human exposure to PHEs in soil.

5.3.2.2 Cadmium

Figure 5.5 showed that Cd was mainly associated with the Zn, Ca and Al-Fe components. Changes in the solid phase distribution of Cd were observed in the more labile components such as the Na-K (porewater/organics) component (soil 3) or the Ca (carbonate) component (Figure 5.6). Cadmium associated with the Ca component increased for time steps T1 to T4, compared to T0 for all the soils, with the exception of soil 7. Increases of Cd associated with the Mg-Ca component were observed in soils 3, 4 and 8, highlighting the potential increases in Cd availability after wetting of dried soils. The results here are similar to other studies where Cd was shown to associate with carbonates after one week of flooding (Khaokaew *et al.,* 2011). It is suggested that this occurs as Cd^{2+} and Ca^{2+} can compete for binding sites on calcite, and calcite was present in the soils used in this study (Chapter 3). Carbonate associated Cd has been shown to contribute to Cd bioaccessibility in this study and in the literature through dissolution in the low pH environment on the stomach (Pelfrêne *et al.,* 2011). Therefore, an increase in carbonate associated Cd may increase Cd exposure to humans from direct exposure to soils.

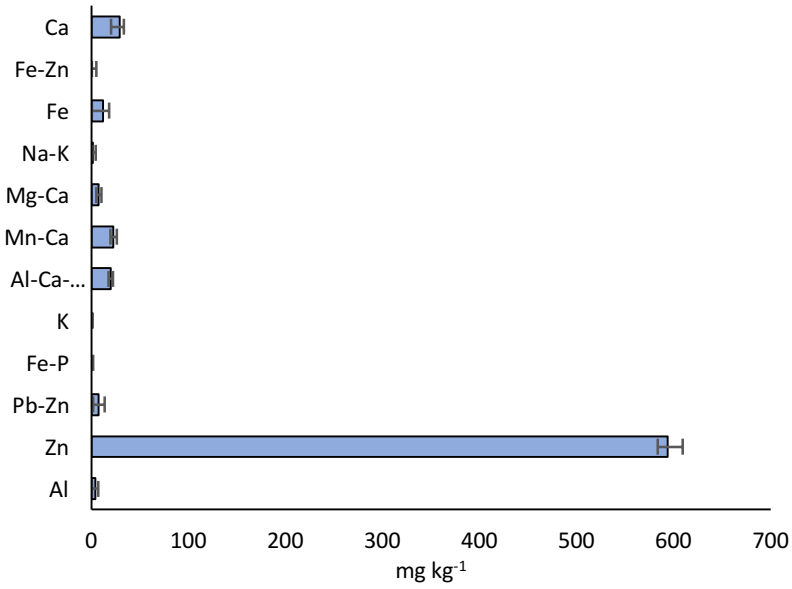

Figure 5.5: Distribution of Cd in CISED extractable components.

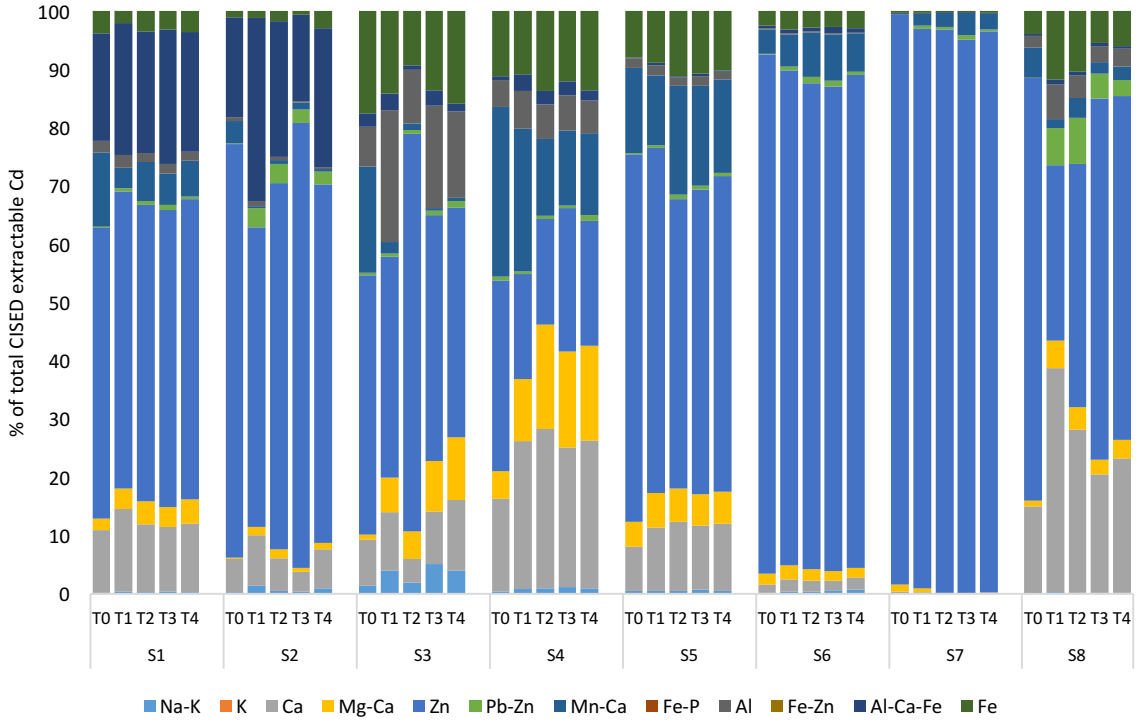

Figure 5.6: CISED stacked bar chart shows the solid phase distribution of cadmium as a % of the total CISED extractable cadmium for each soil at each time step.

5.3.2.3 Copper

Figure 5.7 displays the association of Cu with each component, showing large uncertainty between the Fe-Zn and Al components. The uncertainty associated with these two

components is probably due to the similar extraction profiles of the two components (Figure 5.7). Both the Zn-Fe and Al components are likely to originate from the Al-Fe oxide cluster in Chapter 3. Therefore, the majority of Cu could be associated with either of the two components. Other major hosts of CISED extractable Cu were the Al-Fe oxide component in soils 1 and 2, and the Mg-Ca component in soils 3-6, which is in agreement with the data in Table 3.6.

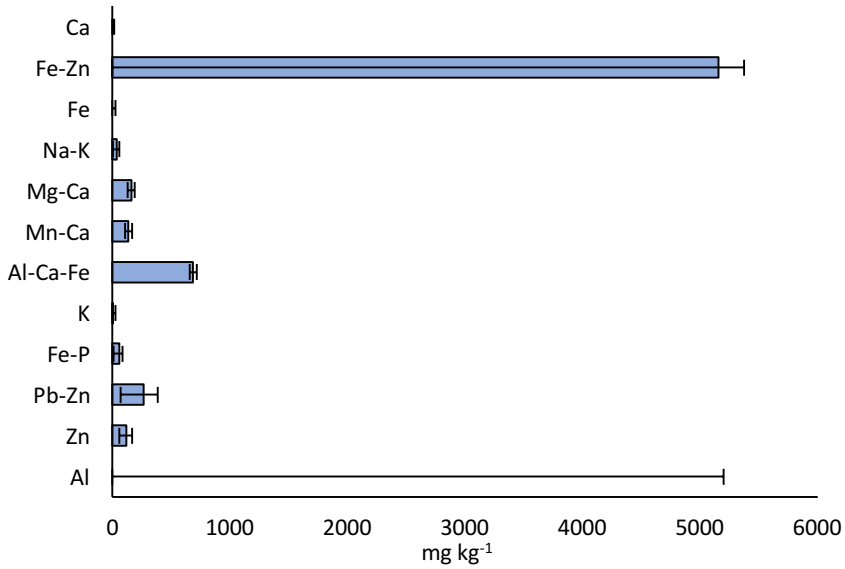

Figure 5.7: Distribution of Cu in CISED extractable components for all soils.

Soils 1 and 2 display similar patterns of flooding induced change within the components (Figure 5.8). There was a small reduction in the mass of extractable Cu associated with the Fe-Zn component, and a concomitant increase of Cu in the Mg-Ca, Pb-Zn and Al-Ca-Fe components. The Mg-Ca and Fe-Zn components were the more easily extractable, suggesting a small increase in Cu associated with the more labile components.

CISED extractable Cu concentrations increased in the K (porewater/organic) component for soils 3 and 6, which were the most organic rich soils (Figure 5.8). This possibly suggests association with organic components during inundation as Cu may become desorbed from other phases during flooding and (re-)associate with organic components (Du Laing *et al.,* 2009). Association with organic components can result in PHEs such as Cu being retained in an exchangeable form, where they are available for uptake by plants (Zeng *et al.,* 2011). Increased uptake by plants in agricultural areas can result in an indirect pathway of PHE exposure to humans through ingestion of PHE enriched plant material. Soil 6 displayed an

increase with the Al-Fe component after flooding, however this component was considered the most inaccessible to humans in the eight soils used in this thesis (Chapter 3).

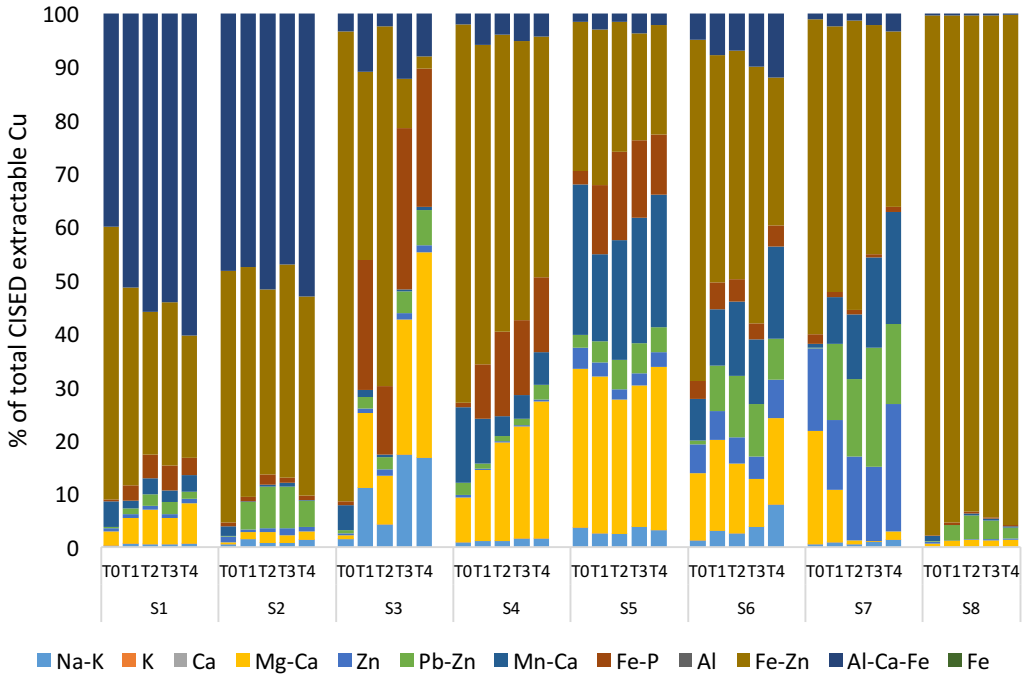

Figure 5.8: CISED stacked bar chart shows the solid phase distribution of copper as a % of the total CISED extractable copper for each soil at each time step.

Soil 4 displayed increases in the Mg-Ca component and the Fe-P component. The Fe-P component was considered to have originated from fertiliser application. Soil 5 displayed an increase in Cu associated with the Fe-P component; little change was observed with the other components.

Soil 8 was dominated by Pb and Zn bearing components (Figure 5.8). Little change was observed in the association of Cu, with Cu being retained in the Pb and Zn dominated components. Little mobilisation of Cu was seen into porewaters in Chapter 4, so Cu associated with the mine spoil tips of similar composition to soil 8 in the upper region of the Tyne catchment were considered to be mostly unreactive and of little concern to human receptors. In contrast, soil 7 had a higher concentration of organic matter and therefore soil 7 Cu behaved differently to that in soil 8 after the wetting and drying cycles. Cu was observed to be associated with a wider range of components and increases were observed in the Pb-Zn and Mn-Ca components after wetting and drying.

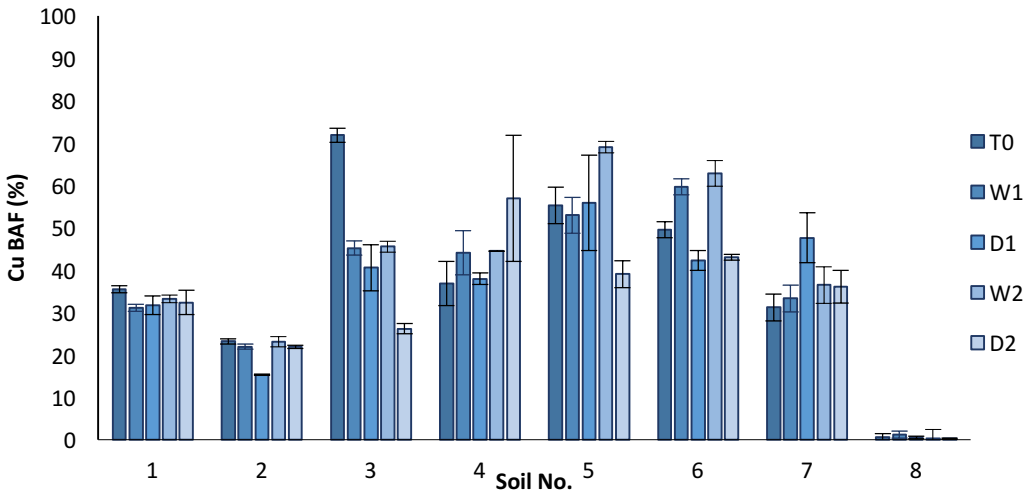

Figure 5.9: The bioaccessible fraction of Cu (%) at each time step. Error bars represent the standard error (n=3). T0 = pre-inundation, W1 = first inundation, D1 = first dying period, W2 = second inundation period and D2 = second drying period.

Flooding induced changes in bioaccessibility of Cu varied between the sampled soils (Figure 5.9). For example, soils 1 and 2 generally displayed little change or a decrease in Cu bioaccessibility during the wetting and drying periods, with the highest bioaccessible Cu concentrations found during the T0 phase. This suggests that dried airborne soils may have higher BAF than those at field capacity. Exposure from airborne particulate fractions (<20 μm) has been reported to be higher than that of bulk samples (<255 μm) because of the smaller particle size and larger surface to volume ratio (Guney *et al.,* 2017). This has implications for human exposure through inhalation should drying and wind erosion take place during periods of drought.

Soil 3 demonstrated a similar pattern to soils 1 and 2. The floodplain soil samples, (4, 5 and 6) all showed flooding induced increases in Cu bioaccessibility. Soil 7, a spoil tip material 'soil' displayed a slight increase in Cu and bioaccessibility whilst Cu remains almost entirely unavailable in soil 8.

5.*3.2.4 Lead*

The majority of Pb was associated with the Pb-Zn component for all soils (Figure 5.10). Increases of Pb associated with the Pb-Zn component were observed for all soils during the wetting and drying cycles, except soils 3 and 4, where Pb also increased in the Al-oxide component (Figure 5.11).

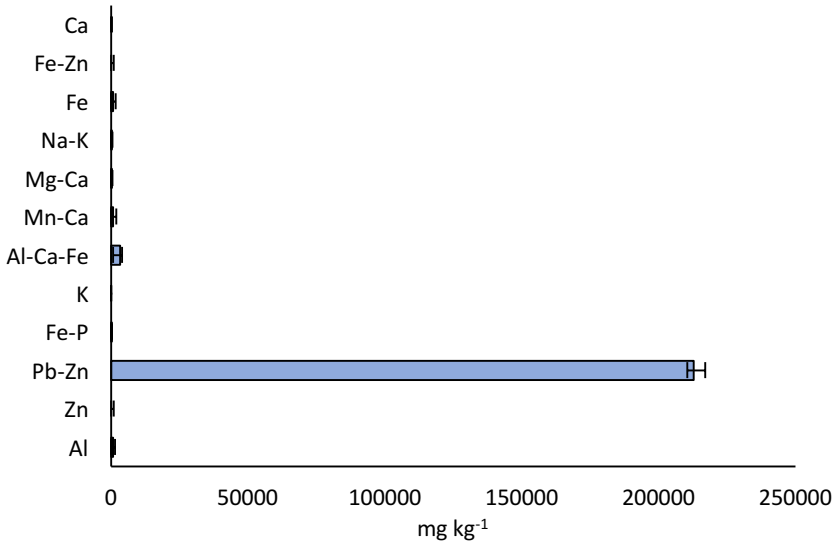

Figure 5.10: Distribution of Pb in CISED extractable components.

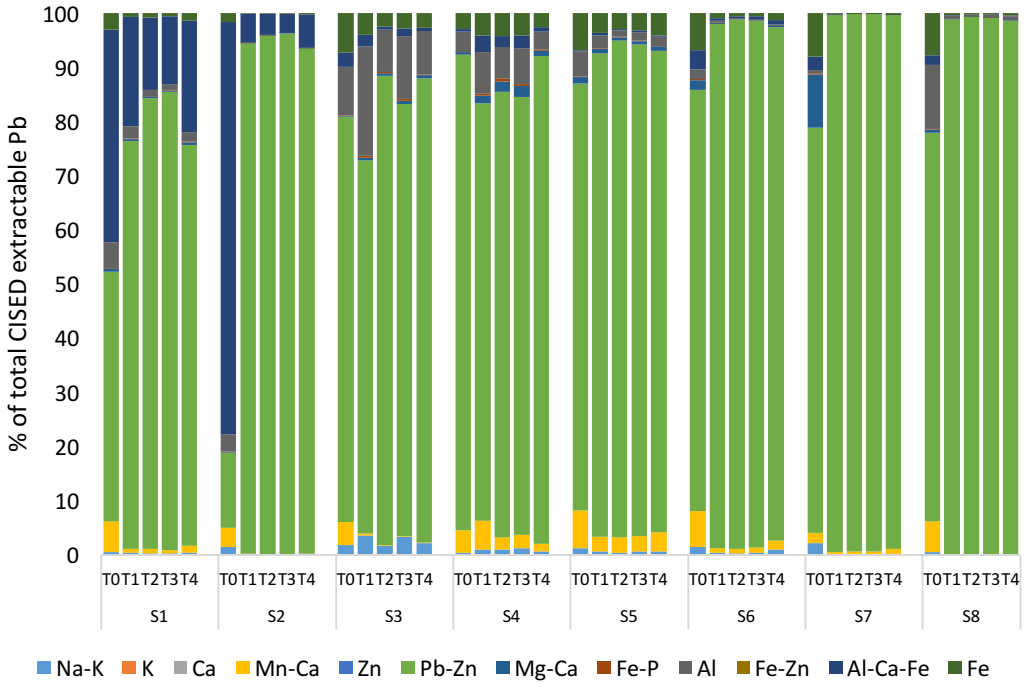

Figure 5.11: CISED stacked bar chart shows the solid phase distribution of lead as a % of the total CISED extractable lead for each soil at each time step.

Soils 1 and 2 had approximately 40-80 % of Pb associated with the Al-Ca-Fe component during the T0 stages but this was reduced after flooding to <20 %. The remaining soils had <5 % associated with this component, which was also reduced during wetting and drying.

The Mn-Ca component and Al-Fe component appeared to be reduced during wetting and drying, resulting in the possible association of Pb with the Pb-Zn component for all soils.

The data suggest a reduction in the Pb associated with the Fe oxides, potentially through the process of dissolution and desorption during wetting periods. Similar results were seen by Lynch *et al.,* (2017) during flooded microcosm studies of Pb and Zn rich mine spoil. The potential environmental implications of this are increased stream loading of Pb in mining impacted catchments (Lynch *et al.,* 2017).

Additionally, an increase in the bioaccessibility of Pb was observed after wetting and drying suggesting that the Mn oxide was a source of bioaccessible Pb (Figure 5.12). This was further corroborated by the results from Chapter 3 where Mn-oxides were shown to contribute to Pb bioaccessibility. Bioaccessible Pb concentrations also exceeded GACs for soil 2, which experienced flooding induced increases in bioaccessibility of approximately 10-30 %, again potentially resulting in increased Pb exposure to human receptors at this particular sampling location.

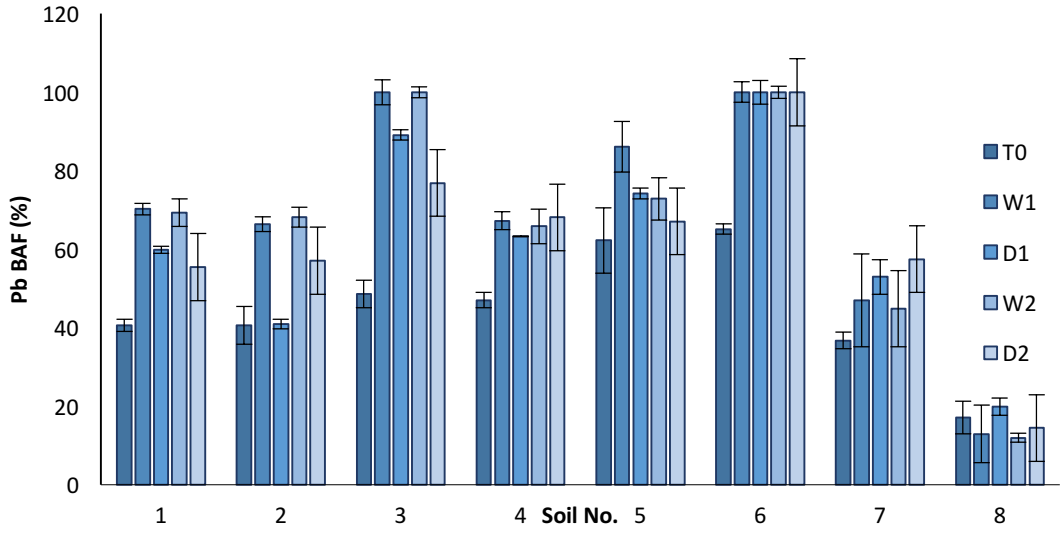

Figure 5.12: The bioaccessible fraction of Pb (%) at each time step. Error bars represent the standard error (n=3). T0 = pre-inundation, W1 = first inundation, D1 = first dying period, W2 = second inundation period and D2 = second drying period.

Lead bioaccessibility was shown in Figure 5.12 to increase during flooding for all soils except 7 and 8, where Pb bioaccessibility was higher during the drying period. This may result from

the oxidation of Pb sulphides during dry periods (Lynch *et al.,* 2014). Pb sulphides (galena) were shown to be present in the mine spoil material (Table 3.4)

5.3.2.5 Zinc

The solid phase distribution of Zn is reported in Figure 5.13 for the Zn, Pb-Zn, Fe and Ca components as four components in Figure 5.13 that contain the majority of extractable Zn. The Fe-Zn and Al component were not considered as their error bars go through 0 (Figure 5.13).

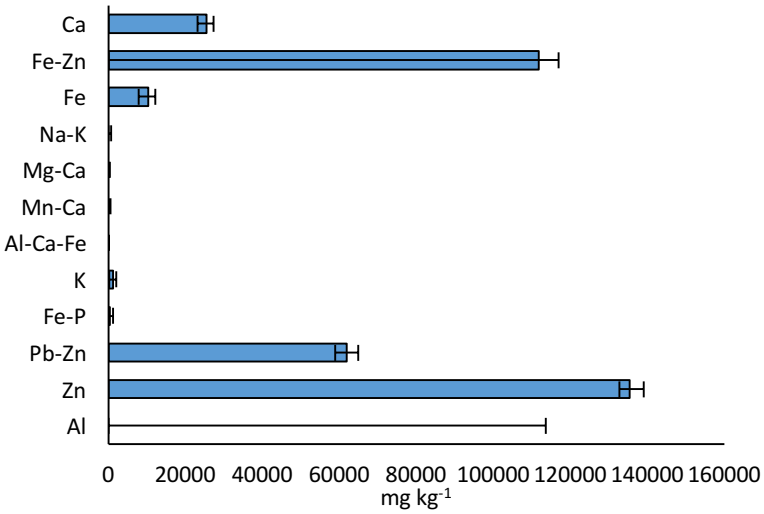

Figure 5.13: Distribution of Zn in CISED extractable components.

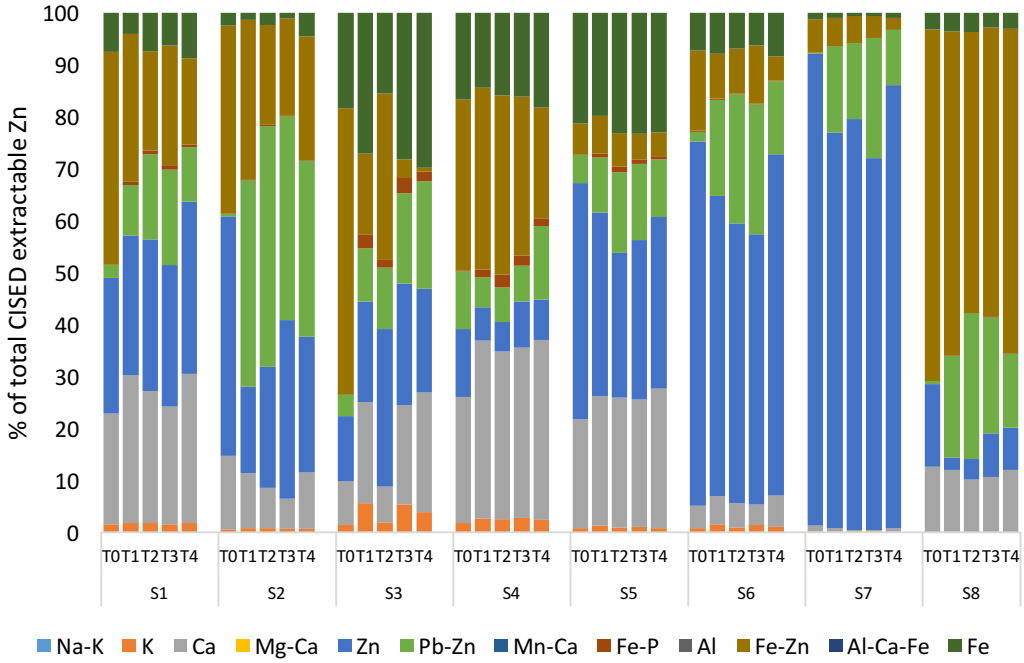

Figure 5.14: CISED stacked bar chart shows the solid phase distribution of zinc as a % of the total CISED extractable zinc for each soil at each time step.

Soils 1, 2, 3, 6, 7 and 8 (Figure 5.14) showed an increase in extractable Zn in the Pb-Zn components after inundation which may be from the increased extractability of the Pb-Zn component, outlined in Table 5.1. An increase in extractable solids associated with the Pb-Zn component can potentially result in an increase in the extractable Zn associated with the Pb-Zn component. The majority of soils also displayed a reduction in the Zn associated with the Zn component and a concomitant increase in the Pb-Zn component. Both the Pb-Zn and Zn components had similar extraction profiles so it may be difficult to distinguish the association of Zn between them. However, because of the similarity of ease of extraction in the Pb-Zn and Zn components, the (re-)distribution of Zn between them had little significance on the overall availability of Zn to human receptors.

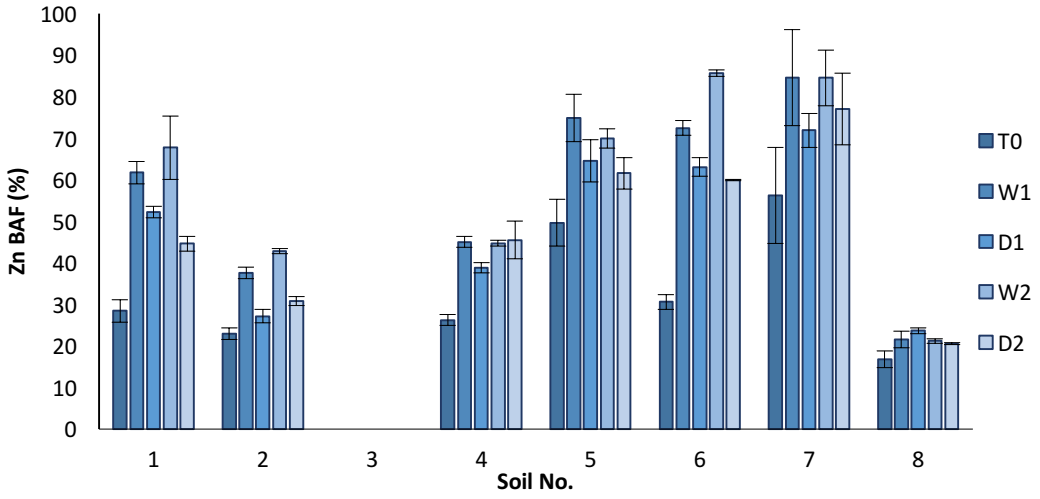

Figure 5.15: The bioaccessible fraction of Zn (%) at each time step. Error bars represent the standard error (n=3). No data are available for soil 3 as bioaccessible Zn was <LOD. T0 = pre-inundation, W1 = first inundation, D1 = first dying period, W2 = second inundation period and D2 = second drying period.

Increases in Zn associated with the Ca component after wetting was observed in soils 1, 3, 4 and 5. A study by Weber *et al.,* (2009) showed an increase in absorbed Zn to the carbonates after 15 days of inundation. The soils in this study all experienced increases in Zn bioaccessibility after flooding and carbonates have been shown to contribute towards Zn bioaccessibility in this study (Chapter 3).

The flooding induced change in the BAF of Zn was broadly similar for all the soils used in this chapter (Figure 5.15). The BAF of Zn was higher during the wetting and drying cycles compared to the T0 step for all soils. The highest BAF values were observed during the wetting periods, where increases of 5 – 10 % were observed over the drying periods.

5.4 Conclusions

The results show that bioaccessibility can be influenced by flooding and drying periods, with an increase being seen for most PHEs during flooding. For example, inundation increased As bioaccessibility in some soils such as 4 and 6 in Figure 5.4 by 20 %, resulting in potentially increased exposure to human receptors. However, changes in PHE bioaccessibility were variable and dependent on soil types and characteristics, which are likely to be caused by differing underlying geology, PHE inputs and the behaviour of individual PHEs. The study has shown that inundation can increase the bioaccessibility for As for the majority of soils used in this study by 5 to 10 %. However, the changes in bioaccessibility witnessed in the soils used in this study were small and the risk to human receptors may be low.

Wetting and dying cycles were shown to result in the redistribution of PHEs between solid phases of the soils, with some PHEs being associated with more labile components. This re-association can increase the potential for uptake, therefore increasing possible PHE exposure. The findings of this chapter are summarised in Table 5.2 below.

Table 5.2: Summary of flooding induced changes in the solid phase distribution and bioaccessibility of PHEs in this chapter

PHE	Flooding induced change in the bioaccessibility of PHEs	Flooding induced change in solid phase distribution of PHEs
As	Generally increased during flooding. Sulphide rich mining material displayed bioaccessibility increases during drying.	Possible redistribution to more labile components, e.g. from Fe to Al-Fe components.
Cd	Not recorded.	Possible redistribution to more labile components, e.g. porewater/organics components and carbonates.
Cu	Reductions in bioaccessibility for the majority of soils, except for 5 and 6. Cu unavailable in soil 8.	Increased with the organic component for soils with higher SOM (3 and 6). Increased with less reactive components, e.g Fe during flooding. Little change in solid phases of Cu for soil 8.
Pb	Generally increased during flooding for soils 1 to 6. Sulphide rich mining material displayed bioaccessibility increases during drying.	Possible redistribution to more labile components, e.g. from Fe Al-Fe to Pb-Zn components.
Zn	Generally increased during flooding for all soils.	Increases in Zn associated with the Ca component. Disassociation and re

Sequential extractions, especially those used in the CISED method, are useful tools for assessing the solid phase distributions of PHEs, providing their limitations are understood. For example, sequential extractions may not be sensitive enough to quantify absolute temporal changes in the concentrations of PHEs in each of the solid phases over short term events (weeks), but they are suitable for highlighting broad patterns of change within soil components and associated PHEs. Such broad patterns can give an indication of the underlying sources of PHE mobilisation into pore and overlying waters, as well as changes in bioaccessibility which can be useful when determining areas within a catchment that have greater chemical mobilisation potential. Datasets such as those in chapters 3, 4 and 5 can complement catchment scale maps of PHE mobility and bioaccessibility in providing the underpinning data and knowledge into why certain areas in a catchment may have a greater risk of flooding induced mobility or bioaccessibility than other areas.

6. PREDICTING THE SPATIAL DISTRIBUTION OF FLOODING INDUCED CHANGES IN THE BIOACCESSIBILITY OF PHES

6.1 Introduction

Floodplain soils in the UK can become enriched with potentially harmful elements (PHEs) originating from the underlying geology or anthropogenic activities such as mining. The toxicity of PHEs, such as those used in this study, means there is a need to understand their potential to cause harm to human and ecological receptors. A primary key human pathway for exposure to PHEs in soil is through accidental ingestion via hand to mouth action. Whilst adults typically ingest 50-200 mg a day (US EPA, 2002), children can ingest up to 20 g (Van der Wiele, 2007), making them more vulnerable to the effects of soil contaminants. Only a proportion of a PHE is dissolved within the gastrointestinal tract and available to be potentially transported across the gastro intestinal wall (Wragg, 2005). This proportion, the bioaccessible fraction, has received international interest with regards to human health and PHE exposure (Broadway *et al.,* 2010; Wragg *et al.,* 2011; Florido *et al.,* 2011; Pelfrêne, *et al.,* 2012; Cave, *et al.,* 2013; Xia *et al.,* 2016).

The production and use of PHE bioaccessibility maps has been recently explored by Wragg *et al.,* (2018) and could provide more realistic estimates of potential exposure compared with the use of total element maps. It has been shown that the bioaccessibility of PHEs varies between different soil types and characteristics in studies (Caboche *et al.,* 2010; Denys *et al.,* 2007; Ruby *et al.,* 2004, Pelfrêne *et al.,* 2012) and Chapter 3 of this thesis. It has also been shown that flooding can influence the bioaccessibility of PHEs (Chapter 5; Florido *et al.,* 2011). Such information can be useful for targeting areas for remediation or the selection of areas within a catchment suitable for flood prevention schemes. For example, if an area within a catchment has a high risk of bioaccessibility increase after flooding, then this area may require further investigative work. This chapter aims to identify these areas using the Tyne catchment as an example.

In this study traditional geospatial tools such as the Inverse Distance Weight (IDW) method have been used and combined with novel machine learning methods such as the Boruta algorithm (Kursa and Rudnicki, 2010), which is a wrapper function for Random Forest (RF) regression models that ranks predictor variable in terms of their importance. This is the first use of this approach to spatially predict the distribution of PHE bioaccessibility in floodplain soils. The aim of this chapter is to firstly geochemically characterise the 48 floodplain soils,

as this information is important in determining the underlying drivers and sources of mobilisation. Secondly, bioaccessibility is predicted from pseudototal datasets prior to spatially mapping the flooding induced changes in PHE bioaccessibility. This is done at a catchment scale using the machine learning and GIS based approaches. Therefore, the specific aims on this chapter are to:

- Characterise the intrinsic soil constituents (ISCs) in the Tyne catchment floodplain soils
- Determine the mobility of PHEs in the Tyne catchment floodplain soils
- Explore the relationships between soil element concentrations and PHE bioaccessibility in soils, using machine learning methods such as RF models.
- Predict bioaccessibility in the Tyne catchment using RF models
- Map PHE bioaccessibility in the Tyne catchment
- Predict flooding induced change in PHE bioaccessibility in the Tyne catchment

6.2 Methods

A full description of the analytical methods is in Chapter 2. An outline of the approach used in this chapter is given below:

6.2.1 Sample locations, sample collection and preparation

Soils were collected from the Tyne catchment (n = 48) from the locations shown in Figure 2.4 and as described in Section 2.4

Soils were processed (Section 2.4.2) and characterised for their metal content using a pseudo-total element digestion process using concentrated nitric acid (HNO_3), loss on ignition (LOI) as a measure of organic carbon, particle size analysis and pH as described in Chapter 2. Understanding these soil characteristics aided the understanding of the controls on element distributions and allowed the generation of a method/protocol to predict PHE concentrations within the South Tyne floodplains and for the determination of intrinsic soil constituents (ISCs), which are described in Section 2.16.

6.2.2 Soil flooding

Microcosms were used to inundate 24 of the 48 soils collected from the Tyne catchment flood plains. The microcosms consisted of 10 g milled soil weighed into 100 ml plastic bottles. The soils were inundated with 30 ml of Tyne river water (pH 7.7), and left on the bench top of the laboratory for 1 week. After 1 week, the volume of overlying water was measured,

and 10 ml was sampled for analysis by ICP-OES to determine the concentrations of PHEs for mass balance calculations. Mass balance calculations were used to quantify the mass of PHE mobilised into the overlying water and what remained in the soil. Soils samples were collected from the bottles once the overlying water had been removed. A 0.3 g surface scrape from the centre of the bottle was taken and immediately subjected to the UBM process, (Section 2.12). The remaining soils were weighed, dried at 1.5 °C for four days and then reweighed to determine the moisture content of the soils. This was necessary to transform the UBM results into a dry weight measure to allow for comparison between the soils as outlined in Section 2.6.

6.2.3 Total element concentration mapping

Pseudo-total concentrations in the 48 samples sites were plotted in the Tyne catchment using ESRI ArcMap 10. Additional spatial soil elemental concentration data were also sourced from the National Soil Index (NSI) which was carried out on a 5 km grid for England and Wales and imported into ArcMap in ascii format. The NSI data were plotted spatially as a layer underneath the sample site data collected during this study (e.g. Figure 6.3) and simple linear regression was carried out to determine if there was relationship between the two datasets and the strength of that relationship if it existed.

The NSI dataset is comprised of soil samples collected in the UK in the 1980s and 1990s on a 5 km orthogonal grid. The upper 15 cm of mineral soils was collected and element content determined by XRFS for approximately 50 elements. The data were interpolated using the IDW function. Further information is provided in Rawlins *et al.* (2012).

6.2.4 Intrinsic Soil Constituents (ISCs)

6.2.4.1 Background

Soils are made up of components such as carbonates, Fe-oxides, humic material, which is dictated by the inputs that led to their formation. PHEs can often be associated with these chemical components and their distribution can affect availability and mobilisation potential. ISCs are defined in this work as a combination of soil particles with similar chemical composition of varying concentrations that have originated from similar geogenic or anthropogenic sources (Wragg, 2005).

ISCs were first modelled to gain an insight into solid phase distribution of PHEs within the 48 soils, compared to the eight soils that underwent the same modelling procedure for the CISED data in Chapter 3 (Section 2.15). ISCs provide a broader look into the solid phase

distribution of PHEs and the method is more suitable that the CISED method for larger datasets where it may not be practical to conduct sequential extractions on a large number of samples. The identified ISCs were used as predictor variables for PHE bioaccessibility in random forest models used to predict PHE bioaccessibility.

The data entered into the algorithm were a matrix containing the total element data for each of the 48 sample sites shown in Figure 2.2. The data for all sample sites were modelled together on the assumption that they are composed of a common set of ISCs as they all originate from similar underlying geologies and from floodplain soils in the South Tyne catchment. Where >75 % of the data for a single element were below the LOD, the element was removed from the data matrix.

The outputs from the total element data are the same as the CISED data, outlined in Section 2.15. However, instead of the profile plot showing the extractable solids over the 14 extraction steps (Figure 2.16), it instead shows the total solids for that ISC associated with each individual sample. The composition plots display the elemental composition of each ISC and the distribution plots show the elemental distribution between ISCs. ISCs were identified in the same manner as the CISED extractable components as outlined in Section 2.15.

6.2.4.2 Difference between ISCs and CISED extractable components

The CISED method and subsequent data analysis using the SMMR identifies the physico-chemical components of the soil that are reactive and therefore extractable and does not include the residual fraction of the soil that is unreactive. As the CISED method identifies the reactive components, it is useful for identifying the components that would be dissolved within the gastrointestinal tract and therefore contribute to bioaccessibility. The identification of ISCs and PHEs associated with them is a broader examination of the soils and solid phase distribution of PHEs and encompasses all fractions of the soil, regardless of their solubility.

6.2.5 Spatially mapping bioaccessibility at a catchment scale

Spatial mapping of bioaccessible PHE concentrations and subsequent flooding induced changes in bioaccessibility was conducted using ESRI ArcMap 10. Spatial datasets of PHE bioaccessibility were imported into ArcMap, in the form of X Y data, using the 'import data' function. Data were then converted to a raster format and clipped to the historic flood outline layer, which was sourced from the Environment Agency (2019). Spatial data for each

PHE was extracted to generate a data matrix of predictor parameters for use in the Random Forest models.

The bioaccessibility data from the samples collected during this study were interpolated using the Inverse Distance Weight (IDW) tool. Values were assigned using a linearly weighted combination of pre-defined sample points, with the weighting being a function of the inverse distance between points. It was assumed that variable importance decreased as the distance between sample points increased. The input data are presented below in Table 6.1.

Table 6.1: Input parameters for IDW tool.

Sampling extent	Search Radius	Number of points	Cell size
Historic Flood Outline Layer	Fixed search radius	6	50 m

Flooding induced change in bioaccessibility was also mapped using the IDW tool. The percentage change between pre- and post- flooding bioaccessibility concentrations were imported into ESRI ArcMap 10 as above.

6.2.6 Modelling bioaccessibility using random forest models

6.2.6.1 Introduction

Random forest models are non-parametric machine learning methods, based on classification and regression trees. They can be used in similar ways to multiple linear regression (MLR) to determine the predictors for the behaviour of a response variable and have been applied to soil studies for the prediction of properties/behaviours (Cave *et al.,* 2013). Random forest models were selected over more conventional MLR methods for the following reasons:

- There was a high level of collinearity in the dataset. The assumptions of MLR would require some of the collinear variables to be removed.
- Random forest can deal well with noisy and non-linear relationships within datasets.
- The risks of overfitting are reduced as multiple decision trees are averaged and therefore variance is reduced.
- They are robust on small datasets. The dataset used here has 48 samples.

Test set error was determined using out of bag error, rather than cross validation. Cross validation is not necessary in random forest models as each tree is constructed by bootstrapping the original data.

Both ISCs and pseudo-total element data were modelled separately as predictors for PHE bioaccessibility, with the model with the highest percentage variance explained being selected as the better performing model. Intrinsic Soil Constituents were modelled from total element data so it was expected the outcomes from using total element and ISCs as predictors would be similar. The RF models that used pseudo-total element data had a higher percentage of variance explained than those using ICs as predictor variables. Therefore, the RF models in this chapter were produced using pseudo-total element data as predictors of PHE bioaccessibility. Five RF models were constructed; one for each of the five PHEs used in this thesis.

The small data set used however meant that it was computationally possible to use a model with 1000 decision trees. Figure 6.38 shows the effect of adding more trees to the model on the out of bag (OOB) data.

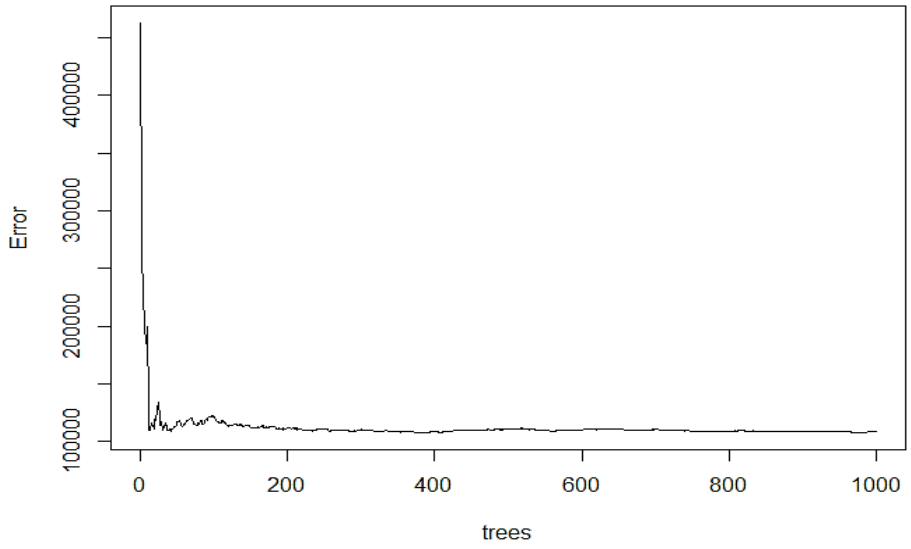

Figure 6.1: The effect of increasing the number of decision trees on the out of bag error.

The decision to predict bioaccessible PHE content in terms of mg kg^{-1} as opposed to the bioaccessible fraction % was made because a map showing a concentration would be more useful for risk assessment purposes than one showing a bioaccessible fraction as a %. This is because it is then possible to compare bioaccessible concentrations to GACs to highlight areas within a catchment that might warrant further investigation. Using the bioaccessible fraction data to produce spatial maps may give an unrealistic idea of where the areas with the greatest hazard exist. For example, an area with a high bioaccessible fraction may come

from a low bioaccessible content (mg kg^{-1}) and therefore the potential hazard of this soil would actually be low.

2.6.6.2 Variable selection using the Boruta package

Selection of variables was conducted using the Boruta package in R. This is an algorithm that works with classification methods such as RF models. The algorithm compares variable importance with those of shadow attributes, which are variables created by randomly shuffling the original variables. Predictor variables that have been classed by the algorithm as less important than shadow attributes are assigned as 'not important' and those with higher importance than the shadow attributes are assigned as 'important'. The user selects the number of iterations to run and each iteration sees the creation of new shadow attributes. The model will run until only the important variables are left, or when the maximum number of iterations assigned has been reached. Variables assigned as 'tentative' are those that are left over when the maximum number of runs has been met. Increasing the number of runs can result in the classification of these variables as either important or unimportant.

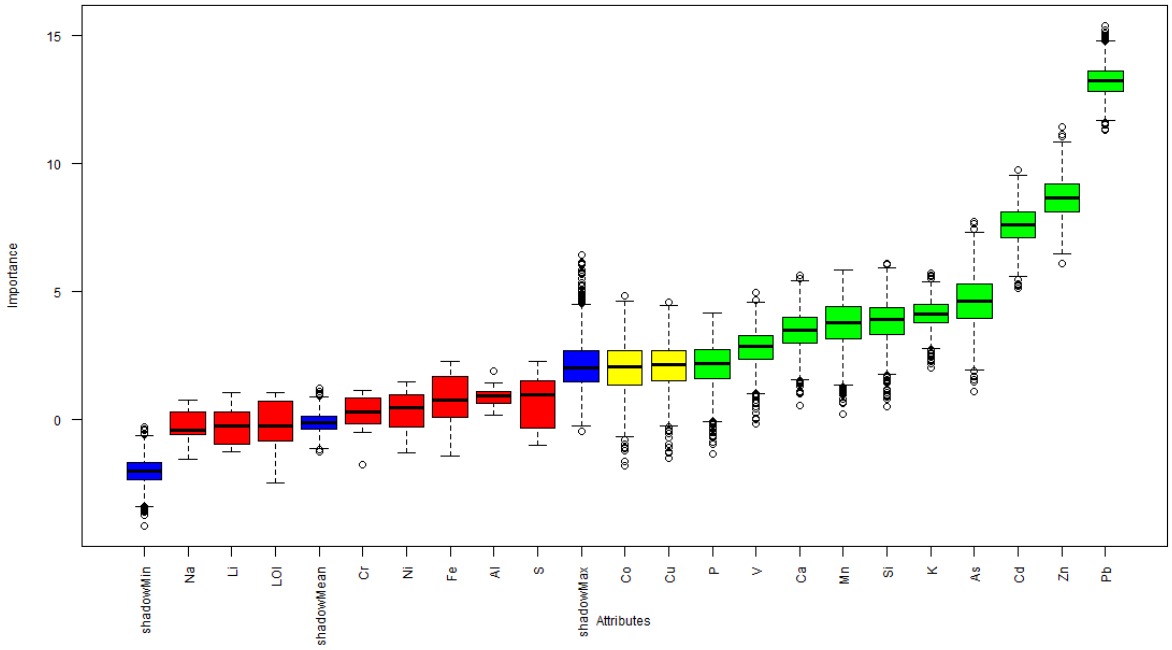

Figure 6.2: Example output from the Boruta algorithm, showing variables assigned as either 'important' in green, 'tentative' in yellow or 'unimportant' in red. Shadow variables are shown in blue.

A second RF model was run for each PHE using the important variables expressed by the Boruta algorithm. This produced a simpler model and improved overall model performance, shown by a higher percentage of variance explained value.

Partial independence plots were used to examine the influence of the predictor variables on PHE bioaccessibility once the five RF models had been constructed. This was done as the 'black box' nature of machine learning algorithms can make interpreting the results of a RF model difficult, and is often a criticism of such analytical methods. However, partial dependence plots can be used to gain an insight into the relationship between predictors and response variables within a RF model, by showing the marginal effect of a predictor on the predicted outcome of a model. Partial dependence plots were therefore generated for each PHE in this study.

6.2.7 The prediction and mapping of flooding induced changes in bioaccessibility

The outputs of the RF models were plotted spatially in ArcMap to provide a comparison between the interpolation of data points collected during this work, and those predicted from the NSI dataset.

A combination of RF models and multiple linear regression (MLR) were used to model flooding induced change in Pb. The dependent variable was the flooding induced change in Pb bioaccessibility from the microcosm inundation work outlined in Section 6.2.2. Input variables were pseudo-total element data, Pb BAF, pH, SOM, clay content, sand content and silt content (n=23).

The Boruta package was used for variable selection as the sample size was small (flooded sample n = 24) and the number of potential variables compared to the sample size was high (n = 23). This would result in over fitting if MLR models were used prior to any variable selection. A combination of models was used as the model performance of MLR after variable selection was better than that of the RF on a sample size of 24.

Of the five PHEs available, Pb was selected because the total concentrations were close to GAC values and therefore was likely to be of most concern with regards to human health. Seven variables (P, Li, Fe, Cr, V, Mn and Si) were selected as important by the Boruta package, and these were subjected to modelling by MLR. Further simplification of the MLR models was conducted by removing insignificant variables until only significant predictors remained, resulting in the final model. Significance was determined if the p-value of a predictor was <0.05.

The NSI dataset was used to predict bioaccessible change in Pb. This was carried out using the 'predict' function in R. The MLR model used to determine flooding induced change on Pb bioaccessibility was used on data from the NSI dataset. A separate dataset was needed as the model had been built using the data collected in this Chapter.

The predicted output values were then entered into ArcMap in the form of X Y data and plotted to produce the final maps. These maps spatially displayed the flooding induced change in the BAF of Pb. The aim of this was to show the potential for combining geochemical characterisation methods, statistical modelling and spatial modelling tools to predict flooding induced changes in PHE bioaccessibility at a catchment scale.

6.3 Results and Discussion

6.3.1 Tyne catchment floodplain soil characteristics

The concentrations of As, Cd and Pb displayed low variation across the 48 soil samples taken in the Tyne catchment (Figure 6.3). Cadmium, Pb and Zn had outlier values, associated with sampling locations 36 and 37, collected from the Nent catchment, this is likely to be as a result of the sampling area being close to, and influenced by, mine spoil material. All soils were predominantly composed of silty material with approximately 10 – 15 % sand and clays (Figure 6.3).

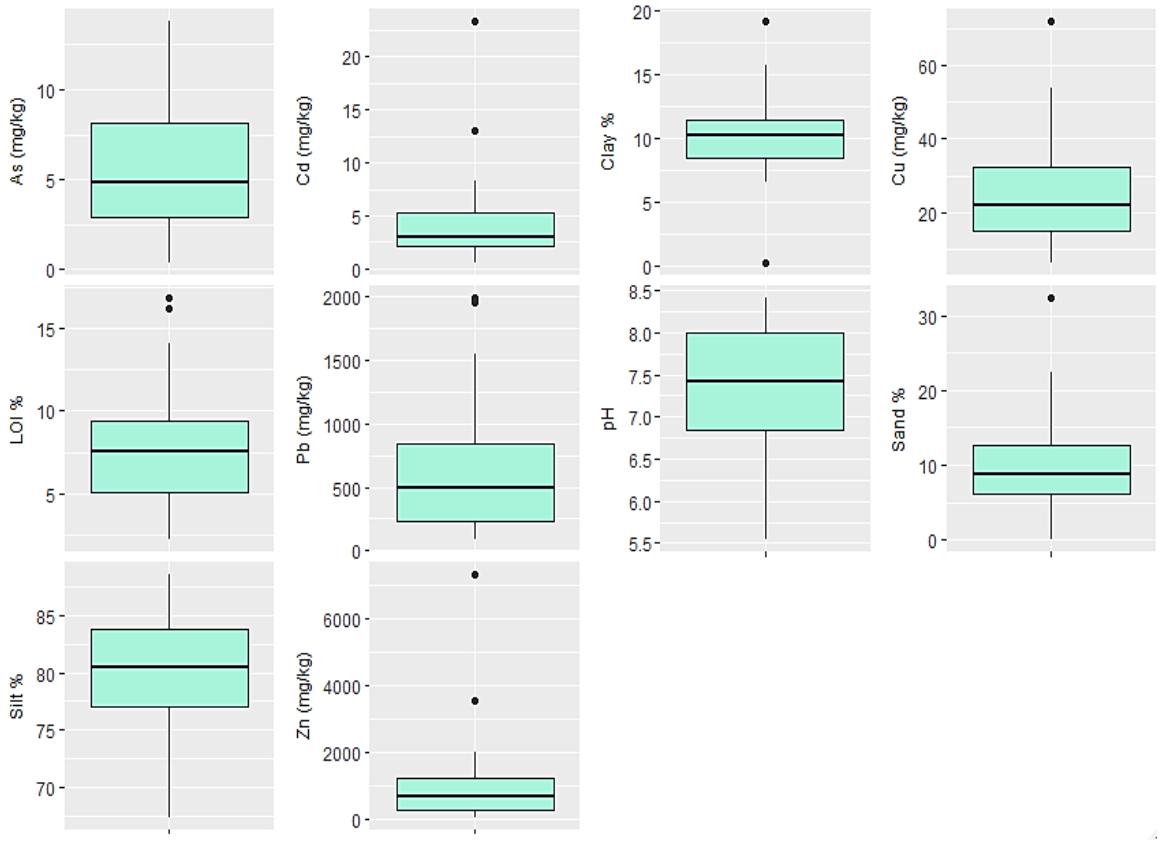

Figure 6.3: Boxplots showing soil characteristics of the Tyne catchment floodplain soil samples (n=48). The full dataset is presented in Table A2.2.

The pH of the soils within the Tyne catchment are mainly between pH 7 and pH 8, likely as a result of the underlying limestones (Figure 6.3). Some soils are more acidic in nature (pH 5.5-6.5), lower pH soils such as 36 and 37 are located in the upper Tyne catchment so pH may be influenced by acid mine drainage from nearby adits and spoil tips (Figure 2.4). The soil organic matter content of the Tyne catchment floodplain soils is high (5-10 %), likely to be a

result of the fine-grained alluvial sediment with high organic matter content that gets deposited by floodwaters (Rinklebe *et al.,* 2007) as well as the high production of living plant matter (Du Laing *et al.,* 2007).

6.3.2 Total concentrations of PHEs within the catchment

Pseudo-total PHE concentrations were determined by a microwave assisted HNO_3 digestion of the 48 soils. The total element concentrations of the 48 soil samples in this study were compared to the total concentration data from the NSI, analysed by wavelength dispersive X-ray fluorescence spectrometry (XRFS).

A comparison between the NSI dataset and the 48 samples in this chapter was conducted to determine the suitability of using the NSI data sets for predicting bioaccessibility within the Tyne catchment. If the NSI data were suitable, this would have allowed an increase in the number of sample points used for predictive modelling of bioaccessibility on the premise that larger datasets can result in more robust models. Secondly, two datasets were needed: one to train and build the RF models, and a second one to spatially predict bioaccessibility.

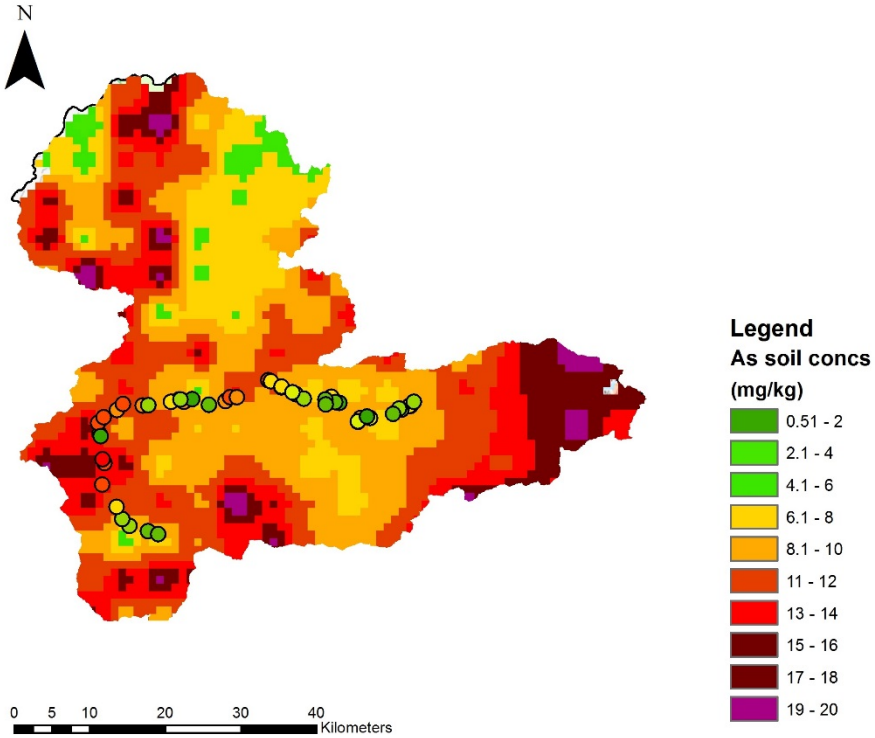

Figure 6.4: IDW interpolation of NSI data and individual points for As measured by pseudo-total digestion.

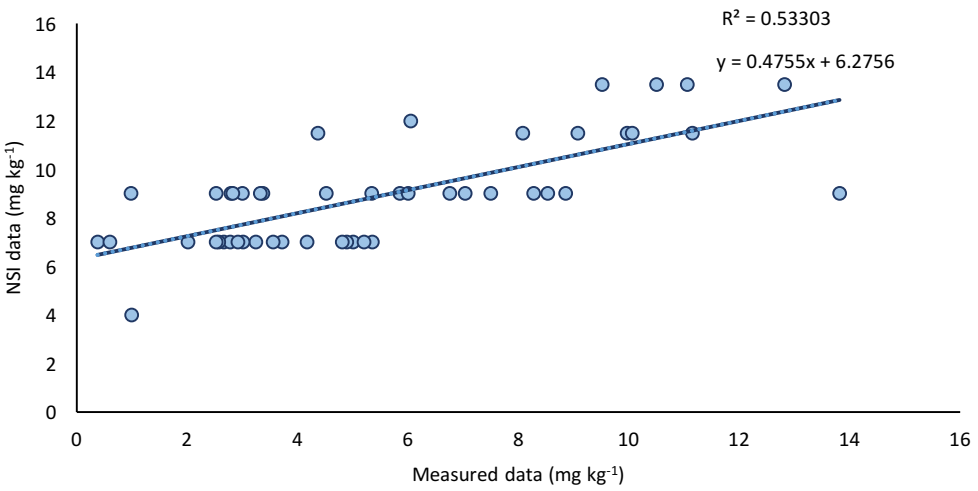

Figure 6.5: Linear regression of spatial samples and NSI data for As. R^2 value shows model fit ($p = < 0.001$)

Concentrations of As were higher in the NSI dataset than the sample site dataset, by approximately 1-3 mg kg^{-1} (Figure 6.4), suggesting the HNO_3 digestion may not be as successful in dissolving 100 % of As. This may be because not all As is fully dissolved during the process. An R^2 value of 0.53 shows a reasonable agreement between the two datasets (Figure 6.5).

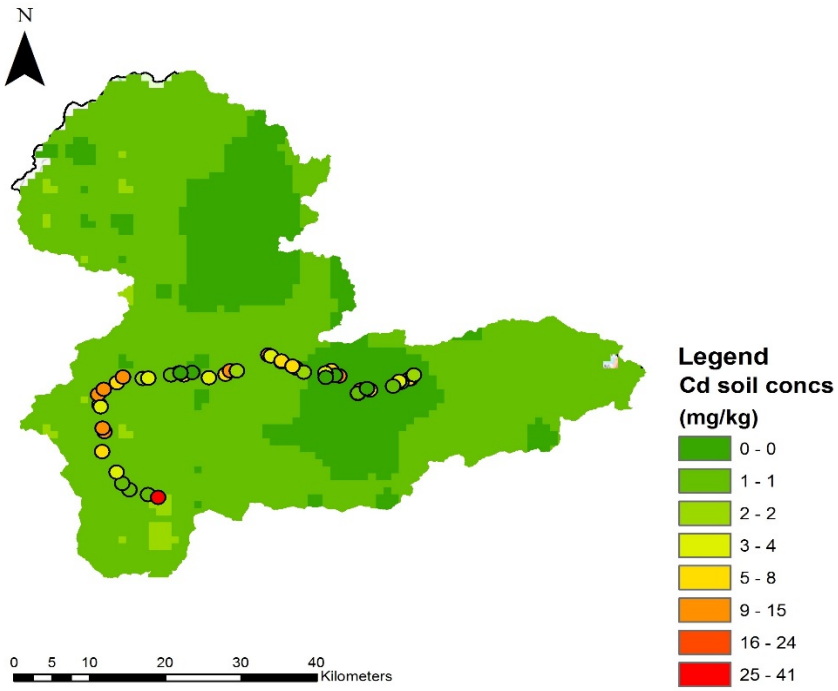

Figure 6.6: IDW interpolation of NSI data and individual points for Cd measured by pseudo-total digestion.

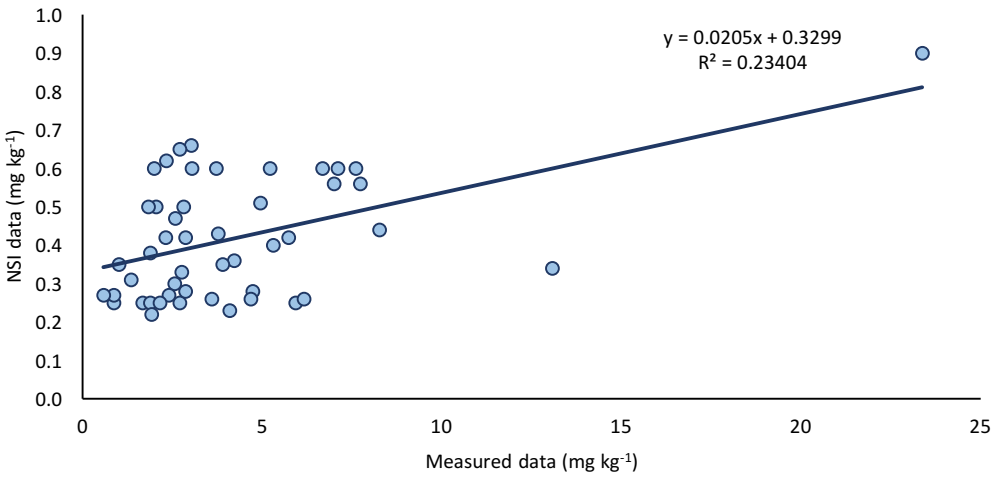

Figure 6.7: Linear regression of spatial samples and NSI data for Cd. R^2 value shows model fit (p = 0.004)

Concentrations of Cd were lower in the NSI dataset than the sample site dataset, by up to an order of magnitude (Figure 6.6). An R^2 value of 0.23 shows a poor agreement between the two datasets (Figure 6.7). This is likely to be because the samples in this study were collected close to the River Tyne and likely to include elevated concentrations of Cd, shown by the outliers in the dataset.

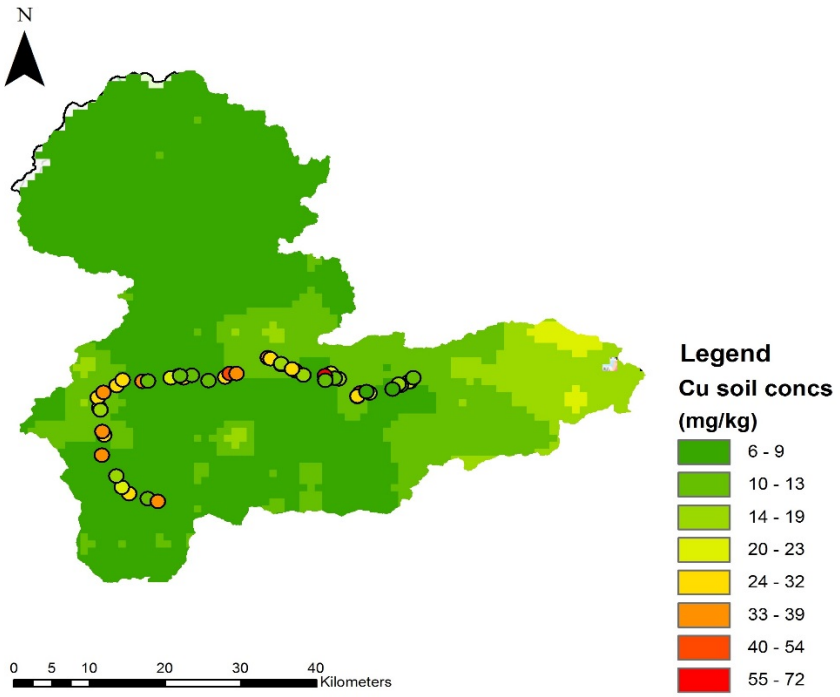

Figure 6.8: IDW interpolation of NSI data and individual points for Cu measured by pseudo-total digestion.

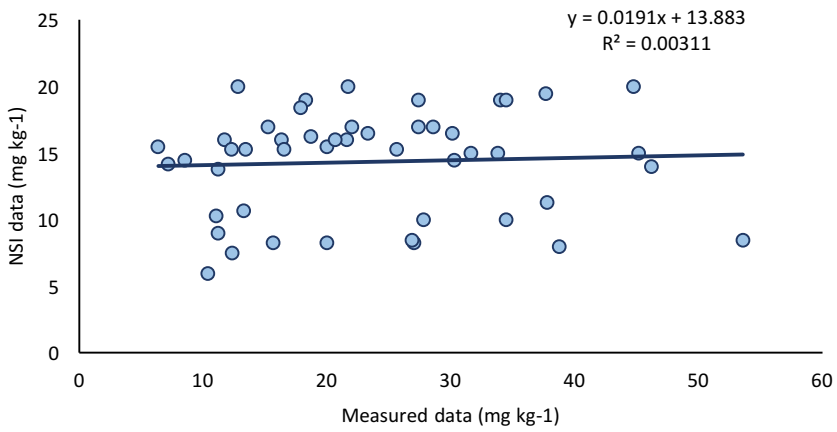

Figure 6.9: Linear regression of spatial samples and NSI data for Cu. R^2 value shows model fit (p = 0.706)

Both datasets were in the same order of magnitude for Cu (Figure 6.8 and 6.9), however, an R^2 value of 0.003 shows a very weak relationship between the two datasets (Figure 6.9). It is likely that sampling locations rather than the analytical method are responsible for the weak relationship shown. For example, the 48 soil samples collected for this chapter in the historic flood areas of the Tyne are point samples and pick up elevated PHE concentrations that have been distributed by the river water. In contrast, the NSI dataset is an interpolated dataset over a 5 km grid and therefore spatial heterogeneity of PHE concentrations could be smoothed out.

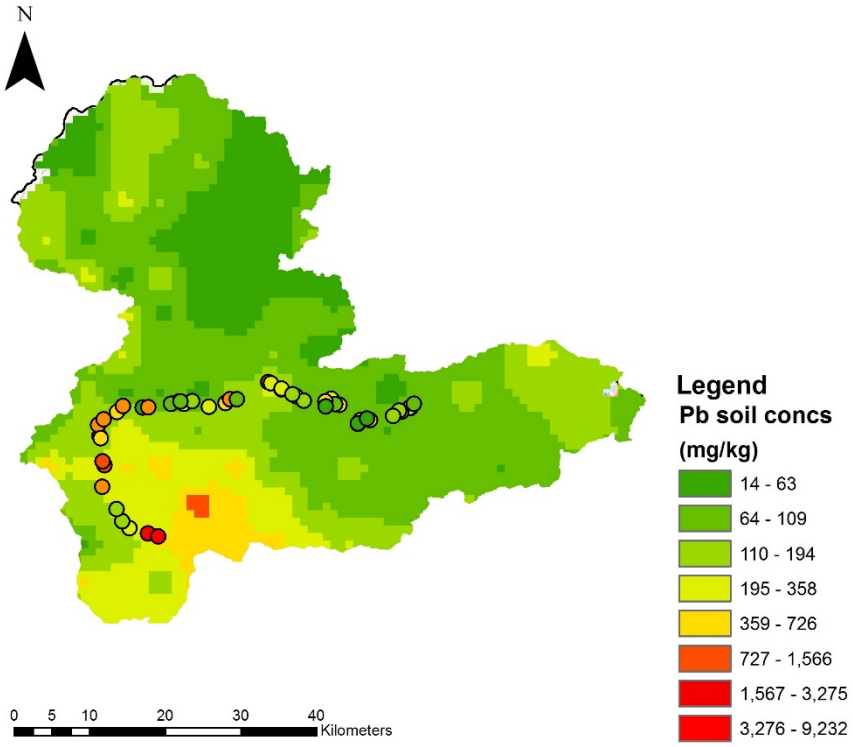

Figure 6.10: IDW interpolation of NSI data and individual points for Pb measured by pseudo-total digestion.

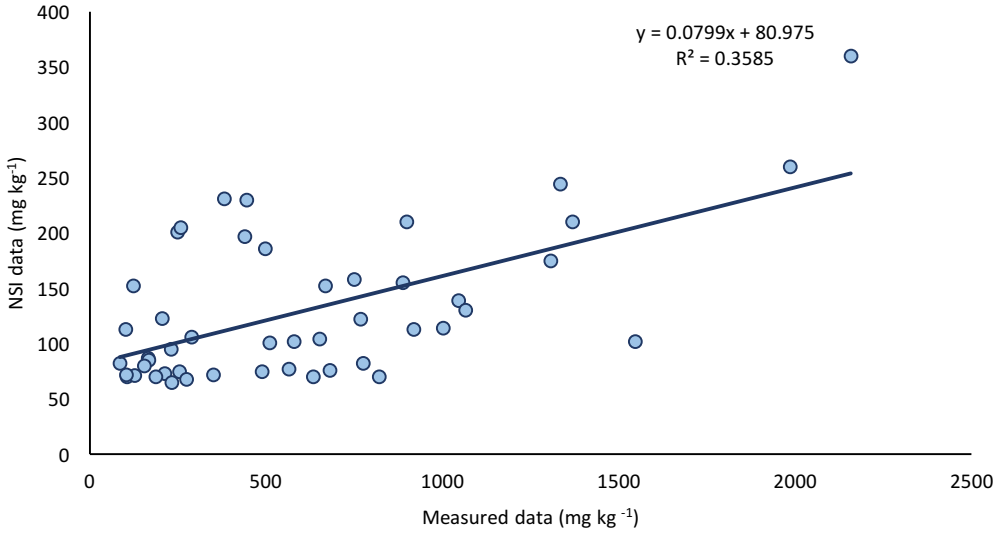

Figure 6.11: Linear regression of spatial samples and NSI data for Pb. R^2 value shows model fit ($p = <0.001$)

Concentrations of Pb were lower in the NSI dataset than the sample site dataset, by up to an order of magnitude (Figure 6.10). An R^2 value of 0.35 shows a poor agreement between the two datasets (Figure 6.11). Again, this is likely to be a result of the resolution and location of the sampling positions for the two datasets.

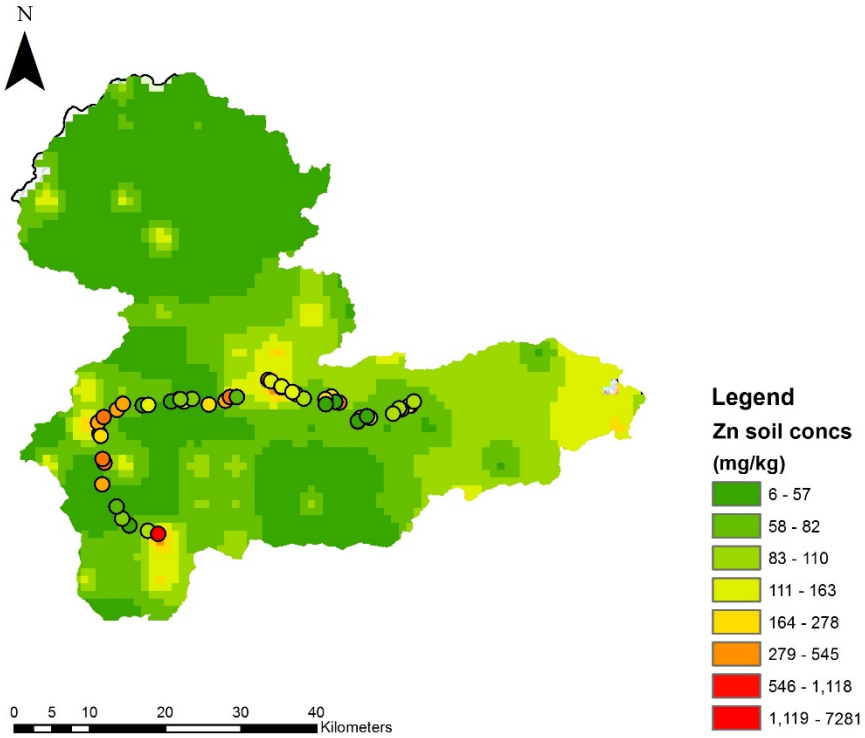

Figure 6.12: IDW interpolation of NSI data and individual points for Zn measured by pseudo-total digestion.

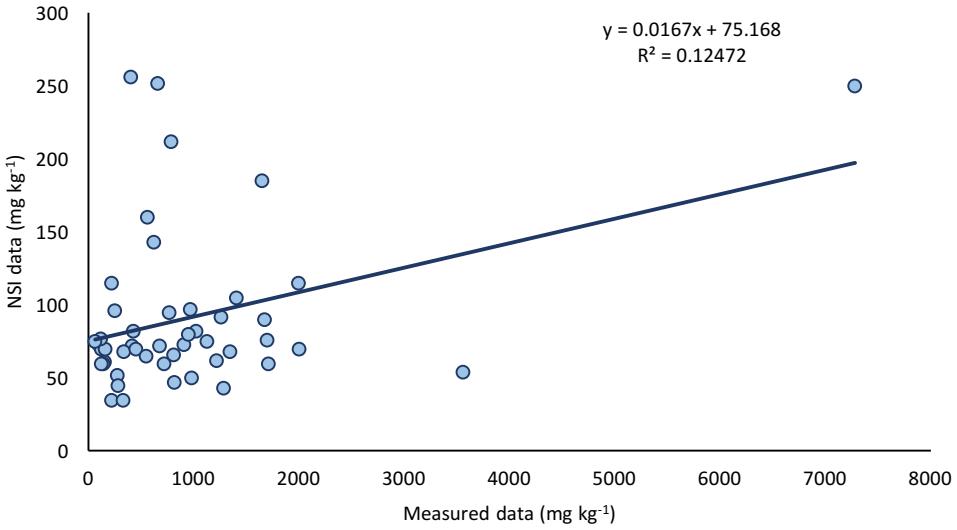

Figure 6.13: Linear regression of spatial samples and NSI data for Zn. R^2 value shows model fit ($p = 0.01$)

Concentrations of Zn were lower in the NSI dataset than the sample site dataset, by up to an order of magnitude (Figure 6.12). An R^2 value of 0.12 shows a poor agreement between the two datasets (Figure 6.13). Again, this is likely to be a result of the resolution and location of the sampling positions for the two datasets.

Apart from As (Figure 6.4), the NSI values tended to be lower than those measured in this work (Figures 6.6, 6.8, 6.10 and 6.12), often by an order of magnitude. The two datasets were determined using different analytical methods – the NSI data were analysed by XRFS whereas this work used a microwave digestion in concentrated HNO_3 method. This is likely to be one reason for the discrepancies between the datasets. Different analytical methods can provide different results, dependent on the analyte of interest. For example, XRFS has been known to report higher concentrations of Pb and Zn than acid digestion techniques (Paveley *et al*., 1988). However, both methods are accepted in the literature for determining pseudo-total concentrations in soils.

Additionally, the samples analysed in this work were collected within historic flood areas of the River Tyne. The documented transport of PHE enriched material down through the catchment may therefore have resulted in the higher concentrations observed (Macklin *et al.,* 1997). The distribution of PHEs in the Tyne catchment has been described as complex with both chemical and physical processes involved in PHE transport and deposition (Macklin *et al.,* 1997). The NSI dataset was collected on a 5 km square grid and therefore samples may have been taken away from localised hotspots close to the river banks. Furthermore, the

subsequent interpolation of the NSI datasets could then result in lower values being seen than in the samples used for this work. This study did not target potential hotspots but sampling locations were randomly generated from the recorded flood outlines of the Tyne, so are generally in closer proximity to the river and hence subject to flooding, than the data from the NSI datasets. Hence, the soils sampled for this thesis may have elevated concentrations of PHEs which can be transported by the river and deposited on floodplain soils.

Simple linear regression was conducted to determine whether the NSI dataset would be suitable for the prediction of bioaccessibility of PHEs within the catchment, or whether the sample site data set should be interpolated to provide additional data for mapping. The best model was seen for As (R^2 = 0.5). The remaining models had R^2 values of <0.3 and therefore it was decided that the sample site data collected during this study should be interpolated for all the PHEs, rather than using the NSI data.

These findings indicate that there is a need for collection of floodplain specific PHE data when modelling PHE distribution in catchments as larger, national spatial datasets are unlikely to have the resolution to capture small scale hotspots that may occur in flood prone areas near the river channel. PHEs that have low mobility in soil, such as Pb, can often accumulate in discrete hotspots as a result of their high residence time (Bower *et al.,* 2017).

6.3.3 Spatially modelling PHE bioaccessibility

Bioaccessibility at a catchment scale was predicted by interpolating the spatial bioaccessibility data collected for this thesis. Only the soils within the historic flood outlines were modelled as these were similar in characteristics to the soils used to build and train the RF models, as described in Section 6.2.5. IDW models were used as these are more suitable for soils with PHE hotspots than other models such as kriging methods (Bower *et al.,* 2017).

GAC values were not exceeded by any floodplain PHE concentrations within the Tyne catchment for the more conservative parkland open space values. Bioaccessible As concentrations ranging from 0.8 to 4.2 mg kg^{-1}, were an order of magnitude below GACs. The highest values were south of Haydon Bridge, which was upstream of the South Tyne confluence. Values below this confluence were generally the lowest, indicating a dilution effect from 'clean' sediment from the North Tyne. Similar examples of dilution with clean sediment were observed by Macklin *et al.,* (1997). This pattern was observed for all PHEs at this location within the catchment.

The spatial distribution of bioaccessible Cd was highest downstream of Haltwhistle and values ranged from 0.4 mg kg^{-1} to 10.8 mg kg^{-1}, likely to originate from the mining areas in the upper catchment. Macklin *et al.* (1997) observed 'pulsed' concentrations of Cd downstream of the mining areas, suggesting that Cd was transported downstream in a series of sediment pulses, possibly from flood events.

Bioaccessible Cu concentrations followed a similar pattern of spatial distribution to As, with higher concentrations (15 mg kg^{-1}) observed downstream of Haydon Bridge (Figure 6.15). Like Cd, the highest bioaccessible Pb concentrations were located downstream of Haltwhistle, with concentrations ranging from 79 mg kg^{-1} to 1,347 mg kg^{-1} (Figure 6.16). Lead concentrations were borderline with its respective GAC value (1,400 mg kg^{-1}) in several areas within the Tyne floodplain. Bioaccessible concentrations of Zn ranged from 44 mg kg^{-1} to 2,922 mg kg^{-1} and followed the same spatial distribution as Pb.

The spatial distribution of the bioaccessible PHE content in Figures 6.14 to 6.18 followed a similar distribution to pseudo-total PHE concentrations in Figures 6.4 to 6.12, suggesting a link between pseudo-total PHE concentrations and bioaccessibility. These relationships are explored in Section 6.3.8 using predictive models of PHE bioaccessibility.

Arsenic

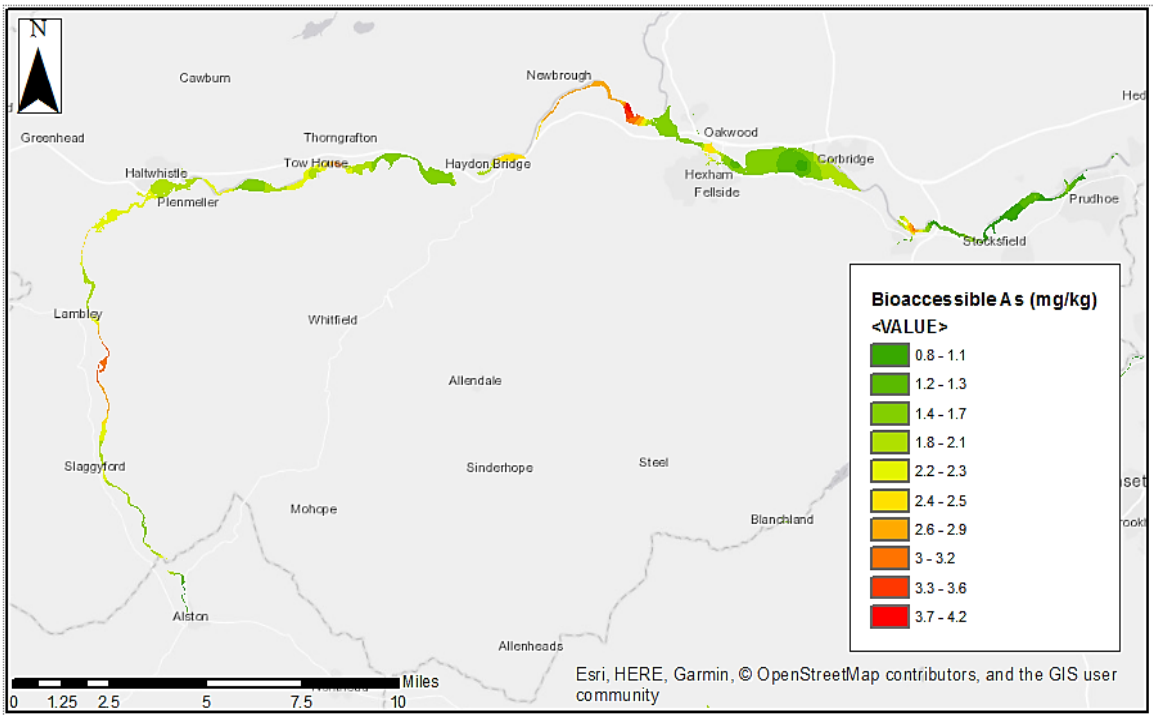

Fig 6.14: Bioaccessible As in soils of the Tyne catchment historic flood outlines. Arsenic allotment GAC = 43 mg kg^{-1}. Arsenic parkland open space GAC = 170 mg kg^{-1}.

Cadmium

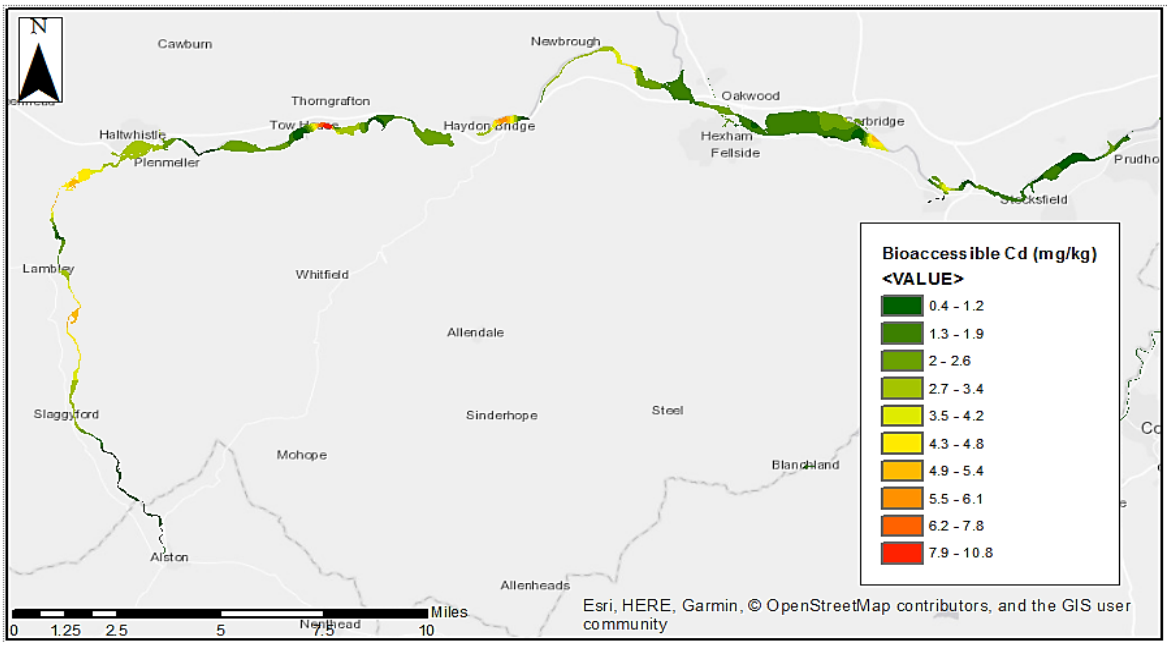

Fig 6.15: Bioaccessible Cd in soils of the Tyne catchment historic flood outlines. Cadmium allotment GAC = 1.9 mg kg^{-1}. Cadmium parkland open space GAC = 560 mg kg^{-1}.

Copper

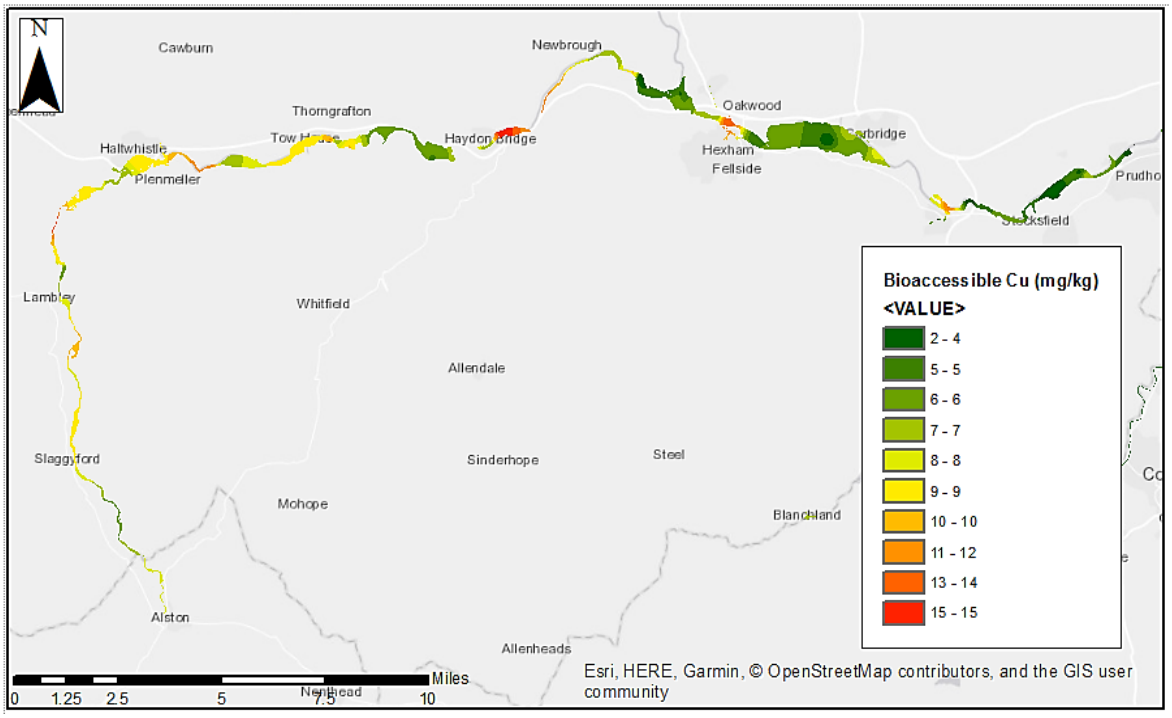

Fig 6.16: Bioaccessible Cu in soils of the Tyne catchment historic flood outlines. Copper allotment GAC = 520 mg kg^{-1}. Copper parkland open space GAC = 44000 mg kg^{-1}.

Lead

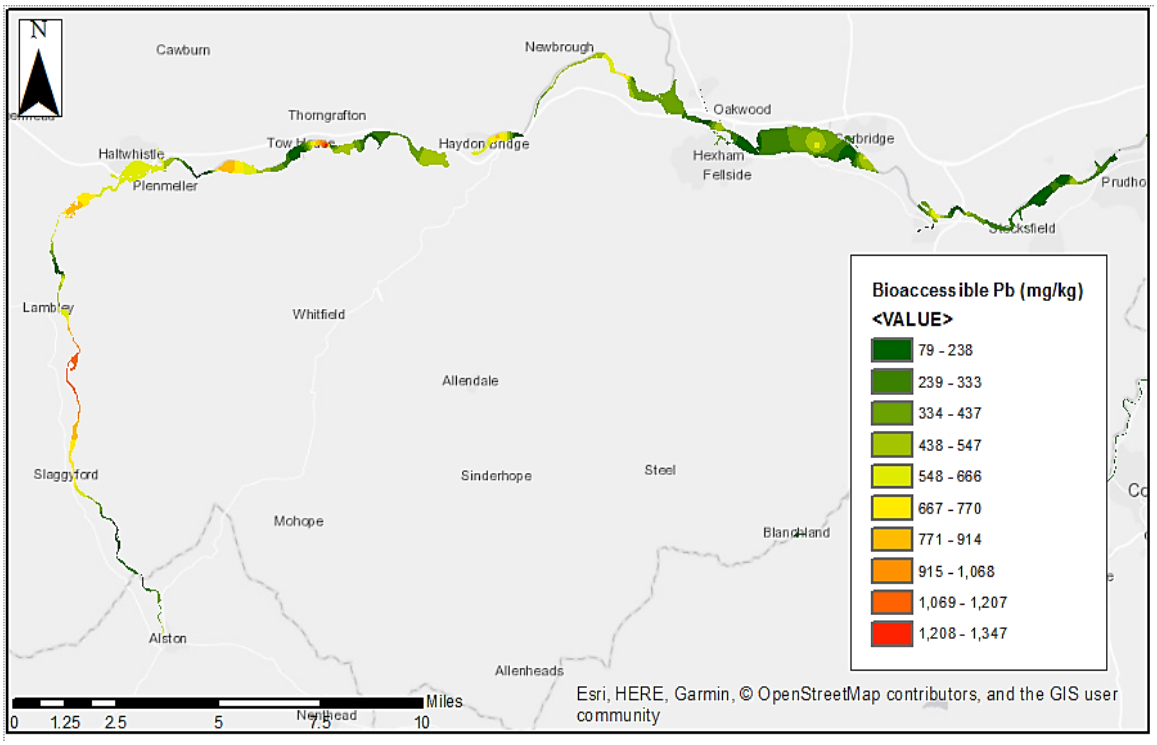

Fig 6.17: Bioaccessible Pb in soils of the Tyne catchment historic flood outlines. Lead allotment GAC = 84 mg kg^{-1}. Lead parkland open space GAC = 1400 mg kg^{-1}.

Zinc

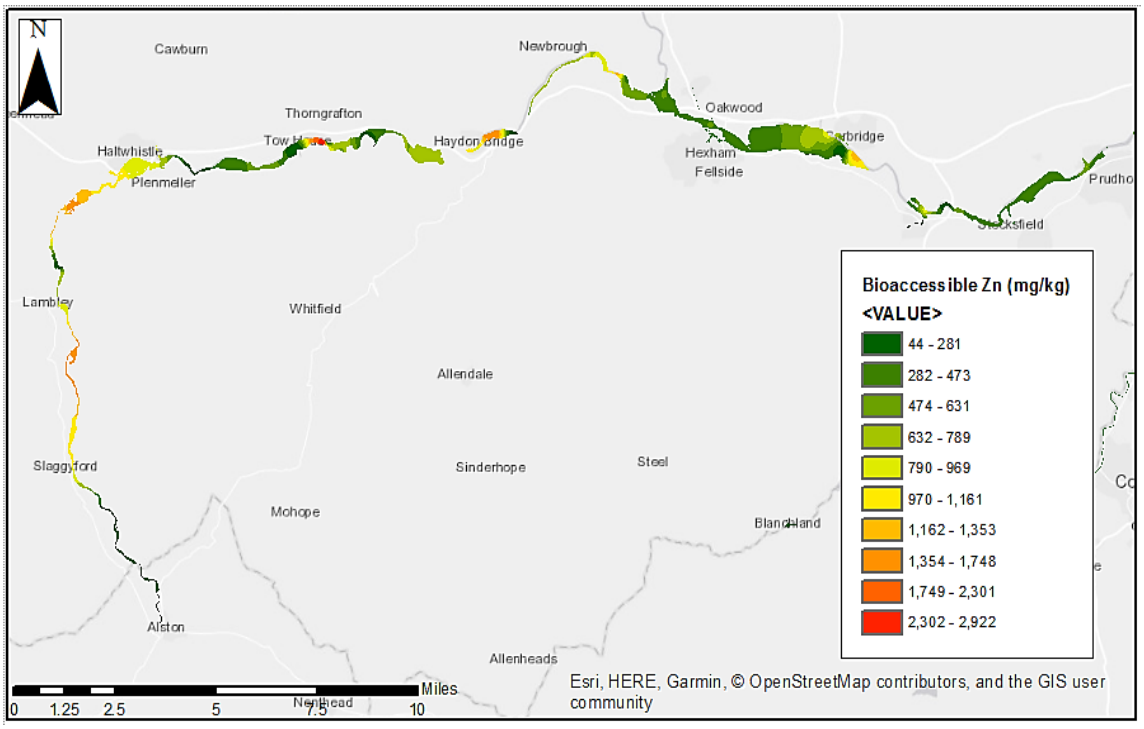

Fig 6.18: Bioaccessible Zn in soils of the Tyne catchment historic flood outlines. Zinc allotment GAC = 620 mg kg^{-1}. Lead parkland open space GAC = 170,000 mg kg^{-1}.

6.3.4 Flooding Induced Mobilisation of PHEs in the Tyne Catchment Floodplain Soils

In addition to spatially mapping the PHE bioaccessibility of soils in the Tyne catchment, their mobility during flooding was also determined. Mobility of PHEs into overlying water after one week of inundation was low for the PHEs investigated in this chapter, ranging from approximately 0.01-2 % (Figure 6.19). Generally, As (0.05 % to 2 %) and Cu (0.19 % to 1.3 %) showed the greatest mobility into overlying waters, with Pb (0.02 % to 0.6 %) and Zn (0.02 % to 1.17 %) being less mobile. This is likely to be a result of the redox sensitivity of As, as shown in Chapter 4, resulting in higher mobility of As over other PHEs. Generally, the variation in PHE mobility between the soils was low, and therefore likely to be a result of the similarity of floodplain soil characteristics (Figure 6.3).

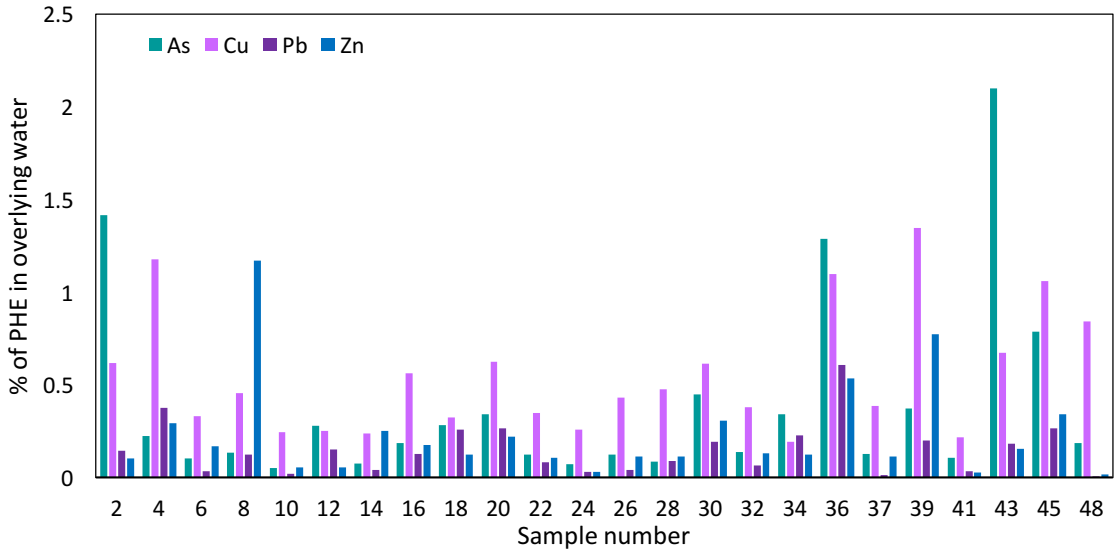

Figure 6.19: Percentage of pseudo-total PHE mobilised into overlying water after 1 week of inundation.

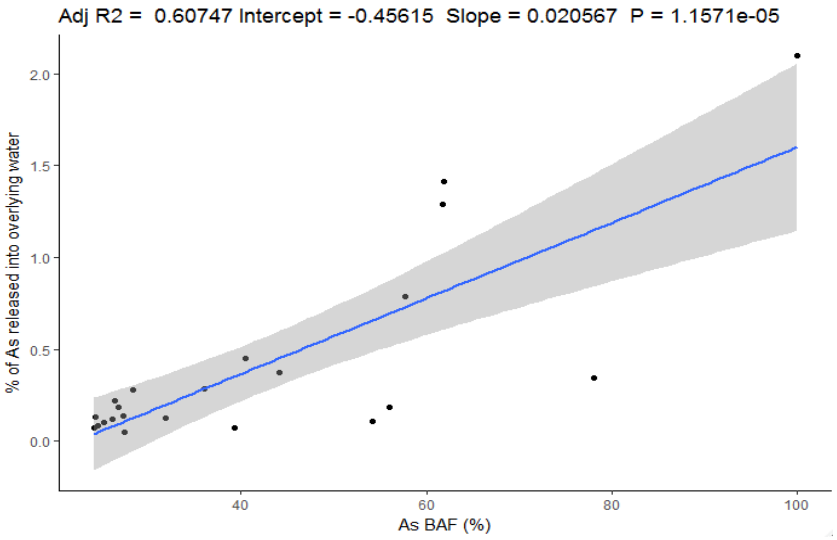

Figure 6.20: Linear regression between the percentage of As released into overlying water and the bioaccessible fraction of As (BAF %) in the sample soils. n=22.

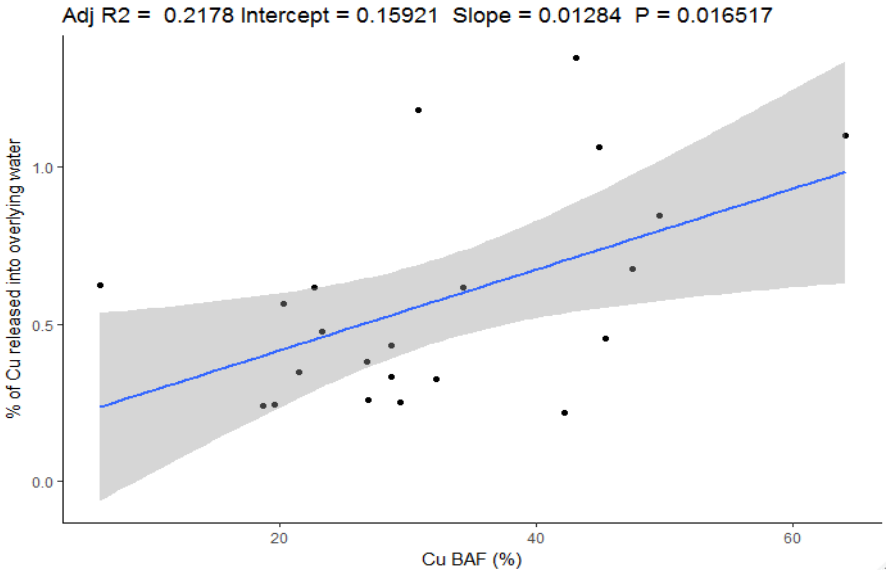

Figure 6.21: Linear regression between the percentage of Cu released into overlying water and the bioaccessible fraction of Cu (BAF %) in the sample soils. n=22.

The relationship between the % of PHE released into overlying waters and the bioaccessible fraction of PHE in soil was modelled to determine if soils with a higher bioaccessible fraction of PHEs also had higher PHE mobility into porewater (Figures 6.20 and 6.21). Both are measures of mobilisation, but mobility into the gastrointestinal tract is expected to be higher than mobility into overlying water as the reagents used in the UBM are of a lower pH (pH 1.2) and therefore more aggressive than river water (pH 7.7). The UBM reagents are aggressive enough to result in mobilisation of PHEs from soil components such as carbonates and metal oxides, as shown in Chapter 3. Changes in redox potential can result in

mobilisation of PHEs from similar components through processes such as desorption and reductive dissolution (Chapter 4), but these processes occur over a greater timescale (usually weeks) with a weaker reagent (water), therefore resulting in lower PHE mobilisation. However, it is hypothesised that soils with a larger proportion of PHE content in more labile components will likely have a higher mobility potential into porewater, as well as the gastrointestinal tract.

Relationships between As and Cu mobility and bioaccessibility showed a positive trend, suggesting that soils with higher bioaccessible PHEs are more likely to have a higher potential for PHE mobilisation during flooding. Linear regression models for Pb and Zn were not significant so are not displayed ($p > 0.05$). Larger sample sizes may improve Pb and Zn models. If such relationships are also present for Pb and Zn (in larger datasets), then this information could be of use for remediation purposes in the Tyne catchment. For example, there may not be a need to predict the risk of PHE mobilisation into overlying water if spatial predictions of bioaccessible PHEs exist if areas with a greater potential for flooding induced change in bioaccessibility are also likely to have a greater risk of PHE mobility into overlying water.

The mobilisation of the PHEs investigated in this chapter into overlying water was low (<2 %), however it does highlight the potential for PHE enriched soils and sediments to be diffuse sources of pollution in PHE enriched areas. Potentially, such mobilisation could have implications for water quality status such as those by the WFD as was shown in Chapter 4 when porewater concentrations were compared to EQS values. Studies have shown elevated concentrations of PHEs in rivers downstream of past mining/industrial areas, with no apparent point sources of PHEs, such as mine adits (Palumbo-Roe *et al.,* 2012), suggesting input from diffuse sources. For example, concentrations of Zn in streambed sediments were predicted to contribute 15-25 % of the Zn load into river waters in the Rookhope catchment in NE England (Banks and Palumbo-Roe, 2010). The Rookhope catchment is geographically close to the Tyne catchment and shares similar underlying geology and soil types, suggesting that the Tyne could see similar loading values from diffuse sources.

6.3.5 Intrinsic Soil Constituents within the Tyne Catchment Floodplain Soils

ISCs can be used as input variables into various models such as MLR and RF models, to predict PHE bioaccessibility in soils. The purposes of generating ISCs in this chapter was to firstly look at the composition of soils within the Tyne catchment, and secondly to generate predictor variables for RF models.

Nine ISCs were identified, although three were grouped into one constituent (Fe-Al Oxides) resulting in seven different ISCs being reported for the Tyne catchment floodplain soils. These are displayed in Figures 6.22 to 6.30. The error bars represent the uncertainty associated with each ISC from the algorithm for each sample.

Fe-Al oxide ISCs

This constituent has been identified as a Fe (~60 %) and Aluminium (~30 %) rich constituent and therefore likely to be Fe-Al oxides. This ISC is present within all soil types, and Fe-Al oxides were identified by the CISED extractions in Chapter 3 as expected, as ISCs are the source of the CISED identified components (Wragg, 2005). Such oxides have a high affinity for PHEs, although only often partly contribute to bioaccessibility because of their relative insolubility (Palumbo-Roe *et al.,* 2015). Figures 6.22 to 6.24 represent the masses of each SC associated with each soil sample. The first and third Fe-Al oxide ISCs (Figures 6.22 and 6.24) are similar in composition, with greater concentrations of Fe (60 %) over Al (20 %). The uncertainty on the Fe-Al ISC 2 (Figure 6.23) is considerably greater as the error bars go through zero for Fe, and there are greater concentrations of Al associated with this ISC (40 %). Fe-Al ISCs are present in all of the soils under investigation. Some soil samples with higher Fe-Al content are located over areas of theolitic basalt in the Tyne catchment, which may account for higher Fe concentrations in soils (Figure 2.2).

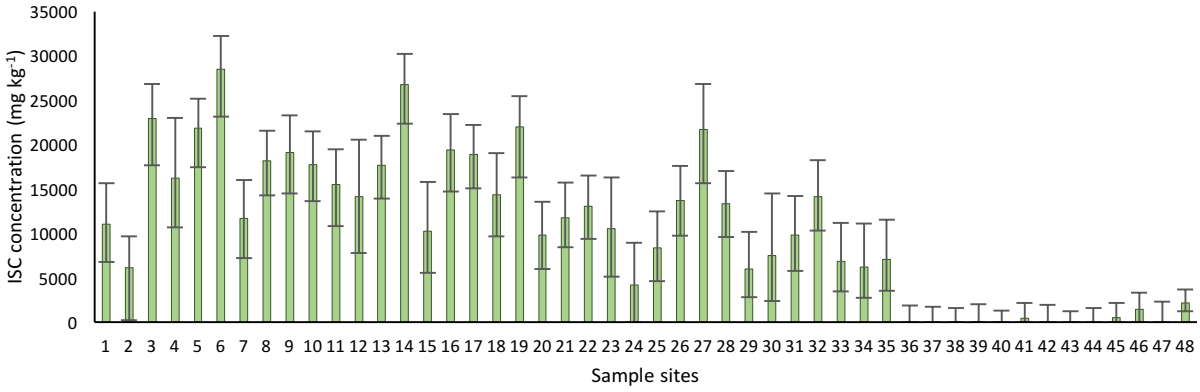

Figure 6.22: Fe-Al ISC 1.

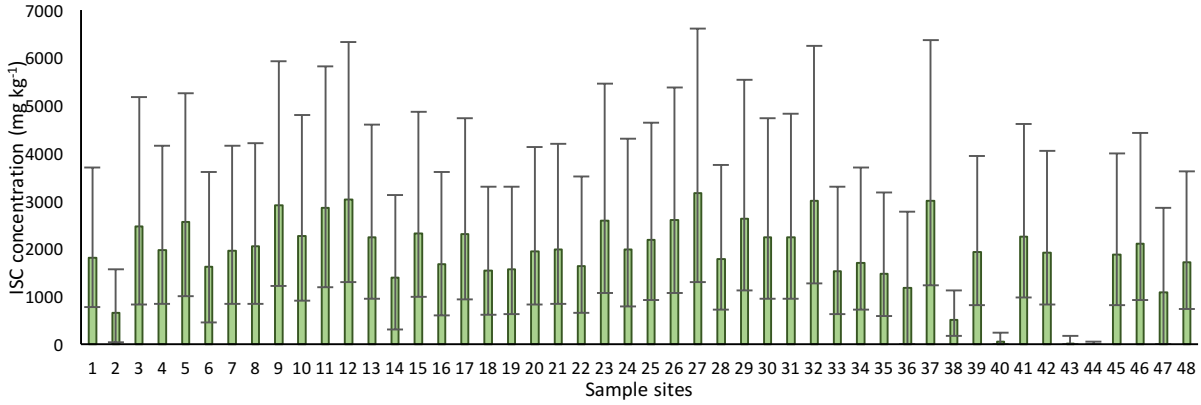

Figure 6.23: Fe-Al ISC 2.

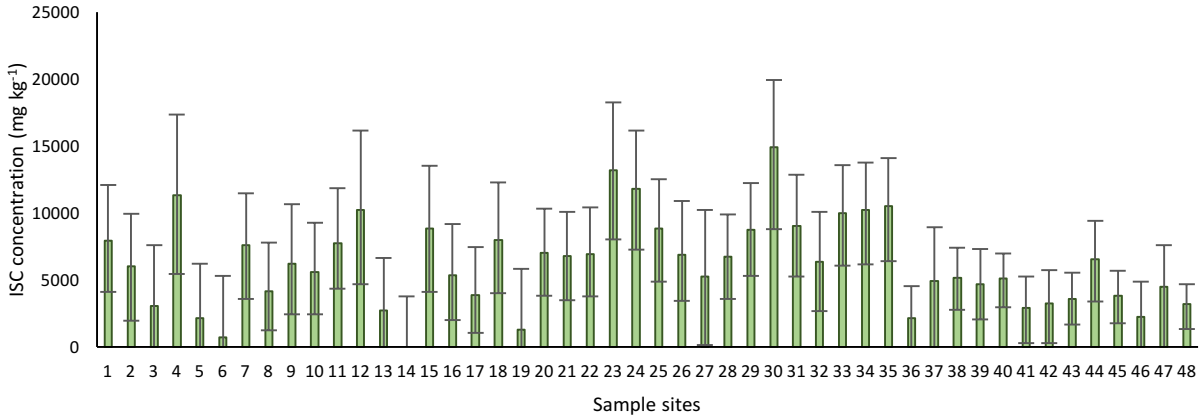

Figure 6.24: Fe-Al ISC 3.

Carbonate ISC

This ISC (Figure 6.25) was identified as a carbonate constituent because of its high Ca percentage (>50 %). Carbonate minerals such as calcite are common in soils and the carbonate ISC is present in all soils with the exception of sample site 4 (Allaby and Allaby, 1999). Carbonates are easily dissolved and therefore they are expected to contribute to PHE bioaccessibility if carbonate associated PHEs are present. Zn (10 %) and Al (10 %) are also both associated with this ISC. Zn is known to form with carbonates to form smithsonite in the Tyne catchment (Hudson-Edwards *et al.,* 1996). The composition of this ISC is similar to the composition of the carbonate component identified by the CISED method in Chapter 3.

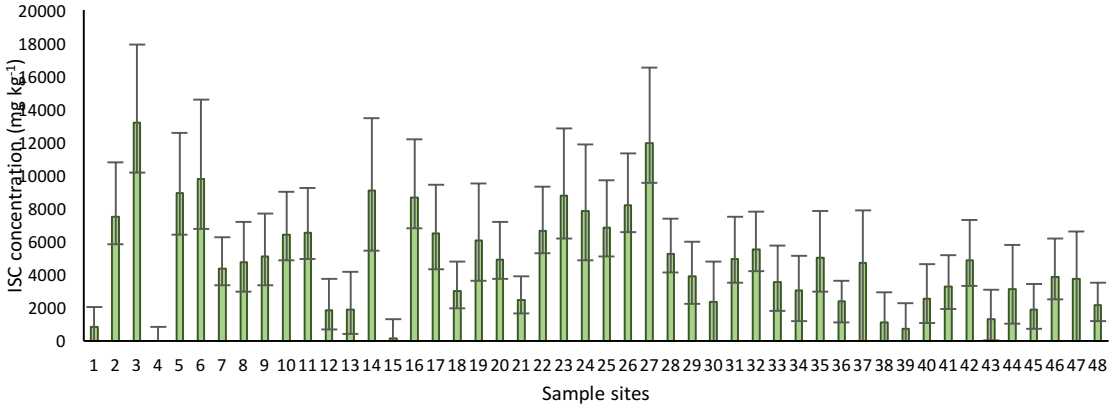

Figure 6.25: Ca dominated ISC.

Ca-Al ISC

The association of Ca and Al has led to the identification of this ISC as an aluminium rich calcite (Figure 6.26), as calcite was identified in the floodplain soils (soils 4 and 5) in Chapter 3 by XRD. It is composed of 50 % Ca, 20 % Al and 10 % Zn and was present in all soils. Sample 47 was sampled from an agricultural field used to grow trees and had the highest concentrations of this ISC. It is hypothesised this may have arisen from the application of lime or fertiliser.

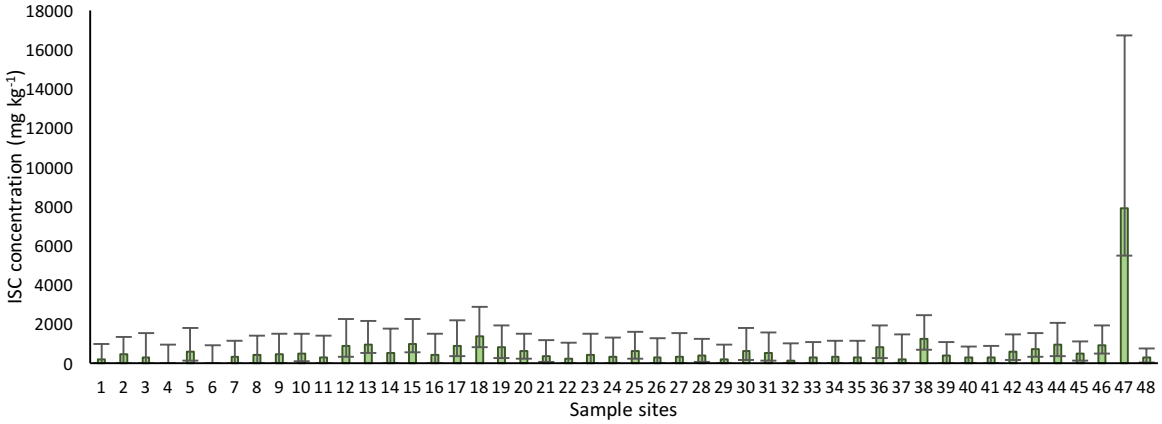

Figure 6.26: Ca-Al ISC.

Al-P ISC

This ISC was mainly composed of Al (60 %) and P (15 %) and trace amounts of K (5 %) with the masses of this ISC varying between sampling locations (Figure 6.27). The presence of P and K suggests that there could be the influence of fertiliser products within this ISC. The

locations from which the samples were collected that contain this ISC were all from arable or improved grassland locations.

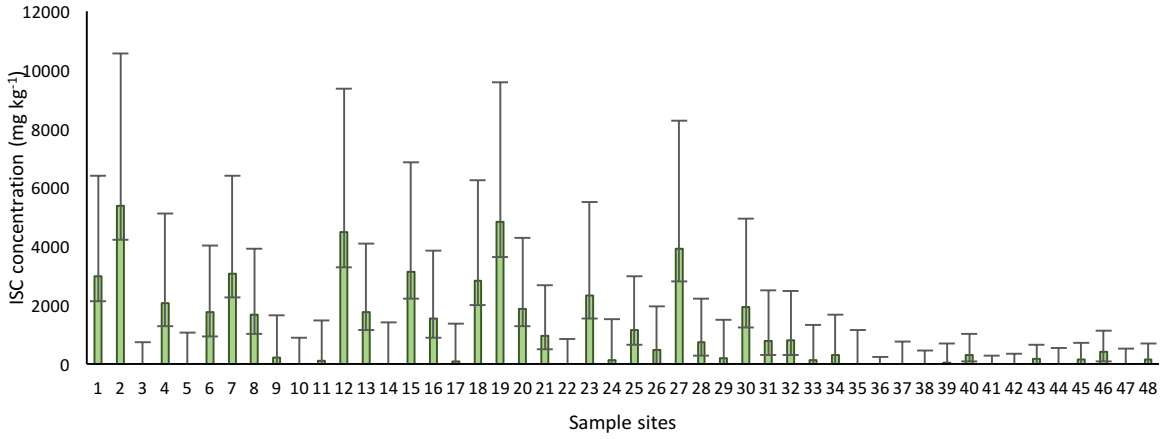

Figure 6.27: Al-P ISC.

Pb-Al-Zn ISC

This ISC was dominated by Pb (50 %), Al (20 %), Zn (15 %) and S (10 %) and was therefore assumed to be Pb dominated minerals, because of the high Pb % (Figure 6.28). These minerals likely originated from mining activities and geogenic sources in the upper reaches of the South Tyne catchment. The presence of sulphur suggests sulphide minerals such as galena (PbS) and sphalerite ZnS). Both of which have been confirmed by XRD as present in the spoil tip material (Chapter 3). The highest concentrations were found in site 36, which was situated near the River Nent confluence, which exits a catchment with numerous mine spoil tips.

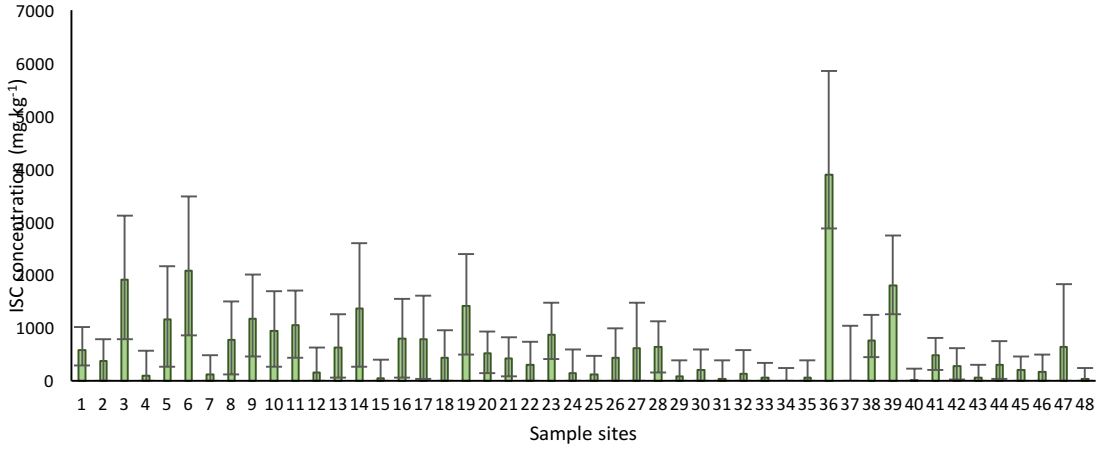

Figure 6.28: Pb-Al-Zn ISC.

Zn-Ca-Pb ISC

This ISC (Figure 6.29) was dominated by Zn (40 %), Ca (25 %), Mn (10 %) and Pb (10 %) and is therefore assumed to be Zn dominated minerals because of the high percentage of Zn and likely or originate from mining activities in the upper reaches of the South Tyne catchment. The highest concentrations were found in site 37, which is situated near the River Nent confluence, which exits a catchment with numerous mine spoil tips.

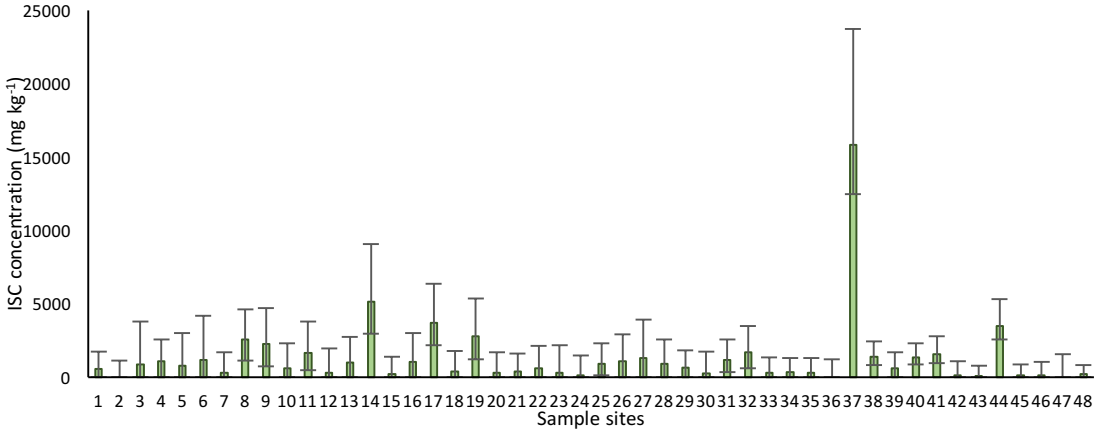

Figure 6.29: Zn-Ca-Pb ISC.

Al-Ca-Mn ISC

This ISC (Figure 6.30) was identified as a mixed metal assemblage ISC because of the presence of Al (50 %) and Mn (15 %). Calcium was also present (20 %). Aluminium oxides and Mn oxides were identified by the CISED extractions in Chapter 3 and therefore may originate from this ISC. This ISC was not present in all samples, and was mostly found in samples 38-48, which are mainly agricultural soils and found within the mid reaches of the Tyne catchment.

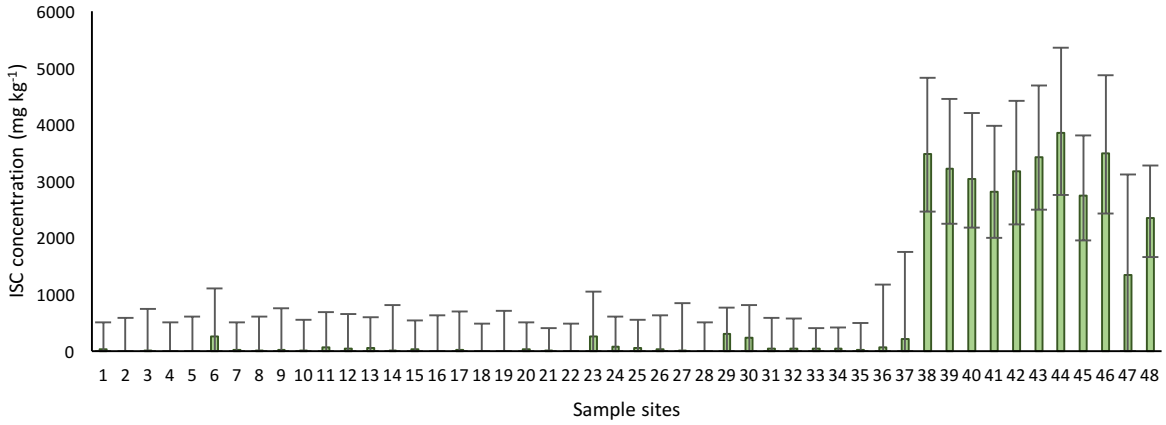

Figure 6.30: Al-Ca-Mn ISC.

6.3.6 PHE distribution within ISCs

Arsenic was found to be mainly associated with the Al-Fe ISCs (Figure 6.31), which was expected because As was found to associated with the Al-Fe cluster in Chapter 3. This relationship is also well documented within the literature (Dixit and Herring, 2003; Burton *et al.,* 2008; Xu *et al.,* 2017). It is therefore assumed that Fe-Al oxides will be a good predictor of pseudo-total As concentrations in catchment soils. As is also known to associate with carbonates (Alloway, 2013), as shown in Figure 6.31.

Cadmium was mainly associated with the Fe-Al ISC (Figure 6.31), the carbonate ISC and the Pb and Zn minerals ISC. Cadmium is known to be associated with Zn bearing minerals (Anju and Banerjee, 2010). High concentrations of Cd found were observed in the Fe dominated ISCs, which was expected, as metal oxides are known to be the most common adsorbents of Cd (Alloway, 2013). The association between Cd and carbonates can occur in higher, more neutral soils such as those found in the Tyne catchment (Chapter 3). This is because precipitates of Cd and carbonates can occur under these conditions (Miller and McFee, 1983). This was corroborated by the positive relationship observed between the Cd content of the Ca ISC and pH, as shown in Figure 6.32 below, suggesting soils with a higher pH have a higher content of Cd associated with the Ca ISC.

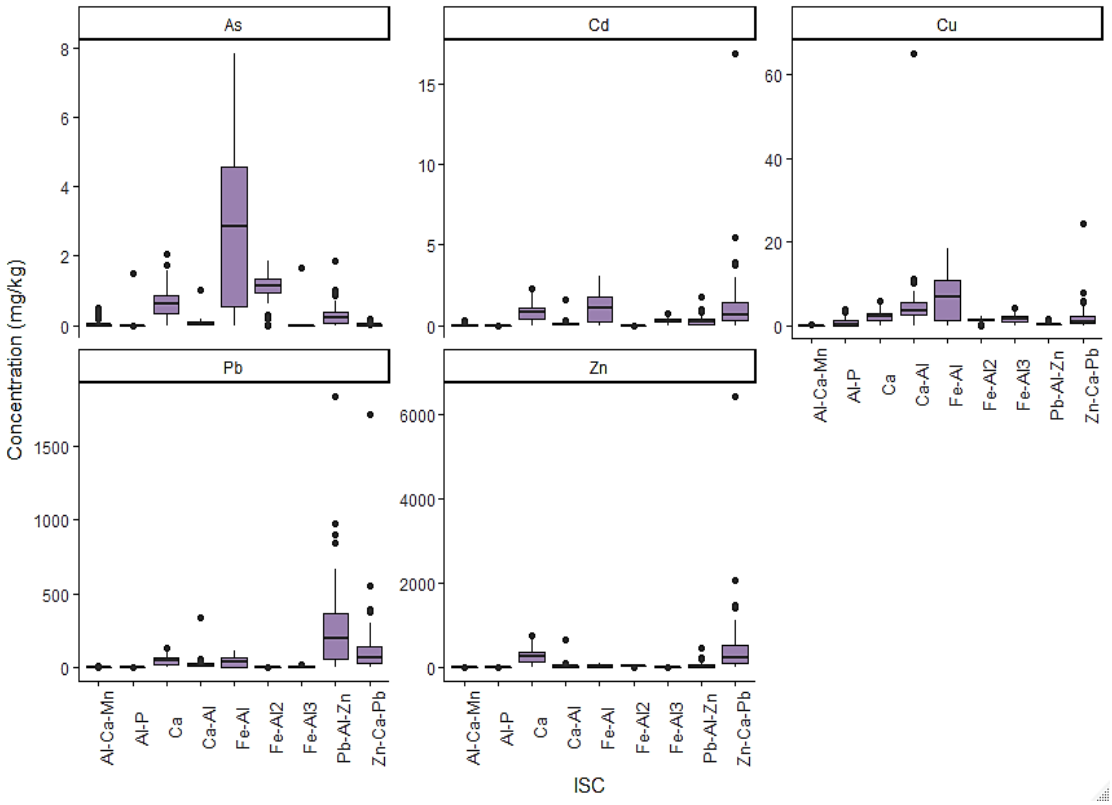

Figure 6.31: Pseudo-total PHE distribution between ISCs in the Tyne catchment soils.

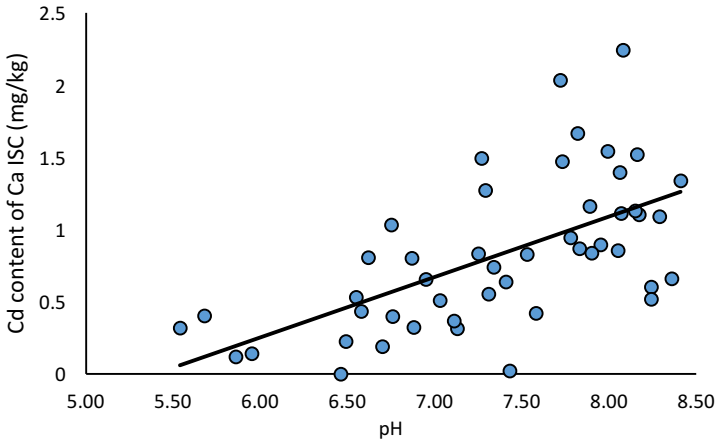

Figure 6.32. Cadmium content of the Ca ISC and pH for the Tyne catchment floodplain soils (n = 48). R_2 is 0.33.

Copper was associated with all the ISCs (Figure 6.31), with the majority of Cu being found in the Fe-Al and Ca-Al ISCs. Copper is reported to be associated with Zn and Pb bearing minerals such as smithsonite and cerussite in the Tyne catchment (Hudson-Edwards *et al.,* 1996), and explains why Cu is seen in the Pb and Zn dominated ISCs.

Lead was distributed between the two Pb and Zn mineral ISCs and the Fe-Al ISC (Figure 6.31). The presence of S in the Pb-Al-Zn ISC suggests the presence of Galena, confirmed by XRD in Chapter 3 and documented in the literature to be present in soils and sediments in the Tyne catchment (Hudson-Edwards *et al.,* 1996). Lead also associates with Fe oxides (Du Laing *et al.,* 2007) and again as seen in the Tyne catchment (Hudson-Edwards *et al.,* 1996).

6.3.7 Flooding induced changes in PHE bioaccessibility at a catchment scale

Bioaccessibility increased for the majority of PHEs after the flooding of soils for 1 week (Figure 6.33). Paired t tests determined if changes were significant, and all PHEs demonstrated a p value of < 0.05, highlighting the potential of flooding events to cause an increase in the bioaccessibility of PHEs. The greatest change in the median concentration occurred for Cu, with Zn showing the smallest change post flooding. Considering individual soils, the changes in the BAF of PHEs ranged from -40 % to 100 % (Figures 6.34 to 6.38). The range in percentage change values highlights the heterogeneity of catchment soils and PHE behaviour. Such variation means suitable tools are needed that can predict the catchment areas that express the greatest potential for PHE mobilisation and increase in bioaccessibility.

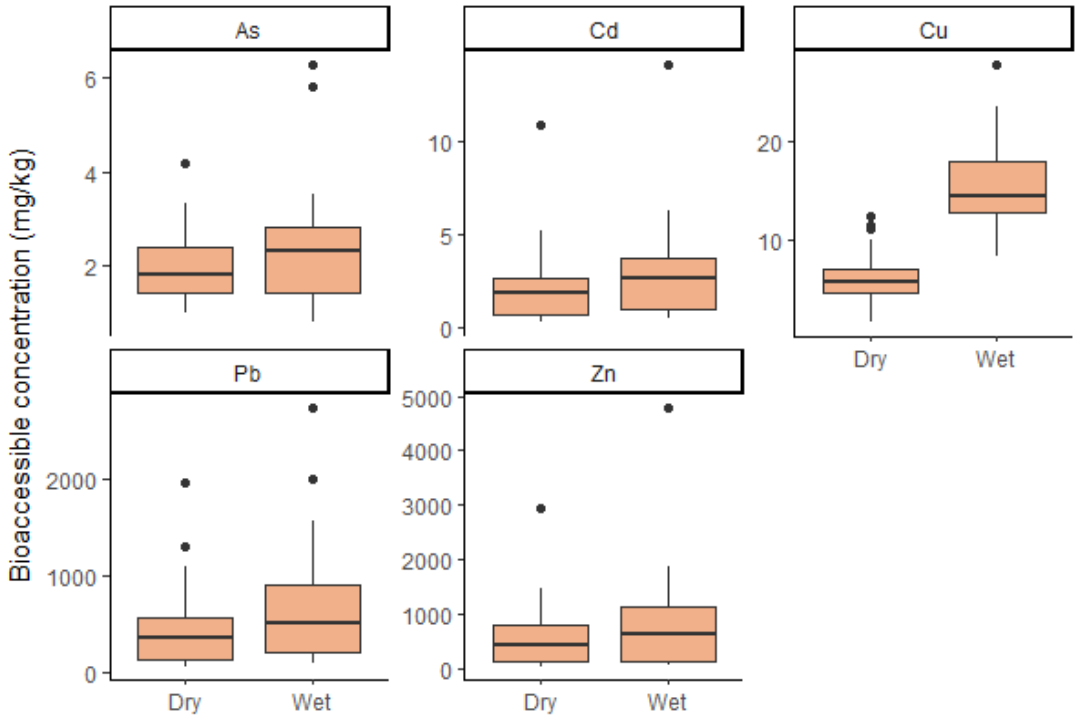

Figure 6.33: Bioaccessible PHE concentrations after wetting and drying for the Tyne floodplain soils (n = 48).

Arsenic was the only PHE studied that showed a reduction in bioaccessibility for some soils after flooding. All other PHEs showed an increase. Arsenic concentrations were low in the sampled soils; therefore, the reduction in bioaccessibility may be a result of values being close to the LOD.

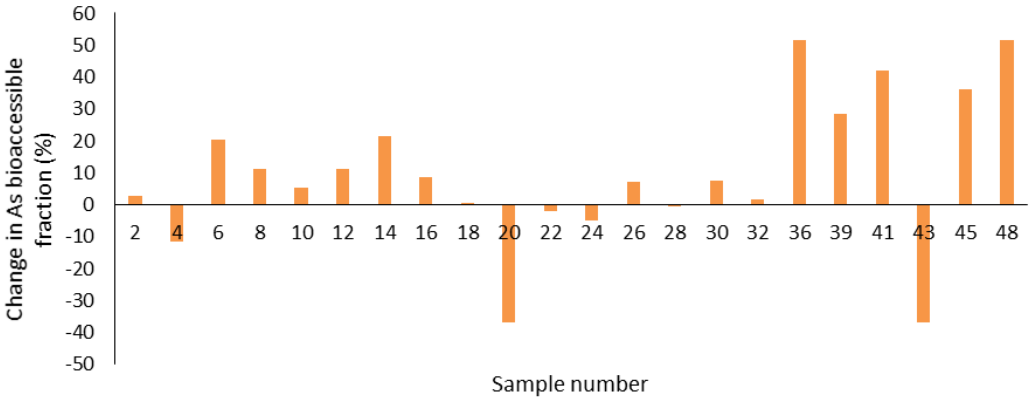

Figure 6.34: Percentage change in As bioaccessibility after flooding.

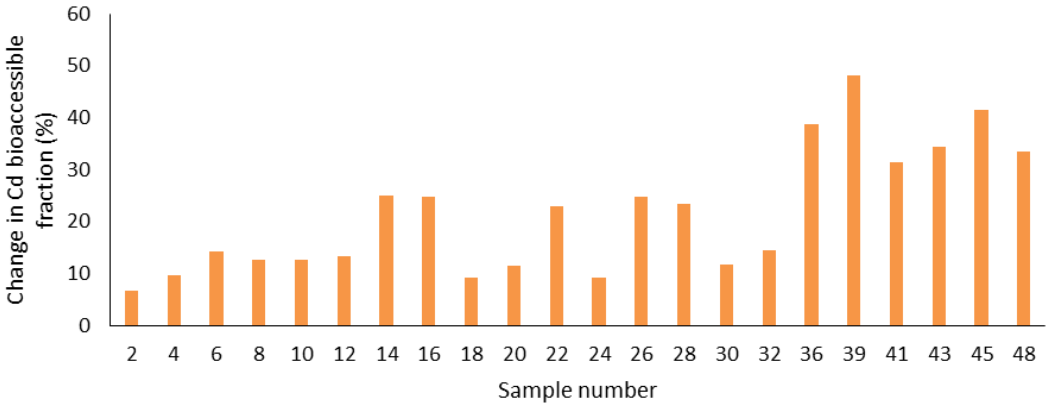

Figure 6.35: Percentage change in Cd bioaccessibility after flooding.

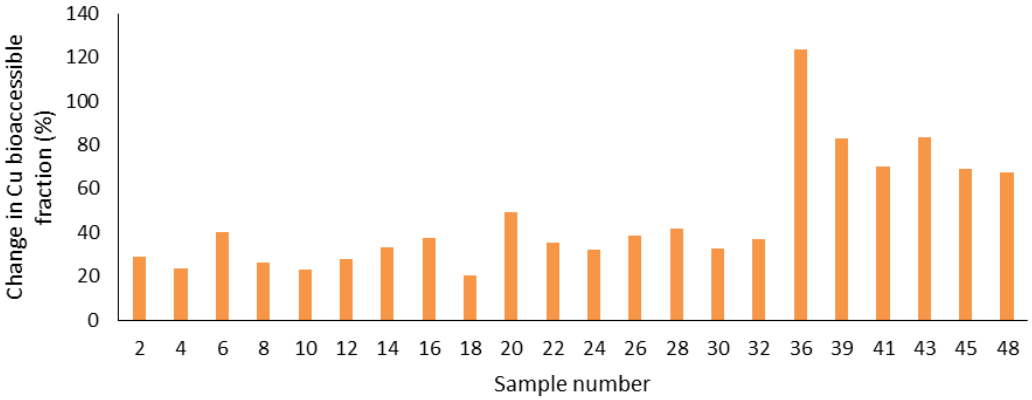

Figure 6.36: Percentage change in Cu bioaccessibility after flooding.

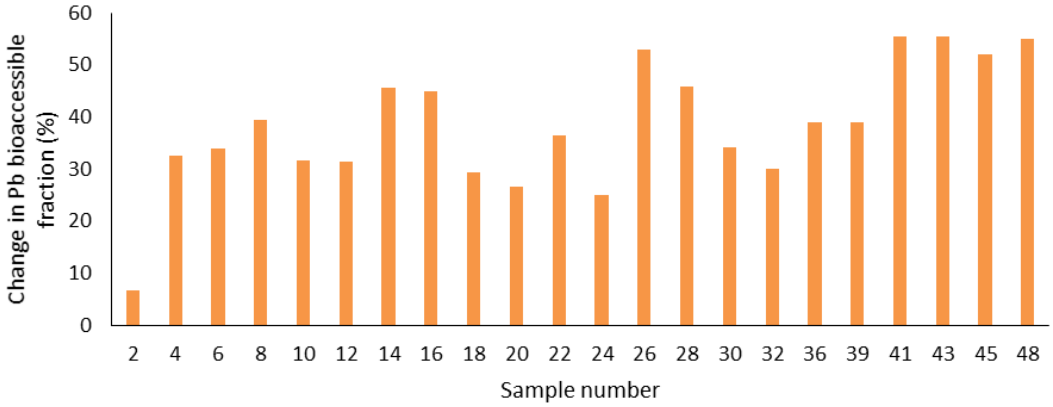

Figure 6.37: Percentage change in Pb bioaccessibility after flooding.

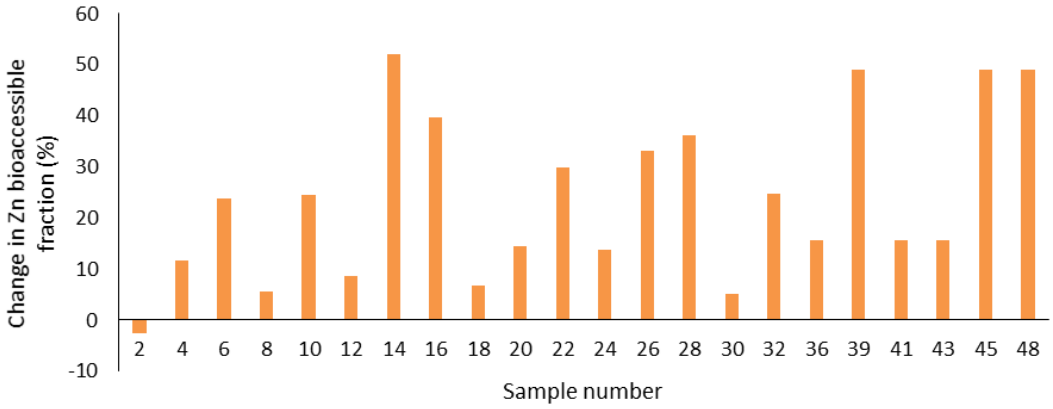

Figure 6.38: Percentage change in Zn bioaccessibility after flooding.

6.3.8 Predicting the bioaccessibility of PHEs within the Tyne catchment using random forest models

Random forest models were used to predict bioaccessible PHE content from total PHE concentrations within the Tyne catchment. The purpose of this was to test the ability of these models to predict bioaccessibility over large spatial scales using datasets of pseudo-total major and trace elements, such as those found in the G-Base datasets. No such high-resolution datasets are currently available for the Tyne catchment, other than the NSI dataset (Figures 6.4, 6.7, 6.9, 6.11 and 6.13) which were shown to have a poor comparison to the sample site data (Section 6.3.2) collected for this study (R^2 0.03 to 0.5). Consequently, the RF models were produced using the data generated by this study alone, and therefore are a proof of concept that bioaccessibility can be predicted in floodplain soils from pseudo-

total datasets. Acquisition of larger spatial datasets in the Tyne catchment floodplain soils would allow for the validation of these models. The use of historic flood outlines could be used as a basis in which to collect more detailed spatial datasets.

6.3.8.1Selection of the most important predictors for each model

Selection of predicators was done using the Boruta package as outlined in section 2.18. The most important parameters for predicting PHE bioaccessibility for each PHE are shown below in Figures 6.39 to 6.43. Values in green are depicted to be the most 'important' variables in the model. Values in yellow are assigned by the model as 'tentative' and those in red are deemed as 'unimportant'. The shadow variables are depicted by the blue boxes.

Arsenic

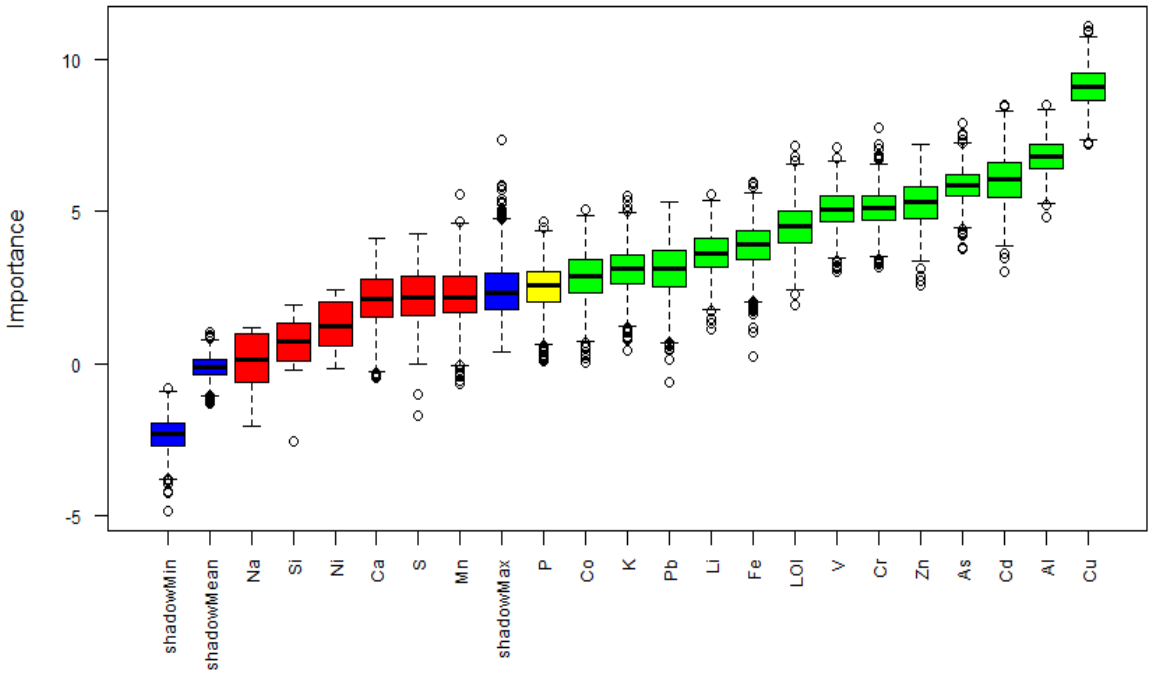

Figure 6.39: Values in green are 'important', yellow are 'tentative' and those in red are deemed as 'unimportant'. Blue boxes represent the shadow variables. The y-axis displays predictor importance.

Cadmium

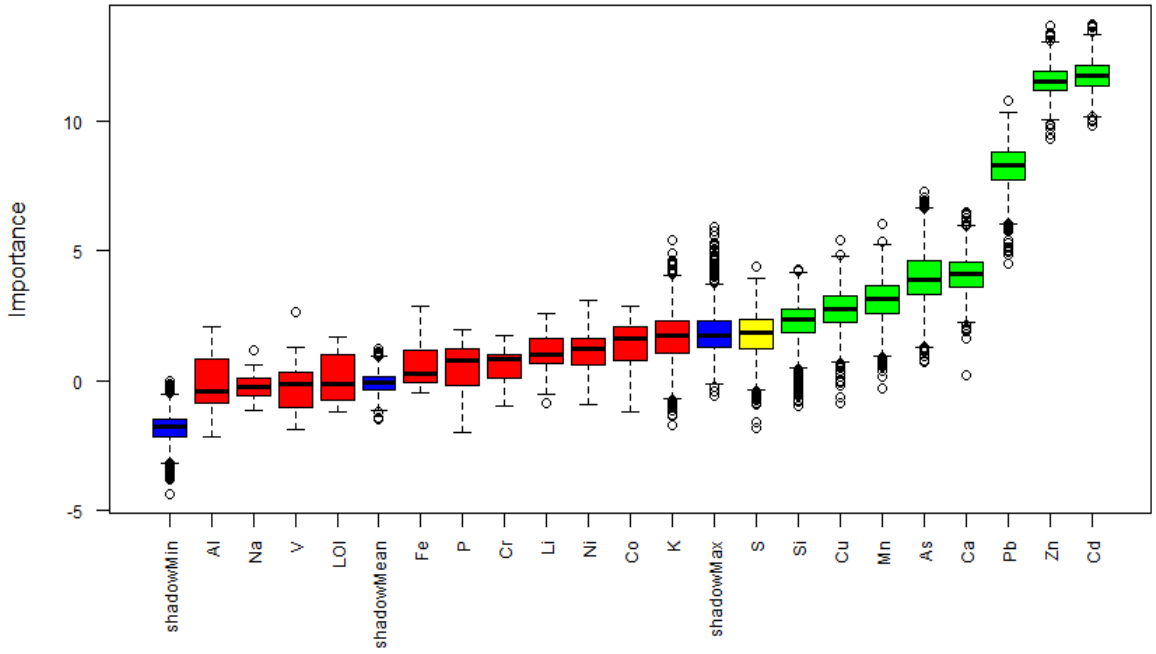

Figure 6.40: Predictor importance for Cd bioaccessibility. Values in green are 'important', yellow are 'tentative' and those in red are deemed as 'unimportant'. Blue boxes represent the shadow variables. The y-axis displays predictor importance.

Copper

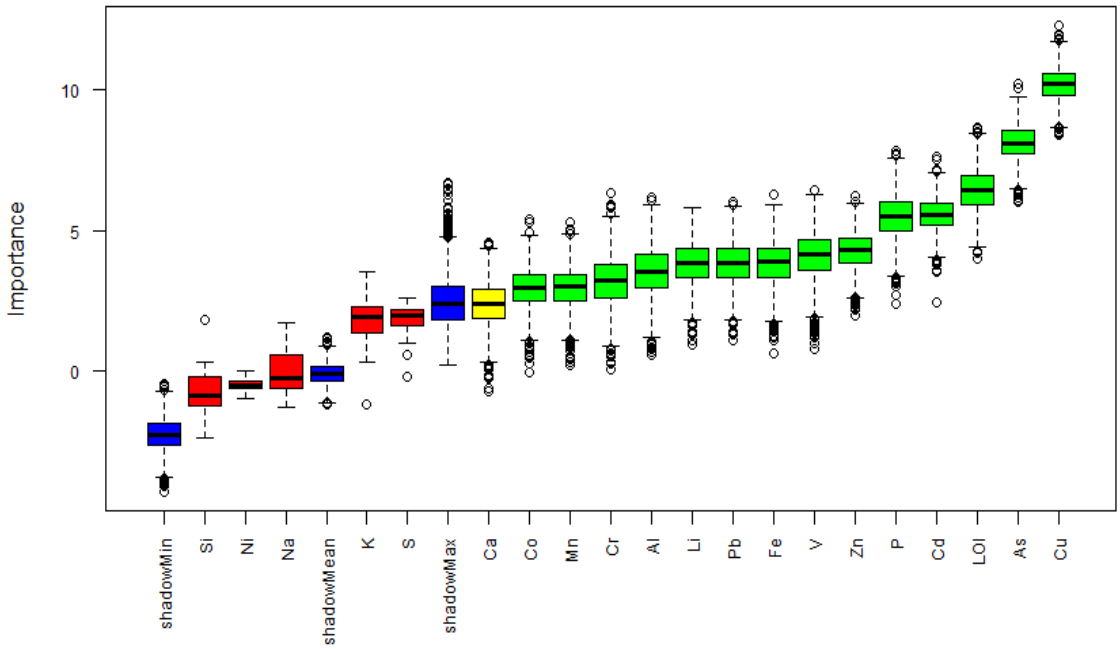

Figure 6.41: Predictor importance for Cu bioaccessibility. Values in green are 'important', yellow are 'tentative' and those in red are deemed as 'unimportant'. Blue boxes represent the shadow variables. The y-axis displays predictor importance.

Lead

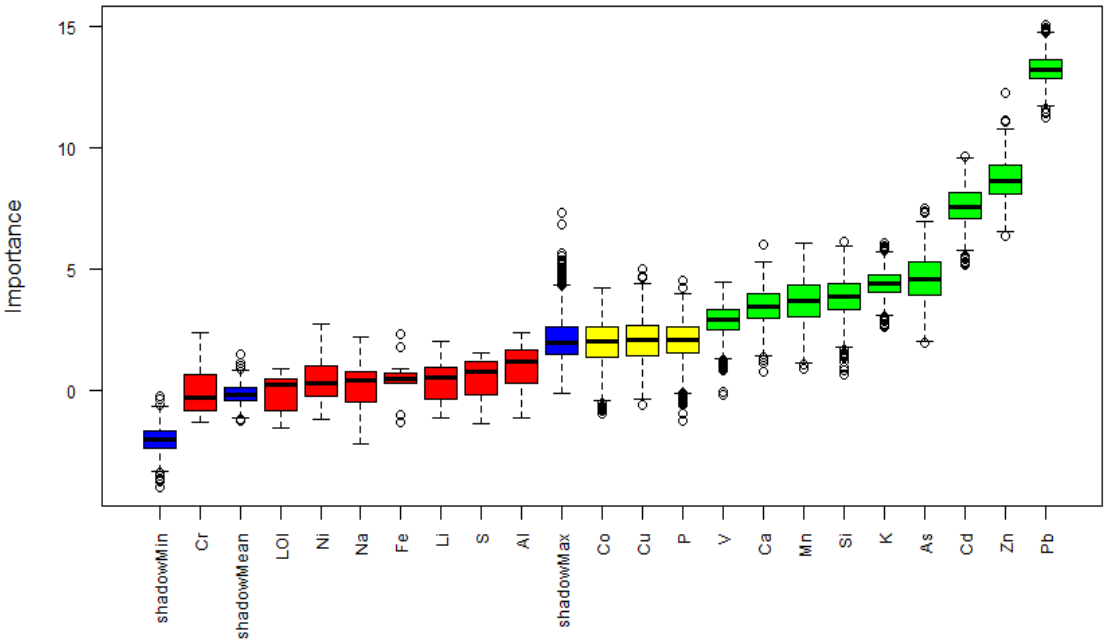

Figure 6.42: Predictor importance for Pb bioaccessibility. Values in green are 'important', yellow are 'tentative' and those in red are deemed as 'unimportant'. Blue boxes represent the shadow variables. The y-axis displays predictor importance.

Zinc

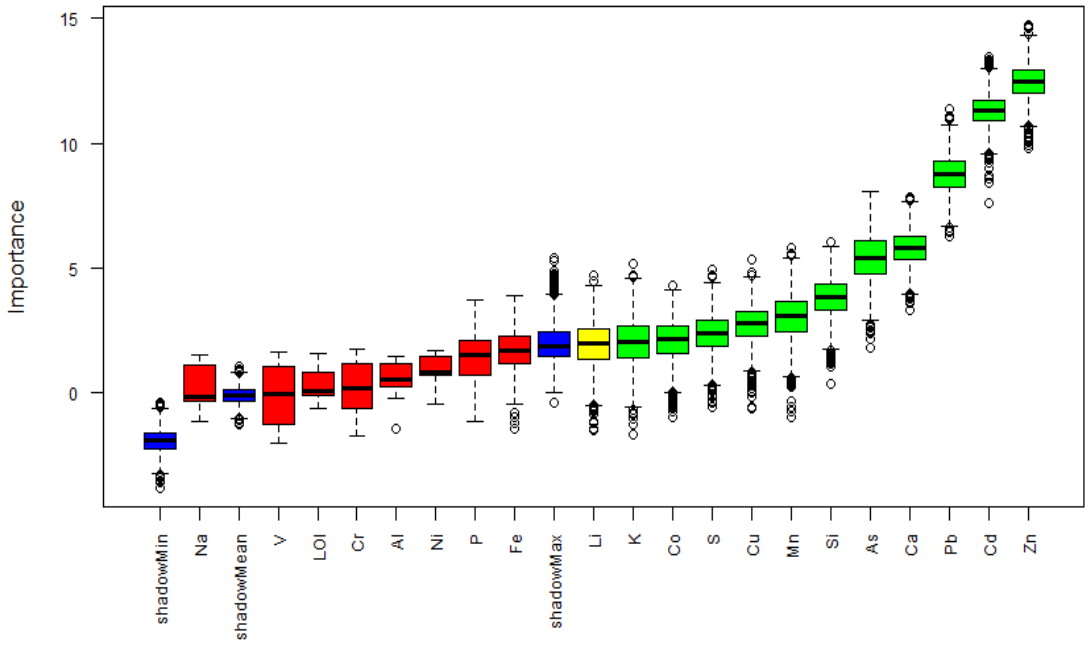

Figure 6.43: Predictor importance for Zn bioaccessibility. Values in green are 'important', yellow are 'tentative' and those in red are deemed as 'unimportant'. Blue boxes represent the shadow variables. The y-axis displays predictor importance.

The predictor variables for each PHE varied in this study and there was no common set of variables for modelling PHE bioaccessibility. Common patterns between the five models above were that the host PHE (e.g. pseudo-total Pb for Pb bioaccessibility) was the most important predictor, with the exception of arsenic. This suggests that, generally, the higher PHE content results in a more PHE bioaccessible concentration, which has been seen elsewhere (e.g. Appleton *et al.,* 2012). PHEs other than the host PHE were also often important predictor variables, with increased bioaccessibility of one PHE often linked to the increased bioaccessibility of another. This suggests possible interaction effects between PHEs occur resulting in the need to examine PHE behaviour and bioaccessibility in mixed chemicals, rather than in isolation.

The most important variables generated by the Boruta package, as shown in Figures 6.39 to 6.43 by the green boxes, were selected and used as an input into a second RF model, as opposed to the first RF model that contained all the predictor variables. The predicted vs actual values for each PHE are shown in Figure 6.44. Most of the points conformed to the line of equivalence for each PHE, suggesting a good model fit. There was a slight under prediction at the top end of the dataset, shown by the deviation of data points from the line

of equivalence, likely to have arisen from fewer samples at the higher end of the range of bioaccessible PHE concentrations.

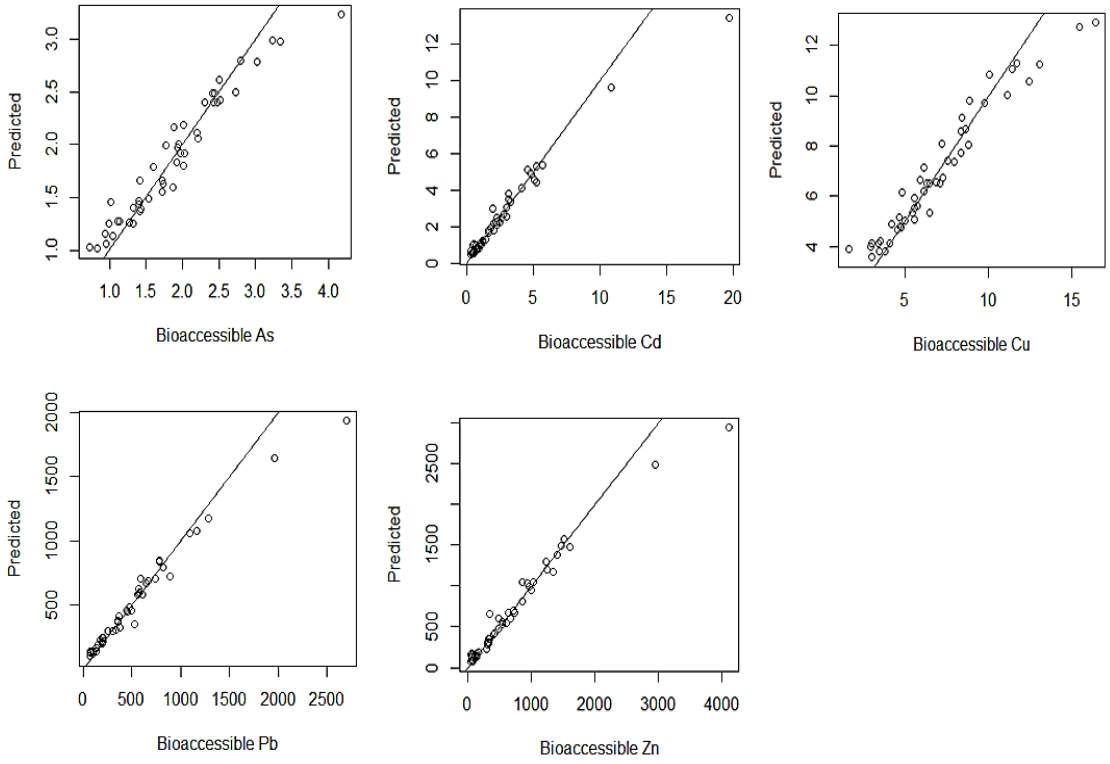

Figure 6.44: Relationship between bioaccessible PHE content (mg kg^{-1}) and predicted bioaccessible PHE content (mg kg^{-1}) from random forest models. Diagonal line represents line of equivalence.

Table 6.2: Percentage of variance explained by each random forest model.

PHE	% of variance explained
As	48
Cd	54
Cu	48
Pb	60
Zn	64

The percentage of variance explained by each model given is an insight into the model's ability to explain the response variable variability. Unexplained variance is likely to be a result of true randomness or lack of fit.

6.3.8.2 Partial dependence plots

Arsenic

The partial dependence plot (Figure 6.45) demonstrated the partial effect of the x-axis variable on the y-axis variable (PHE bioaccessibility). Positive relationships were seen with the other PHEs used in this study (Figure 6.45), suggesting that bioaccessible As content was greater where there were greater PHE concentrations in soils. This could result from PHEs being hosted in similar ISCs, however no PHEs shared a common set of predictor variables so this is unlikely. Additionally, the boxplots in Figure 6.31 show the PHEs generally tend to associate with different ISCs. Another explanation could be the PHEs shared similar inputs, arising from the land use at each site. For example, an input of mine soil could result in the input of multiple PHEs to the soil, therefore resulting in elevated concentrations of all PHEs. This may explain the positive associations seen between PHEs and As bioaccessibility. The positive relationship between bioaccessible As and pseudo-total content of Cu, Cd, Zn and Pb may also indicate potential interaction effects between PHEs and their bioaccessibility, which is not described well in the literature and therefore a knowledge gap.

A positive relationship was seen with Al, suggesting higher concentrations of Al oxides may result in higher As bioaccessibility. Al-Fe oxides were shown to contribute to As bioaccessibility in some soils in Chapter 3. Concentrations of Fe displayed a negative trend with As bioaccessibility up to about 16,000 mg kg^{-1}, after which the trend becomes positive. This may be because Fe oxides only contribute partially to As bioaccessibility (Palumbo-Roe and Klinck, 2007; Meunier *et al.,* 2010), resulting in the variability observed in Figure 6.38. Generally, Fe-oxides are not as soluble as other soil constituents are, because they are less easily extractable, depending on their crystallinity (Palumbo-Roe *et al.,* 2015). For example, pseudo-total Fe content will include both crystalline and more newly formed Fe oxides. Cave *et al.* (2013) observed, when predicting As bioaccessibility from soil properties, that crystalline Fe oxides display a negative trend with As bioaccessibility, and less crystalline Fe oxides display a positive trend. Therefore, the presence of both crystalline and newly formed Fe oxides may result in the negative trend at lower Fe values and the positive trend higher Fe concentrations seen here.

The main predictors of As identified in Chapter 3 showed some differences to the data presented here. For example, Mn-oxides were shown to be hosts of As in the eight soils samples in the Tyne catchment in Chapter 3, but Mn was not an important predictor of the 48 Tyne catchment flood plain soils sampled for this chapter. This may be because the Tyne

floodplains soils do not contain ISC identifiable quantities of Mn oxides in all the soils, as shown in Figure 6.30. The Tyne catchment floodplain soils analysed in this chapter are much more similar in their characteristics than the eight soils used in Chapter 3, which were purposefully selected to be different form each other with regards to their soil characteristics and components.

Carbonates were also identified in Chapter 3 to be hosts of bioaccessible As and were deemed as 'unimportant' predictors for bioaccessibility in the Tyne catchment floodplain soils here. Carbonates were identified as an ISC in these soils, and therefore it is assumed that they are not hosts of bioaccessible As. This result highlights the change in predictors that can occur at differing spatial scales.

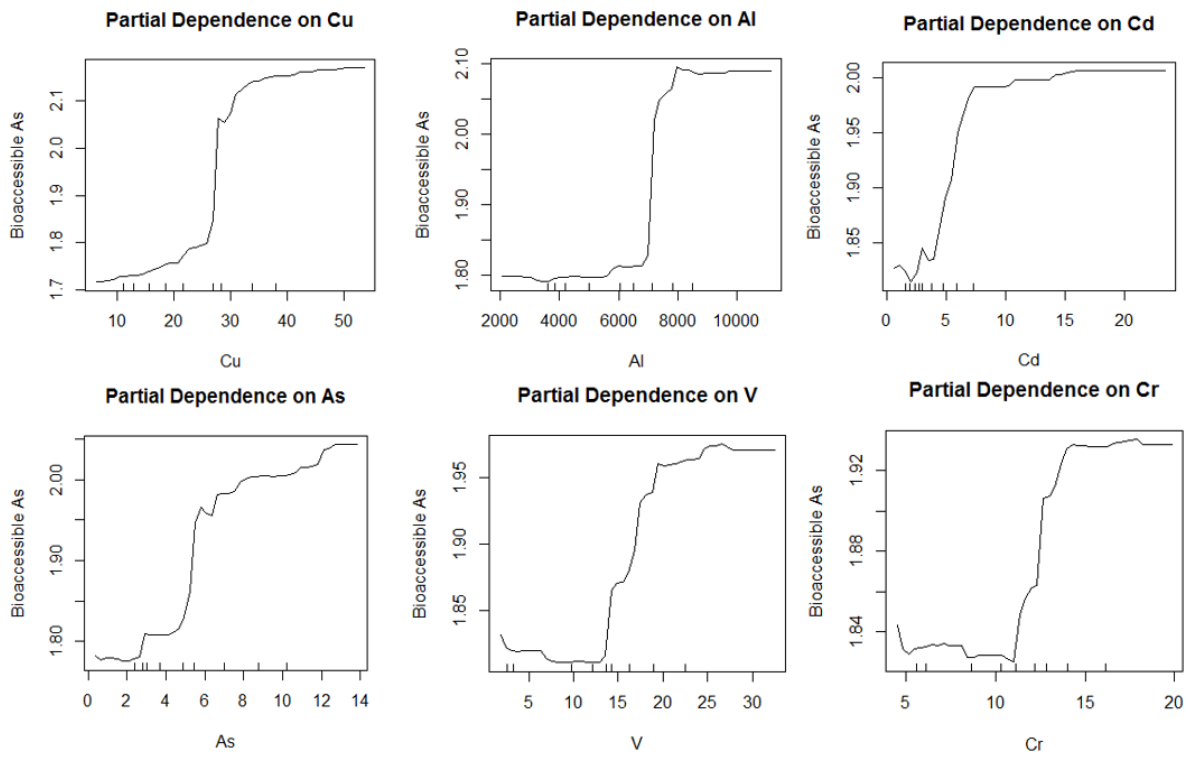

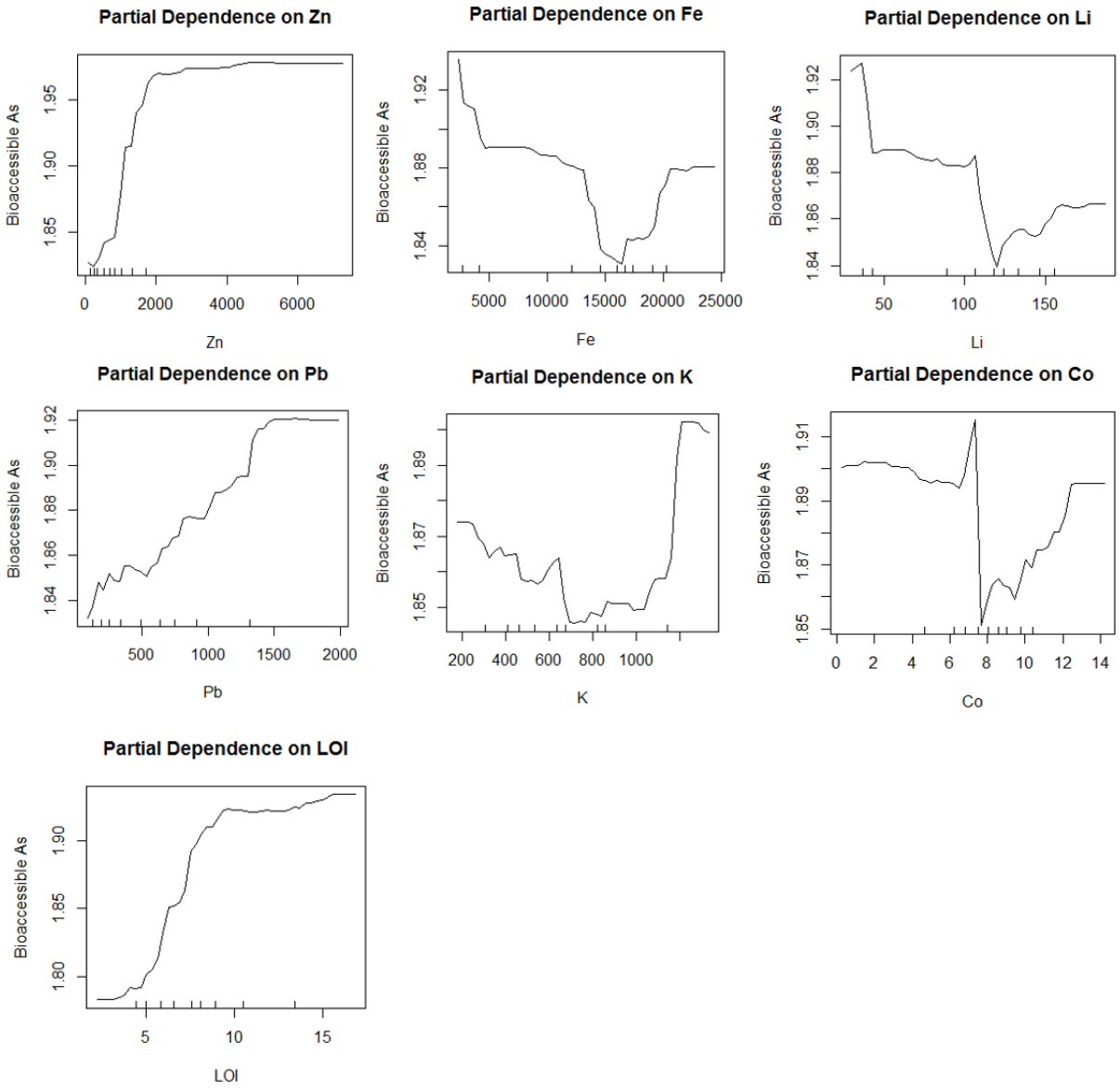

Figure 6.45: Partial dependence plots for As bioaccessibility. Plots are ordered by importance. Units are mg kg^{-1} for all elements and % for LOI.

Cadmium

Pelfrêne *et al.,* (2013) reported that the most influential factors for predicting Cd bioaccessibility were carbonates, SOM, P, Fe-oxides, Al, Cd and Pb. This differs from the results here and highlights the importance of catchment specific modelling, as no single model will be able to predict PHE bioaccessibility in every catchment. Pseudo-total Cd and Zn both have positive partial effects on Cd bioaccessibility. This is likely because Cd and Zn are often both associated with similar soil constituents and minerals; increases of Cd are therefore likely to result in increases in the bioaccessible concentration of Cd as seen in Figure 6.46. The relationships between Cd and its predictor variables were all positive. Like

As, there are positive relationships between the other PHEs of interest in this study, as well as the major elements. Ca was shown to be an important predictor (a similar finding to that of Pelfrêne *et al.,* (2013)). Manganese was shown to be a significant predictor of Cd bioaccessibility, similar to the results seen in Chapter 3, where manganese oxides were shown to be hosts of bioaccessible Cd for the eight selected soils studied.

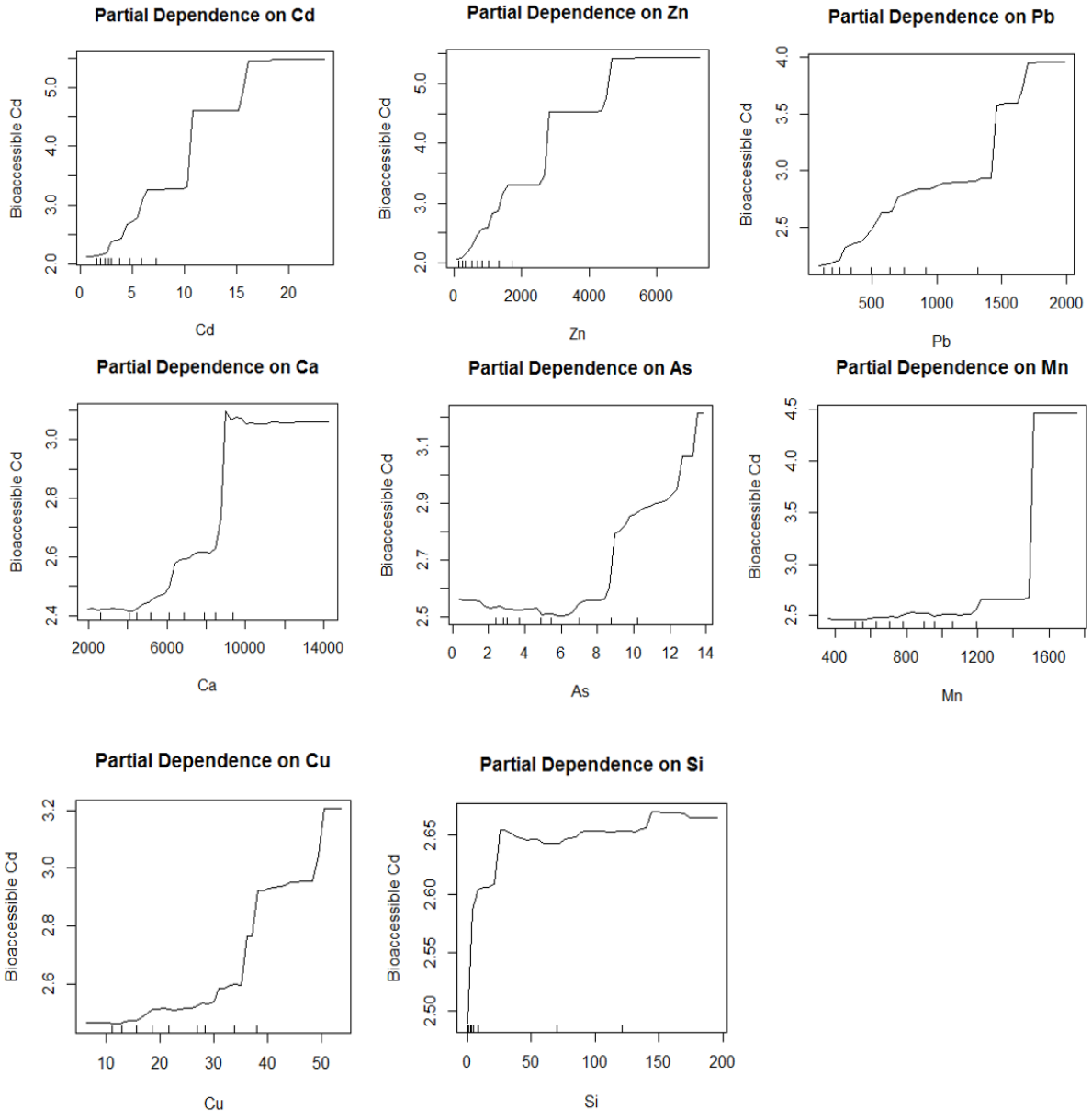

Figure 6.46: Partial dependence plots for Cd bioaccessibility. Plots are ordered by importance. Units are mg kg^{-1} for all elements and % for LOI.

Copper

Positive relationships were observed for Cu and the remaining PHEs (Figure 6.47). The positive relationship with soil organic matter (LOI) suggests that Cu bound to organic matter contributes to Cu bioaccessibility (Figure 6.47). This result is contradictory to the literature as studies have reported mobility of Cu into mobility to be negatively affected by soil organic matter content (Pouschat and Zagury, 2008; Cui *et al.,* 2016), and such relationships are mentioned in Chapter 4. Other studies have reported that Cu bioaccessibility can be positively correlated with SOM in the gastrointestinal tract and a near neutral pH environment. This is because organic compounds in the gastrointestinal fluids such as pancreatin and pepsin can bind with Cu at near neutral pH bringing it in to solution (Cai *et al.,* 2016). However, this chapter presents data from the gastric extract, which uses reagents with a pH of approximately 1.2. Therefore, it is hypothesised that some desorption of Cu from SOM may take place in the gastric fluid. Higher concentrations of Cu are likely to be associated with soils with greater masses of SOM, therefore resulting in the positive relationship observed between SOM and bioaccessible Cu.

A negative relationship was observed with Al though, suggesting that Cu bound to Al-oxides does not contribute to Cu bioaccessibility. Similar results were observed in chapter 3, where Al bearing components did not contribute to Cu bioaccessibility. Chapter 3 results also showed Mn-oxides to be hosts of bioaccessible Cu, and similar conclusions can be made here from a positive relationship between Mn and Cu.

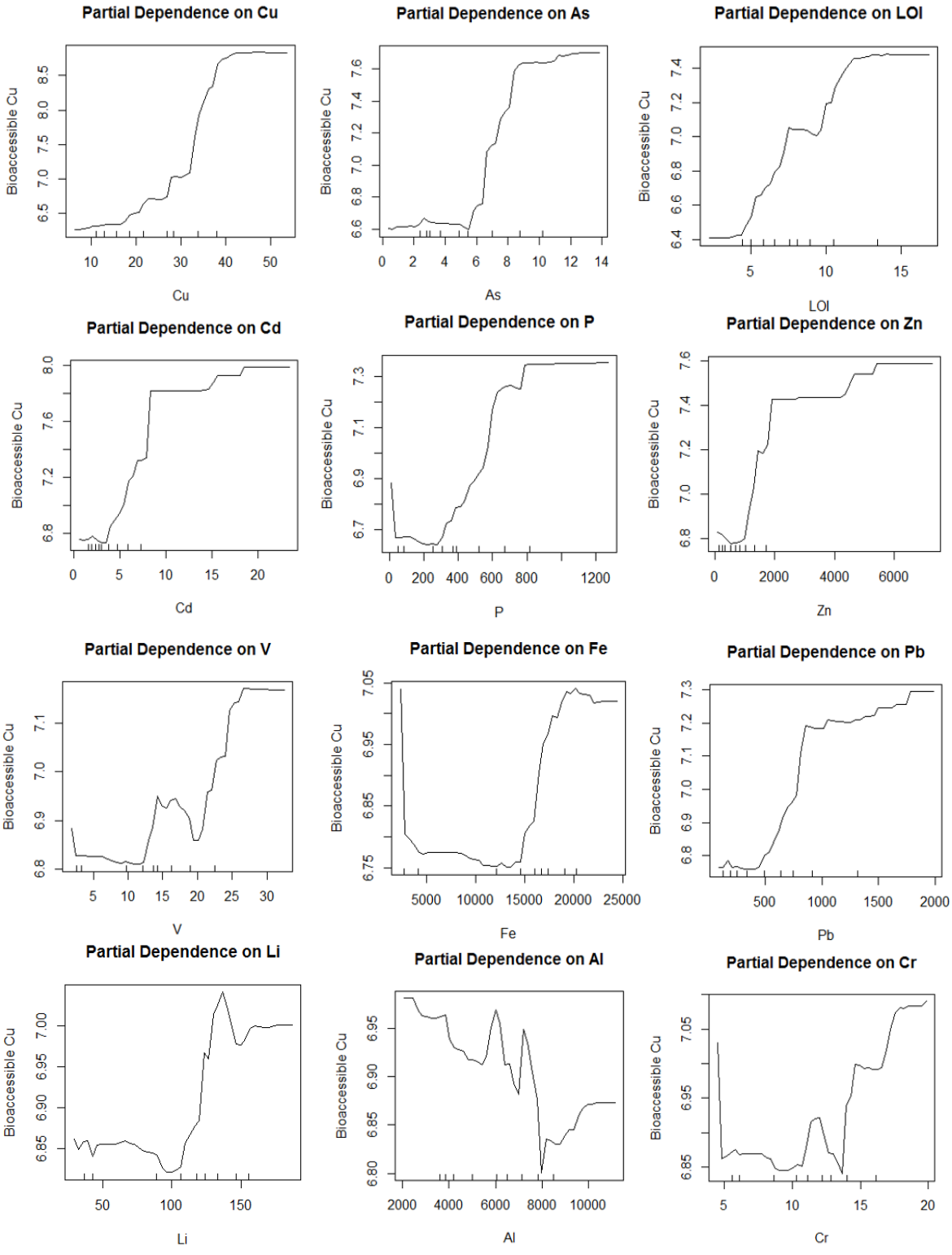
Partial Dependence on Cu
Bioaccessible Cu
Cu
Partial Dependence on As
As
Partial Dependence on LOI
LOI
Partial Dependence on Cd
Cd
Partial Dependence on P
P
Partial Dependence on Zn
Zn
Partial Dependence on V
V
Partial Dependence on Fe
Fe
Partial Dependence on Pb
Pb
Partial Dependence on Li
Li
Partial Dependence on Al
Al
Partial Dependence on Cr
Cr

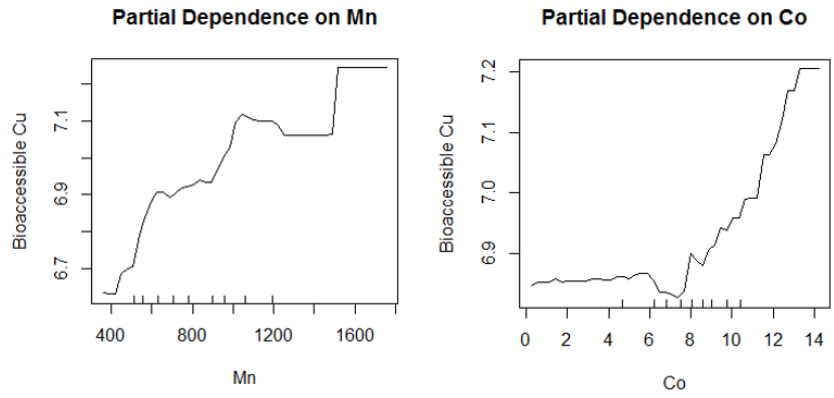

Figure 6.47: Partial dependence plots for Cu bioaccessibility. Plots are ordered by importance. Units are mg kg^{-1} for all elements and % for LOI.

Lead

Figure 6.48 displays the partial dependence plots for Pb bioaccessibility. A linear increasing trend was observed between Pb and Pb bioaccessibility (Figure 6.40), indicating that higher pseudo-total Pb concentrations in soil may contribute to higher bioaccessible concentrations of Pb. Similar results were seen by Appleton *et al.,* (2012). Positive linear trends with the PHEs Zn, Cd and As were also observed. This is likely to be a result of the association of these elements in mine spoil material. A negative relationship was seen with K. Potassium is known to be generally present in organic compounds within the soil, which could explain the negative trend seen as PHEs can be immobilised by organic material and therefore could reduce bioaccessibility of Pb (Tang *et al.,* 2008).

The positive association with Mn (Figure 6.48) suggests that Mn oxides are hosts of bioaccessible Pb, as shown in Chapter 3 and in the literature (e.g. Courtin-Nomade *et al.,* 2016; Rinklebe *et al.,* 2016). A non-linear, parabolic trend was seen between Pb bioaccessibility and Ca, suggesting that lower concentrations of Ca result in a negative relationship with Pb bioaccessibility up to about 4,000 mg kg^{-1} where the trend relationship changes to a positive one. This could be an effect of Ca concentrations on the pH of soil as pH is known to be an important factor in Pb availability. For example, Pelfrêne *et al.,* (2013) reported higher Pb bioaccessibility in carbonate soils, suggesting that Pb bound to carbonates was released in the acidic environment of the stomach. Carbonates were shown to contribute to bioaccessibility in the soils studied in Chapter 3. Both P and V showed a negative non-linear trend with Pb bioaccessibility. The formation of insoluble lead phosphate minerals may explain the negative relationship between P and Pb, suggesting that soils in the

Tyne with higher P content, such as agricultural fields, have reduced Pb bioaccessibility (Ruby *et al.,* 1999; Pelfrêne *et al.,* 2013).

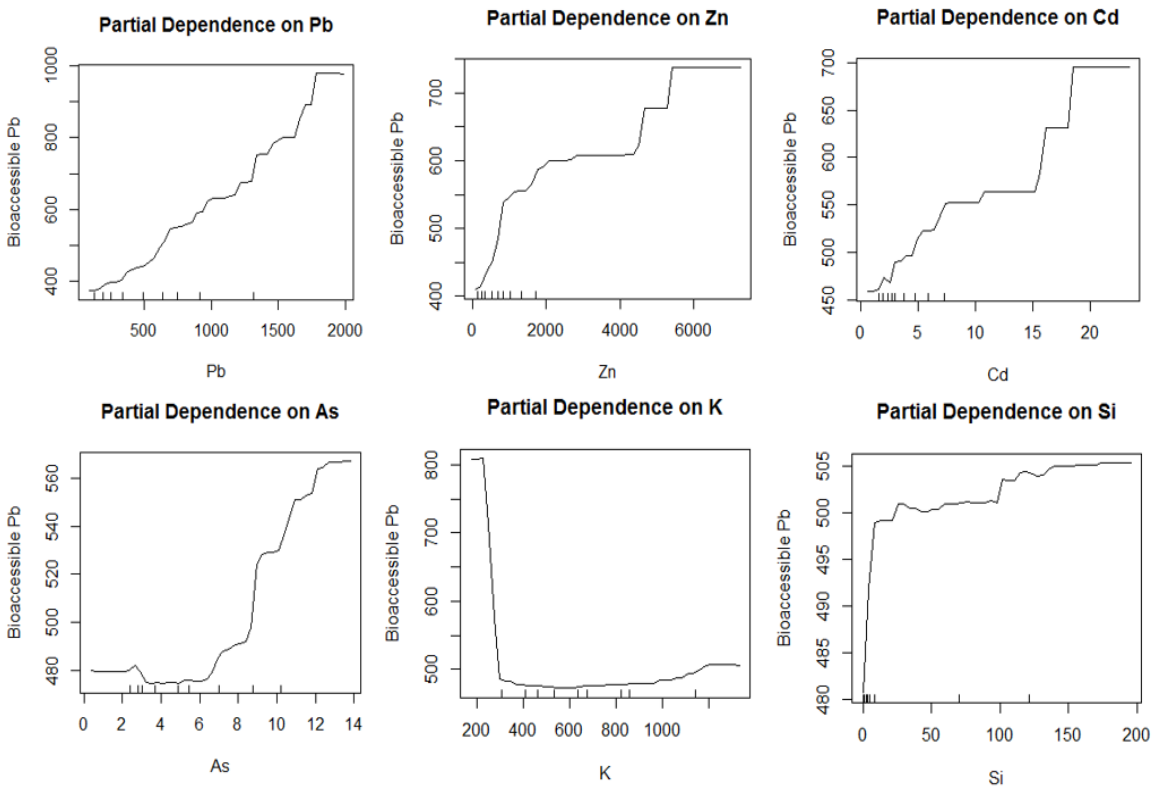

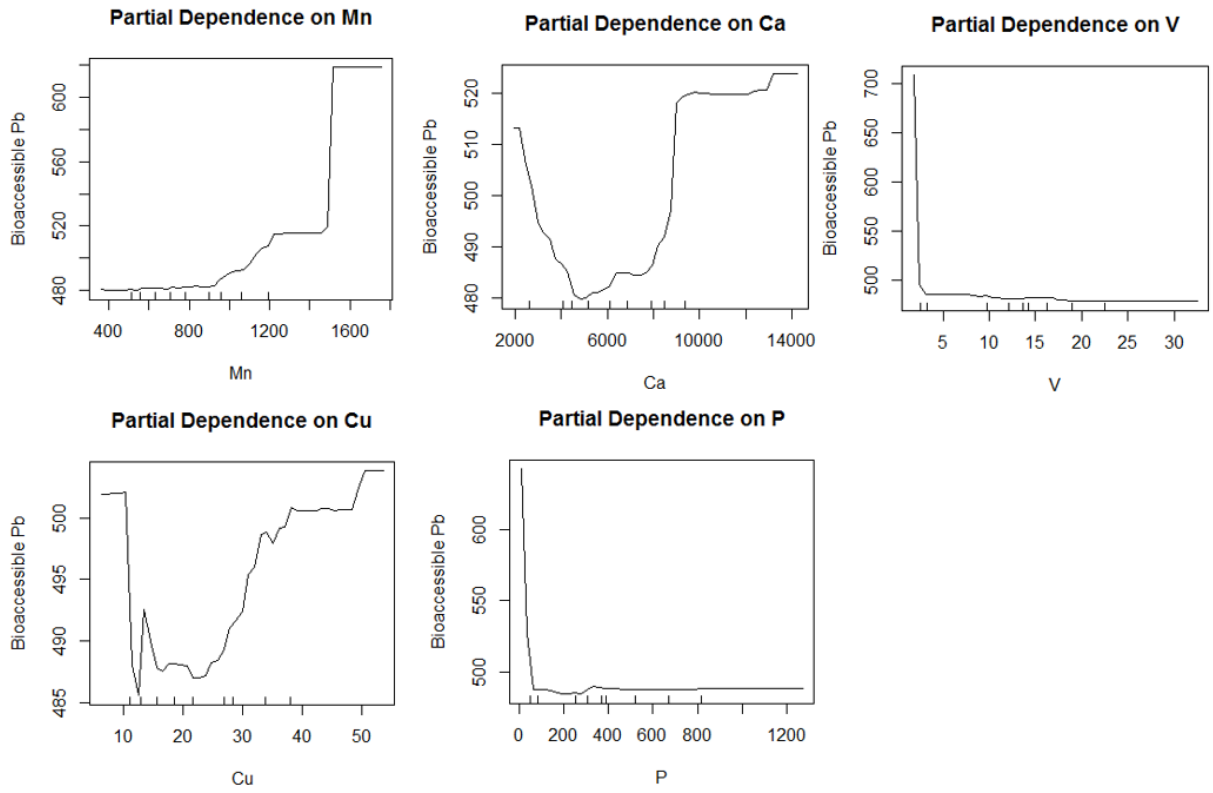

Figure 6.48: Partial dependence plots for Pb bioaccessibility. Plots are ordered by importance. Units are mg kg^{-1} for all elements and % for LOI.

Zinc

Positive trends were observed between Zn and the PHEs under investigation in this study (Figure 6.49), which was likely to be a result of soils with higher concentrations of bioaccessible Zn having higher concentrations of other PHEs in general. Calcium content was also shown to be potentially related to Zn concentrations (Figure 6.49), suggesting that higher Ca concentrations could result in higher bioaccessible Zn. Positive relationships were also observed with Mn. Mn oxides were shown to contribute to the bioaccessible content of Zn (Chapter 3) and therefore soils in the Tyne with higher Mn content may have a higher affinity for accessible Zn (Brümmer *et al.,* 1983).

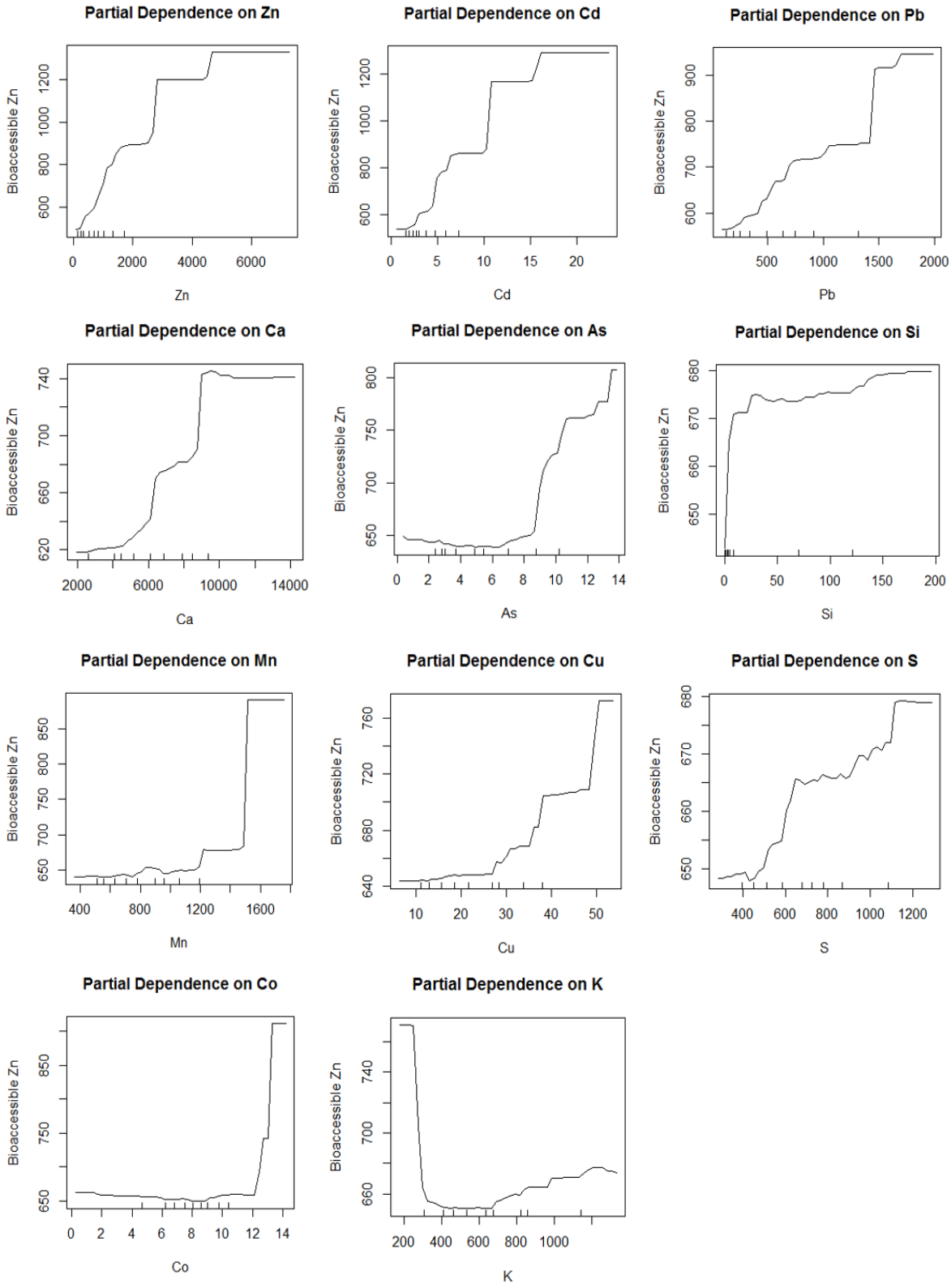

Figure 6.49: Partial dependence plots for Zn bioaccessibility. Plots are ordered by importance. Units are mg kg^{-1} for all elements and % for LOI.

Broad comparisons can be made to the clusters identified in Chapter 3, which showed the bioaccessible hosts of the PHEs studied in this work. Chapter 3 and this chapter used different techniques to determine the potential relationships between the solid phases of soils and PHE bioaccessibility. This was done because the determination of ISCs was much less time consuming on the Tyne floodplain soil sample size (n = 48). Only eight soils were used in Chapters 3, 4 and 5, so it was possible to conduct the CISED method on the smaller sample size.

Similarities were observed between the components that contribute to bioaccessibility in Chapter 3 and the relationships between PHEs and major elements in this chapter, showing the potential of both methods for identifying soil characteristics that are influential on PHE bioaccessibility. However, the differences between the ISCs in this chapter and the clusters in Chapter 3 are likely to be a result of the spatial scales over which the samples for each chapter were collected. For example, the soils in Chapter 3 were not linked spatially (Figure 2.6) and were purposefully selected to be different from each other in terms of their soil characteristics and solid phase components. Therefore, they do not always match with the ISCs generated from the 48 samples used in this chapter. The soil samples in this chapter were collected from the Tyne catchment floodplains in the upper and mid catchment (Figure 2.7) and are more likely to have similar characteristics than with the soils in Chapter 3. The differences in the components that contribute to bioaccessibility are to be expected between the soils analysed in the two chapters. However, both ISCs and clustering are useful for examining the underlying contributors towards PHE bioaccessibility, and both have their advantages.

The components identified by the CISED method are derived from ISCs and provide a more detailed snapshot of the solid phase distribution of PHEs. For example, several Fe-oxide components come from one Fe dominated ISC. The ISCs generated in this chapter give a broader look at the distribution of PHEs using a less time-consuming digestion process than the CISED extraction method. Consequently, the results in this thesis support the use of ISCs to predict PHE bioaccessibility on a catchment scale dataset to geochemically characterise the soils in more detail than just the pseudo-total element content. This has been shown to identify the main influential components of PHEs through machine learning methods and successfully predict bioaccessibility in floodplain soils, providing a better estimation of the risk of PHE exposure to humans. The CISED method is useful for looking at soils of interest in more detail. For example, any particular areas in a catchment that may have elevated levels

of bioaccessible PHEs. The CISED method may provide more detailed information on the geochemical characterisation of these soils that can be used to unpick why bioaccessibility concentrations are elevated.

6.3.9 Predicting flooding induced change in PHE bioaccessibility

A combination of RF and linear regression models were used to determine the predictor variables needed for the prediction of flooding induced change in bioaccessibility. Lead was used as a model PHE as Pb is known to be a pollutant of interest in the Tyne catchment and bioaccessible Pb concentrations did exceed parkland S4UL values in certain locations. Significant predictors ($p < 0.01$, $R_2 = 0.65$) were Si, Li and P. Their partial effects are shown in Figure 6.50.

Both Si and Li are suggested to positively influence flooding induced change in Pb bioaccessibility, indicating that areas with a higher Si and Li content will experience greater change in Pb bioaccessibility (Figure 6.50). Phosphorus displayed a negative linear relationship with Pb bioaccessibility change, suggesting higher concentrations of P retard change in Pb bioaccessibility. This result agrees with the literature as phosphates have been shown to reduce Pb bioaccessibility through the formation of insoluble lead phosphates (Ruby *et al.,* 2004; Hettiarachchi and Pierzynski, 2002). Therefore, it is plausible to assume that the higher mass of lead phosphates in soil, the smaller the change in Pb bioaccessibility as a result of flooding.

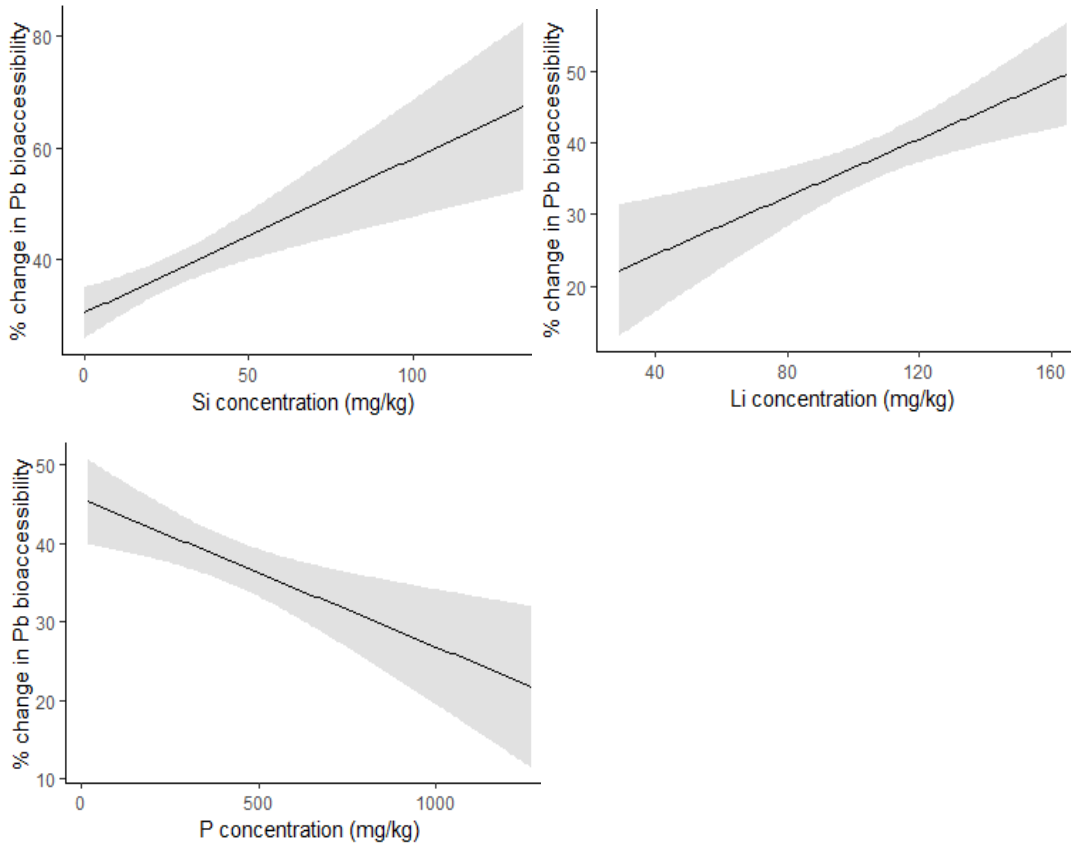

Figure 6.50: Partial dependence plots for the three predictor variables. Partial dependence plots can show whether the effect of a predictor to a response variable is linear or not, when all other predictor variables are held constant around their mean. The grey shaded areas represent the 95 % confidence intervals.

The NSI dataset was used as a different set of input variables for the RF models to be able to predict bioaccessibility at a larger and finer scale than the IDW tool utilised in Section 6.3.3, as there were more sample points (n=103) The relationship between the data from the 48 soils sample in this study and the NSI dataset was shown to be poor (section 6.3.2). However, the NSI dataset was used to provide a proof of concept for the ability of RF models to predict bioaccessibility and consequent flooding induced change at a catchment scale. The NSI dataset is an interpolated dataset and therefore there is likely to be uncertainty associated with these data. Information on these errors were not accessible and therefore consideration of uncertainty has not been incorporated into the prediction of bioaccessibility using RF models.

Li is not included in the NSI dataset. To overcome this issue, Li data were interpolated from the 48 samples collected within the Tyne catchment. This was done because Li is a predictor variable for determining flooding induced change in Pb bioaccessibility and was therefore needed as a model input.

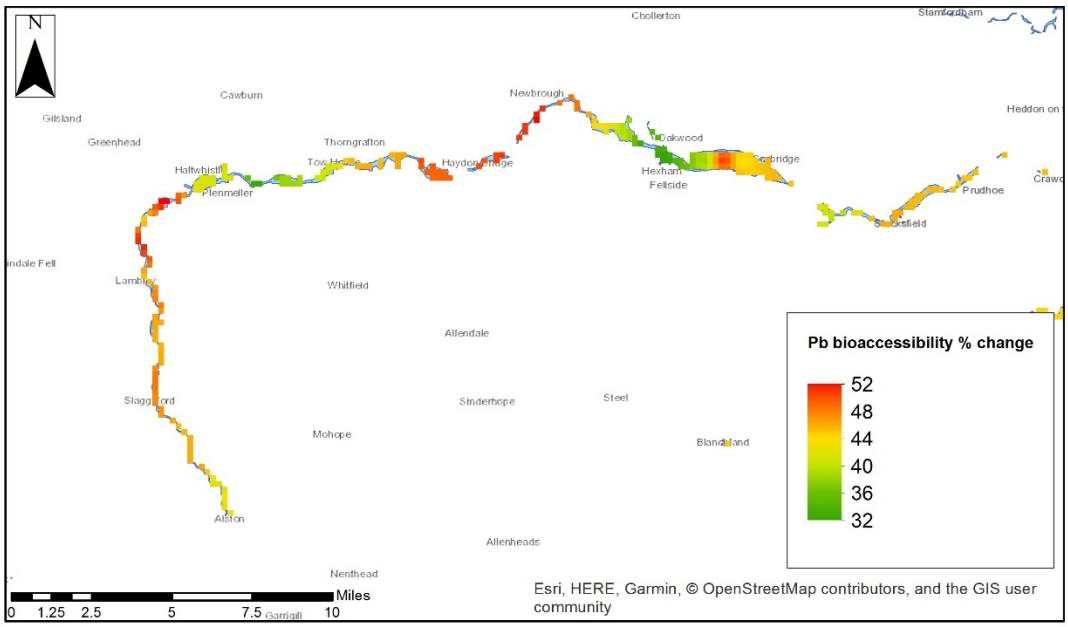

Figure 6.51: Map of the Tyne catchment showing the modelled percentage change in bioaccessibility after flooding.

Figure 6.51 shows that the majority of historic flood areas within the Tyne catchment showed an increase of bioaccessibility of between 44 % and 52 %. A few areas around the towns of Hexham and Haltwhistle predicted lower increases in bioaccessibility, ranging from 32 % to 44 %. Lead concentrations around Haltwhistle and Hexham range from 79 to 547 mg/kg (Figure 6.16). GACs for Pb vary from 84 mg kg^{-1} for allotments to 330 mg kg^{-1} for residential areas with no home grown produce. The predicted change in bioaccessibility results in soil lead concentrations around the towns of Hexham and Haltwhistle potentially exceeding these GACs; increasing the risk of PHE exposure to humans utilising these areas. The percentage change seen in the lower agricultural areas of the catchment are also likely to exceed the more conservative GACs for Pb. Even though this work did not assess changes in the phytoavailability of PHEs, it can be hypothesised that plant uptake would likely increase after flooding events. This is supported by the evidence in Chapter 5, where Pb was shown to re-associate with more labile components of some soils within the Tyne catchment.

6.3.10 Implications for Risk Assessment

The use of random forest models for the spatial prediction of PHE bioaccessibility over large geographic areas, such as at a catchment scale, has been shown. Predicting bioaccessibility

spatially using modelling approaches such as those outlined here is advantageous because it reduces the need for costly and time-consuming bioaccessibility extraction tests on large datasets, allowing for an estimation of PHE exposure over large spatial areas. Spatial datasets are also becoming more common, such as those by the BGS Geochemical Baseline Survey of the England (GBASE) and the UK Soil and Herbage Survey (UKSHS). The ability to predict and therefore use bioaccessibility data in risk assessment is likely to result in less costly remediation, compared with basing such assessments on pseudo-total data. For example, over conservative risk assessments in England have been suggested to have cost £200 million (DEFRA, 2012).

The spatial prediction of bioaccessibility can use pseudo-total element concentrations that are commonly used in human health risk assessment and provide a more realistic and potentially less conservative estimation of potential risk of PHE exposure to humans. For example, the ability to determine the soils within a catchment with the greatest risk of mobilisation can allow for targeted remediation strategies or highlight areas that need further investigation, such as geochemical characterisation. Additionally, the spatial prediction of flooding induced change in bioaccessibility may be used to highlight suitable areas within a catchment that require flood alleviation measures. For example, areas with a lower risk of PHE mobility may be more suitable for natural flood water retention methods. Sensitive areas within a catchment may benefit from flood alleviation measures to reduce the risk of flooding and potential PHE mobilisation. However, it is suggested that the spatial prediction of flooding induced change in bioaccessibility should be used to compliment existing datasets such as land use, topography and flood modelling outputs.

Catchment soils that are under agriculture are particularly susceptible to anthropogenic pressures though food production, recreation and redevelopment for housing. Therefore, the ability to model bioaccessibility and flooding induced change in bioaccessibility is important for human health risk assessment purposes for sites undergoing a change in land use. Additionally, changes in land use can alter the physico-chemical properties of soil and therefore potentially change PHE bioaccessibility.

It should be noted that such models are catchment specific and therefore random forest models need to be trained on individual catchment data sets; a finding also reported by Zhu *et al.* (2016).

6.4 Conclusions

The combination of the modelling approaches utilised within this chapter, and regional spatial data sets on soil elements to characterise the behaviour and mobility potential of PHEs in floodplain soils at a catchment level has been demonstrated. For example, the modelling of ISCs can determine the geochemical sources of PHEs and such information is useful for understanding the drivers of PHE mobility and availability, as demonstrated in Chapters 3 and 4.

Inundation of the Tyne catchment floodplain soils displayed low mobility into overlying waters (<2 %), however, it was determined that continuous inputs from elevated diffuse sources of PHE could lead to poor water quality status. The predicted frequency and size of flooding events in the UK suggest that the Tyne catchment will see an increased stream loading of PHEs (particularly Pb and Zn). Bioaccessibility increased after inundation for all PHEs in most of the soils, again suggesting that the predicted increase in flood events may result in greater PHE exposure from soils to humans in the Tyne catchment. These results were further corroborated by the production of a map (Figure 6.51) showing the predicted flooding induced change in Pb bioaccessibility in the Tyne catchment. This illustrated that inundation of soils was likely to increase Pb bioaccessibility in soils by approximately 30 % to 50 %. The implications for this are that bioaccessible Pb values may be raised above GAC values after periods of inundation. Pb values that are above GAC values may result in an increased risk of adverse health effects from Pb exposure in the Tyne catchment.

The partial dependence plots from the random forest models for each PHE showed different sets of predictor variables, emphasising the need to build independent PHE and catchment specific models. The fact that other PHEs are significant predictors suggests that there may be potential interaction effects occurring. For example, the increase of one PHE may result in the consequent increase in the bioaccessibility of another, through competition for binding sites and studies have shown that Pb can be preferentially absorbed over Cd, increasing Cd solubility (Xia *et al.,* 2017). Lead concentrations were shown to be positively related with Cd bioaccessible concentration; therefore, a possible interaction may be present. There is currently a knowledge gap in the literature regarding interaction effects between PHEs and how this can affect their overall bioaccessibility and toxicity to humans. The work in this chapter emphasises the need for further research into this area.

7. CONCLUSIONS

This project aimed to gain an understanding of the fate and behaviour of PHEs in a selection of soils from the Tyne catchment in North East England during wetting and drying events. The work is driven by the need for a better understanding of the influences of flooding on PHE behaviour, stemming from an increasing reliance by humans on floodplains and a predicted increase in the frequency and magnitude of flood events in the UK. Floodplain soils and sediments are known to be potential sinks and sources of PHEs (Macklin *et al.,* 1997; Overesch *et al.,*2007; Schulz-Zunkel, 2009), therefore any changes in the availability and mobility of PHEs in these soils could result in new exposure pathways to human and ecological receptors. The research here is specific to the soils of the Tyne catchment and has shown that:

- Flooding can mobilise PHEs (As, Cd, Cu, Pb and Zn) into overlying water and porewaters, even over short-term events
- Bioaccessibility of PHEs increases for some PHEs post flooding
- Wetting and drying events can change the solid phase distribution of PHEs
- It is possible to predict and consequently map PHEs and flooding induced change in PHE bioaccessibility in soils at a catchment scale

The following sections outline these findings in more detail.

7.1 Flooding induced mobility of PHEs

Flooding has been shown to result in the mobilisation of the PHEs investigated in this work to porewaters and overlying waters. Redox potential was shown to mainly follow the patterns of wetting and drying for the Tyne catchment soils: declining during wetting and increasing during drying. Flooding was shown to have little influence on the redox potential of mine spoil material. The patterns of porewater mobilisation varied between PHEs and soils, however some general patterns and trends can be outlined. Arsenic tended to follow the trend of redox potential, increasing in porewaters during declines in redox potential and decreasing in porewater during increasing redox potential. Copper generally showed the opposite pattern to As, decreasing during inundation and increasing post flooding. Zinc patterns were varied and inconsistent between soils.

7.2 Flooding induced change in PHE bioaccessibility

Flooding was shown to have the potential to increase PHE exposure to humans, but the risk from increased PHE exposure from the PHEs in this study is deemed to be low for the majority of soils. However, GACs were exceeded for bioaccessible concentrations of As for soil 1 and Pb by soils 2, 6, 7 and 8. Therefore, these soils present a greater risk of increases of PHE exposure to humans.

7.3 Flooding induced change in the solid phase distribution of PHEs

The results of this study suggest redox induced change occurs during wetting and drying events, even during short term wetting and drying events such as those in this study. Broad scale changes in the solid phase distribution of PHEs varied between soils. For arsenic, generally the greatest change was observed in the iron oxide components. Other PHEs exhibited redistribution between soil components, often to those that were more labile. A re-association of PHEs with more labile soil components can result in increased availability to human, wildlife or plant receptors and an greater mobilisation potential. The main findings of Chapters 3, 4 and 5 are summarised below in Table 7.1.

Table 7.1 Summary of the behaviour of PHEs in the eight soils used in chapters 3, 4 and 5.

PHE	Associated with:	Main drivers of mobilisation:	Flooding induced change in the bioaccessibility of PHEs	Flooding induced change in solid phase distribution of PHEs
As	Al-Fe oxides.	Reductive dissolution of Fe(III)(hydr)oxides.	Generally increased during flooding. Sulphide rich mining material displayed bioaccessibility increases during drying.	Possible redistribution to more labile components. E.g. From Fe to Al-Fe components.
Cd	Zn bearing minerals.	Not recorded.	Not recorded.	Possible redistribution to more labile components. E.g. porewater/organics components and carbonates.
Cu	Organics, exchangeable, Al-Fe oxides, Pb and Zn minerals.	Oxidation of Cu sulphide complexes and SOM complexes during soil drying.	Reductions in bioaccessibility for the majority of soils, except for 5 and 6. Cu inaccessible in soil 8. Increases observed during soil drying	Increase with the organic component for soils with higher SOM (3 and 6). Increases with less reactive components. E.g. Fe during flooding. Little change in solid phases of Cu for soil 8.
Pb	Pb bearing minerals, Mn oxides, Al-Fe oxides.	Not recorded.	Generally increased during flooding for soils 1 to 6. Sulphide rich mining material displayed bioaccessibility increases during drying.	Possible redistribution to more labile components. E.g. From Fe Al-Fe to Pb-Zn components.
Zn	Zn and Pb bearing minerals.	Variable but likely to include the reductive dissolution of Mn, Al and Fe oxides.	Generally increased during flooding for all soils.	Increases in Zn associated with the Ca component. Disassociation and re association between Zn and Pb-Zn components

7.4 Spatial predictions of PHE bioaccessibility and flooding induced change in bioaccessibility

PHEs were shown to be distributed between all ISCs, especially the Fe oxide, carbonate and lead and zinc bearing ISCs. Spatial modelling of bioaccessibility showed broad spatial patterns between the PHEs and the effect of sediment dilution below the North and South Tyne confluence, resulting in an area of lower PHE bioaccessibility. Broad spatial patterns of PHE bioaccessibility showed higher bioaccessible concentrations in the upper reaches of the South Tyne, and lower concentrations in the lower reaches, with various local hotspots in between. Mobilisation into overlying waters was generally low for the soils, and As and Cu had a positive relationship with bioaccessibility, suggesting that more bioaccessible soils have greater As and Cu mobility.

Random forest models were constructed to predict PHE bioaccessibility from pseudo-total element concentrations and ISCs. The pseudo-total metals were shown to produce a better performing model for predicting PHE bioaccessibility in the Tyne catchment floodplain soils than ISCs, although this outcome may change using a dataset from a different catchment. A similar approach was used by Wragg *et al.,* (2018) using ISCs as predictors for As bioaccessibility as opposed to pseudo-total element concentrations. It would be expected that the outcomes from model using ISCs and pseudo-total concentrations would be similar, as ISCS are modelled from pseudo-total concentrations. Therefore, it is suggested that models are built using both ISCs and pseudo-total concentrations, and the better performing model selected for the work required.

This work has shown that using a selection of geochemical characterisation tools such as bioaccessibility testing, the CISED methodology and the determination of ISCs can provide enough data to help understand the drivers of flooding induced change in mobility and bioaccessibility of PHEs, as well as being able to map these changes. Whilst verification of the final models was not possible because of time constraints, the methods employed here demonstrate the ability of random forest and multiple linear regression models to spatially predict bioaccessibility and subsequent flooding induced change in PHE bioaccessibility at a catchment scale.

With additional time, validation of the final model may be conducted using soil samples collected from neighbouring catchments of similar soil types and underlying geologies. The

model outline in Chapter 6 could be used to determine the areas within the second catchment that undergo the greatest change in flooding induced change in bioaccessibility. The required spatial elemental data would either need to be acquired through spatial sampling and physicochemical characterisation or by using a pre-existing dataset such as the NSI spatial datasets. Once the most vulnerable areas within the catchment had been highlighted by the model, repetition of the inundation and bioaccessibility work in Chapter 6 may be used to verify the model output.

7.5 Limitations of this work

The main limitations of this study are that the predictions made are based on soils within the Tyne catchment and cannot be extrapolated to other soils or geographical areas. This is because the models used in Chapter 6 of this work were built on the properties of the soils within the Tyne catchment. Other soils may result in different model outcomes, for example, studies on different soils by Pelfrêne *et al.,* (2013) and Wragg *et al.,* (2018) reported different significant predictor variables than those in this thesis. Additionally, different datasets may not meet the assumptions of all the models used within this work. For example, multiple linear regression requires that the response variable has a linear relationship with the predictor variables.

Secondly, the ability of the CISED method to detect redox induced changes in the solid phase distribution of PHEs can only really be used to determine overall patterns, rather than actual values. This is because of the propagation of error throughout the sequential extraction procedure and subsequent chemometric modelling.

Interaction effects between the differing PHEs were not accounted for in this study, as this was outside of the scope of work undertaken. However, interaction effects can occur through competition for binding sites, so the presence of one PHE may affect the availability and mobility of another. Interaction effects were suggested in this thesis (Section 6.3.8.2).

Finally, the models and methods used to spatially predict the bioaccessibility and flooding induced change in PHE bioaccessibility are in need of verification and application to other catchments to further test their suitability, as suggested in section 7.4. This work demonstrates the first steps in using such methods to build tools and models that may be of benefit to risk assessment processes in the future, especially in light of recent climate change predictions that forecast a greater change of flood events.

7.6 Future recommendations

There is scope for further research into the fate and behaviour of PHEs during wetting and drying events. The main recommendations arising from this work are to:

- Better understand redox induced change in PHE behaviour through the investigation of changes in PHE speciation. This will allow for a more detailed understanding of the change of PHE toxicity to receptors.
- Apply this work to different PHEs e.g other metals or organic contaminants such as polychlorinated biphenyls (PCBs) or polyaromatic hydrocarbons (PAHs).
- Conduct similar experiments on soils of differing characteristics and land uses to gain a broader understanding of the effect of these parameters on PHE behaviour during wetting and drying events.
- Undertake field experiments to upscale the results from laboratory scale studies to those of the field.
- Investigate the effects of interaction effects between PHEs on mobility and bioaccessibility as evidence has been shown in this work to suggest possible interaction effects between PHEs on their bioaccessibility.
- Validation of the final models of this thesis using neighbouring catchments with a similar underlying geology and soil type, as outlined in section 7.4

8. REFERENCE LIST

Abrahams, P.W. and Blackwell, N.L., 2013. The importance of ingested soils in supplying fluorine and lead to sheep grazing contaminated pastures in the Peak District mining area of Derbyshire, UK. *Environmental Science and Pollution Research*, *20*(12), pp.8729-8738.

Aceves, M.B., Grace, C., Ansorena, J., Dendooven, L. and Brookes, P.C., 1999. Soil microbial biomass and organic C in a gradient of zinc concentrations in soils around a mine spoil tip. *Soil Biology and Biochemistry*, *31*(6), pp.867-876.

Adaptation Sub-Committee. 2011 Adapting to climate change in the UK – Measuring progress.

Agency for Toxic Substances and Disease Registry (ATSDR). 2012. Toxicological profile for Cadmium. Atlanta, GA: U.S. Department of Health and Human Services, Public Health Service.

Albering, H.J., van Leusen, S.M., Moonen, E.J., Hoogewerff, J.A. and Kleinjans, J.C., 1999. Human health risk assessment: A case study involving heavy metal soil contamination after the flooding of the river Meuse during the winter of 1993-1994. *Environmental health perspectives*, *107*(1), p.37.

Allen, S. E., Grimshaw, H. M., Parkinson, J. A. & Quarmby, C., 1989. Chemical analysis of ecological materials. Blackwell, Scientific Publications, Oxford.

Allinson, D.W., and C. Dzialo. 1981. The influence of lead, cadmium and nickel on the growth of ryegrass and oats. *Plant Soil, 62*, pp.81–89.

Alloway, B.J. and Davies, B.E., 1971. Trace element content of soils affected by base metal mining in Wales. *Geoderma, 5*(3), pp.197-208.

Alloway, B.J., 2013. Sources of heavy metals and metalloids in soils. In *Heavy metals in soils* Springer, Dordrecht.

Alloway, B.J., 1995. Cadmium. In Heavy Metals in Soils (2nd edn.). (ed. B.J. Alloway). London: Blackie Academic & Professional.

Ander, E.L., Cave, M.R., Johnson, C.C. and Palumbo Roe, B., 2011. Normal background concentrations of contaminants in the soils of England. Available data and data exploration. *British Geological Survey Commissioned Report,* CR/11/145. p124

Anju, M. and Banerjee, D.K., 2011. Associations of cadmium, zinc, and lead in soils from a lead and zinc mining area as studied by single and sequential extractions. *Environmental Monitoring and Assessment*, *176*(1), pp.67-85.

Antić-Mladenović, S., Frohne, T., Kresović, M., Stärk, H.J., Tomić, Z., Ličina, V. and Rinklebe, J., 2017. Biogeochemistry of Ni and Pb in a periodically flooded arable soil: fractionation and redox-induced (im) mobilization. *Journal of Environmental Management*, 186, pp.141-150.

Appleton, J.D., Cave, M.R. and Wragg, J., 2012. Modelling lead bioaccessibility in urban topsoils based on data from Glasgow, London, Northampton and Swansea, UK. *Environmental Pollution*, *171*, pp.265-272.

Armitage, P.D., Bowes, M.J. and Vincent, H.M., 2007. Long-term changes in macroinvertebrate communities of a heavy metal polluted stream: the river Nent (Cumbria, UK) after 28 years. *River Research and Applications*, *23*(9), pp.997-1015.

Baldin, D.S., 1996. Effects of exposure to air and subsequent drying on the phosphate sorption characteristics of sediments from a eutrophic reservoir. *Journal of Limnology and Oceanography*. pp.1725-1732.

Bambra C, Robertson S, Kasim A, Smith J, Cairns-Nagi J M, Copeland A, Finlay N, Johnson K, 2014. "Healthy land? An examination of the area-level association between brownfield land and morbidity and mortality in England" *Environment and Planning. 46*(2), pp.433 – 454

Banks, V.J. Palumbo-Roe, B**.**, 2010. Synoptic monitoring as an approach to discriminating between point and diffuse source contributions to zinc loads in mining impacted catchments. *Journal of Environmental Monitoring*, *12*(9), pp.1684-1698.

Beane, S.J., Comber, S.D., Rieuwerts, J. and Long, P., 2016. Abandoned metal mines and their impact on receiving waters: a case study from Southwest England. *Chemosphere*, *153,* pp.294-306.

Bell, V., Kay, A., Cole, S., Jones, R., Moore, R. and Reynard, N., 2012. How might climate change affect river flows across the Thames Basin? An area-wide analysis using the UKCP09 Regional Climate Model ensemble. *Journal of Hydrology, 442*, 89-104.

Bergmann, J.D., Metker, L.W., McCain, W.C., Beall, P.A., Michie, M.W. and Lee, R.B., 2000. Intratracheal instillation of zinc-cadmium sulfide (ZnCdS) in Fischer 344 rats. *Inhalation Toxicology, 12*(4), pp.331-346.

Barker, L., Hannaford, J., Muchan, K., Turner, S. and Parry, S., 2016. The winter 2015/2016 floods in the UK: a hydrological appraisal. *Weather,* 71(12), pp.324-333.

Bissen, M., and Frimmel, F. H., 2003. Arsenic—a review. Part I: occurrence, toxicity, speciation, mobility. *Acta hydrochimica et hydrobiologica*, *31*(1), pp.9-18.

Blaylock, M.J., Salt, D.E., Dushenkov, S., Zakharova, O., Gussman, C., Kapulnik, Y., Ensley, B.D. and Raskin, I., 1997. Enhanced accumulation of Pb in Indian mustard by soil-applied chelating agents. *Environmental Science & Technology*, *31*(3), pp.860-865.

Bonneville, S., Van Cappellen, P. and Behrends, T., 2004. Microbial reduction of iron (III) oxyhydroxides: effects of mineral solubility and availability. *Chemical Geology*, *212*(3-4), pp.255-268.

Bower, J.A., Lister, S., Hazebrouck, G. and Perdrial, N., 2017. Geospatial evaluation of lead bioaccessibility and distribution for site specific prediction of threshold limits. *Environmental Pollution*, *229*, pp.290-299.

Brandon, E.F., Oomen, A.G., Rompelberg, C.J., Versantvoort, C.H., van Engelen, J.G. and Sips, A.J., 2006. Consumer product in vitro digestion model: bioaccessibility of contaminants and its application in risk assessment. *Regulatory Toxicology and Pharmacology, 44*(2), pp.161-171.

Breshears, D. D., Kirchner, T. B., Whicker, J. J., Field, J. P., & Allen, C. D., 2012. Modelling aeolian transport in response to succession, disturbance and future climate: Dynamic long-term risk assessment for contaminant redistribution. *Aeolian Research, 3*(4), pp.445-457.

Broadley, M.R., White, P.J., Hammond, J.P., Zelko, I. and Lux, A., 2007. Zinc in plants. *New Phytologist*, *173*, pp.677-702.

Brümmer, G., Tiller, K.G., Herms, U. and Clayton, P.M., 1983. Adsorption—desorption and/or precipitation—dissolution processes of zinc in soils. *Geoderma*, *31*(4), pp.337-354.

Calabrese, E.J., Stanek, E.J. and Gilbert, C.E., 1991. Evidence of soil-pica behaviour and quantification of soil ingested. *Human and Experimental Toxicology*, *10*(4), pp.245-249.

Canadian Council of Ministers of the Environment., 1999. Canadian soil quality guidelines for the protection of environmental and human health: Lead (1999). *Canadian environmental quality guidelines, 1999*, Canadian Council of Ministers of the Environment, Winnipeg.

Cave, M., Wragg, J. & Harrison, H., 2013. Measurement modelling and mapping of arsenic bioaccessibility in Northampton. United Kingdom. *Journal of Environmental Science and Health, Part A: Toxic/Hazardous Substances and Environmental Engineering, 48*, pp.629-640.

Cave, M.R., Milodowski, A.E. and Friel, E.N., 2004. Evaluation of a method for identification of host physico-chemical phases for trace metals and measurement of their solid-phase partitioning in soil samples by nitric acid extraction and chemometric mixture resolution. *Geochemistry: Exploration, Environment, Analysis, 4*(1), pp.71-86.

Chapman, P. and others ,1998. Ecotoxicology of metals in aquatic sediments: binding and release, bioavailability, risk assessment, and remediation, *55*, pp.2221-2243.

Charlatchka, R. and Cambier, P., 2000. Influence of reducing conditions on solubility of trace metals in contaminated soils. *Water, Air, And Soil Pollution, 118*, pp.143-168.

Charlton, M.B. & Arnell, N.W., 2014. Assessing the impacts of climate change on river flows in England using the UKCP09 climate change projections. *Journal of Hydrology, 519,* pp.1723-1738.

Chatterjee, S., 2009. Calcite and calcium oxalate sequestration of heavy metals. Temple University.

Ciscar, J. C., Iglesias, A., Feyen, L., Szabó, L., Van Regemorter, D., Amelung, B. and Soria, A., 2011. Physical and economic consequences of climate change in Europe. *Proceedings of the National Academy of Sciences, 108*(7), pp.2678-2683.

CL:AIRE (2010) Soil Generic Assessment Criteria for Human Health Risk Assessment. London. ISBN 978-1-905046-20-1

Coulthard, T., Ramirez, J., Fowler, H. and Glenis, V., 2012. Using the UKCP09 probabilistic scenarios to model the amplified impact of climate change on drainage basin sediment yield. *Hydrology and Earth System Sciences, 16*, pp.4401-4416.

Coulthard, T.J. and Macklin, M.G., 2003. Modelling long-term contamination in river systems from historical metal mining. *Geology, 31*, pp.451-454.

Courtin-Nomade, A., Waltzing, T., Evrard, C., Soubrand, M., Lenain, J.F., Ducloux, E., Ghorbel, S., Grosbois, C. and Bril, H., 2016. Arsenic and lead mobility: From tailing materials to the aqueous compartment. *Applied Geochemistry*, *64*, pp.10-21.

Cox, S.F., Chelliah, M.C., McKinley, J.M., Palmer, S., Ofterdinger, U., Young, M.E., Cave, M.R. and Wragg, J., 2013. The importance of solid-phase distribution on the oral bioaccessibility of Ni and Cr in soils overlying Palaeogene basalt lavas, Northern Ireland. *Environmental Geochemistry and Health, 35*(5), pp.553-567.

Cui, H., Fan, Y., Fang, G., Zhang, H., Su, B. and Zhou, J., 2016. Leachability, availability and bioaccessibility of Cu and Cd in a contaminated soil treated with apatite, lime and charcoal: a five-year field experiment. *Ecotoxicology and Environmental Safety*, *134*, pp.148-155.

Das, P., Samantaray, S. and Rout, G., 1997. Studies on cadmium toxicity in plants: a review. *Environmental Pollution, 98,* pp.29-36.

Dean, J.R., Elom, N.I. and Entwistle, J.A., 2017. Use of simulated epithelial lung fluid in assessing the human health risk of Pb in urban street dust. *Science of the Total Environment*, *579*, pp.387-395.

DEFRA (2012), Defra, Environmental Protection Act 1990: Part 2A Contaminated Land Statutory Guidance, in, Department for Environment, Food and Rural Affairs (Defra), 2012.

DEFRA, 2014. SP1010: Development of Category 4 Screening Levels for Assessment of Land Affected by Contamination – Policy Companion Document.

Dennis, I.A., Macklin, M.G., Coulthard, T.J. and Brewer, P.A., 2003. The impact of the October–November 2000 floods on contaminant metal dispersal in the River Swale catchment, North Yorkshire, UK. *Hydrological Processes, 17*(8), pp.1641-1657.

Denys, S., Caboche, J., Tack, K., Rychen, G., Wragg, J., Cave, M., Jondreville, C. and Feidt, C., 2012. *In vivo* validation of the unified BARGE method to assess the bioaccessibility of arsenic, antimony, cadmium, and lead in soils. *Environmental Science & Technology, 46*(11), pp.6252-6260.

Dong, D., Liu, L., Hua, X. and Lu, Y., 2007. Comparison of lead, cadmium, copper and cobalt adsorption onto metal oxides and organic materials in natural surface coatings. *Microchemical Journal, 85*(2), pp.270-275.

Du Laing, G., Rinklebe, J., Vandecasteele, B., Meers, E. and Tack, F. (2009). Trace metal behaviour in estuarine and riverine floodplain soils and sediments: a review. *Science of the Total Environment, 407*, pp.3972-3985.

Du Laing, G., Vanthuyne, D., Vandecasteele, B., Tack, F. and Verloo, M., 2007. Influence of hydrological regime on porewater metal concentrations in a contaminated sediment-derived soil. *Environmental Pollution, 147,* pp.615-625.

Eggleton, J. & Thomas, K., 2004. A review of factors affecting the release and bioavailability of contaminants during sediment disturbance events. *Environment International, 30*, pp.973-980.

Entwistle, J.A., Amaibi, P.M., Dean, J.R., Deary, M.E., Medock, D., Morton, J., Rodushkin, I. and Bramwell, L., 2019. An apple a day? Assessing gardeners' lead exposure in urban agriculture sites to improve the derivation of soil assessment criteria. *Environment international*, *122*, pp.130-141.

Environment Agency, 2007. Inter-laboratory comparison of in vitro bioaccessibility measurements for arsenic lead and nickel in soil, Science Report SC040060/SR2. Bristol: Environment Agency.

Environment Agency, 2009a. Soil guideline values for As in soil. Science Report SC050021/Arsenic SGV. Bristol: Environment Agency.

Environment Agency, 2009b. Soil guideline values for Cd in soil. Science Report SC050021/Cadmium SGV. Bristol: Environment Agency.

Environment Agency, 2011. Adapting to Climate Change: Advice for Flood and Coastal Erosion Risk Management Authorities. Environment Agency, September 2011, pp.29

Environment Agency, 2007. UK Soil and Herbage Pollutant Survey. Report No. 7: Environmental concentrations of heavy metals in UK soil and herbage. UKSHS Report 7. Bristol: Environment Agency.

Environment Agency, 2009. Soil Guideline Values for inorganic arsenic in soil Science Report SC050021/ arsenic SGV. Bristol: Environment Agency.

Environment Agency, 2019. GIS layer - Recorded flood outlines. Available from: https://data.gov.uk/dataset/16e32c53-35a6-4d54-a111-ca09031eaaaf/recorded-flood-outlines [Accessed September 2018]

EPA, U. 2003. Child-specific exposure factors handbook. National Center for Environmental Assessment, Washington, pp.121-135.

European Commission 2006. Proposal for a directive of the European Parliament and of the council on environmental quality standards in the field of water policy and amending Directive 2000/60/EC.

Filgueiras, A.V., Lavilla, I. and Bendicho, C., 2004. Evaluation of distribution, mobility and binding behaviour of heavy metals in surficial sediments of Louro River (Galicia, Spain) using chemometric analysis: a case study. *Science of the Total Environment, 330*, pp.115-129.

Florido, M.C., Madrid, F. and Ajmone-Marsan, F., 2011. Variations of metal availability and bio-accessibility in water-logged soils with various metal contents: in vitro experiments. *Water, Air, & Soil Pollution, 217*, pp.149-156.

Forstner, U., Heise, S., Schwartz, R., Westrich, B. and Ahlf, W., 2004. Historical Contaminated Sediments and Soils at the River Basin Scale. *Journal of Soils and Sediments, 4*, pp.247-260.

Fosmire, G.J., 1990. Zinc toxicity. *The American Journal of Clinical Nutrition, 51*, pp.225-227.

Foulds, S.A., Brewer, P.A., Macklin, M.G., Haresign, W., Betson, R.E. and Rassner, S.M.E., 2014. Flood-related contamination in catchments affected by historical metal mining: an unexpected and emerging hazard of climate change. *Science of the Total Environment, 476,* pp.165-180.

Fraga, C.G., 2005. Relevance, essentiality and toxicity of trace elements in human health. *Molecular Aspects of Medicine, 26,* 235-244.

Frohne, T., Rinklebe, J., Diaz-Bone, R.A., Du Laing and G., 2011. Controlled variation of redox conditions in a floodplain soil: Impact on metal mobilisation and biomethylation of arsenic and antimony. *Geoderma, 160,* pp.414-424.

Furman, O., Strawn, D.G. and McGeehan, S., 2007. Sample drying effects on lead bioaccessibility in reduced soil. *Journal of Environmental Quality, 36*, pp.899-903.

Garrett, R.G., 2000. Natural sources of metals to the environment. *Human and Ecological Risk Assessment, 6*, pp.945-963.

Gasser, U.G., Walker, W.J., Dahlgren, R.A., Borch, R.S. and Burau R.G., 1996. Lead release from smelter and mine waste impacted materials under simulated gastric conditions s and relation to speciation. *Environmental Science and Technology, 30*, pp.761–769

Geeson, N.A., Abrahams, P.W., Murphy, M.P. and Thornton, I., 1998. Fluorine and metal enrichment of soils and pasture herbage in the old mining areas of Derbyshire, UK. *Agriculture, Ecosystems & Environment, 68*(3), pp.217-231.

Goldhaber, S.B., 2003. Trace element risk assessment: essentiality vs. toxicity. *Regulatory Toxicology and Pharmacology, 38*(2), pp.232-242.

Gozzard, E., Mayes, W.M., Potter, H.A.B. and Jarvis, A.P., 2011. Seasonal and spatial variation of diffuse (non-point) source zinc pollution in a historically metal mined river catchment, UK. *Environmental Pollution*, *159*(10), pp.3113-3122.

Green, I., Boughey, K. and Diaz, A., 2014. Potentially Toxic Metals in Historic Landfill Sites: Implications for Grazing Animals. *Water, Air and Soil Pollution, 225*, pp.1-12.

Greenwood, P., Walling, D.E. and Quine, T.A., 2013. Using caesium-134 and cobalt-60 as tracers to assess the remobilisation of recently deposited overbank-derived sediment on river floodplains during subsequent inundation events. *Earth Surface Processes and Landforms, 39*, pp.228-244.

Grybos, M., Davranche, M., Gruau, G. and Petitjean, P., 2007. Is trace metal release in wetland soils controlled by organic matter mobility or Fe-oxyhydroxides reduction. *Journal of Colloid and Interface Science, 314*(2), pp.490-501.

Guney, M., Bourges, C.M.J., Chapuis, R.P. and Zagury, G.J., 2017. Lung bioaccessibility of As, Cu, Fe, Mn, Ni, Pb, and Zn in fine fraction (< 20 µm) from contaminated soils and mine tailings. *Science of the Total Environment*, *579*, pp.378-386.

Haines, A., Kovats, R. S., Campbell-Lendrum, D., and Corvalán, C., 2006. Climate change and human health: impacts, vulnerability and public health. *Public Health, 120*(7), pp.585-596.

Nagajyoti, P.C., Lee, K.D. and Sreekanth, T.V.M., 2010. Heavy metals, occurrence and toxicity for plants: a review. *Environmental Chemistry Letters*, *8*(3), pp.199-216.

Hamilton, E.M., Barlow, T.S., Gowing, C.J. and Watts, M.J., 2015. Bioaccessibility performance data for fifty-seven elements in guidance material BGS 102. *Microchemical Journal*, 123, pp.131-138.

Harris, K. L., Banks, L. D., Mantey, J. A., Huderson, A. C., and Ramesh, A., 2013. Bioaccessibility of polycyclic aromatic hydrocarbons: relevance to toxicity and carcinogenesis. *Expert Opinion on Drug Metabolism and Toxicology. 9,* pp.1465-1480.

Hettiarachchi, G.M. and Pierzynski, G.M., 2002. In situ stabilization of soil lead using phosphorus and manganese oxide. *Journal of Environmental Quality*, *31*(2), pp.564-572.

Hettiarachchi, G.M. and Pierzynski, G.M., 2004. Soil lead bioavailability and in situ remediation of lead-contaminated soils: A review. *Environmental Progress, 23*, pp.78-93.

Hofacker, A.F., Voegelin, A., Kaegi, R., Weber, F.A. and Kretzschmar, R., 2013. Temperature-dependent formation of metallic copper and metal sulfide nanoparticles during flooding of a contaminated soil. *Geochimica et Cosmochimica Acta*, *103*, pp.316-332.

Hogan, K., Marcus, A., Smith, R. and White, P., 1998. Integrated exposure uptake biokinetic model for lead in children: empirical comparisons with epidemiologic data. *Environmental Health Perspectives, 106*(6), p.1557.

Honma, T., Ohba, H., Kaneko-Kadokura, A., Makino, T., Nakamura, K. and Katou, H., 2016. Optimal soil Eh, pH, and water management for simultaneously minimizing arsenic and cadmium concentrations in rice grains. *Environmental Science and Technology*, *50*(8), pp.4178-4185.

Hughes, M.F., 2002. Arsenic toxicity and potential mechanisms of action. *Toxicology Letters, 133*, pp.1-16.

Huang, J.H., 2014. Impact of microorganisms on arsenic biogeochemistry: a review. *Water, Air, & Soil Pollution*, *225*(2), p.1848.

Huang, H., Jia, Y., Sun, G.X. and Zhu, Y.G., 2012. Arsenic speciation and volatilization from flooded paddy soils amended with different organic matters. *Environmental Science and Technology, 46*(4), pp.2163-2168.

Hysong, T. A., Burgess, J. L., Garcia, M. E. C., and O'Rourke, M. K., 2003. House dust and inorganic urinary arsenic in two Arizona mining towns. *Journal of Exposure Science and Environmental Epidemiology,13(*3), pp.211-218.

ICRCL. 1990. Notes on the restoration and aftercare of metalliferous mining sites for pasture and grazing. Interdepartmental Committee on the Redevelopment of Contaminated Land Guidance Note 70/90. London: Department of the Environment. P.14

Indraratne, S.P. and Kumaragamage, D., 2017. Flooding-induced mobilisation of potentially toxic trace elements from uncontaminated, calcareous agricultural soils. *Canadian Journal of Soil Science, 98*(1), pp.103-113.

Intergovermental Panel on Climate Change., 2018. *Global Warming of 1.5 °C*. Switzerland. ISBN 978-92-9169-151-7

Järup, L., Rogenfelt, A., Elinder, C.G., Nogawa, K. and Kjellström, T., 1983. Biological half-time of cadmium in the blood of workers after cessation of exposure. *Scandinavian Journal of Work, Environment and Health*, pp.327-331.

Jenkins, G. J., Murphy, J. M., Sexton, D. M. H., Lowe, J. A., Jones, P. and Kilsby, C. G., 2009. *UK Climate Projections: Briefing report.* Met Office Hadley Centre, Exeter, UK.

Jenne, E.A., 1997. Trace element sorption by soils and sediments. Sites and processes, *Proceedings of the Symposium on Molybdenum in the Environment, vol. 2,* Dekker, New York. pp. 425-553

Jones, M.R., Fowler, H.J., Kilsby, C.G. and Blenkinsop, S., 2013. An assessment of changes in seasonal and annual extreme rainfall in the UK between 1961 and 2009. *International Journal of Climatology, 33,* pp.1178-1194.

Joubert, A.V.P., Lucas, L., Garrido, F., Joulian, C. and Jauzein, M., 2007. Effect of temperature, gas phase composition, pH and microbial activity on As, Zn, Pb and Cd mobility in selected soils in the Ebro and Meuse Basins in the context of global change. *Environmental pollution*, *148*(3), pp.749-758.

Jurjanz, S. and Rychen, G., 2007. *In Vitro* Bioaccessibility of Soil-Bound Polycyclic Aromatic Hydrocarbons in Successive Digestive Compartments in Cows. *Journal of Agricultural Food Chemistry, 55,* pp.8800-8805.

Kapaj, S., Peterson, H., Liber, K., & Bhattacharya, P., 2006. Human health effects from chronic arsenic poisoning–a review. *Journal of Environmental Science and Health Part A,* 41, pp.2399-2428.

Kay, A. and Jones, R., 2012. Comparison of the use of alternative UKCP09 products for modelling the impacts of climate change on flood frequency. *Climatic Change, 114*, pp.211-230.

Khan, H.M., Chaudhry, Z.S., Ismail, M. and Khan, K., 2010. Assessment of radionuclides, trace metals and radionuclide transfer from soil to food of Jhangar Valley (Pakistan) using gamma-ray spectrometry. *Water, Air, and Soil Pollution, 213,* pp.353-362.

Khaokaew, S., Chaney, R.L., Landrot, G., Ginder-Vogel, M. and Sparks, D.L., 2011. Speciation and release kinetics of cadmium in an alkaline paddy soil under various flooding periods and draining conditions. *Environmental Science and Technology*, *45*(10), pp.4249-4255.

Kierczak, J., Neel, C., Aleksander-Kwaterczak, U., Helios-Rybicka, E., Bril, H. and Puziewicz, J., 2008. Solid speciation and mobility of potentially toxic elements from natural and contaminated soils: a combined approach. *Chemosphere, 73*(5), pp.776-784.

Kinouchi, T., Yoshimura, K. and Omata, T., 2015. Modeling radiocesium transport from a river catchment based on a physically-based distributed hydrological and sediment erosion model. *Journal of Environmental Radioactivity, 139*, pp.407-415.

Komárek, M., Ettler, V., Chrastný, V. and Mihaljevič, M., 2008. Lead isotopes in environmental sciences: a review. *Environment International,* 34, pp.562-577.

Kursa, M.B. and Rudnicki, W.R., 2010. Feature selection with the Boruta package. *Journal of Statistical Software*, *36*(11), pp.1-13.

Lake, I.R., Foxall, C.D., Fernandes, A., Lewis, M., Rose, M., White, O., Lovett, A.A., White, S., Dowding, A. and Mortimer, D., 2015. The effects of flooding on dioxin and PCB levels in food produced on industrial river catchments. *Environment International*, *77*, pp.106-115.

Li, J., Xue, Q., Wang, P., Li, Z. and Liu, L., 2014. Effect of drying-wetting cycles on leaching behaviour of cement solidified lead-contaminated soil. *Chemosphere, 117*, pp.10-13.

Li, X., Poon, C. S., and Liu, P. S., 2001. Heavy metal contamination of urban soils and street dusts in Hong Kong. *Applied Geochemistry, 16,* pp.1361-1368.

Lieser, K., 1995. Radionuclides in the geosphere: sources, mobility, reactions in natural waters and interactions with solids. *Radiochimca Acta, 70*, pp.355-376.

Lijzen, J.P.A., Baars, A.J., Otte, P.F., Rikken, M., Swartjes, F.A., Verbruggen, E.M.J. and Van Wezel, A.P., 2001. Technical evaluation of the Intervention Values for Soil/sediment and Groundwater. Human and ecotoxicological risk assessment and derivation of risk limits for soil, aquatic sediment and groundwater.

Lin, J., Zhang, S., Liu, D., Yu, Z., Zhang, L., Cui, J., Xie, K., Li, T. and Fu, C., 2018. Mobility and potential risk of sediment-associated heavy metal fractions under continuous drought-rewetting cycles. *Science of The Total Environment*, 625, pp.79-86.

Liu, B., Qu, D., Chen, X., Li, Q. and Peng, L., 2013. Effects of flooding and ferrhydrite on copper fractionation in paddy soil. *Procedia Environmental Sciences*, *18*, pp.135-142.

Lowe, J.A., Bernie, D., Bett, P., Bricheno, L., Brown, S., Calvert, D., Eagle, K. *et al.,* 2018. UKCP18 Science Overview report. Crown Copyright. Met office.

Luo, C., Liu, C., Wang, Y., Liu, X., Li, F., Zhang, G., and Li, X., 2011. Heavy metal contamination in soils and vegetables near an e-waste processing site, south China. *Journal of Hazardous Materials*, *186,* pp.481-490.

Lynch, S.F., Batty, L.C. and Byrne, P., 2014. Environmental risk of metal mining contaminated river bank sediment at redox-transitional zones. *Minerals, 4*, pp.52-73.

Macklin, M.G., Brewer, P.A., Hudson-Edwards, K.A., Bird, G., Coulthard, T.J., Dennis, I.A., Lechler, P.J., Miller, J.R. and Turner, J.N., 2006. A geomorphological approach to the management of rivers contaminated by metal mining. *Geomorphology*, *79*(3), pp.423-447.

Macklin, M.G., Hudson-Edwards, K.A. and Dawson, E.J., 1997. The significance of pollution from historic metal mining in the Pennine orefields on river sediment contaminant fluxes to the North Sea. *Science of the Total Environment*, *194*, pp.391-397.

Macklin, M.G., Ridgway, J., Passmore, D.G. and Rumsby, B.T., 1994. The use of overbank sediment for geochemical mapping and contamination assessment: results from selected English and Welsh floodplains. *Applied Geochemistry*, *9*(6), pp.689-700.

Madrid, F., Biasoili, M. and Ajmone-Marsan, F., 2008. Availability and Bioaccessibility of Metals in Fine Particles of Some Urban Soils. *Archives of Environmental Contamination and Toxicology, 55,* pp.21-32.

Magalhaes, M., 2002. Arsenic. An environmental problem limited by solubility. *Pure and Applied Chemistry, 74*(10), pp.1843-1850.

Martin, J.M., Nirel, P. and Thomas, A.J., 1987. Sequential extraction techniques: promises and problems. *Marine Chemistry*, *22*(2-4), pp.313-341.

Masscheleyn, P.H., Delaune, R.D. and Patrick Jr, W.H., 1991. Effect of redox potential and pH on arsenic speciation and solubility in a contaminated soil. *Environmental Science and Technology, 25*(8), pp.1414-1419.

Matinho Reis, A.P., Shepherd, T., Nowell, G. Cahcada, A., Duarte, A.C., Cave, M., Wgarr, J., Patinha, C., Dias, A., Rocha, F., Ferreira da Silva, E., Sousa, A.J., Prazeres, C. and Batista, M.J. 2016. Source and pathway analysis of lead and polycyclic aromatic hydrocarbons in Lisbon urban soils. *Science of the Total Environment, 573,* pp.324–336

Mayes, W.M., Johnston, D., Potter, H.A.B. and Jarvis, A.P., 2009. A national strategy for identification, prioritisation and management of pollution from abandoned non-coal mine sites in England and Wales. I.: methodology development and initial results. *Science of the Total Environment*, *407*(21), pp.5435-5447.

McCann, C.M., Gray, N.D., Tourney, J., Davenport, R.J., Wade, M., Finlay, N., Hudson-Edwards, K.A. and Johnson, K.L., 2015. Remediation of a historically Pb contaminated soil using a model natural Mn oxide waste. *Chemosphere*, *138*, pp.211-217.

McCauley, C. Jones and J. Jacobsen (2009) Soil pH and Organic Matter. Nutrient management modules 8, #4449-8 Montana State University Extension Service, Bozeman, Montana pp. 1–12

Meharg, A.A. and Hartley-Whitaker, J., 2002. Arsenic uptake and metabolism in arsenic resistant and nonresistant plant species. *New Phytologist, 154*, pp.29-43.

Meunier, L., Walker, S.R., Wragg, J., Parsons, M.B., Koch, I., Jamieson, H.E. and Reimer, K.J., 2010. Effects of soil composition and mineralogy on the bioaccessibility of arsenic from tailings and soil in gold mine districts of Nova Scotia. *Environmental Science & Technology, 44*(7), pp.2667-2674.

Mielke, H.W., Gonzales, C.R., Smith, M.K. and Mielke, P.W., 1999. The urban environment and children's health: soils as an integrator of lead, zinc, and cadmium in New Orleans, Louisiana, USA. *Environmental Research, 81*(2), pp.117-129.

Miller, W.P. and Mc Fee, W.W., 1983. Distribution of Cadmium, Zinc, Copper, and Lead in Soils of Industrial Northwestern Indiana 1. *Journal of Environmental Quality*, *12*(1), pp.29-33.

Mitsunobu, S., Harada, T. and Takahashi, Y., 2006. Comparison of antimony behavior with that of arsenic under various soil redox conditions. *Environmental Science and Technology, 40,* pp.7270-7276.

Molina, R.M., Schaider, L.A., Donaghey, T.C., Shine, J.P. and Brain, J.D., 2013. Mineralogy affects geoavailability, bioaccessibility and bioavailability of zinc. *Environmental Pollution, 182,* pp.217-224.

Müller-Höcker, J., Meyer, U., Wiebecke, B., Hübner, G., Eife, R., Kellner, M. and Schramel, P., 1988. Copper storage disease of the liver and chronic dietary copper intoxication in two further German infants mimicking Indian childhood cirrhosis. *Pathology-Research and Practice, 183*(1), pp.39-45.

Nagajyoti, P.C., Lee, K.D. and Sreekanth, T.V.M., 2010. Heavy metals, occurrence and toxicity for plants: a review. *Environmental Chemistry Letters*, *8*(3), pp.199-216.

Naidu, R., Semple, K.T., Megharaj, M., Juhasz, A.L., Bolan, N.S., Gupta, S.K., Clothier, B.E. and Schulin, R., 2008. Bioavailability: Definition, assessment and implications for risk assessment. *Developments in Soil Science*, *32*, pp.39-51.

Nathanail, C.P., McCaffrey, C., Gillet, A.G., Ogden, R.C. and Nathanail, J.F., 2015. The LQM/CIEH S4ULs for Human Health Risk Assessment. Land Quality Press, Nottingham

Nelson, C.M., Li, K., Obenour, D.R., Miller, J., Misenheimer, J.C., Scheckel, K., Betts, A., Juhasz, A., Thomas, D.J. and Bradham, K.D., 2018. Relating soil geochemical properties to arsenic bioaccessibility through hierarchical modelling. *Journal of Toxicology and Environmental Health, Part A, 81*(6), pp.160-172.

Newhook, R., Hirtle, H., Byrne, K. and Meek, M., 2003. Releases from copper smelters and refineries and zinc plants in Canada: human health exposure and risk characterization. *Science of the Total Environment, 301,* pp.23-41.

Nicholson, F.A., Smith, S.R., Alloway, B.J., Carlton-Smith, C. & Chambers, B.J., 2003. An inventory of heavy metals inputs to agricultural soils in England and Wales. *Science of the Total Environment, 311*, pp.205-219.

Nuttall, C.A. and Younger, P.L., 1999, Reconnaissance hydrogeochemical evaluation of an abandoned Pb–Zn orefield, Nent Valley, Cumbria, UK. *In Proceedings of the Yorkshire Geological and Polytechnic Society*, *52*(4), pp.395-405

Nuttall, C.A. and Younger, P.L., 2002. Secondary minerals in the abandoned mines of Nenthead, Cumbria as sinks for pollutant metals. *Geological Society, London, Special Publications, 198,* pp.241-250

Okorie, A., Entwistle, J. and Dean, J.R., 2010. The optimization of microwave digestion procedures and application to an evaluation of potentially toxic element contamination on a former industrial site. *Talanta*, *82*(4), pp.1421-1425.

Okorie, A., Entwistle, J. and Dean, J.R., 2011. The application of in vitro gastrointestinal extraction to assess oral bioaccessibility of potentially toxic elements from an urban recreational site. *Applied Geochemistry, 26*(5), pp.789-796.

O'Reilly, S.E. and Hochella, M.F., 2003. Lead sorption efficiencies of natural and synthetic Mn and Fe-oxides. *Geochimica et Cosmochimica Acta, 67*(23), pp.4471-4487.

Overesch, M., Rinklebe, J., Broll, G. and Neue, H.U., 2007. Metals and arsenic in soils and corresponding vegetation at Central Elbe river floodplains (Germany). *Environmental Pollution*, *145*(3), pp.800-812.

Palumbo-Roe, B. and Klinck, B., 2007. Bioaccessibility of arsenic in mine waste-contaminated soils: A case study from an abandoned arsenic mine in SW England (UK). *Journal of Environmental Science and Health Part A, 42*(9), pp.1251-1261.

Palumbo-Roe, B., Cave, M., Klinck, B., Wragg, J., Taylor, H., O'Donnell, K. et al., (2005). Bioaccessibility of arsenic in soils developed over Jurassic ironstones in eastern England. *Environmental Geochemistry and Health, 27*, pp.121-130.

Palumbo-Roe, B., Wragg, J. and Cave, M., 2015. Linking selective chemical extraction of iron oxyhydroxides to arsenic bioaccessibility in soil. *Environmental pollution, 207*, pp.256-265.

Pan, J., Plant, J. A., Voulvoulis, N., Oates, C. J., and Ihlenfeld, C., 2010. Cadmium levels in Europe: implications for human health. *Environmental Geochemistry and Health, 32*, pp.1-12.

Park, J. H., Choppala, G. K., Bolan, N. S., Chung, J. W., and Chuasavathi, T., 2011. Biochar reduces the bioavailability and phytotoxicity of heavy metals. *Plant and Soil, 348*, pp.439-451.

Pedersen, H.D., Postma, D. and Jakobsen, R., 2006. Release of arsenic associated with the reduction and transformation of iron oxides. *Geochimica et Cosmochimica Acta, 70*(16), pp.4116-4129.

Pelfrêne, A., Waterlot, C. and Douay, F., 2013. Influence of land use on human bioaccessibility of metals in smelter-impacted soils. *Environmental Pollution, 178*, pp.80-88.

Pelfrêne, A., Waterlot, C., Mazzuca, M., Nisse, C., Cuny, D., Richard, A., Denys, S., Heyman, C., Roussel, H., Bidar, G. and Douay, F., 2012. Bioaccessibility of trace elements as affected by soil parameters in

smelter-contaminated agricultural soils: A statistical modelling approach. *Environmental Pollution, 160,* pp.130-138.

Pelfrêne, A., Waterlot, C., Mazzuca, M., Nisse, C., Bidar, G. and Douay, F., 2011. Assessing Cd, Pb, Zn human bioaccessibility in smelter-contaminated agricultural topsoils (northern France). *Environmental Geochemistry and Health*, *33*(5), pp.477-493.

Pimentel, D., Harvey, C., Resosudarmo, P., Sinclair, K., Kurz, D., McNair, M. and Blair, R., 1995. Environmental and economic costs of soil erosion and conservation benefits. Science-AAAS-Weekly *Paper Edition, 267*(5201), pp.1117-1122.

Pinto, A., Mota, A., De Varennes, A. and Pinto, F., 2004. Influence of organic matter on the uptake of cadmium, zinc, copper and iron by sorghum plants. *Science of the Total Environment, 326*, pp.239-247.

Pouschat, P. and Zagury, G.J., 2008. Bioaccessibility of chromium and copper in soils near CCA-treated wood poles. *Practice Periodical of Hazardous, Toxic, and Radioactive Waste Management*, *12*(3), pp.216-223.

Ratnaike, R.N., 2003. Acute and chronic arsenic toxicity. *Postgraduate Medical Journal, 79*(933), pp.391-396.

Rawlins, B G, McGrath, S P, Scheib, A J, Breward, N, Cave, M, Lister, T R, Ingham, M, Gowing, C and Carter, S. 2012. *The Advanced Soil Geochemical Atlas of England and Wales*. Keyworth, Nottingham: British Geological Survey.

Reis, A.P., Patinha, C., Wragg, J., Dias, A.C., Cave, M., Sousa, A.J., Costa, C., Cachada, A., Da Silva, E.F., Rocha, F. and Duarte, A., 2014. Geochemistry, mineralogy, solid-phase fractionation and oral bioaccessibility of lead in urban soils of Lisbon. *Environmental Geochemistry and Health, 36*(5), pp.867-881.

Rinklebe, J., Franke, C. and Neue, H.U., 2007. Aggregation of floodplain soils based on classification principles to predict concentrations of nutrients and pollutants. *Geoderma*, *141*(3-4), pp.210-223.

Rinklebe, J., Shaheen, S.M., Schröter, F. and Rennert, T., 2016. Exploiting biogeochemical and spectroscopic techniques to assess the geochemical distribution and release dynamics of chromium and lead in a contaminated floodplain soil. *Chemosphere*, *150*, pp.390-397.

Robson, T.C., Braungardt, C.B., Rieuwerts, J. and Worsfold, P., 2014. Cadmium contamination of agricultural soils and crops resulting from sphalerite weathering. *Environmental Pollution*, *184*, pp.283-289.

Roussel, H., Waterlot, C., Pelfrêne, A., Pruvot, C., Mazzuca, M. and Douay, F., 2010. Cd, Pb and Zn oral bioaccessibility of urban soils contaminated in the past by atmospheric emissions from two lead and zinc smelters. *Archives of Environmental Contamination and Toxicology, 58*(4), pp.945-954.

Rowland, C.S.; Morton, R.D.; Carrasco, L.; McShane, G.; O'Neil, A.W.; Wood, C.M. 2017 Land Cover Map 2015 (25m raster, GB). NERC Environmental Information Data Centre. https://doi.org/10.5285/bb15e200-9349-403c-bda9-b430093807c7

Roy, M. and McDonald, L.M., 2015. Metal Uptake in Plants and Health Risk Assessments in Metal-Contaminated Smelter Soils. *Land Degradation & Development, 26*(8), pp.785-792.

Ruby, M.V., Davis, A., Link, T.E., Schoof, R., Chaney, R.L., Freeman, G.B. and Bergstrom, P., 1993. Development of an in vitro screening test to evaluate the *in vivo* bioaccessibility of ingested mine-waste lead. *Environmental science & technology, 27*(13), pp.2870-2877.

Ruby, M.V., Schoof, R., Brattin, W., Goldade, M., Post, G., Harnois, M., Mosby, D.E., Casteel, S.W., Berti, W., Carpenter, M. and Edwards, D., 1999. Advances in evaluating the oral bioavailability of inorganics in soil for use in human health risk assessment. *Environmental Science & Technology*, *33*(21), pp.3697-3705.

Ruby, M.V. and Lowney, Y.W., 2012. Selective soil particle adherence to hands: implications for understanding oral exposure to soil contaminants. *Environmental Science and Technology*, *46*(23), pp.12759-12771.

Sarkar, Deepayan (2008) Lattice: Multivariate Data Visualization with R. Springer, New York. ISBN 978-0-387-75968-5

Sauve, S., McBride, M. and Hendershot, W., 1998. Soil solution speciation of lead (II): Effects of organic matter and pH. *Soil Science Society of America Journal, 62*, pp.618-621.

Schaider, L.A., Senn, D.B., Brabander, D.J., McCarthy, K.D. and Shine, J.P., 2007. Characterization of zinc, lead, and cadmium in mine waste: implications for transport, exposure, and bioavailability. *Environmental Science and Technology, 41*(11), pp.4164-4171.

Schönbrunner, I.M., Preiner, S. and Hein, T. (2012). Impact of drying and re-flooding of sediment on phosphorus dynamics of river-floodplain systems. *Science of the Total Environment, 432,* pp.329-337.

Schulz-Zunkel, C. and Krueger, F., 2009. Trace metal dynamics in floodplain soils of the River Elbe: a review. *Journal of environmental quality, 38,* pp.1349-1362.

Sharma, S.K., Sehkon, N.S., Deswal, S. and John, S., 2009. Transport and fate of copper in soils. *International Journal of Civil and Environmental Engineering*, *1*(1), pp.19-39.

Shore, R.F. and Douben, P.E. (1994). The ecotoxicological significance of cadmium intake and residues in terrestrial small mammals. *Ecotoxicology and Environmental Safety, 29*, pp.101-112.

Singer, M.B., Aalto, R., James, L.A., Kilham, N.E., Higson, J.L. and Ghoshal, S., 2013. Enduring legacy of a toxic fan via episodic redistribution of California gold mining debris. *Proceedings of the National Academy of Sciences of the United States of America, 110,* pp.18436-18441.

Sipter, E., Rózsa, E., Gruiz, K., Tátrai, E. and Morvai, V., 2008. Site-specific risk assessment in contaminated vegetable gardens. *Chemosphere*, *71*(7), pp.1301-1307.

Skerfving, S., Löfmark, L., Lundh, T., Mikoczy, Z. and Strömberg, U., 2015. Late effects of low blood lead concentrations in children on school performance and cognitive functions. *Neurotoxicology*, 49, pp.114-120.

Smedley, P.L. and Kinniburgh, D.G., 2013. Arsenic in groundwater and the environment. *In Essentials of Medical Geology*. Springer Netherlands. pp. 279-310

Smith, L., Liang, Q., James, P. and Lin, W., 2017. Assessing the utility of social media as a data source for flood risk management using a real-time modelling framework. *Journal of Flood Risk Management*, 10(3), pp.370-380.

Smith, E., Naidu, R. and Alston, A.M., 1998. Arsenic in the soil environment: a review. *Advances in Agronomy, 64*, pp.149-195.

Smith, K.M., Abrahams, P.W., Dagleish, M.P. and Steigmajer, J., 2009. The intake of lead and associated metals by sheep grazing mining-contaminated floodplain pastures in mid-Wales, UK: I. Soil ingestion, soil–metal partitioning and potential availability to pasture herbage and livestock. *Science of the Total Environment, 407*(12), pp.3731-3739.

Smith, S. R., 2009. A critical review of the bioavailability and impacts of heavy metals in municipal solid waste composts compared to sewage sludge. *Environment International, 35*(1), 142-156.

Tack, F.M.G., Van Ranst, E., L., C. and Vandenberghe, R.E. (2006). Soil solution Cd Cu and Zn concentrations as affected by short-time drying or wetting: The role of hydrous oxides of Fe and Mn. *Geoderma, 137,* pp.83-89.

Tangahu, B.V., Abdullah, S., Rozaimah, S., Basri, H., Idris, M., Anuar, N. and Mukhlisin, M., 2011. A review on heavy metals (As, Pb, and Hg) uptake by plants through phytoremediation. *International Journal of Chemical Engineering*, *2011*.

Tessier, A., Campbell, P.G. and Bisson, M., 1979. Sequential extraction procedure for the speciation of particulate trace metals. *Analytical Chemistry*, *51*(7), pp.844-851.

Teuchies, J., Singh, G., Bervoets, L. and Meire, P., 2013. Land use changes and metal mobility: Multi-approach study on tidal marsh restoration in a contaminated estuary. *Science of The Total Environment, 449,* pp.174-183.

Thompson, J. and Bannigan, J., 2008. Cadmium: toxic effects on the reproductive system and the embryo. *Reproductive Toxicology, 25,* pp.304-315.

Tong, S., Schirnding, Y.E.V. and Prapamontol, T., 2000. Environmental lead exposure: a public health problem of global dimensions. *Bulletin of the World Health Organization, 78*(9), pp.1068-1077.

Vahter, M. and Concha, G., 2001. Role of metabolism in arsenic toxicity. *Pharmacology & Toxicology: MiniReview*, *89*(1), pp.1-5.

Van de Wiele, T. R., Oomen, A. G., Wragg, J., Cave, M., Minekus, M., Hack, A. and Sips, A. J. 2007. Comparison of five *in vitro* digestion models to *in vivo* experimental results: lead bioaccessibility in the human gastrointestinal tract. *Journal of Environmental Science and Health Part A, 42(*9), pp.1203-1211.

Van der Geest, Harm, G. and Paumen, M.L., 2008. Dynamics of metal availability and toxicity in historically polluted floodplain sediments. *Science of the Total Environment, 406*, pp.419-425.

Verstraeten, S.V., Aimo, L. and Oteiza, P.I., 2008. Aluminium and lead: molecular mechanisms of brain toxicity. *Archives of Toxicology, 82*(11), pp.789-802.

Visser, A., Kroes, J., van Vliet, M.T., Blenkinsop, S., Fowler, H.J. and Broers, H.P., 2012. Climate change impacts on the leaching of a heavy metal contamination in a small lowland catchment. *Journal of Contaminant Hydrology, 127*, pp.47-64.

Wang, S. and Mulligan, C.N., 2006. Effect of natural organic matter on arsenic release from soils and sediments into groundwater. *Environmental Geochemistry and Health*, *28*(3), pp.197-214.

Wentworth, C.K., 1922. A Scale of Grade and Class Terms for Clastic Sediments. *The Journal of geology* 30, 377.

WFD-UKTAG. 2012a. Development and use of the copper bioavailability assessment tool (draft). Report SC080021/8a-a. Water Framework Directive - United Kingdom Technical Advisory Group (WFD-UKTAG), SNIFFER, Edinburgh, Scotland, UK.

WFD-UKTAG. 2012b. Estimation of background reference concentrations for metals in UK freshwaters Report SC080021/1a. Water Framework Directive - United Kingdom Technical Advisory Group (WFD-UKTAG), SNIFFER, Edinburgh, Scotland, UK.

WFD-UKTAG. 2013. Development and use of the zinc bioavailability assessment tool (draft). Report SC080021/1g-a. Water Framework Directive - United Kingdom Technical Advisory Group (WFD-UKTAG), SNIFFER, Edinburgh, Scotland, UK.

Whitehead, D.C. 2000. Nutrient Elements in Grassland: Soil-plant-animal Relationships. CABI. Pp.163-164

Wijnhoven, S., Van Der Velde, G., Leuven, R.S.E.W., Eijsackers, H.J.P. and Smits, A.J.M., 2006. Metal accumulation risks in regularly flooded and non-flooded parts of floodplains of the river Rhine: Extractability and exposure through the food chain. *Chemistry and Ecology, 22(*6), pp.463-477.

Wilson, S.C., Lockwood, P.V., Ashley, P.M. and Tighe, M., 2010. The chemistry and behaviour of antimony in the soil environment with comparisons to arsenic: a critical review. *Environmental Pollution, 158*, pp.1169-1181.

Wölz, J., Cofalla, C., Hudjetz, S., Roger, S., Brinkmann, M., Schmidt, B., Schäffer, A., Kammann, U., Lennartz, G., Hecker, M. and Schüttrumpf, H., 2009. In search for the ecological and toxicological relevance of sediment re-mobilisation and transport during flood events. *Journal of Soils and Sediments*, *9*(1), pp.1-5.

World Health Organisation (1992) Cadmium – environmental aspects. Environmental Health Criteria 135. Geneva.

Wragg, J., Cave, M., Basta, N., Brandon, E., Casteel, S., Denys, S., Gron, C., Oomen, A., Reime, K., Tack, K., and Van de Wiele, T. 2011. An Inter-Laboratory Trial of the Unified {BARGE} Bioaccessability Method for Arsenic, Cadmium and Lead in Soil. *Science of the Total Environment, 409*, pp.4016-4030.

Wragg, J. and Cave, M., 2012. Assessment of a geochemical extraction procedure to determine the solid phase fractionation and bioaccessibility of potentially harmful elements in soils: A case study using the NIST 2710 reference soil. *Analytica Chimica Acta, 722*, pp.43-54.

Wragg, J., 2005. A study of the relationship between arsenic bioaccessibility and its solid phase distribution in Wellingborough soils (Doctoral dissertation, University of Nottingham).

Wragg, J., 2009. Certificate of Analysis: BGS Guidance Material 102 Ironstone Soil.

Wragg, J., Cave, M. and Gregory, S., 2014. The solid phase distribution and bioaccessibility of arsenic, chromium, and nickel in natural ironstone soils in the UK. *Applied and Environmental Soil Science*. 12. Article ID 924891.

Wragg, J., Cave, M. and Nathanail, P., 2007. A study of the relationship between arsenic bioaccessibility and its solid-phase distribution in soils from Wellingborough, UK. *Journal of Environmental Science and Health Part A, 42*(9), pp.1303-1315.

Wragg, J., Cave, M., Basta, N., Brandon, E., Casteel, S., Denys, S., Gron, C., Oomen, A., Reimer, K., Tack, K. and Van de Wiele, T., 2011. An inter-laboratory trial of the unified BARGE bioaccessibility method for arsenic, cadmium and lead in soil. *Science of the Total Environment, 409*(19), pp.4016-4030.

Wragg, J., Cave, M., Hamilton, E. and Lister, T., 2018. The link between soil geochemistry in South-West England and human exposure to soil arsenic. *Minerals,* 8(12), p.570.

Xia, Q., Lamb, D., Peng, C. and Ng, J.C., 2017. Interaction effects of As, Cd and Pb on their respective bioaccessibility with time in co-contaminated soils assessed by the Unified BARGE Method. *Environmental Science and Pollution Research, 24*(6), pp.5585-5594.

Zhang, H., Davison, W. and Ottley, C., 1999. Remobilisation of major ions in freshly deposited lacustrine sediment at overturn. *Aquatic Sciences, 61*, pp.354-361.

Zhao, F., Ma, J., Meharg, A. and McGrath, S., 2009. Arsenic uptake and metabolism in plants. *New Phytologist, 181,* pp.777-794.

Zhao, Y. and Marriott, S.B., 2013. Dispersion and remobilisation of heavy metals in the River Severn system, UK. *Procedia Environmental Sciences*, *18*, pp.167-173.

Zeng, F., Ali, S., Zhang, H., Ouyang, Y., Qiu, B., Wu, F. and Zhang, G., 2011. The influence of pH and organic matter content in paddy soil on heavy metal availability and their uptake by rice plants. *Environmental Pollution, 159*(1), pp.84-91.

Zhong, X.I., Zhou, S., Zhu, Q. and Zhao, Q., 2011. Fraction distribution and bioavailability of soil heavy metals in the Yangtze River Delta—A case study of Kunshan City in Jiangsu Province, China. *Journal of Hazardous Materials, 198,* pp.13-21.

Zhu, X., Yang, F., Wei, C. and Liang, T., 2016. Bioaccessibility of heavy metals in soils cannot be predicted by a single model in two adjacent areas. *Environmental Geochemistry and Health*, *38*(1), pp.233-241.

Zimdahl, R.L. and Skogerboe, R.K., 1977. Behaviour of Lead in Soil. *Environmental Science and Technology, 11*, pp.1202-1207.

APPENDICES

Appendix 1

Outputs from the SMMR for the eight soils in Chapter 3

Soil 1

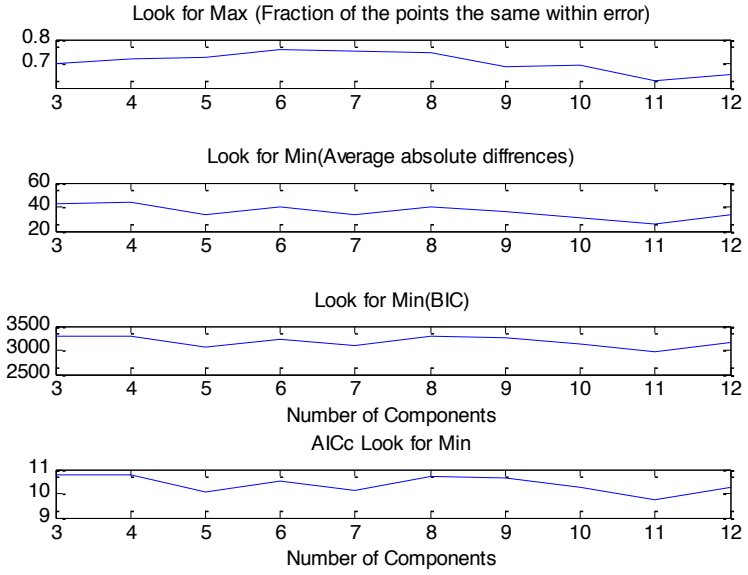

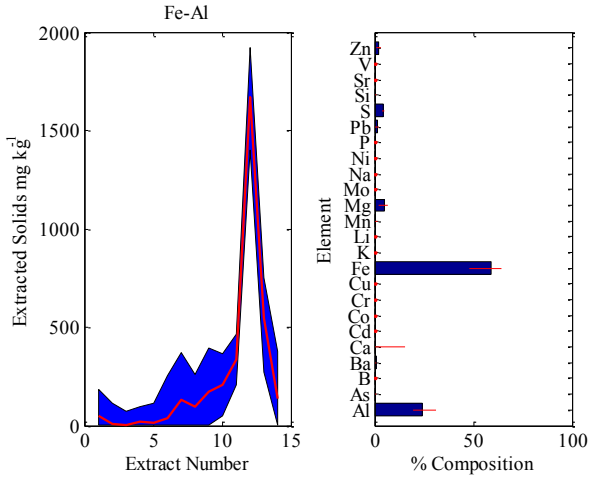
Fe-Al
Extracted Solids mg kg-1
Extract Number
Element
% Composition
Zn
V
Sr
Si
S
Pb
P
Ni
Na
Mo
Mg
Mn
Li
K
Fe
Cu
Cr
Co
Cd
Ca
Ba
B
As
Al

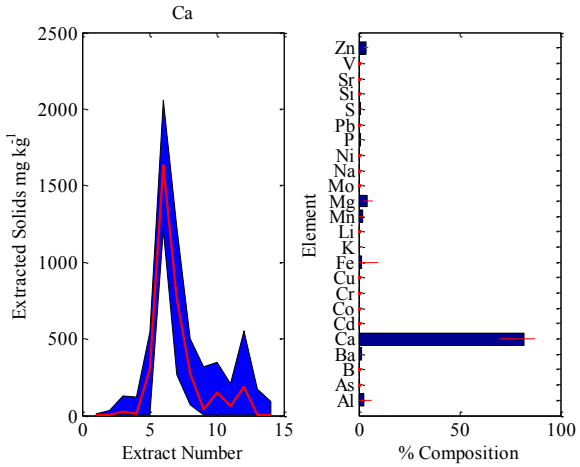
Ca
Extracted Solids mg kg-1
Extract Number
Element
% Composition
Zn
V
Sr
Si
S
Pb
P
Ni
Na
Mo
Mg
Mn
Li
K
Fe
Cu
Cr
Co
Cd
Ca
Ba
B
As
Al

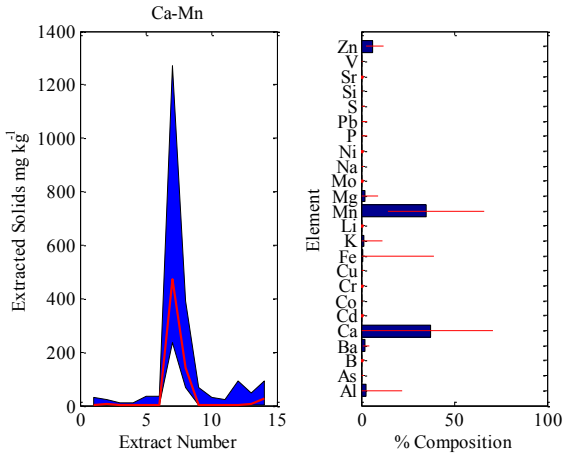
Ca-Mn
Extracted Solids mg kg-1
Extract Number
Element
% Composition
Zn
V
Sr
Si
S
Pb
P
Ni
Na
Mo
Mg
Mn
Li
K
Fe
Cu
Cr
Co
Cd
Ca
Ba
B
As
Al

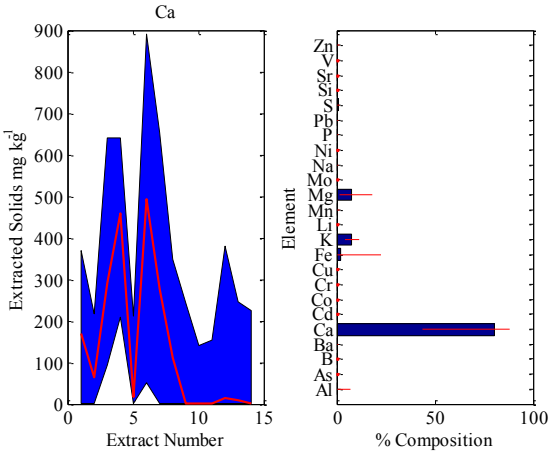
Ca
Extracted Solids mg kg-1
Extract Number
Element
% Composition
Zn
V
Sr
Si
S
Pb
P
Ni
Na
Mo
Mg
Mn
Li
K
Fe
Cu
Cr
Co
Cd
Ca
Ba
B
As
Al

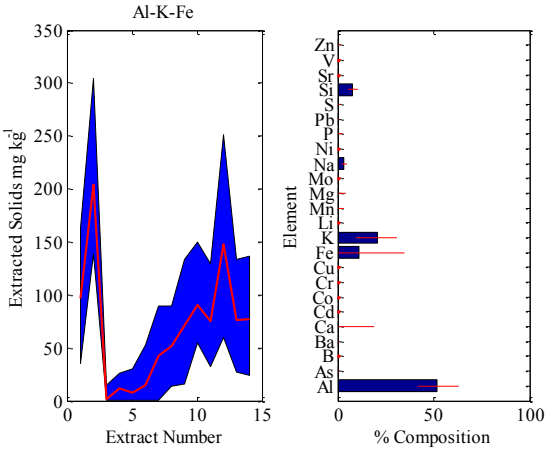
Al-K-Fe
Extracted Solids mg kg-1
Extract Number
Element
% Composition
Zn
V
Sr
Si
S
Pb
P
Ni
Na
Mo
Mg
Mn
Li
K
Fe
Cu
Cr
Co
Cd
Ca
Ba
B
As
Al

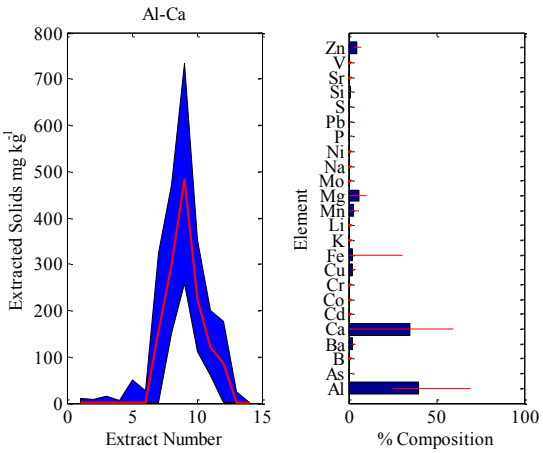
Al-Ca
Extracted Solids mg kg-1
Extract Number
Element
% Composition
Zn
V
Sr
Si
S
Pb
P
Ni
Na
Mo
Mg
Mn
Li
K
Fe
Cu
Cr
Co
Cd
Ca
Ba
B
As
Al

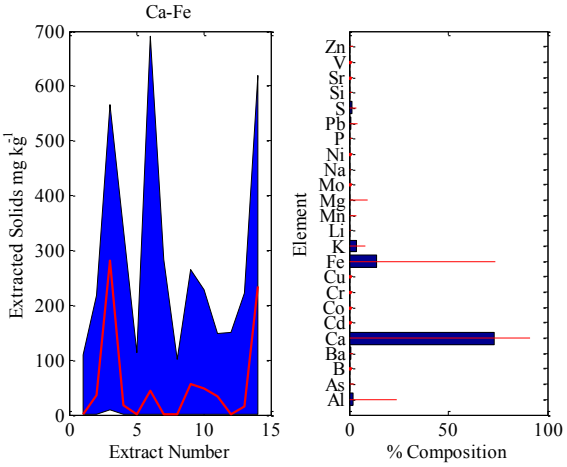
Ca-Fe
Extracted Solids mg kg-1
Extract Number
Element
% Composition
Zn
V
Sr
Si
S
Pb
P
Ni
Na
Mo
Mg
Mn
Li
K
Fe
Cu
Cr
Co
Cd
Ca
Ba
B
As
Al

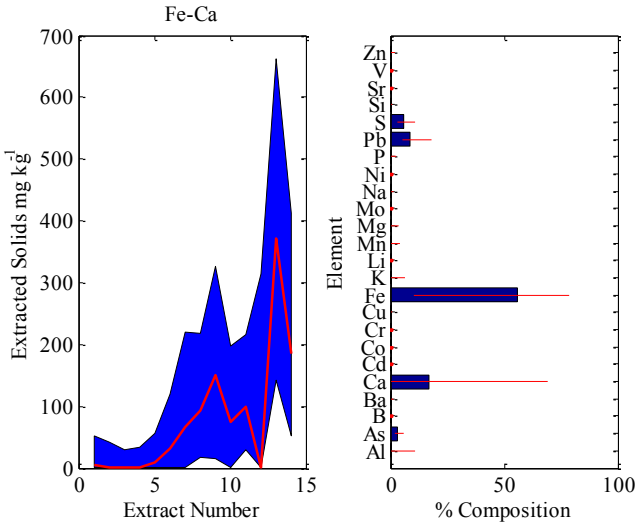
Fe-Ca
Extracted Solids mg kg-1
Extract Number
Element
% Composition
Zn
V
Sr
Si
S
Pb
P
Ni
Na
Mo
Mg
Mn
Li
K
Fe
Cu
Cr
Co
Cd
Ca
Ba
B
As
Al

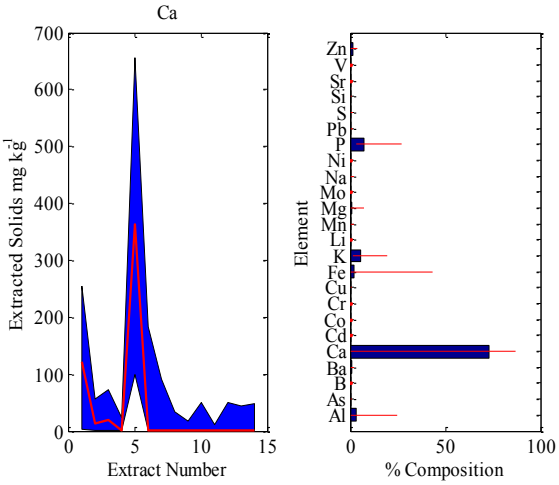
Ca
Extracted Solids mg kg-1
Extract Number
Element
% Composition
Zn
V
Sr
Si
S
Pb
P
Ni
Na
Mo
Mg
Mn
Li
K
Fe
Cu
Cr
Co
Cd
Ca
Ba
B
As
Al

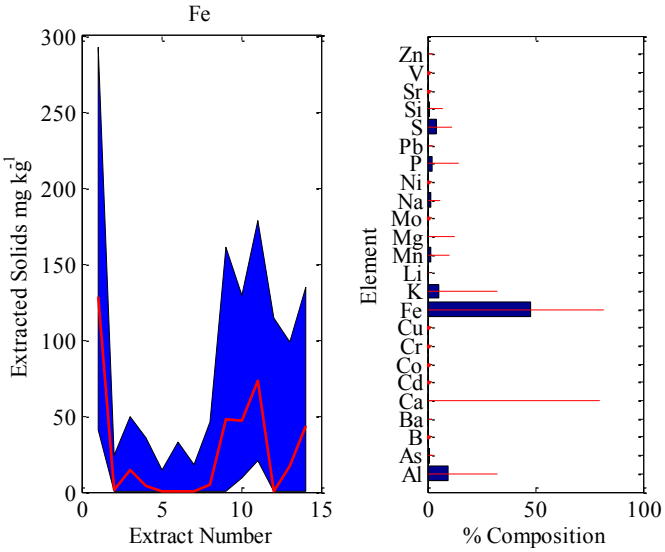
Fe
Extracted Solids mg kg-1
Extract Number
Element
% Composition
Zn
V
Sr
Si
S
Pb
P
Ni
Na
Mo
Mg
Mn
Li
K
Fe
Cu
Cr
Co
Cd
Ca
Ba
B
As
Al

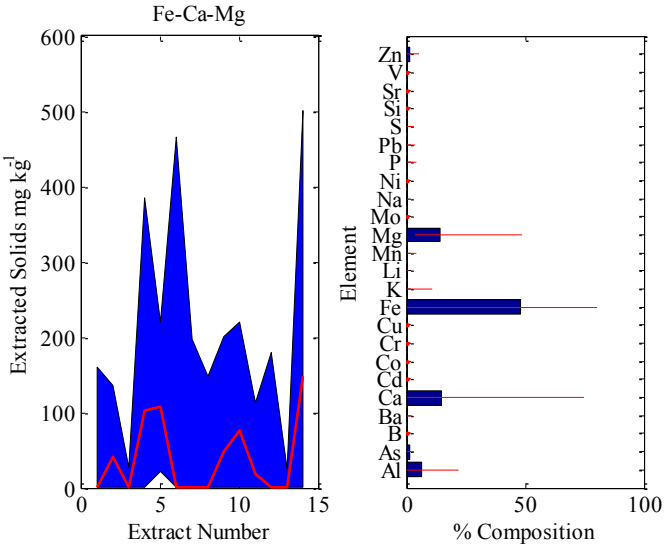
Fe-Ca-Mg
Extracted Solids mg kg-1
Extract Number
Element
% Composition
Zn
V
Sr
Si
S
Pb
P
Ni
Na
Mo
Mg
Mn
Li
K
Fe
Cu
Cr
Co
Cd
Ca
Ba
B
As
Al

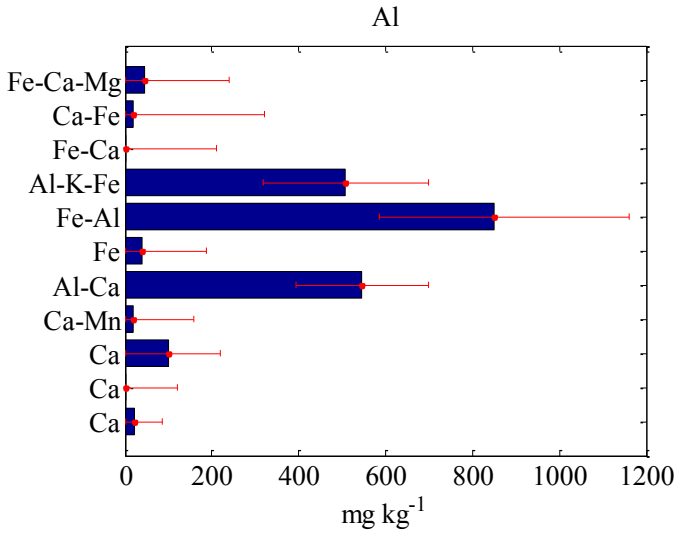
Al
Fe-Ca-Mg
Ca-Fe
Fe-Ca
Al-K-Fe
Fe-Al
Fe
Al-Ca
Ca-Mn
Ca
Ca
Ca
0
200
400
600
800
1000
1200
mg kg-1

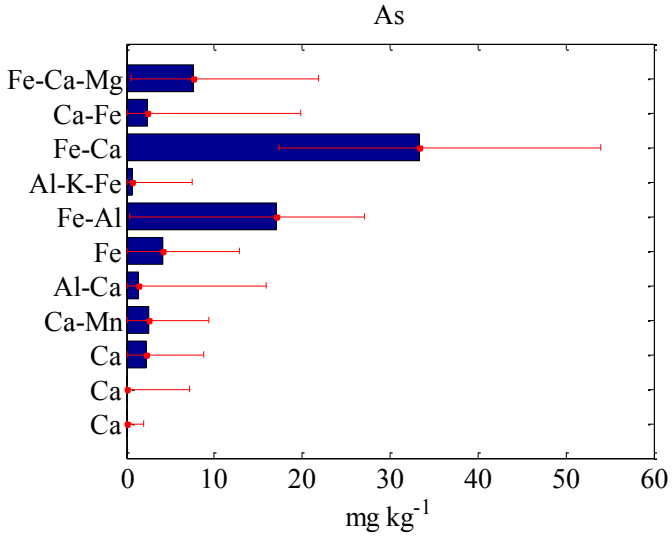
As
Fe-Ca-Mg
Ca-Fe
Fe-Ca
Al-K-Fe
Fe-Al
Fe
Al-Ca
Ca-Mn
Ca
Ca
Ca
0
10
20
30
40
50
60
mg kg-1

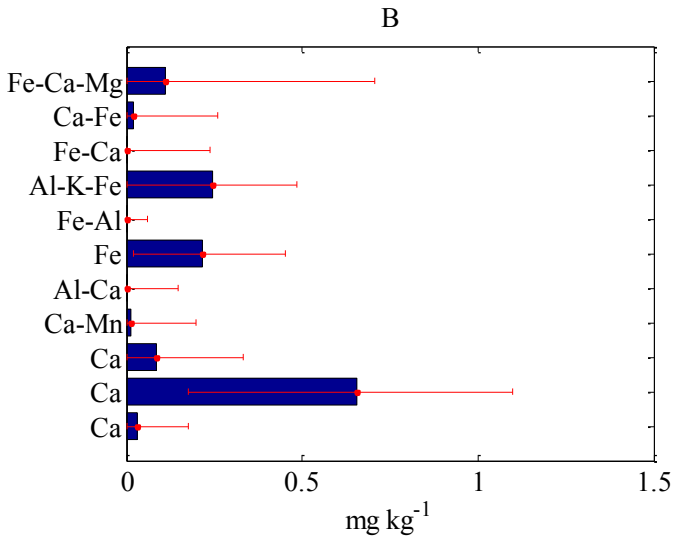
B
Fe-Ca-Mg
Ca-Fe
Fe-Ca
Al-K-Fe
Fe-Al
Fe
Al-Ca
Ca-Mn
Ca
Ca
Ca
0
0.5
1
1.5
mg kg-1

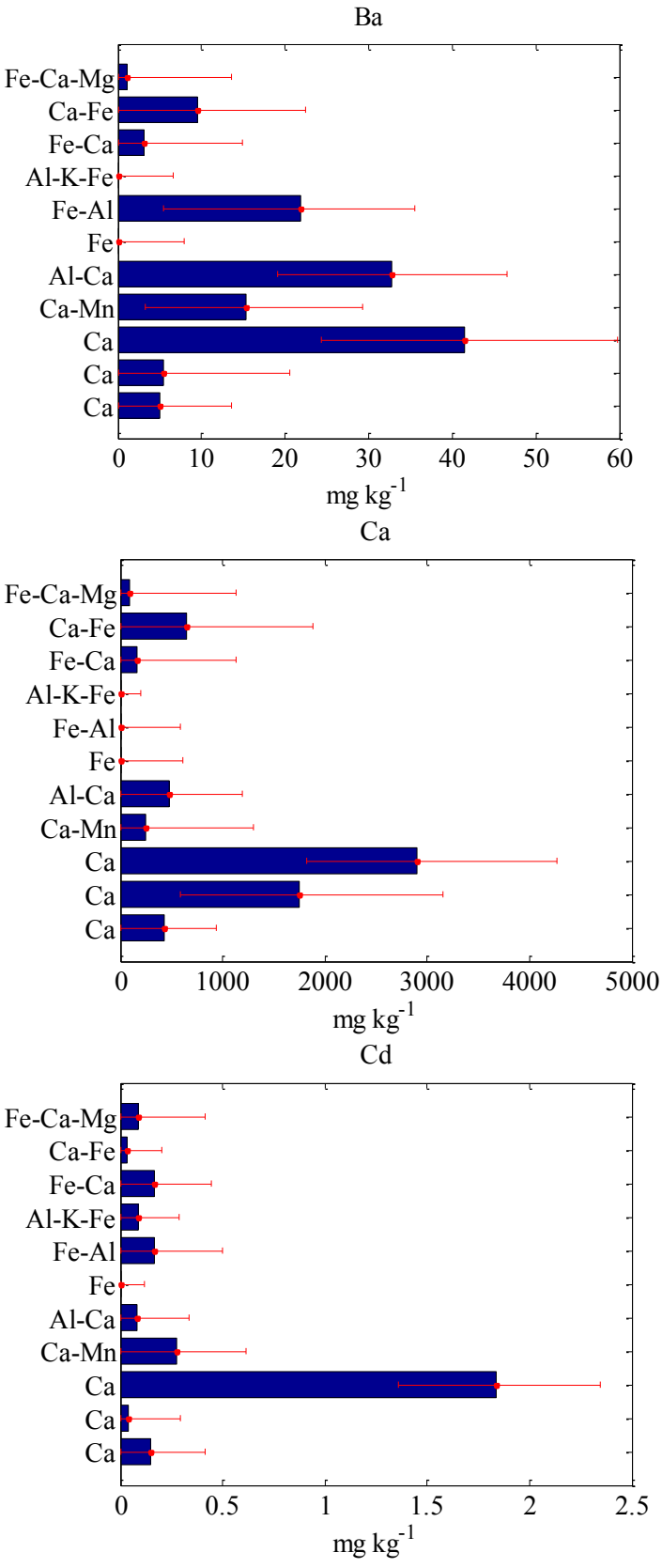
Ba
Fe-Ca-Mg
Ca-Fe
Fe-Ca
Al-K-Fe
Fe-Al
Fe
Al-Ca
Ca-Mn
Ca
Ca
Ca
0
10
20
30
40
50
60
mg kg-1
Ca
Fe-Ca-Mg
Ca-Fe
Fe-Ca
Al-K-Fe
Fe-Al
Fe
Al-Ca
Ca-Mn
Ca
Ca
Ca
0
1000
2000
3000
4000
5000
mg kg-1
Cd
Fe-Ca-Mg
Ca-Fe
Fe-Ca
Al-K-Fe
Fe-Al
Fe
Al-Ca
Ca-Mn
Ca
Ca
Ca
0
0.5
1
1.5
2
2.5
mg kg-1

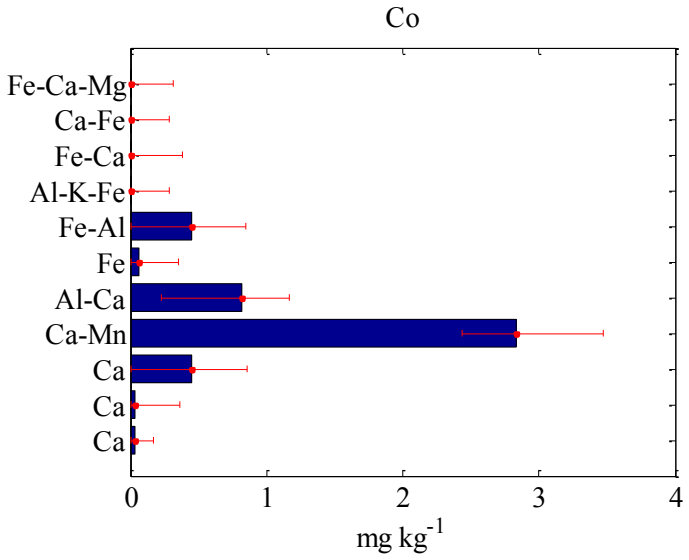
Co
Fe-Ca-Mg
Ca-Fe
Fe-Ca
Al-K-Fe
Fe-Al
Fe
Al-Ca
Ca-Mn
Ca
Ca
Ca
0
1
2
3
4
mg kg-1

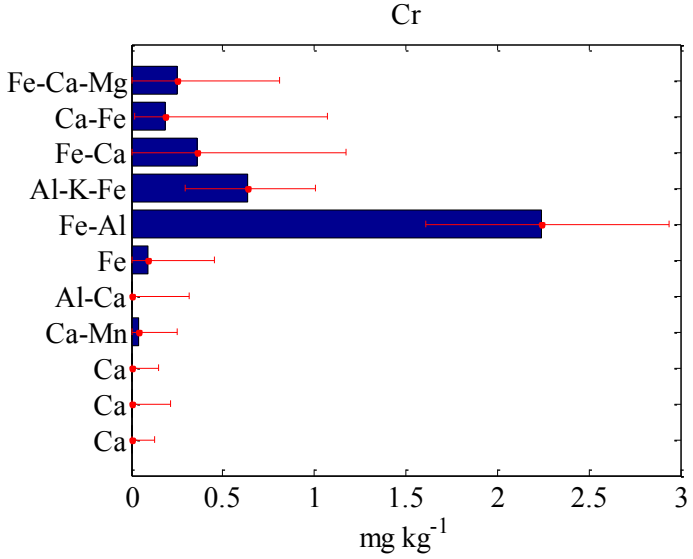
Cr
Fe-Ca-Mg
Ca-Fe
Fe-Ca
Al-K-Fe
Fe-Al
Fe
Al-Ca
Ca-Mn
Ca
Ca
Ca
0
0.5
1
1.5
2
2.5
3
mg kg-1

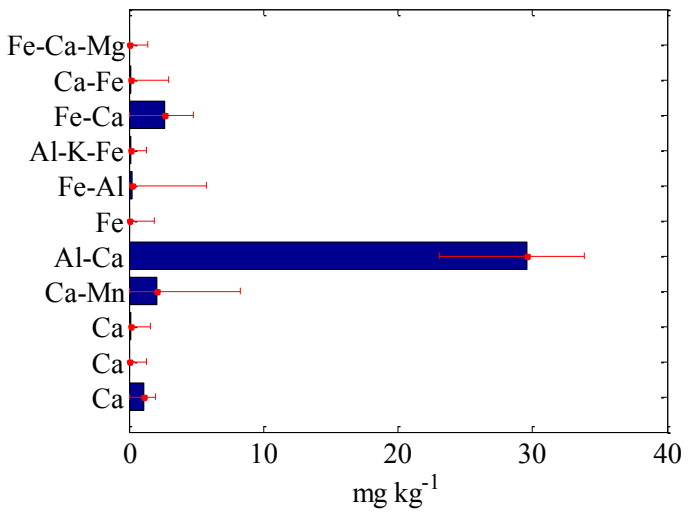
Cu
Fe-Ca-Mg
Ca-Fe
Fe-Ca
Al-K-Fe
Fe-Al
Fe
Al-Ca
Ca-Mn
Ca
Ca
Ca
0
10
20
30
40
mg kg-1

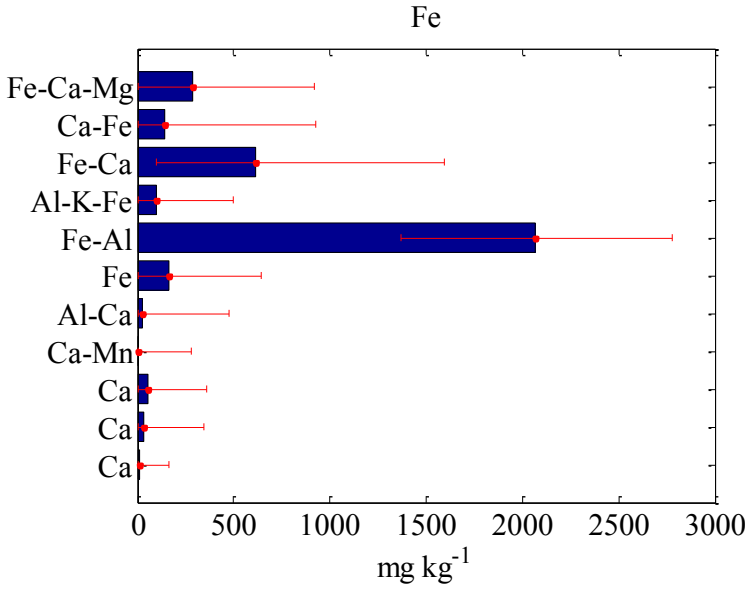
Fe
Fe-Ca-Mg
Ca-Fe
Fe-Ca
Al-K-Fe
Fe-Al
Fe
Al-Ca
Ca-Mn
Ca
Ca
Ca
0
500
1000
1500
2000
2500
3000
mg kg-1

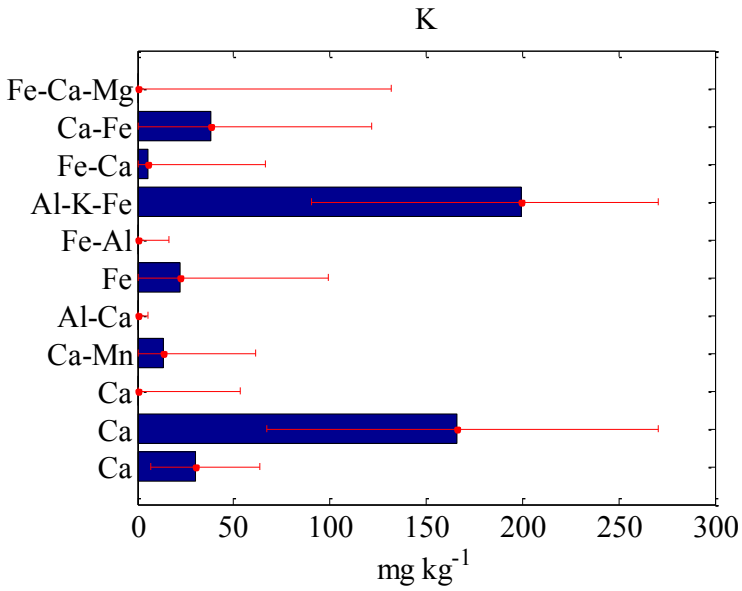
K
Fe-Ca-Mg
Ca-Fe
Fe-Ca
Al-K-Fe
Fe-Al
Fe
Al-Ca
Ca-Mn
Ca
Ca
Ca
0
50
100
150
200
250
300
mg kg-1

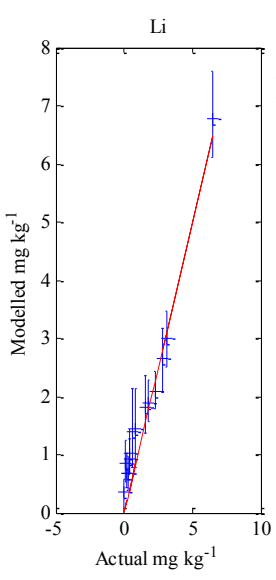
Li
Modelled mg kg-1
Actual mg kg-1
0
1
2
3
4
5
6
7
8
-5
0
5
10

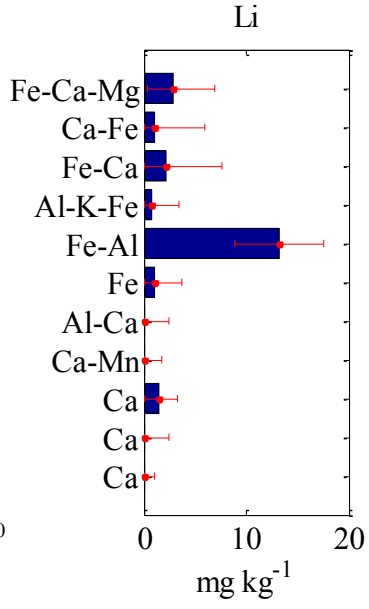
Li
Fe-Ca-Mg
Ca-Fe
Fe-Ca
Al-K-Fe
Fe-Al
Fe
Al-Ca
Ca-Mn
Ca
Ca
Ca
0
10
20
mg kg-1

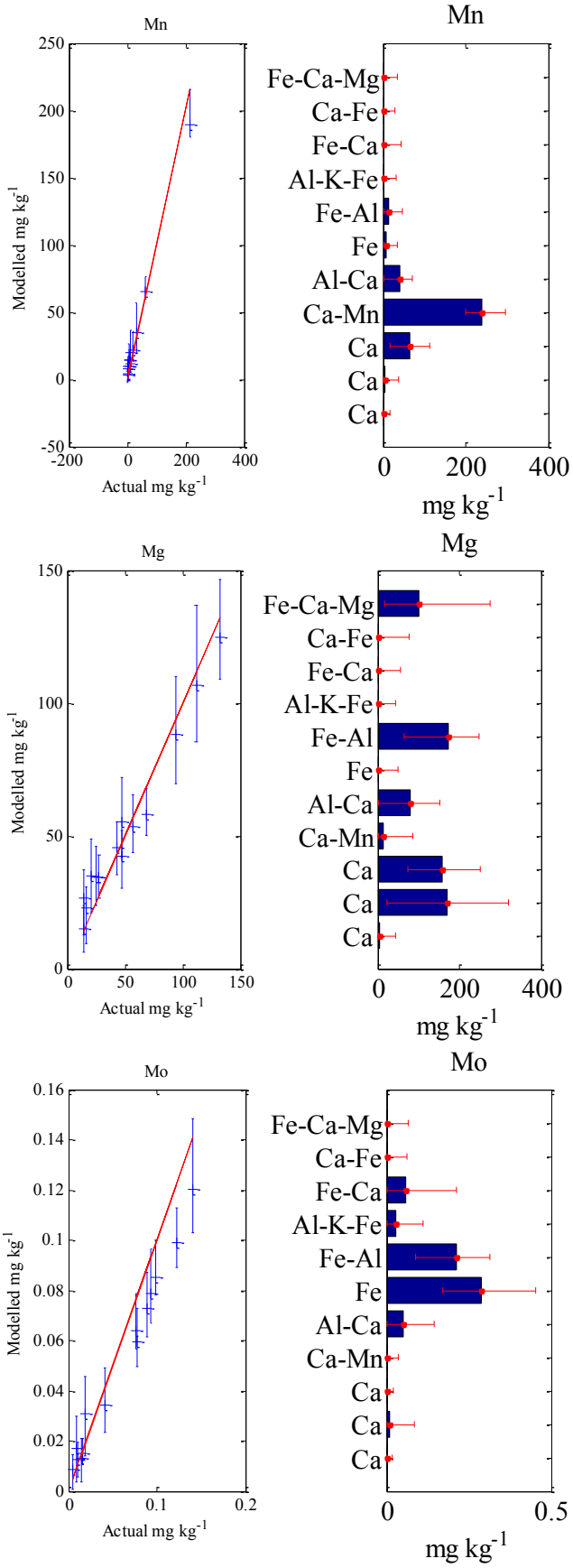
Mn
Modelled mg kg-1
Actual mg kg-1
Mn
Fe-Ca-Mg
Ca-Fe
Fe-Ca
Al-K-Fe
Fe-Al
Fe
Al-Ca
Ca-Mn
Ca
Ca
Ca
mg kg-1
Mg
Modelled mg kg-1
Actual mg kg-1
Mg
Fe-Ca-Mg
Ca-Fe
Fe-Ca
Al-K-Fe
Fe-Al
Fe
Al-Ca
Ca-Mn
Ca
Ca
Ca
mg kg-1
Mo
Modelled mg kg-1
Actual mg kg-1
Mo
Fe-Ca-Mg
Ca-Fe
Fe-Ca
Al-K-Fe
Fe-Al
Fe
Al-Ca
Ca-Mn
Ca
Ca
Ca
mg kg-1

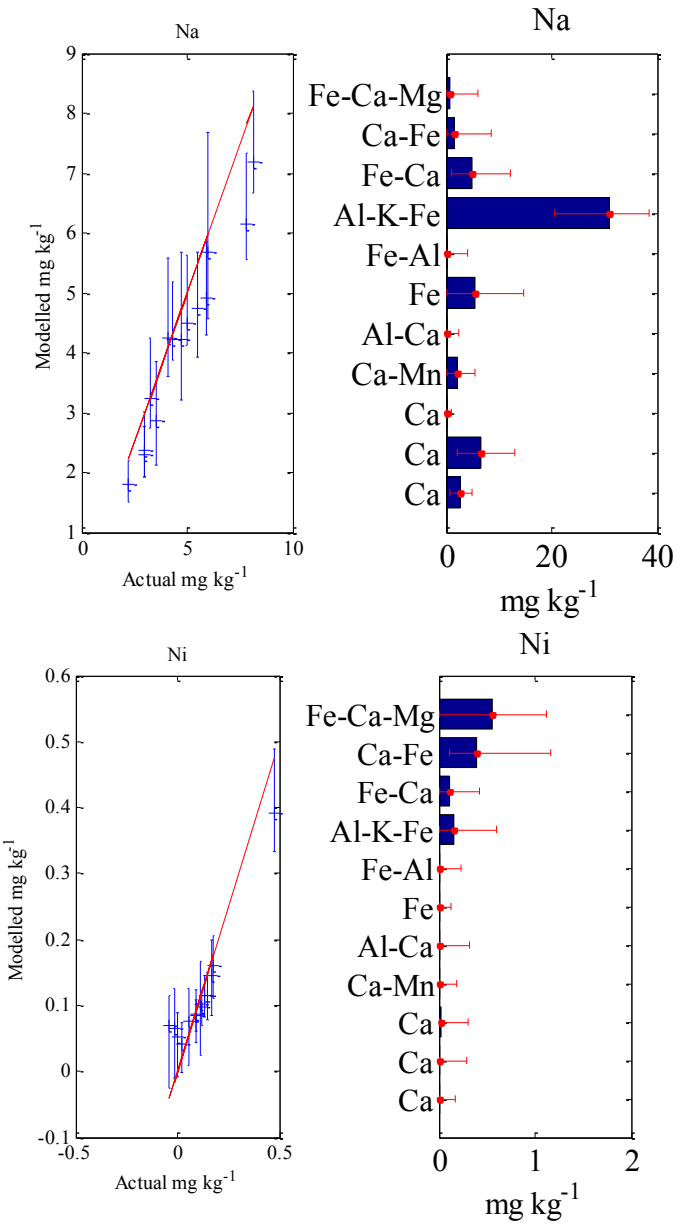
Na
Modelled mg kg-1
Actual mg kg-1
Na
Fe-Ca-Mg
Ca-Fe
Fe-Ca
Al-K-Fe
Fe-Al
Fe
Al-Ca
Ca-Mn
Ca
Ca
Ca
mg kg-1
Ni
Modelled mg kg-1
Actual mg kg-1
Ni
Fe-Ca-Mg
Ca-Fe
Fe-Ca
Al-K-Fe
Fe-Al
Fe
Al-Ca
Ca-Mn
Ca
Ca
Ca
mg kg-1

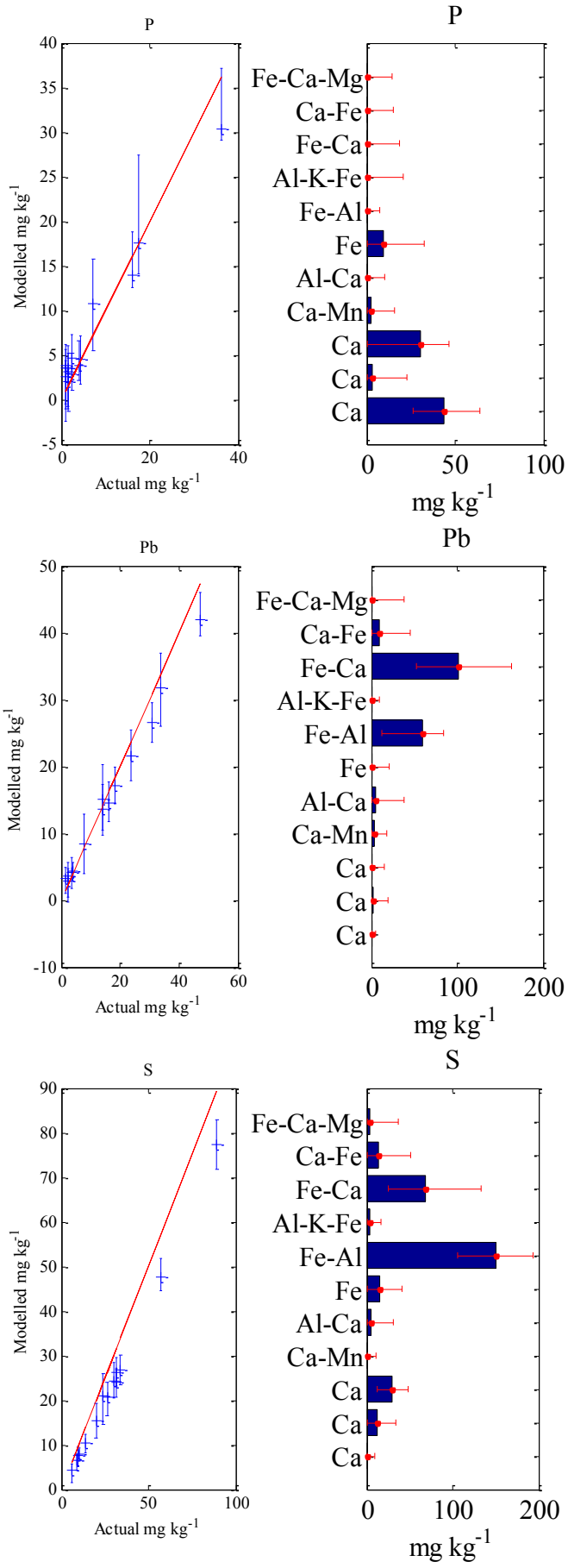
P
Modelled mg kg-1
Actual mg kg-1
P
Fe-Ca-Mg
Ca-Fe
Fe-Ca
Al-K-Fe
Fe-Al
Fe
Al-Ca
Ca-Mn
Ca
Ca
Ca
mg kg-1
Pb
Modelled mg kg-1
Actual mg kg-1
Pb
Fe-Ca-Mg
Ca-Fe
Fe-Ca
Al-K-Fe
Fe-Al
Fe
Al-Ca
Ca-Mn
Ca
Ca
Ca
mg kg-1
S
Modelled mg kg-1
Actual mg kg-1
S
Fe-Ca-Mg
Ca-Fe
Fe-Ca
Al-K-Fe
Fe-Al
Fe
Al-Ca
Ca-Mn
Ca
Ca
Ca
mg kg-1

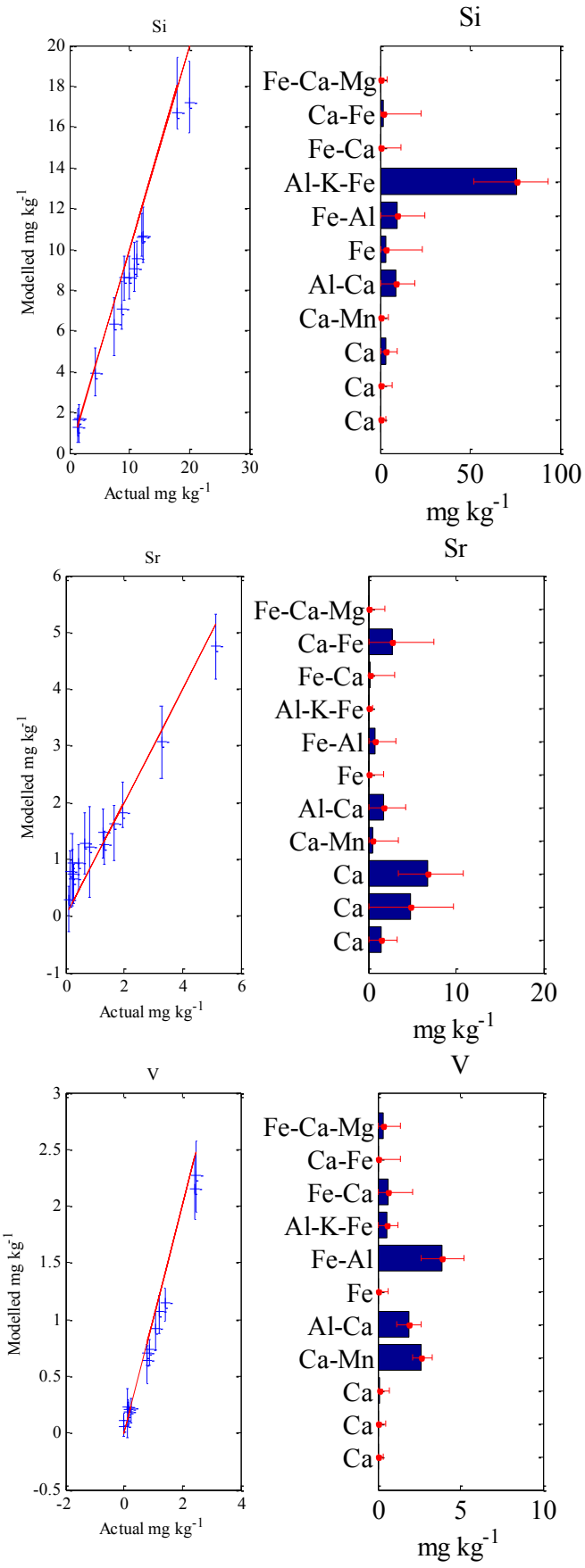
Si
Modelled mg kg-1
Actual mg kg-1
Si
Fe-Ca-Mg
Ca-Fe
Fe-Ca
Al-K-Fe
Fe-Al
Fe
Al-Ca
Ca-Mn
Ca
Ca
Ca
mg kg-1
Sr
Modelled mg kg-1
Actual mg kg-1
Sr
Fe-Ca-Mg
Ca-Fe
Fe-Ca
Al-K-Fe
Fe-Al
Fe
Al-Ca
Ca-Mn
Ca
Ca
Ca
mg kg-1
V
Modelled mg kg-1
Actual mg kg-1
V
Fe-Ca-Mg
Ca-Fe
Fe-Ca
Al-K-Fe
Fe-Al
Fe
Al-Ca
Ca-Mn
Ca
Ca
Ca
mg kg-1

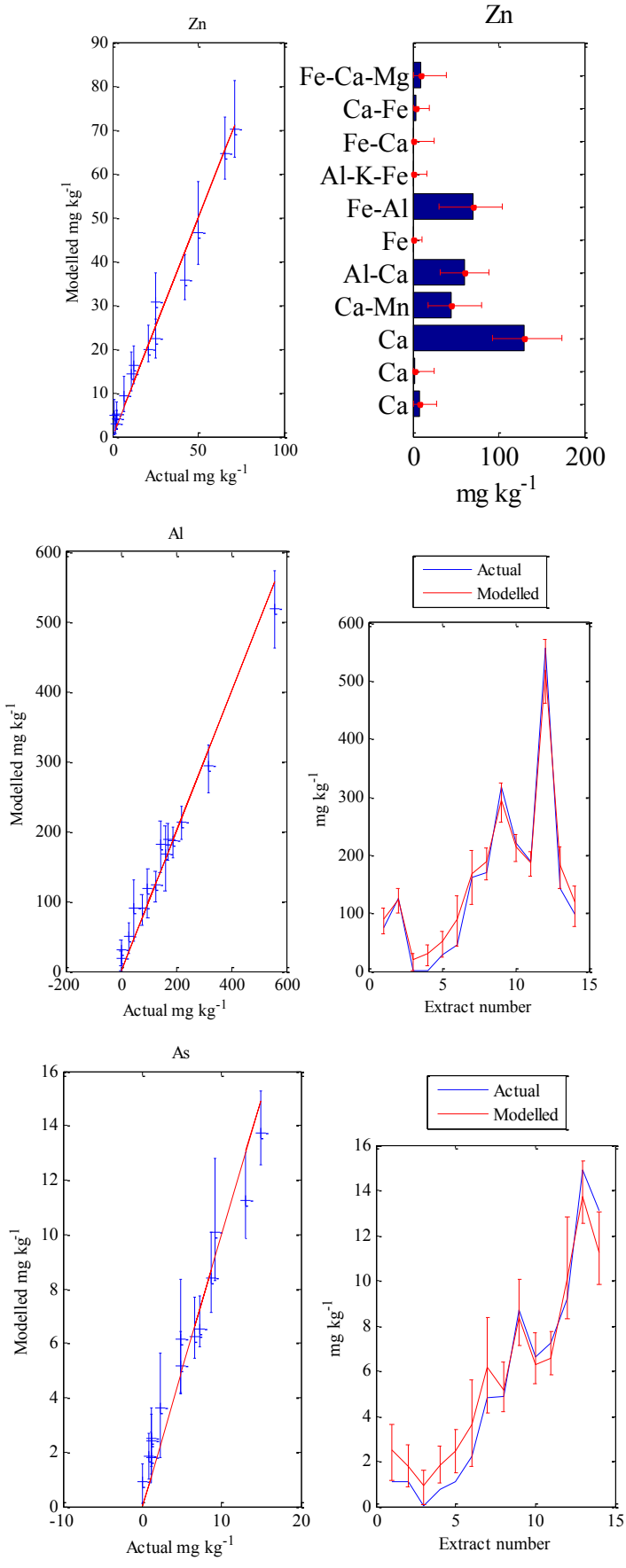
Zn
Modelled mg kg-1
Actual mg kg-1
Zn
Fe-Ca-Mg
Ca-Fe
Fe-Ca
Al-K-Fe
Fe-Al
Fe
Al-Ca
Ca-Mn
Ca
Ca
Ca
mg kg-1
Al
Modelled mg kg-1
Actual mg kg-1
Actual
Modelled
mg kg-1
Extract number
As
Modelled mg kg-1
Actual mg kg-1
Actual
Modelled
mg kg-1
Extract number

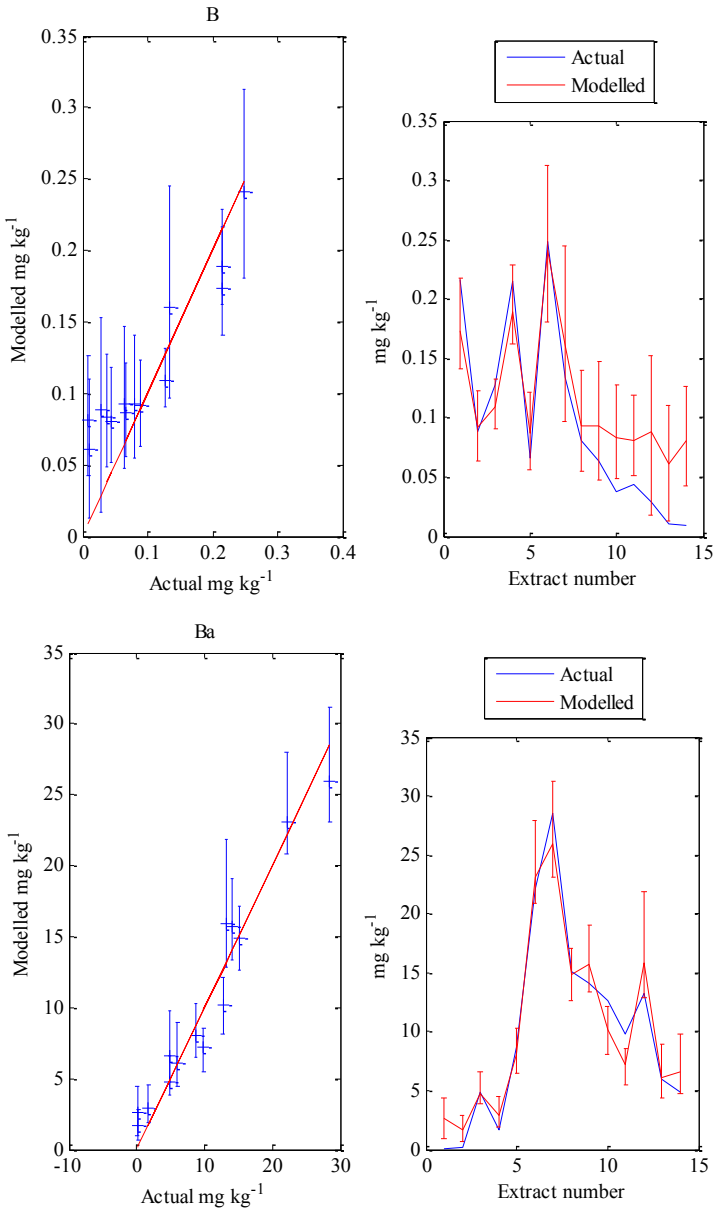
B
Modelled mg kg-1
Actual mg kg-1
Actual
Modelled
mg kg-1
Extract number
Ba
Modelled mg kg-1
Actual mg kg-1
Actual
Modelled
mg kg-1
Extract number

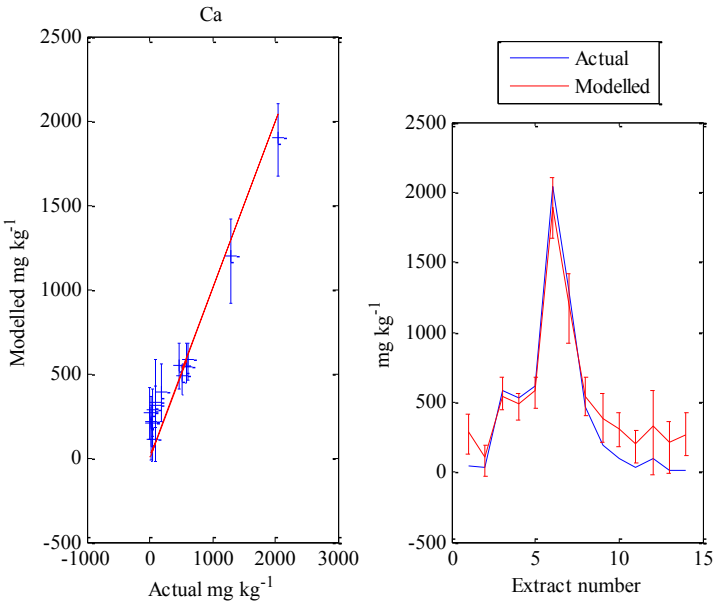
Ca
Modelled mg kg-1
Actual mg kg-1
Actual
Modelled
mg kg-1
Extract number

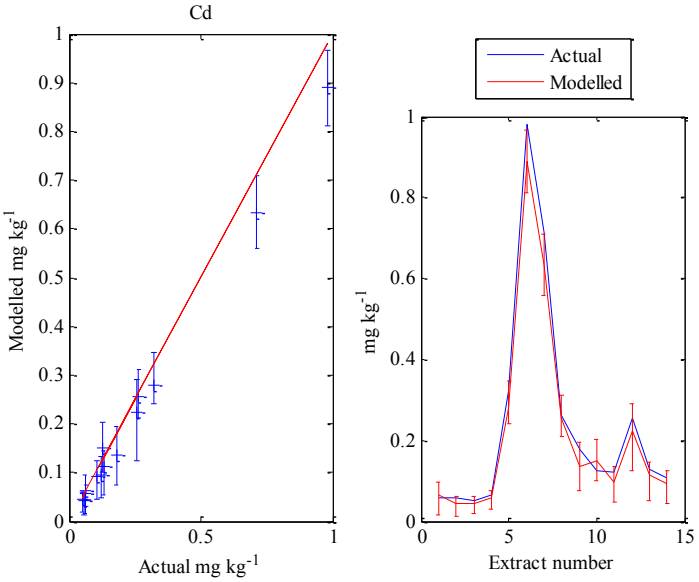
Cd
Modelled mg kg-1
Actual mg kg-1
Actual
Modelled
mg kg-1
Extract number

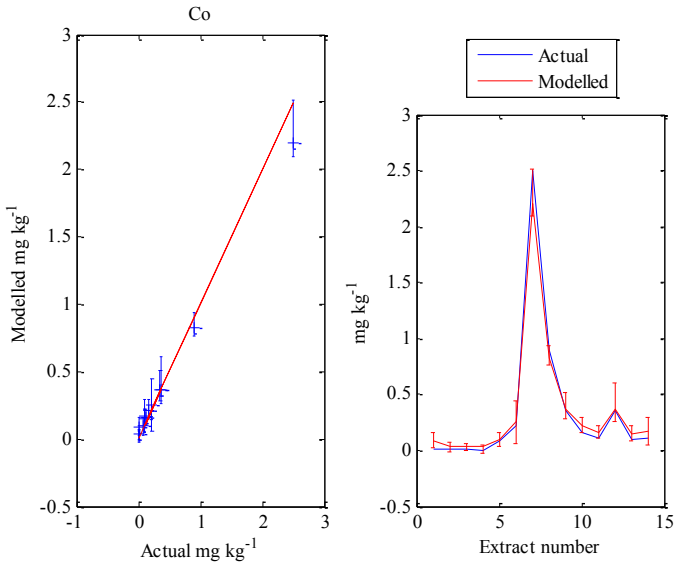
Co
Modelled mg kg-1
Actual mg kg-1
Actual
Modelled
mg kg-1
Extract number

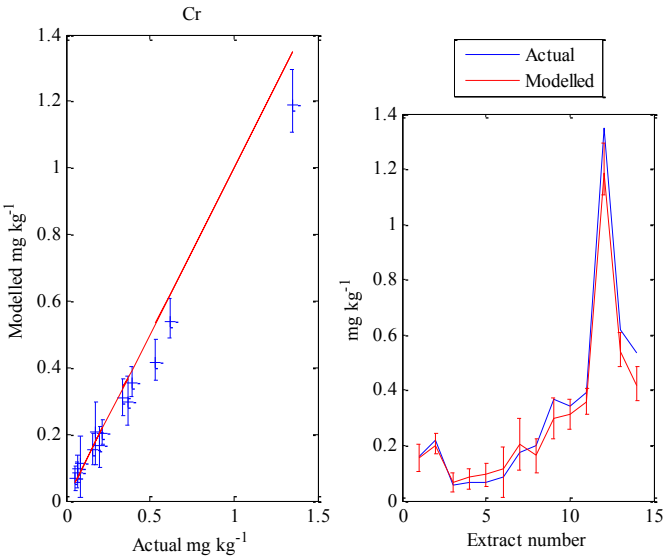
Cr
Modelled mg kg-1
Actual mg kg-1
Actual
Modelled
mg kg-1
Extract number

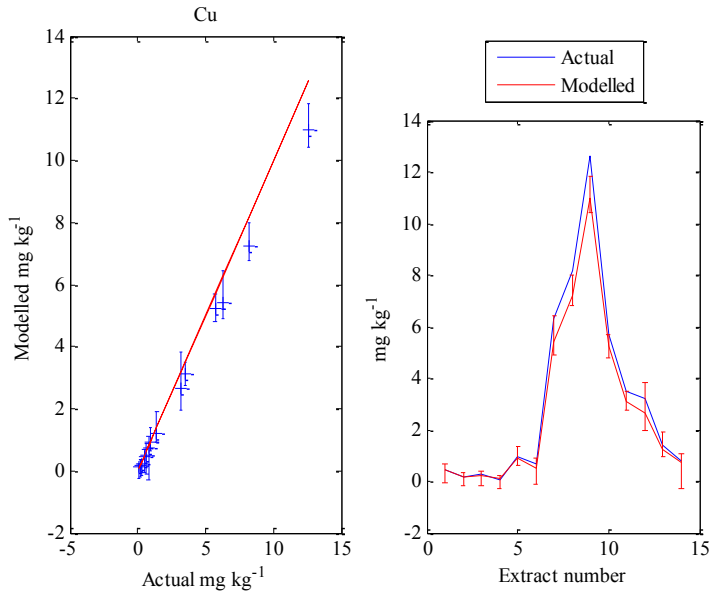
Cu
Modelled mg kg-1
Actual mg kg-1
Actual
Modelled
mg kg-1
Extract number

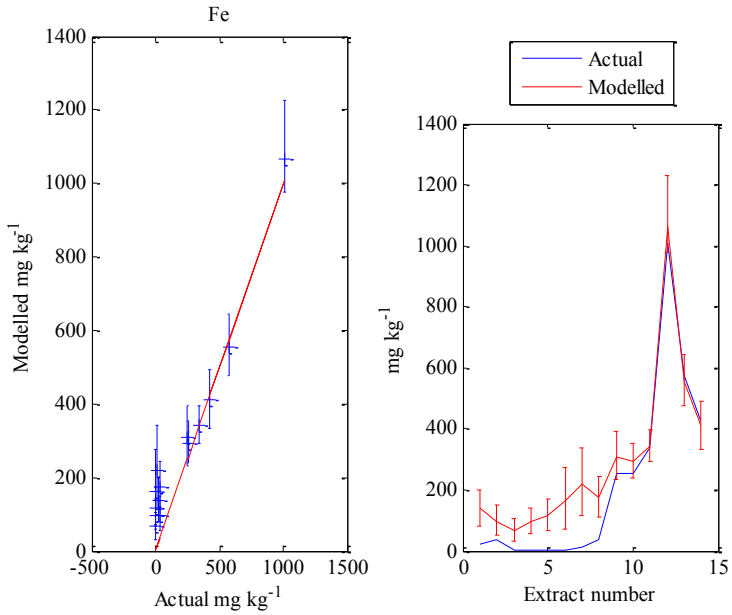
Fe
Modelled mg kg-1
Actual mg kg-1
Actual
Modelled
mg kg-1
Extract number

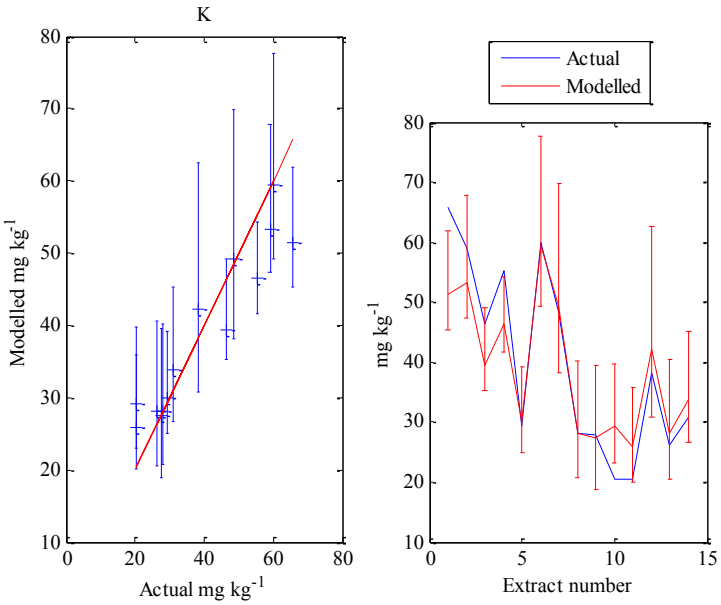
K
Modelled mg kg-1
Actual mg kg-1
Actual
Modelled
mg kg-1
Extract number

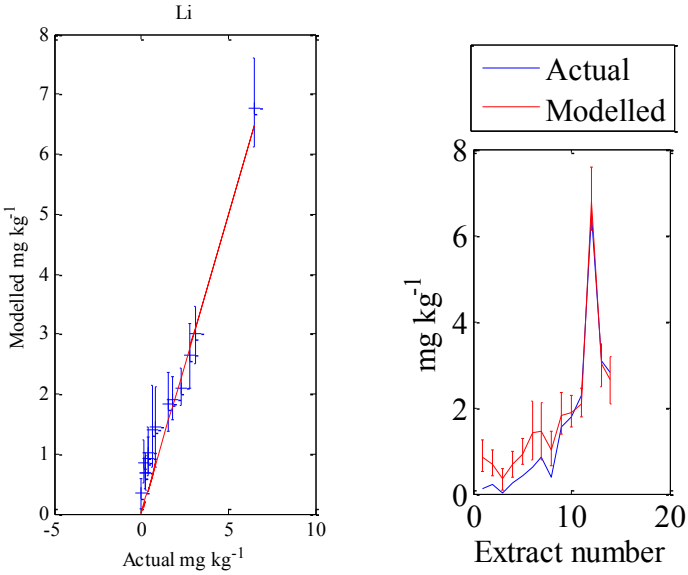
Li
Modelled mg kg-1
Actual mg kg-1
Actual
Modelled
mg kg-1
Extract number

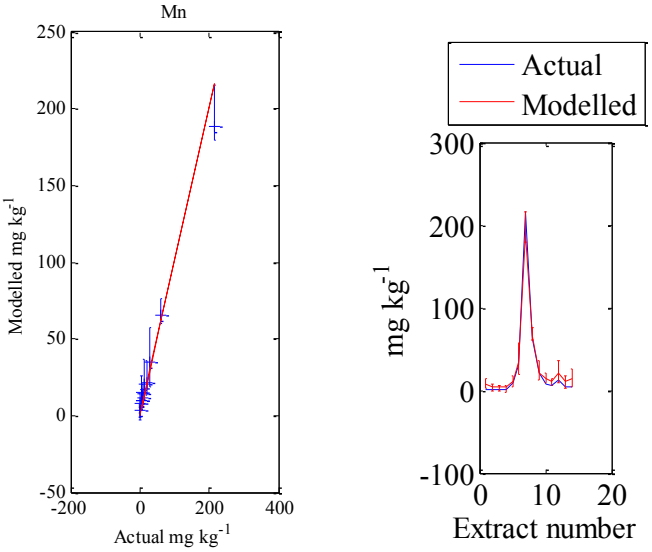
Mn
Modelled mg kg-1
Actual mg kg-1
Actual
Modelled
mg kg-1
Extract number

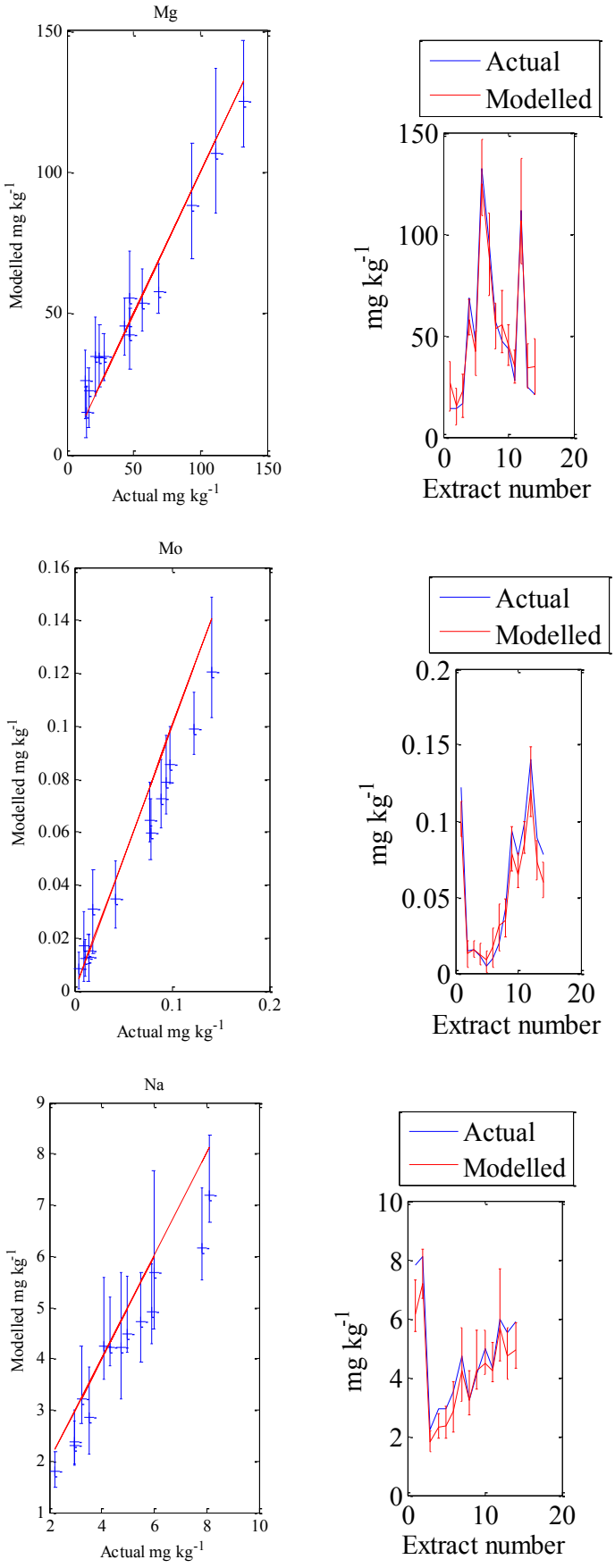
Mg
Modelled mg kg-1
Actual mg kg-1
Actual
Modelled
mg kg-1
Extract number
Mo
Modelled mg kg-1
Actual mg kg-1
Actual
Modelled
mg kg-1
Extract number
Na
Modelled mg kg-1
Actual mg kg-1
Actual
Modelled
mg kg-1
Extract number

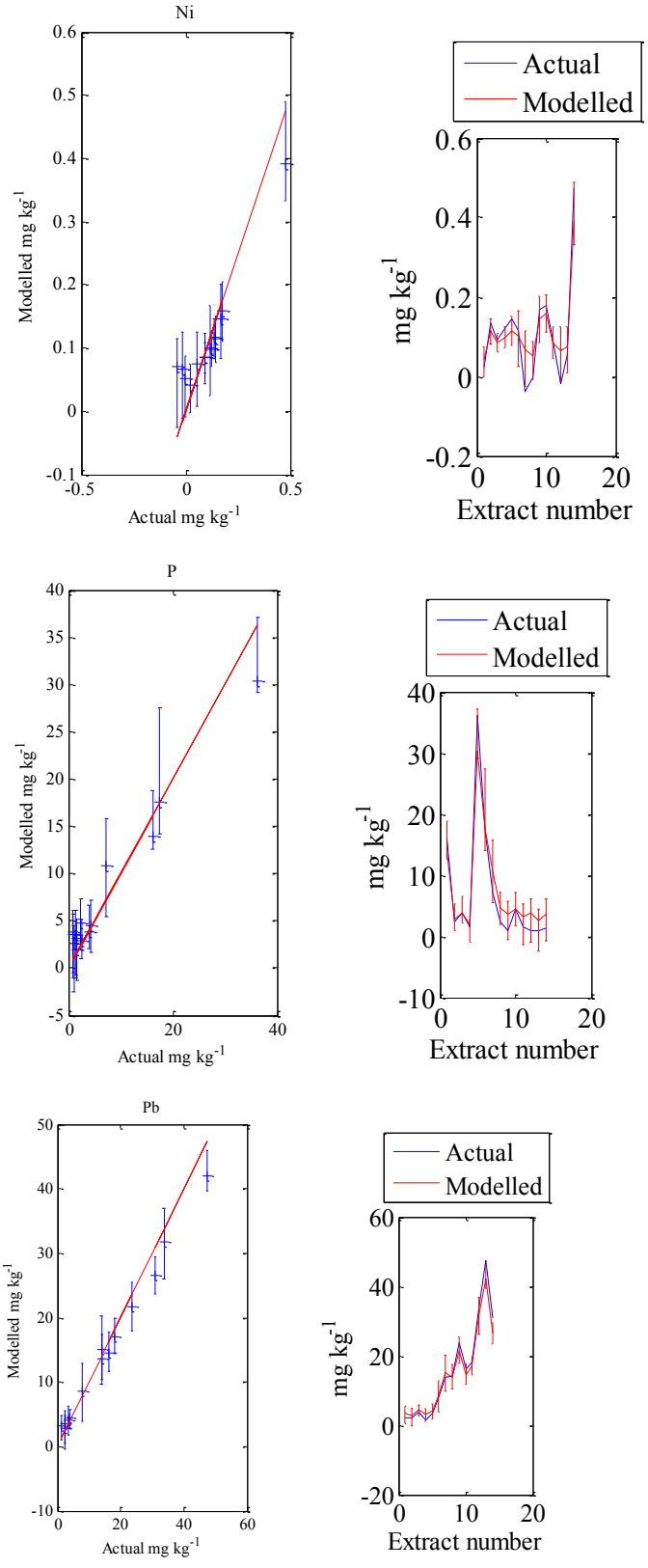
Ni
Modelled mg kg-1
Actual mg kg-1
Actual
Modelled
mg kg-1
Extract number
P
Modelled mg kg-1
Actual mg kg-1
Actual
Modelled
mg kg-1
Extract number
Pb
Modelled mg kg-1
Actual mg kg-1
Actual
Modelled
mg kg-1
Extract number

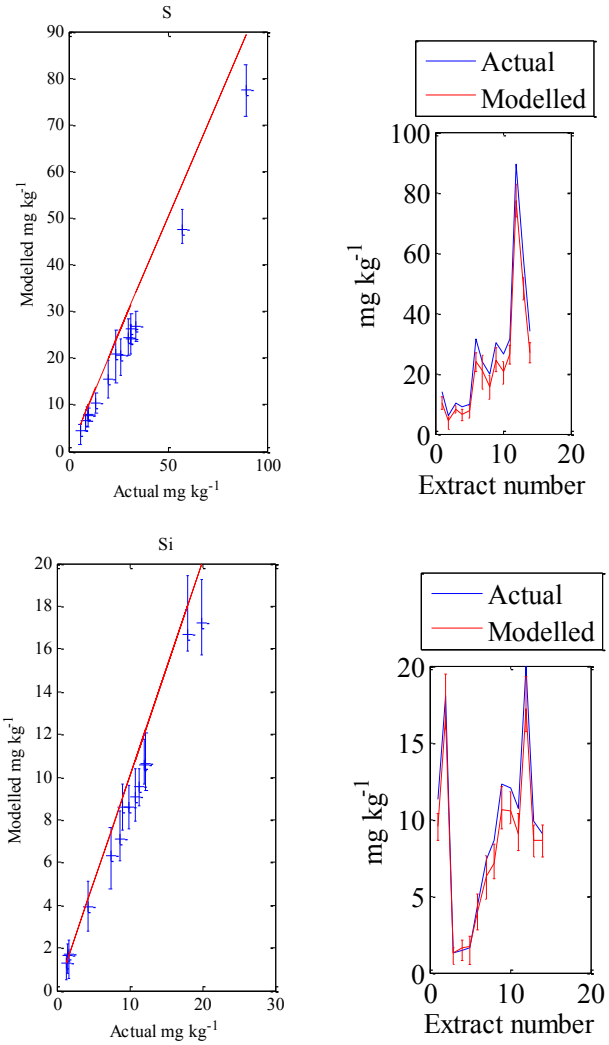
S
Modelled mg kg-1
Actual mg kg-1
Actual
Modelled
mg kg-1
Extract number
Si
Modelled mg kg-1
Actual mg kg-1
Actual
Modelled
mg kg-1
Extract number

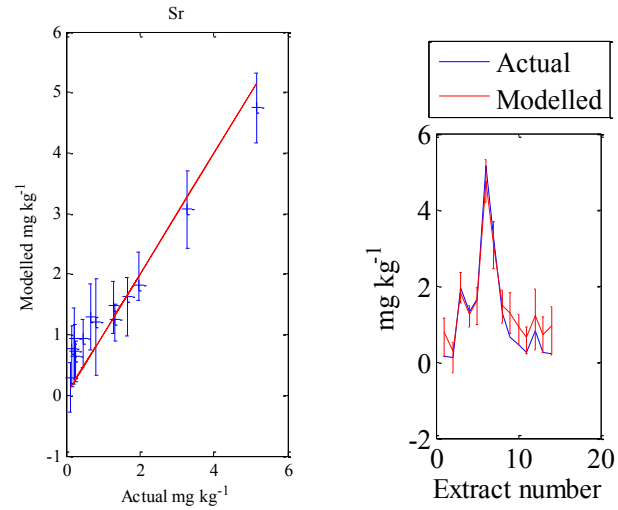
Sr
Modelled mg kg-1
Actual mg kg-1

Actual
Modelled
mg kg-1
Extract number

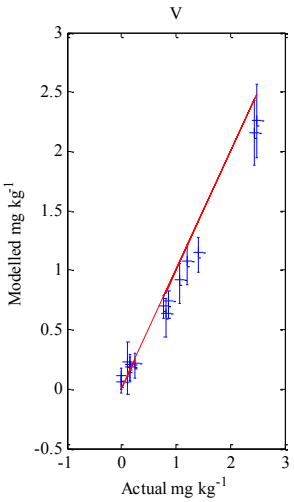
V
Modelled mg kg-1
Actual mg kg-1

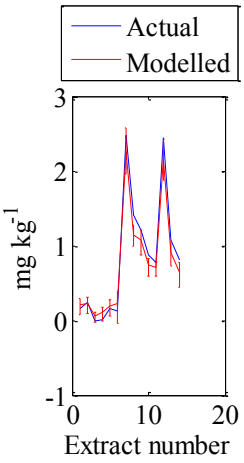
Actual
Modelled
mg kg-1
Extract number

Soil 2

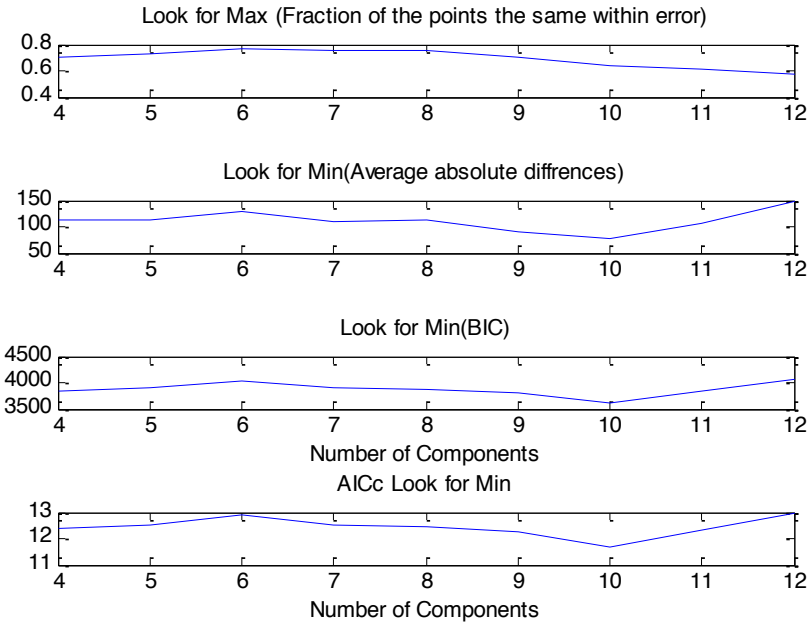
Look for Max (Fraction of the points the same within error)
0.8
0.6
0.4
4 5 6 7 8 9 10 11 12
Look for Min(Average absolute diffrences)
150
100
50
4 5 6 7 8 9 10 11 12
Look for Min(BIC)
4500
4000
3500
4 5 6 7 8 9 10 11 12
Number of Components
AICc Look for Min
13
12
11
4 5 6 7 8 9 10 11 12
Number of Components

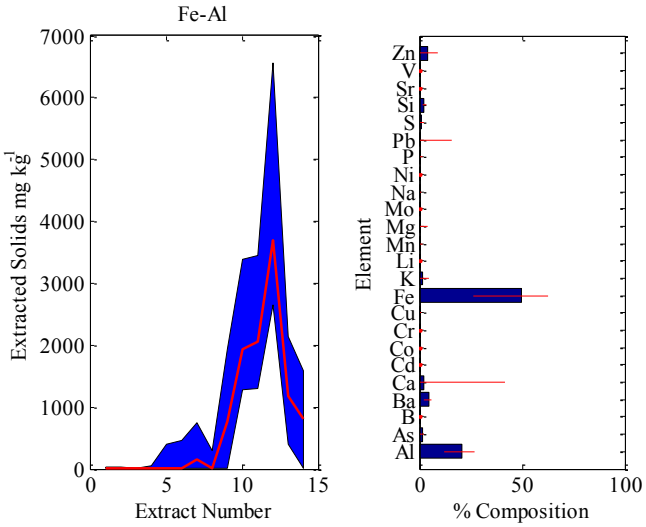
Fe-Al
Extracted Solids mg kg-1
Extract Number
Element
% Composition
Zn
V
Sr
Si
S
Pb
P
Ni
Na
Mo
Mg
Mn
Li
K
Fe
Cu
Cr
Co
Cd
Ca
Ba
B
As
Al

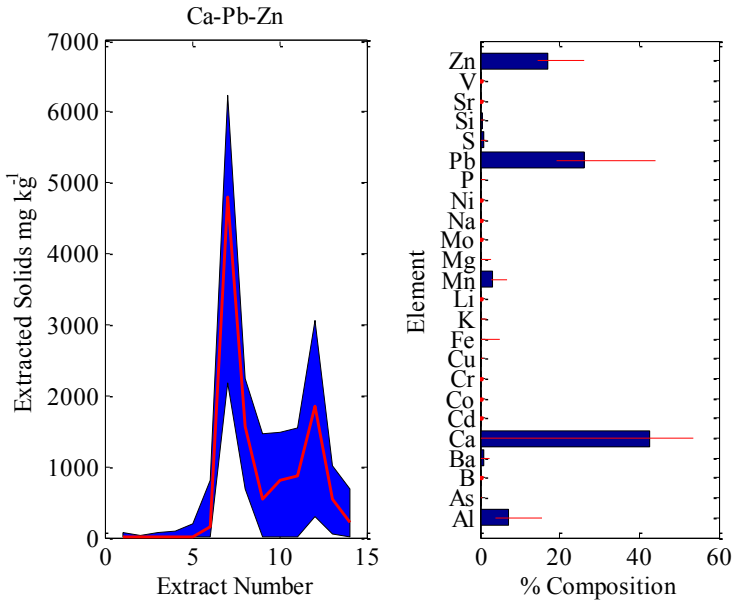
Ca-Pb-Zn
Extracted Solids mg kg-1
Extract Number
Element
% Composition
Zn
V
Sr
Si
S
Pb
P
Ni
Na
Mo
Mg
Mn
Li
K
Fe
Cu
Cr
Co
Cd
Ca
Ba
B
As
Al

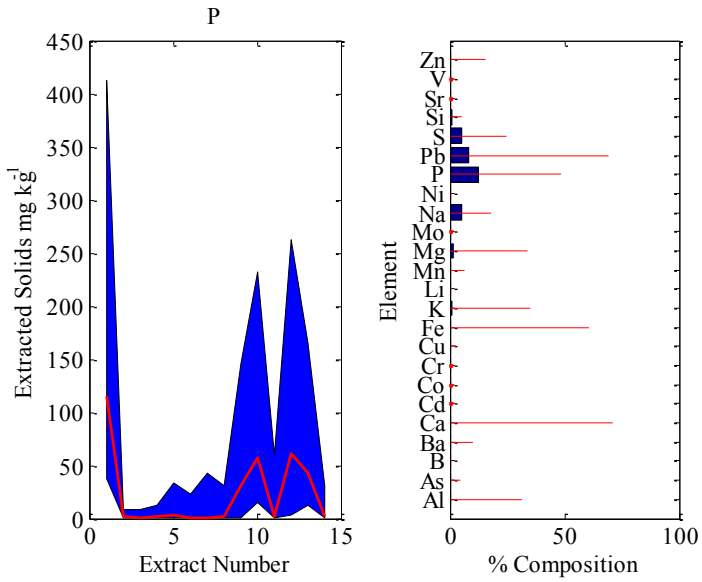
P
Extracted Solids mg kg-1
Extract Number
Element
% Composition
Zn
V
Sr
Si
S
Pb
P
Ni
Na
Mo
Mg
Mn
Li
K
Fe
Cu
Cr
Co
Cd
Ca
Ba
B
As
Al

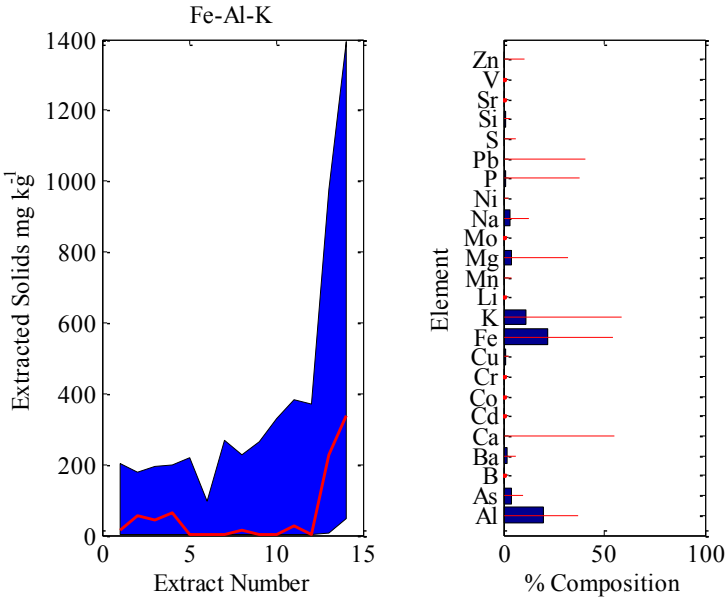
Fe-Al-K
Extracted Solids mg kg-1
Extract Number
Element
% Composition
Zn
V
Sr
Si
S
Pb
P
Ni
Na
Mo
Mg
Mn
Li
K
Fe
Cu
Cr
Co
Cd
Ca
Ba
B
As
Al

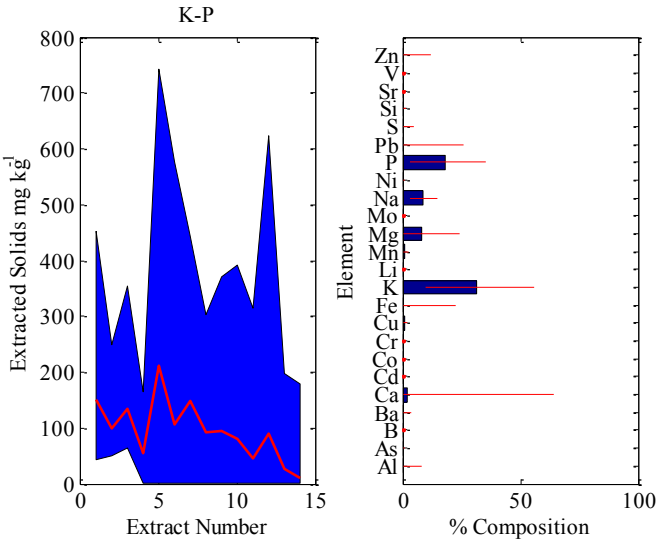
K-P
Extracted Solids mg kg-1
Extract Number
Element
% Composition
Zn
V
Sr
Si
S
Pb
P
Ni
Na
Mo
Mg
Mn
Li
K
Fe
Cu
Cr
Co
Cd
Ca
Ba
B
As
Al

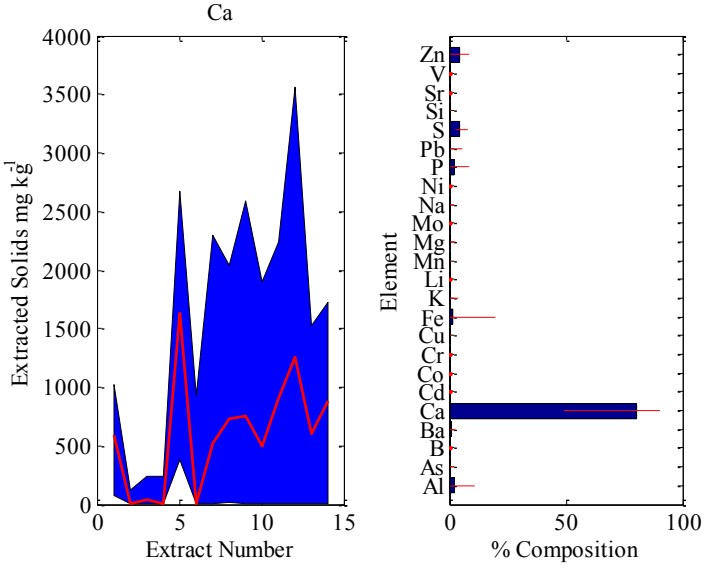
Ca
Extracted Solids mg kg-1
Extract Number
Element
% Composition
Zn
V
Sr
Si
S
Pb
P
Ni
Na
Mo
Mg
Mn
Li
K
Fe
Cu
Cr
Co
Cd
Ca
Ba
B
As
Al

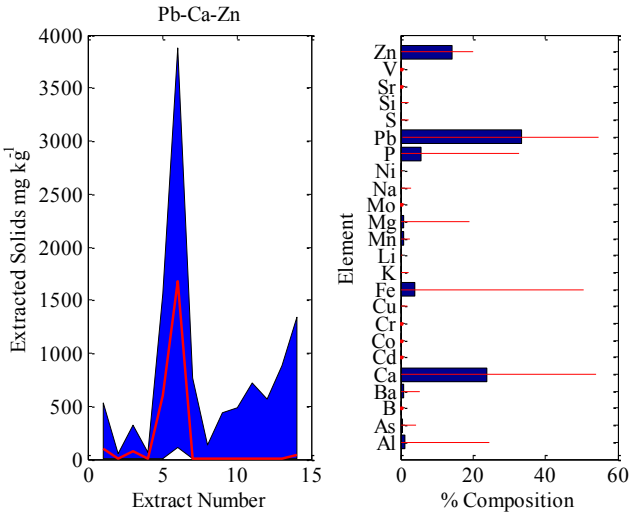
Pb-Ca-Zn
Extracted Solids mg kg-1
Extract Number
Element
% Composition
Zn
V
Sr
Si
S
Pb
P
Ni
Na
Mo
Mg
Mn
Li
K
Fe
Cu
Cr
Co
Cd
Ca
Ba
B
As
Al

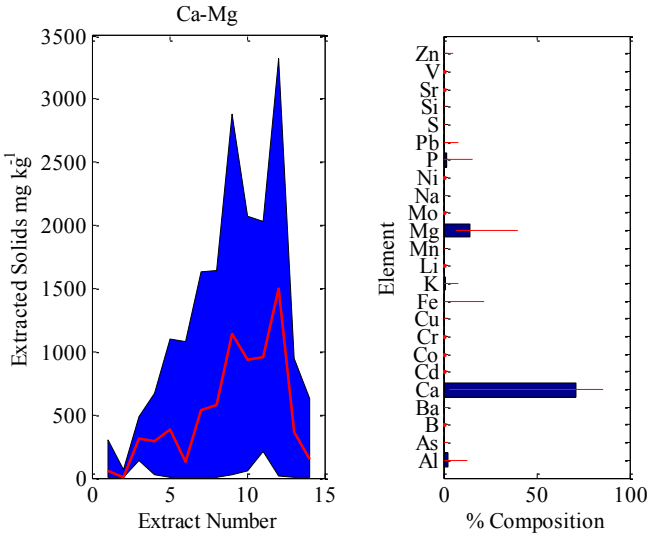
Ca-Mg
Extracted Solids mg kg-1
Extract Number
Element
% Composition
Zn
V
Sr
Si
S
Pb
P
Ni
Na
Mo
Mg
Mn
Li
K
Fe
Cu
Cr
Co
Cd
Ca
Ba
B
As
Al

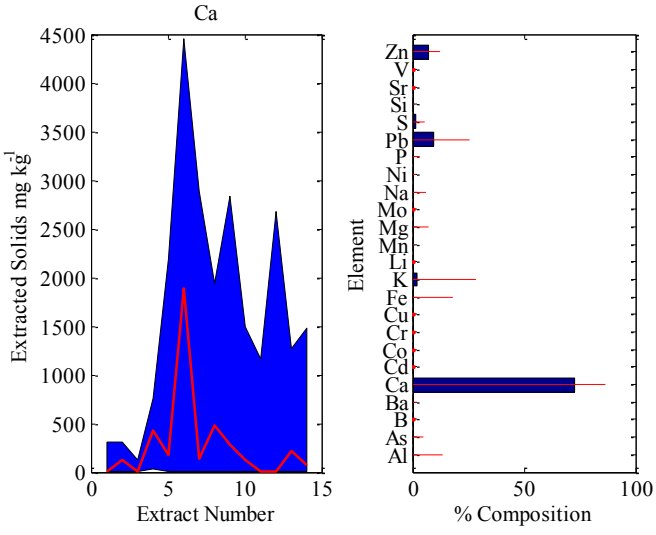
Ca
Extracted Solids mg kg-1
Extract Number
Element
% Composition
Zn
V
Sr
Si
S
Pb
P
Ni
Na
Mo
Mg
Mn
Li
K
Fe
Cu
Cr
Co
Cd
Ca
Ba
B
As
Al

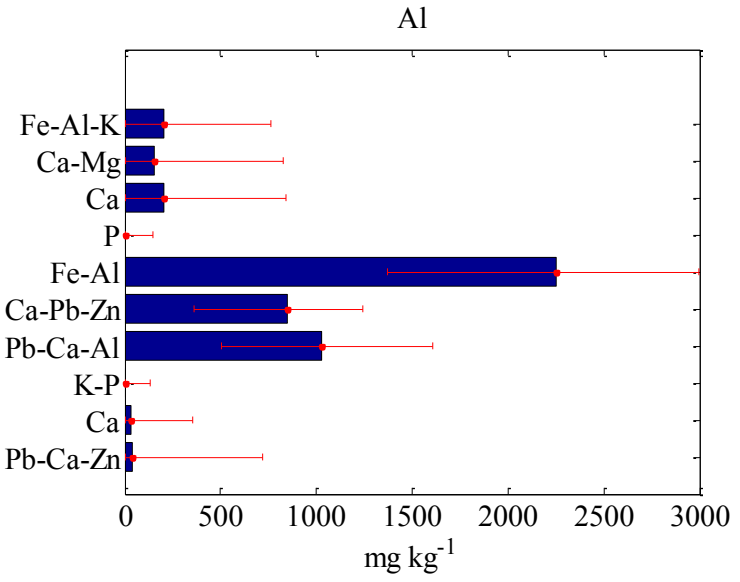
Al
Fe-Al-K
Ca-Mg
Ca
P
Fe-Al
Ca-Pb-Zn
Pb-Ca-Al
K-P
Ca
Pb-Ca-Zn
0
500
1000
1500
2000
2500
3000
mg kg-1

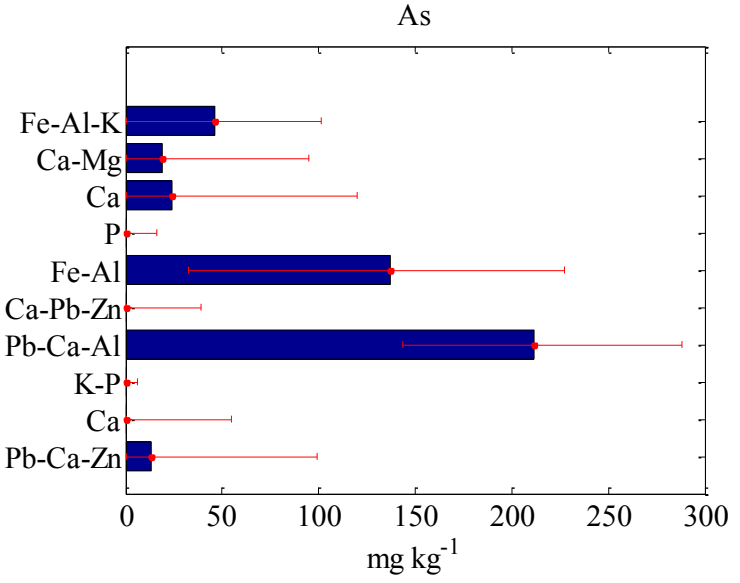
As
Fe-Al-K
Ca-Mg
Ca
P
Fe-Al
Ca-Pb-Zn
Pb-Ca-Al
K-P
Ca
Pb-Ca-Zn
0
50
100
150
200
250
300
mg kg-1

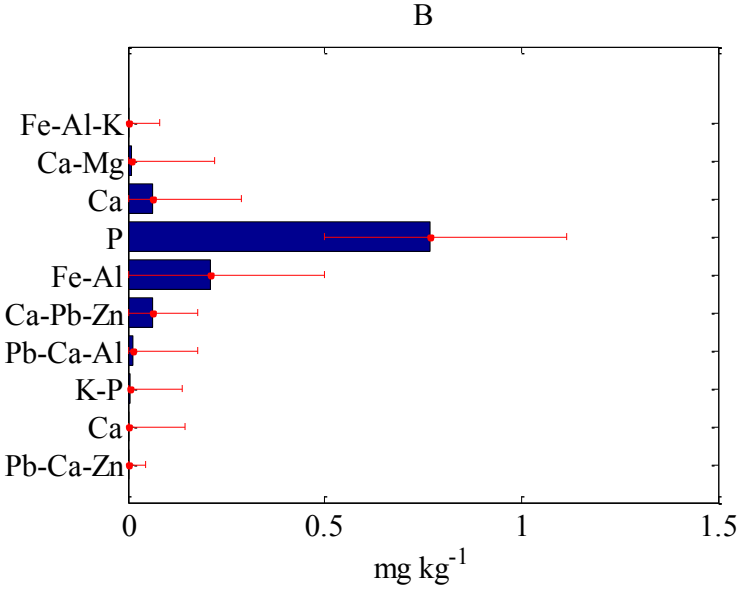
B
Fe-Al-K
Ca-Mg
Ca
P
Fe-Al
Ca-Pb-Zn
Pb-Ca-Al
K-P
Ca
Pb-Ca-Zn
0
0.5
1
1.5
mg kg-1

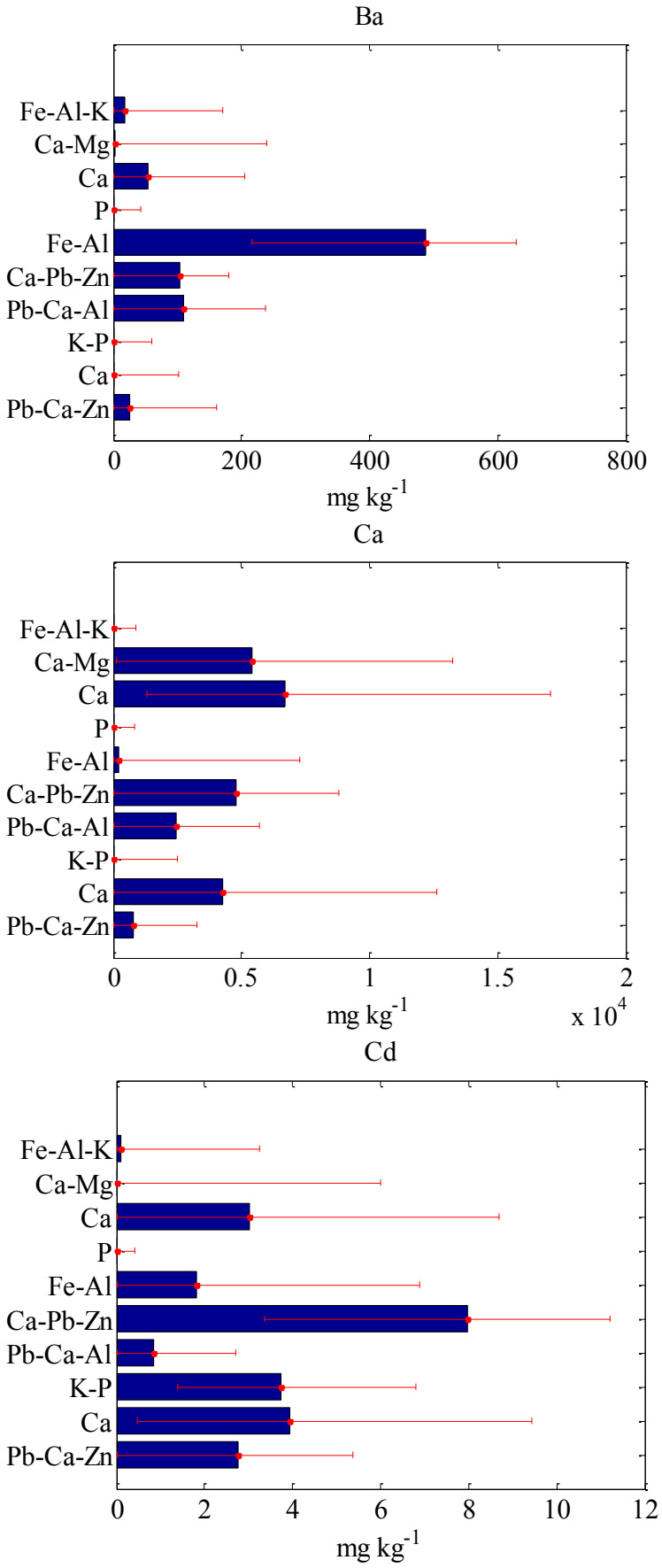
Ba
Fe-Al-K
Ca-Mg
Ca
P
Fe-Al
Ca-Pb-Zn
Pb-Ca-Al
K-P
Ca
Pb-Ca-Zn
0
200
400
600
800
mg kg-1
Ca
Fe-Al-K
Ca-Mg
Ca
P
Fe-Al
Ca-Pb-Zn
Pb-Ca-Al
K-P
Ca
Pb-Ca-Zn
0
0.5
1
1.5
2
mg kg-1
x 10^4
Cd
Fe-Al-K
Ca-Mg
Ca
P
Fe-Al
Ca-Pb-Zn
Pb-Ca-Al
K-P
Ca
Pb-Ca-Zn
0
2
4
6
8
10
12
mg kg-1

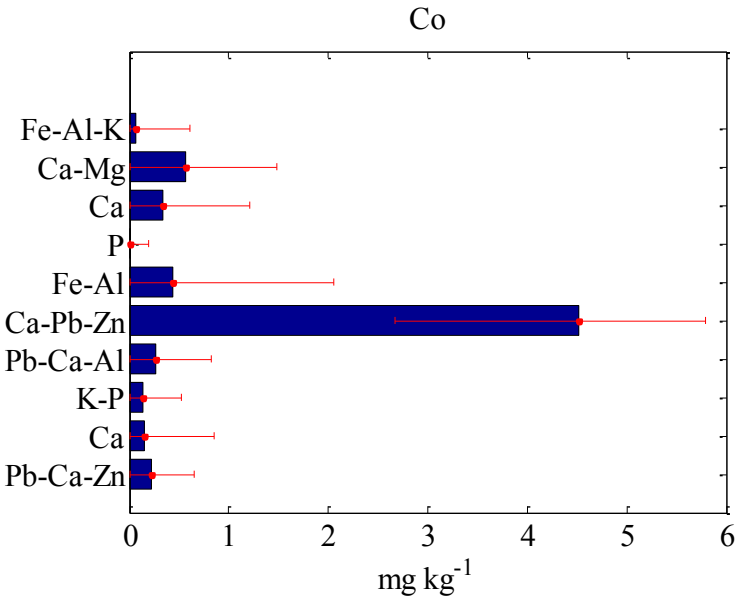
Co
Fe-Al-K
Ca-Mg
Ca
P
Fe-Al
Ca-Pb-Zn
Pb-Ca-Al
K-P
Ca
Pb-Ca-Zn
0
1
2
3
4
5
6
mg kg-1

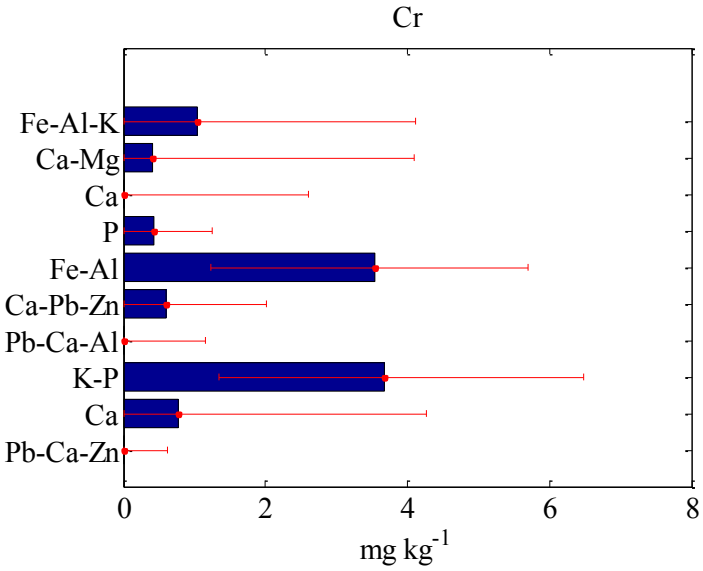
Cr
Fe-Al-K
Ca-Mg
Ca
P
Fe-Al
Ca-Pb-Zn
Pb-Ca-Al
K-P
Ca
Pb-Ca-Zn
0
2
4
6
8
mg kg-1

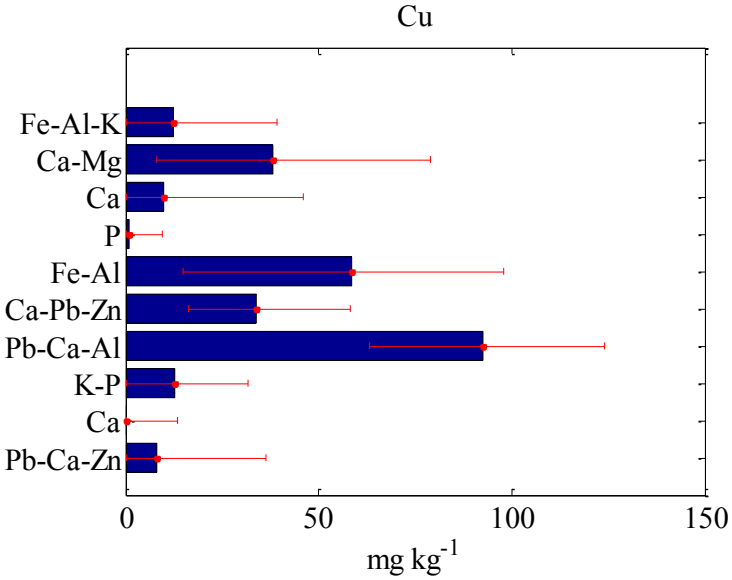
Cu
Fe-Al-K
Ca-Mg
Ca
P
Fe-Al
Ca-Pb-Zn
Pb-Ca-Al
K-P
Ca
Pb-Ca-Zn
0
50
100
150
mg kg-1

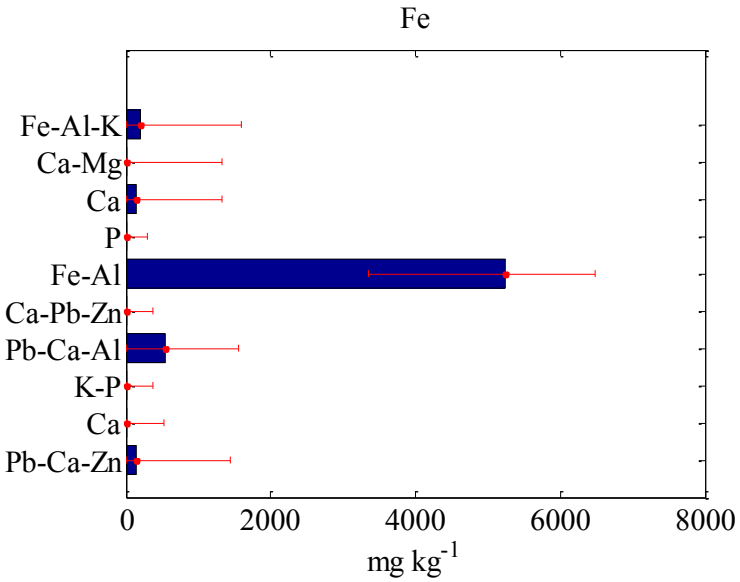
Fe
Fe-Al-K
Ca-Mg
Ca
P
Fe-Al
Ca-Pb-Zn
Pb-Ca-Al
K-P
Ca
Pb-Ca-Zn
0
2000
4000
6000
8000
mg kg-1

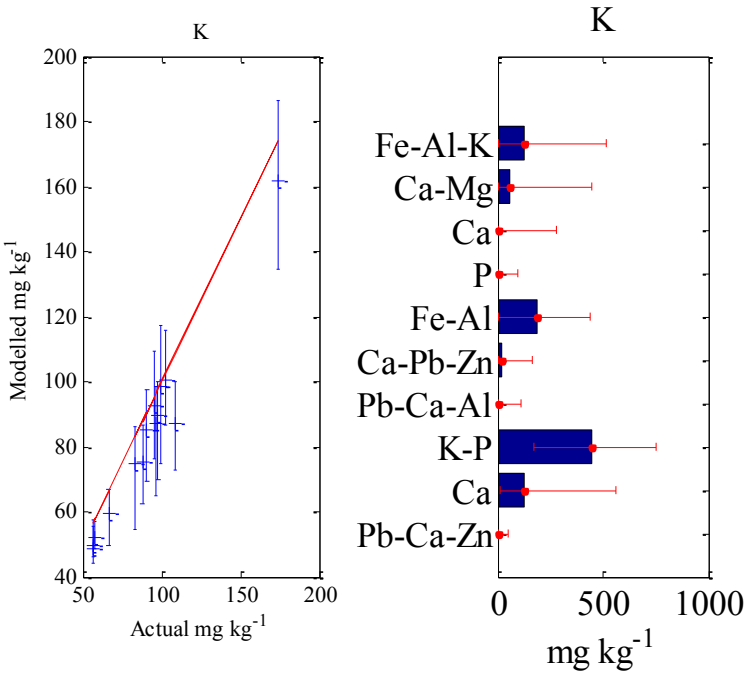
K
200
180
160
140
120
100
80
60
40
Modelled mg kg-1
50
100
150
200
Actual mg kg-1
K
Fe-Al-K
Ca-Mg
Ca
P
Fe-Al
Ca-Pb-Zn
Pb-Ca-Al
K-P
Ca
Pb-Ca-Zn
0
500
1000
mg kg-1

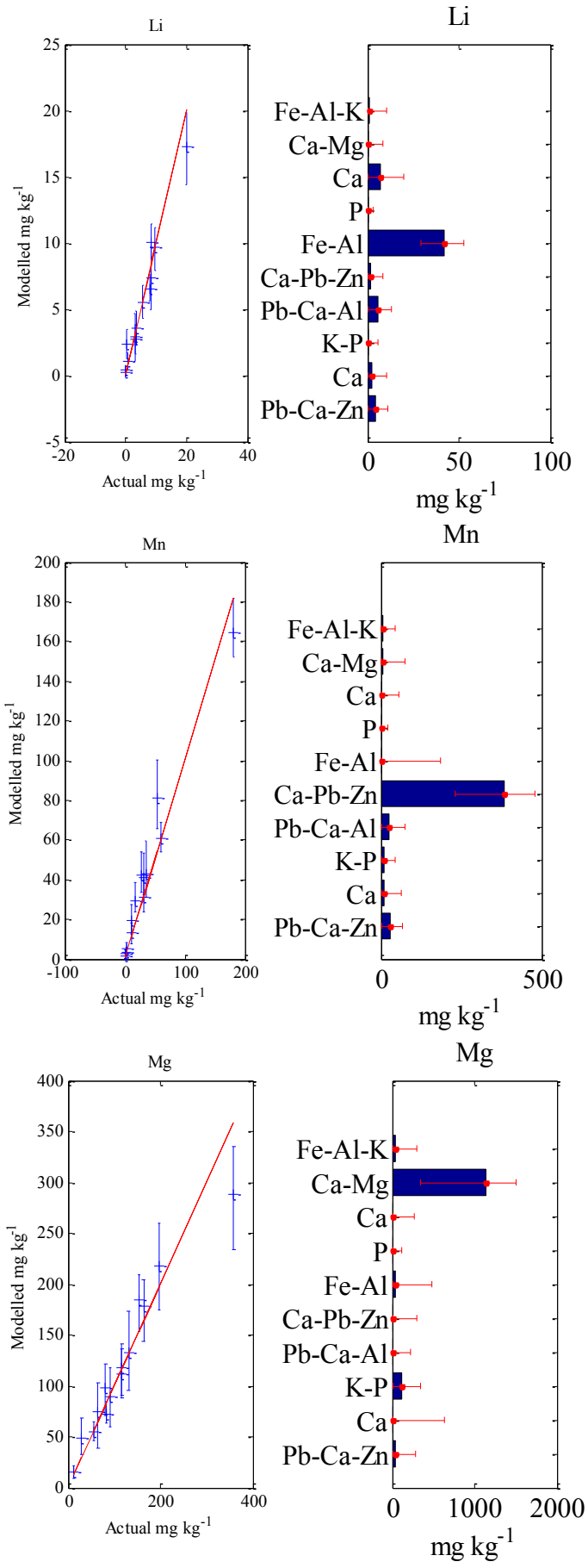
Li
Modelled mg kg-1
Actual mg kg-1
Li
Fe-Al-K
Ca-Mg
Ca
P
Fe-Al
Ca-Pb-Zn
Pb-Ca-Al
K-P
Ca
Pb-Ca-Zn
mg kg-1
Mn
Modelled mg kg-1
Actual mg kg-1
Mn
Fe-Al-K
Ca-Mg
Ca
P
Fe-Al
Ca-Pb-Zn
Pb-Ca-Al
K-P
Ca
Pb-Ca-Zn
mg kg-1
Mg
Modelled mg kg-1
Actual mg kg-1
Mg
Fe-Al-K
Ca-Mg
Ca
P
Fe-Al
Ca-Pb-Zn
Pb-Ca-Al
K-P
Ca
Pb-Ca-Zn
mg kg-1

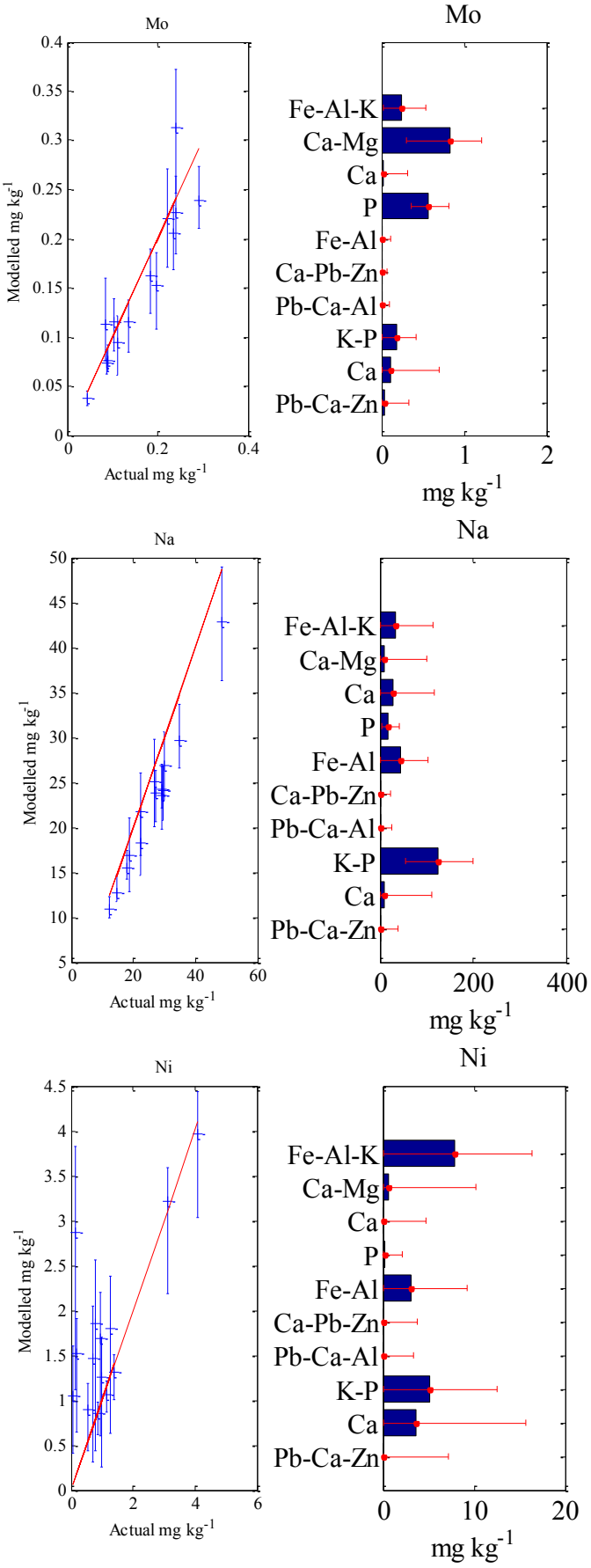
Mo
Modelled mg kg-1
Actual mg kg-1
Mo
Fe-Al-K
Ca-Mg
Ca
P
Fe-Al
Ca-Pb-Zn
Pb-Ca-Al
K-P
Ca
Pb-Ca-Zn
mg kg-1
Na
Modelled mg kg-1
Actual mg kg-1
Na
Fe-Al-K
Ca-Mg
Ca
P
Fe-Al
Ca-Pb-Zn
Pb-Ca-Al
K-P
Ca
Pb-Ca-Zn
mg kg-1
Ni
Modelled mg kg-1
Actual mg kg-1
Ni
Fe-Al-K
Ca-Mg
Ca
P
Fe-Al
Ca-Pb-Zn
Pb-Ca-Al
K-P
Ca
Pb-Ca-Zn
mg kg-1

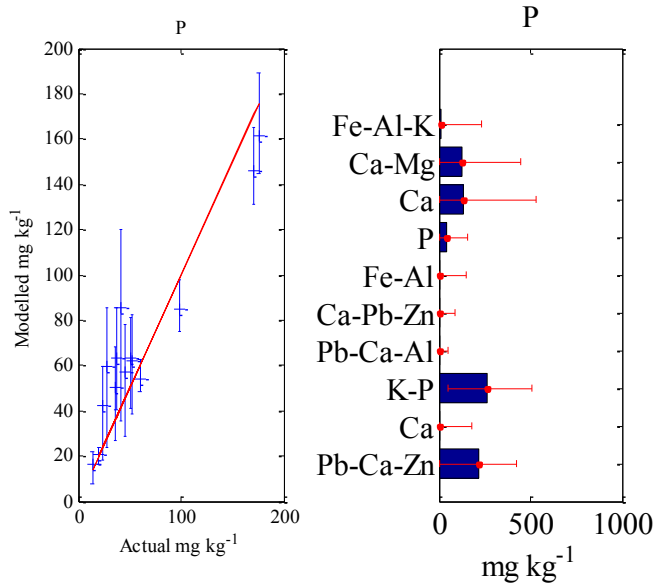
P
Modelled mg kg-1
Actual mg kg-1
0
20
40
60
80
100
120
140
160
180
200
0
100
200
P
Fe-Al-K
Ca-Mg
Ca
P
Fe-Al
Ca-Pb-Zn
Pb-Ca-Al
K-P
Ca
Pb-Ca-Zn
0
500
1000
mg kg-1

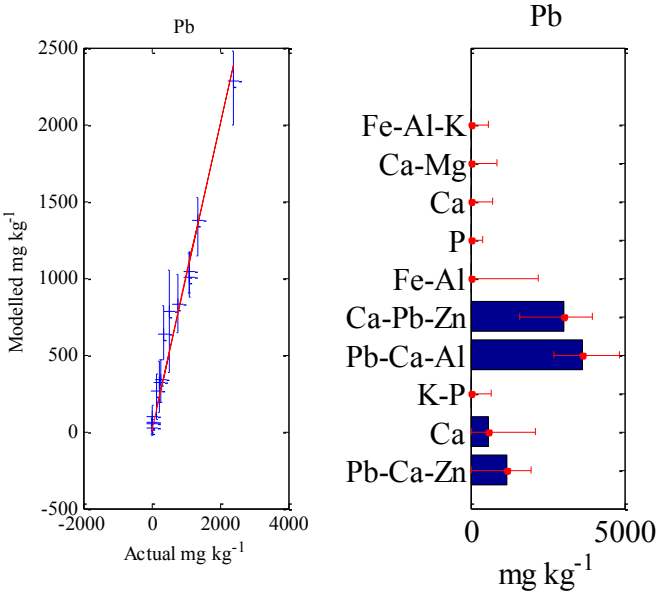
Pb
Modelled mg kg-1
Actual mg kg-1
-500
0
500
1000
1500
2000
2500
-2000
0
2000
4000
Pb
Fe-Al-K
Ca-Mg
Ca
P
Fe-Al
Ca-Pb-Zn
Pb-Ca-Al
K-P
Ca
Pb-Ca-Zn
0
5000
mg kg-1

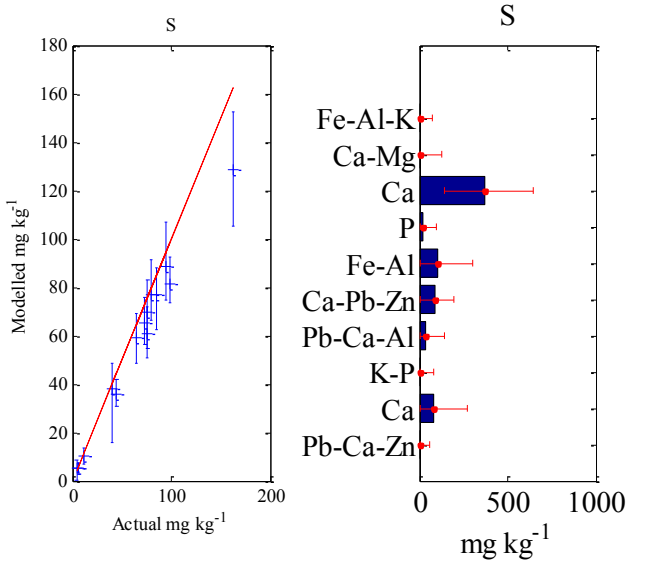
S
Modelled mg kg-1
Actual mg kg-1
0
20
40
60
80
100
120
140
160
180
0
100
200
S
Fe-Al-K
Ca-Mg
Ca
P
Fe-Al
Ca-Pb-Zn
Pb-Ca-Al
K-P
Ca
Pb-Ca-Zn
0
500
1000
mg kg-1

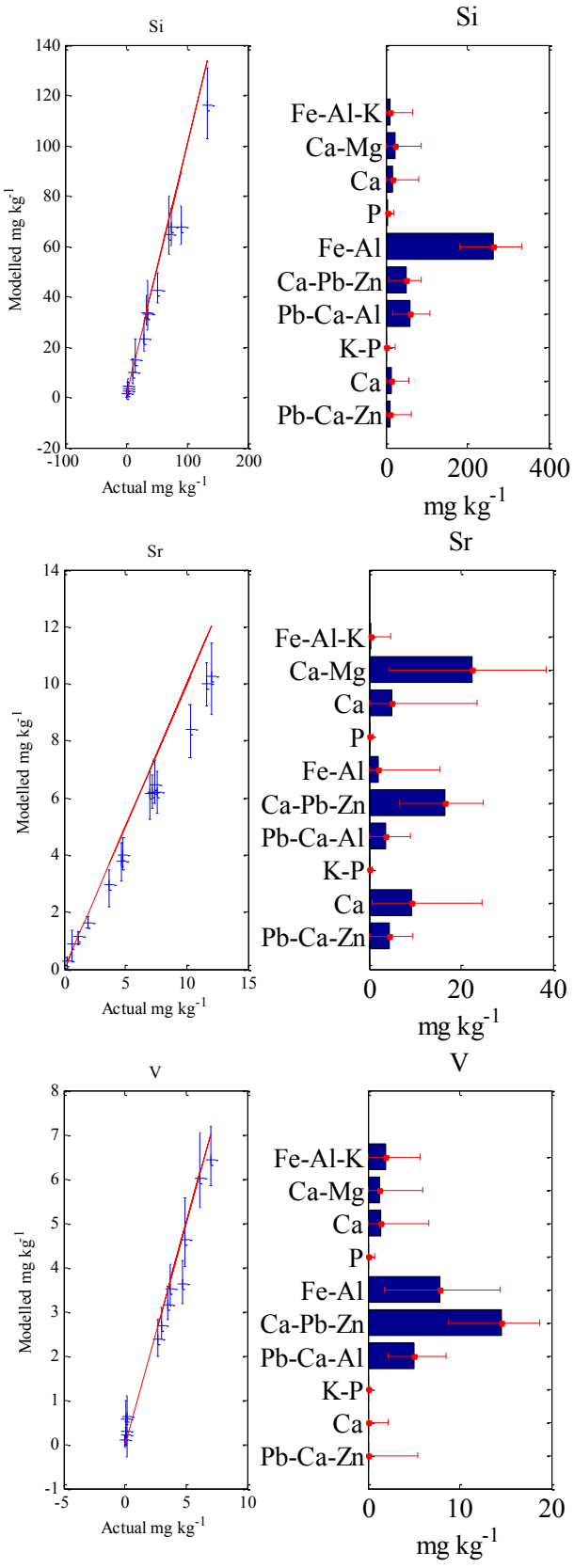
Si
Modelled mg kg-1
Actual mg kg-1
Si
Fe-Al-K
Ca-Mg
Ca
P
Fe-Al
Ca-Pb-Zn
Pb-Ca-Al
K-P
Ca
Pb-Ca-Zn
mg kg-1
Sr
Modelled mg kg-1
Actual mg kg-1
Sr
Fe-Al-K
Ca-Mg
Ca
P
Fe-Al
Ca-Pb-Zn
Pb-Ca-Al
K-P
Ca
Pb-Ca-Zn
mg kg-1
V
Modelled mg kg-1
Actual mg kg-1
V
Fe-Al-K
Ca-Mg
Ca
P
Fe-Al
Ca-Pb-Zn
Pb-Ca-Al
K-P
Ca
Pb-Ca-Zn
mg kg-1

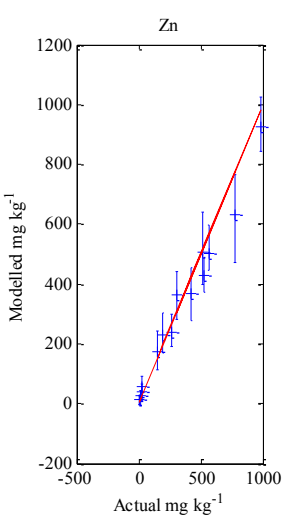
Zn
Modelled mg kg-1
Actual mg kg-1

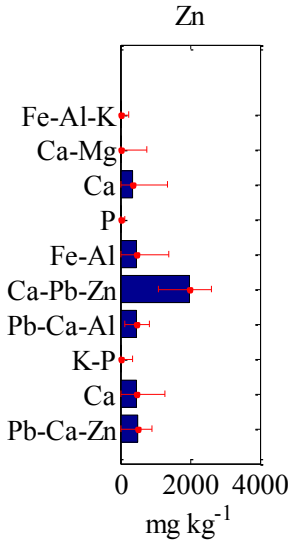
Zn
Fe-Al-K
Ca-Mg
Ca
P
Fe-Al
Ca-Pb-Zn
Pb-Ca-Al
K-P
Ca
Pb-Ca-Zn
mg kg-1

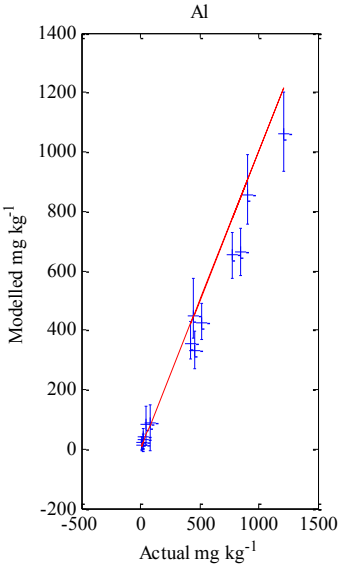
Al
Modelled mg kg-1
Actual mg kg-1

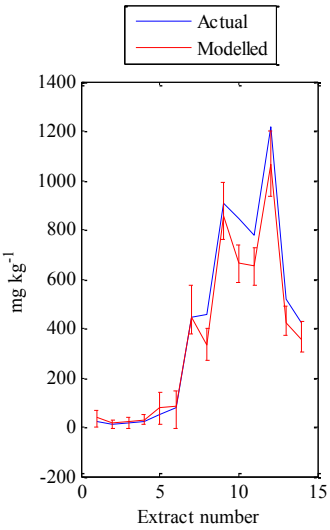
Actual
Modelled
mg kg-1
Extract number

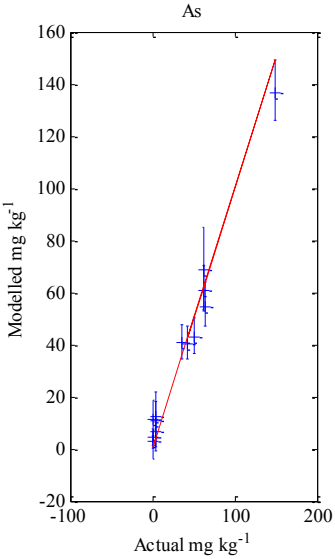
As
Modelled mg kg-1
Actual mg kg-1

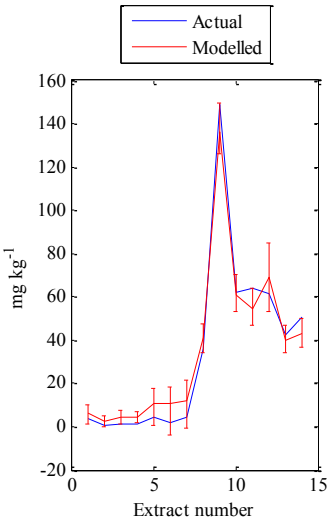
Actual
Modelled
mg kg-1
Extract number

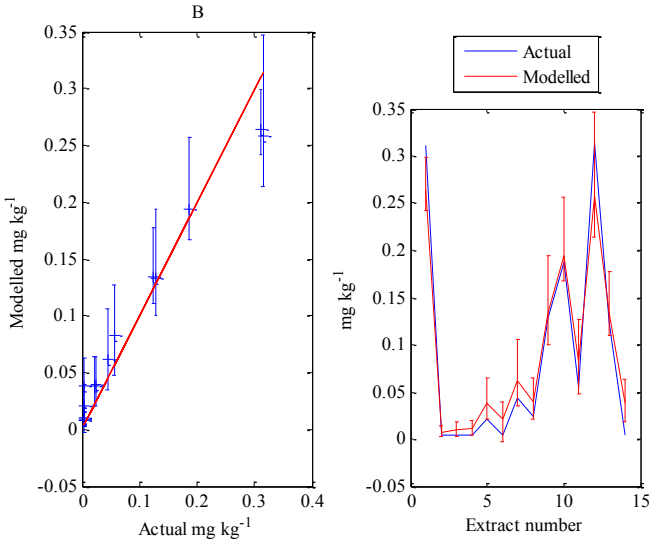
B
Modelled mg kg-1
Actual mg kg-1
Actual
Modelled
mg kg-1
Extract number

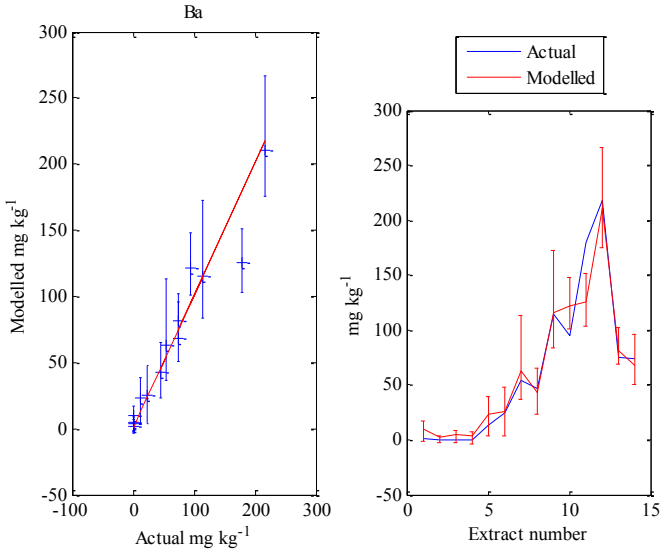
Ba
Modelled mg kg-1
Actual mg kg-1
Actual
Modelled
mg kg-1
Extract number

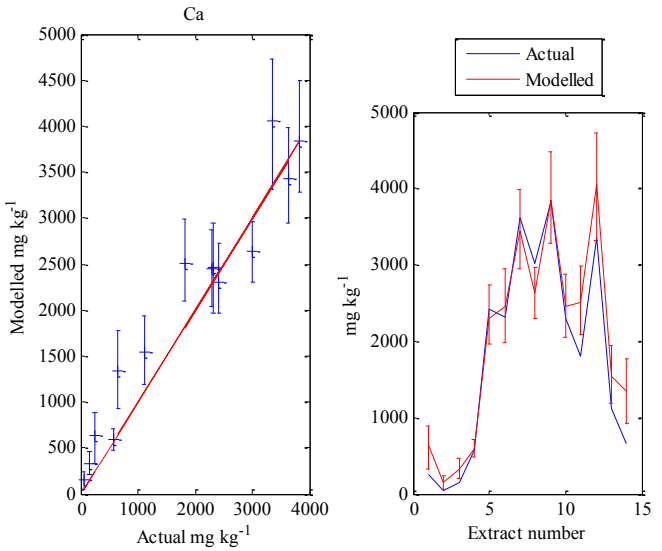
Ca
Modelled mg kg-1
Actual mg kg-1
Actual
Modelled
mg kg-1
Extract number

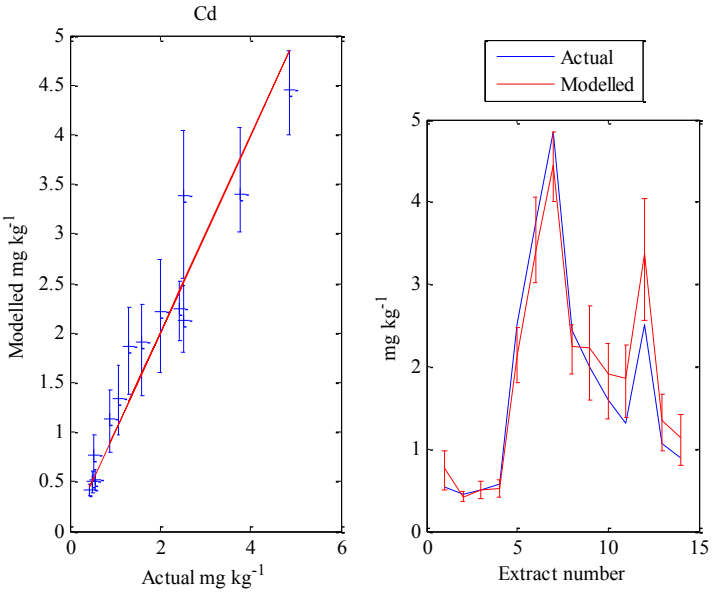
Cd
Modelled mg kg-1
Actual mg kg-1
Actual
Modelled
mg kg-1
Extract number

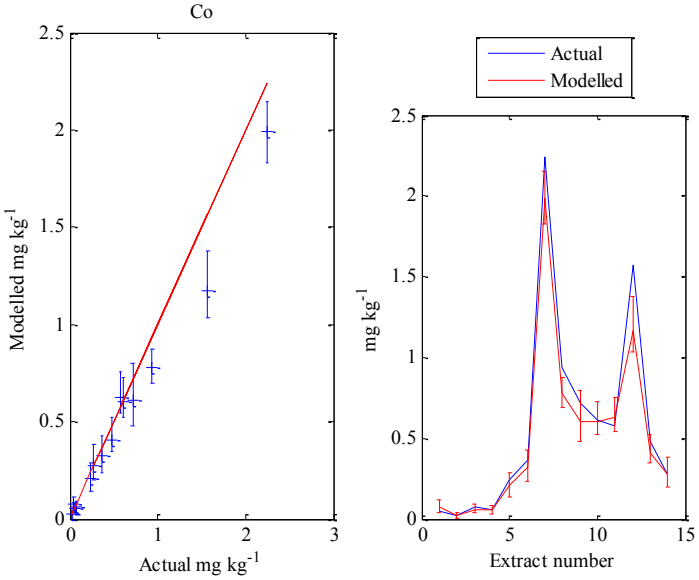
Co
Modelled mg kg-1
Actual mg kg-1
Actual
Modelled
mg kg-1
Extract number

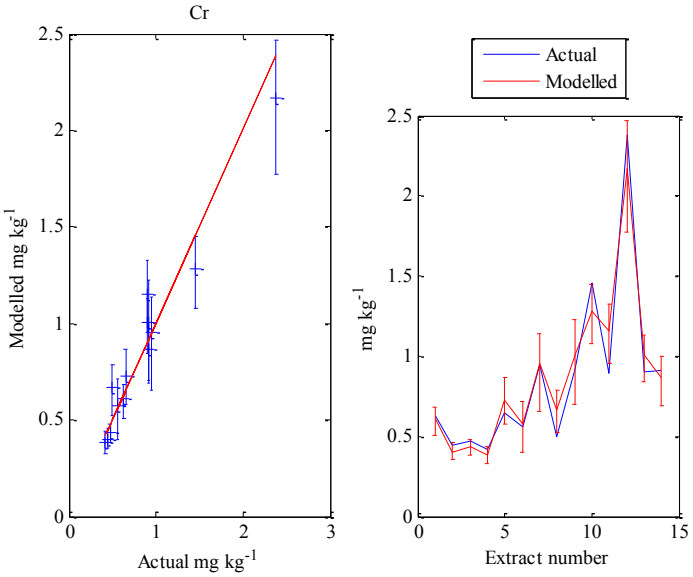
Cr
Modelled mg kg-1
Actual mg kg-1
Actual
Modelled
mg kg-1
Extract number

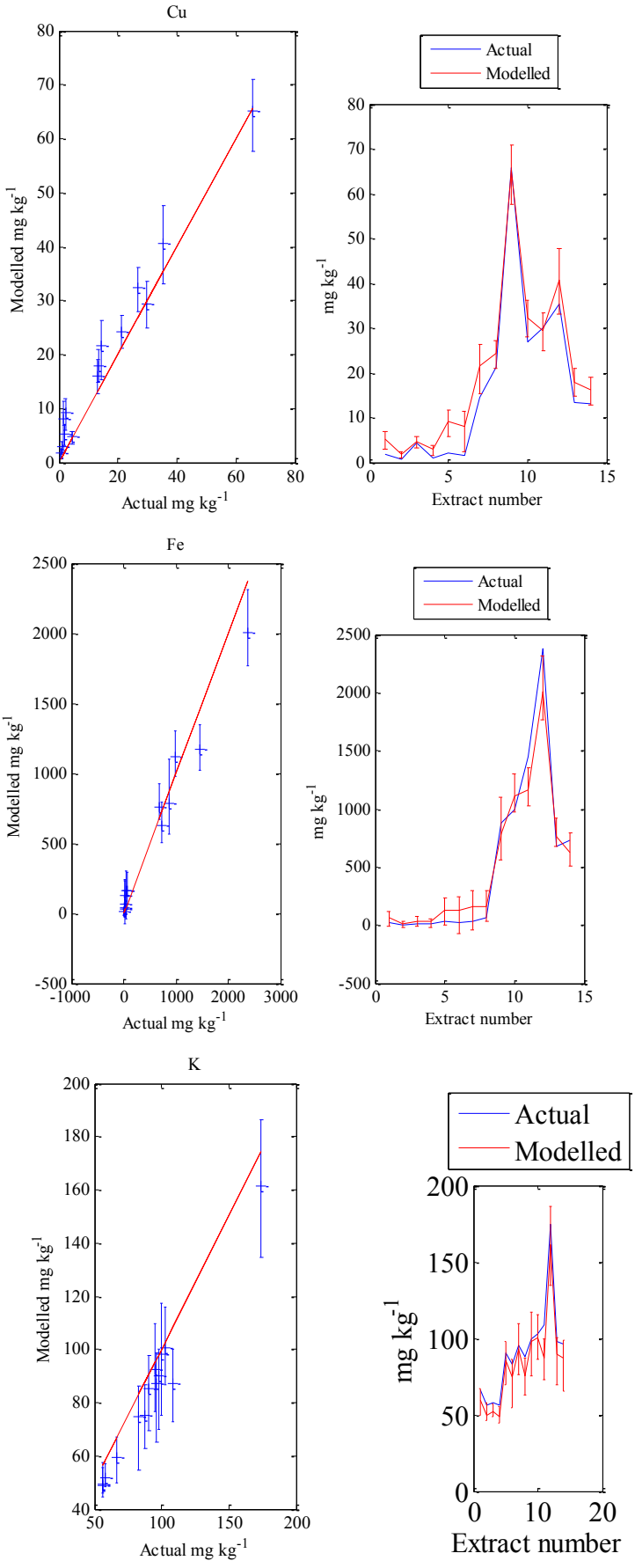
Cu
Modelled mg kg-1
Actual mg kg-1
Actual
Modelled
mg kg-1
Extract number
Fe
Modelled mg kg-1
Actual mg kg-1
Actual
Modelled
mg kg-1
Extract number
K
Modelled mg kg-1
Actual mg kg-1
Actual
Modelled
mg kg-1
Extract number

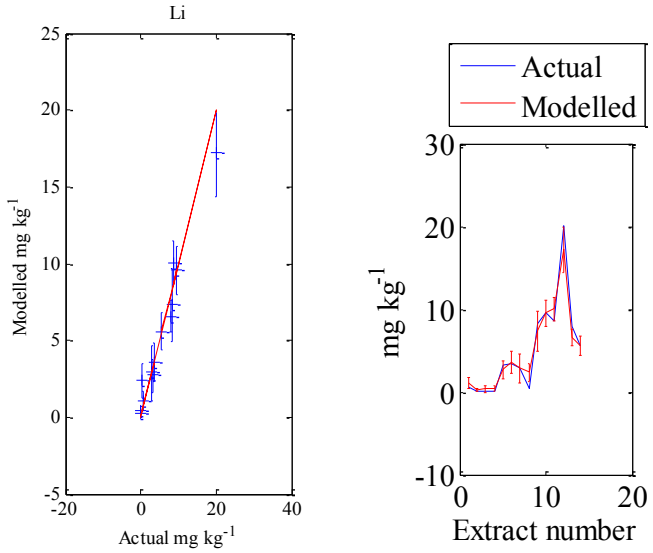
Li
Modelled mg kg-1
Actual mg kg-1
Actual
Modelled
mg kg-1
Extract number

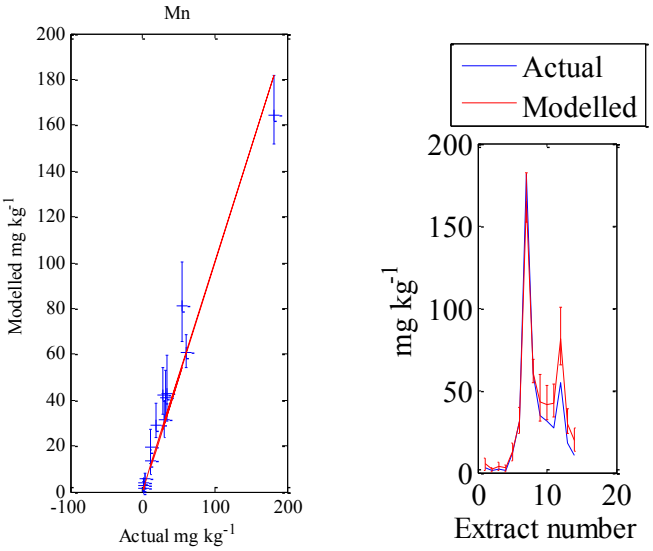
Mn
Modelled mg kg-1
Actual mg kg-1
Actual
Modelled
mg kg-1
Extract number

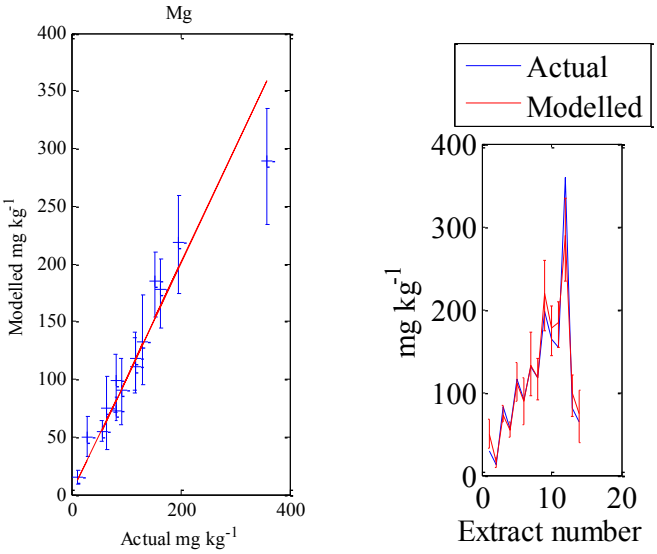
Mg
Modelled mg kg-1
Actual mg kg-1
Actual
Modelled
mg kg-1
Extract number

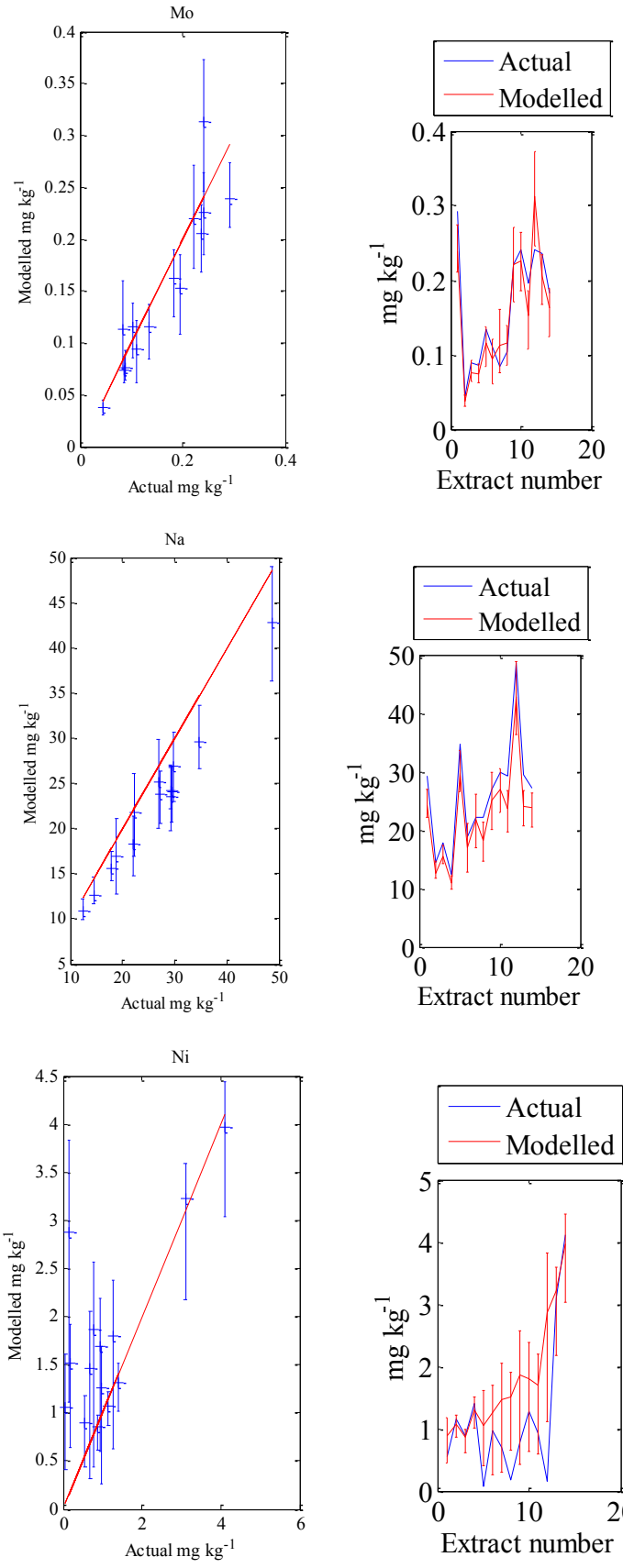
Mo
Modelled mg kg-1
Actual mg kg-1
Actual
Modelled
mg kg-1
Extract number
Na
Modelled mg kg-1
Actual mg kg-1
Actual
Modelled
mg kg-1
Extract number
Ni
Modelled mg kg-1
Actual mg kg-1
Actual
Modelled
mg kg-1
Extract number

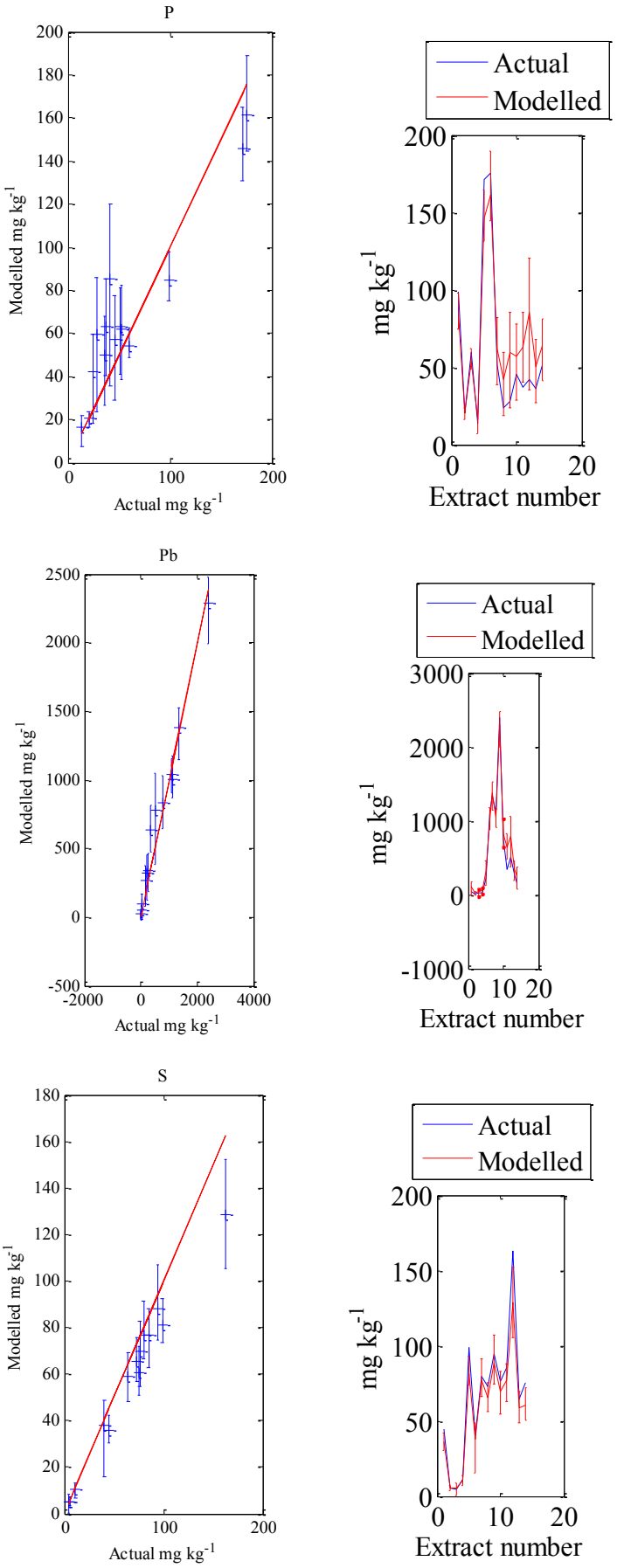
P
Modelled mg kg-1
Actual mg kg-1
0
20
40
60
80
100
120
140
160
180
200
0
100
200
Actual
Modelled
mg kg-1
0
50
100
150
200
0
10
20
Extract number
Pb
Modelled mg kg-1
Actual mg kg-1
-500
0
500
1000
1500
2000
2500
-2000
0
2000
4000
Actual
Modelled
mg kg-1
-1000
0
1000
2000
3000
0
10
20
Extract number
S
Modelled mg kg-1
Actual mg kg-1
0
20
40
60
80
100
120
140
160
180
0
100
200
Actual
Modelled
mg kg-1
0
50
100
150
200
0
10
20
Extract number

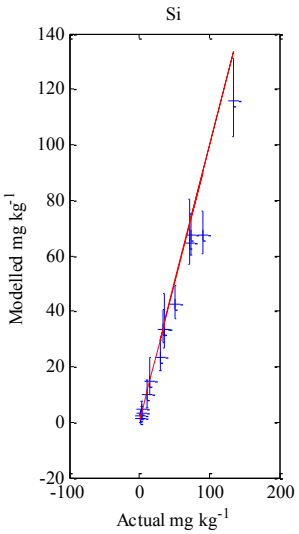
Si
Modelled mg kg-1
Actual mg kg-1

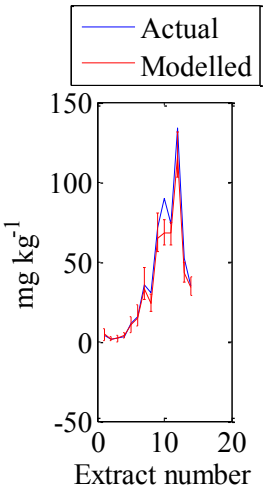
Actual
Modelled
mg kg-1
Extract number

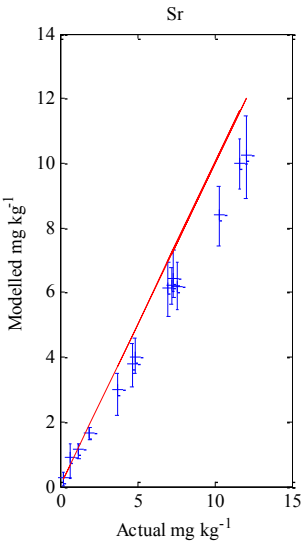
Sr
Modelled mg kg-1
Actual mg kg-1

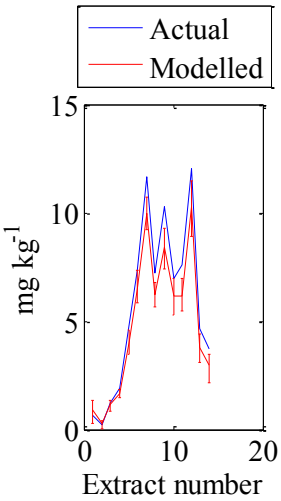
Actual
Modelled
mg kg-1
Extract number

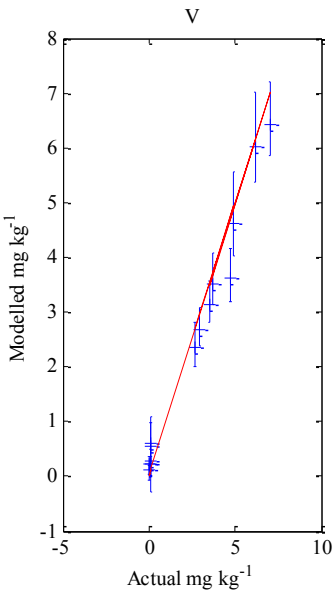
V
Modelled mg kg-1
Actual mg kg-1

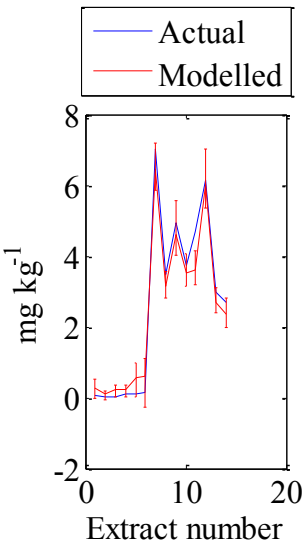
Actual
Modelled
mg kg-1
Extract number

Soil 3

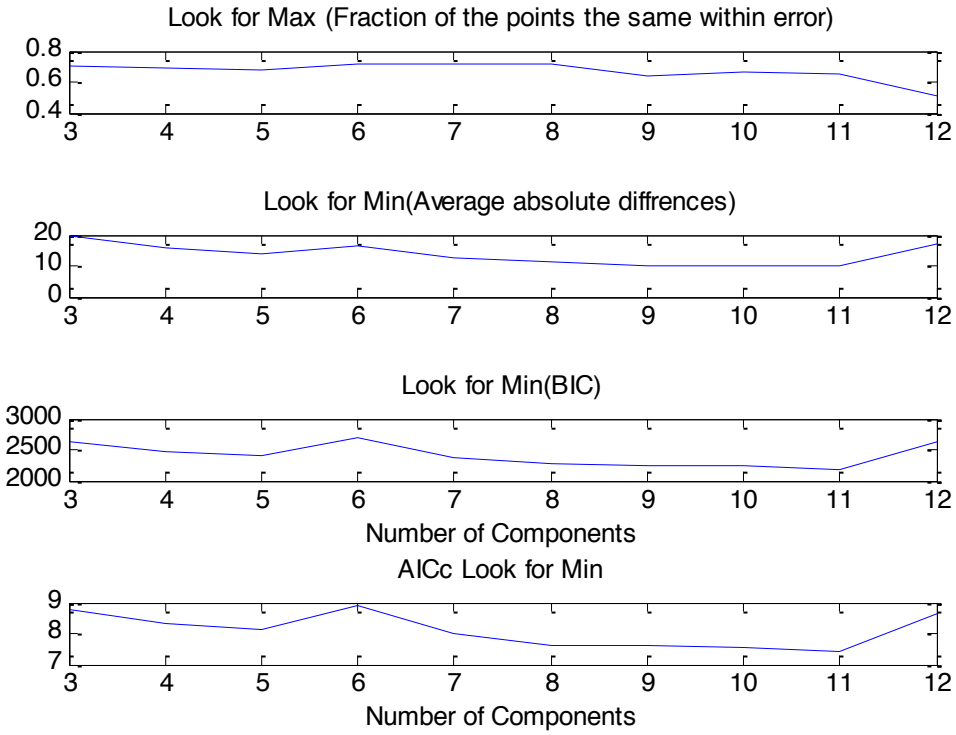
Look for Max (Fraction of the points the same within error)
0.8
0.6
0.4
3 4 5 6 7 8 9 10 11 12
Look for Min(Average absolute diffrences)
20
10
0
3 4 5 6 7 8 9 10 11 12
Look for Min(BIC)
3000
2500
2000
3 4 5 6 7 8 9 10 11 12
Number of Components
AICc Look for Min
9
8
7
3 4 5 6 7 8 9 10 11 12
Number of Components

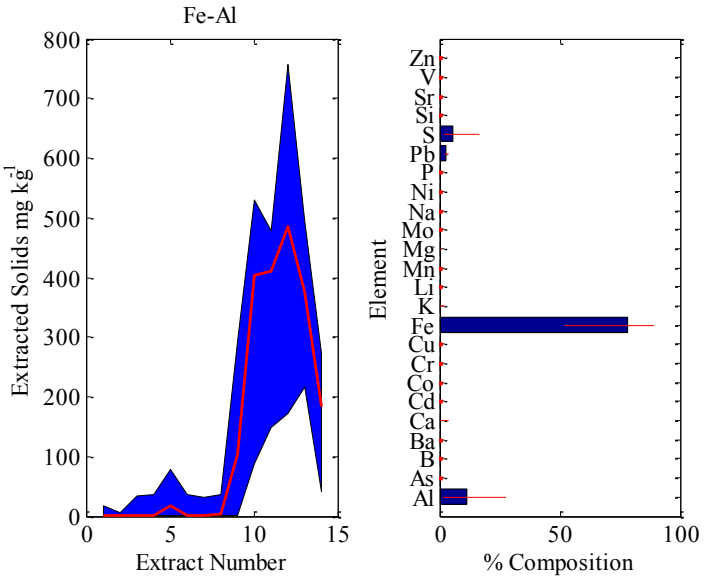
Fe-Al
Extracted Solids mg kg-1
800
700
600
500
400
300
200
100
0
0 5 10 15
Extract Number
Element
Zn
V
Sr
Si
S
Pb
P
Ni
Na
Mo
Mg
Mn
Li
K
Fe
Cu
Cr
Co
Cd
Ca
Ba
B
As
Al
0 50 100
% Composition

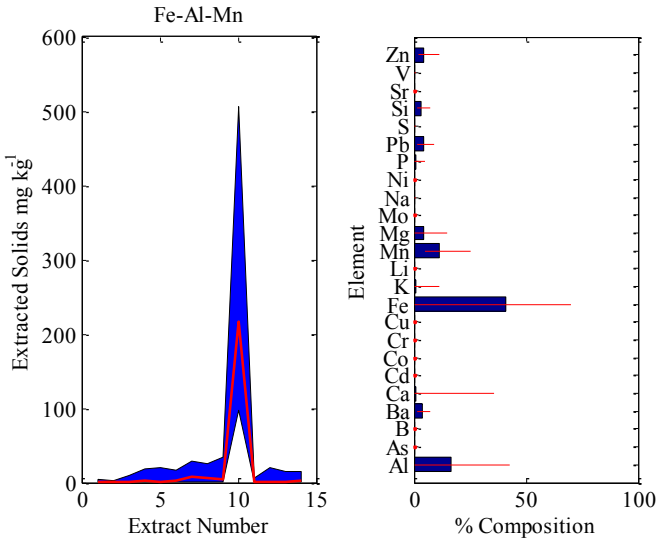
Fe-Al-Mn
Extracted Solids mg kg-1
Extract Number
Element
% Composition
Zn
V
Sr
Si
S
Pb
P
Ni
Na
Mo
Mg
Mn
Li
K
Fe
Cu
Cr
Co
Cd
Ca
Ba
B
As
Al

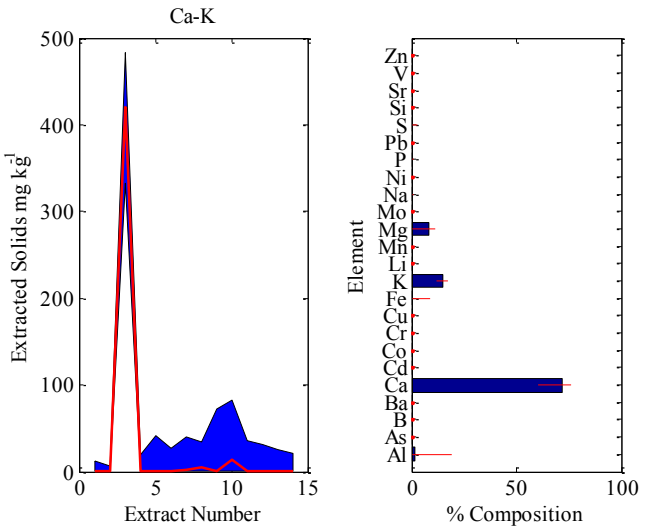
Ca-K
Extracted Solids mg kg-1
Extract Number
Element
% Composition
Zn
V
Sr
Si
S
Pb
P
Ni
Na
Mo
Mg
Mn
Li
K
Fe
Cu
Cr
Co
Cd
Ca
Ba
B
As
Al

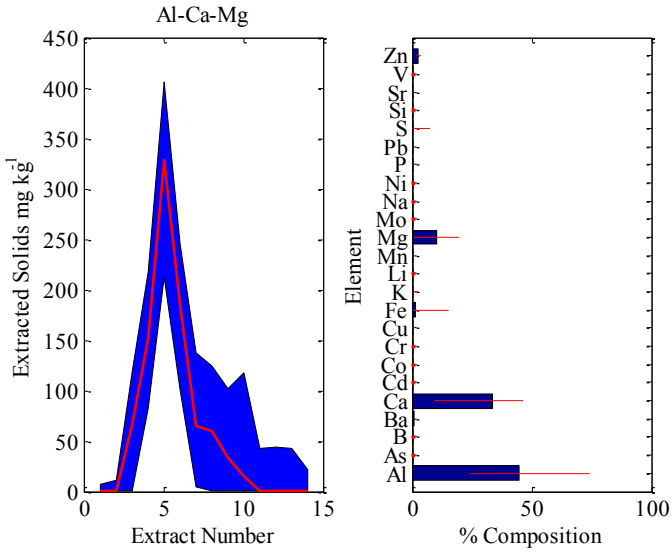
Al-Ca-Mg
Extracted Solids mg kg-1
Extract Number
Element
% Composition
Zn
V
Sr
Si
S
Pb
P
Ni
Na
Mo
Mg
Mn
Li
K
Fe
Cu
Cr
Co
Cd
Ca
Ba
B
As
Al

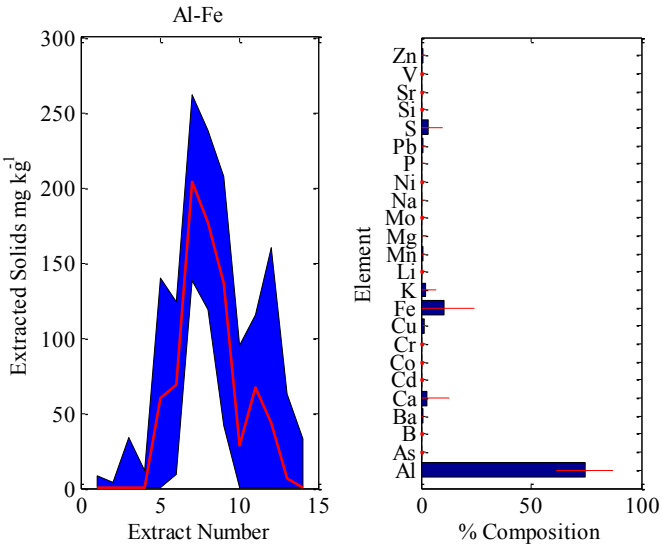
Al-Fe
Extracted Solids mg kg-1
Extract Number
Element
% Composition
Zn
V
Sr
Si
S
Pb
P
Ni
Na
Mo
Mg
Mn
Li
K
Fe
Cu
Cr
Co
Cd
Ca
Ba
B
As
Al

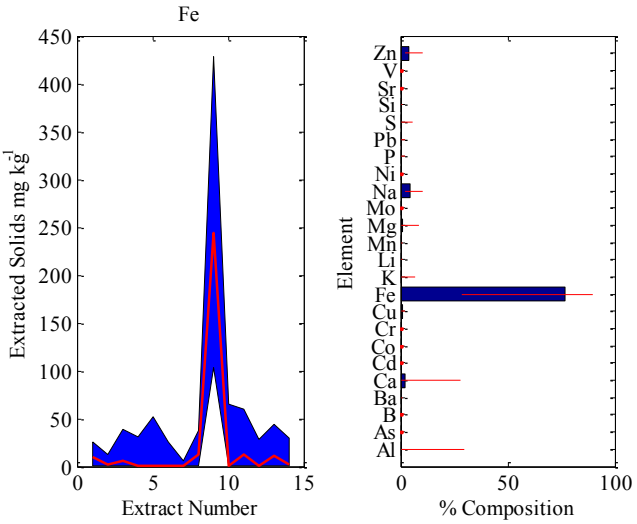
Fe
Extracted Solids mg kg-1
Extract Number
Element
% Composition
Zn
V
Sr
Si
S
Pb
P
Ni
Na
Mo
Mg
Mn
Li
K
Fe
Cu
Cr
Co
Cd
Ca
Ba
B
As
Al

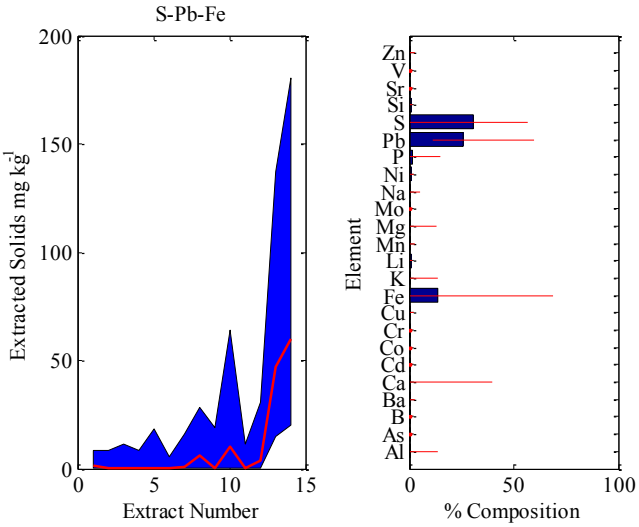
S-Pb-Fe
Extracted Solids mg kg-1
Extract Number
Element
% Composition
Zn
V
Sr
Si
S
Pb
P
Ni
Na
Mo
Mg
Mn
Li
K
Fe
Cu
Cr
Co
Cd
Ca
Ba
B
As
Al

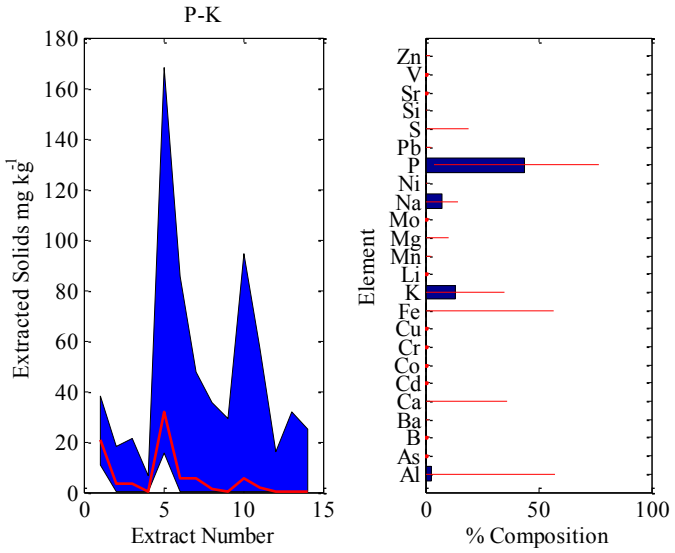
P-K
Extracted Solids mg kg-1
Extract Number
Element
% Composition
Zn
V
Sr
Si
S
Pb
P
Ni
Na
Mo
Mg
Mn
Li
K
Fe
Cu
Cr
Co
Cd
Ca
Ba
B
As
Al

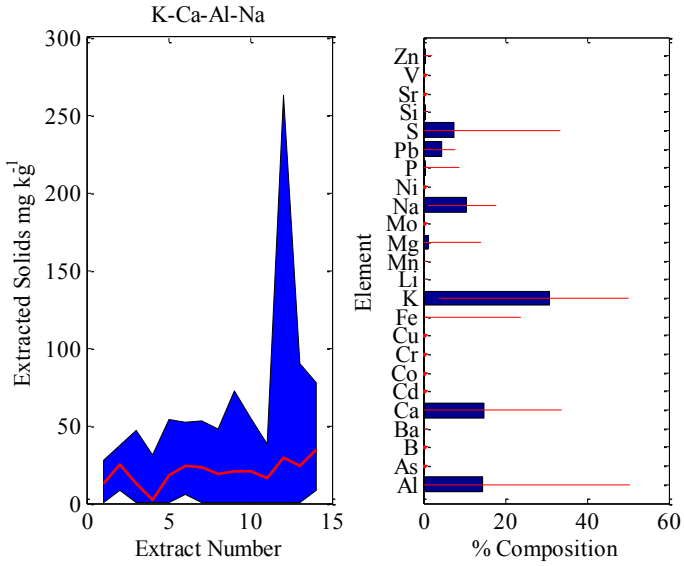
K-Ca-Al-Na
Extracted Solids mg kg-1
Extract Number
Element
% Composition
Zn
V
Sr
Si
S
Pb
P
Ni
Na
Mo
Mg
Mn
Li
K
Fe
Cu
Cr
Co
Cd
Ca
Ba
B
As
Al

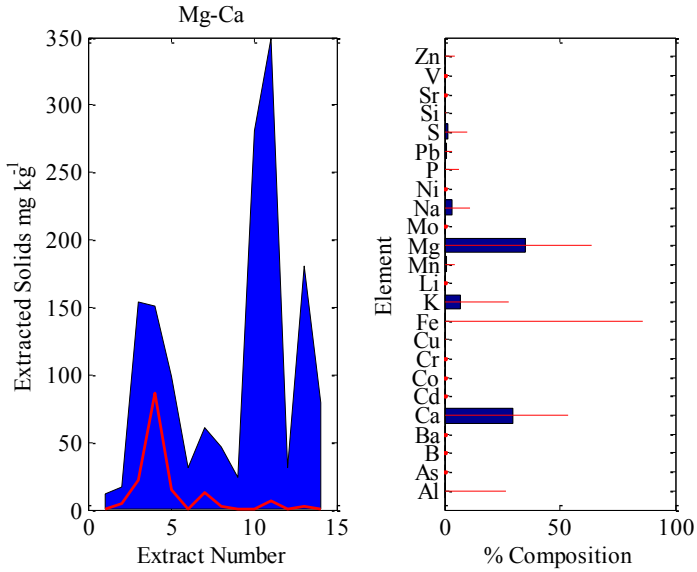
Mg-Ca
Extracted Solids mg kg-1
Extract Number
Element
% Composition
Zn
V
Sr
Si
S
Pb
P
Ni
Na
Mo
Mg
Mn
Li
K
Fe
Cu
Cr
Co
Cd
Ca
Ba
B
As
Al

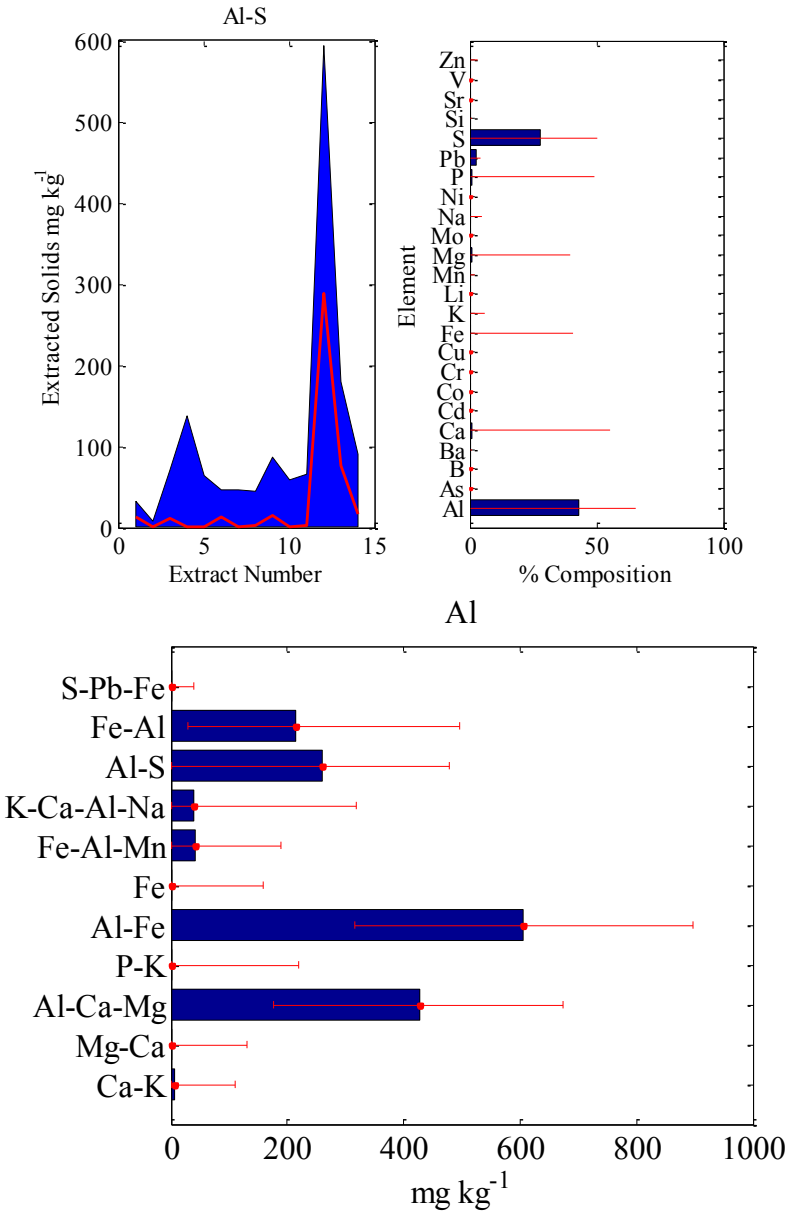
Al-S
Extracted Solids mg kg-1
Extract Number
Element
% Composition
Zn
V
Sr
Si
S
Pb
P
Ni
Na
Mo
Mg
Mn
Li
K
Fe
Cu
Cr
Co
Cd
Ca
Ba
B
As
Al
Al
S-Pb-Fe
Fe-Al
Al-S
K-Ca-Al-Na
Fe-Al-Mn
Fe
Al-Fe
P-K
Al-Ca-Mg
Mg-Ca
Ca-K
mg kg-1

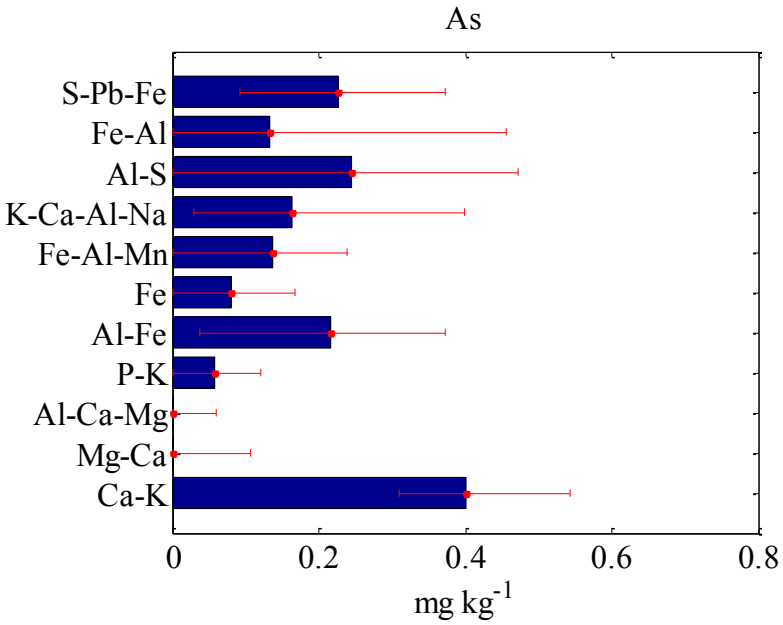
As
S-Pb-Fe
Fe-Al
Al-S
K-Ca-Al-Na
Fe-Al-Mn
Fe
Al-Fe
P-K
Al-Ca-Mg
Mg-Ca
Ca-K
0
0.2
0.4
0.6
0.8
mg kg-1

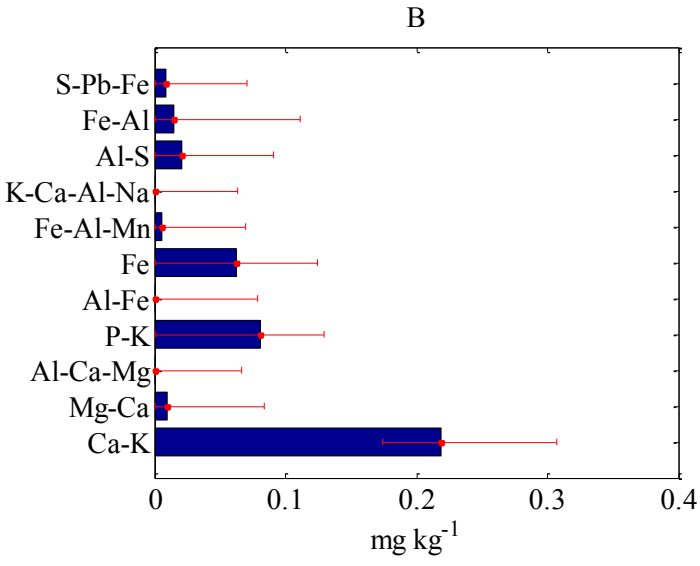
B
S-Pb-Fe
Fe-Al
Al-S
K-Ca-Al-Na
Fe-Al-Mn
Fe
Al-Fe
P-K
Al-Ca-Mg
Mg-Ca
Ca-K
0
0.1
0.2
0.3
0.4
mg kg-1

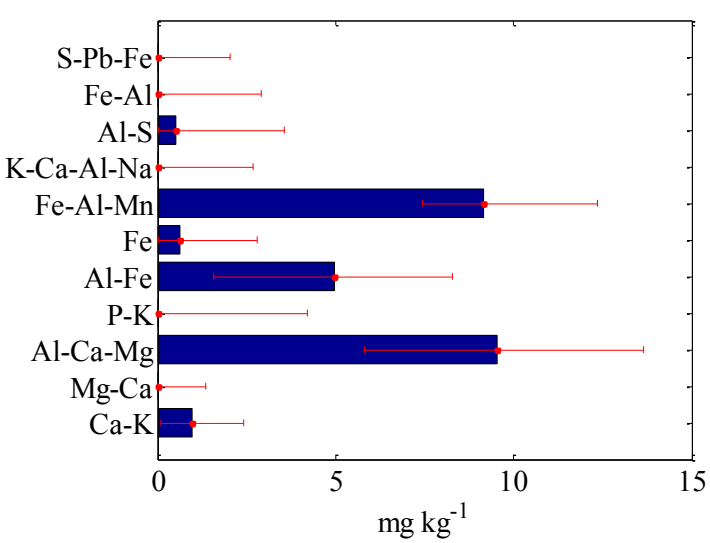
Ba
S-Pb-Fe
Fe-Al
Al-S
K-Ca-Al-Na
Fe-Al-Mn
Fe
Al-Fe
P-K
Al-Ca-Mg
Mg-Ca
Ca-K
0
5
10
15
mg kg-1

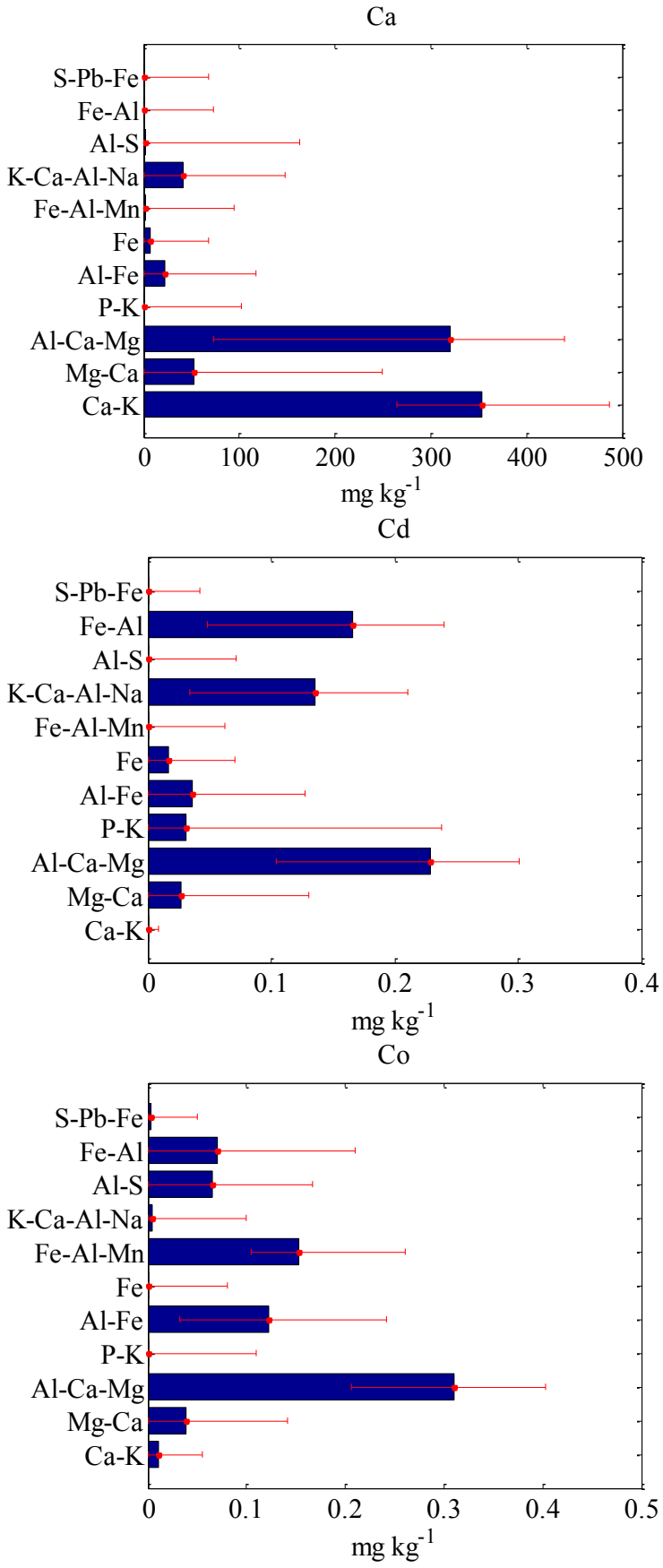
Ca
S-Pb-Fe
Fe-Al
Al-S
K-Ca-Al-Na
Fe-Al-Mn
Fe
Al-Fe
P-K
Al-Ca-Mg
Mg-Ca
Ca-K
0
100
200
300
400
500
mg kg-1
Cd
S-Pb-Fe
Fe-Al
Al-S
K-Ca-Al-Na
Fe-Al-Mn
Fe
Al-Fe
P-K
Al-Ca-Mg
Mg-Ca
Ca-K
0
0.1
0.2
0.3
0.4
mg kg-1
Co
S-Pb-Fe
Fe-Al
Al-S
K-Ca-Al-Na
Fe-Al-Mn
Fe
Al-Fe
P-K
Al-Ca-Mg
Mg-Ca
Ca-K
0
0.1
0.2
0.3
0.4
0.5
mg kg-1

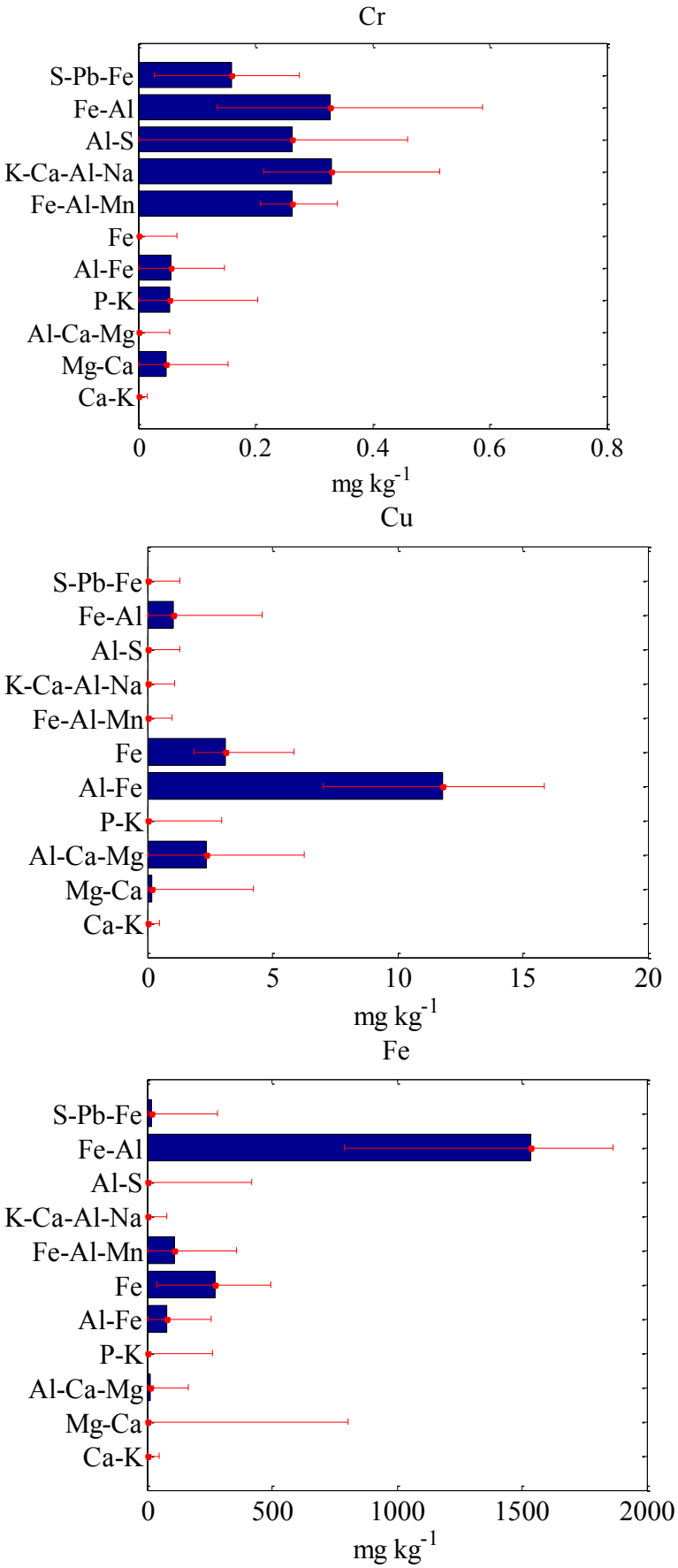
Cr
S-Pb-Fe
Fe-Al
Al-S
K-Ca-Al-Na
Fe-Al-Mn
Fe
Al-Fe
P-K
Al-Ca-Mg
Mg-Ca
Ca-K
0
0.2
0.4
0.6
0.8
mg kg-1
Cu
S-Pb-Fe
Fe-Al
Al-S
K-Ca-Al-Na
Fe-Al-Mn
Fe
Al-Fe
P-K
Al-Ca-Mg
Mg-Ca
Ca-K
0
5
10
15
20
mg kg-1
Fe
S-Pb-Fe
Fe-Al
Al-S
K-Ca-Al-Na
Fe-Al-Mn
Fe
Al-Fe
P-K
Al-Ca-Mg
Mg-Ca
Ca-K
0
500
1000
1500
2000
mg kg-1

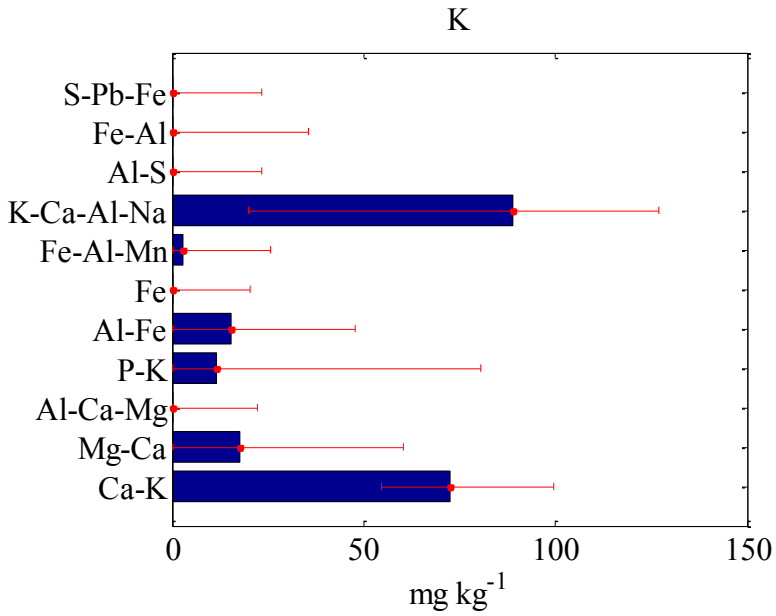
K
S-Pb-Fe
Fe-Al
Al-S
K-Ca-Al-Na
Fe-Al-Mn
Fe
Al-Fe
P-K
Al-Ca-Mg
Mg-Ca
Ca-K
0
50
100
150
mg kg-1

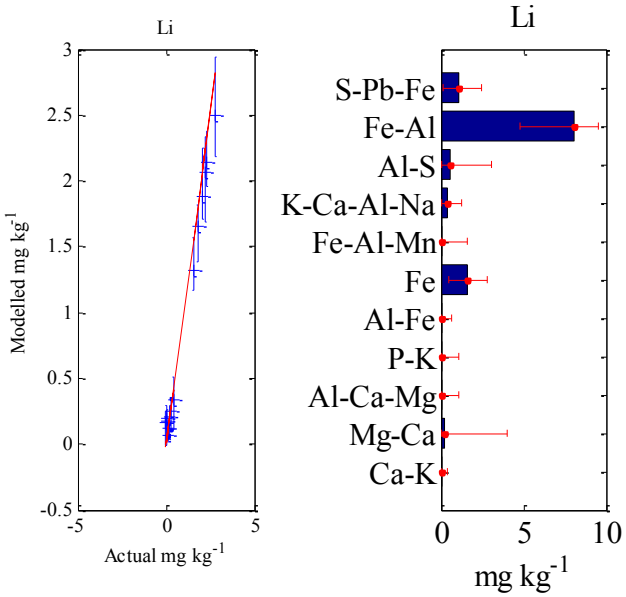
Li
Modelled mg kg-1
Actual mg kg-1
Li
S-Pb-Fe
Fe-Al
Al-S
K-Ca-Al-Na
Fe-Al-Mn
Fe
Al-Fe
P-K
Al-Ca-Mg
Mg-Ca
Ca-K
0
5
10
mg kg-1

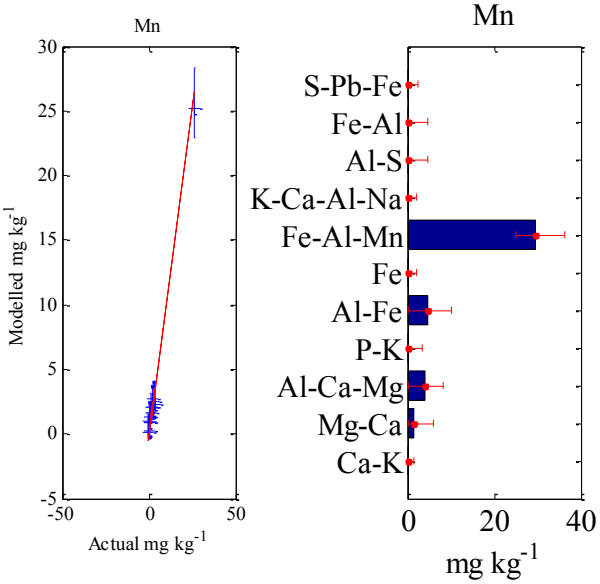
Mn
Modelled mg kg-1
Actual mg kg-1
Mn
S-Pb-Fe
Fe-Al
Al-S
K-Ca-Al-Na
Fe-Al-Mn
Fe
Al-Fe
P-K
Al-Ca-Mg
Mg-Ca
Ca-K
0
20
40
mg kg-1

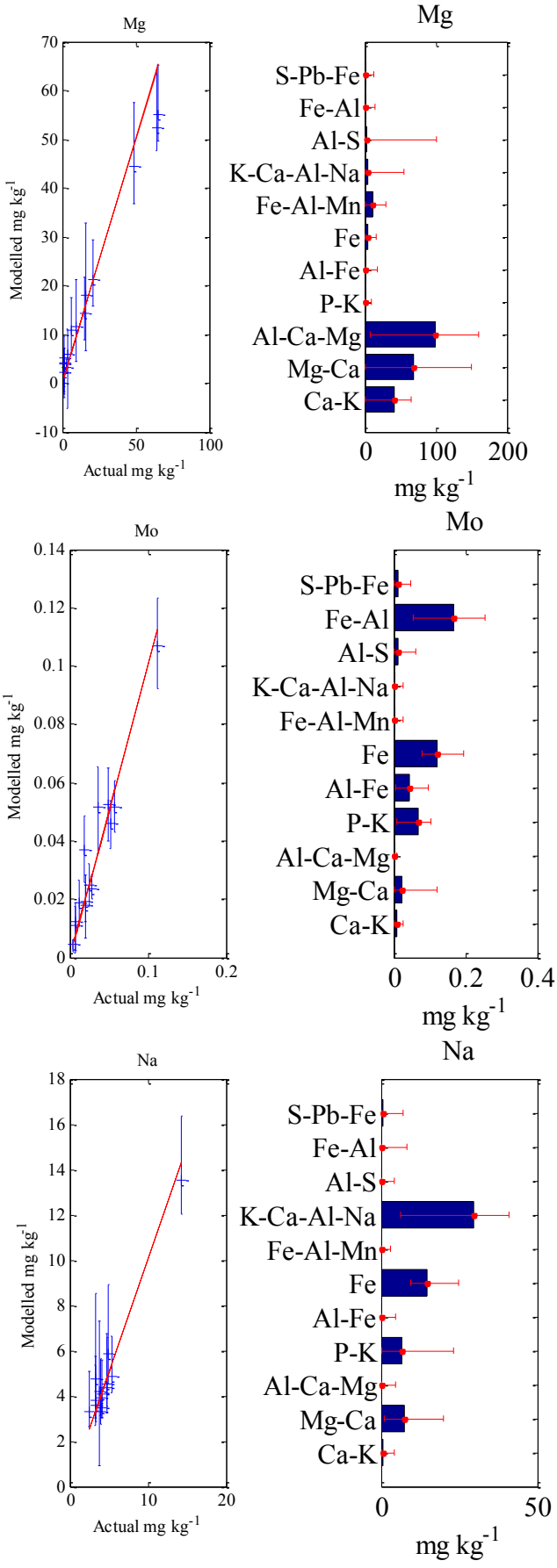
Mg
Modelled mg kg-1
Actual mg kg-1
Mg
S-Pb-Fe
Fe-Al
Al-S
K-Ca-Al-Na
Fe-Al-Mn
Fe
Al-Fe
P-K
Al-Ca-Mg
Mg-Ca
Ca-K
mg kg-1
Mo
Modelled mg kg-1
Actual mg kg-1
Mo
mg kg-1
Na
Modelled mg kg-1
Actual mg kg-1
Na
mg kg-1

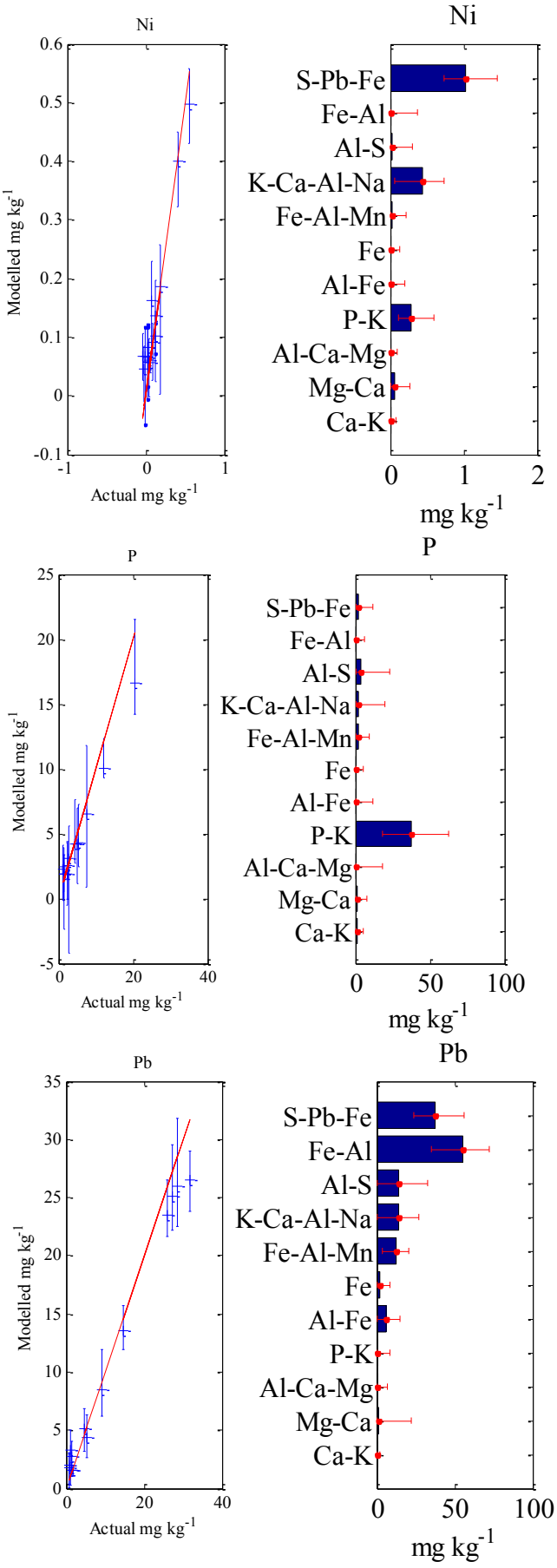
Ni
Modelled mg kg-1
Actual mg kg-1
Ni
S-Pb-Fe
Fe-Al
Al-S
K-Ca-Al-Na
Fe-Al-Mn
Fe
Al-Fe
P-K
Al-Ca-Mg
Mg-Ca
Ca-K
mg kg-1
P
Modelled mg kg-1
Actual mg kg-1
P
mg kg-1
Pb
Modelled mg kg-1
Actual mg kg-1
Pb
mg kg-1

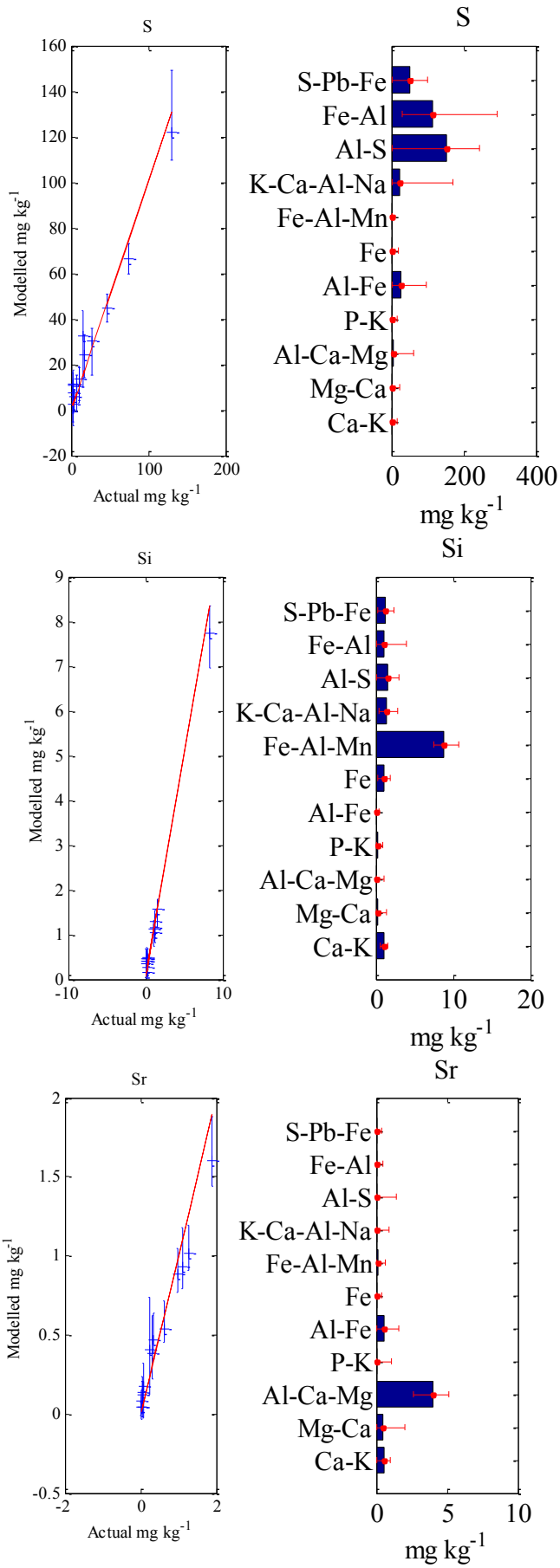
S
Modelled mg kg-1
Actual mg kg-1
S
S-Pb-Fe
Fe-Al
Al-S
K-Ca-Al-Na
Fe-Al-Mn
Fe
Al-Fe
P-K
Al-Ca-Mg
Mg-Ca
Ca-K
mg kg-1
Si
Modelled mg kg-1
Actual mg kg-1
Si
S-Pb-Fe
Fe-Al
Al-S
K-Ca-Al-Na
Fe-Al-Mn
Fe
Al-Fe
P-K
Al-Ca-Mg
Mg-Ca
Ca-K
mg kg-1
Sr
Modelled mg kg-1
Actual mg kg-1
Sr
S-Pb-Fe
Fe-Al
Al-S
K-Ca-Al-Na
Fe-Al-Mn
Fe
Al-Fe
P-K
Al-Ca-Mg
Mg-Ca
Ca-K
mg kg-1

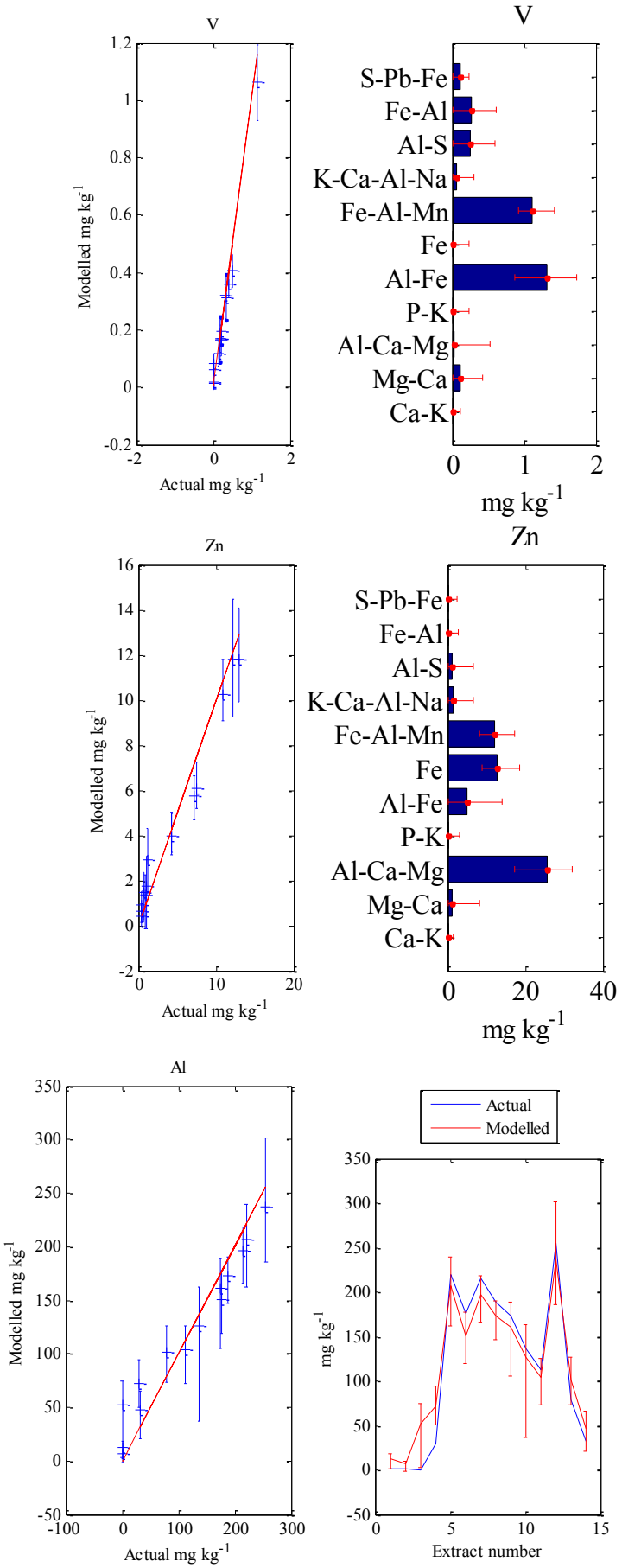
V
Modelled mg kg-1
Actual mg kg-1
V
S-Pb-Fe
Fe-Al
Al-S
K-Ca-Al-Na
Fe-Al-Mn
Fe
Al-Fe
P-K
Al-Ca-Mg
Mg-Ca
Ca-K
mg kg-1
Zn
Modelled mg kg-1
Actual mg kg-1
Zn
S-Pb-Fe
Fe-Al
Al-S
K-Ca-Al-Na
Fe-Al-Mn
Fe
Al-Fe
P-K
Al-Ca-Mg
Mg-Ca
Ca-K
mg kg-1
Al
Modelled mg kg-1
Actual mg kg-1
Actual
Modelled
mg kg-1
Extract number

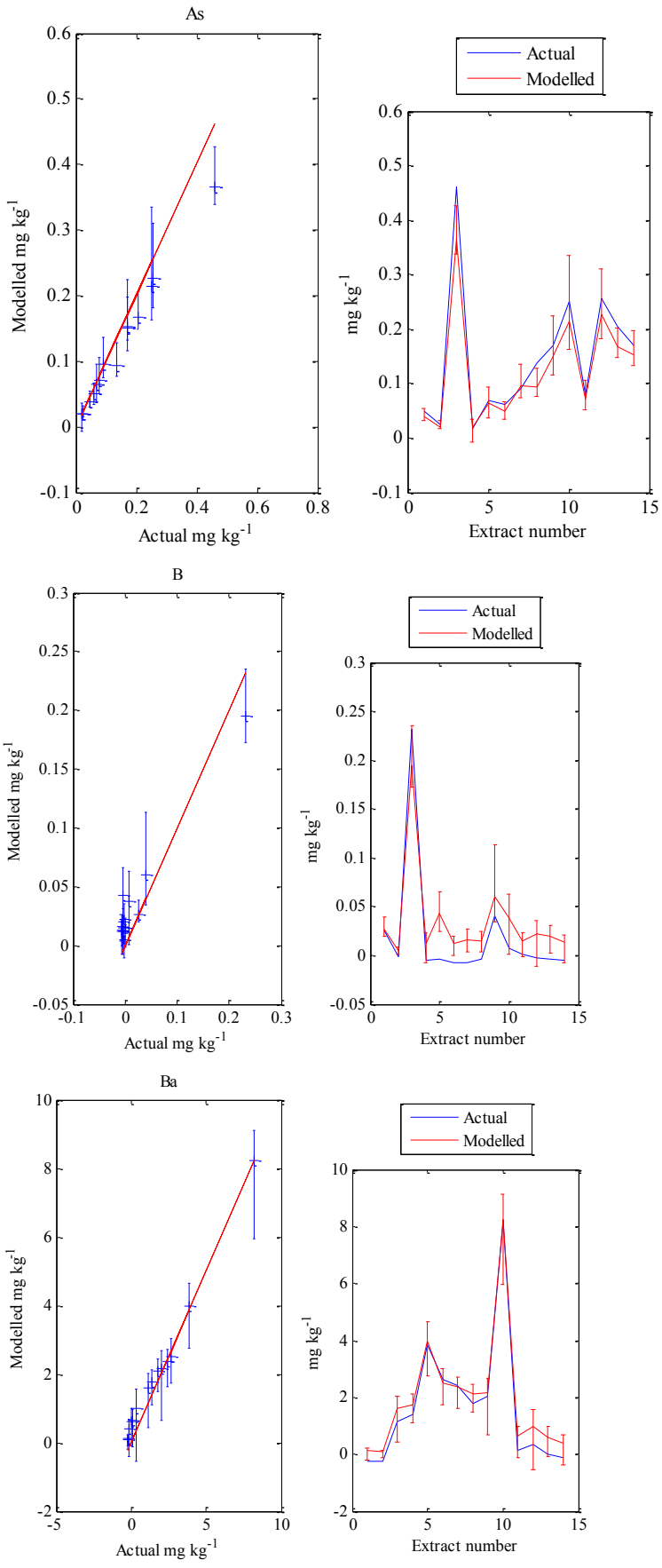
As
Modelled mg kg-1
Actual mg kg-1
Actual
Modelled
mg kg-1
Extract number
B
Modelled mg kg-1
Actual mg kg-1
Actual
Modelled
mg kg-1
Extract number
Ba
Modelled mg kg-1
Actual mg kg-1
Actual
Modelled
mg kg-1
Extract number

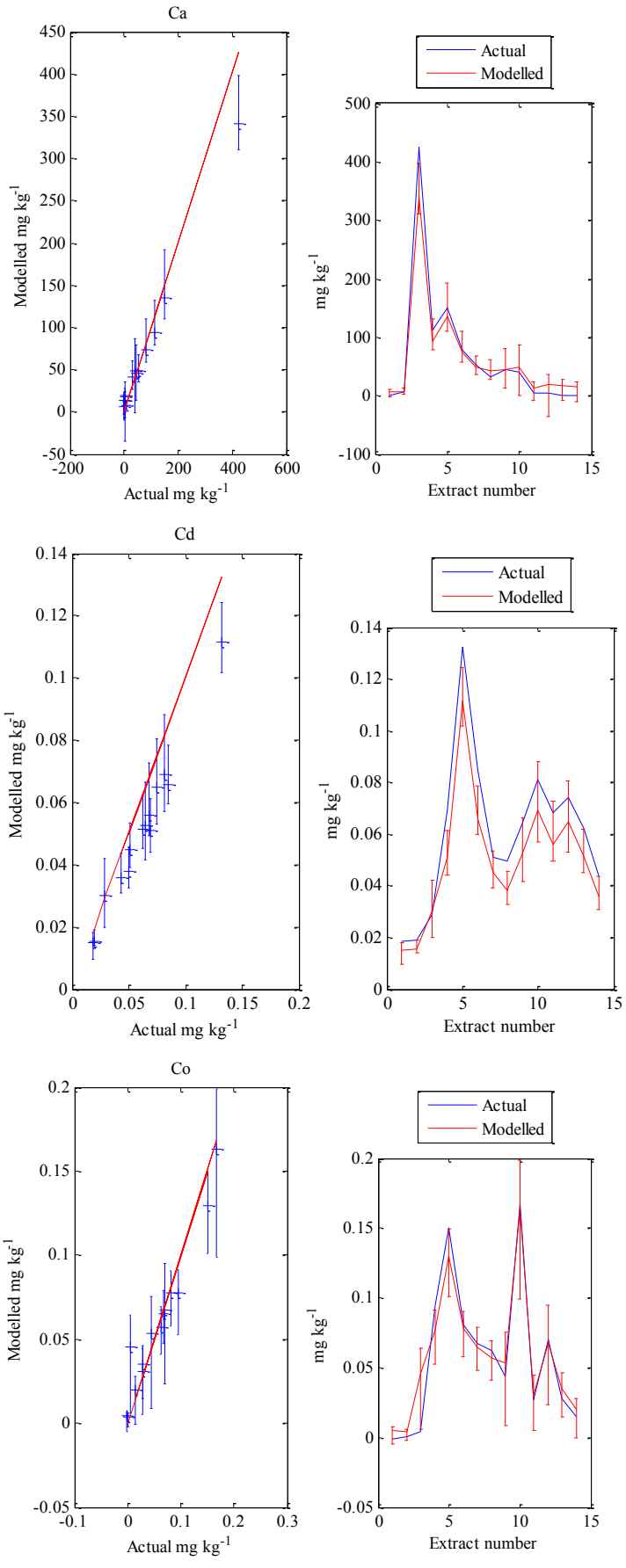
Ca
Modelled mg kg-1
Actual mg kg-1
Actual
Modelled
mg kg-1
Extract number
Cd
Modelled mg kg-1
Actual mg kg-1
Actual
Modelled
mg kg-1
Extract number
Co
Modelled mg kg-1
Actual mg kg-1
Actual
Modelled
mg kg-1
Extract number

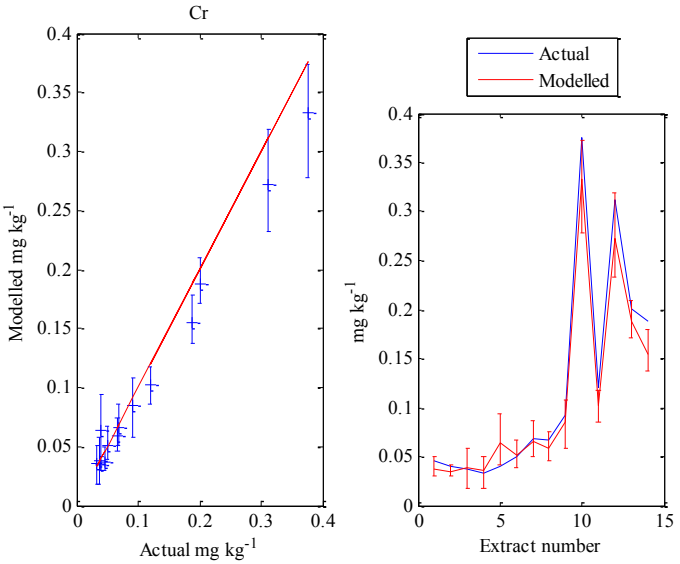
Cr
Modelled mg kg-1
Actual mg kg-1
Actual
Modelled
mg kg-1
Extract number

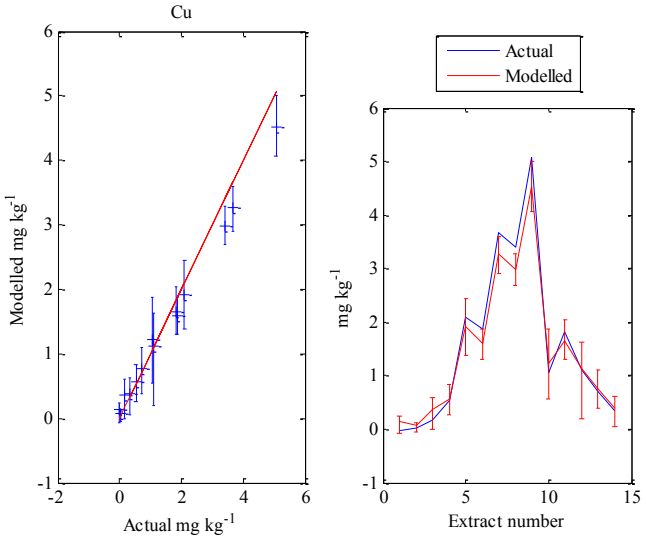
Cu
Modelled mg kg-1
Actual mg kg-1
Actual
Modelled
mg kg-1
Extract number

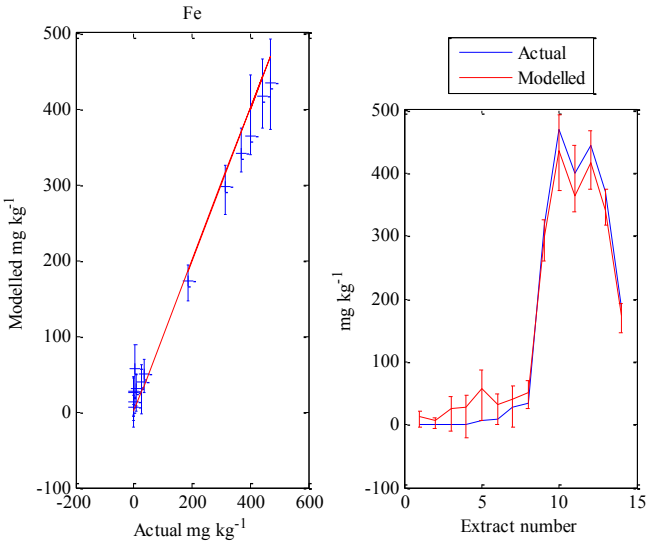
Fe
Modelled mg kg-1
Actual mg kg-1
Actual
Modelled
mg kg-1
Extract number

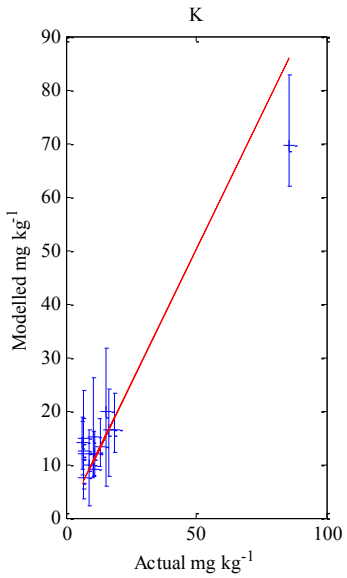
K
Modelled mg kg-1
Actual mg kg-1
0
10
20
30
40
50
60
70
80
90
0
50
100

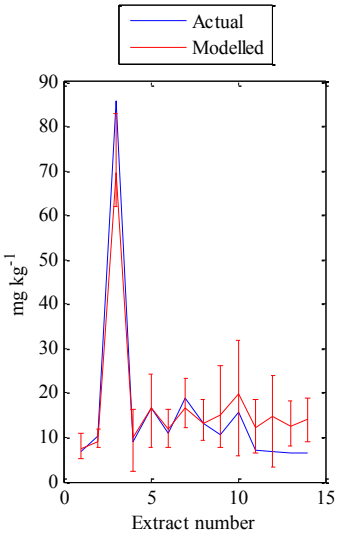
Actual
Modelled
mg kg-1
Extract number
0
10
20
30
40
50
60
70
80
90
0
5
10
15

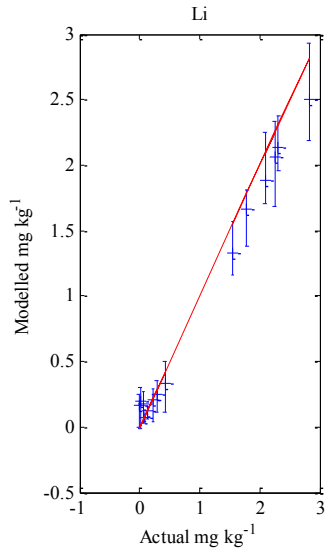
Li
Modelled mg kg-1
Actual mg kg-1
-0.5
0
0.5
1
1.5
2
2.5
3
-1
0
1
2
3

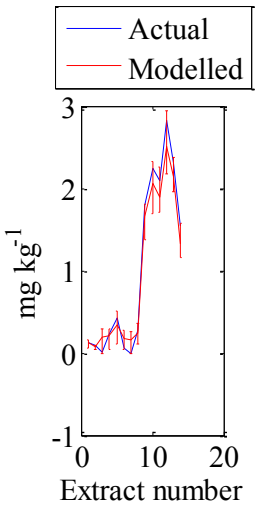
Actual
Modelled
mg kg-1
Extract number
-1
0
1
2
3
0
10
20

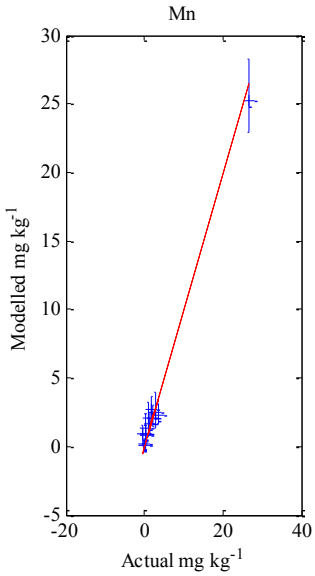
Mn
Modelled mg kg-1
Actual mg kg-1
-5
0
5
10
15
20
25
30
-20
0
20
40

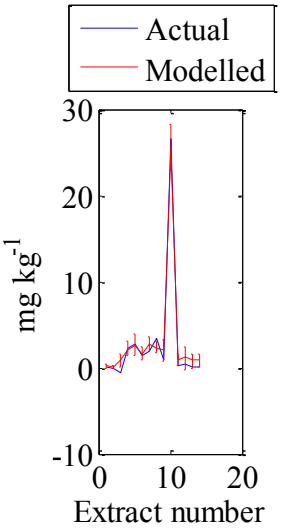
Actual
Modelled
mg kg-1
Extract number
-10
0
10
20
30
0
10
20

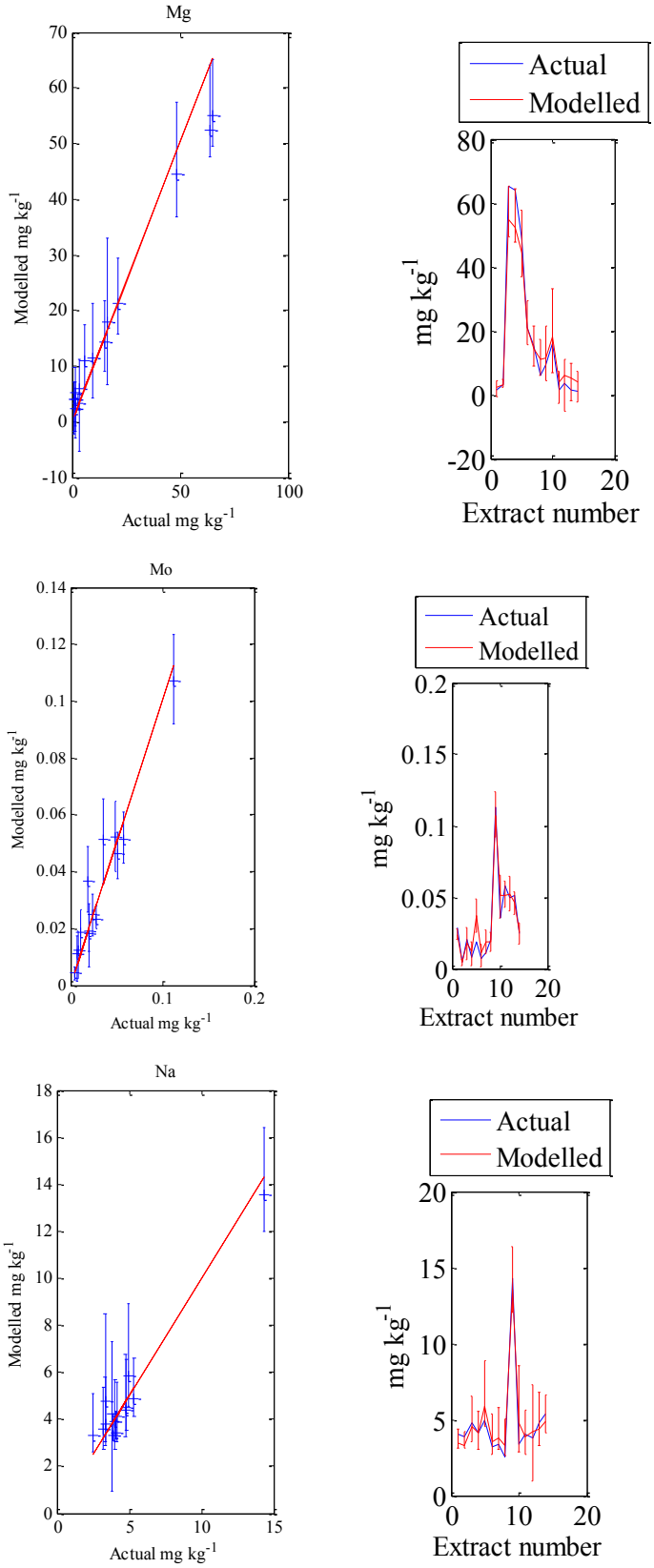
Mg
Modelled mg kg-1
Actual mg kg-1
Actual
Modelled
mg kg-1
Extract number
Mo
Modelled mg kg-1
Actual mg kg-1
Actual
Modelled
mg kg-1
Extract number
Na
Modelled mg kg-1
Actual mg kg-1
Actual
Modelled
mg kg-1
Extract number

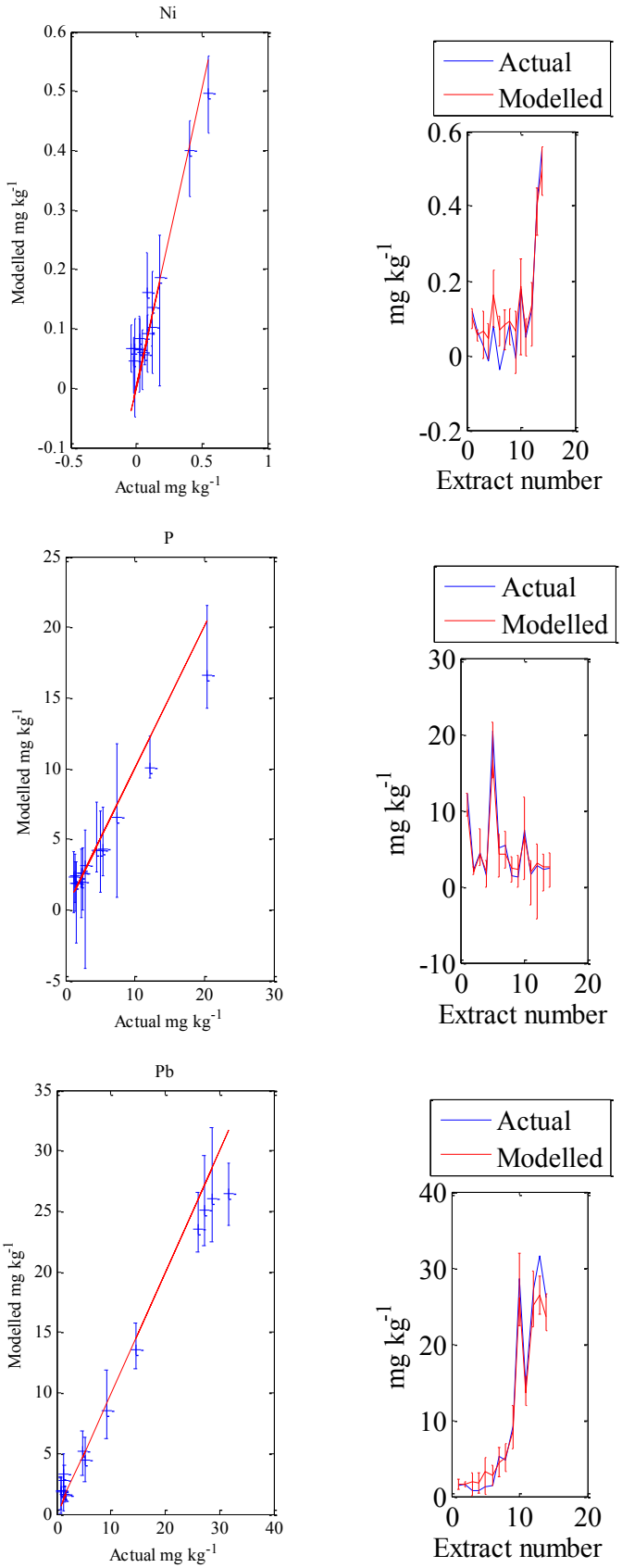
Ni
Modelled mg kg-1
Actual mg kg-1
Actual
Modelled
mg kg-1
Extract number
P
Modelled mg kg-1
Actual mg kg-1
Actual
Modelled
mg kg-1
Extract number
Pb
Modelled mg kg-1
Actual mg kg-1
Actual
Modelled
mg kg-1
Extract number

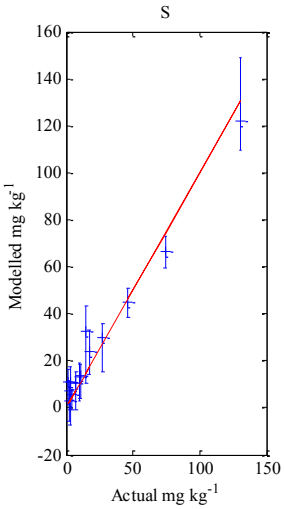
S
Modelled mg kg-1
Actual mg kg-1
160
140
120
100
80
60
40
20
0
-20
0
50
100
150

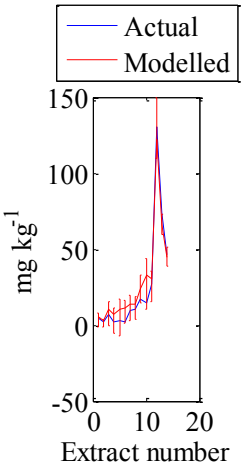
Actual
Modelled
mg kg-1
Extract number
150
100
50
0
-50
0
10
20

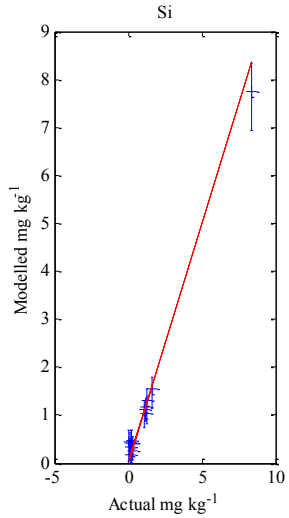
Si
Modelled mg kg-1
Actual mg kg-1
9
8
7
6
5
4
3
2
1
0
-5
0
5
10

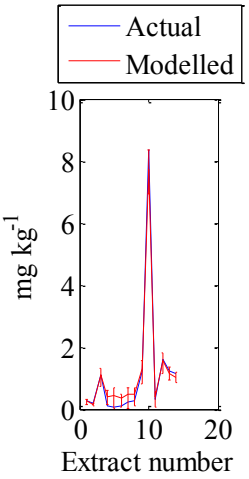
Actual
Modelled
mg kg-1
Extract number
10
8
6
4
2
0
0
10
20

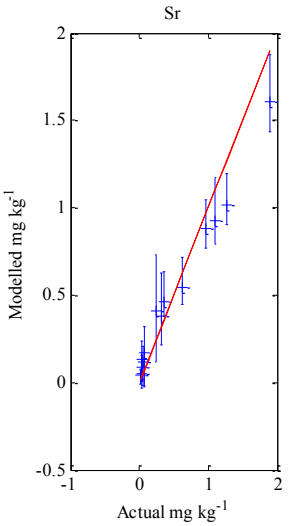
Sr
Modelled mg kg-1
Actual mg kg-1
2
1.5
1
0.5
0
-0.5
-1
0
1
2

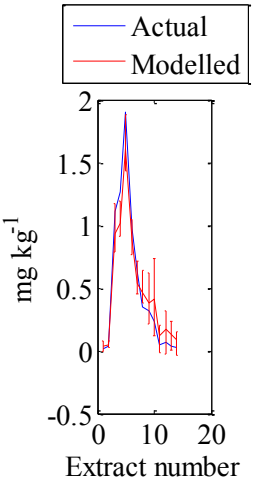
Actual
Modelled
mg kg-1
Extract number
2
1.5
1
0.5
0
-0.5
0
10
20

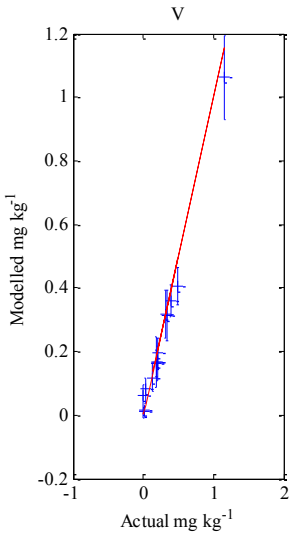
V
Modelled mg kg-1
Actual mg kg-1
1.2
1
0.8
0.6
0.4
0.2
0
-0.2
-1
0
1
2

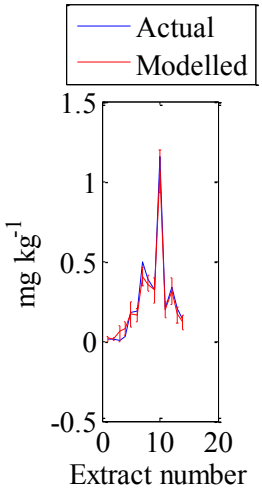
Actual
Modelled
mg kg-1
Extract number
1.5
1
0.5
0
-0.5
0
10
20

Soil 4

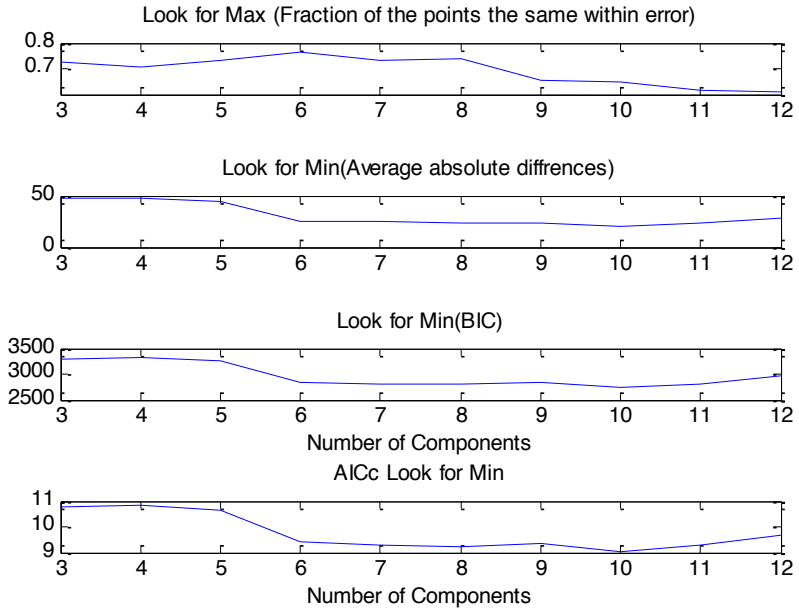
Look for Max (Fraction of the points the same within error)
0.8
0.7
3 4 5 6 7 8 9 10 11 12
Look for Min(Average absolute diffrences)
50
0
3 4 5 6 7 8 9 10 11 12
Look for Min(BIC)
3500
3000
2500
3 4 5 6 7 8 9 10 11 12
Number of Components
AICc Look for Min
11
10
9
3 4 5 6 7 8 9 10 11 12
Number of Components

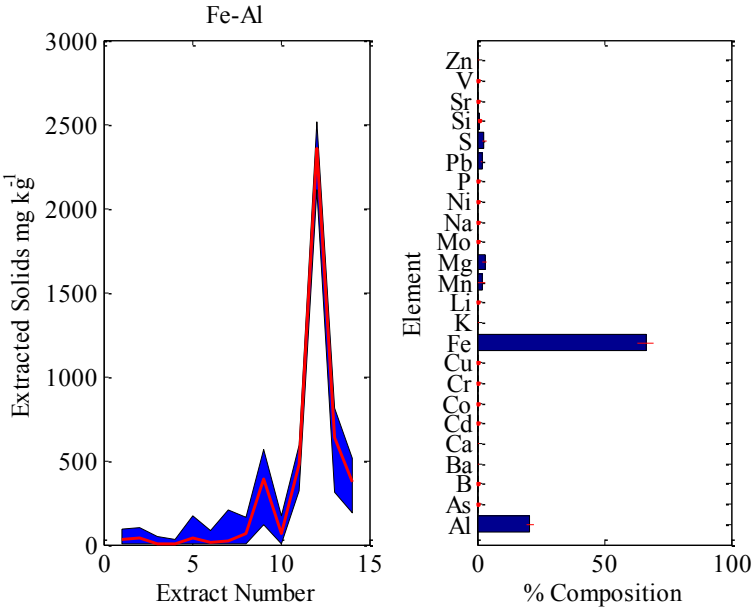
Fe-Al
Extracted Solids mg kg-1
3000
2500
2000
1500
1000
500
0
0 5 10 15
Extract Number
Element
Zn
V
Sr
Si
S
Pb
P
Ni
Na
Mo
Mg
Mn
Li
K
Fe
Cu
Cr
Co
Cd
Ca
Ba
B
As
Al
0 50 100
% Composition

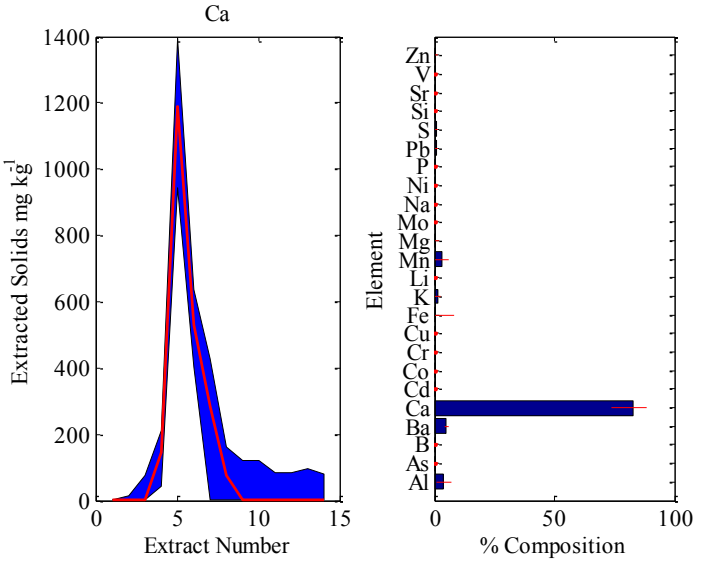
Ca
Extracted Solids mg kg-1
Extract Number
Element
% Composition
Zn
V
Sr
Si
S
Pb
P
Ni
Na
Mo
Mg
Mn
Li
K
Fe
Cu
Cr
Co
Cd
Ca
Ba
B
As
Al

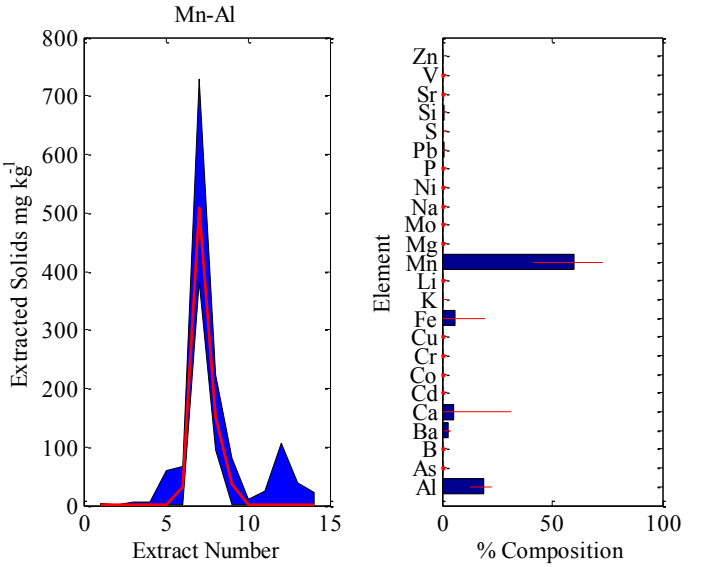
Mn-Al
Extracted Solids mg kg-1
Extract Number
Element
% Composition
Zn
V
Sr
Si
S
Pb
P
Ni
Na
Mo
Mg
Mn
Li
K
Fe
Cu
Cr
Co
Cd
Ca
Ba
B
As
Al

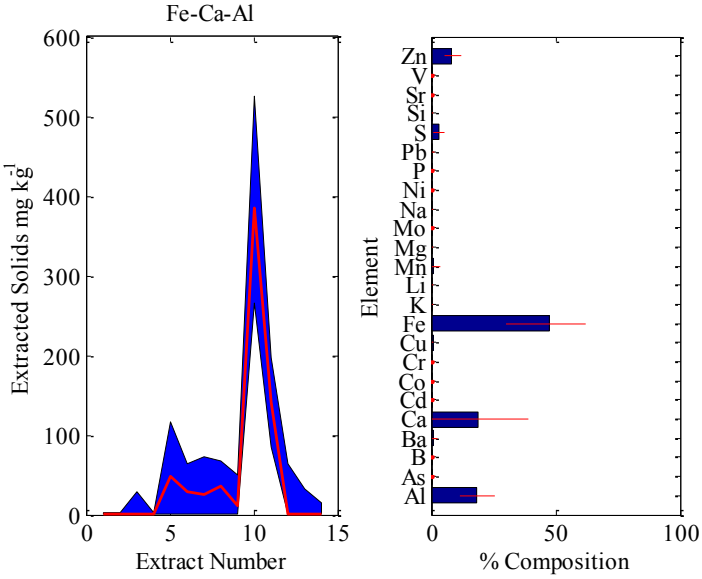
Fe-Ca-Al
Extracted Solids mg kg-1
Extract Number
Element
% Composition
Zn
V
Sr
Si
S
Pb
P
Ni
Na
Mo
Mg
Mn
Li
K
Fe
Cu
Cr
Co
Cd
Ca
Ba
B
As
Al

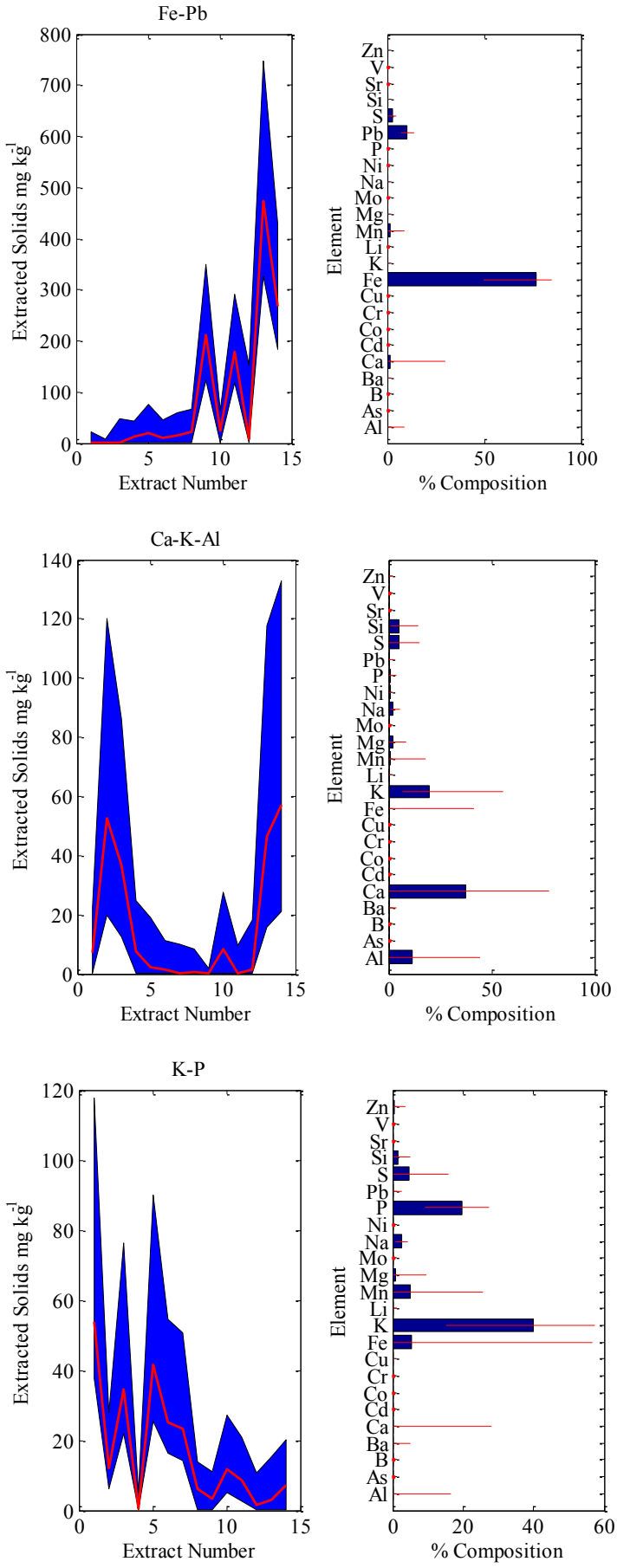
Fe-Pb
Extracted Solids mg kg-1
Extract Number
Element
% Composition
Ca-K-Al
Extracted Solids mg kg-1
Extract Number
Element
% Composition
K-P
Extracted Solids mg kg-1
Extract Number
Element
% Composition

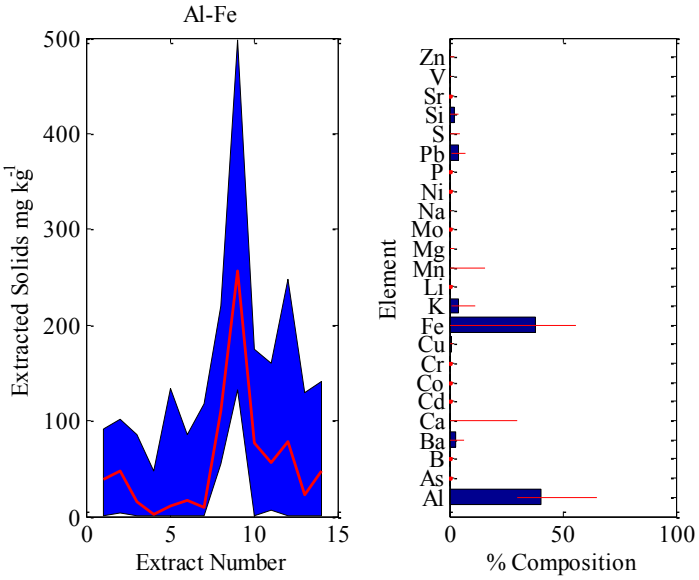
Al-Fe
Extracted Solids mg kg-1
Extract Number
Element
% Composition
Zn
V
Sr
Si
S
Pb
P
Ni
Na
Mo
Mg
Mn
Li
K
Fe
Cu
Cr
Co
Cd
Ca
Ba
B
As
Al

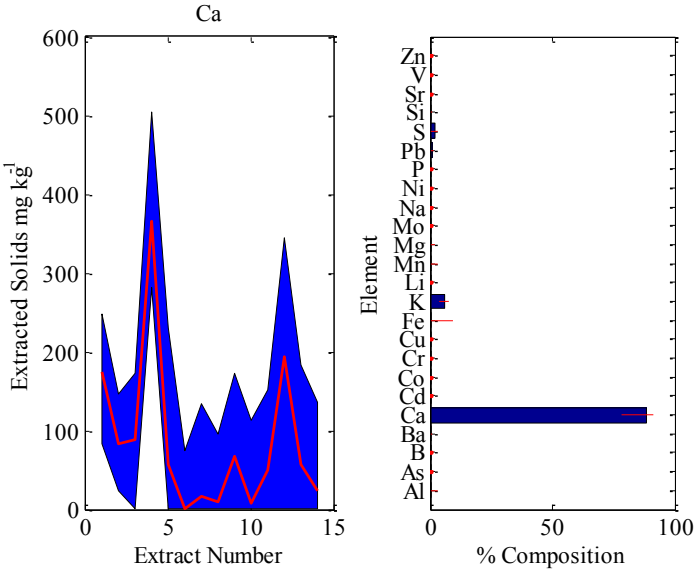
Ca
Extracted Solids mg kg-1
Extract Number
Element
% Composition
Zn
V
Sr
Si
S
Pb
P
Ni
Na
Mo
Mg
Mn
Li
K
Fe
Cu
Cr
Co
Cd
Ca
Ba
B
As
Al

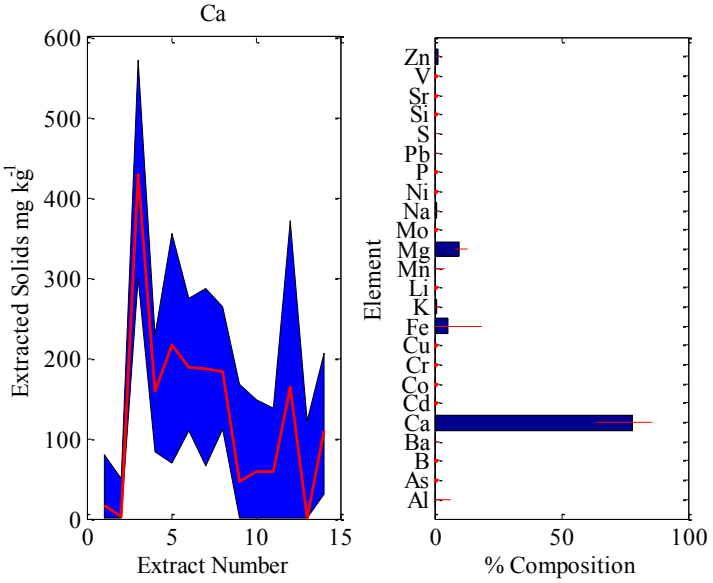
Ca
Extracted Solids mg kg-1
Extract Number
Element
% Composition
Zn
V
Sr
Si
S
Pb
P
Ni
Na
Mo
Mg
Mn
Li
K
Fe
Cu
Cr
Co
Cd
Ca
Ba
B
As
Al

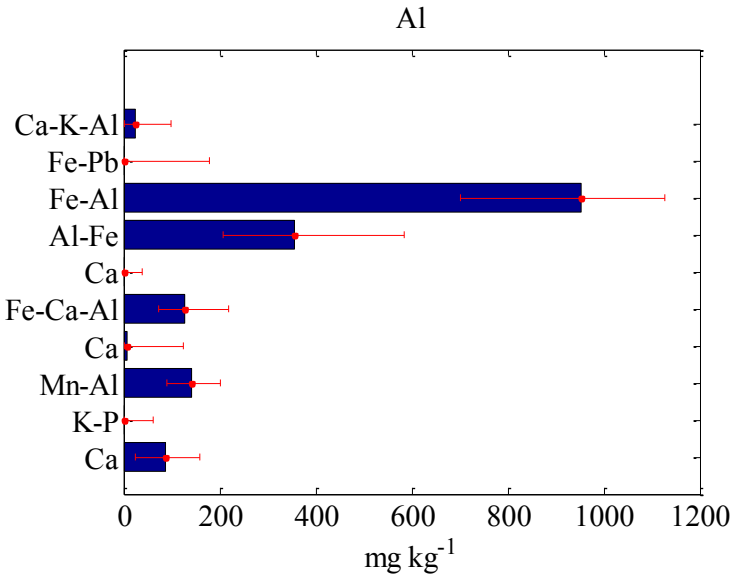
Al
Ca-K-Al
Fe-Pb
Fe-Al
Al-Fe
Ca
Fe-Ca-Al
Ca
Mn-Al
K-P
Ca
0
200
400
600
800
1000
1200
mg kg-1

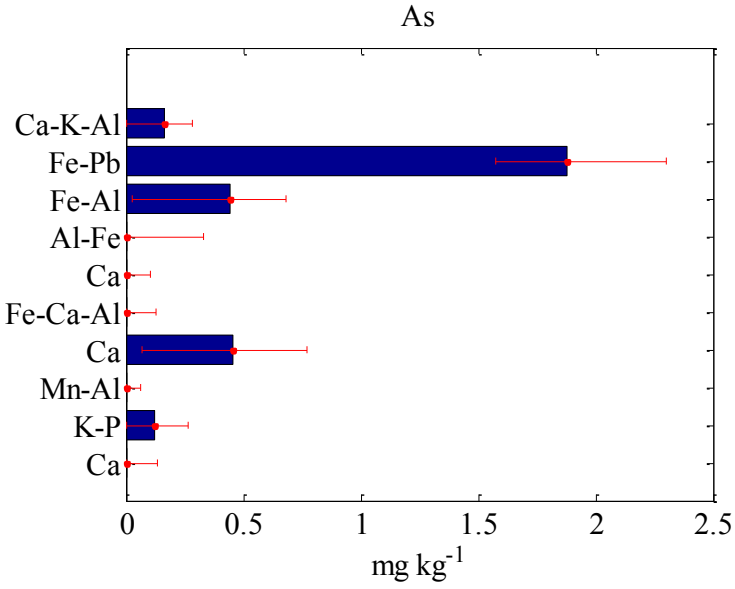
As
Ca-K-Al
Fe-Pb
Fe-Al
Al-Fe
Ca
Fe-Ca-Al
Ca
Mn-Al
K-P
Ca
0
0.5
1
1.5
2
2.5
mg kg-1

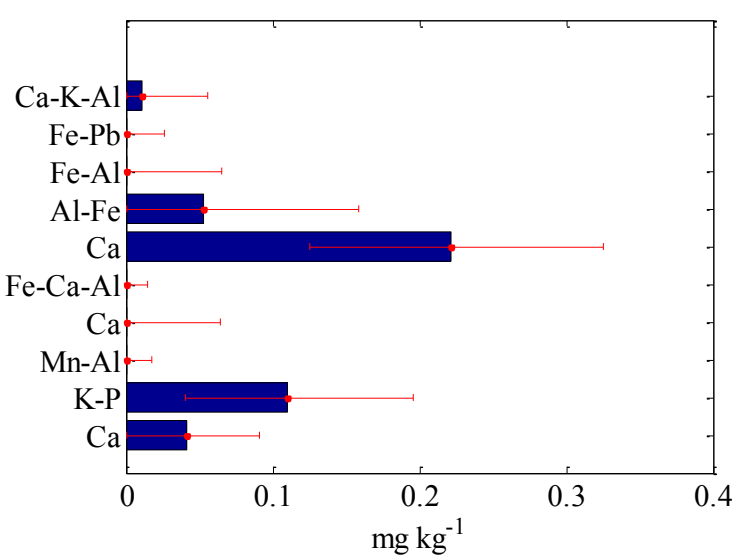
B
Ca-K-Al
Fe-Pb
Fe-Al
Al-Fe
Ca
Fe-Ca-Al
Ca
Mn-Al
K-P
Ca
0
0.1
0.2
0.3
0.4
mg kg-1

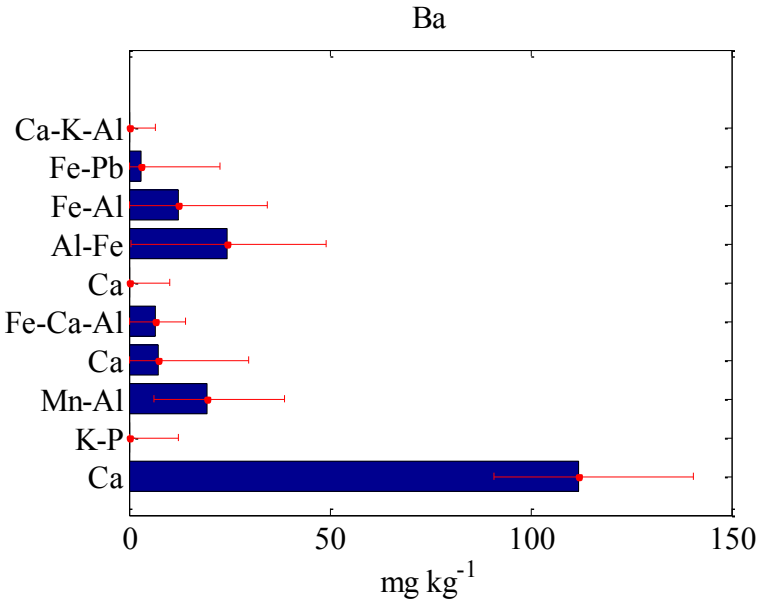
Ba
Ca-K-Al
Fe-Pb
Fe-Al
Al-Fe
Ca
Fe-Ca-Al
Ca
Mn-Al
K-P
Ca
0
50
100
150
mg kg-1

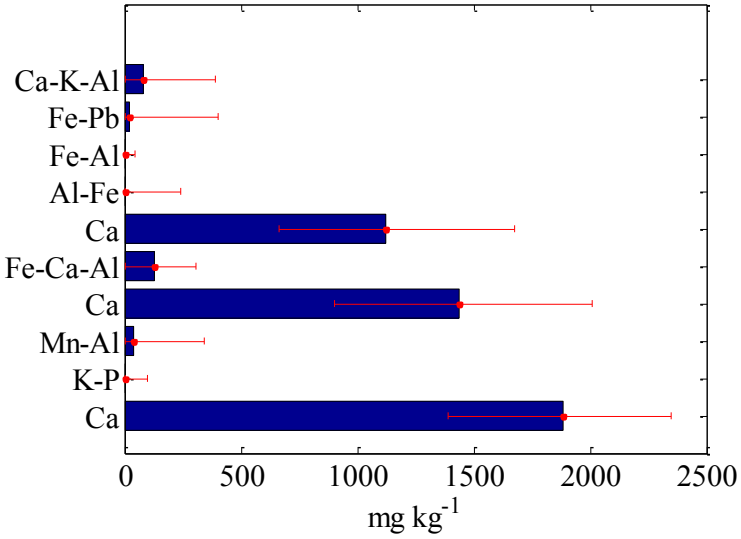
Ca
Ca-K-Al
Fe-Pb
Fe-Al
Al-Fe
Ca
Fe-Ca-Al
Ca
Mn-Al
K-P
Ca
0
500
1000
1500
2000
2500
mg kg-1

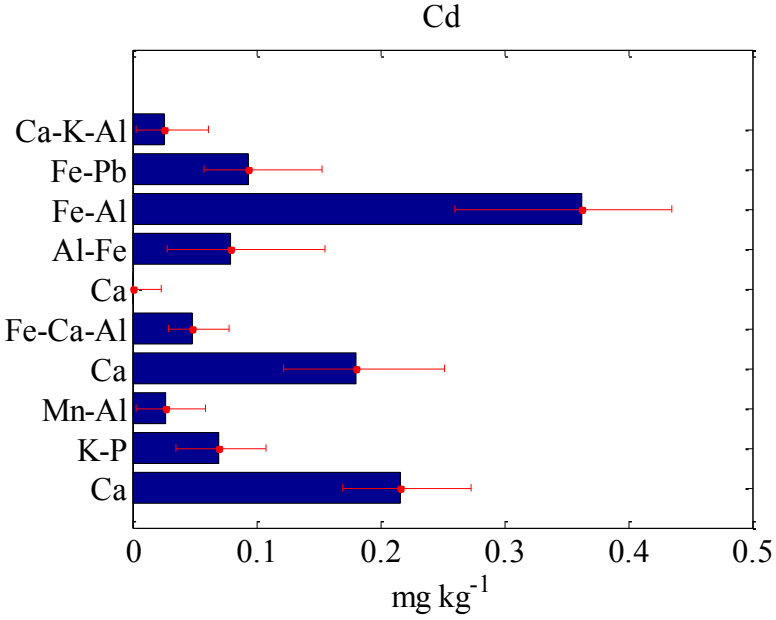
Cd
Ca-K-Al
Fe-Pb
Fe-Al
Al-Fe
Ca
Fe-Ca-Al
Ca
Mn-Al
K-P
Ca
0
0.1
0.2
0.3
0.4
0.5
mg kg-1

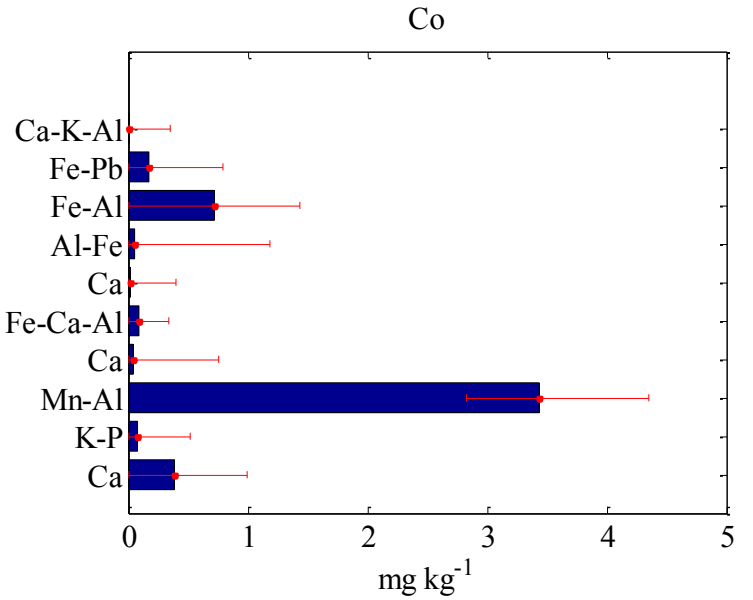
Co
Ca-K-Al
Fe-Pb
Fe-Al
Al-Fe
Ca
Fe-Ca-Al
Ca
Mn-Al
K-P
Ca
0
1
2
3
4
5
mg kg-1

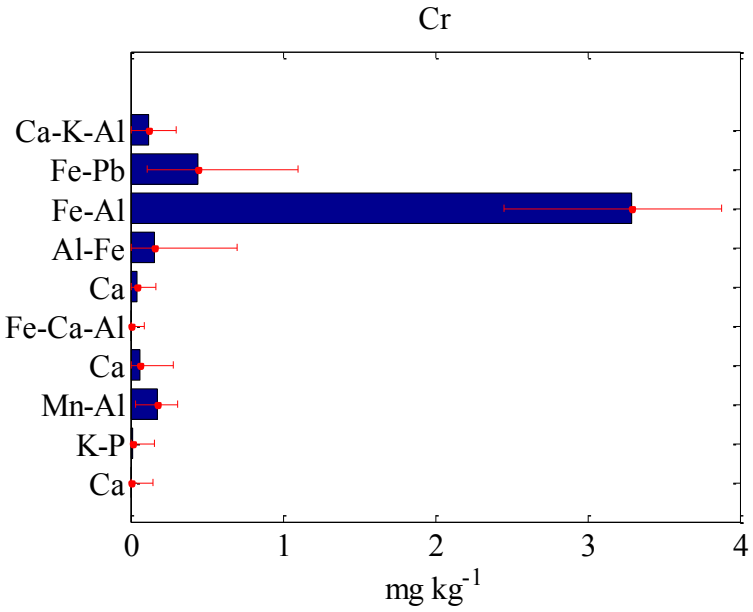
Cr
Ca-K-Al
Fe-Pb
Fe-Al
Al-Fe
Ca
Fe-Ca-Al
Ca
Mn-Al
K-P
Ca
0
1
2
3
4
mg kg-1

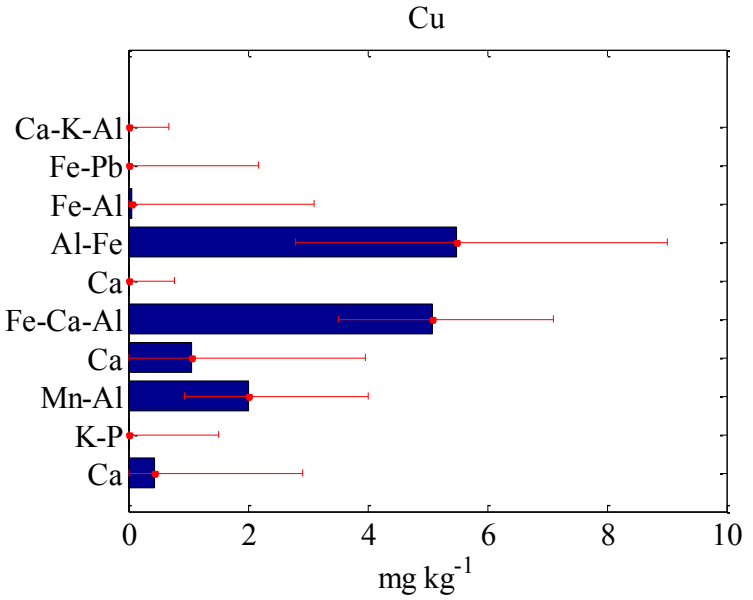
Cu
Ca-K-Al
Fe-Pb
Fe-Al
Al-Fe
Ca
Fe-Ca-Al
Ca
Mn-Al
K-P
Ca
0
2
4
6
8
10
mg kg-1

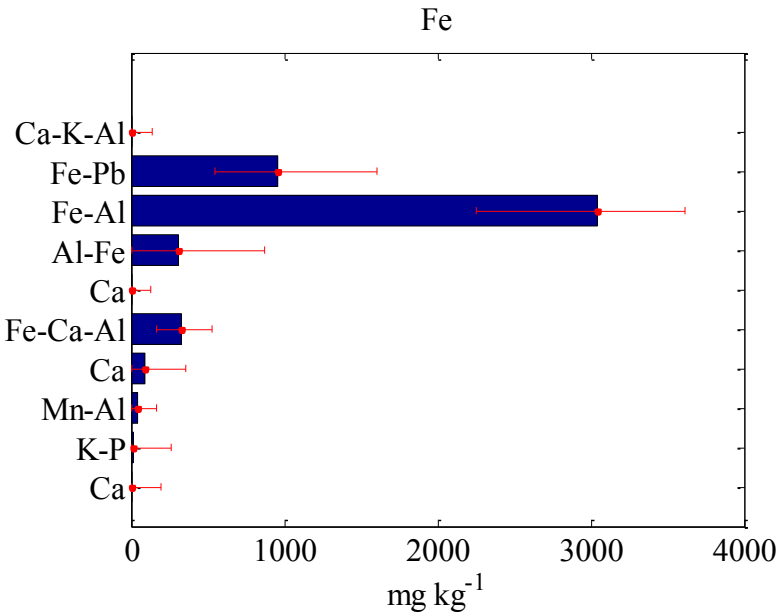
Fe
Ca-K-Al
Fe-Pb
Fe-Al
Al-Fe
Ca
Fe-Ca-Al
Ca
Mn-Al
K-P
Ca
0
1000
2000
3000
4000
mg kg-1

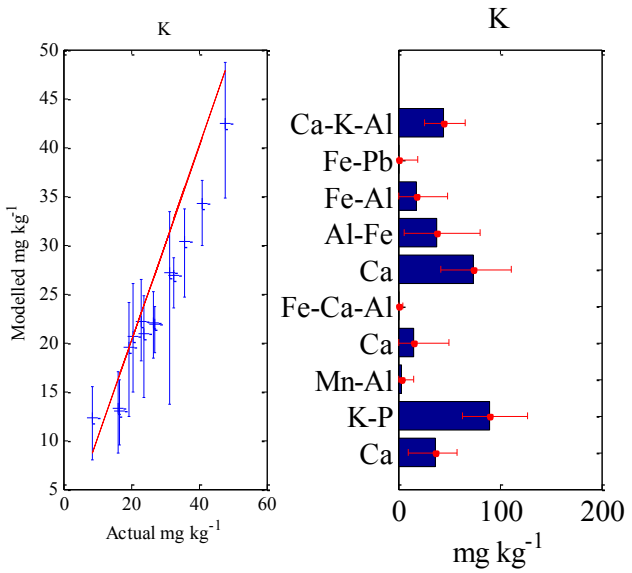
K
Modelled mg kg-1
Actual mg kg-1
K
Ca-K-Al
Fe-Pb
Fe-Al
Al-Fe
Ca
Fe-Ca-Al
Ca
Mn-Al
K-P
Ca
0
100
200
mg kg-1

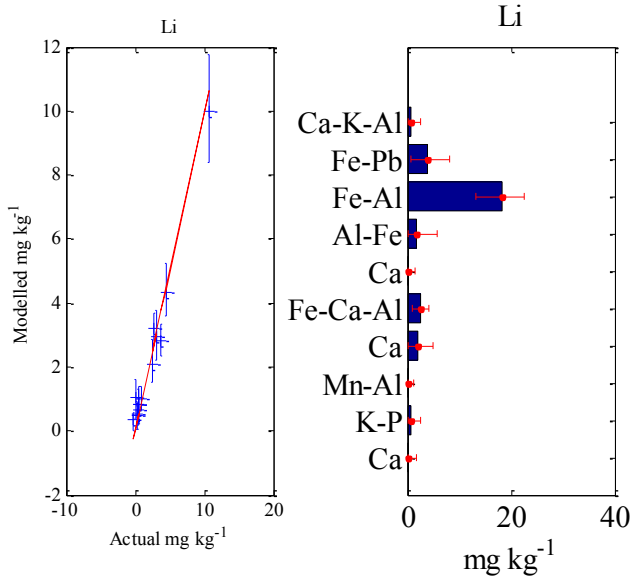
Li
Modelled mg kg-1
Actual mg kg-1
Li
Ca-K-Al
Fe-Pb
Fe-Al
Al-Fe
Ca
Fe-Ca-Al
Ca
Mn-Al
K-P
Ca
0
20
40
mg kg-1

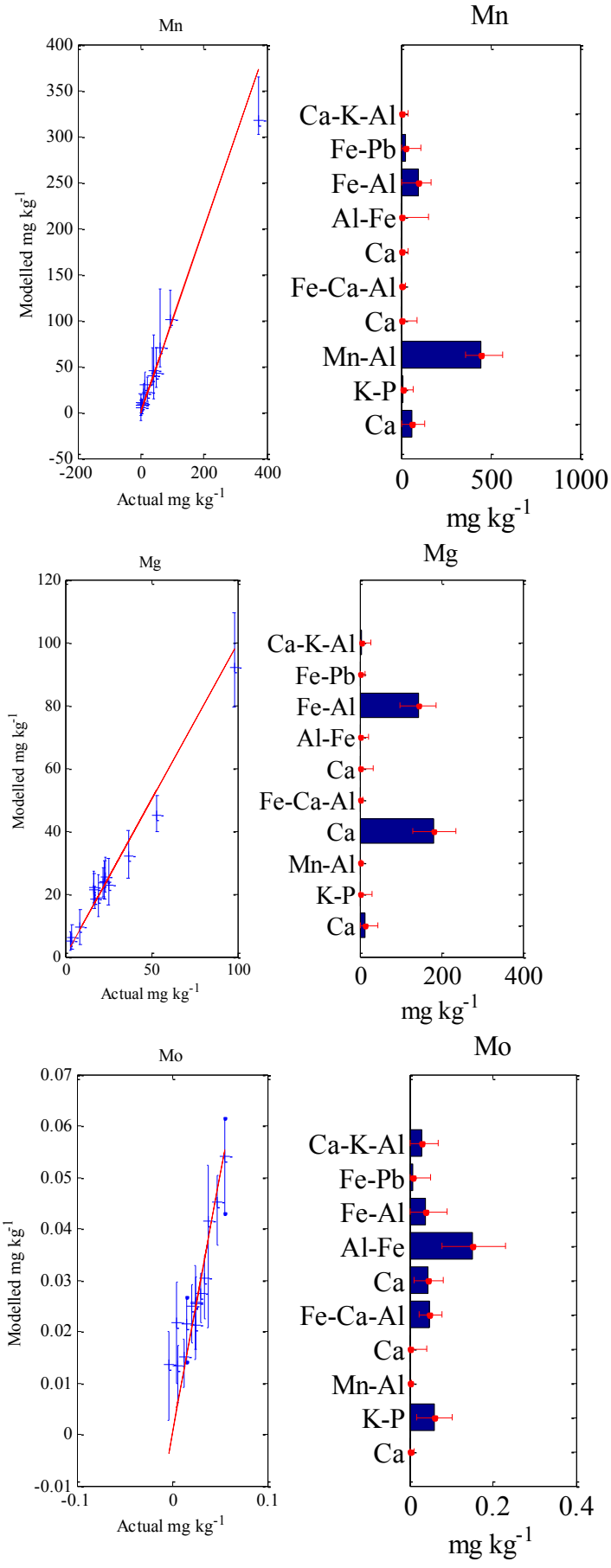
Mn
Modelled mg kg-1
Actual mg kg-1
400
350
300
250
200
150
100
50
0
-50
-200
0
200
400
Mn
Ca-K-Al
Fe-Pb
Fe-Al
Al-Fe
Ca
Fe-Ca-Al
Ca
Mn-Al
K-P
Ca
0
500
1000
mg kg-1
Mg
Modelled mg kg-1
Actual mg kg-1
120
100
80
60
40
20
0
0
50
100
Mg
Ca-K-Al
Fe-Pb
Fe-Al
Al-Fe
Ca
Fe-Ca-Al
Ca
Mn-Al
K-P
Ca
0
200
400
mg kg-1
Mo
Modelled mg kg-1
Actual mg kg-1
0.07
0.06
0.05
0.04
0.03
0.02
0.01
0
-0.01
-0.1
0
0.1
Mo
Ca-K-Al
Fe-Pb
Fe-Al
Al-Fe
Ca
Fe-Ca-Al
Ca
Mn-Al
K-P
Ca
0
0.2
0.4
mg kg-1

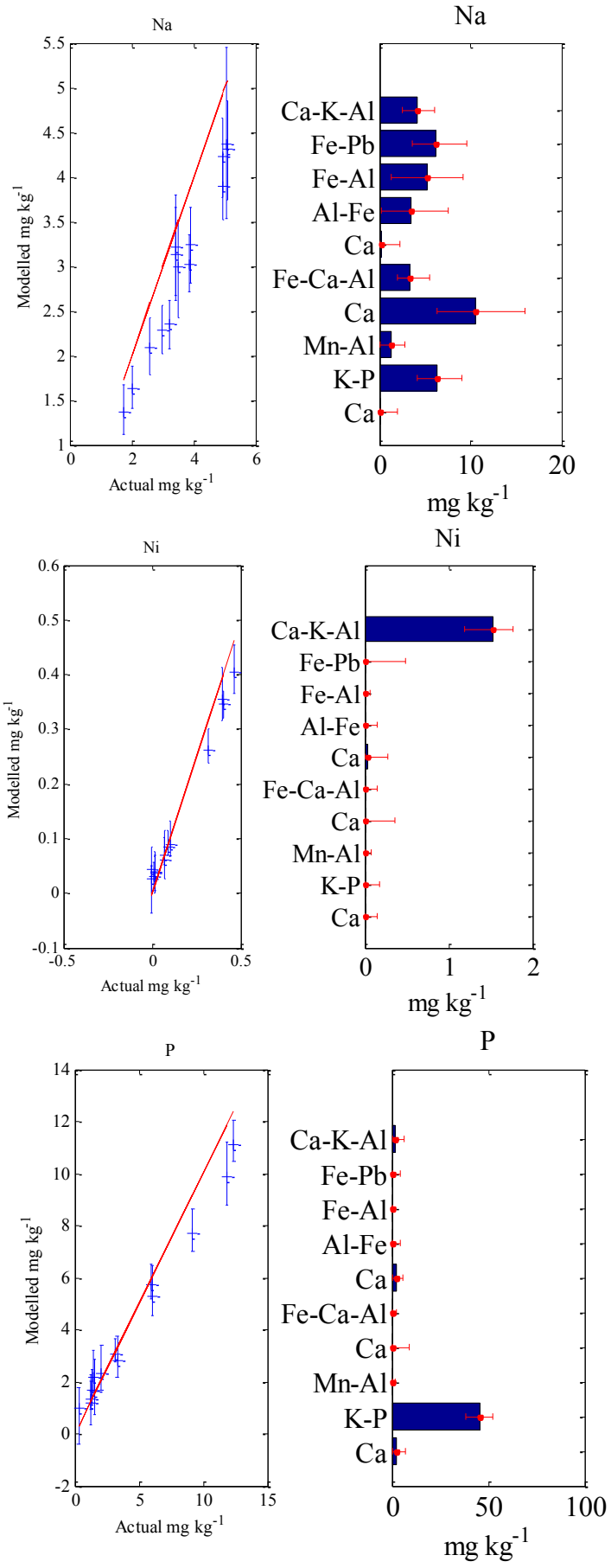
Na
Modelled mg kg-1
Actual mg kg-1
Na
Ca-K-Al
Fe-Pb
Fe-Al
Al-Fe
Ca
Fe-Ca-Al
Ca
Mn-Al
K-P
Ca
mg kg-1
Ni
Modelled mg kg-1
Actual mg kg-1
Ni
Ca-K-Al
Fe-Pb
Fe-Al
Al-Fe
Ca
Fe-Ca-Al
Ca
Mn-Al
K-P
Ca
mg kg-1
P
Modelled mg kg-1
Actual mg kg-1
P
Ca-K-Al
Fe-Pb
Fe-Al
Al-Fe
Ca
Fe-Ca-Al
Ca
Mn-Al
K-P
Ca
mg kg-1

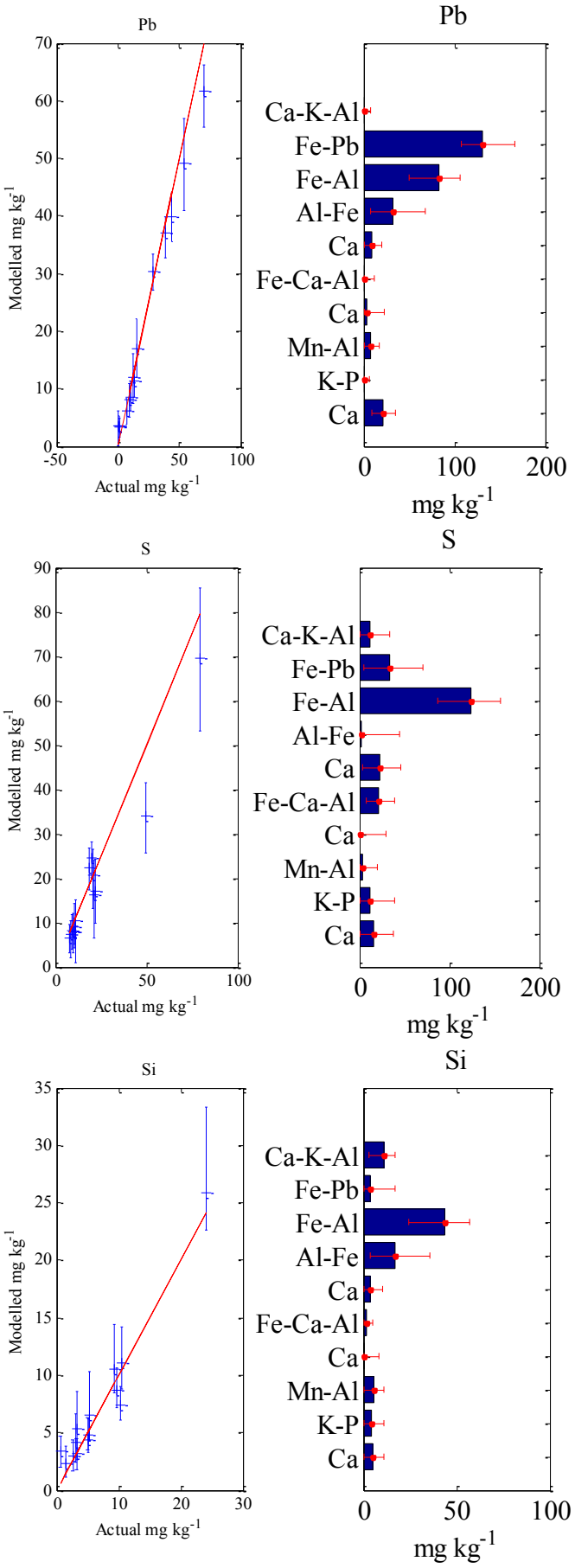
Pb
Modelled mg kg-1
Actual mg kg-1
Pb
Ca-K-Al
Fe-Pb
Fe-Al
Al-Fe
Ca
Fe-Ca-Al
Ca
Mn-Al
K-P
Ca
mg kg-1
S
Modelled mg kg-1
Actual mg kg-1
S
Ca-K-Al
Fe-Pb
Fe-Al
Al-Fe
Ca
Fe-Ca-Al
Ca
Mn-Al
K-P
Ca
mg kg-1
Si
Modelled mg kg-1
Actual mg kg-1
Si
Ca-K-Al
Fe-Pb
Fe-Al
Al-Fe
Ca
Fe-Ca-Al
Ca
Mn-Al
K-P
Ca
mg kg-1

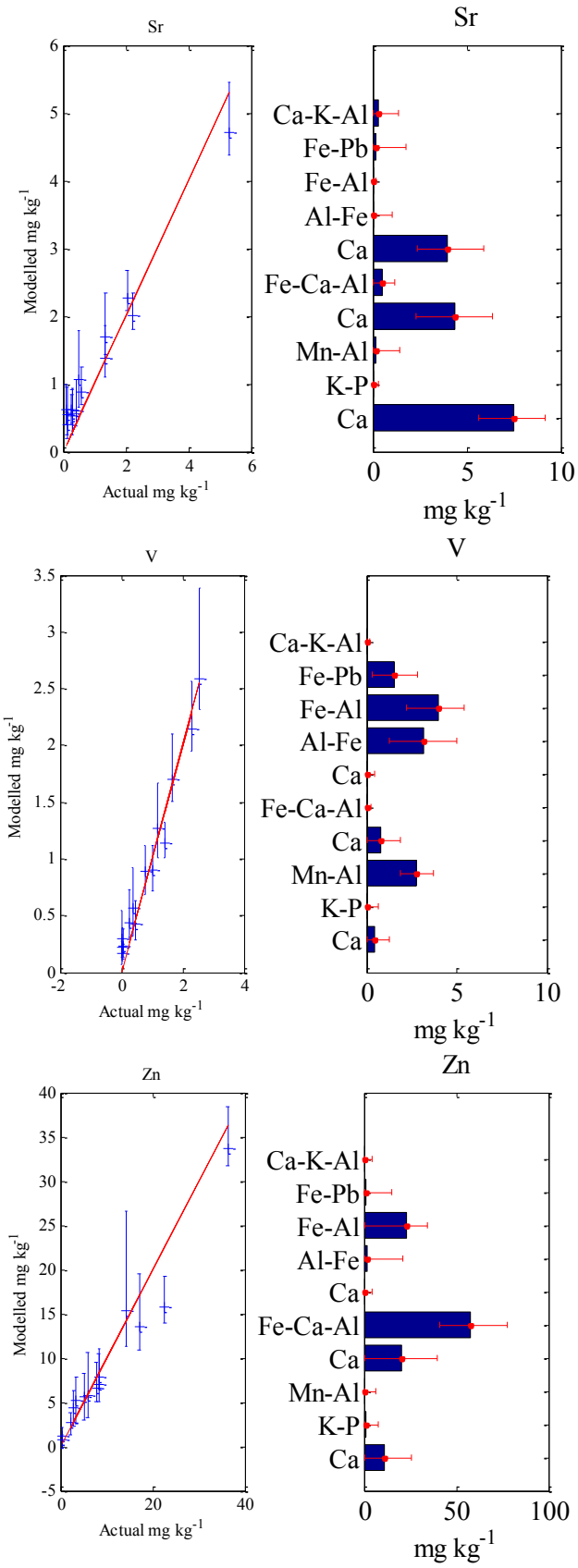
Sr
Modelled mg kg-1
Actual mg kg-1
0
1
2
3
4
5
6
Sr
Ca-K-Al
Fe-Pb
Fe-Al
Al-Fe
Ca
Fe-Ca-Al
Ca
Mn-Al
K-P
Ca
0
5
10
mg kg-1
V
Modelled mg kg-1
Actual mg kg-1
0
0.5
1
1.5
2
2.5
3
3.5
-2
0
2
4
V
Ca-K-Al
Fe-Pb
Fe-Al
Al-Fe
Ca
Fe-Ca-Al
Ca
Mn-Al
K-P
Ca
0
5
10
mg kg-1
Zn
Modelled mg kg-1
Actual mg kg-1
0
5
10
15
20
25
30
35
40
-5
0
20
40
Zn
Ca-K-Al
Fe-Pb
Fe-Al
Al-Fe
Ca
Fe-Ca-Al
Ca
Mn-Al
K-P
Ca
0
50
100
mg kg-1

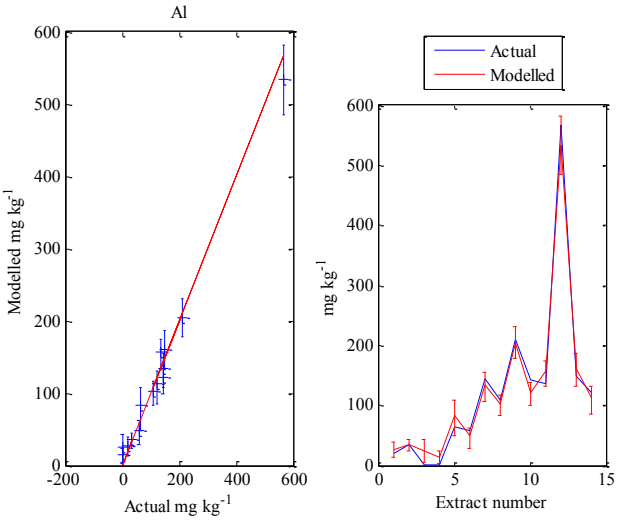
Al
Modelled mg kg-1
Actual mg kg-1
Actual
Modelled
mg kg-1
Extract number

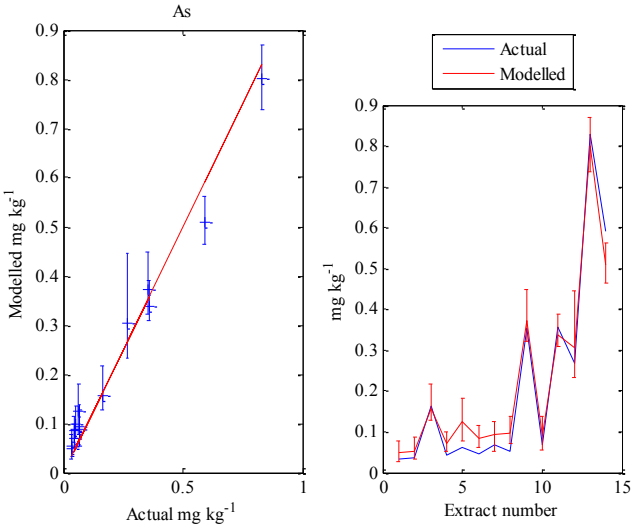
As
Modelled mg kg-1
Actual mg kg-1
Actual
Modelled
mg kg-1
Extract number

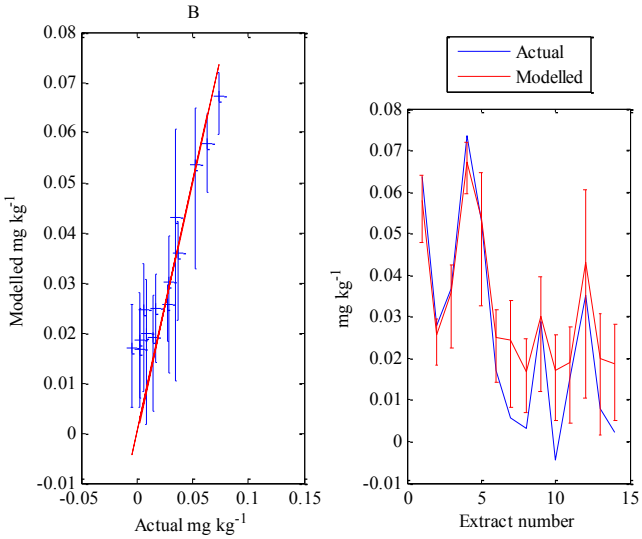
B
Modelled mg kg-1
Actual mg kg-1
Actual
Modelled
mg kg-1
Extract number

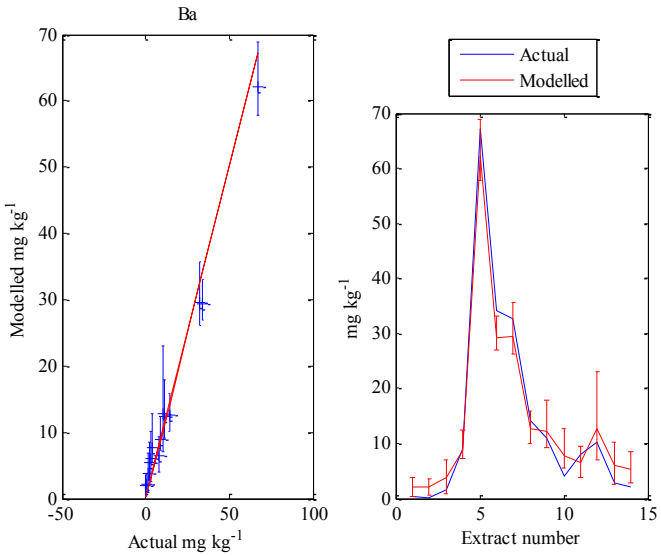
Ba
Modelled mg kg-1
Actual mg kg-1
Actual
Modelled
mg kg-1
Extract number

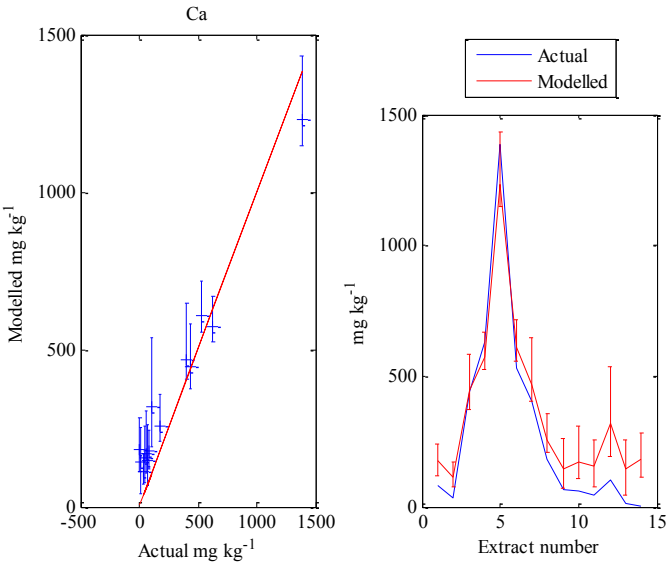
Ca
Modelled mg kg-1
Actual mg kg-1
Actual
Modelled
mg kg-1
Extract number

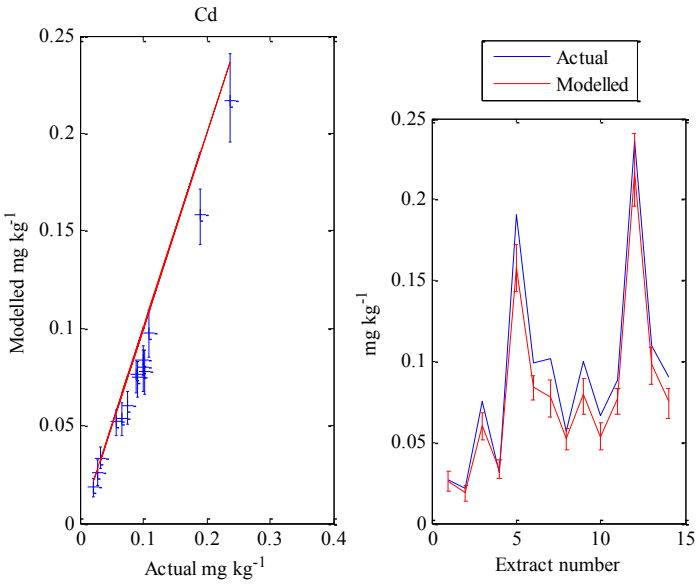
Cd
Modelled mg kg-1
Actual mg kg-1
Actual
Modelled
mg kg-1
Extract number

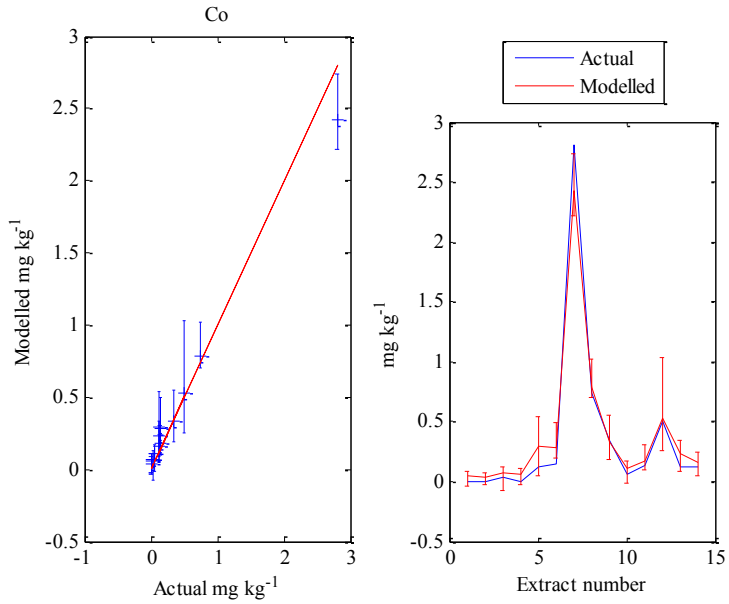
Co
Modelled mg kg-1
Actual mg kg-1
Actual
Modelled
mg kg-1
Extract number

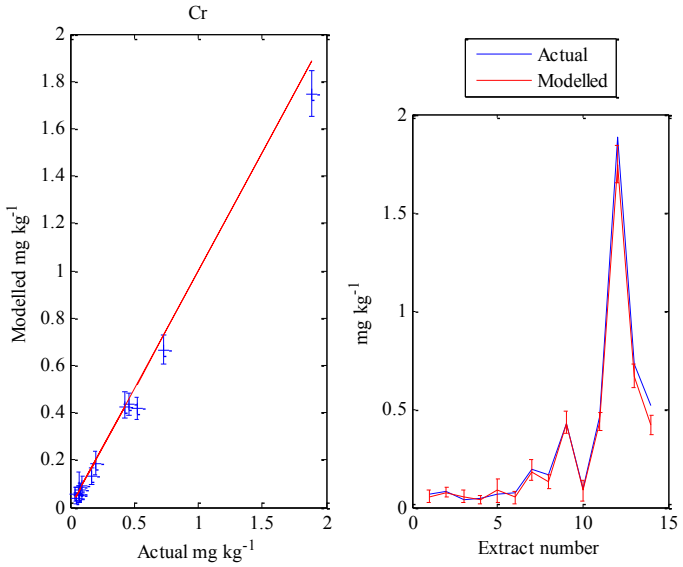
Cr
Modelled mg kg-1
Actual mg kg-1
Actual
Modelled
mg kg-1
Extract number

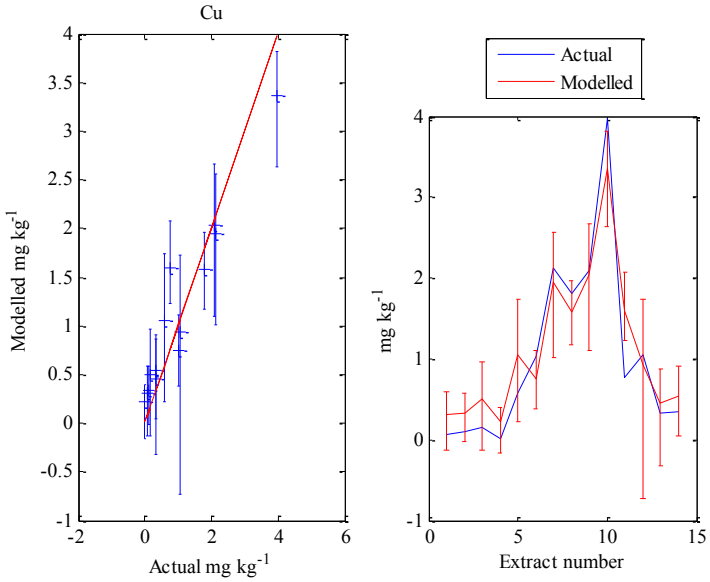
Cu
Modelled mg kg-1
Actual mg kg-1
Actual
Modelled
mg kg-1
Extract number

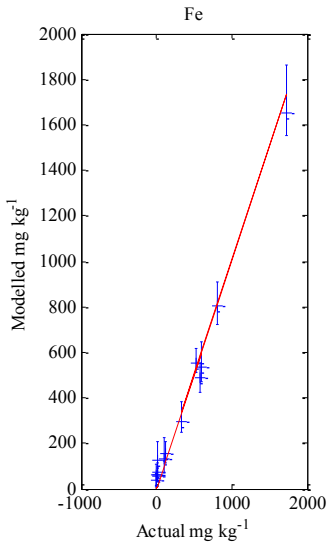
Fe
Modelled mg kg-1
Actual mg kg-1
2000
1800
1600
1400
1200
1000
800
600
400
200
0
-1000
0
1000
2000

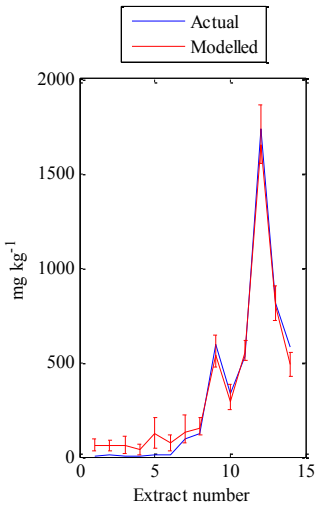
Actual
Modelled
mg kg-1
Extract number
2000
1500
1000
500
0
0
5
10
15

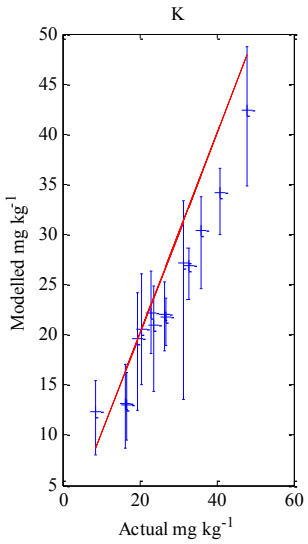
K
Modelled mg kg-1
Actual mg kg-1
50
45
40
35
30
25
20
15
10
5
0
20
40
60

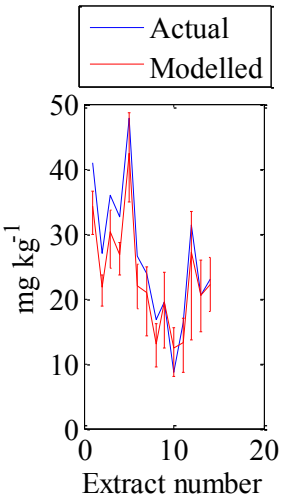
Actual
Modelled
mg kg-1
Extract number
50
40
30
20
10
0
0
10
20

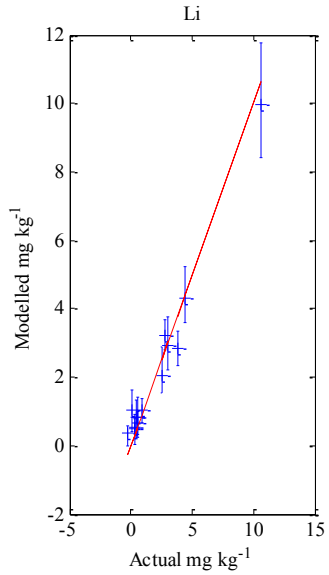
Li
Modelled mg kg-1
Actual mg kg-1
12
10
8
6
4
2
0
-2
-5
0
5
10
15

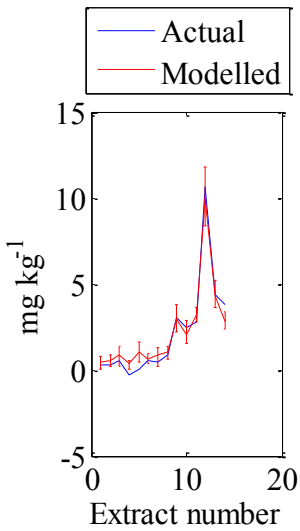
Actual
Modelled
mg kg-1
Extract number
15
10
5
0
-5
0
10
20

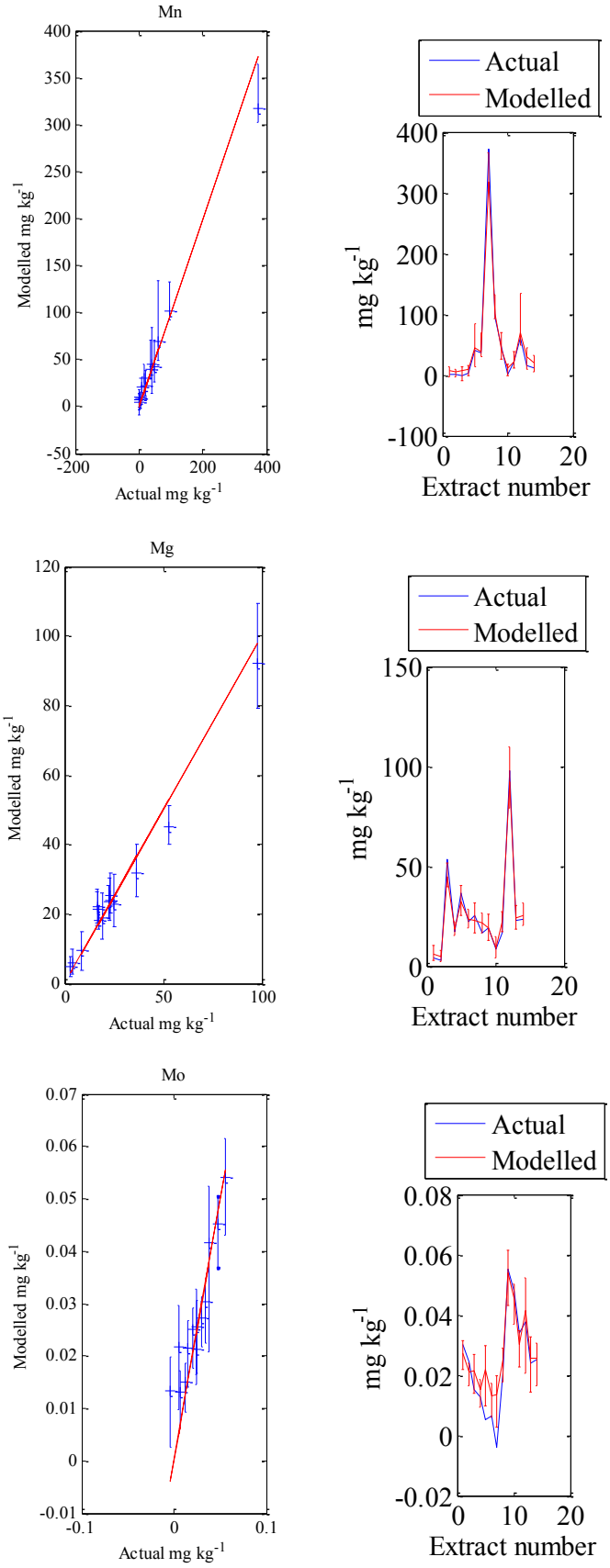
Mn
Modelled mg kg-1
Actual mg kg-1
Actual
Modelled
mg kg-1
Extract number
Mg
Modelled mg kg-1
Actual mg kg-1
Actual
Modelled
mg kg-1
Extract number
Mo
Modelled mg kg-1
Actual mg kg-1
Actual
Modelled
mg kg-1
Extract number

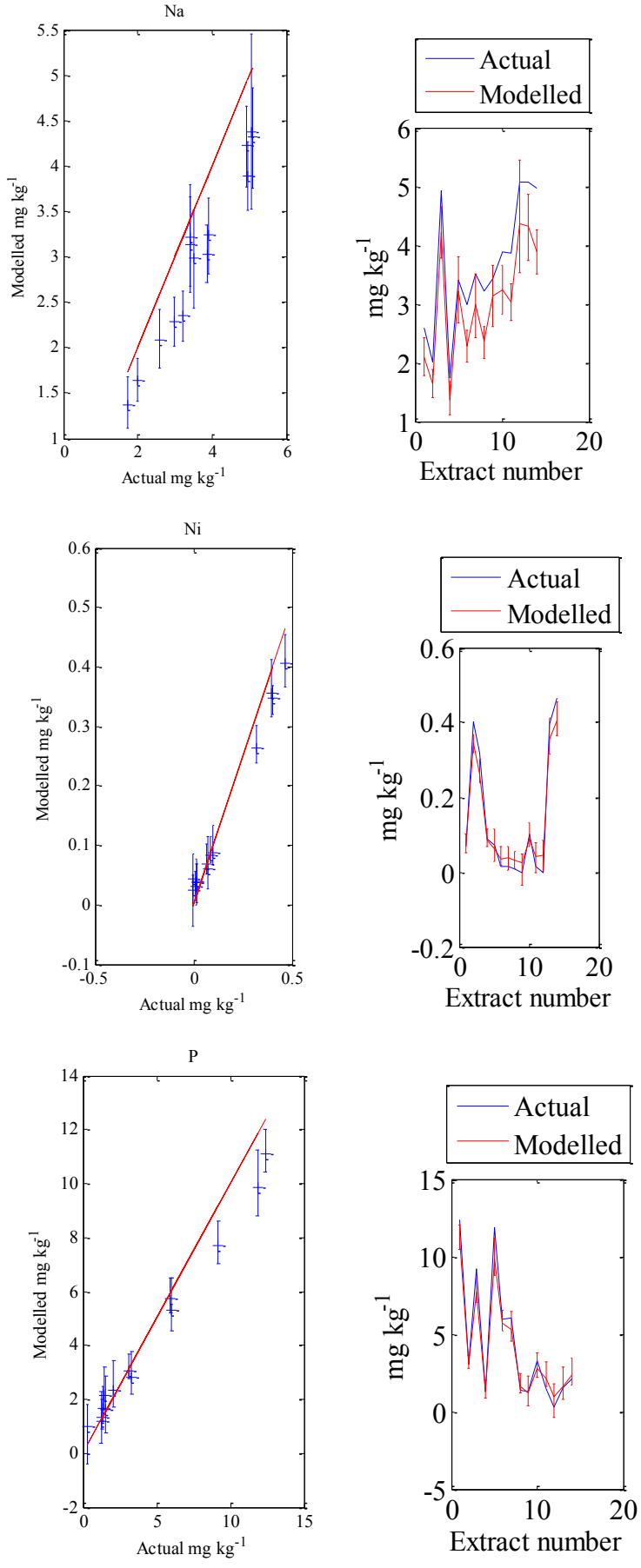
Na
Modelled mg kg-1
Actual mg kg-1
Actual
Modelled
mg kg-1
Extract number
Ni
Modelled mg kg-1
Actual mg kg-1
Actual
Modelled
mg kg-1
Extract number
P
Modelled mg kg-1
Actual mg kg-1
Actual
Modelled
mg kg-1
Extract number

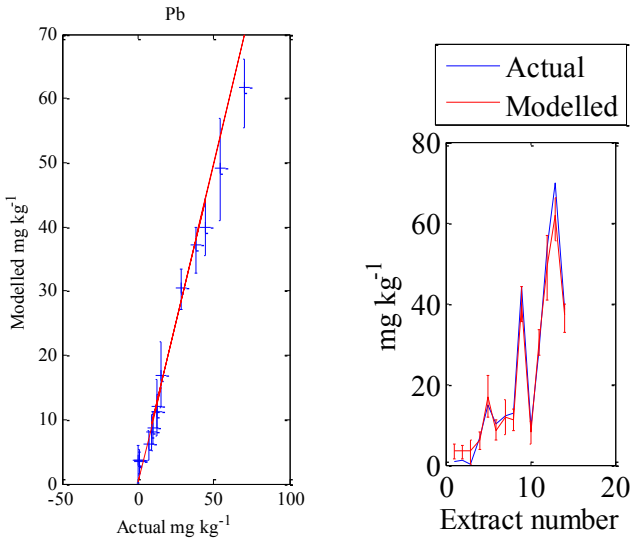
Pb
Modelled mg kg-1
Actual mg kg-1
70
60
50
40
30
20
10
0
-50
0
50
100

Actual
Modelled
mg kg-1
Extract number
80
60
40
20
0
0
10
20

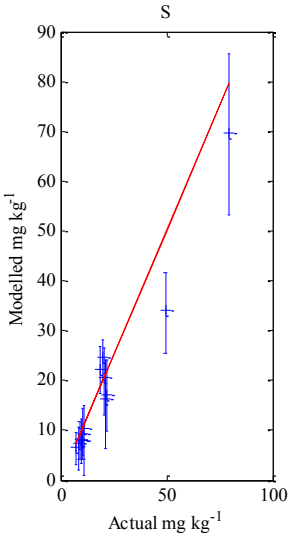
S
Modelled mg kg-1
Actual mg kg-1
90
80
70
60
50
40
30
20
10
0
0
50
100

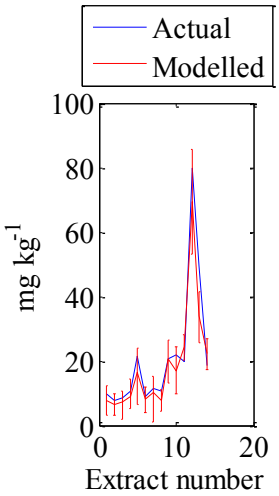
Actual
Modelled
mg kg-1
Extract number
100
80
60
40
20
0
0
10
20

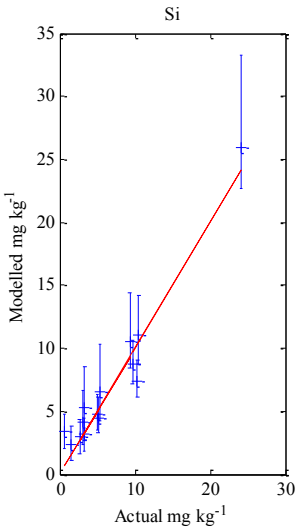
Si
Modelled mg kg-1
Actual mg kg-1
35
30
25
20
15
10
5
0
0
10
20
30

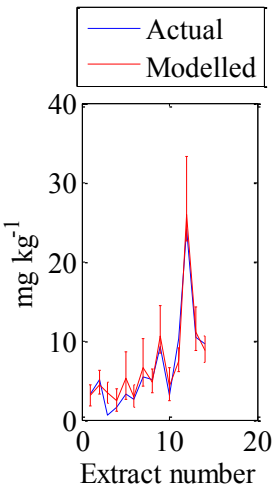
Actual
Modelled
mg kg-1
Extract number
40
30
20
10
0
0
10
20

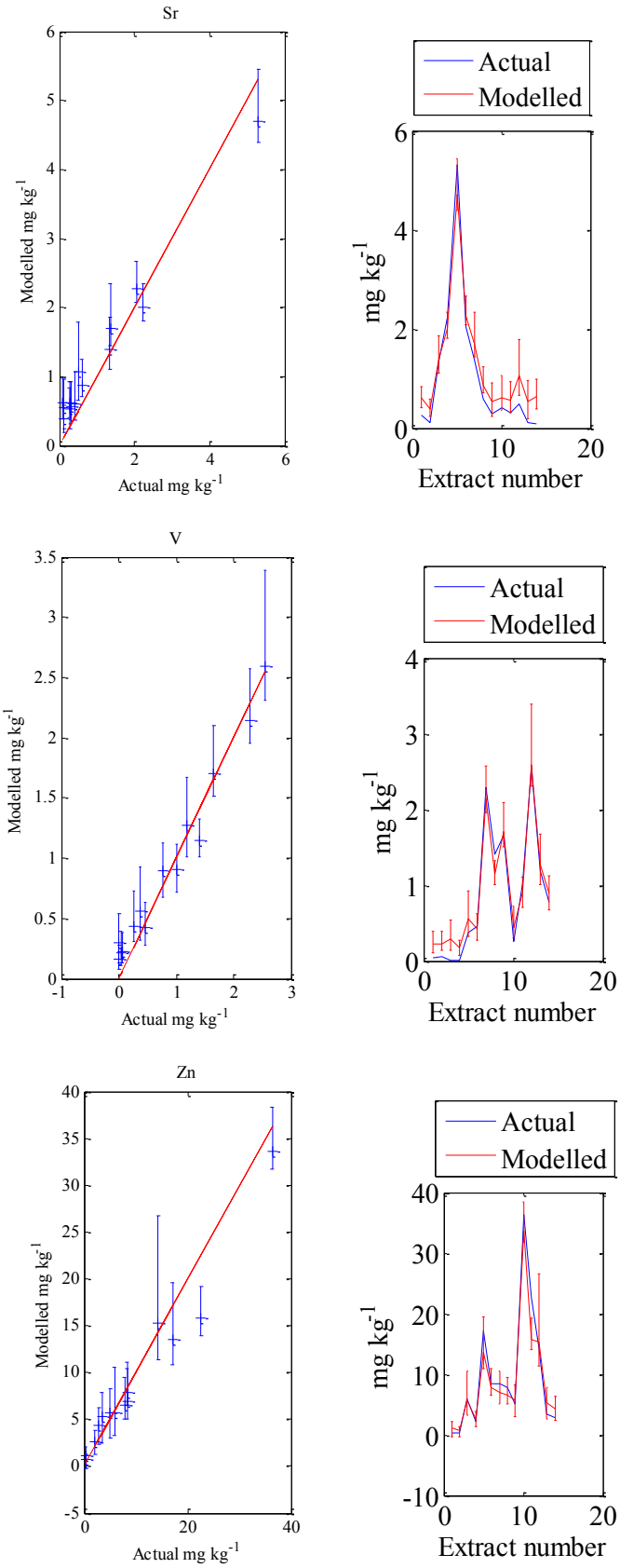
Sr
Modelled mg kg-1
Actual mg kg-1
Actual
Modelled
mg kg-1
Extract number
V
Modelled mg kg-1
Actual mg kg-1
Actual
Modelled
mg kg-1
Extract number
Zn
Modelled mg kg-1
Actual mg kg-1
Actual
Modelled
mg kg-1
Extract number

Soil 5

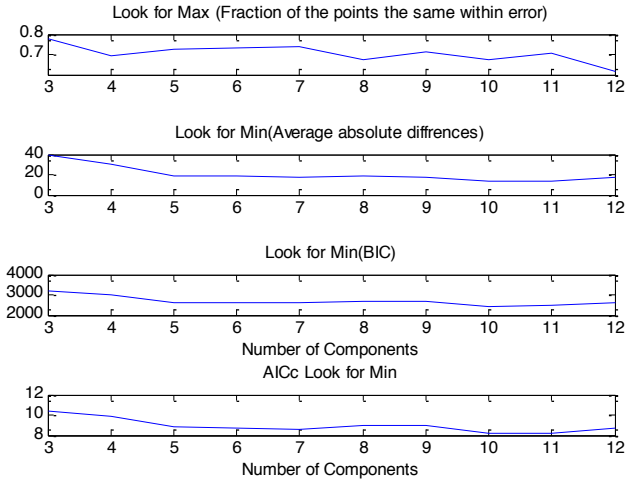
Look for Max (Fraction of the points the same within error)
Look for Min(Average absolute diffrences)
Look for Min(BIC)
Number of Components
AICc Look for Min
Number of Components

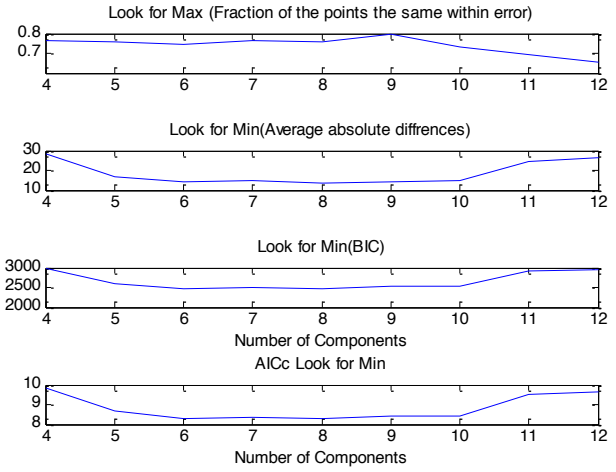
Look for Max (Fraction of the points the same within error)
Look for Min(Average absolute diffrences)
Look for Min(BIC)
Number of Components
AICc Look for Min
Number of Components

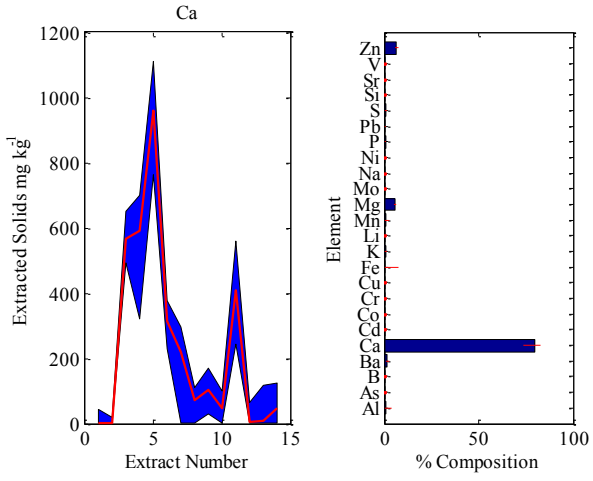
Ca
Extracted Solids mg kg-1
Extract Number
Element
% Composition
Zn
V
Sr
Si
S
Pb
P
Ni
Na
Mo
Mg
Mn
Li
K
Fe
Cu
Cr
Co
Cd
Ca
Ba
B
As
Al

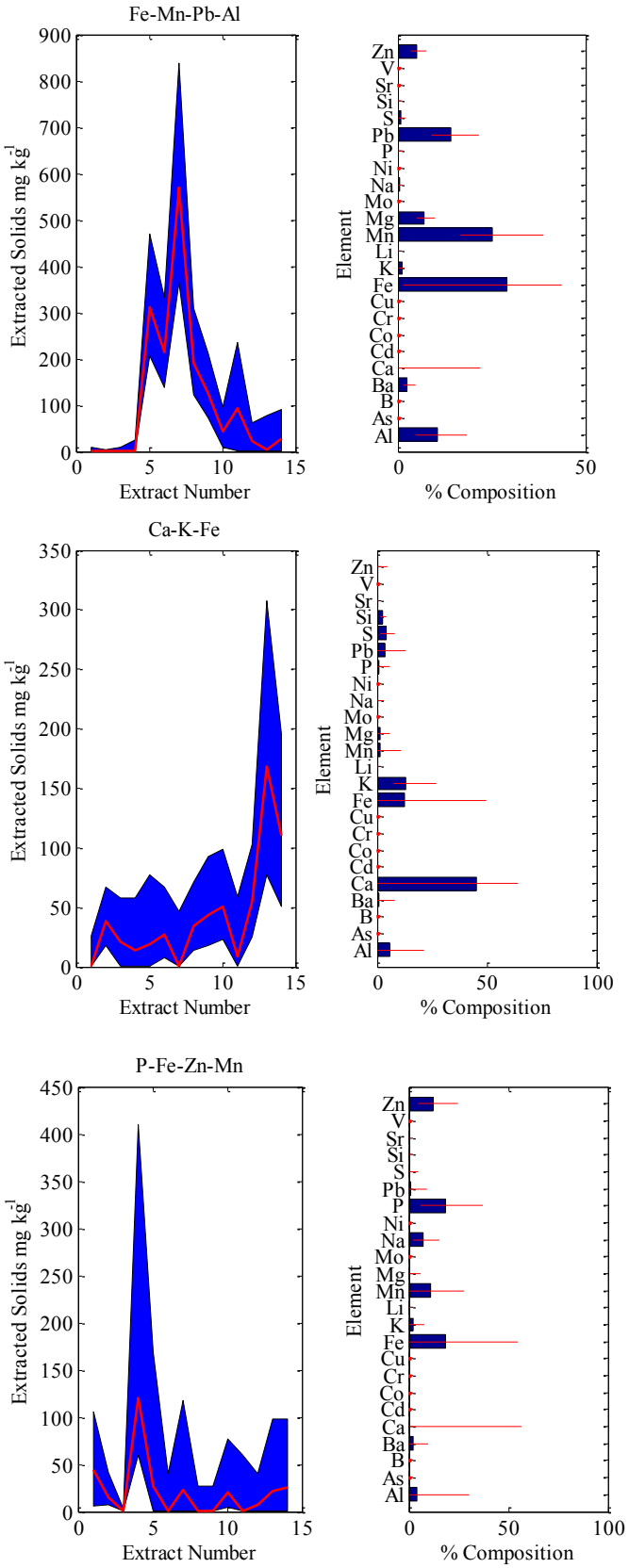
Fe-Mn-Pb-Al
Extracted Solids mg kg-1
Extract Number
Element
% Composition
Ca-K-Fe
Extracted Solids mg kg-1
Extract Number
Element
% Composition
P-Fe-Zn-Mn
Extracted Solids mg kg-1
Extract Number
Element
% Composition

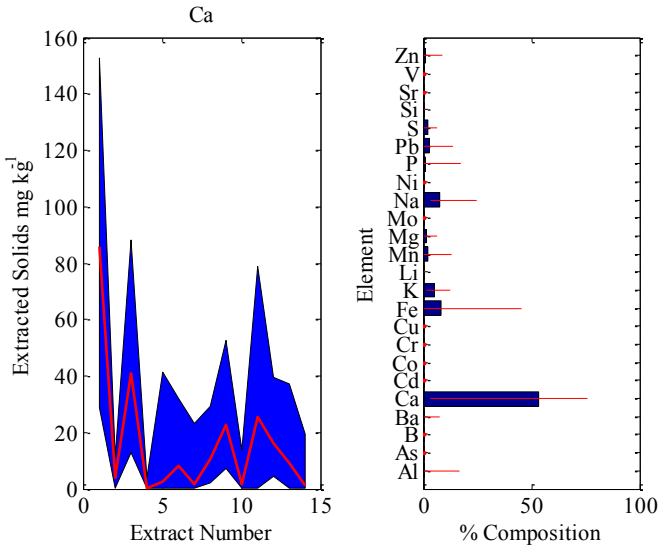
Ca
Extracted Solids mg kg-1
Extract Number
Element
% Composition
Zn
V
Sr
Si
S
Pb
P
Ni
Na
Mo
Mg
Mn
Li
K
Fe
Cu
Cr
Co
Cd
Ca
Ba
B
As
Al

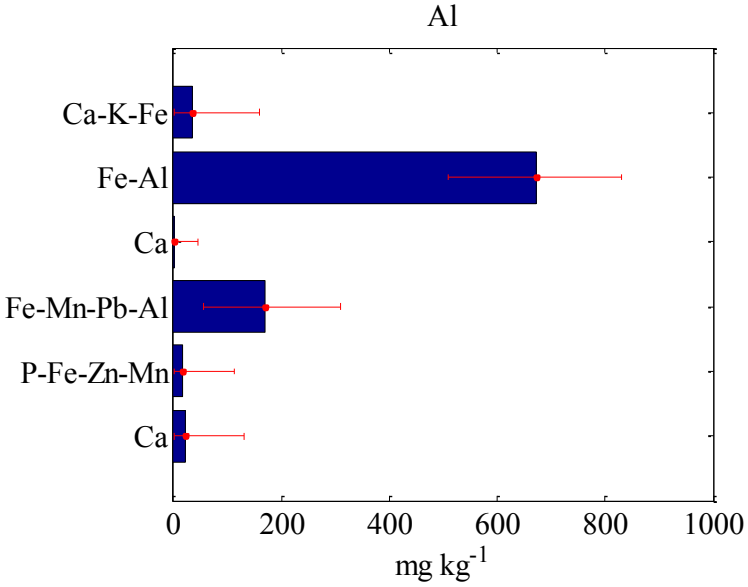
Al
Ca-K-Fe
Fe-Al
Ca
Fe-Mn-Pb-Al
P-Fe-Zn-Mn
Ca
mg kg-1

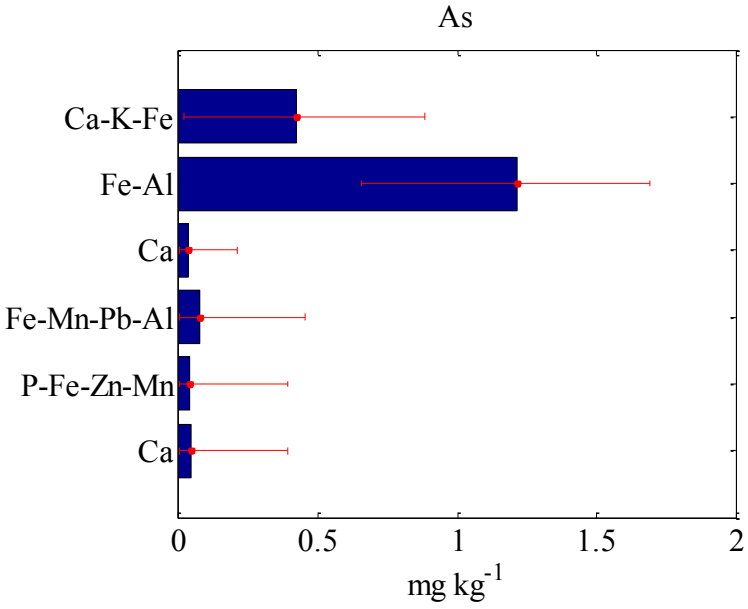
As
Ca-K-Fe
Fe-Al
Ca
Fe-Mn-Pb-Al
P-Fe-Zn-Mn
Ca
mg kg-1

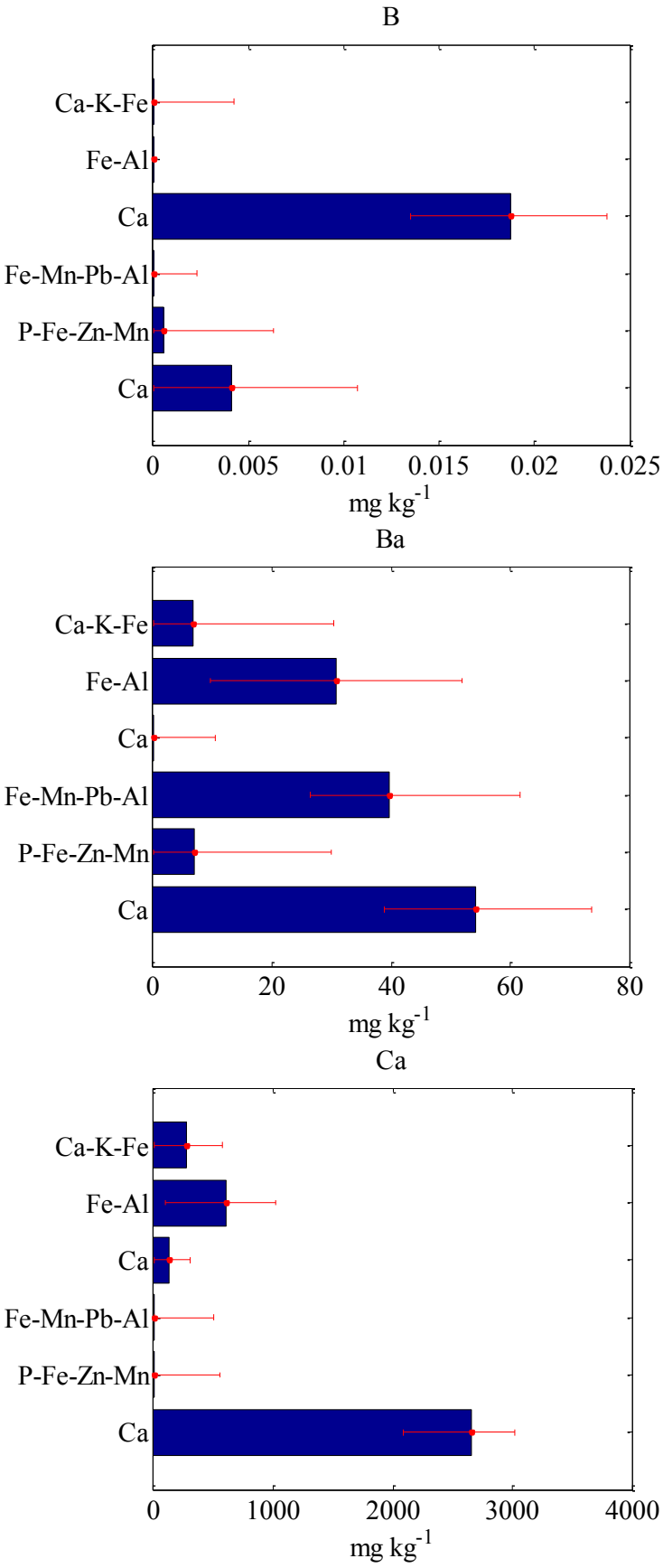
B
Ca-K-Fe
Fe-Al
Ca
Fe-Mn-Pb-Al
P-Fe-Zn-Mn
Ca
0
0.005
0.01
0.015
0.02
0.025
mg kg-1
Ba
Ca-K-Fe
Fe-Al
Ca
Fe-Mn-Pb-Al
P-Fe-Zn-Mn
Ca
0
20
40
60
80
mg kg-1
Ca
Ca-K-Fe
Fe-Al
Ca
Fe-Mn-Pb-Al
P-Fe-Zn-Mn
Ca
0
1000
2000
3000
4000
mg kg-1

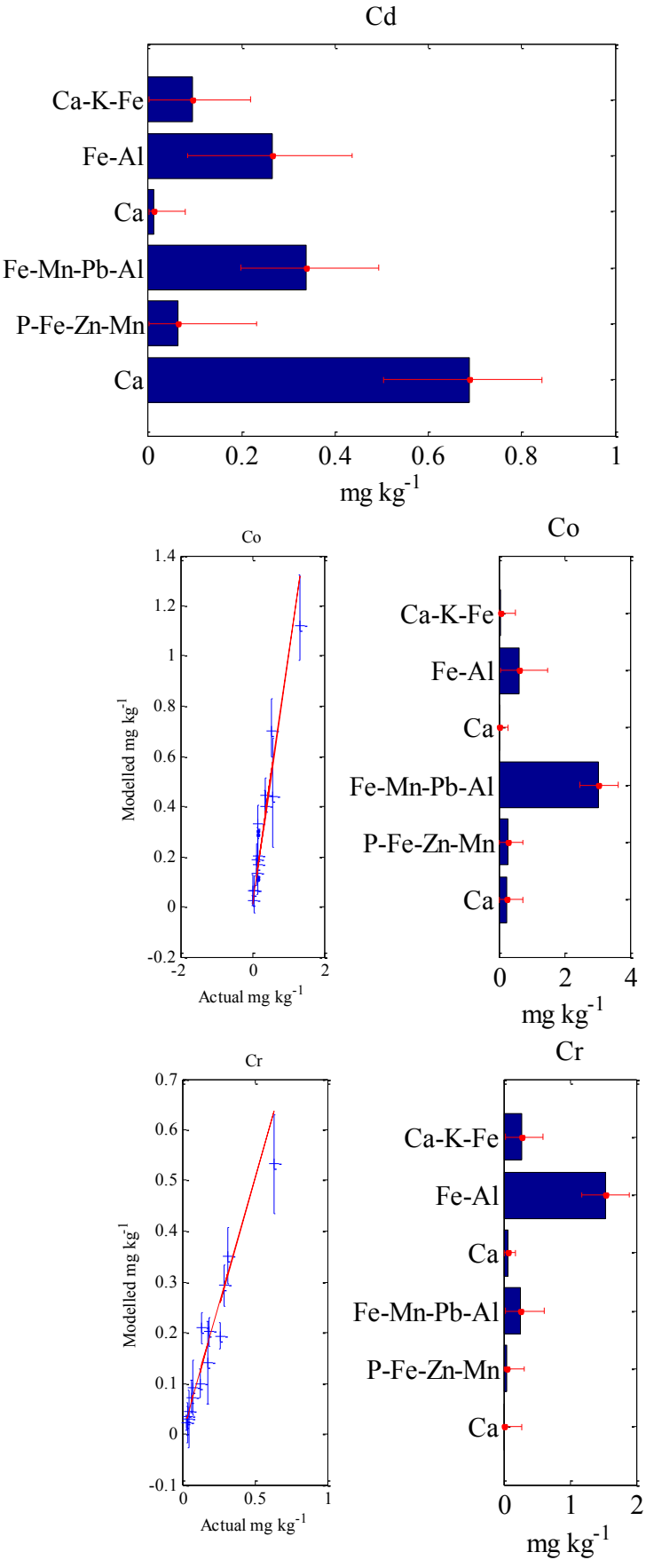
Cd
Ca-K-Fe
Fe-Al
Ca
Fe-Mn-Pb-Al
P-Fe-Zn-Mn
Ca
0
0.2
0.4
0.6
0.8
1
mg kg-1
Co
Modelled mg kg-1
Actual mg kg-1
Co
Ca-K-Fe
Fe-Al
Ca
Fe-Mn-Pb-Al
P-Fe-Zn-Mn
Ca
mg kg-1
Cr
Modelled mg kg-1
Actual mg kg-1
Cr
Ca-K-Fe
Fe-Al
Ca
Fe-Mn-Pb-Al
P-Fe-Zn-Mn
Ca
mg kg-1

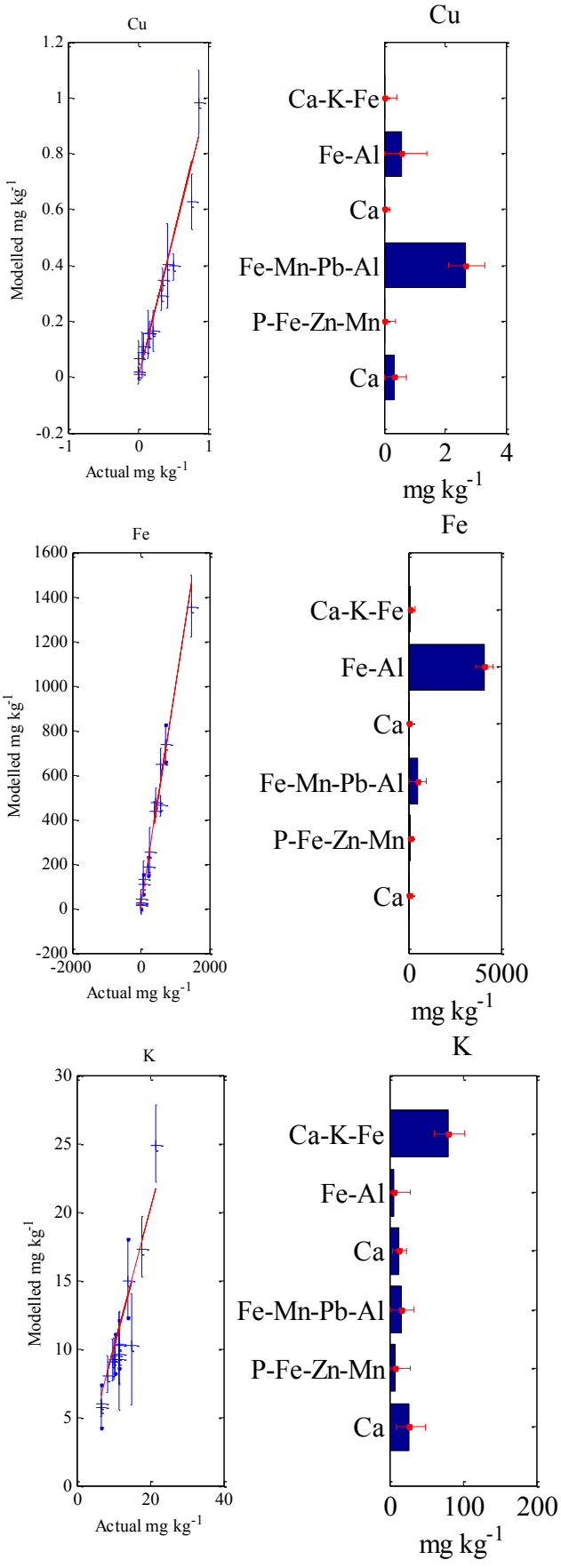
Cu
Modelled mg kg-1
Actual mg kg-1
Cu
Ca-K-Fe
Fe-Al
Ca
Fe-Mn-Pb-Al
P-Fe-Zn-Mn
Ca
mg kg-1
Fe
Modelled mg kg-1
Actual mg kg-1
Fe
Ca-K-Fe
Fe-Al
Ca
Fe-Mn-Pb-Al
P-Fe-Zn-Mn
Ca
mg kg-1
K
Modelled mg kg-1
Actual mg kg-1
K
Ca-K-Fe
Fe-Al
Ca
Fe-Mn-Pb-Al
P-Fe-Zn-Mn
Ca
mg kg-1

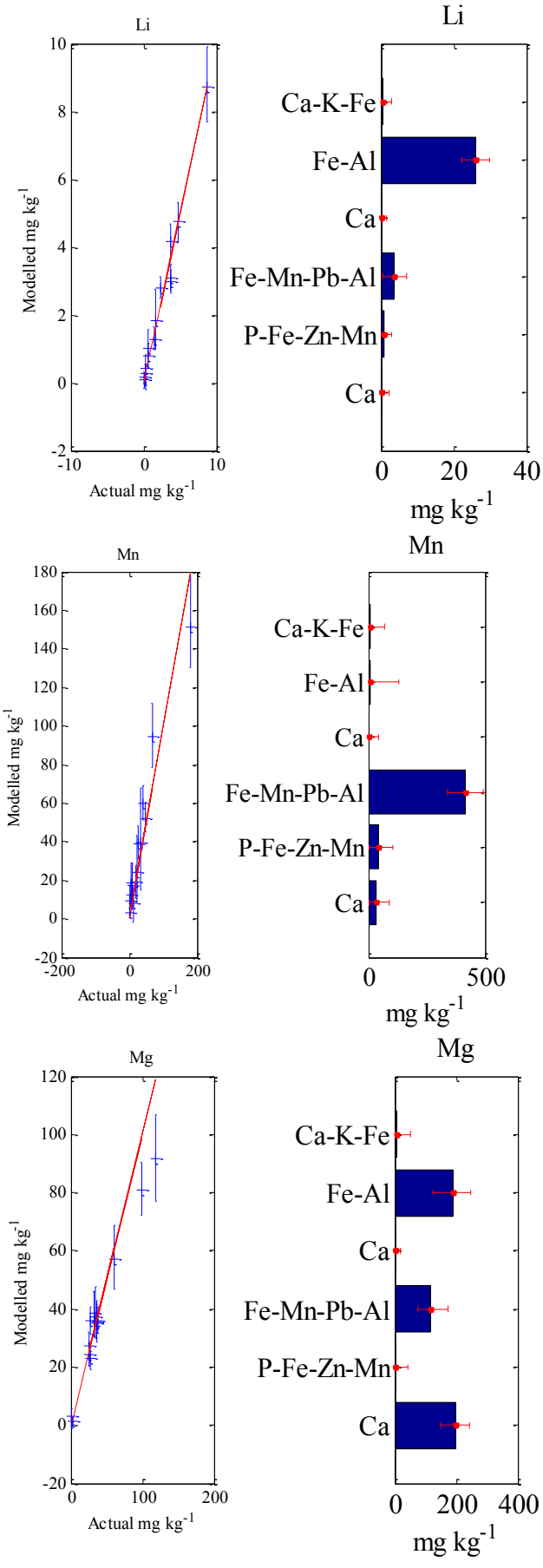
Li
Modelled mg kg-1
Actual mg kg-1
Li
Ca-K-Fe
Fe-Al
Ca
Fe-Mn-Pb-Al
P-Fe-Zn-Mn
Ca
mg kg-1
Mn
Modelled mg kg-1
Actual mg kg-1
Mn
Ca-K-Fe
Fe-Al
Ca
Fe-Mn-Pb-Al
P-Fe-Zn-Mn
Ca
mg kg-1
Mg
Modelled mg kg-1
Actual mg kg-1
Mg
Ca-K-Fe
Fe-Al
Ca
Fe-Mn-Pb-Al
P-Fe-Zn-Mn
Ca
mg kg-1

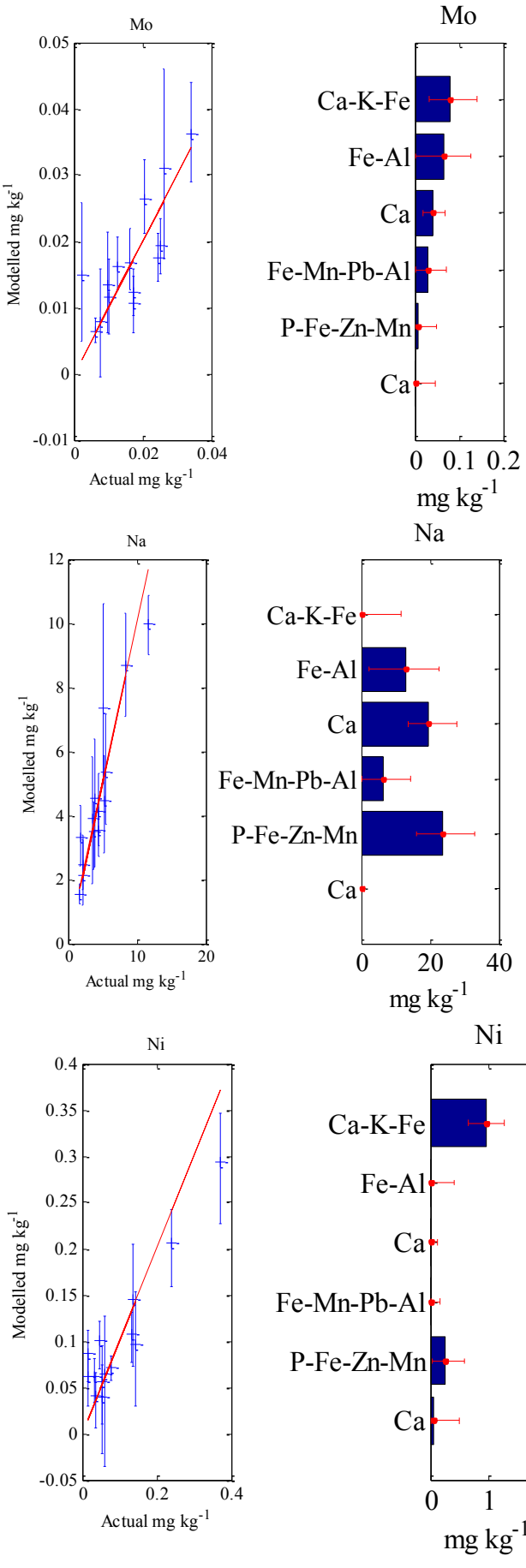
Mo
Modelled mg kg-1
Actual mg kg-1
0.05
0.04
0.03
0.02
0.01
0
-0.01
0
0.02
0.04
Mo
Ca-K-Fe
Fe-Al
Ca
Fe-Mn-Pb-Al
P-Fe-Zn-Mn
Ca
0
0.1
0.2
mg kg-1
Na
Modelled mg kg-1
Actual mg kg-1
12
10
8
6
4
2
0
0
10
20
Na
Ca-K-Fe
Fe-Al
Ca
Fe-Mn-Pb-Al
P-Fe-Zn-Mn
Ca
0
20
40
mg kg-1
Ni
Modelled mg kg-1
Actual mg kg-1
0.4
0.35
0.3
0.25
0.2
0.15
0.1
0.05
0
-0.05
0
0.2
0.4
Ni
Ca-K-Fe
Fe-Al
Ca
Fe-Mn-Pb-Al
P-Fe-Zn-Mn
Ca
0
1
2
mg kg-1

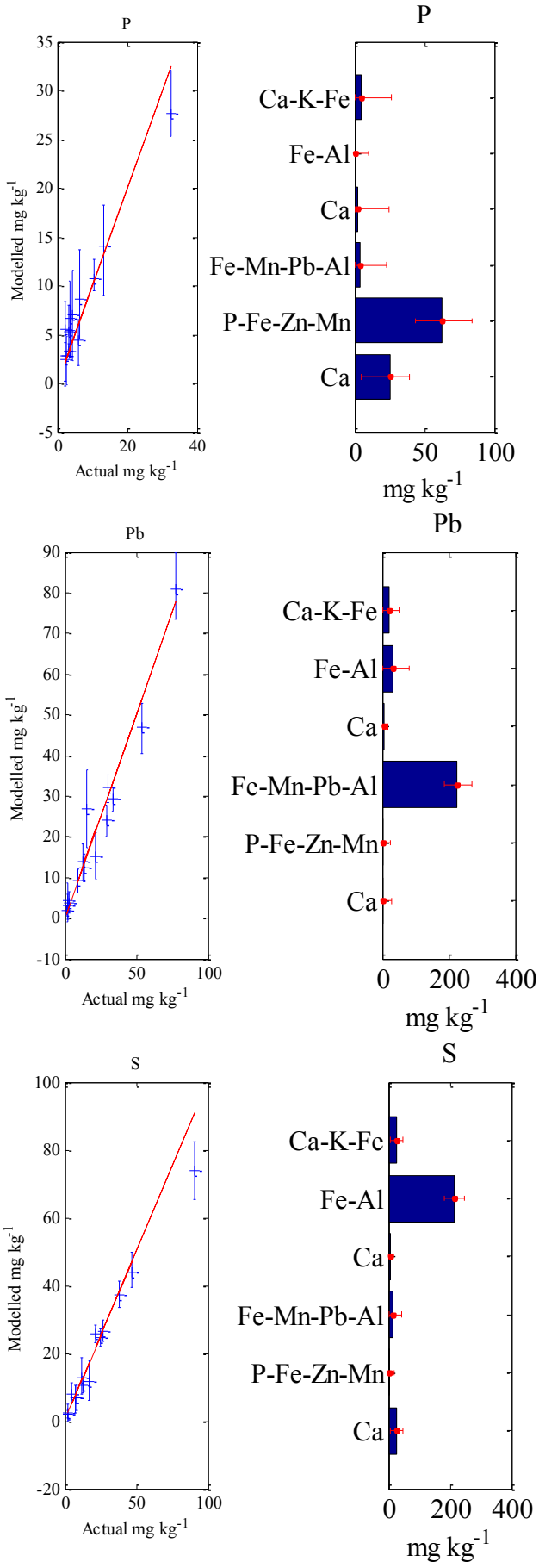
P
Modelled mg kg-1
Actual mg kg-1
P
Ca-K-Fe
Fe-Al
Ca
Fe-Mn-Pb-Al
P-Fe-Zn-Mn
Ca
mg kg-1
Pb
Modelled mg kg-1
Actual mg kg-1
Pb
Ca-K-Fe
Fe-Al
Ca
Fe-Mn-Pb-Al
P-Fe-Zn-Mn
Ca
mg kg-1
S
Modelled mg kg-1
Actual mg kg-1
S
Ca-K-Fe
Fe-Al
Ca
Fe-Mn-Pb-Al
P-Fe-Zn-Mn
Ca
mg kg-1

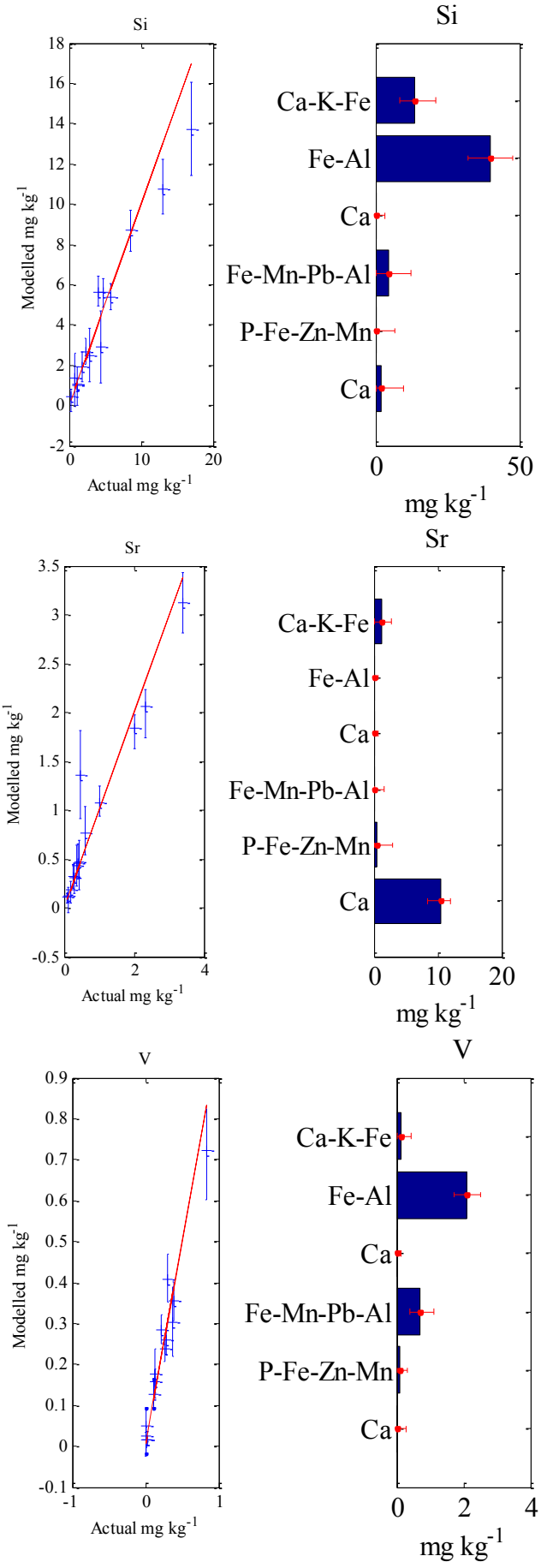
Si
Modelled mg kg-1
Actual mg kg-1
Si
Ca-K-Fe
Fe-Al
Ca
Fe-Mn-Pb-Al
P-Fe-Zn-Mn
Ca
mg kg-1
Sr
Modelled mg kg-1
Actual mg kg-1
Sr
Ca-K-Fe
Fe-Al
Ca
Fe-Mn-Pb-Al
P-Fe-Zn-Mn
Ca
mg kg-1
V
Modelled mg kg-1
Actual mg kg-1
V
Ca-K-Fe
Fe-Al
Ca
Fe-Mn-Pb-Al
P-Fe-Zn-Mn
Ca
mg kg-1

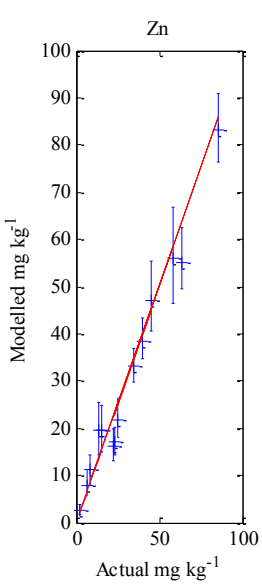
Zn
Modelled mg kg-1
Actual mg kg-1
0
10
20
30
40
50
60
70
80
90
100
0
50
100

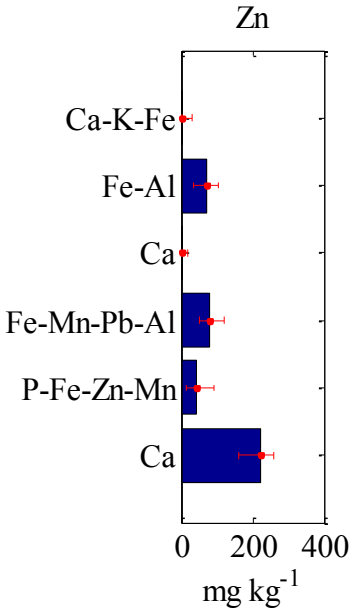
Zn
Ca-K-Fe
Fe-Al
Ca
Fe-Mn-Pb-Al
P-Fe-Zn-Mn
Ca
0
200
400
mg kg-1

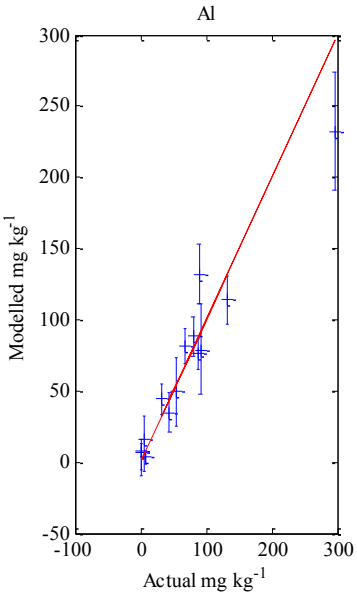
Al
Modelled mg kg-1
Actual mg kg-1
-50
0
50
100
150
200
250
300
-100
0
100
200
300

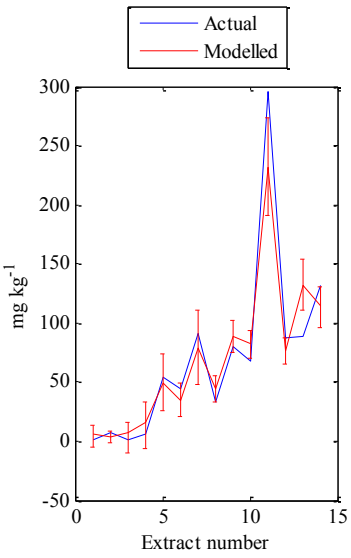
Actual
Modelled
mg kg-1
Extract number
-50
0
50
100
150
200
250
300
0
5
10
15

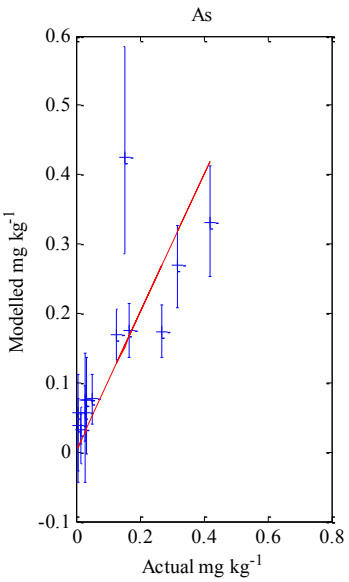
As
Modelled mg kg-1
Actual mg kg-1
-0.1
0
0.1
0.2
0.3
0.4
0.5
0.6
0
0.2
0.4
0.6
0.8

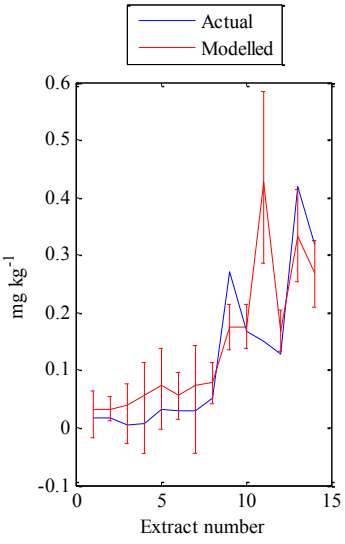
Actual
Modelled
mg kg-1
Extract number
-0.1
0
0.1
0.2
0.3
0.4
0.5
0.6
0
5
10
15

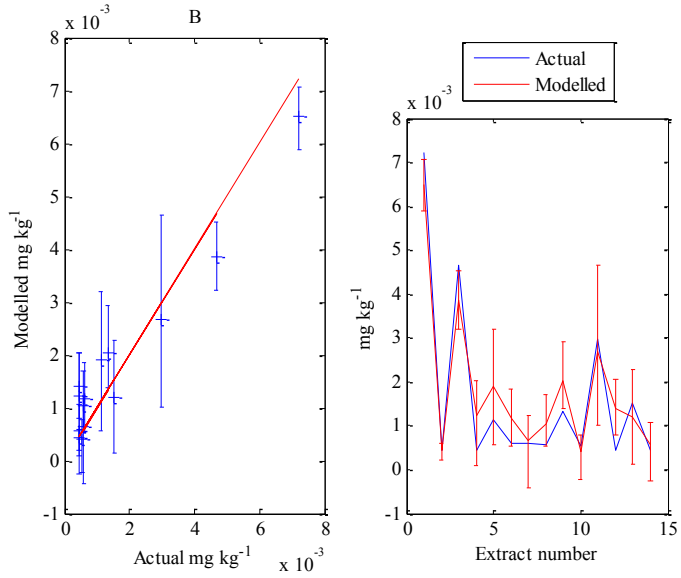
B
x 10^-3
Modelled mg kg^-1
Actual mg kg^-1
x 10^-3
Actual
Modelled
mg kg^-1
Extract number

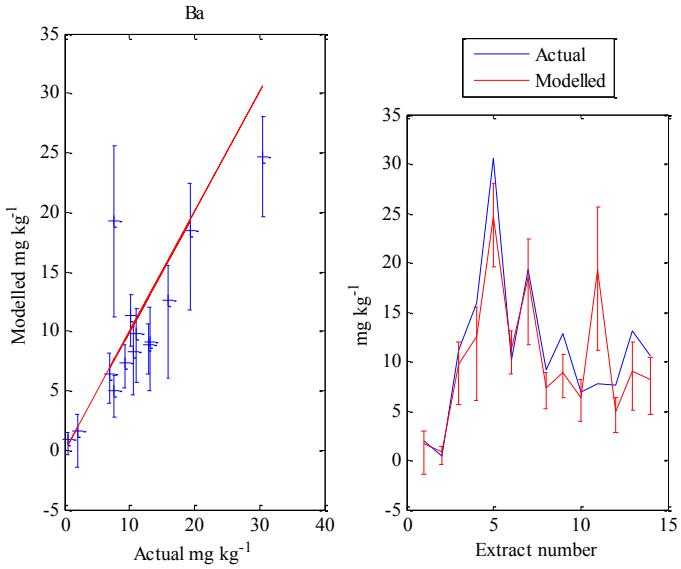
Ba
Modelled mg kg^-1
Actual mg kg^-1
Actual
Modelled
mg kg^-1
Extract number

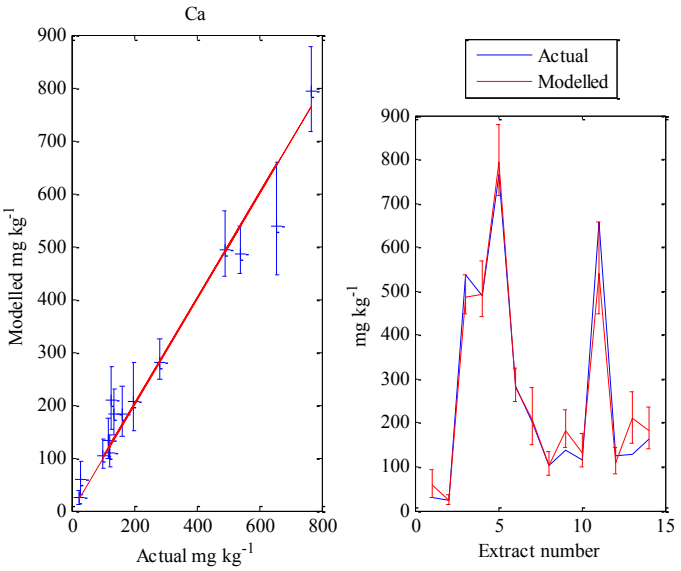
Ca
Modelled mg kg^-1
Actual mg kg^-1
Actual
Modelled
mg kg^-1
Extract number

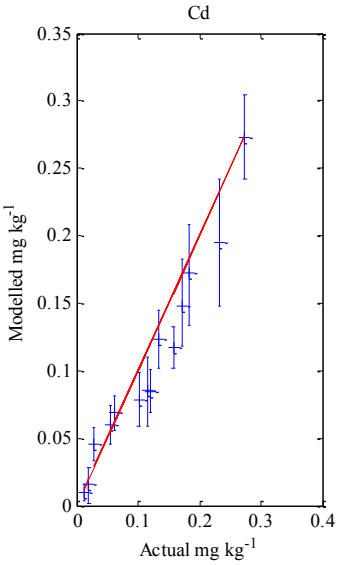
Cd
Modelled mg kg-1
Actual mg kg-1
0.35
0.3
0.25
0.2
0.15
0.1
0.05
0
0 0.1 0.2 0.3 0.4

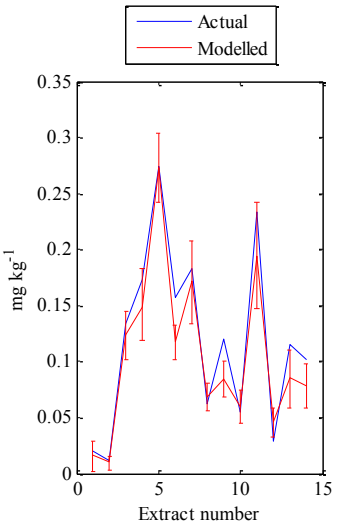
Actual
Modelled
mg kg-1
Extract number
0.35
0.3
0.25
0.2
0.15
0.1
0.05
0
0 5 10 15

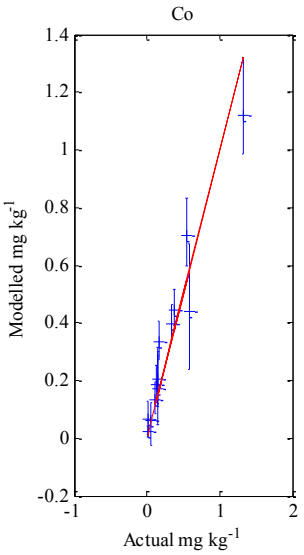
Co
Modelled mg kg-1
Actual mg kg-1
1.4
1.2
1
0.8
0.6
0.4
0.2
0
-0.2
-1 0 1 2

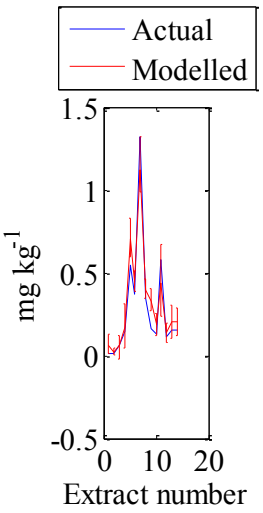
Actual
Modelled
mg kg-1
Extract number
1.5
1
0.5
0
-0.5
0 10 20

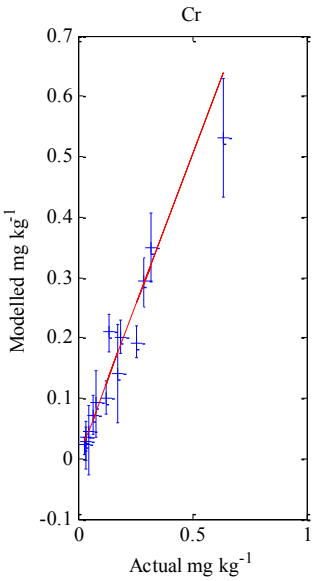
Cr
Modelled mg kg-1
Actual mg kg-1
0.7
0.6
0.5
0.4
0.3
0.2
0.1
0
-0.1
0 0.5 1

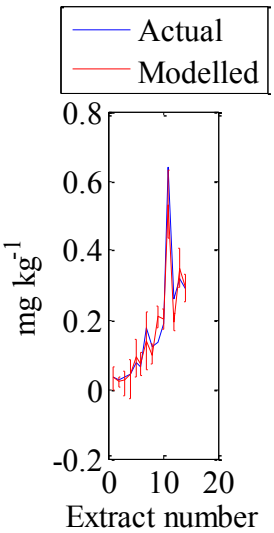
Actual
Modelled
mg kg-1
Extract number
0.8
0.6
0.4
0.2
0
-0.2
0 10 20

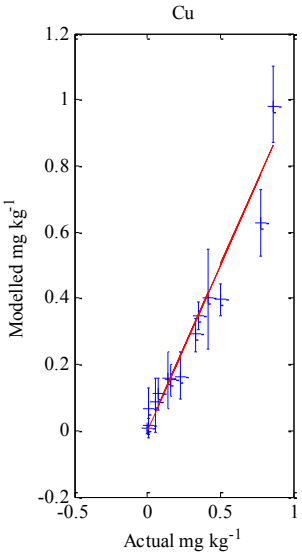
Cu
Modelled mg kg-1
Actual mg kg-1

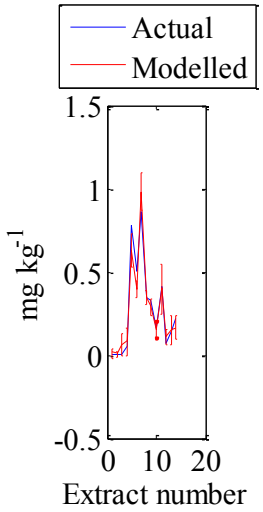
Actual
Modelled
mg kg-1
Extract number

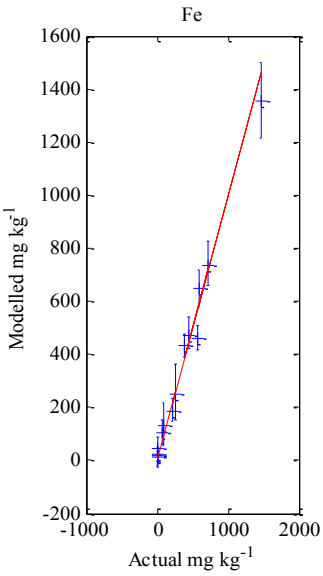
Fe
Modelled mg kg-1
Actual mg kg-1

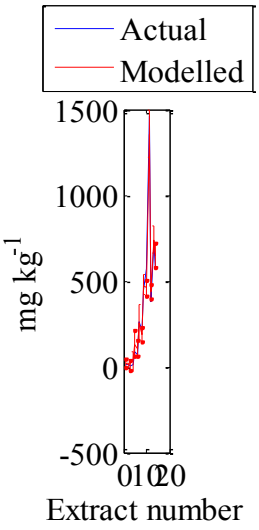
Actual
Modelled
mg kg-1
Extract number

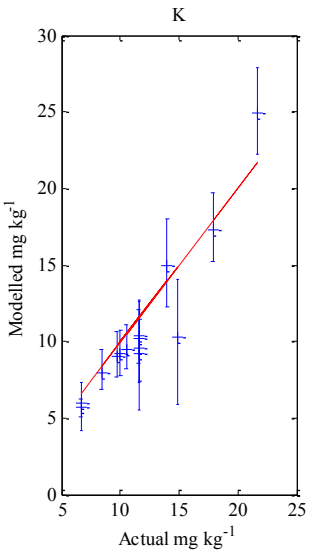
K
Modelled mg kg-1
Actual mg kg-1

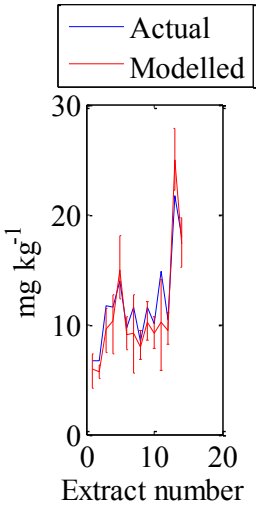
Actual
Modelled
mg kg-1
Extract number

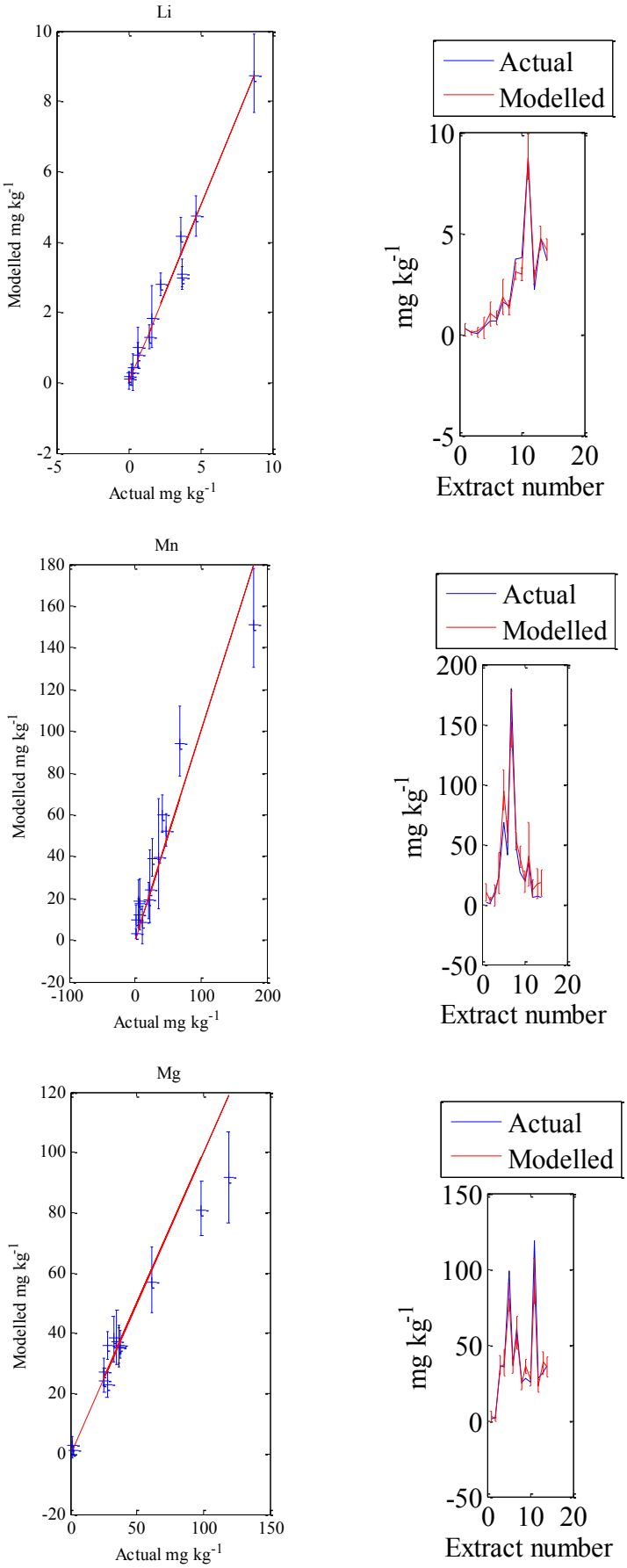
Li
Modelled mg kg-1
Actual mg kg-1
Actual
Modelled
mg kg-1
Extract number
Mn
Modelled mg kg-1
Actual mg kg-1
Actual
Modelled
mg kg-1
Extract number
Mg
Modelled mg kg-1
Actual mg kg-1
Actual
Modelled
mg kg-1
Extract number

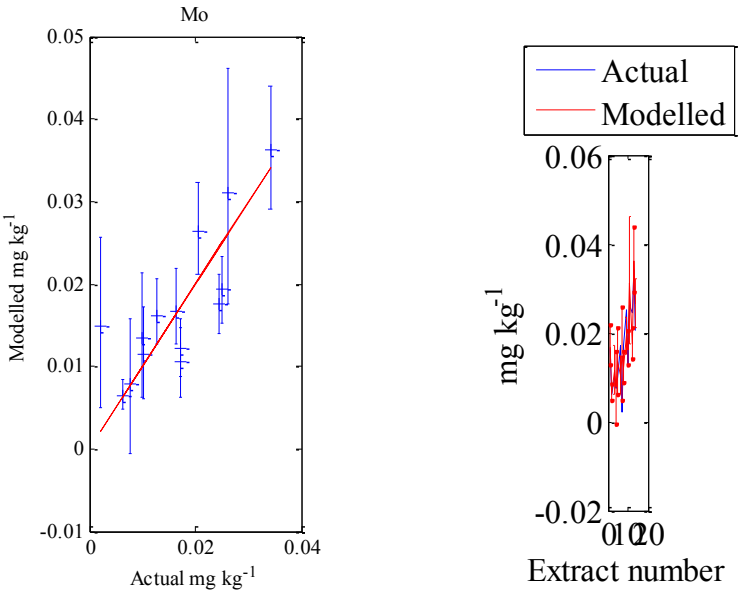
Mo
Modelled mg kg-1
Actual mg kg-1
0.05
0.04
0.03
0.02
0.01
0
-0.01
0
0.02
0.04
Actual
Modelled
mg kg-1
0.06
0.04
0.02
0
-0.02
0
10
20
Extract number

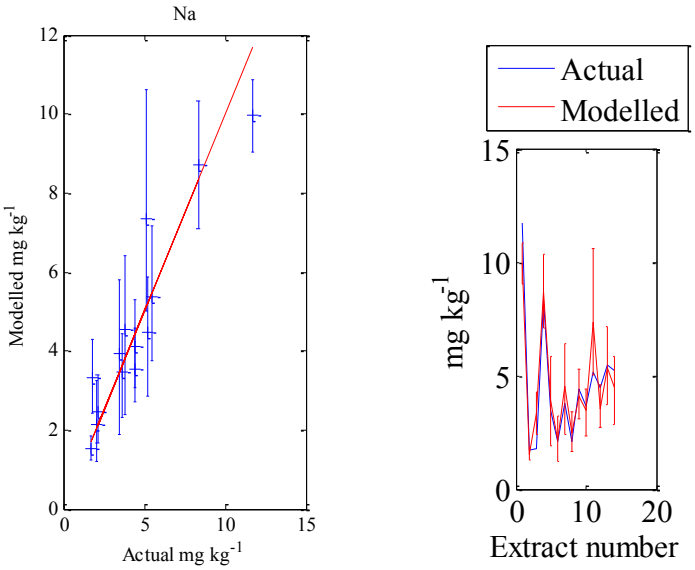
Na
Modelled mg kg-1
Actual mg kg-1
12
10
8
6
4
2
0
0
5
10
15
Actual
Modelled
mg kg-1
15
10
5
0
0
10
20
Extract number

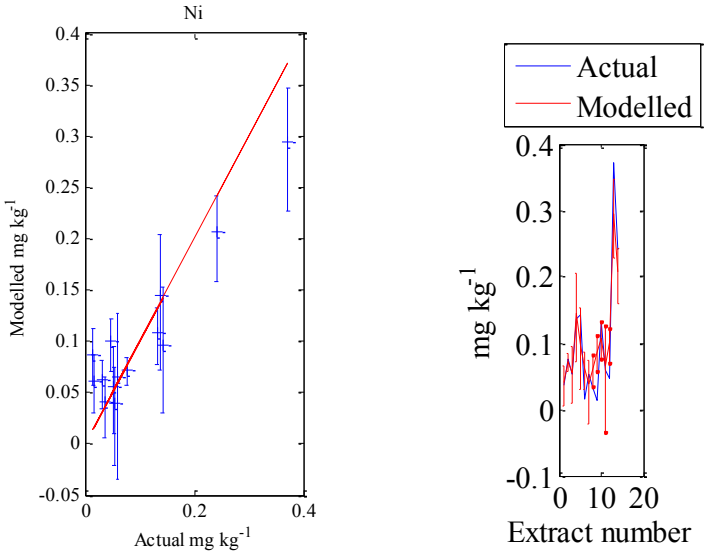
Ni
Modelled mg kg-1
Actual mg kg-1
0.4
0.35
0.3
0.25
0.2
0.15
0.1
0.05
0
-0.05
0
0.2
0.4
Actual
Modelled
mg kg-1
0.4
0.3
0.2
0.1
0
-0.1
0
10
20
Extract number

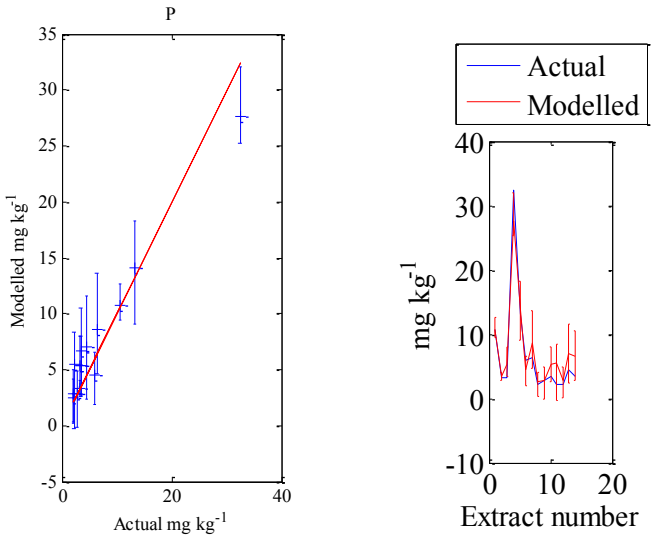
P
Modelled mg kg-1
Actual mg kg-1
Actual
Modelled
mg kg-1
Extract number

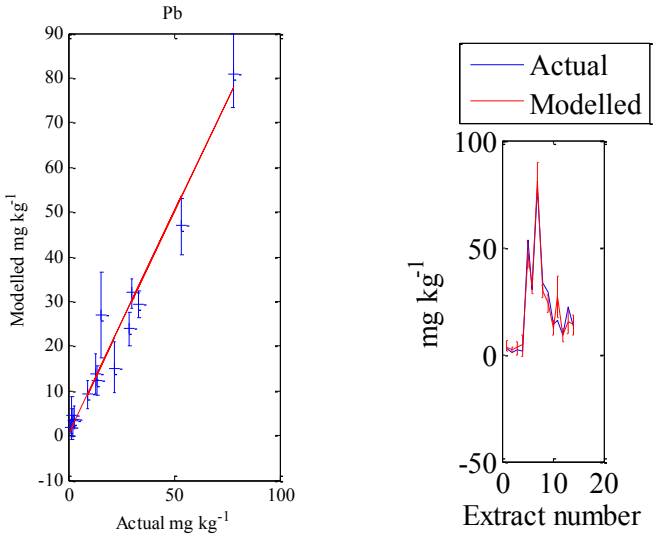
Pb
Modelled mg kg-1
Actual mg kg-1
Actual
Modelled
mg kg-1
Extract number

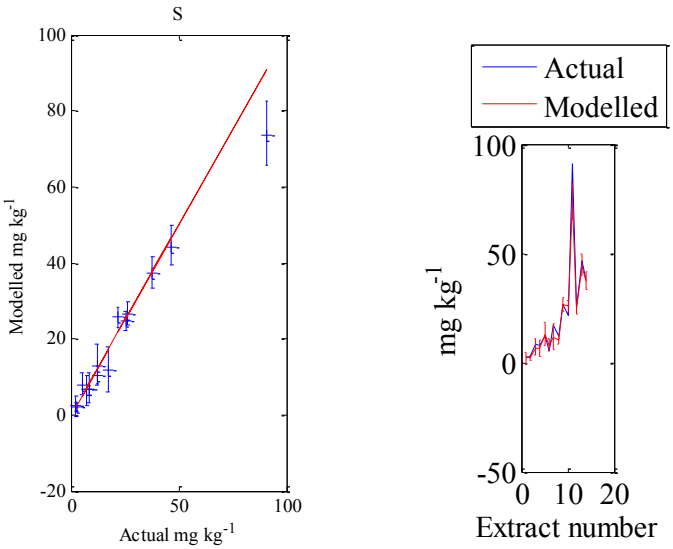
S
Modelled mg kg-1
Actual mg kg-1
Actual
Modelled
mg kg-1
Extract number

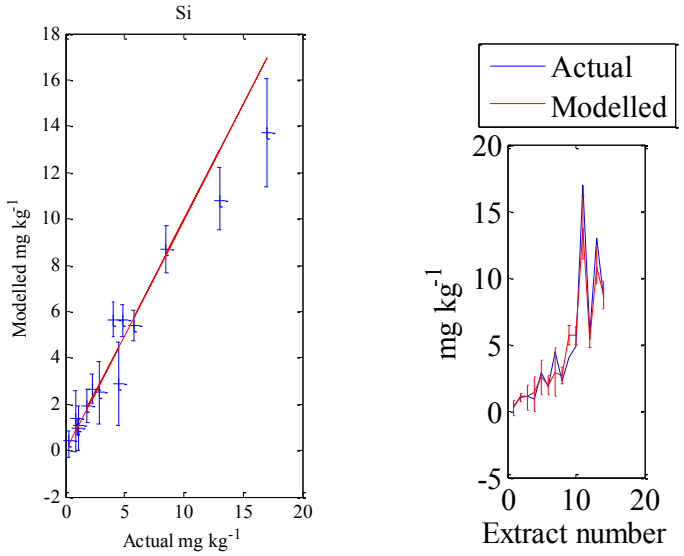
Si
Modelled mg kg-1
Actual mg kg-1
Actual
Modelled
mg kg-1
Extract number

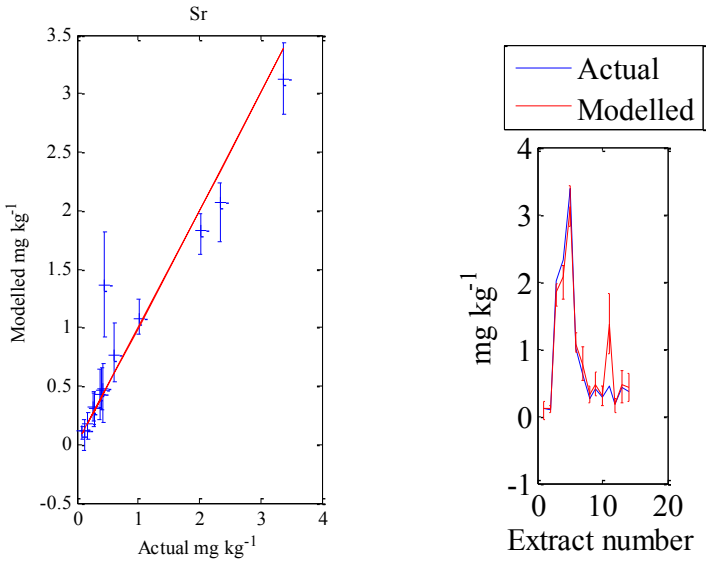
Sr
Modelled mg kg-1
Actual mg kg-1
Actual
Modelled
mg kg-1
Extract number

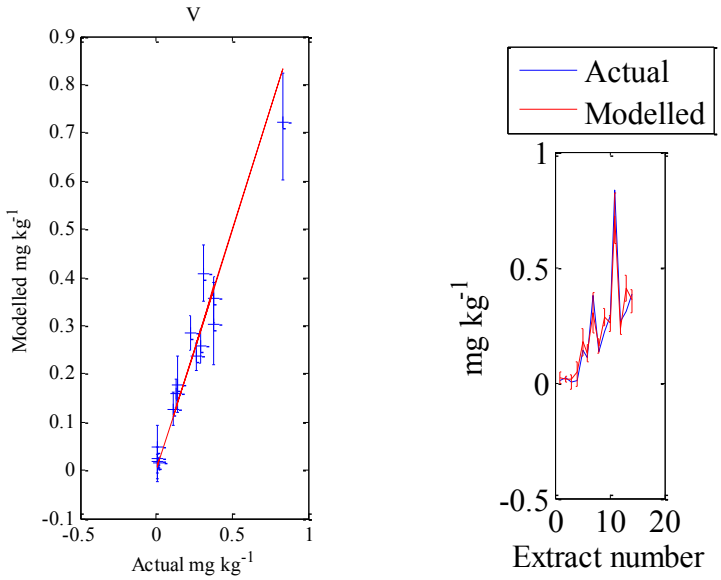
V
Modelled mg kg-1
Actual mg kg-1
Actual
Modelled
mg kg-1
Extract number

Soil 6

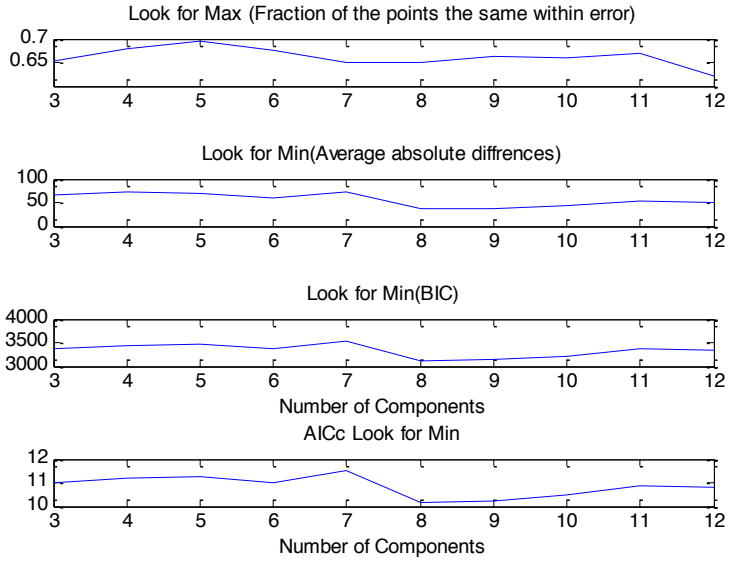
Look for Max (Fraction of the points the same within error)
0.7
0.65
3 4 5 6 7 8 9 10 11 12
Look for Min(Average absolute diffrences)
100
50
0
3 4 5 6 7 8 9 10 11 12
Look for Min(BIC)
4000
3500
3000
3 4 5 6 7 8 9 10 11 12
Number of Components
AICc Look for Min
12
11
10
3 4 5 6 7 8 9 10 11 12
Number of Components

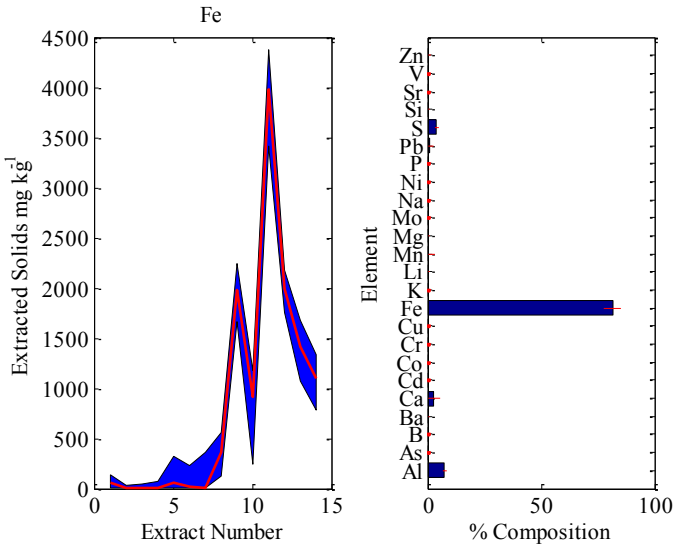
Fe
Extracted Solids mg kg-1
4500
4000
3500
3000
2500
2000
1500
1000
500
0
0 5 10 15
Extract Number
Element
Zn
V
Sr
Si
S
Pb
P
Ni
Na
Mo
Mg
Mn
Li
K
Fe
Cu
Cr
Co
Cd
Ca
Ba
B
As
Al
0 50 100
% Composition

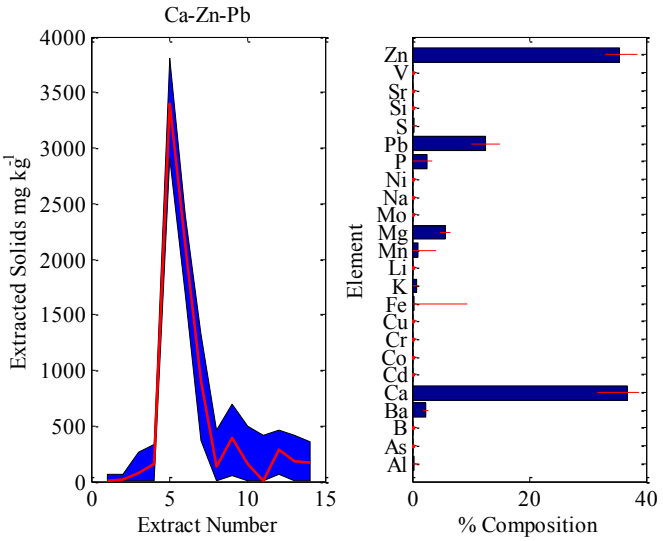
Ca-Zn-Pb
Extracted Solids mg kg-1
Extract Number
Element
% Composition
Zn
V
Sr
Si
S
Pb
P
Ni
Na
Mo
Mg
Mn
Li
K
Fe
Cu
Cr
Co
Cd
Ca
Ba
B
As
Al

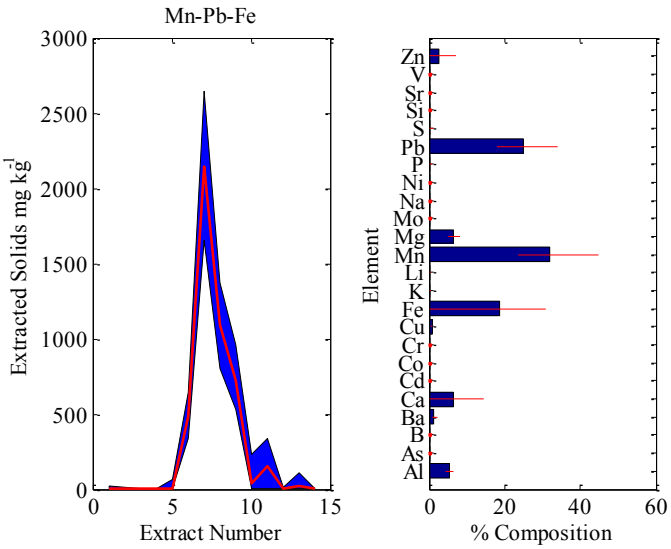
Mn-Pb-Fe
Extracted Solids mg kg-1
Extract Number
Element
% Composition
Zn
V
Sr
Si
S
Pb
P
Ni
Na
Mo
Mg
Mn
Li
K
Fe
Cu
Cr
Co
Cd
Ca
Ba
B
As
Al

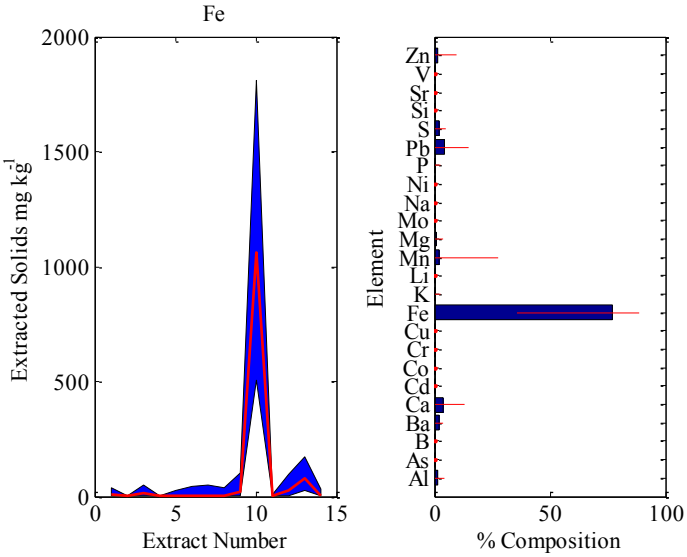
Fe
Extracted Solids mg kg-1
Extract Number
Element
% Composition
Zn
V
Sr
Si
S
Pb
P
Ni
Na
Mo
Mg
Mn
Li
K
Fe
Cu
Cr
Co
Cd
Ca
Ba
B
As
Al

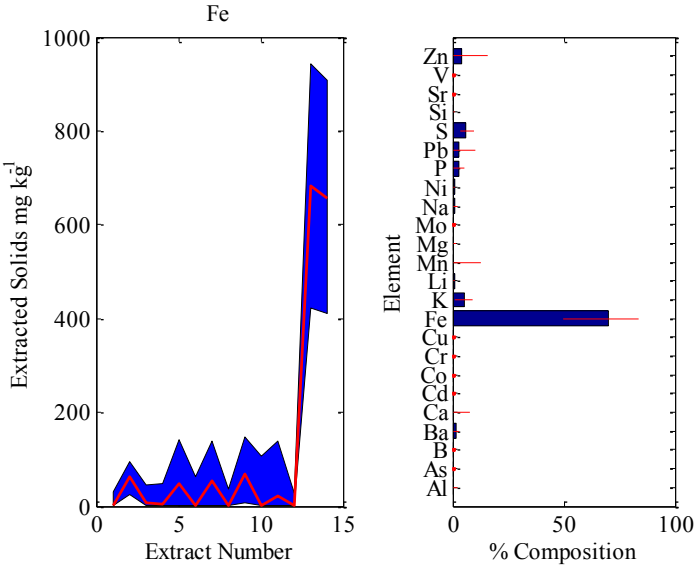
Fe
Extracted Solids mg kg-1
Extract Number
Element
% Composition
Zn
V
Sr
Si
S
Pb
P
Ni
Na
Mo
Mg
Mn
Li
K
Fe
Cu
Cr
Co
Cd
Ca
Ba
B
As
Al

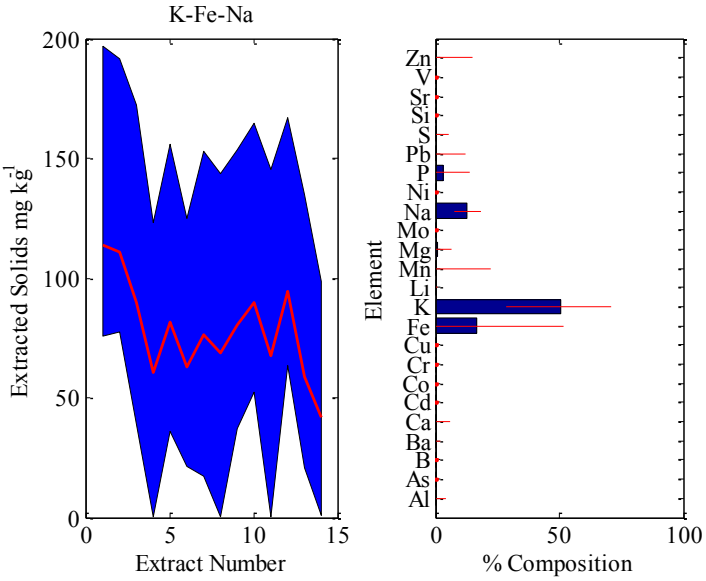
K-Fe-Na
Extracted Solids mg kg-1
Extract Number
Element
% Composition
Zn
V
Sr
Si
S
Pb
P
Ni
Na
Mo
Mg
Mn
Li
K
Fe
Cu
Cr
Co
Cd
Ca
Ba
B
As
Al

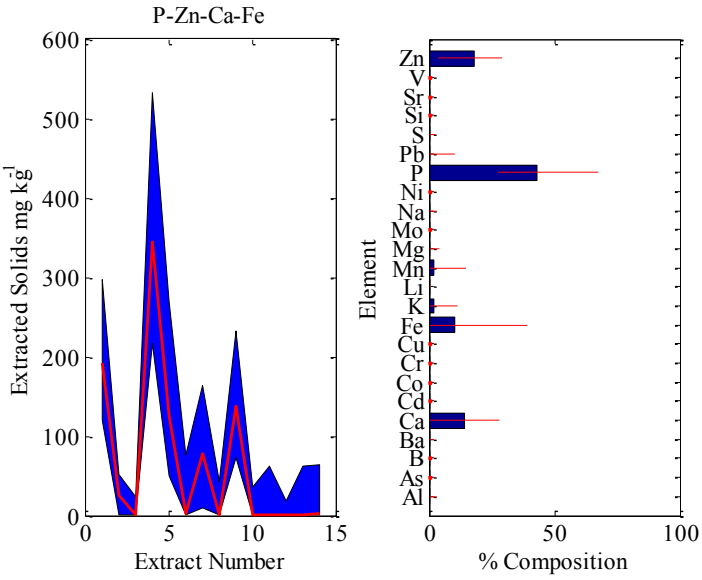
P-Zn-Ca-Fe
Extracted Solids mg kg-1
Extract Number
Element
% Composition
Zn
V
Sr
Si
S
Pb
P
Ni
Na
Mo
Mg
Mn
Li
K
Fe
Cu
Cr
Co
Cd
Ca
Ba
B
As
Al

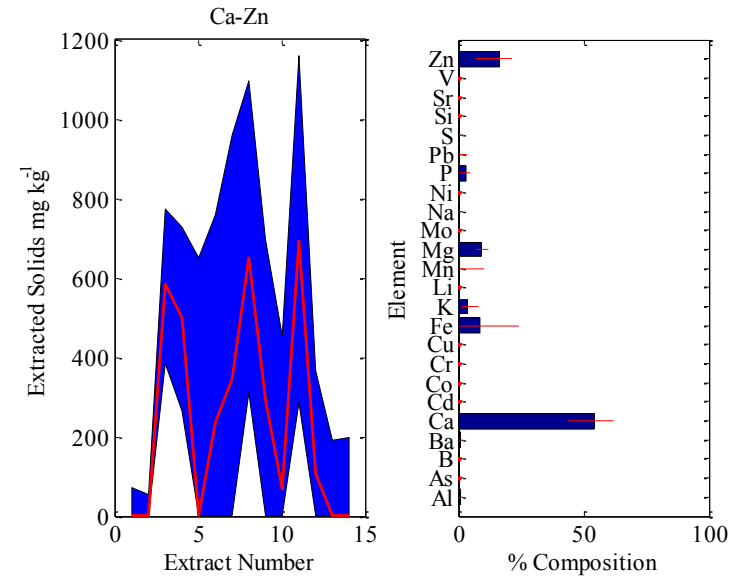
Ca-Zn
Extracted Solids mg kg-1
Extract Number
Element
% Composition
Zn
V
Sr
Si
S
Pb
P
Ni
Na
Mo
Mg
Mn
Li
K
Fe
Cu
Cr
Co
Cd
Ca
Ba
B
As
Al

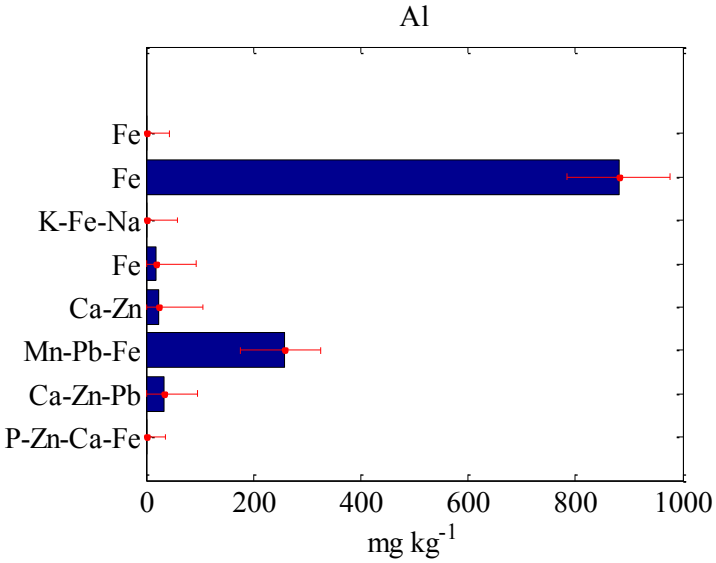
Al
Fe
Fe
K-Fe-Na
Fe
Ca-Zn
Mn-Pb-Fe
Ca-Zn-Pb
P-Zn-Ca-Fe
mg kg-1

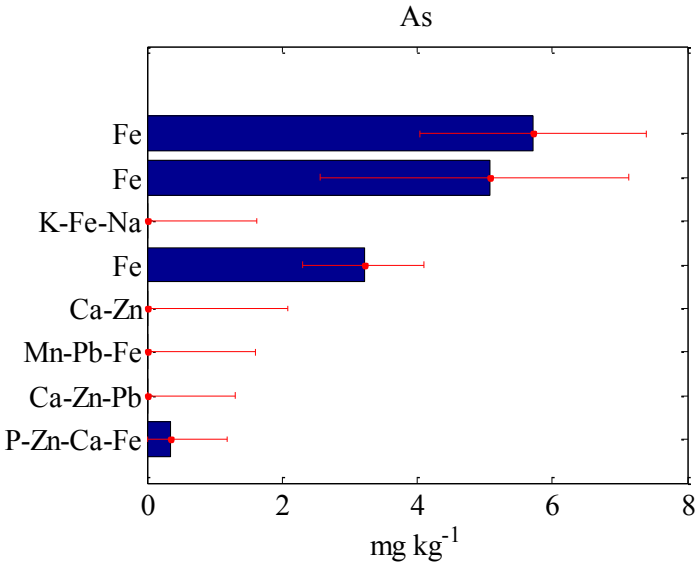
As
Fe
Fe
K-Fe-Na
Fe
Ca-Zn
Mn-Pb-Fe
Ca-Zn-Pb
P-Zn-Ca-Fe
mg kg-1

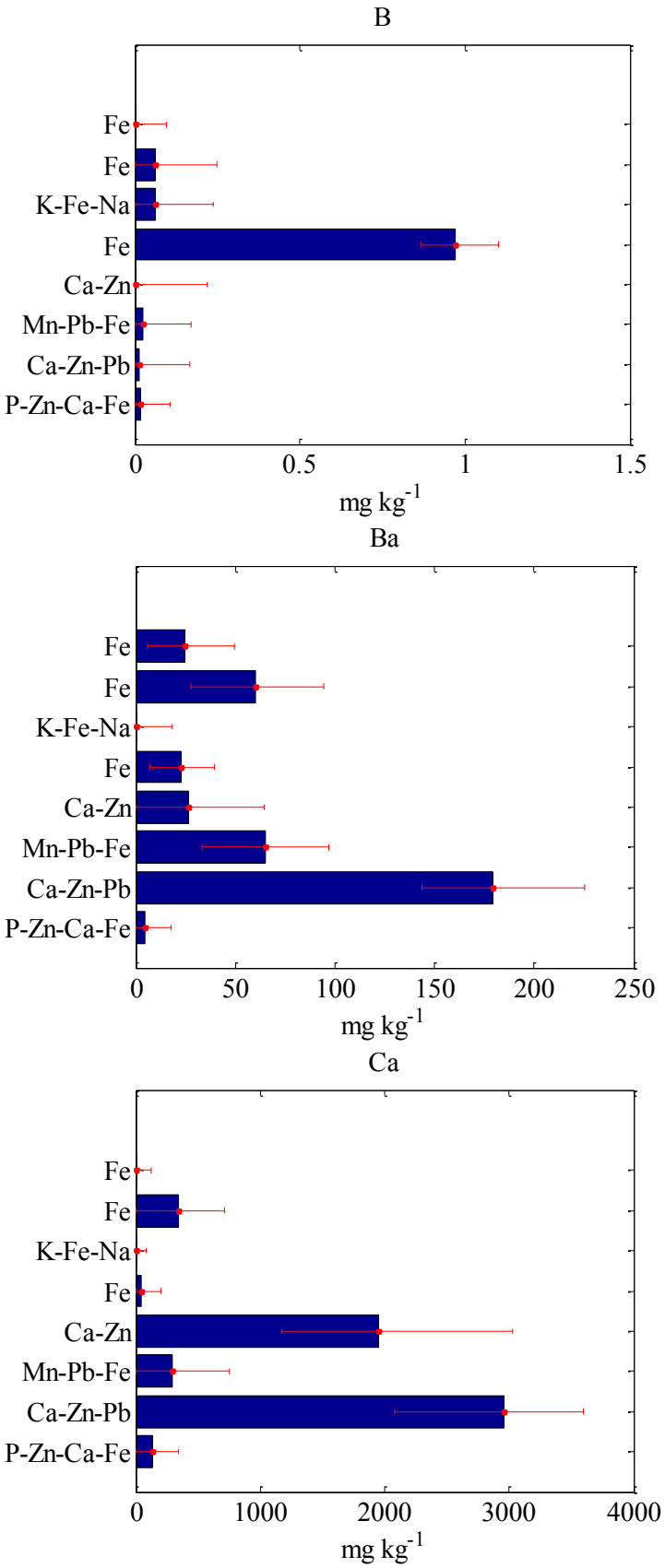
B
Fe
Fe
K-Fe-Na
Fe
Ca-Zn
Mn-Pb-Fe
Ca-Zn-Pb
P-Zn-Ca-Fe
0
0.5
1
1.5
mg kg-1
Ba
Fe
Fe
K-Fe-Na
Fe
Ca-Zn
Mn-Pb-Fe
Ca-Zn-Pb
P-Zn-Ca-Fe
0
50
100
150
200
250
mg kg-1
Ca
Fe
Fe
K-Fe-Na
Fe
Ca-Zn
Mn-Pb-Fe
Ca-Zn-Pb
P-Zn-Ca-Fe
0
1000
2000
3000
4000
mg kg-1

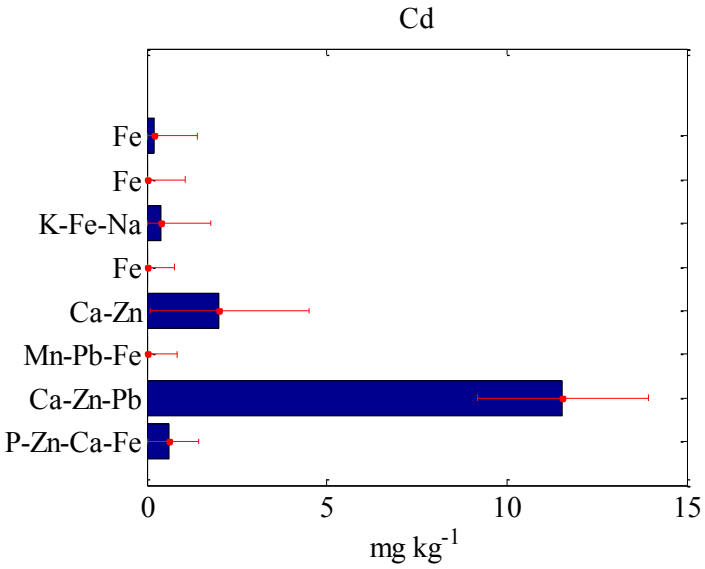
Cd
Fe
Fe
K-Fe-Na
Fe
Ca-Zn
Mn-Pb-Fe
Ca-Zn-Pb
P-Zn-Ca-Fe
0
5
10
15
mg kg-1

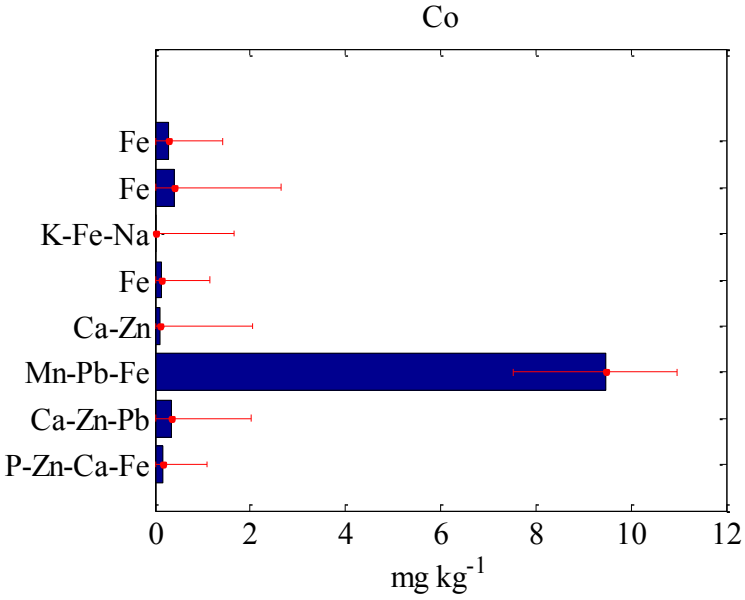
Co
Fe
Fe
K-Fe-Na
Fe
Ca-Zn
Mn-Pb-Fe
Ca-Zn-Pb
P-Zn-Ca-Fe
0
2
4
6
8
10
12
mg kg-1

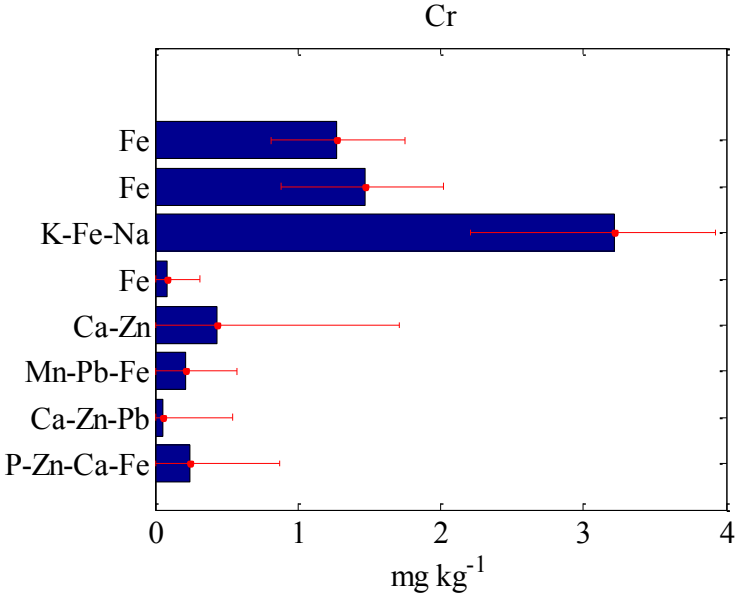
Cr
Fe
Fe
K-Fe-Na
Fe
Ca-Zn
Mn-Pb-Fe
Ca-Zn-Pb
P-Zn-Ca-Fe
0
1
2
3
4
mg kg-1

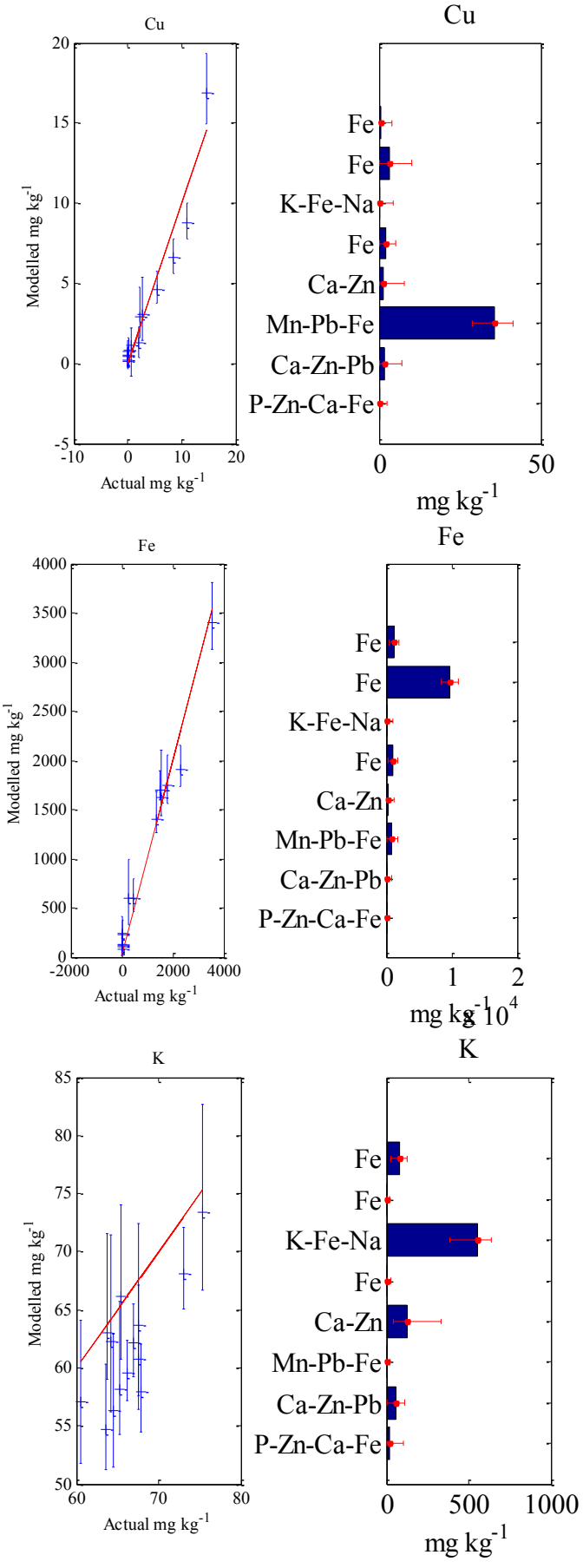
Cu
Modelled mg kg-1
Actual mg kg-1
20
15
10
5
0
-5
-10
0
10
20
Cu
Fe
Fe
K-Fe-Na
Fe
Ca-Zn
Mn-Pb-Fe
Ca-Zn-Pb
P-Zn-Ca-Fe
0
50
mg kg-1
Fe
Modelled mg kg-1
Actual mg kg-1
4000
3500
3000
2500
2000
1500
1000
500
0
-2000
0
2000
4000
Fe
Fe
Fe
K-Fe-Na
Fe
Ca-Zn
Mn-Pb-Fe
Ca-Zn-Pb
P-Zn-Ca-Fe
0
1
2
mg kg-1
x 10^4
K
Modelled mg kg-1
Actual mg kg-1
85
80
75
70
65
60
55
50
60
70
80
K
Fe
Fe
K-Fe-Na
Fe
Ca-Zn
Mn-Pb-Fe
Ca-Zn-Pb
P-Zn-Ca-Fe
0
500
1000
mg kg-1

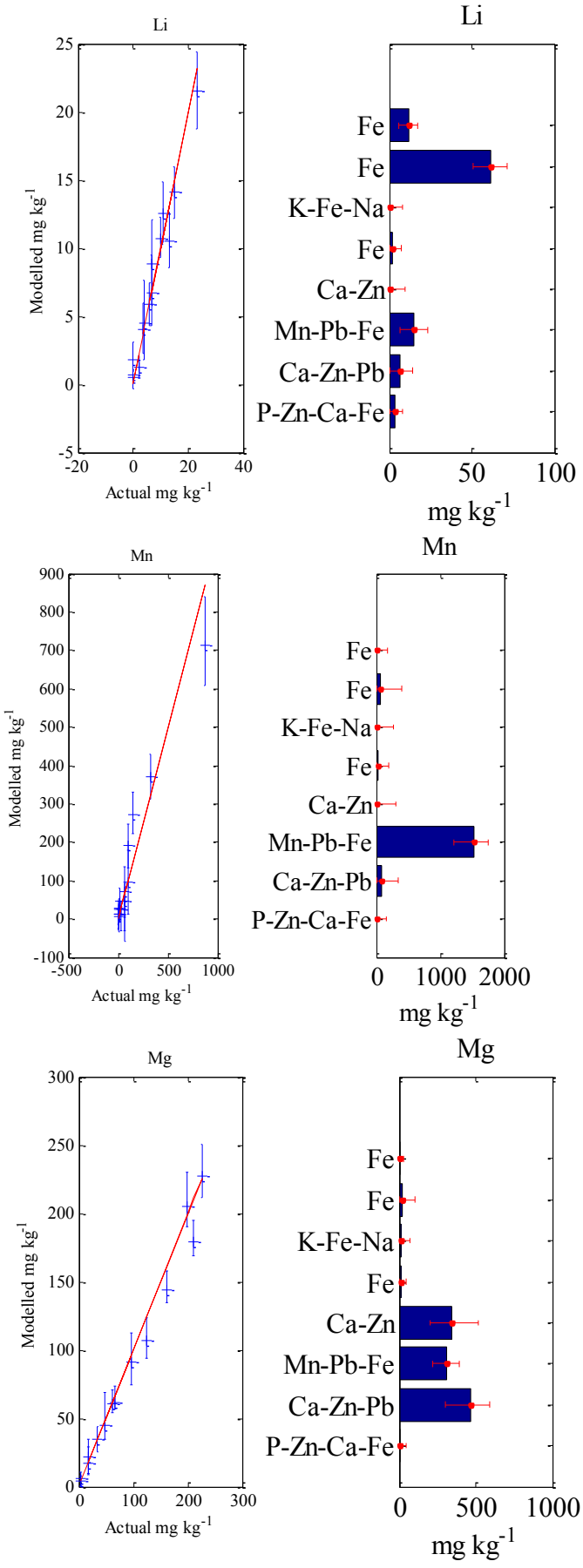
Li
Modelled mg kg-1
Actual mg kg-1
Li
Fe
Fe
K-Fe-Na
Fe
Ca-Zn
Mn-Pb-Fe
Ca-Zn-Pb
P-Zn-Ca-Fe
mg kg-1
Mn
Modelled mg kg-1
Actual mg kg-1
Mn
Fe
Fe
K-Fe-Na
Fe
Ca-Zn
Mn-Pb-Fe
Ca-Zn-Pb
P-Zn-Ca-Fe
mg kg-1
Mg
Modelled mg kg-1
Actual mg kg-1
Mg
Fe
Fe
K-Fe-Na
Fe
Ca-Zn
Mn-Pb-Fe
Ca-Zn-Pb
P-Zn-Ca-Fe
mg kg-1

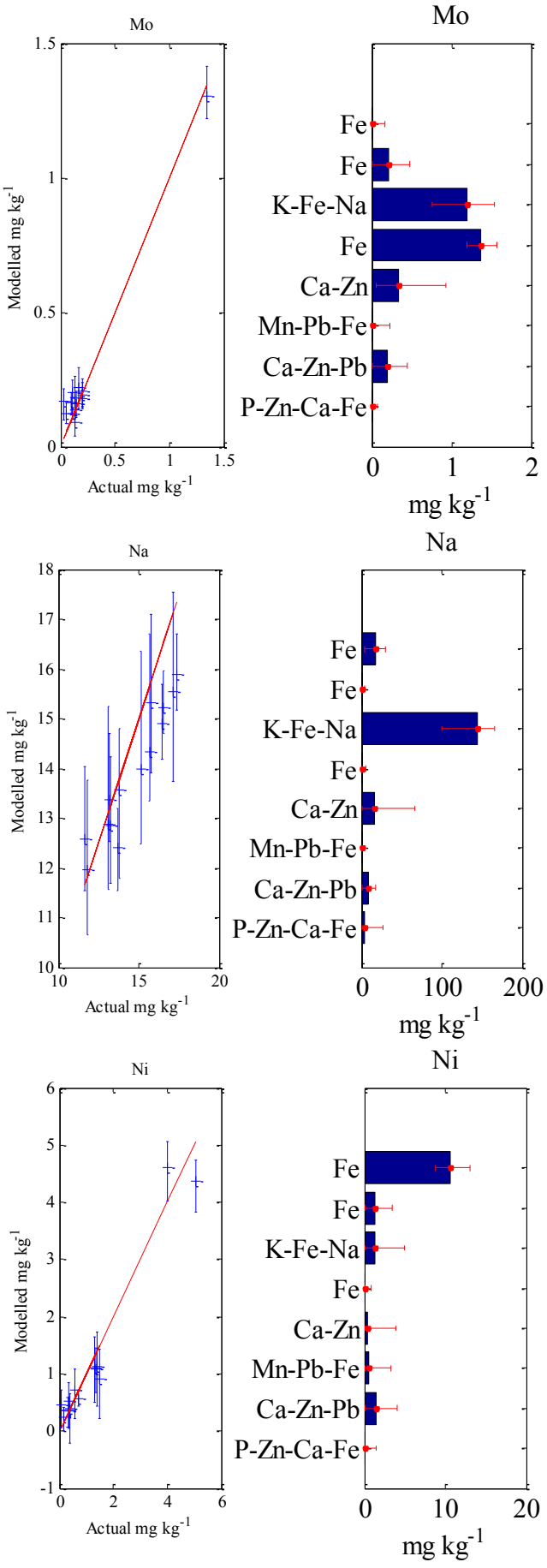
Mo
Modelled mg kg-1
Actual mg kg-1
Mo
Fe
Fe
K-Fe-Na
Fe
Ca-Zn
Mn-Pb-Fe
Ca-Zn-Pb
P-Zn-Ca-Fe
mg kg-1
Na
Modelled mg kg-1
Actual mg kg-1
Na
Fe
Fe
K-Fe-Na
Fe
Ca-Zn
Mn-Pb-Fe
Ca-Zn-Pb
P-Zn-Ca-Fe
mg kg-1
Ni
Modelled mg kg-1
Actual mg kg-1
Ni
Fe
Fe
K-Fe-Na
Fe
Ca-Zn
Mn-Pb-Fe
Ca-Zn-Pb
P-Zn-Ca-Fe
mg kg-1

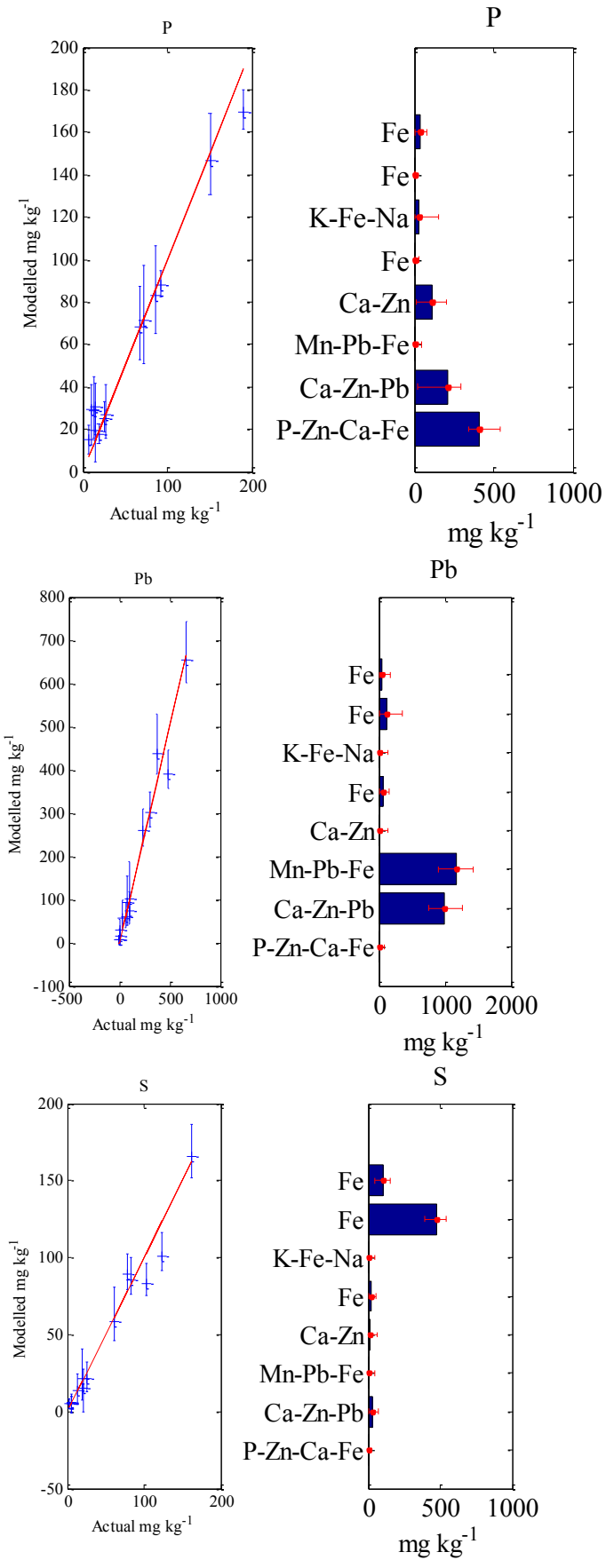
P
Modelled mg kg-1
Actual mg kg-1
0
20
40
60
80
100
120
140
160
180
200
0
100
200
P
Fe
Fe
K-Fe-Na
Fe
Ca-Zn
Mn-Pb-Fe
Ca-Zn-Pb
P-Zn-Ca-Fe
0
500
1000
mg kg-1
Pb
Modelled mg kg-1
Actual mg kg-1
-100
0
100
200
300
400
500
600
700
800
-500
0
500
1000
Pb
Fe
Fe
K-Fe-Na
Fe
Ca-Zn
Mn-Pb-Fe
Ca-Zn-Pb
P-Zn-Ca-Fe
0
1000
2000
mg kg-1
S
Modelled mg kg-1
Actual mg kg-1
-50
0
50
100
150
200
0
100
200
S
Fe
Fe
K-Fe-Na
Fe
Ca-Zn
Mn-Pb-Fe
Ca-Zn-Pb
P-Zn-Ca-Fe
0
500
1000
mg kg-1

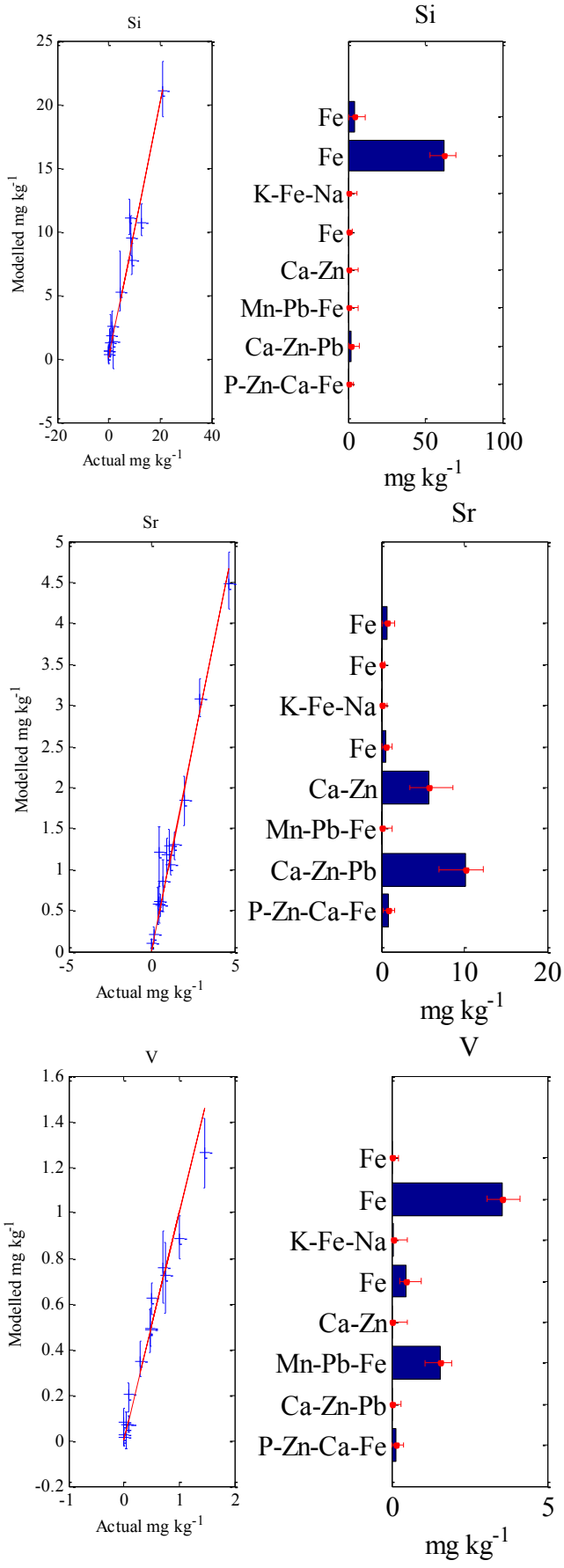
Si
Modelled mg kg-1
Actual mg kg-1
Si
Fe
Fe
K-Fe-Na
Fe
Ca-Zn
Mn-Pb-Fe
Ca-Zn-Pb
P-Zn-Ca-Fe
mg kg-1
Sr
Modelled mg kg-1
Actual mg kg-1
Sr
Fe
Fe
K-Fe-Na
Fe
Ca-Zn
Mn-Pb-Fe
Ca-Zn-Pb
P-Zn-Ca-Fe
mg kg-1
V
Modelled mg kg-1
Actual mg kg-1
V
Fe
Fe
K-Fe-Na
Fe
Ca-Zn
Mn-Pb-Fe
Ca-Zn-Pb
P-Zn-Ca-Fe
mg kg-1

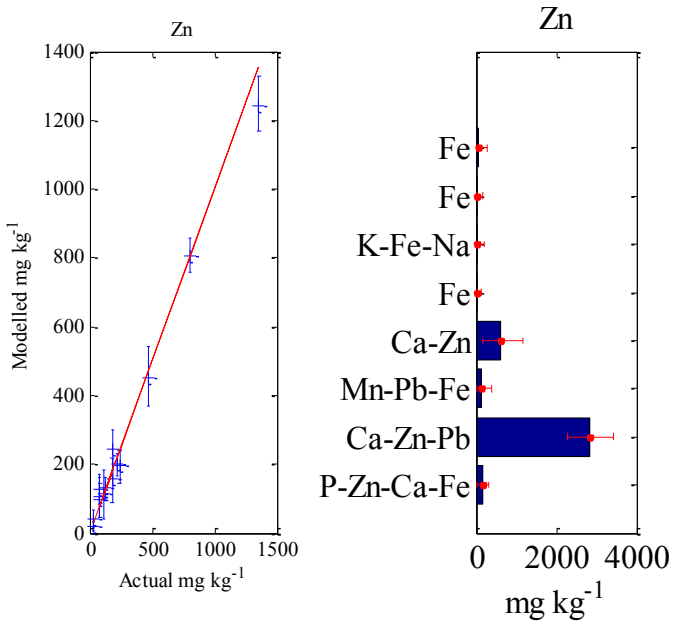
Zn
Modelled mg kg-1
Actual mg kg-1
0
200
400
600
800
1000
1200
1400
0
500
1000
1500
Zn
Fe
Fe
K-Fe-Na
Fe
Ca-Zn
Mn-Pb-Fe
Ca-Zn-Pb
P-Zn-Ca-Fe
0
2000
4000
mg kg-1

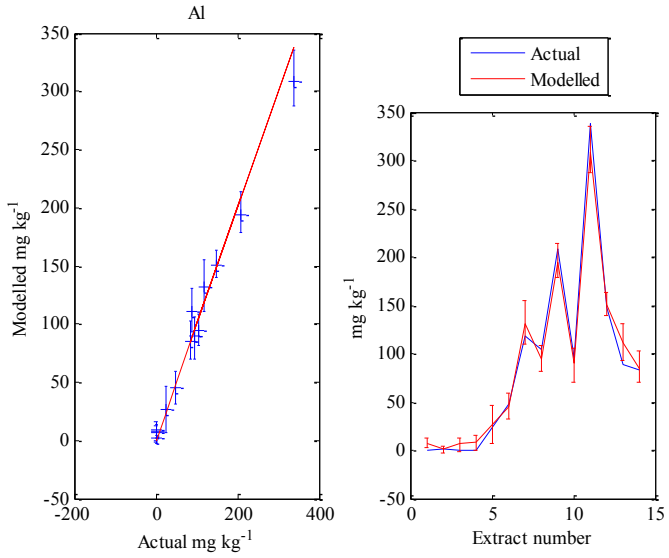
Al
Modelled mg kg-1
Actual mg kg-1
-50
0
50
100
150
200
250
300
350
-200
0
200
400
Actual
Modelled
mg kg-1
Extract number
-50
0
50
100
150
200
250
300
350
0
5
10
15

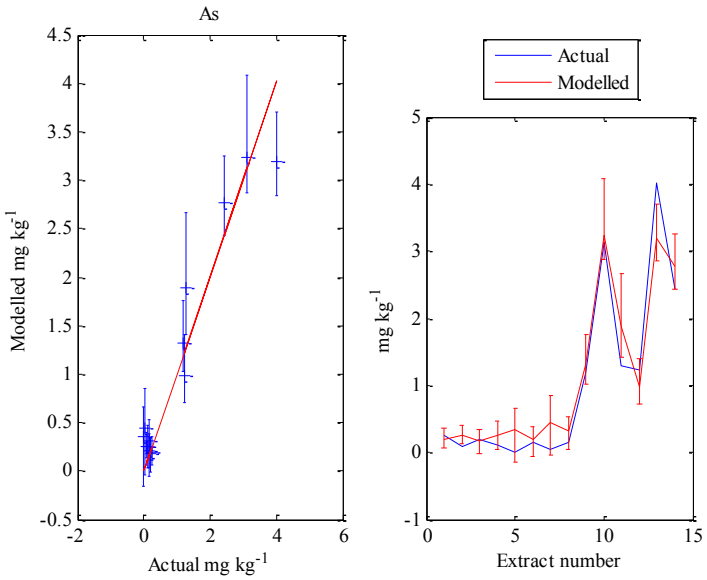
As
Modelled mg kg-1
Actual mg kg-1
-0.5
0
0.5
1
1.5
2
2.5
3
3.5
4
4.5
-2
0
2
4
6
Actual
Modelled
mg kg-1
Extract number
-1
0
1
2
3
4
5
0
5
10
15

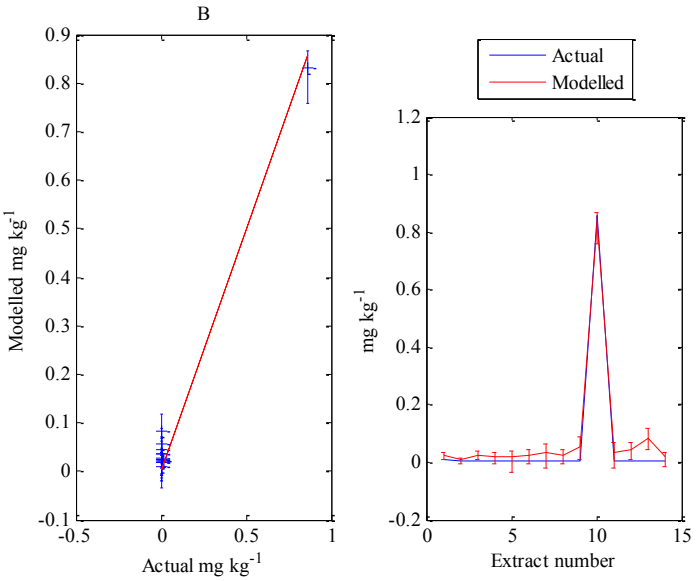
B
Modelled mg kg-1
Actual mg kg-1
Actual
Modelled
mg kg-1
Extract number

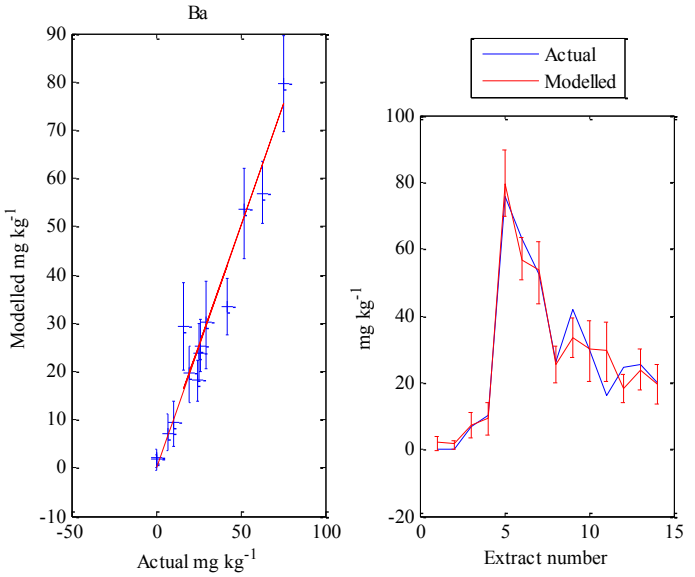
Ba
Modelled mg kg-1
Actual mg kg-1
Actual
Modelled
mg kg-1
Extract number

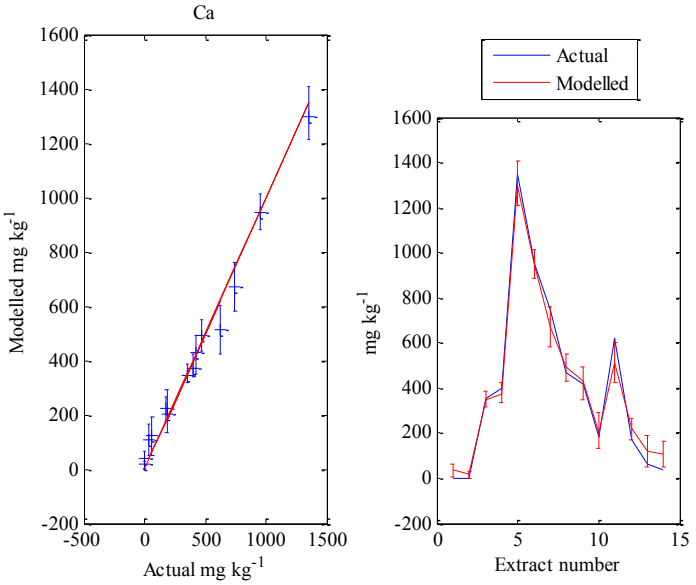
Ca
Modelled mg kg-1
Actual mg kg-1
Actual
Modelled
mg kg-1
Extract number

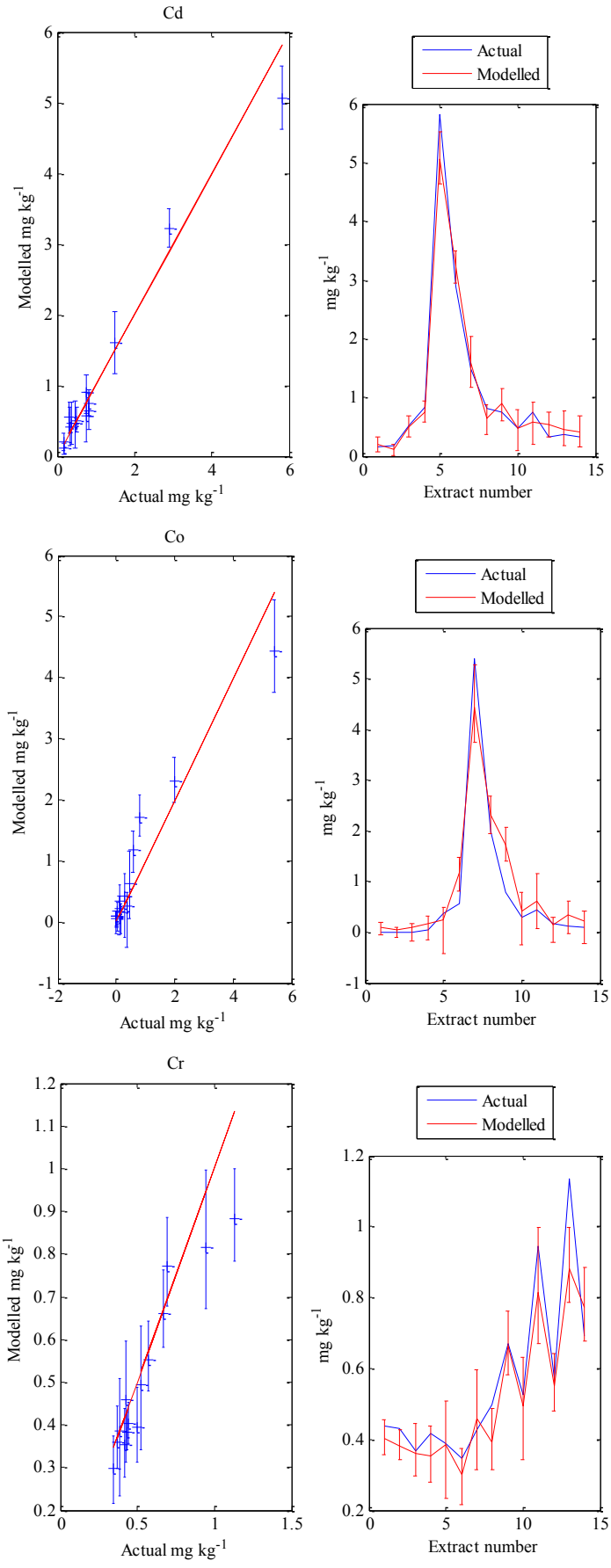
Cd
Modelled mg kg-1
Actual mg kg-1
Actual
Modelled
mg kg-1
Extract number
Co
Modelled mg kg-1
Actual mg kg-1
Actual
Modelled
mg kg-1
Extract number
Cr
Modelled mg kg-1
Actual mg kg-1
Actual
Modelled
mg kg-1
Extract number

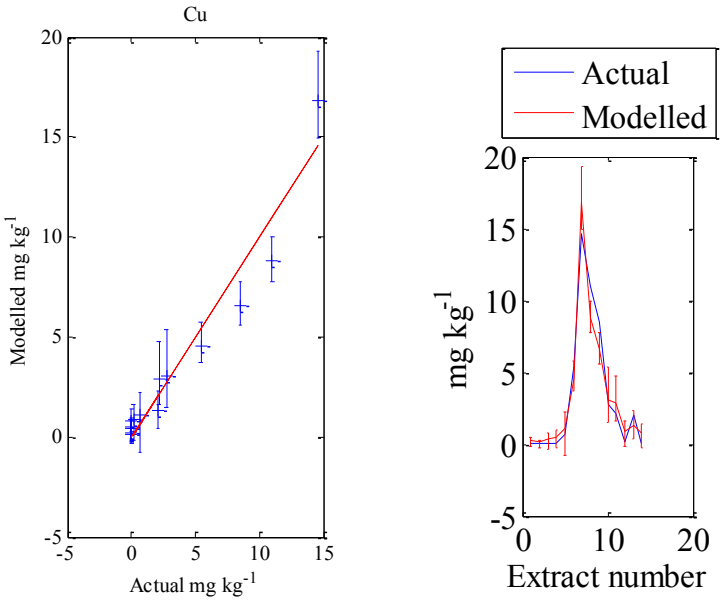
Cu
Modelled mg kg-1
Actual mg kg-1
Actual
Modelled
mg kg-1
Extract number

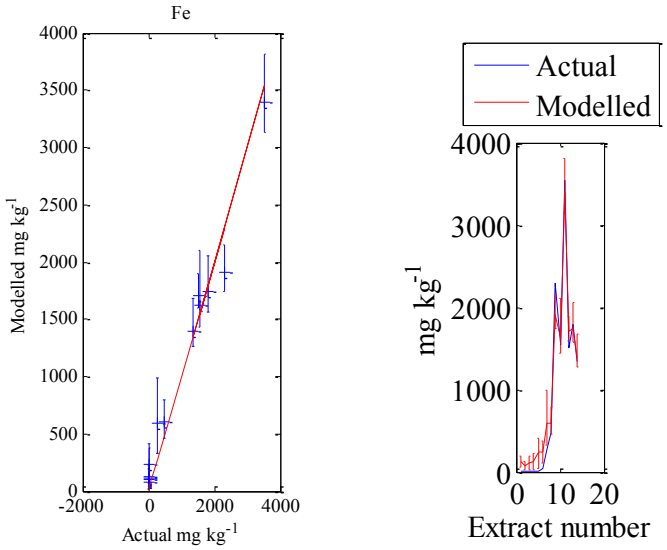
Fe
Modelled mg kg-1
Actual mg kg-1
Actual
Modelled
mg kg-1
Extract number

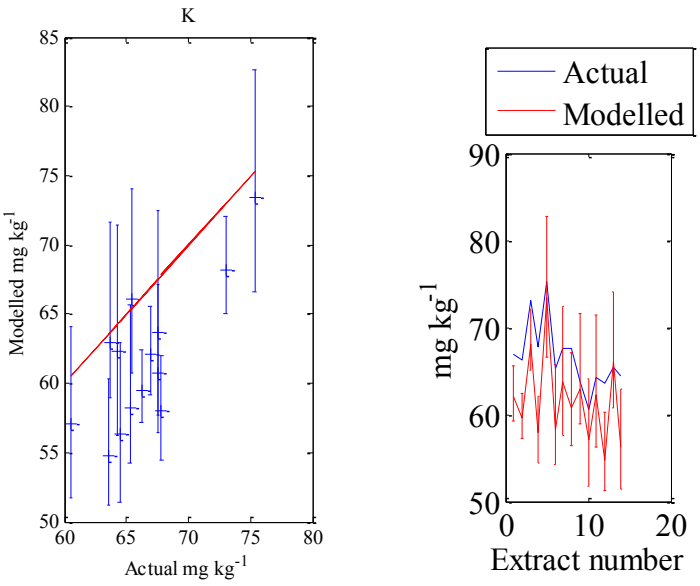
K
Modelled mg kg-1
Actual mg kg-1
Actual
Modelled
mg kg-1
Extract number

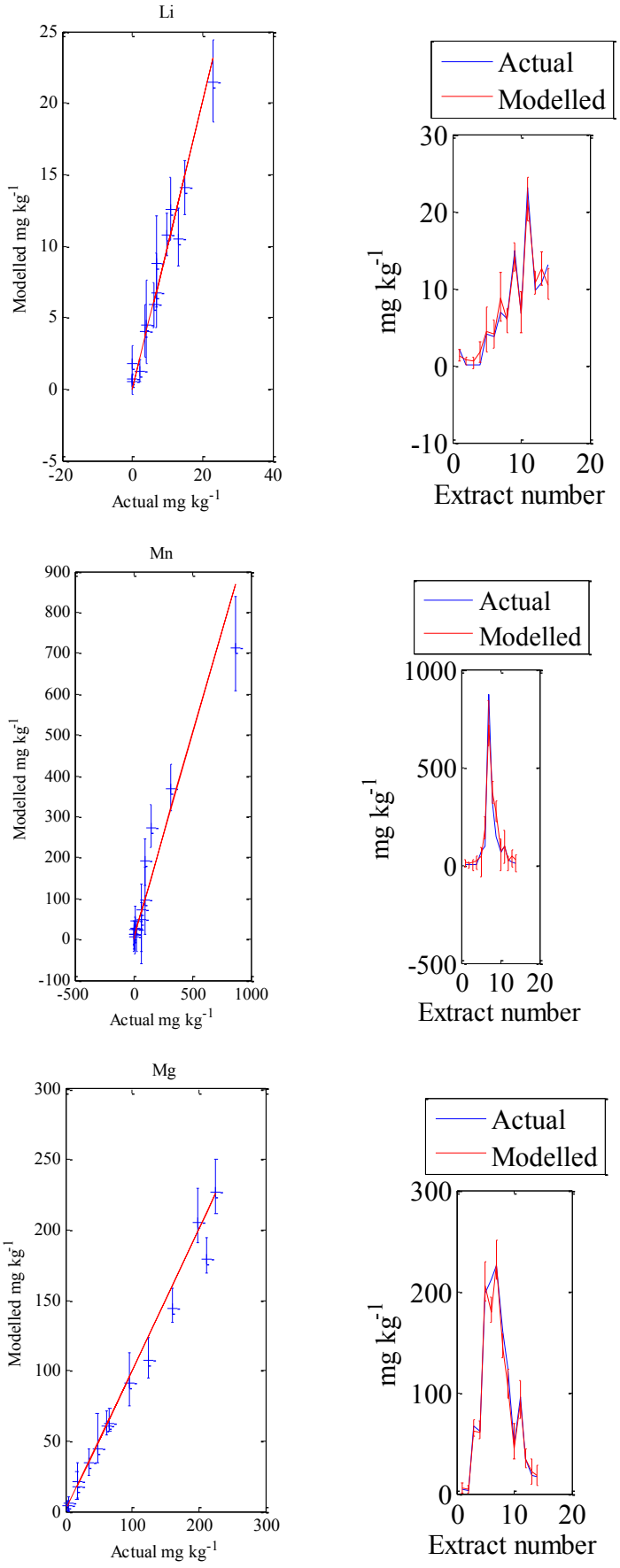
Li
Modelled mg kg-1
Actual mg kg-1
Actual
Modelled
mg kg-1
Extract number
Mn
Modelled mg kg-1
Actual mg kg-1
Actual
Modelled
mg kg-1
Extract number
Mg
Modelled mg kg-1
Actual mg kg-1
Actual
Modelled
mg kg-1
Extract number

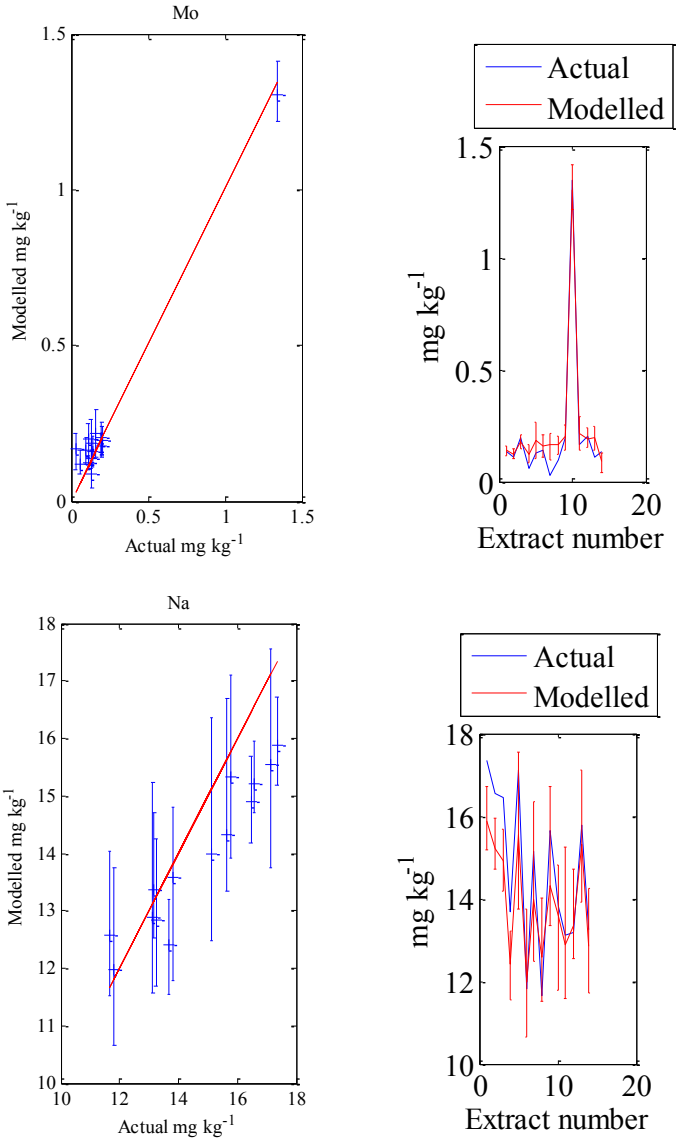
Mo
Modelled mg kg-1
Actual mg kg-1
Actual
Modelled
mg kg-1
Extract number
Na
Modelled mg kg-1
Actual mg kg-1
Actual
Modelled
mg kg-1
Extract number
Ni
Modelled mg kg-1
Actual mg kg-1
Actual
Modelled
mg kg-1
Extract number

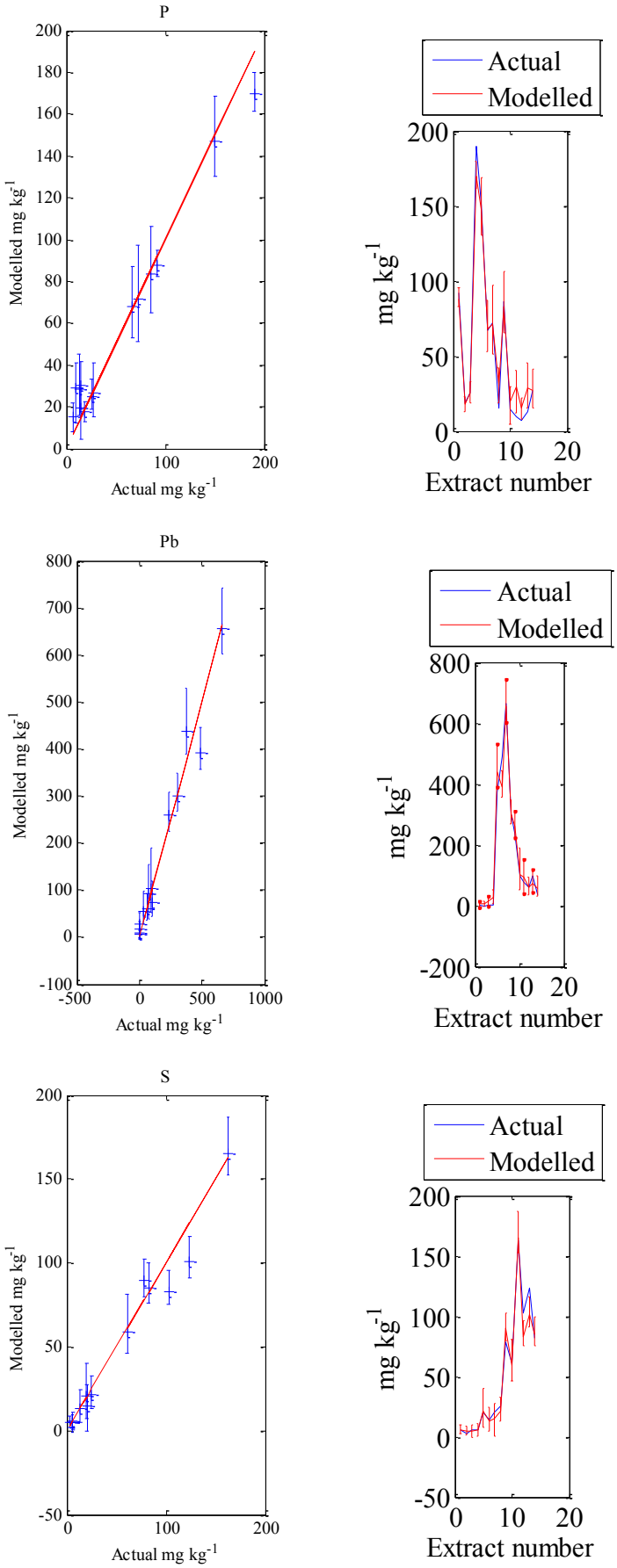
P
Modelled mg kg-1
Actual mg kg-1
Actual
Modelled
mg kg-1
Extract number
Pb
Modelled mg kg-1
Actual mg kg-1
Actual
Modelled
mg kg-1
Extract number
S
Modelled mg kg-1
Actual mg kg-1
Actual
Modelled
mg kg-1
Extract number

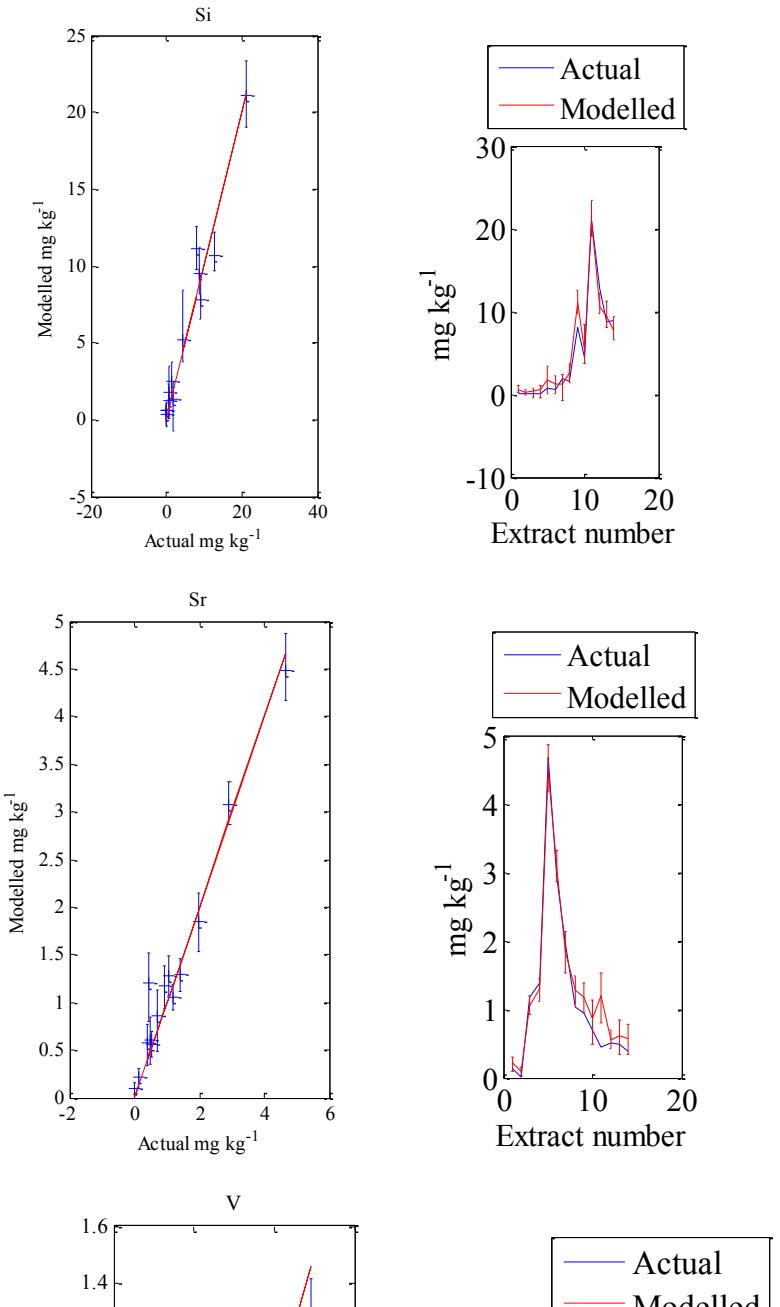
Si
Modelled mg kg-1
Actual mg kg-1
Actual
Modelled
mg kg-1
Extract number
Sr
Modelled mg kg-1
Actual mg kg-1
Actual
Modelled
mg kg-1
Extract number
V
Modelled mg kg-1
Actual mg kg-1
Actual
Modelled
mg kg-1
Extract number

Soil 7

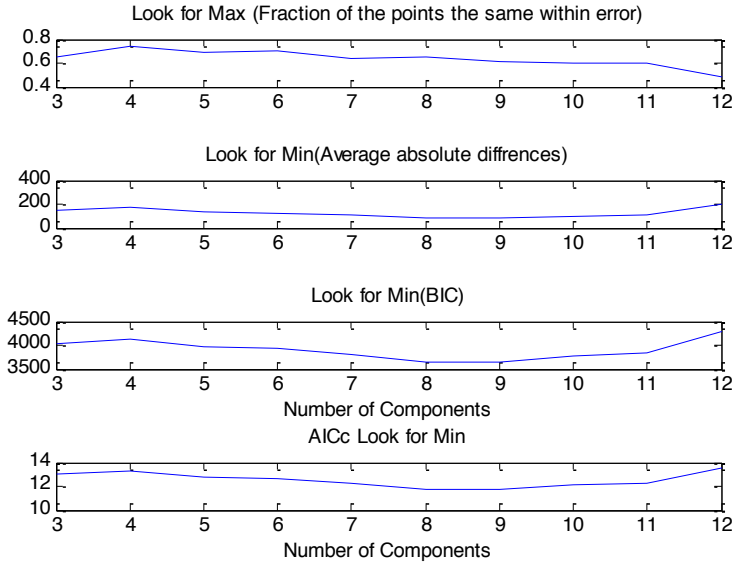
Look for Max (Fraction of the points the same within error)
0.8
0.6
0.4
3 4 5 6 7 8 9 10 11 12
Look for Min(Average absolute diffrences)
400
200
0
3 4 5 6 7 8 9 10 11 12
Look for Min(BIC)
4500
4000
3500
3 4 5 6 7 8 9 10 11 12
Number of Components
AICc Look for Min
14
12
10
3 4 5 6 7 8 9 10 11 12
Number of Components

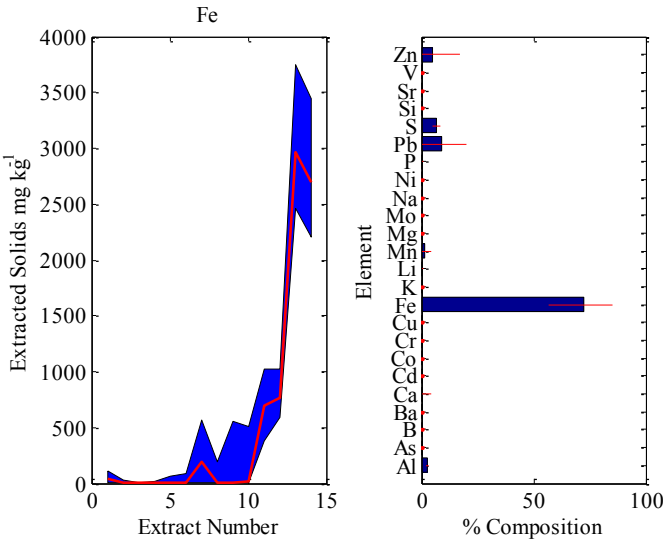
Fe
Extracted Solids mg kg-1
4000
3500
3000
2500
2000
1500
1000
500
0
0 5 10 15
Extract Number
Element
Zn
V
Sr
Si
S
Pb
P
Ni
Na
Mo
Mg
Mn
Li
K
Fe
Cu
Cr
Co
Cd
Ca
Ba
B
As
Al
0 50 100
% Composition

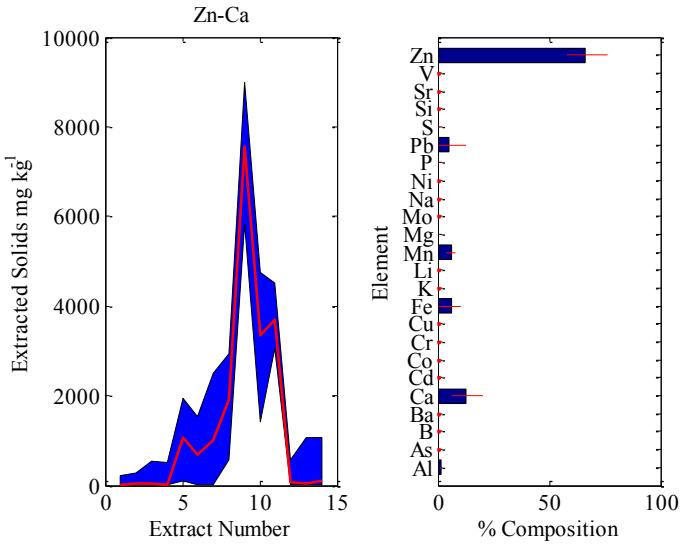
Zn-Ca
Extracted Solids mg kg-1
Extract Number
Element
% Composition
Zn
V
Sr
Si
S
Pb
P
Ni
Na
Mo
Mg
Mn
Li
K
Fe
Cu
Cr
Co
Cd
Ca
Ba
B
As
Al

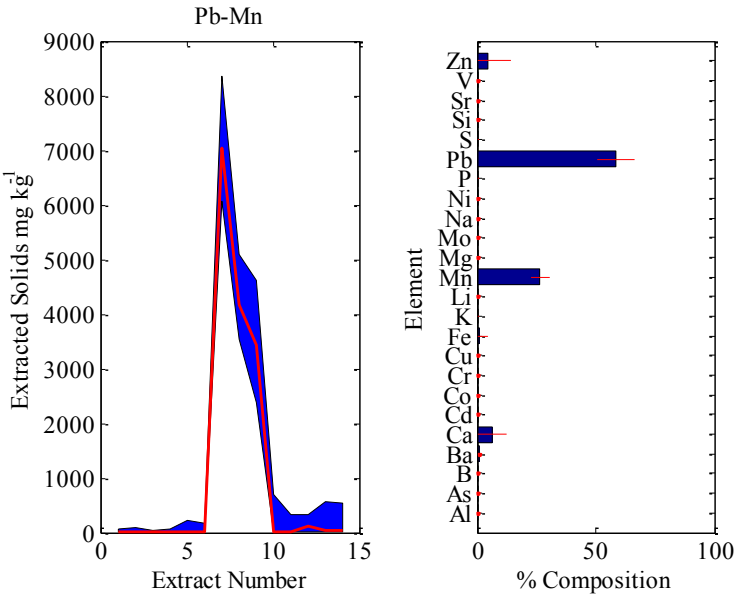
Pb-Mn
Extracted Solids mg kg-1
Extract Number
Element
% Composition
Zn
V
Sr
Si
S
Pb
P
Ni
Na
Mo
Mg
Mn
Li
K
Fe
Cu
Cr
Co
Cd
Ca
Ba
B
As
Al

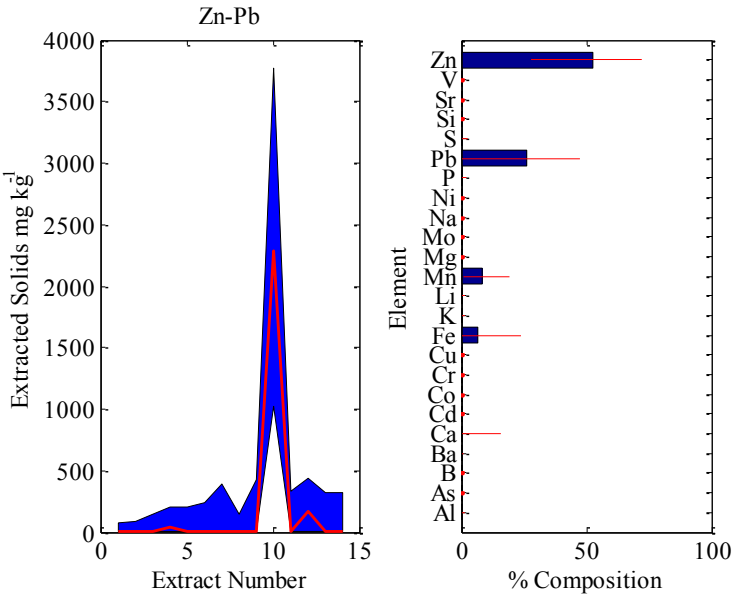
Zn-Pb
Extracted Solids mg kg-1
Extract Number
Element
% Composition
Zn
V
Sr
Si
S
Pb
P
Ni
Na
Mo
Mg
Mn
Li
K
Fe
Cu
Cr
Co
Cd
Ca
Ba
B
As
Al

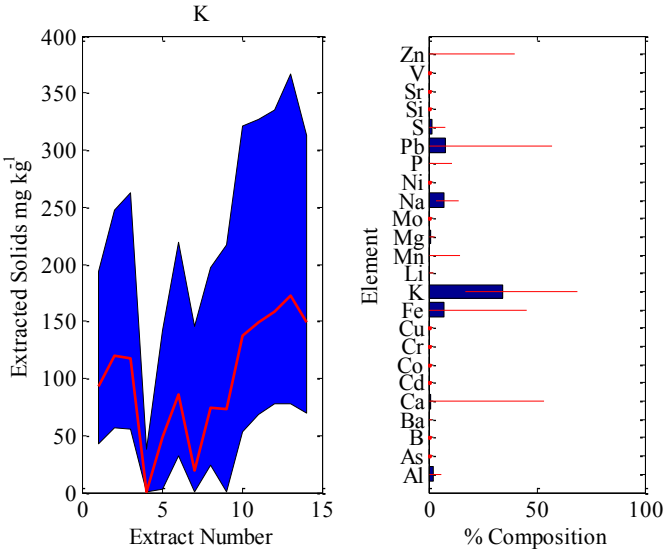
K
Extracted Solids mg kg-1
Extract Number
Element
% Composition
Zn
V
Sr
Si
S
Pb
P
Ni
Na
Mo
Mg
Mn
Li
K
Fe
Cu
Cr
Co
Cd
Ca
Ba
B
As
Al

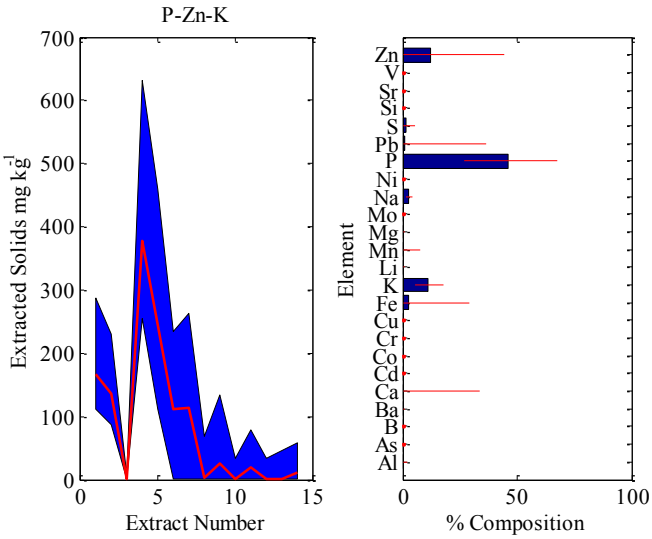
P-Zn-K
Extracted Solids mg kg-1
Extract Number
Element
% Composition
Zn
V
Sr
Si
S
Pb
P
Ni
Na
Mo
Mg
Mn
Li
K
Fe
Cu
Cr
Co
Cd
Ca
Ba
B
As
Al

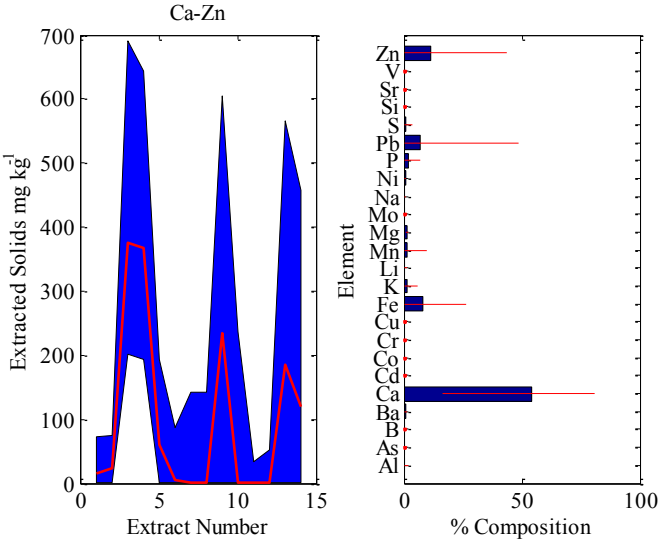
Ca-Zn
Extracted Solids mg kg-1
Extract Number
Element
% Composition
Zn
V
Sr
Si
S
Pb
P
Ni
Na
Mo
Mg
Mn
Li
K
Fe
Cu
Cr
Co
Cd
Ca
Ba
B
As
Al

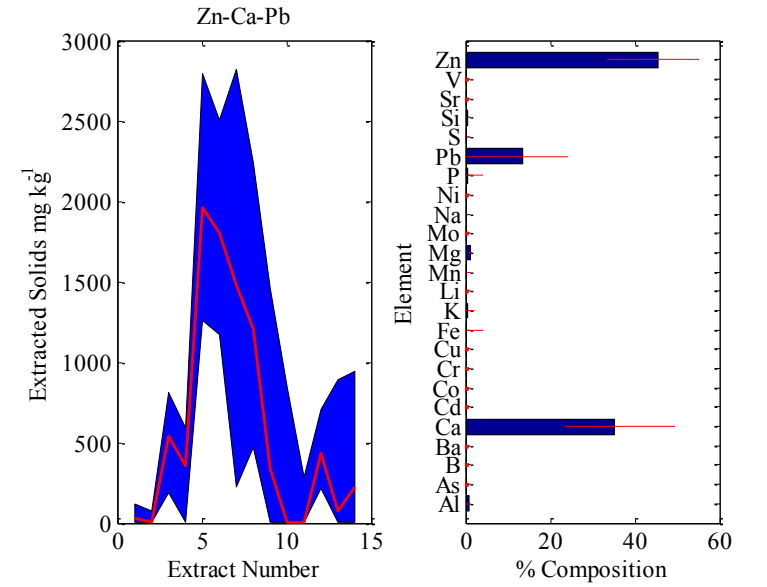
Zn-Ca-Pb
Extracted Solids mg kg-1
Extract Number
Element
% Composition
Zn
V
Sr
Si
S
Pb
P
Ni
Na
Mo
Mg
Mn
Li
K
Fe
Cu
Cr
Co
Cd
Ca
Ba
B
As
Al

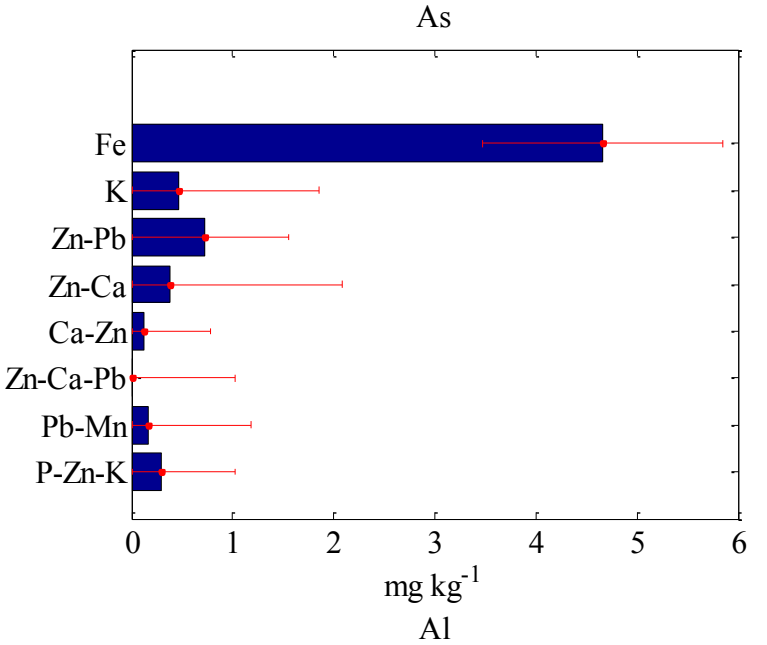
As
Fe
K
Zn-Pb
Zn-Ca
Ca-Zn
Zn-Ca-Pb
Pb-Mn
P-Zn-K
mg kg-1

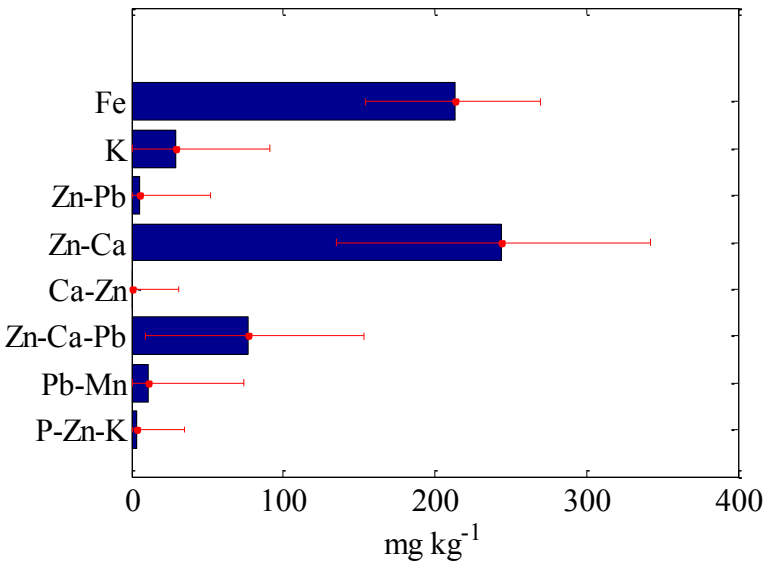
Al
Fe
K
Zn-Pb
Zn-Ca
Ca-Zn
Zn-Ca-Pb
Pb-Mn
P-Zn-K
mg kg-1

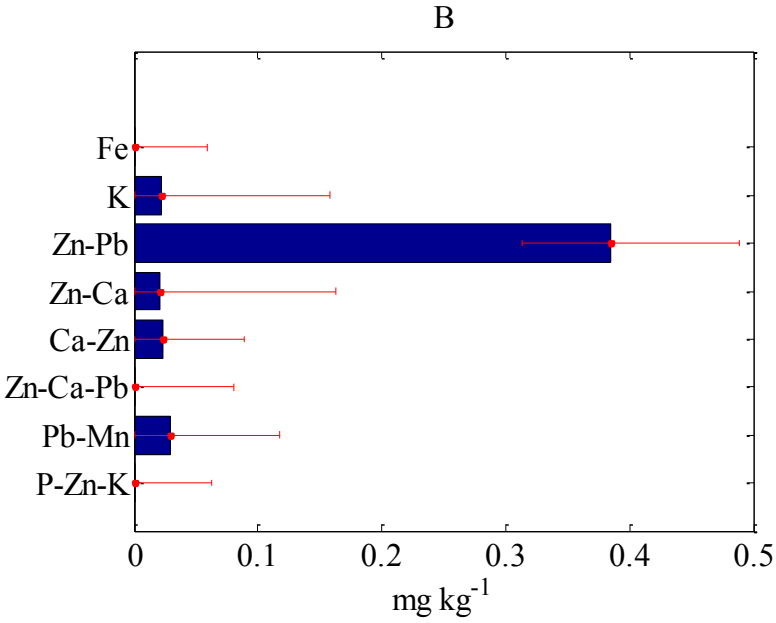
B
Fe
K
Zn-Pb
Zn-Ca
Ca-Zn
Zn-Ca-Pb
Pb-Mn
P-Zn-K
0
0.1
0.2
0.3
0.4
0.5
mg kg-1

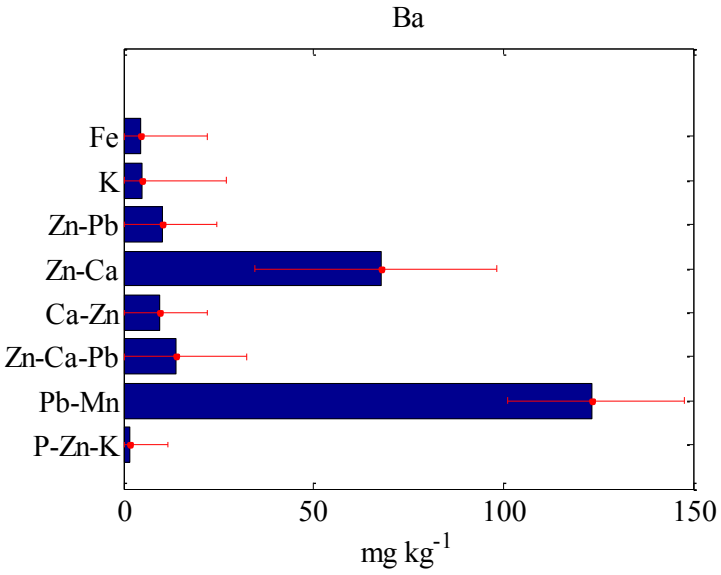
Ba
Fe
K
Zn-Pb
Zn-Ca
Ca-Zn
Zn-Ca-Pb
Pb-Mn
P-Zn-K
0
50
100
150
mg kg-1

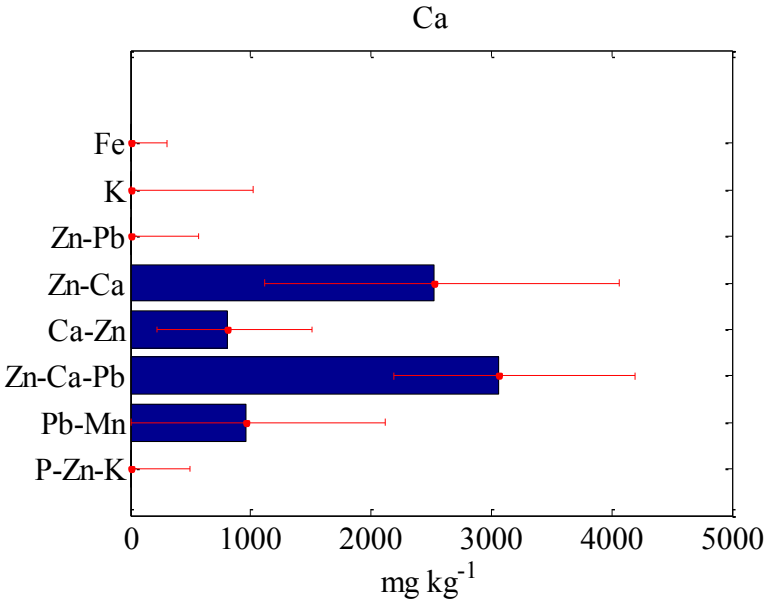
Ca
Fe
K
Zn-Pb
Zn-Ca
Ca-Zn
Zn-Ca-Pb
Pb-Mn
P-Zn-K
0
1000
2000
3000
4000
5000
mg kg-1

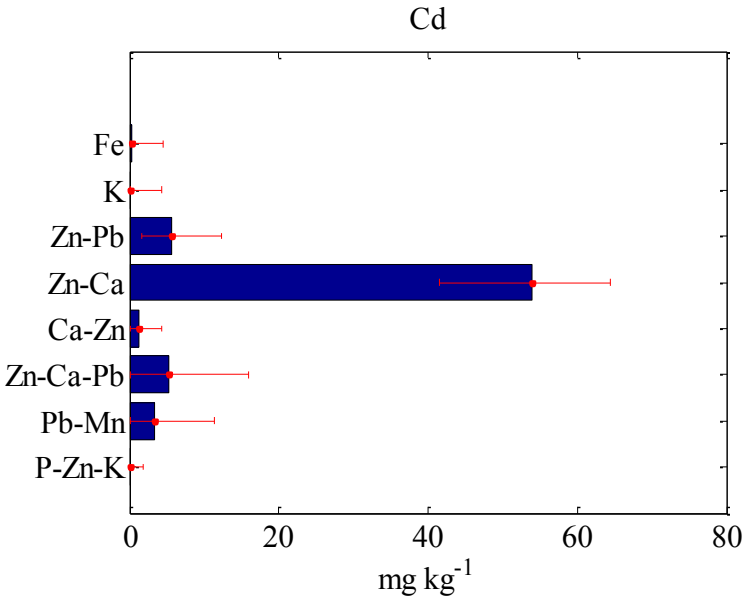
Cd
Fe
K
Zn-Pb
Zn-Ca
Ca-Zn
Zn-Ca-Pb
Pb-Mn
P-Zn-K
0
20
40
60
80
mg kg-1

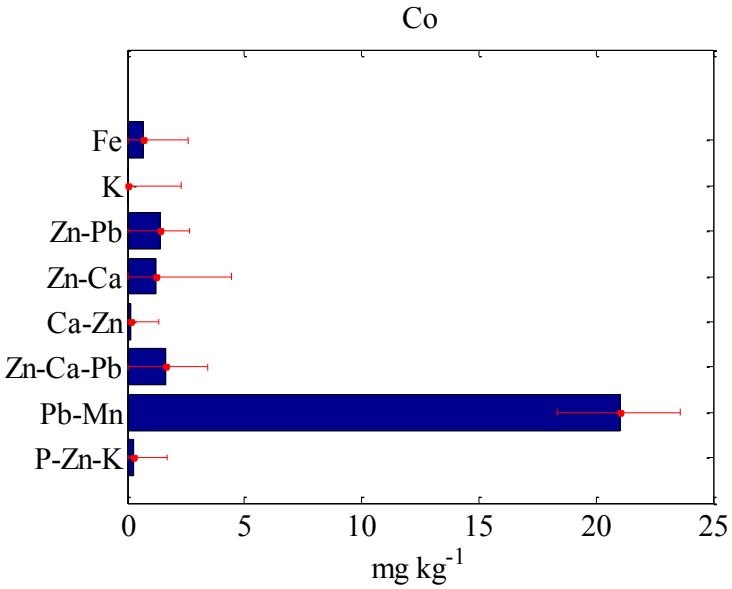
Co
Fe
K
Zn-Pb
Zn-Ca
Ca-Zn
Zn-Ca-Pb
Pb-Mn
P-Zn-K
0
5
10
15
20
25
mg kg-1

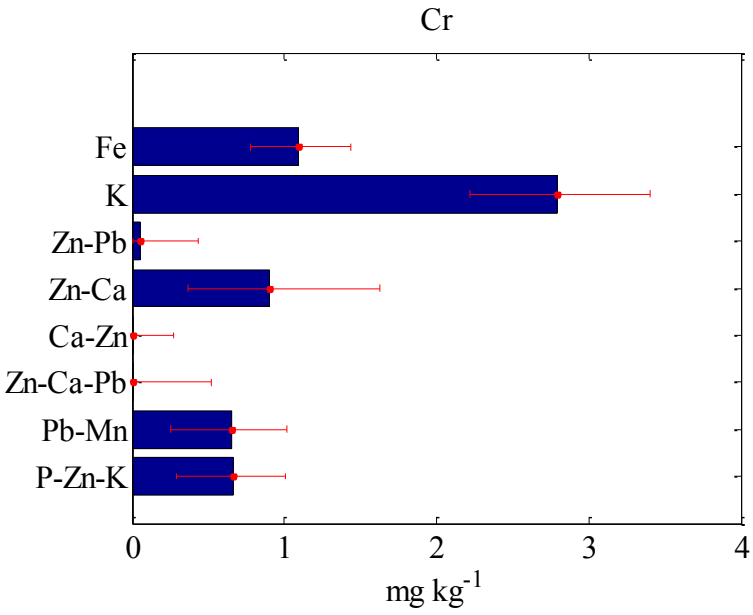
Cr
Fe
K
Zn-Pb
Zn-Ca
Ca-Zn
Zn-Ca-Pb
Pb-Mn
P-Zn-K
0
1
2
3
4
mg kg-1

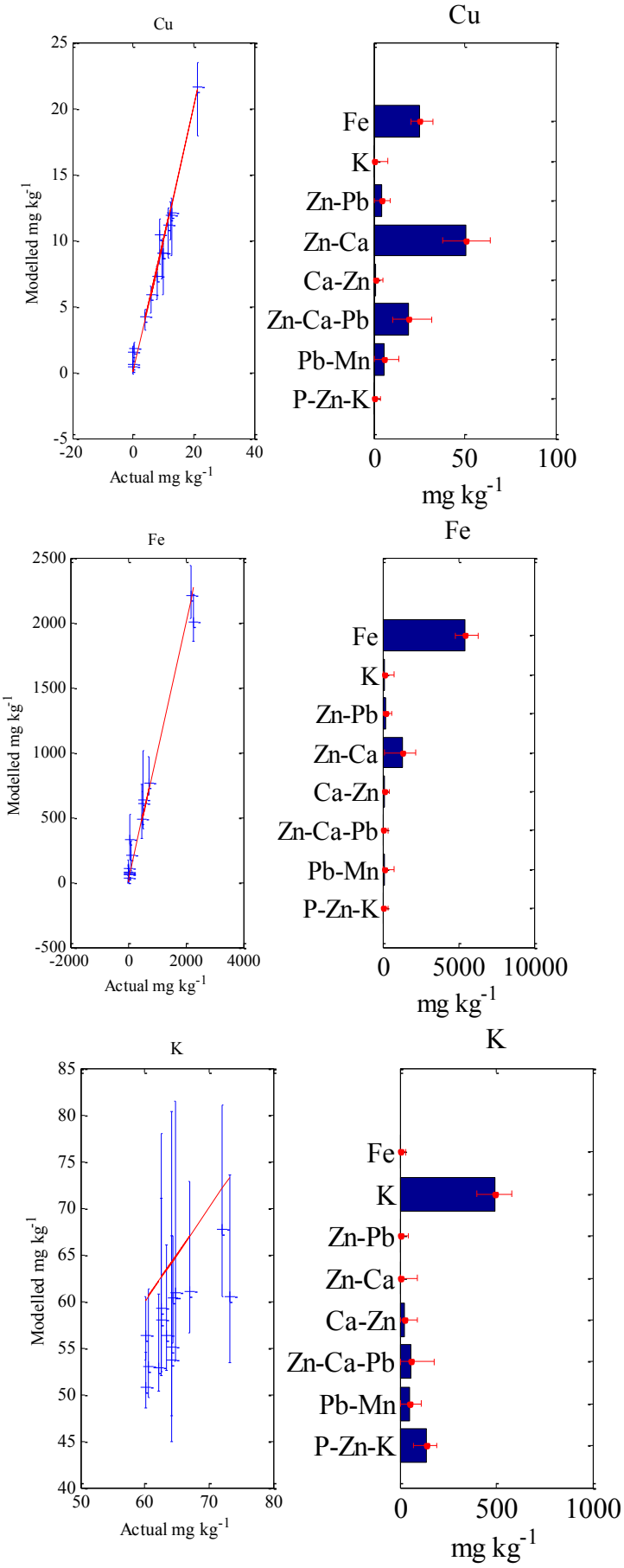
Cu
Modelled mg kg-1
Actual mg kg-1
Cu
Fe
K
Zn-Pb
Zn-Ca
Ca-Zn
Zn-Ca-Pb
Pb-Mn
P-Zn-K
mg kg-1
Fe
Modelled mg kg-1
Actual mg kg-1
Fe
mg kg-1
K
Modelled mg kg-1
Actual mg kg-1
K
mg kg-1

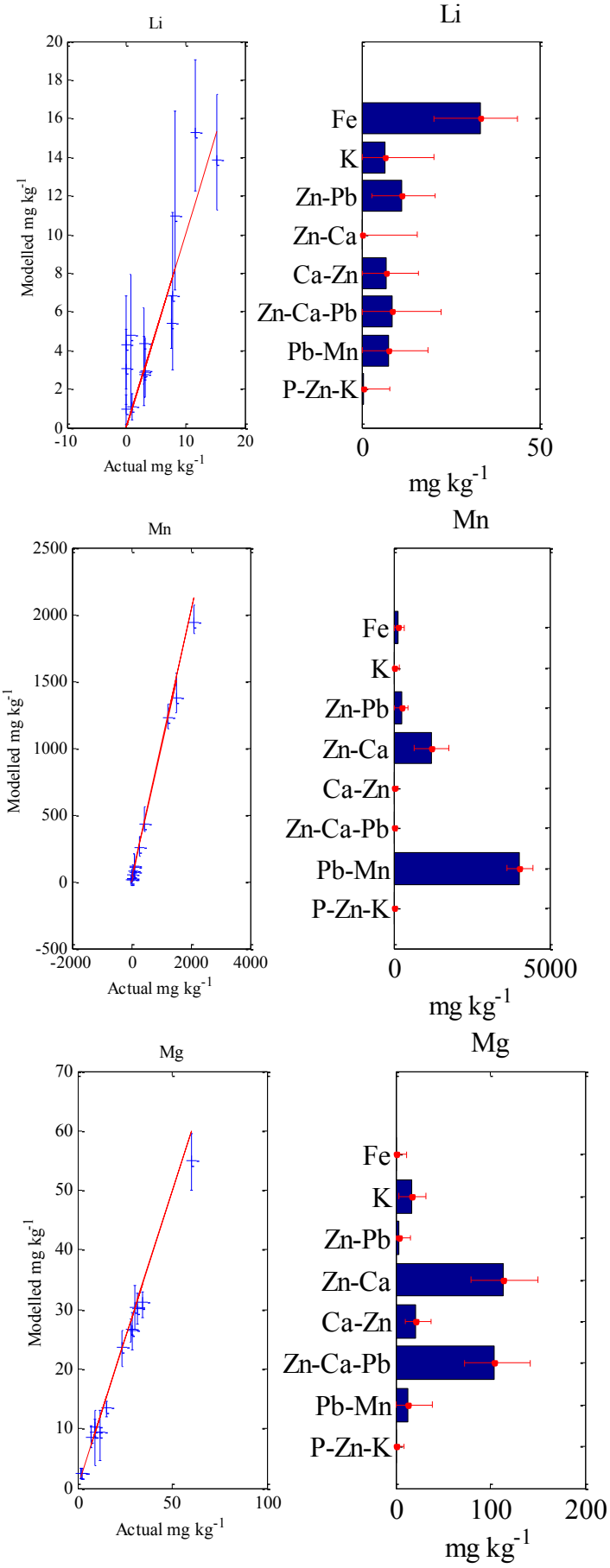
Li
Modelled mg kg-1
Actual mg kg-1
Li
Fe
K
Zn-Pb
Zn-Ca
Ca-Zn
Zn-Ca-Pb
Pb-Mn
P-Zn-K
mg kg-1
Mn
Modelled mg kg-1
Actual mg kg-1
Mn
Fe
K
Zn-Pb
Zn-Ca
Ca-Zn
Zn-Ca-Pb
Pb-Mn
P-Zn-K
mg kg-1
Mg
Modelled mg kg-1
Actual mg kg-1
Mg
Fe
K
Zn-Pb
Zn-Ca
Ca-Zn
Zn-Ca-Pb
Pb-Mn
P-Zn-K
mg kg-1

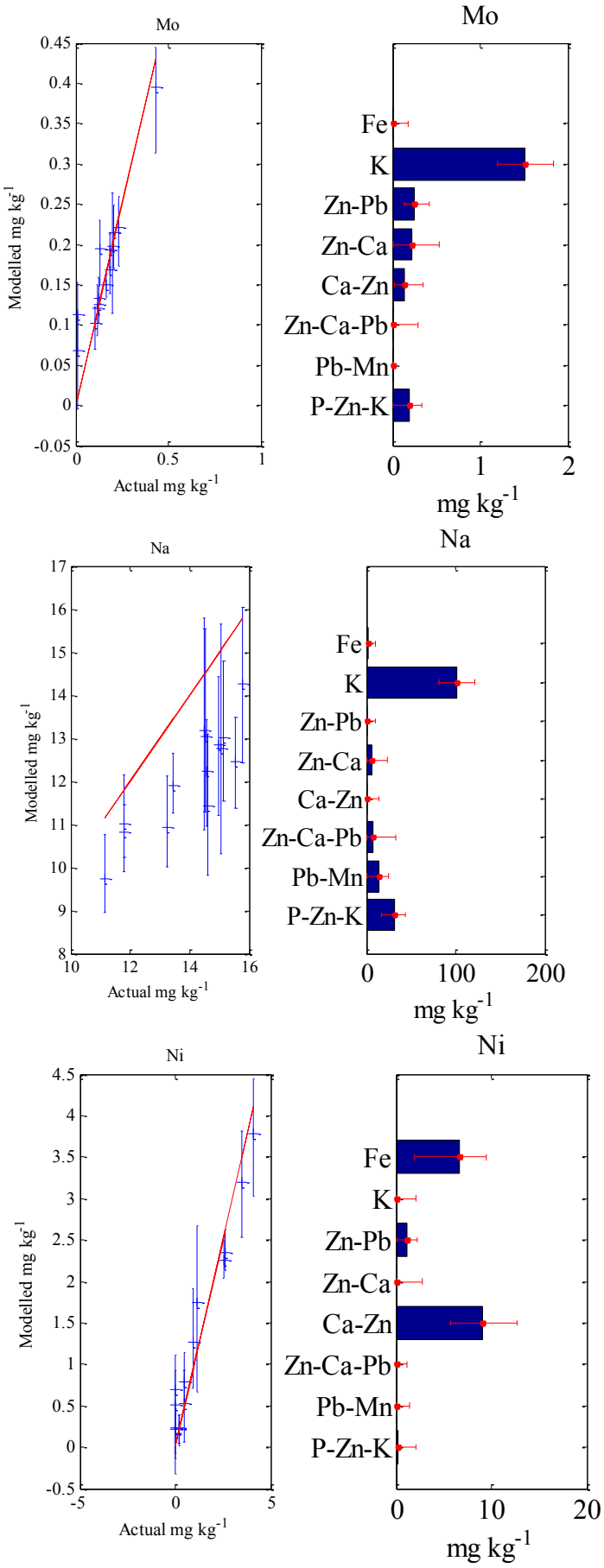
Mo
Modelled mg kg-1
Actual mg kg-1
0.45
0.4
0.35
0.3
0.25
0.2
0.15
0.1
0.05
0
-0.05
0
0.5
1
Mo
Fe
K
Zn-Pb
Zn-Ca
Ca-Zn
Zn-Ca-Pb
Pb-Mn
P-Zn-K
0
1
2
mg kg-1
Na
Modelled mg kg-1
Actual mg kg-1
17
16
15
14
13
12
11
10
9
8
10
12
14
16
Na
Fe
K
Zn-Pb
Zn-Ca
Ca-Zn
Zn-Ca-Pb
Pb-Mn
P-Zn-K
0
100
200
mg kg-1
Ni
Modelled mg kg-1
Actual mg kg-1
4.5
4
3.5
3
2.5
2
1.5
1
0.5
0
-0.5
-5
0
5
Ni
Fe
K
Zn-Pb
Zn-Ca
Ca-Zn
Zn-Ca-Pb
Pb-Mn
P-Zn-K
0
10
20
mg kg-1

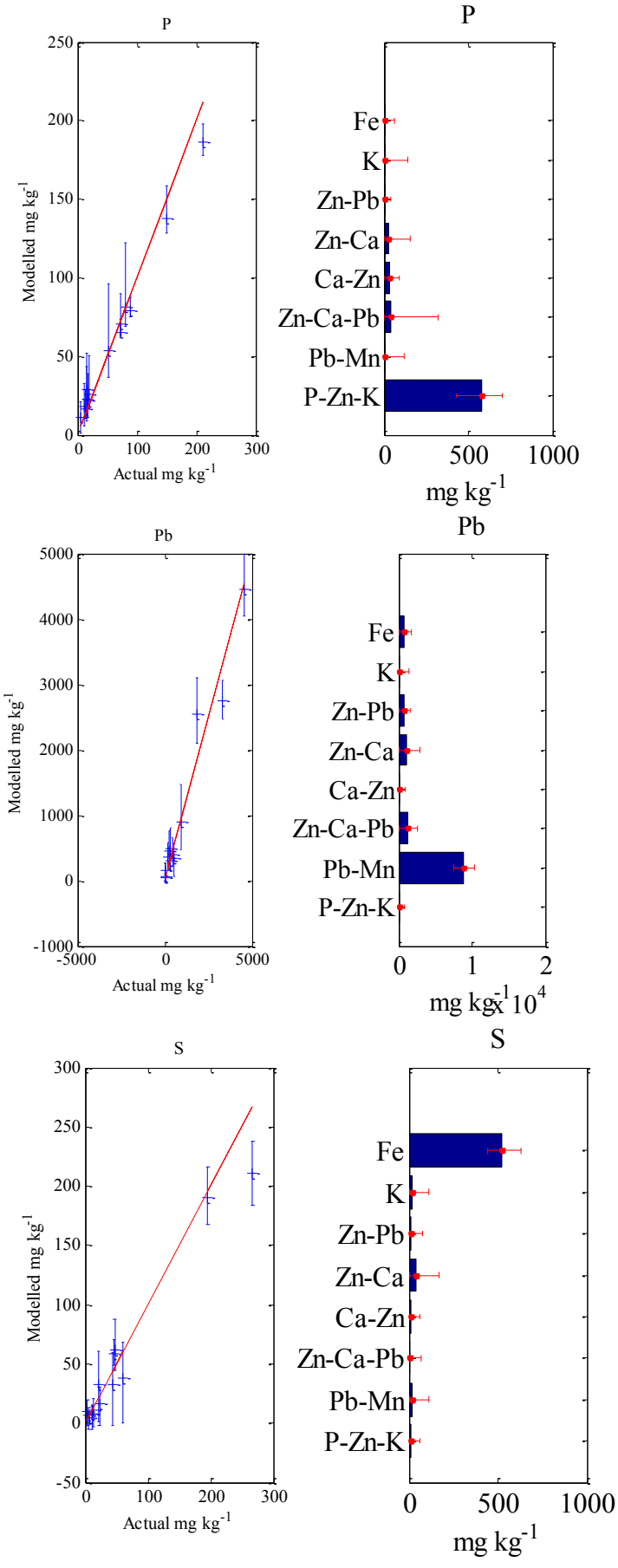
P
Modelled mg kg-1
Actual mg kg-1
0
50
100
150
200
250
0
100
200
300
P
Fe
K
Zn-Pb
Zn-Ca
Ca-Zn
Zn-Ca-Pb
Pb-Mn
P-Zn-K
0
500
1000
mg kg-1
Pb
Modelled mg kg-1
Actual mg kg-1
-1000
0
1000
2000
3000
4000
5000
-5000
0
5000
Pb
Fe
K
Zn-Pb
Zn-Ca
Ca-Zn
Zn-Ca-Pb
Pb-Mn
P-Zn-K
0
1
2
mg kg-1 x 10^4
S
Modelled mg kg-1
Actual mg kg-1
-50
0
50
100
150
200
250
300
0
100
200
300
S
Fe
K
Zn-Pb
Zn-Ca
Ca-Zn
Zn-Ca-Pb
Pb-Mn
P-Zn-K
0
500
1000
mg kg-1

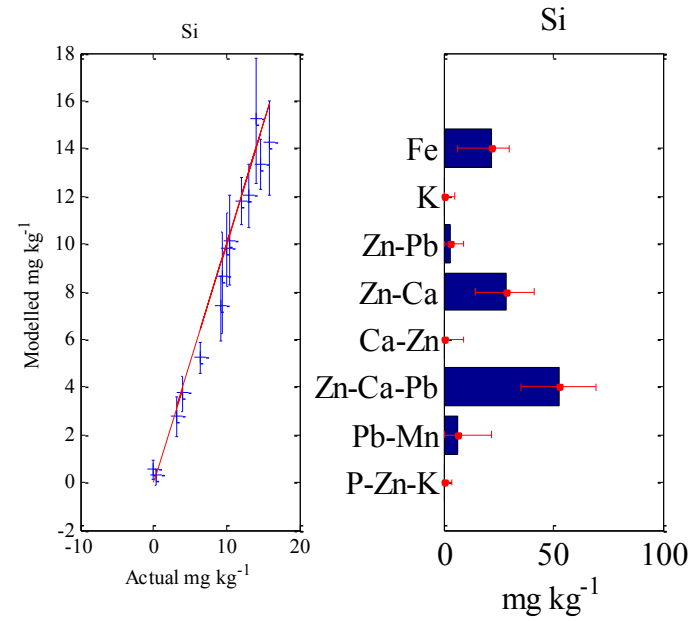
Si
Modelled mg kg-1
Actual mg kg-1
Si
Fe
K
Zn-Pb
Zn-Ca
Ca-Zn
Zn-Ca-Pb
Pb-Mn
P-Zn-K
mg kg-1

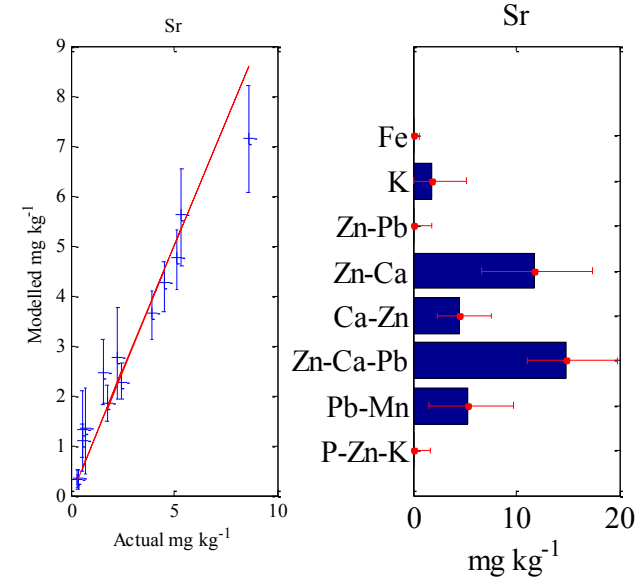
Sr
Modelled mg kg-1
Actual mg kg-1
Sr
Fe
K
Zn-Pb
Zn-Ca
Ca-Zn
Zn-Ca-Pb
Pb-Mn
P-Zn-K
mg kg-1

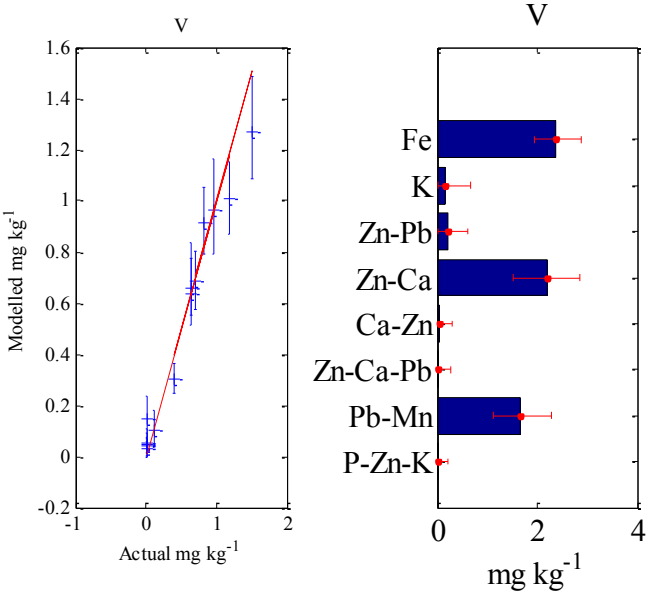
V
Modelled mg kg-1
Actual mg kg-1
V
Fe
K
Zn-Pb
Zn-Ca
Ca-Zn
Zn-Ca-Pb
Pb-Mn
P-Zn-K
mg kg-1

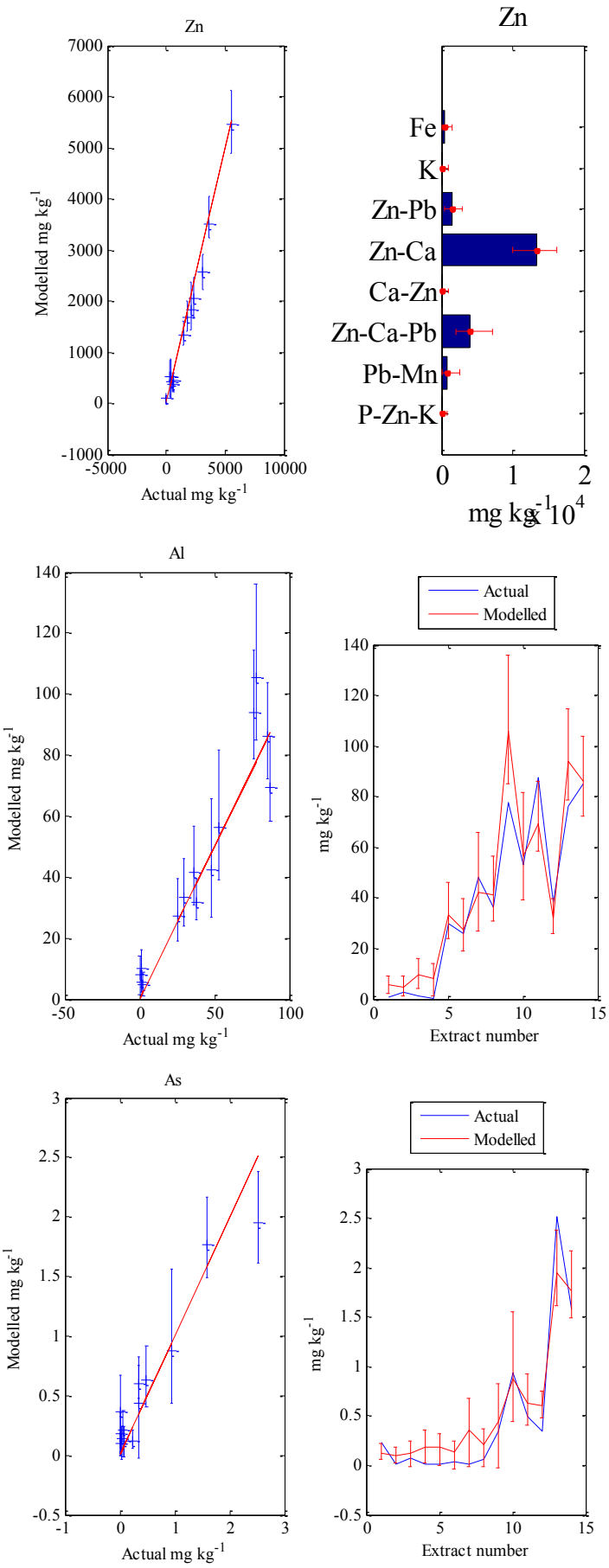
Zn
Modelled mg kg-1
Actual mg kg-1
Zn
Fe
K
Zn-Pb
Zn-Ca
Ca-Zn
Zn-Ca-Pb
Pb-Mn
P-Zn-K
mg kg-1 x 10^4
Al
Modelled mg kg-1
Actual mg kg-1
Actual
Modelled
mg kg-1
Extract number
As
Modelled mg kg-1
Actual mg kg-1
Actual
Modelled
mg kg-1
Extract number

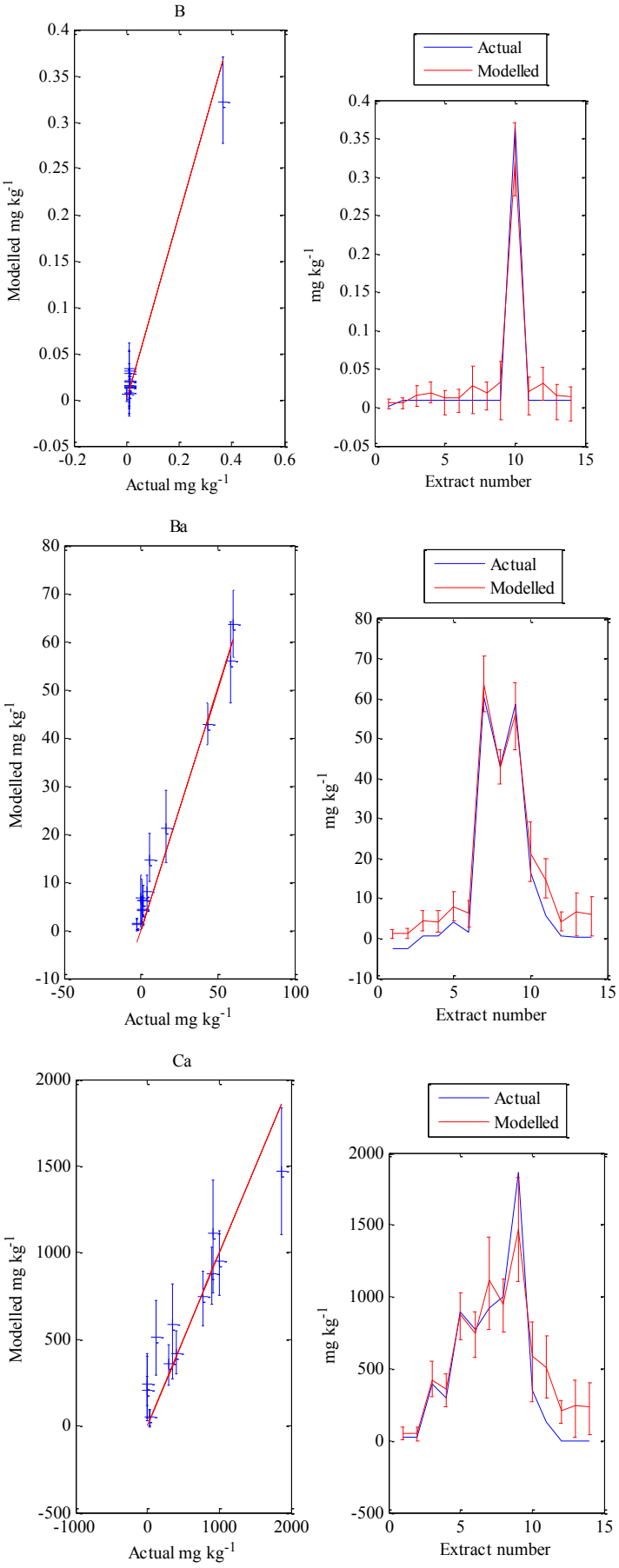
B
Modelled mg kg-1
Actual mg kg-1
Actual
Modelled
mg kg-1
Extract number
Ba
Modelled mg kg-1
Actual mg kg-1
Actual
Modelled
mg kg-1
Extract number
Ca
Modelled mg kg-1
Actual mg kg-1
Actual
Modelled
mg kg-1
Extract number

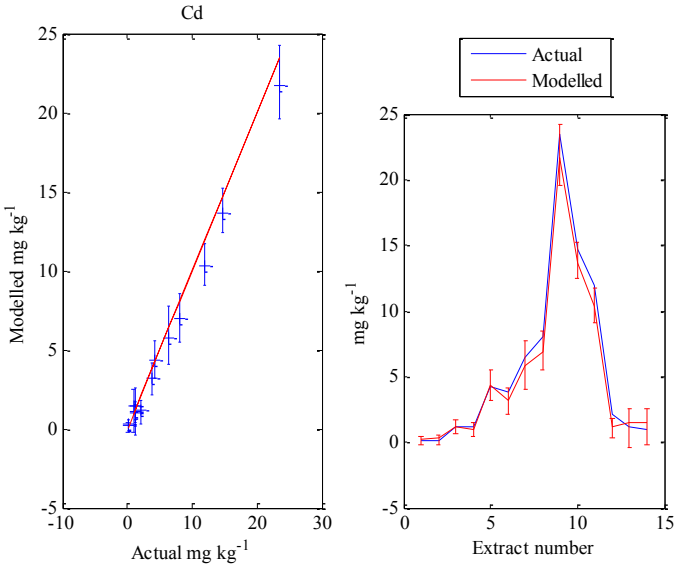
Cd
Modelled mg kg-1
Actual mg kg-1
Actual
Modelled
mg kg-1
Extract number

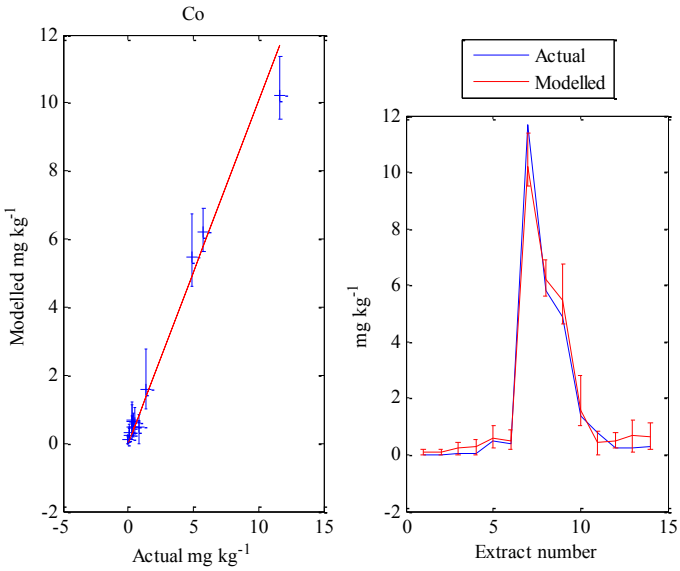
Co
Modelled mg kg-1
Actual mg kg-1
Actual
Modelled
mg kg-1
Extract number

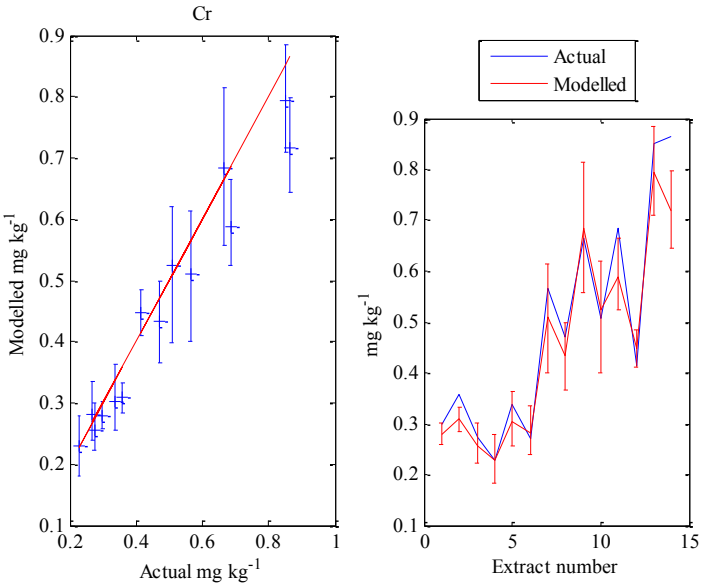
Cr
Modelled mg kg-1
Actual mg kg-1
Actual
Modelled
mg kg-1
Extract number

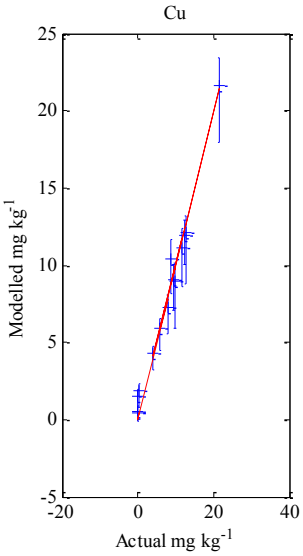
Cu
Modelled mg kg-1
Actual mg kg-1

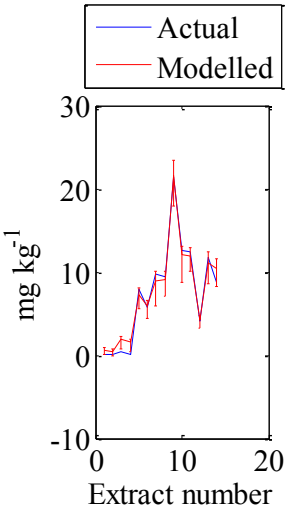
Actual
Modelled
mg kg-1
Extract number

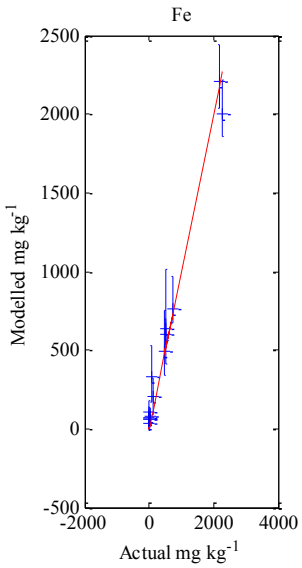
Fe
Modelled mg kg-1
Actual mg kg-1

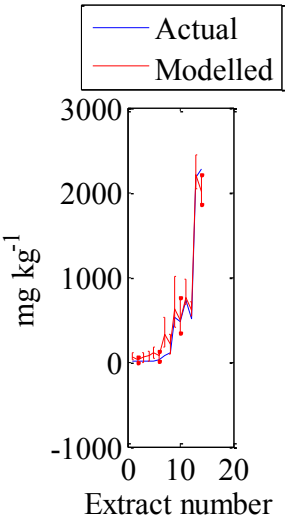
Actual
Modelled
mg kg-1
Extract number

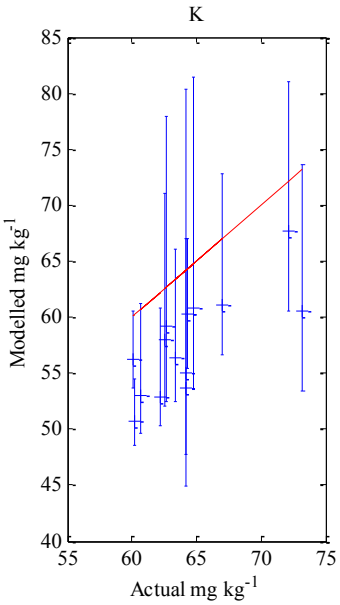
K
Modelled mg kg-1
Actual mg kg-1

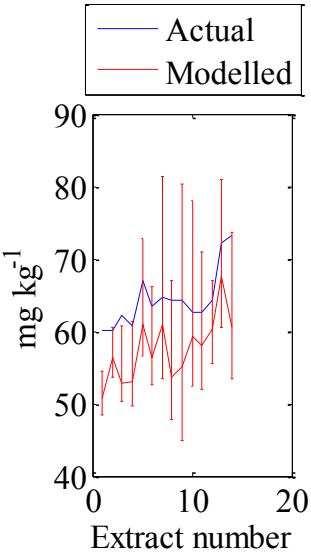
Actual
Modelled
mg kg-1
Extract number

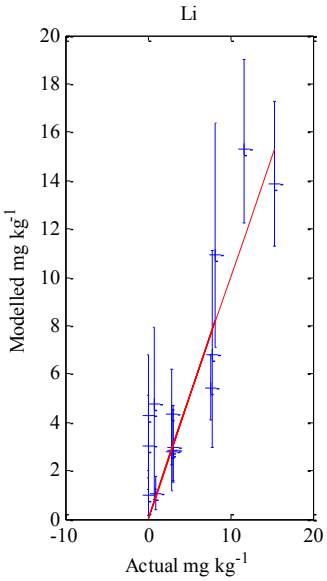
Li
Modelled mg kg-1
Actual mg kg-1

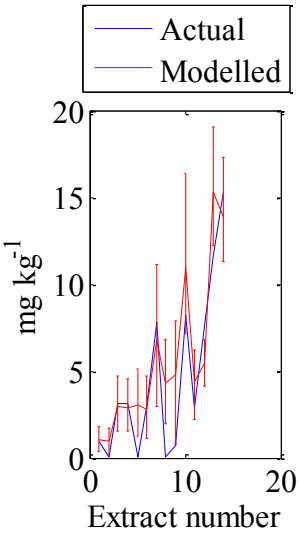
Actual
Modelled
mg kg-1
Extract number

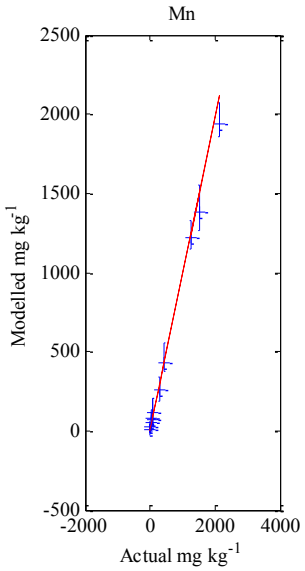
Mn
Modelled mg kg-1
Actual mg kg-1

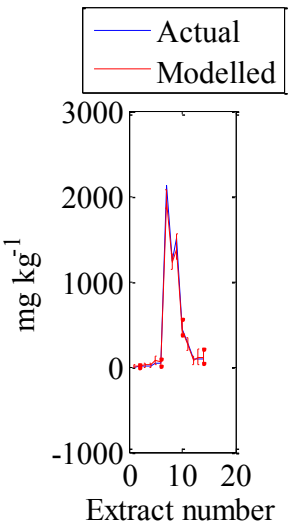
Actual
Modelled
mg kg-1
Extract number

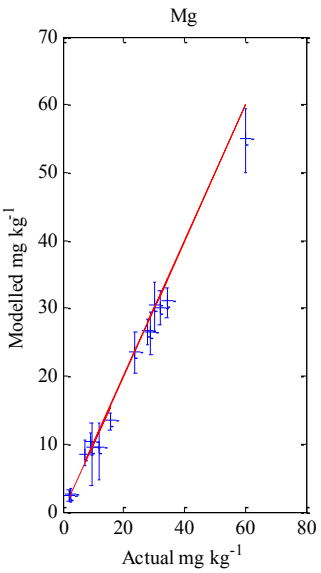
Mg
Modelled mg kg-1
Actual mg kg-1

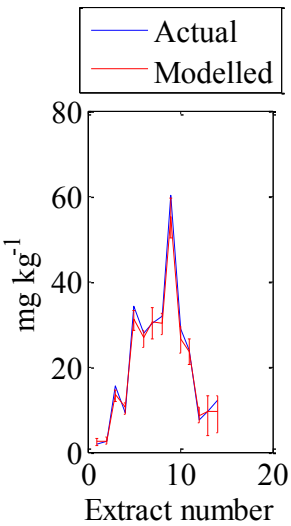
Actual
Modelled
mg kg-1
Extract number

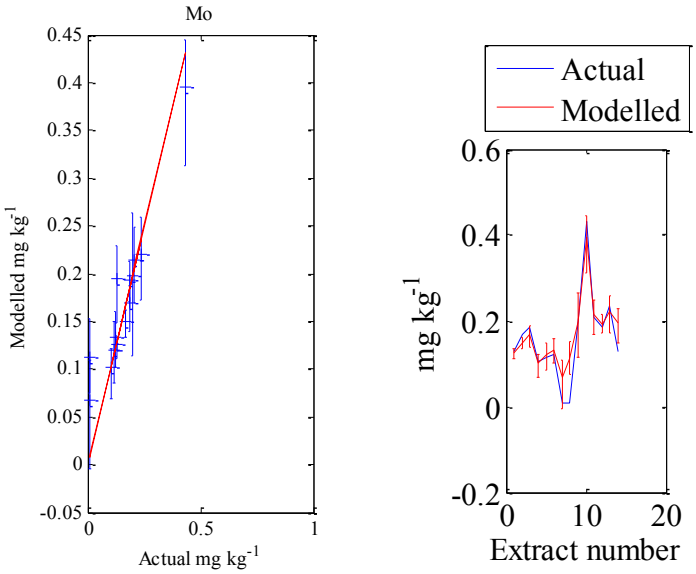
Mo
Modelled mg kg-1
Actual mg kg-1
Actual
Modelled
mg kg-1
Extract number

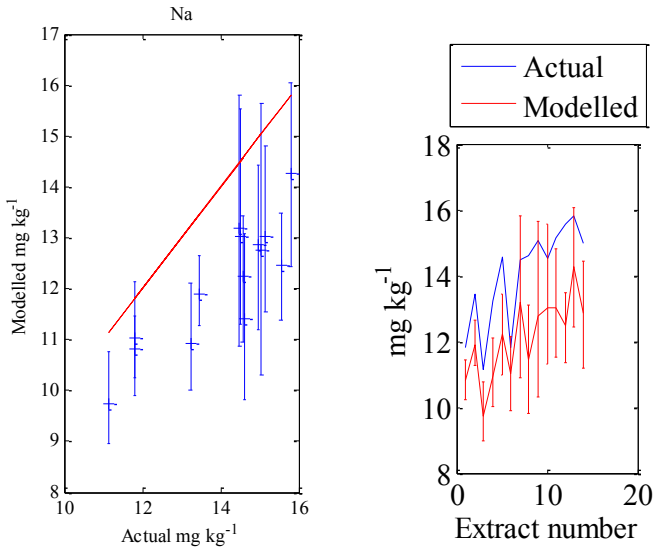
Na
Modelled mg kg-1
Actual mg kg-1
Actual
Modelled
mg kg-1
Extract number

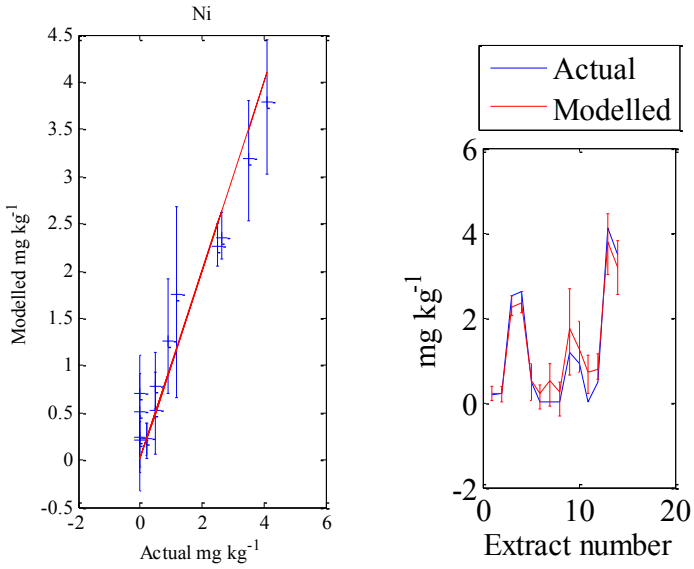
Ni
Modelled mg kg-1
Actual mg kg-1
Actual
Modelled
mg kg-1
Extract number

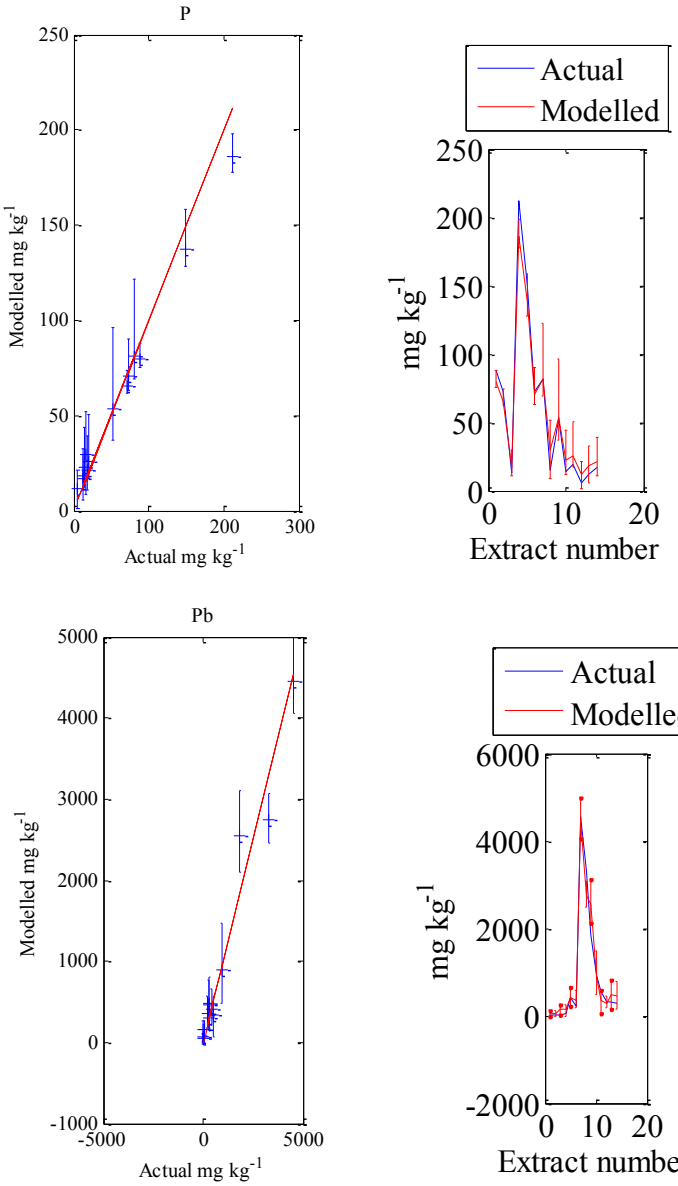
P
Modelled mg kg-1
Actual mg kg-1
Actual
Modelled
mg kg-1
Extract number
Pb
Modelled mg kg-1
Actual mg kg-1
Actual
Modelled
mg kg-1
Extract number
S
Modelled mg kg-1
Actual mg kg-1
Actual
Modelled
mg kg-1
Extract number

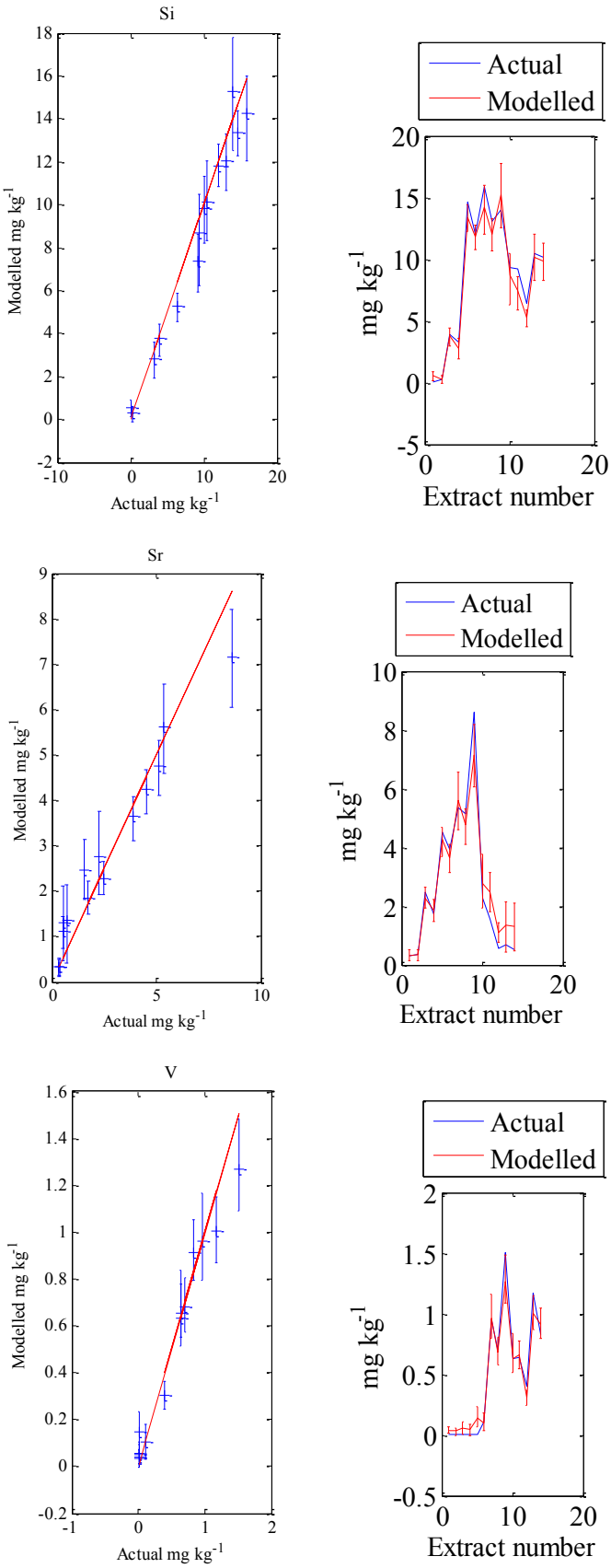
Si
Modelled mg kg-1
Actual mg kg-1
Actual
Modelled
mg kg-1
Extract number
Sr
Modelled mg kg-1
Actual mg kg-1
Actual
Modelled
mg kg-1
Extract number
V
Modelled mg kg-1
Actual mg kg-1
Actual
Modelled
mg kg-1
Extract number

Soil 8

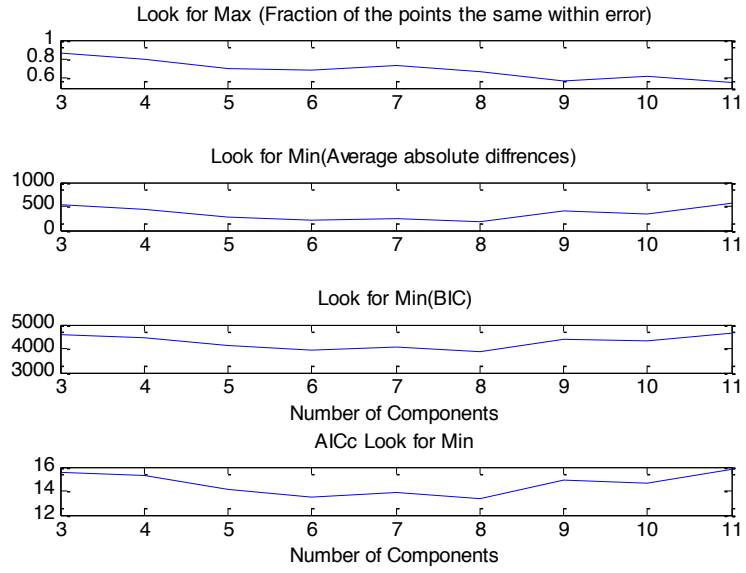
Look for Max (Fraction of the points the same within error)
Look for Min(Average absolute diffrences)
Look for Min(BIC)
Number of Components
AICc Look for Min
Number of Components

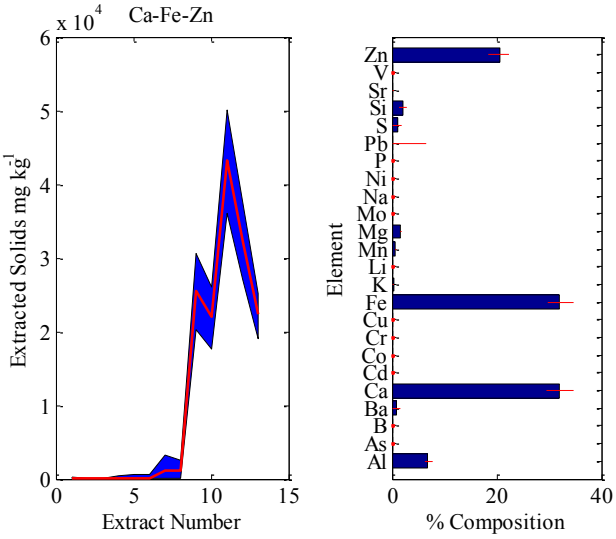
Ca-Fe-Zn
x 10^4
Extracted Solids mg kg-1
Extract Number
Element
% Composition
Zn
V
Sr
Si
S
Pb
P
Ni
Na
Mo
Mg
Mn
Li
K
Fe
Cu
Cr
Co
Cd
Ca
Ba
B
As
Al

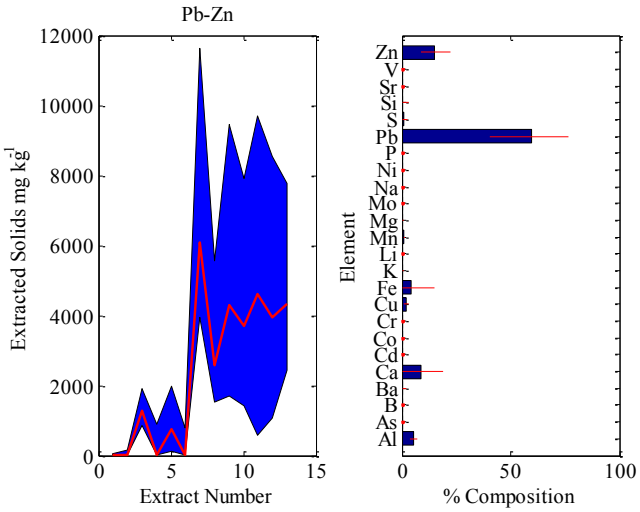
Pb-Zn
Extracted Solids mg kg-1
Extract Number
Element
% Composition
Zn
V
Sr
Si
S
Pb
P
Ni
Na
Mo
Mg
Mn
Li
K
Fe
Cu
Cr
Co
Cd
Ca
Ba
B
As
Al

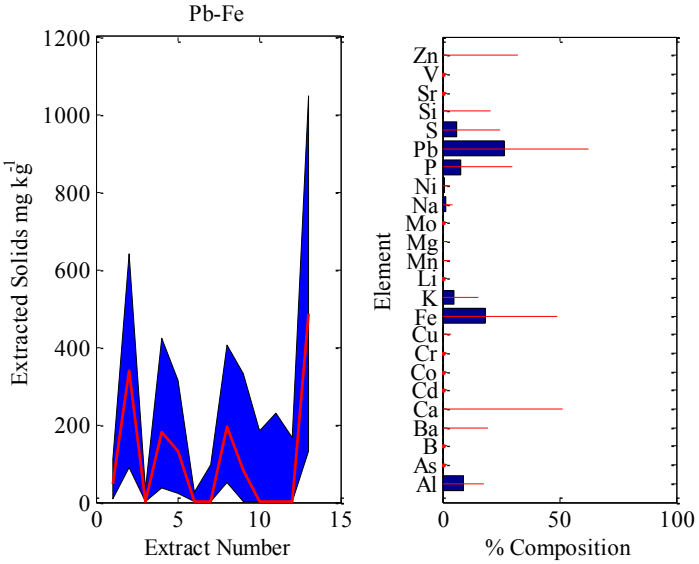
Pb-Fe
Extracted Solids mg kg-1
Extract Number
Element
% Composition
Zn
V
Sr
Si
S
Pb
P
Ni
Na
Mo
Mg
Mn
Li
K
Fe
Cu
Cr
Co
Cd
Ca
Ba
B
As
Al

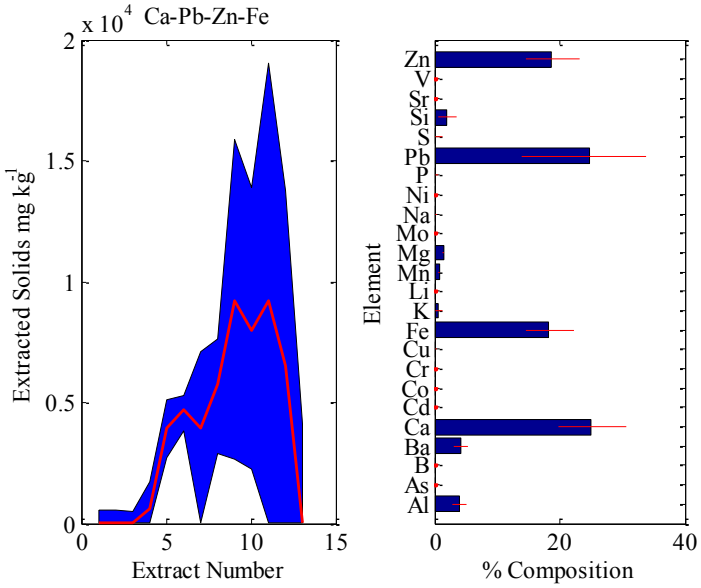
x 10^4
Ca-Pb-Zn-Fe
Extracted Solids mg kg-1
Extract Number
Element
% Composition
Zn
V
Sr
Si
S
Pb
P
Ni
Na
Mo
Mg
Mn
Li
K
Fe
Cu
Cr
Co
Cd
Ca
Ba
B
As
Al

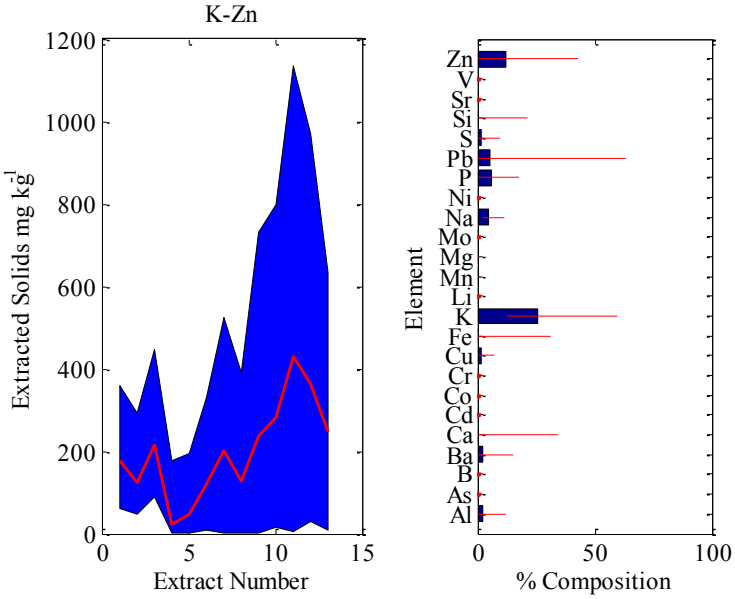
K-Zn
Extracted Solids mg kg-1
Extract Number
Element
% Composition
Zn
V
Sr
Si
S
Pb
P
Ni
Na
Mo
Mg
Mn
Li
K
Fe
Cu
Cr
Co
Cd
Ca
Ba
B
As
Al

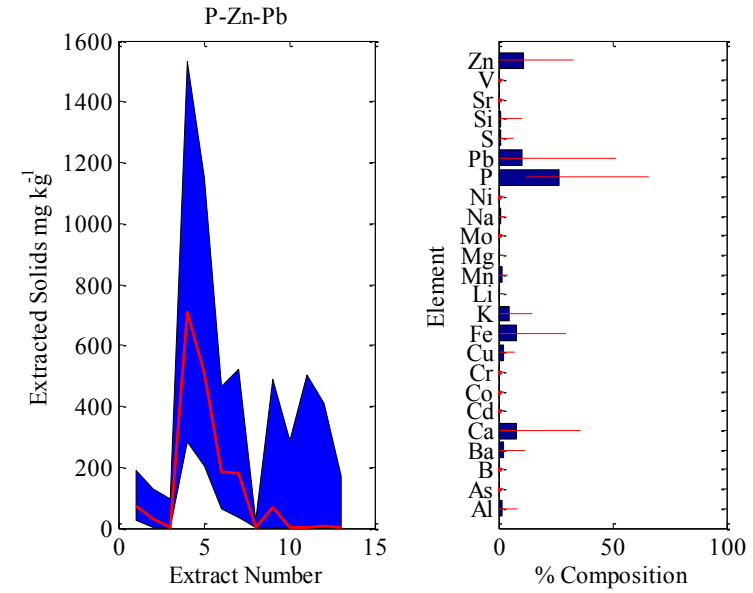
P-Zn-Pb
Extracted Solids mg kg-1
Extract Number
Element
% Composition
Zn
V
Sr
Si
S
Pb
P
Ni
Na
Mo
Mg
Mn
Li
K
Fe
Cu
Cr
Co
Cd
Ca
Ba
B
As
Al

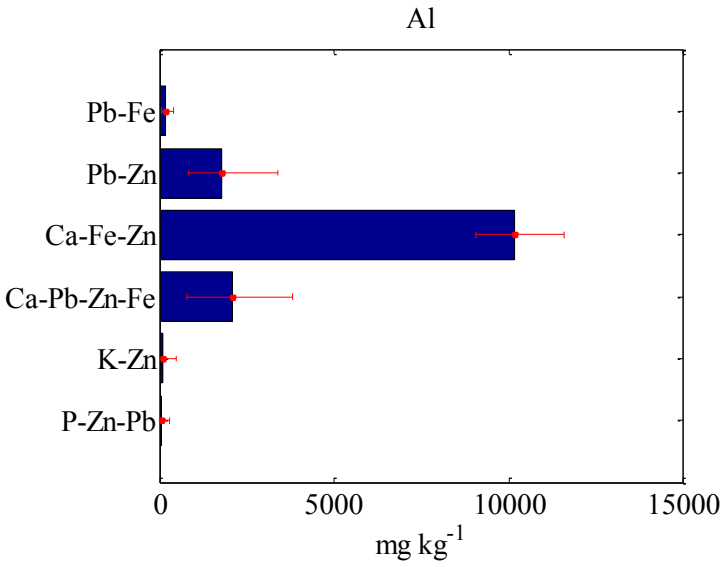
Al
Pb-Fe
Pb-Zn
Ca-Fe-Zn
Ca-Pb-Zn-Fe
K-Zn
P-Zn-Pb
mg kg-1

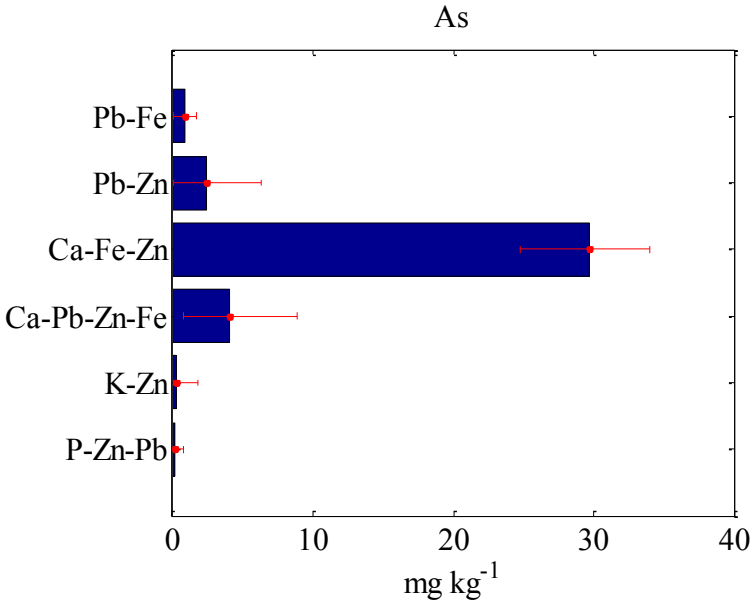
As
Pb-Fe
Pb-Zn
Ca-Fe-Zn
Ca-Pb-Zn-Fe
K-Zn
P-Zn-Pb
mg kg-1

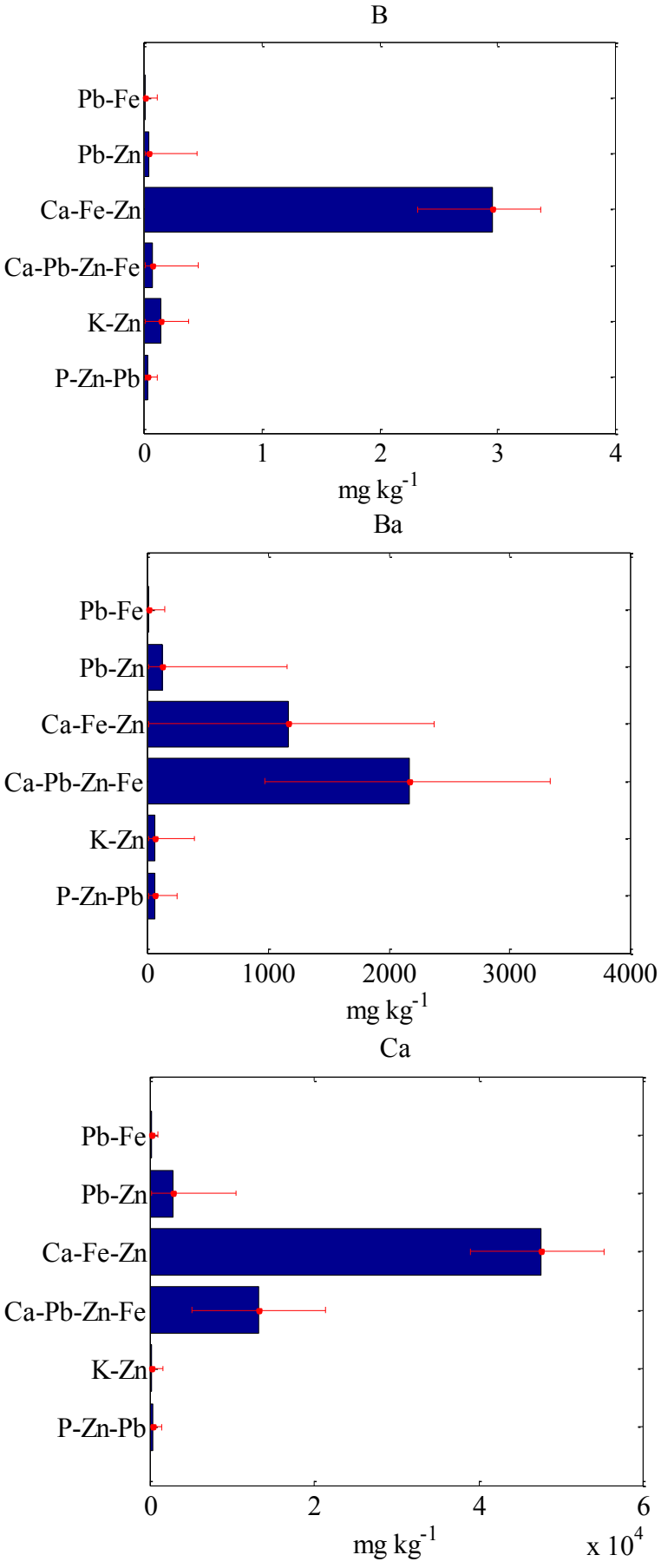
B
Pb-Fe
Pb-Zn
Ca-Fe-Zn
Ca-Pb-Zn-Fe
K-Zn
P-Zn-Pb
0
1
2
3
4
mg kg-1
Ba
Pb-Fe
Pb-Zn
Ca-Fe-Zn
Ca-Pb-Zn-Fe
K-Zn
P-Zn-Pb
0
1000
2000
3000
4000
mg kg-1
Ca
Pb-Fe
Pb-Zn
Ca-Fe-Zn
Ca-Pb-Zn-Fe
K-Zn
P-Zn-Pb
0
2
4
6
mg kg-1
x 10^4

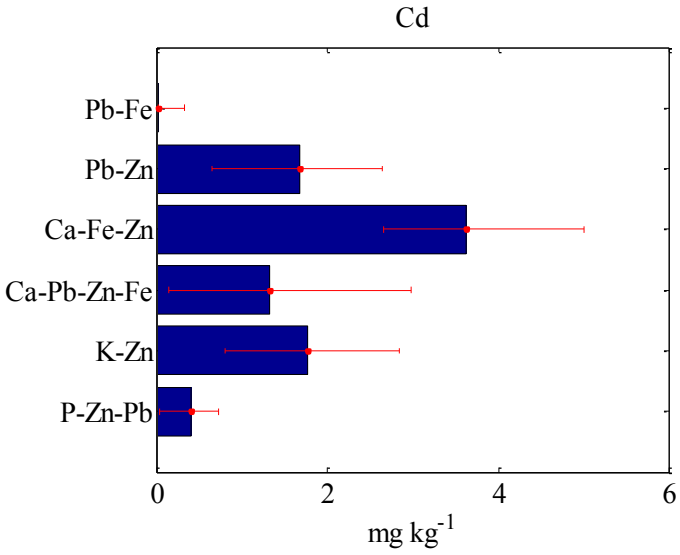
Cd
Pb-Fe
Pb-Zn
Ca-Fe-Zn
Ca-Pb-Zn-Fe
K-Zn
P-Zn-Pb
0
2
4
6
mg kg-1

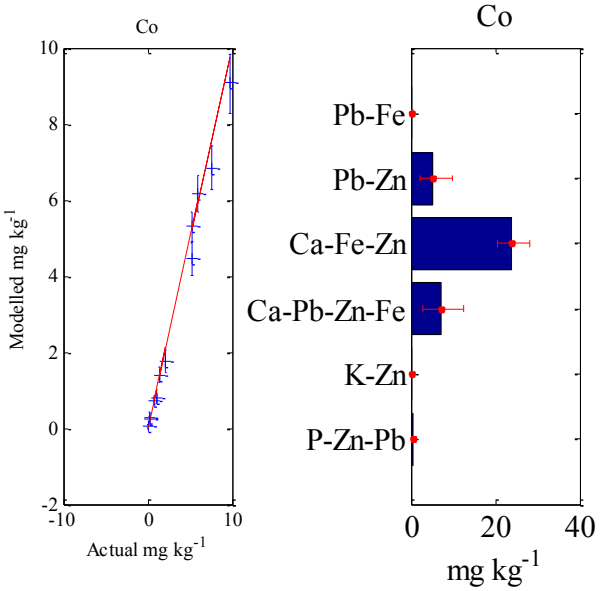
Co
Modelled mg kg-1
Actual mg kg-1
Co
Pb-Fe
Pb-Zn
Ca-Fe-Zn
Ca-Pb-Zn-Fe
K-Zn
P-Zn-Pb
0
20
40
mg kg-1

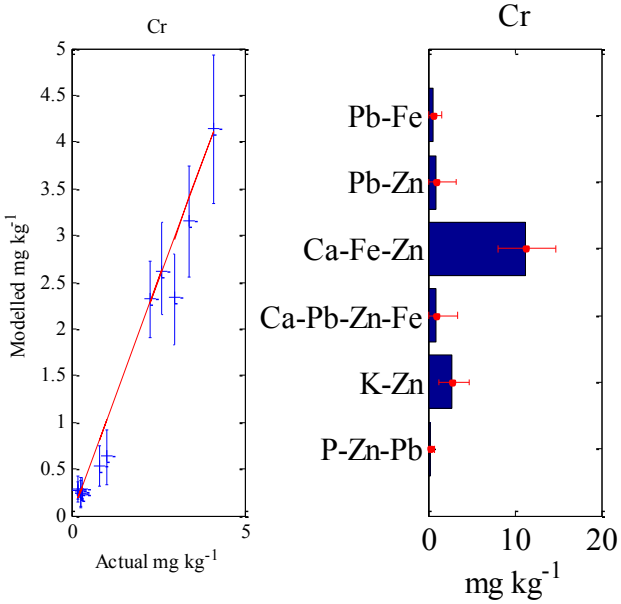
Cr
Modelled mg kg-1
Actual mg kg-1
Cr
Pb-Fe
Pb-Zn
Ca-Fe-Zn
Ca-Pb-Zn-Fe
K-Zn
P-Zn-Pb
0
10
20
mg kg-1

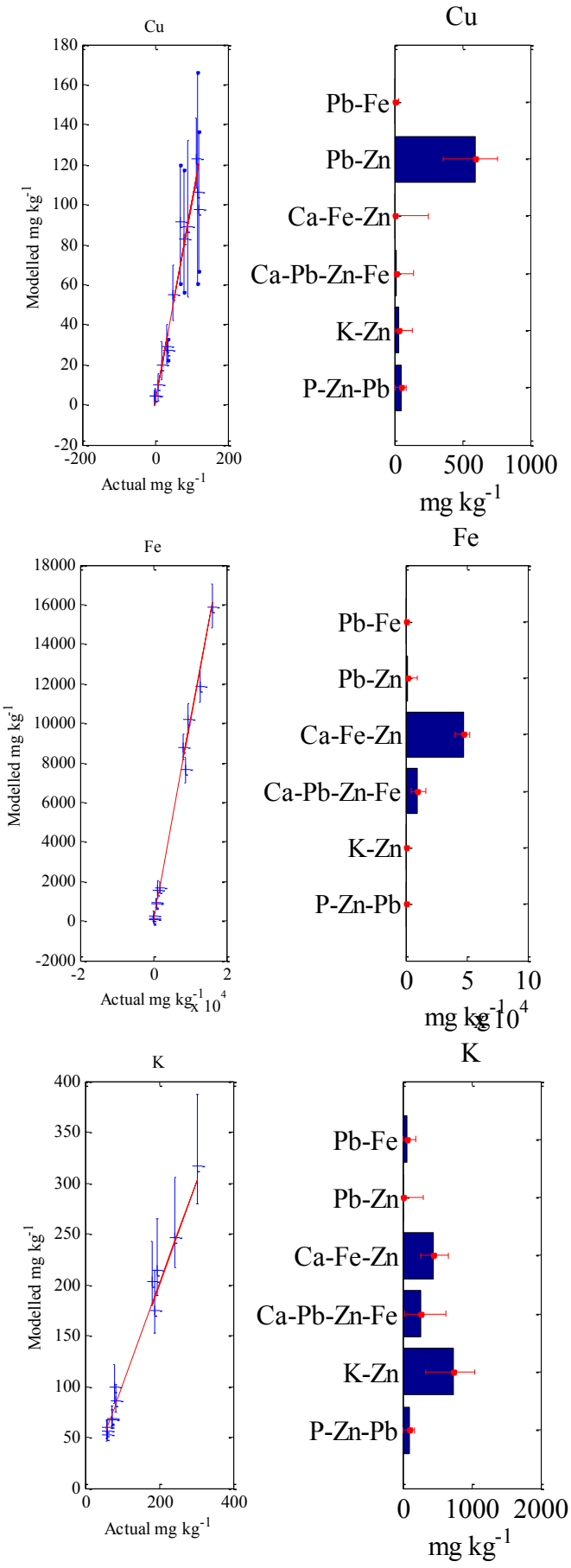
Cu
Modelled mg kg-1
Actual mg kg-1
Cu
Pb-Fe
Pb-Zn
Ca-Fe-Zn
Ca-Pb-Zn-Fe
K-Zn
P-Zn-Pb
mg kg-1
Fe
Modelled mg kg-1
Actual mg kg-1 x 10^4
Fe
mg kg-1 x 10^4
K
Modelled mg kg-1
Actual mg kg-1
K
mg kg-1

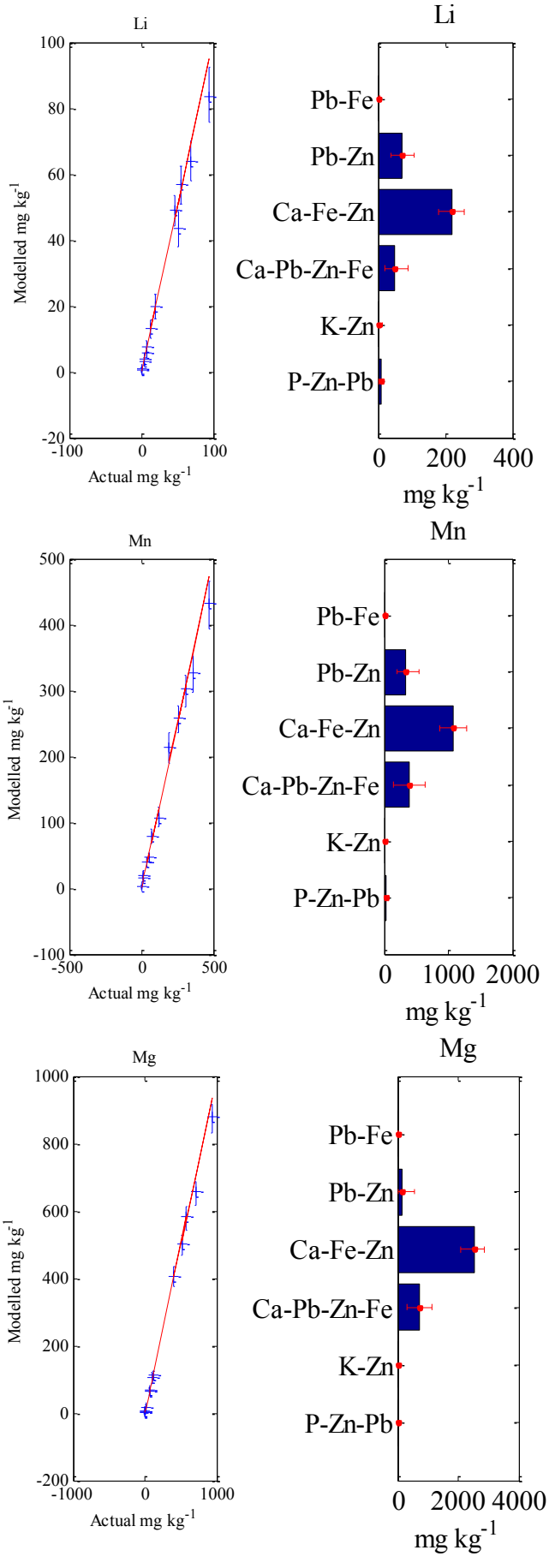
Li
Modelled mg kg-1
Actual mg kg-1
100
80
60
40
20
0
-20
-100
0
100
Li
Pb-Fe
Pb-Zn
Ca-Fe-Zn
Ca-Pb-Zn-Fe
K-Zn
P-Zn-Pb
0
200
400
mg kg-1
Mn
Modelled mg kg-1
Actual mg kg-1
500
400
300
200
100
0
-100
-500
0
500
Mn
Pb-Fe
Pb-Zn
Ca-Fe-Zn
Ca-Pb-Zn-Fe
K-Zn
P-Zn-Pb
0
1000
2000
mg kg-1
Mg
Modelled mg kg-1
Actual mg kg-1
1000
800
600
400
200
0
-200
-1000
0
1000
Mg
Pb-Fe
Pb-Zn
Ca-Fe-Zn
Ca-Pb-Zn-Fe
K-Zn
P-Zn-Pb
0
2000
4000
mg kg-1

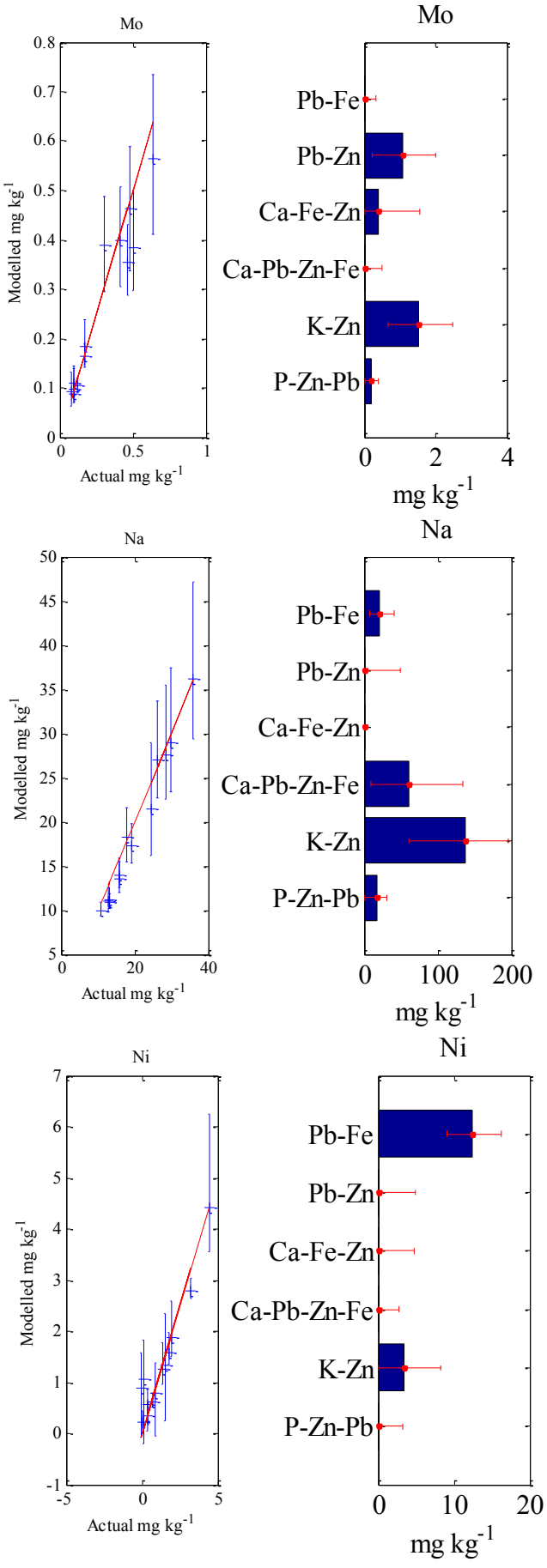
Mo
Modelled mg kg-1
Actual mg kg-1
0
0.1
0.2
0.3
0.4
0.5
0.6
0.7
0.8
0.5
1
Mo
Pb-Fe
Pb-Zn
Ca-Fe-Zn
Ca-Pb-Zn-Fe
K-Zn
P-Zn-Pb
0
2
4
mg kg-1
Na
Modelled mg kg-1
Actual mg kg-1
5
10
15
20
25
30
35
40
45
50
0
20
40
Na
Pb-Fe
Pb-Zn
Ca-Fe-Zn
Ca-Pb-Zn-Fe
K-Zn
P-Zn-Pb
0
100
200
mg kg-1
Ni
Modelled mg kg-1
Actual mg kg-1
-1
0
1
2
3
4
5
6
7
-5
0
5
Ni
Pb-Fe
Pb-Zn
Ca-Fe-Zn
Ca-Pb-Zn-Fe
K-Zn
P-Zn-Pb
0
10
20
mg kg-1

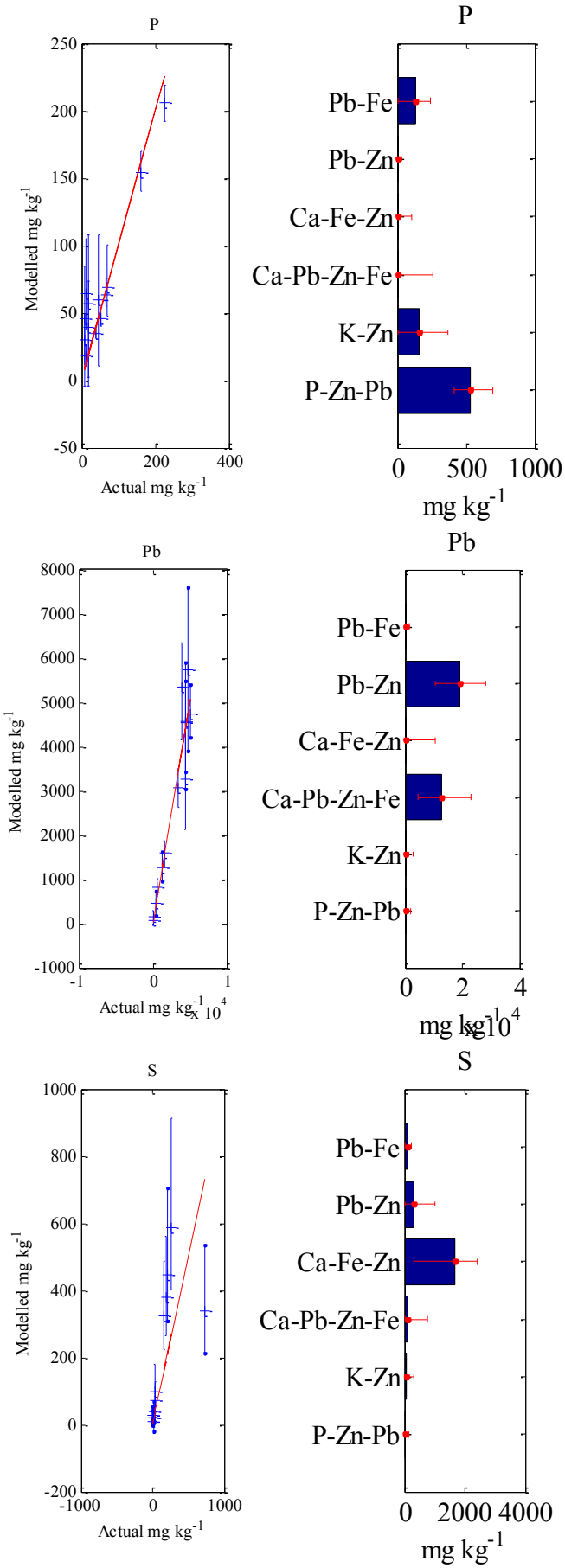
P
Modelled mg kg-1
Actual mg kg-1
250
200
150
100
50
0
-50
0
200
400
P
Pb-Fe
Pb-Zn
Ca-Fe-Zn
Ca-Pb-Zn-Fe
K-Zn
P-Zn-Pb
0
500
1000
mg kg-1
Pb
Modelled mg kg-1
Actual mg kg-1 x 10^4
8000
7000
6000
5000
4000
3000
2000
1000
0
-1000
-1
0
1
Pb
Pb-Fe
Pb-Zn
Ca-Fe-Zn
Ca-Pb-Zn-Fe
K-Zn
P-Zn-Pb
0
2
4
mg kg-1 x 10^4
S
Modelled mg kg-1
Actual mg kg-1
1000
800
600
400
200
0
-200
-1000
0
1000
S
Pb-Fe
Pb-Zn
Ca-Fe-Zn
Ca-Pb-Zn-Fe
K-Zn
P-Zn-Pb
0
2000
4000
mg kg-1

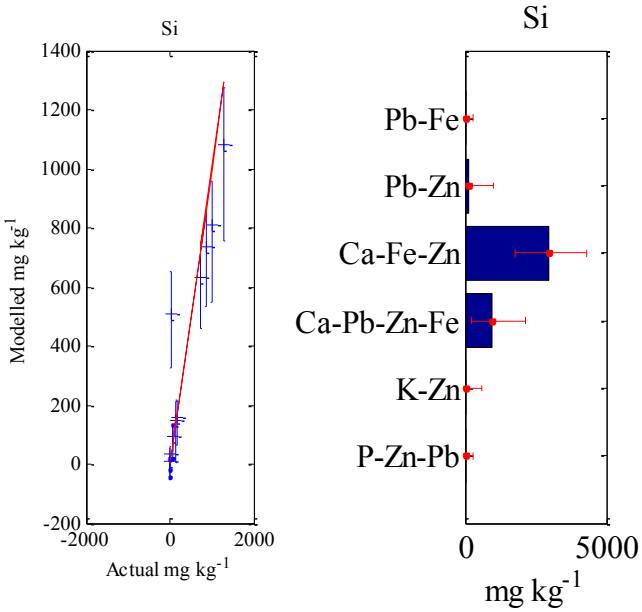
Si
Modelled mg kg-1
Actual mg kg-1
1400
1200
1000
800
600
400
200
0
-200
-2000
0
2000
Si
Pb-Fe
Pb-Zn
Ca-Fe-Zn
Ca-Pb-Zn-Fe
K-Zn
P-Zn-Pb
0
5000
mg kg-1

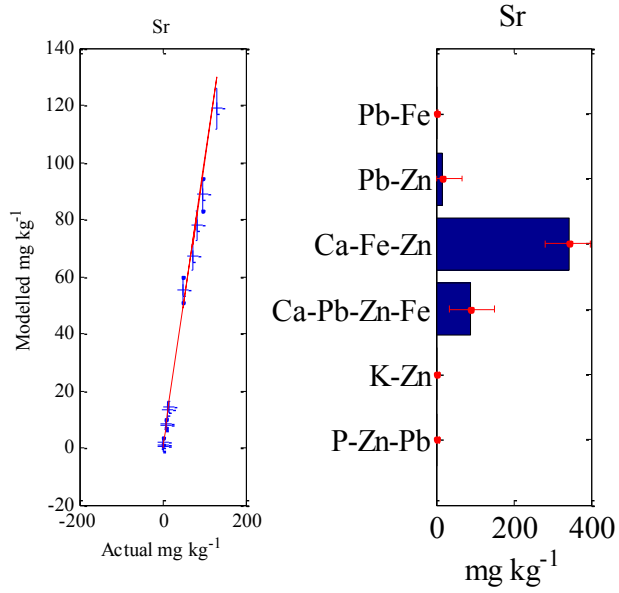
Sr
Modelled mg kg-1
Actual mg kg-1
140
120
100
80
60
40
20
0
-20
-200
0
200
Sr
Pb-Fe
Pb-Zn
Ca-Fe-Zn
Ca-Pb-Zn-Fe
K-Zn
P-Zn-Pb
0
200
400
mg kg-1

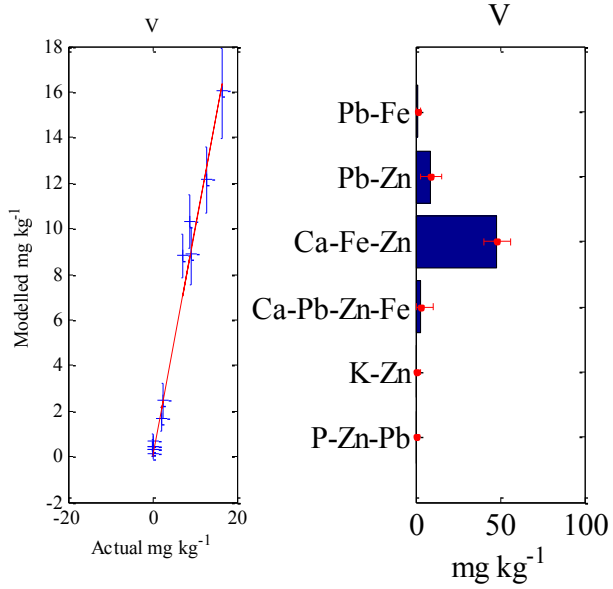
V
Modelled mg kg-1
Actual mg kg-1
18
16
14
12
10
8
6
4
2
0
-2
-20
0
20
V
Pb-Fe
Pb-Zn
Ca-Fe-Zn
Ca-Pb-Zn-Fe
K-Zn
P-Zn-Pb
0
50
100
mg kg-1

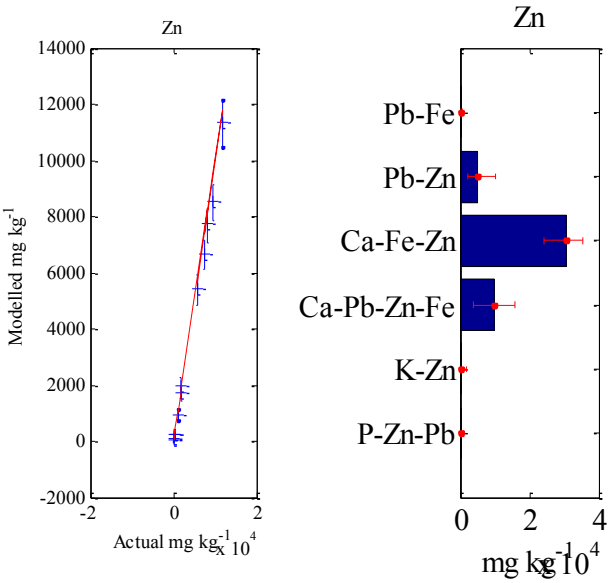
Zn
Modelled mg kg-1
Actual mg kg-1
x 10^4
Zn
Pb-Fe
Pb-Zn
Ca-Fe-Zn
Ca-Pb-Zn-Fe
K-Zn
P-Zn-Pb
mg kg-1
x 10^4

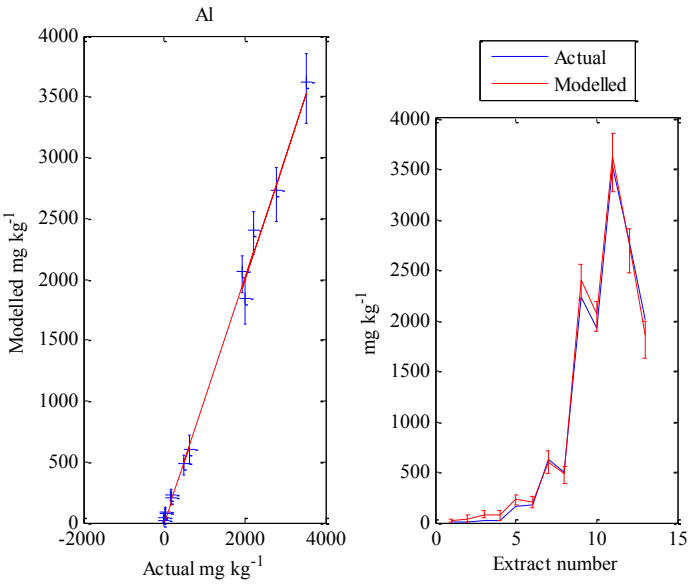
Al
Modelled mg kg-1
Actual mg kg-1
Actual
Modelled
mg kg-1
Extract number

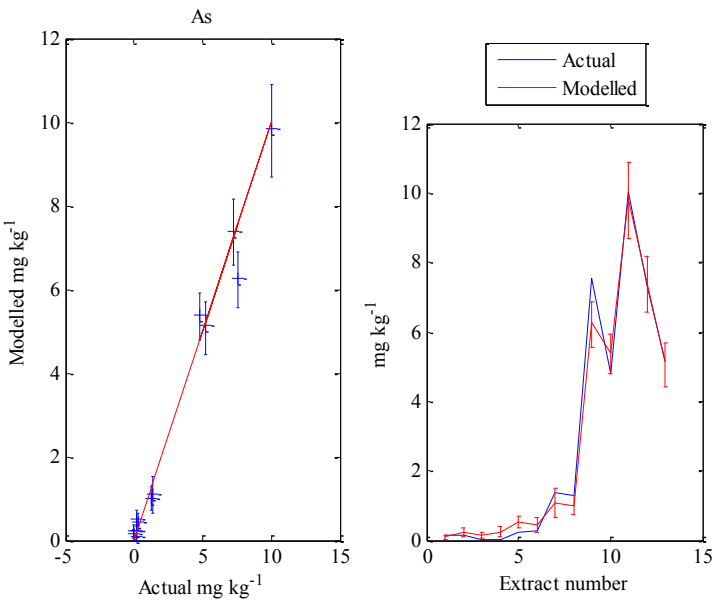
As
Modelled mg kg-1
Actual mg kg-1
Actual
Modelled
mg kg-1
Extract number

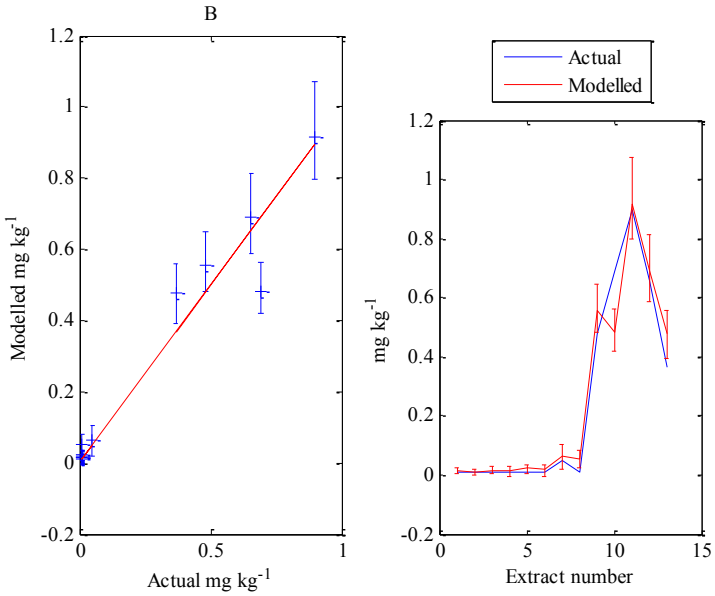
B
Modelled mg kg-1
Actual mg kg-1
Actual
Modelled
mg kg-1
Extract number

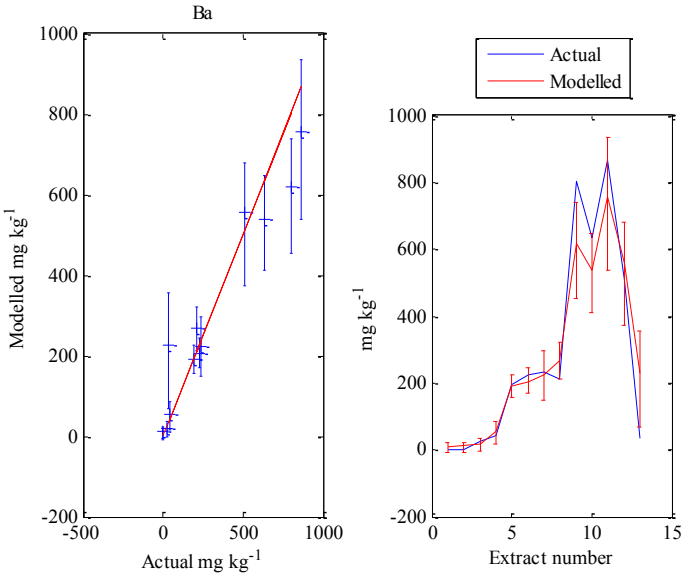
Ba
Modelled mg kg-1
Actual mg kg-1
Actual
Modelled
mg kg-1
Extract number

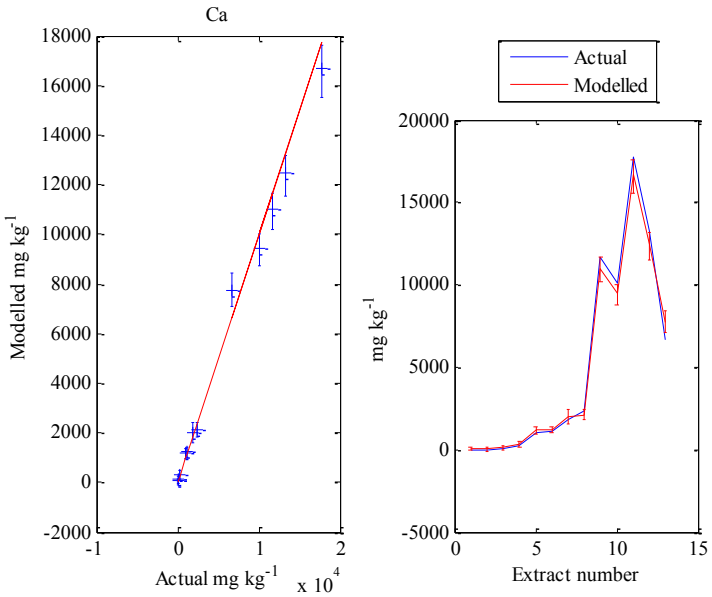
Ca
Modelled mg kg-1
Actual mg kg-1
x 10^4
Actual
Modelled
mg kg-1
Extract number

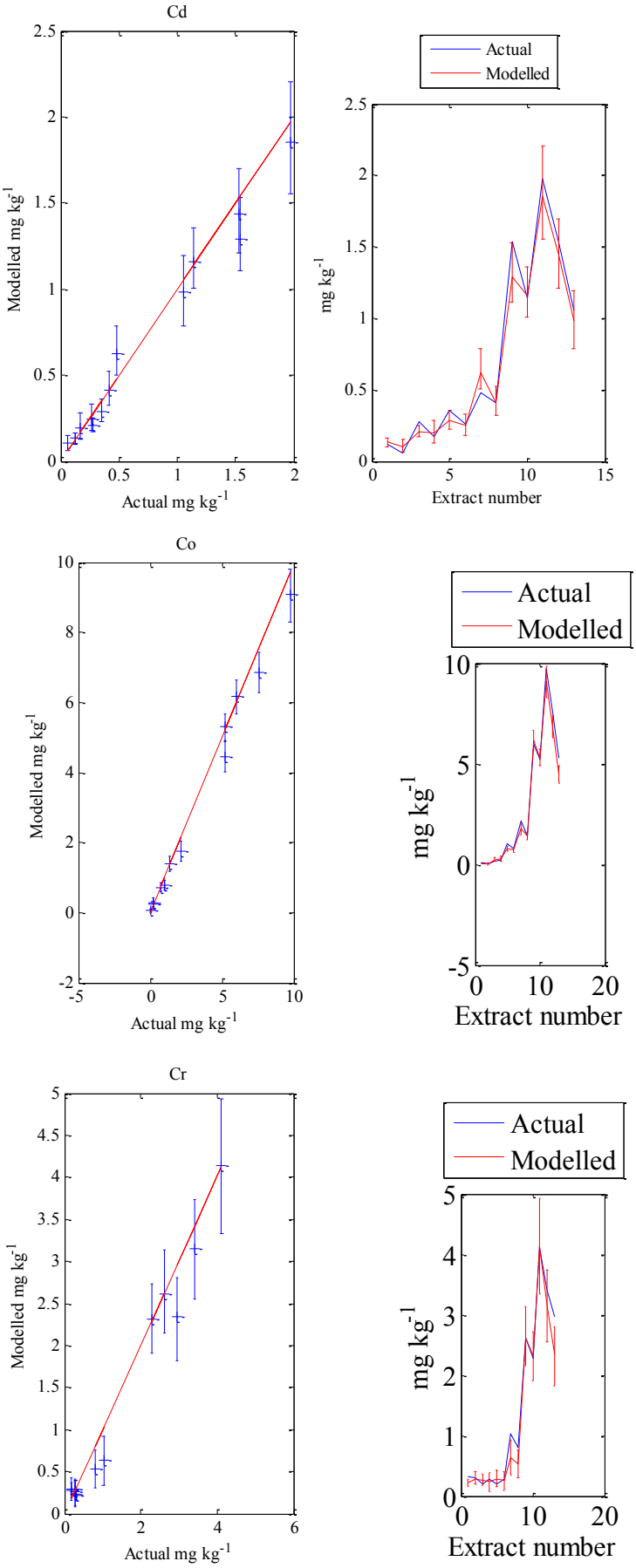
Cd
Modelled mg kg-1
Actual mg kg-1
Actual
Modelled
mg kg-1
Extract number
Co
Modelled mg kg-1
Actual mg kg-1
Actual
Modelled
mg kg-1
Extract number
Cr
Modelled mg kg-1
Actual mg kg-1
Actual
Modelled
mg kg-1
Extract number

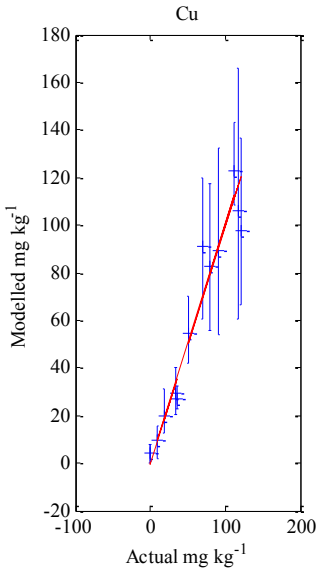
Cu
Modelled mg kg-1
Actual mg kg-1
180
160
140
120
100
80
60
40
20
0
-20
-100
0
100
200

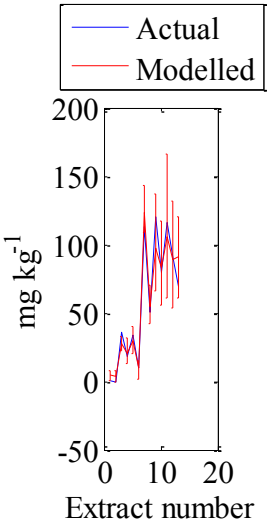
Actual
Modelled
mg kg-1
Extract number
200
150
100
50
0
-50
0
10
20

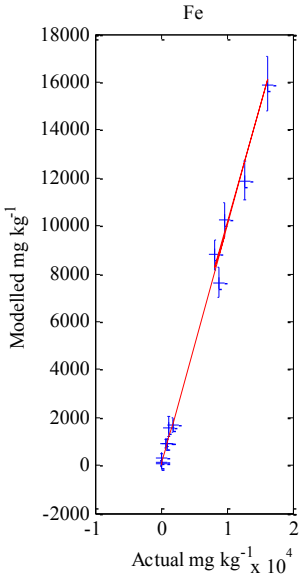
Fe
Modelled mg kg-1
Actual mg kg-1 x 10^4
18000
16000
14000
12000
10000
8000
6000
4000
2000
0
-2000
-1
0
1
2

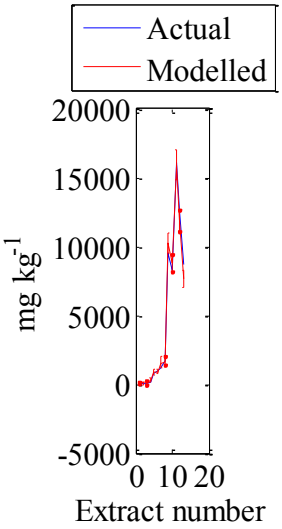
Actual
Modelled
mg kg-1
Extract number
20000
15000
10000
5000
0
-5000
0
10
20

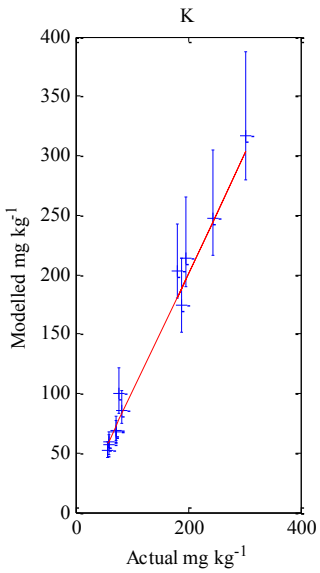
K
Modelled mg kg-1
Actual mg kg-1
400
350
300
250
200
150
100
50
0
0
200
400

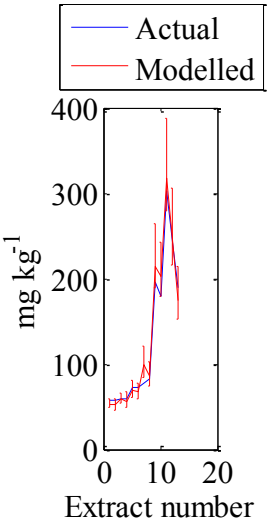
Actual
Modelled
mg kg-1
Extract number
400
300
200
100
0
0
10
20

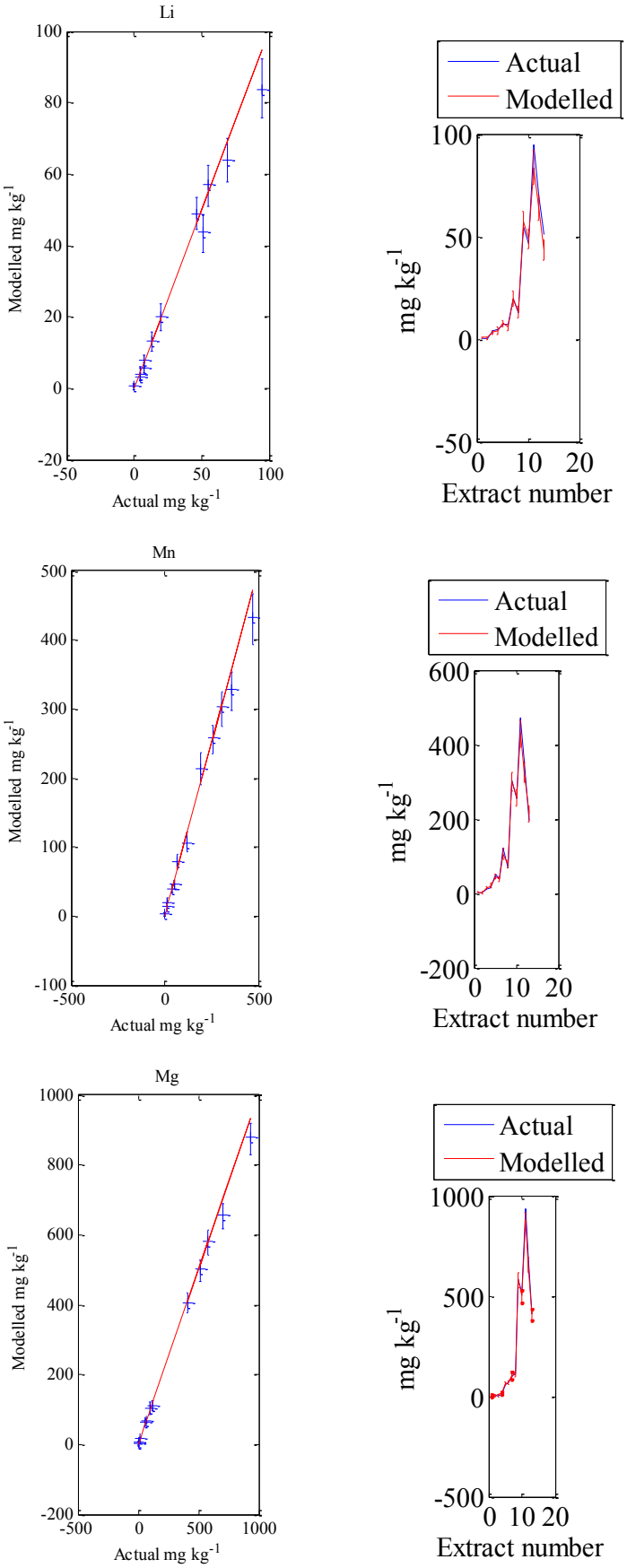
Li
Modelled mg kg-1
Actual mg kg-1
Actual
Modelled
mg kg-1
Extract number
Mn
Modelled mg kg-1
Actual mg kg-1
Actual
Modelled
mg kg-1
Extract number
Mg
Modelled mg kg-1
Actual mg kg-1
Actual
Modelled
mg kg-1
Extract number

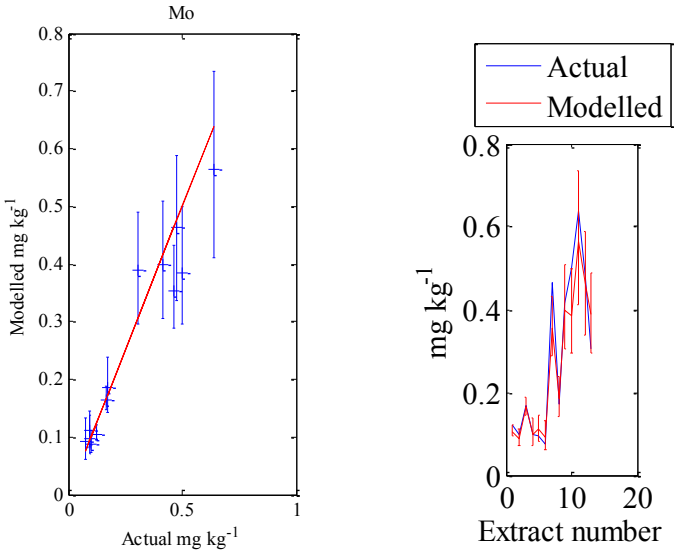
Mo
Modelled mg kg-1
Actual mg kg-1
Actual
Modelled
mg kg-1
Extract number

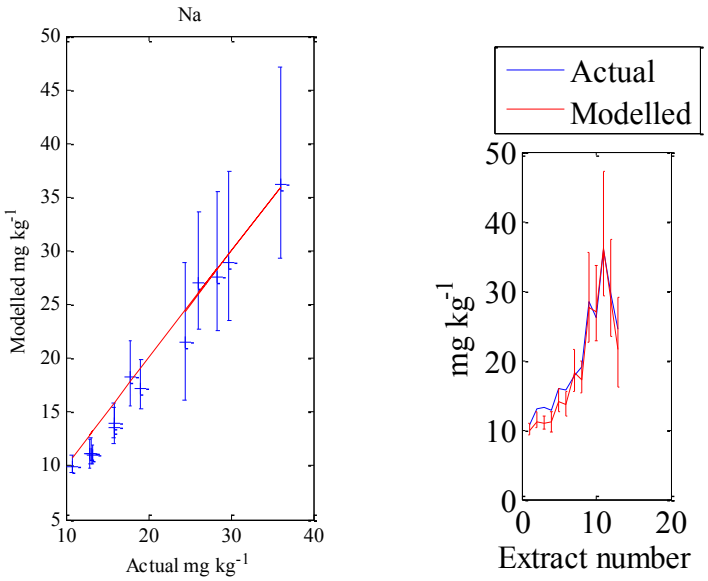
Na
Modelled mg kg-1
Actual mg kg-1
Actual
Modelled
mg kg-1
Extract number

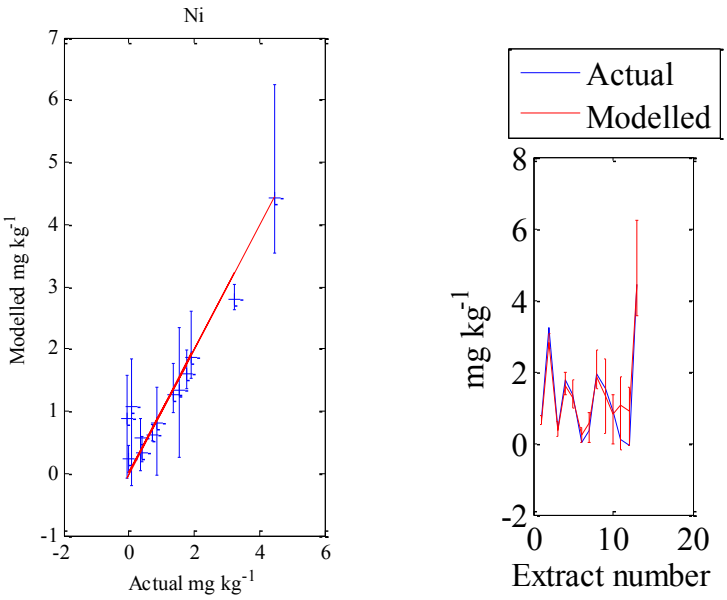
Ni
Modelled mg kg-1
Actual mg kg-1
Actual
Modelled
mg kg-1
Extract number

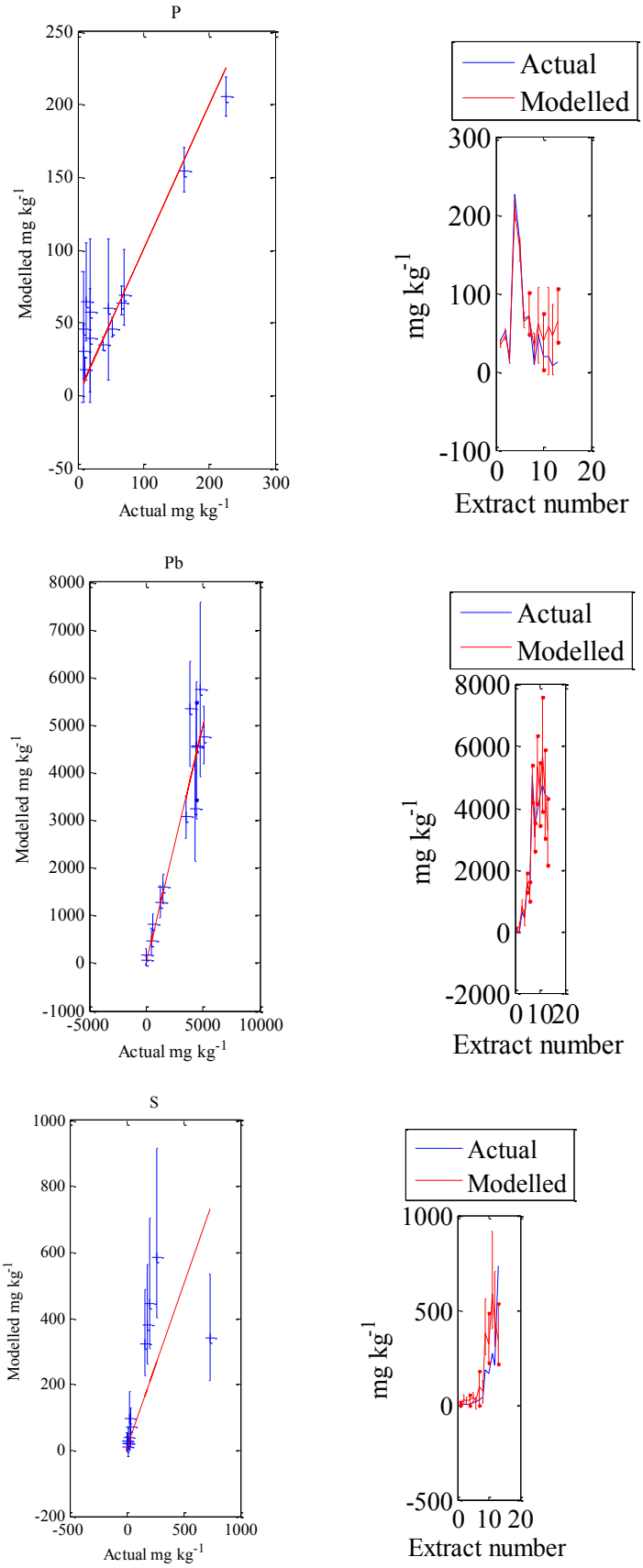
P
Modelled mg kg-1
Actual mg kg-1
Actual
Modelled
mg kg-1
Extract number
Pb
Modelled mg kg-1
Actual mg kg-1
Actual
Modelled
mg kg-1
Extract number
S
Modelled mg kg-1
Actual mg kg-1
Actual
Modelled
mg kg-1
Extract number

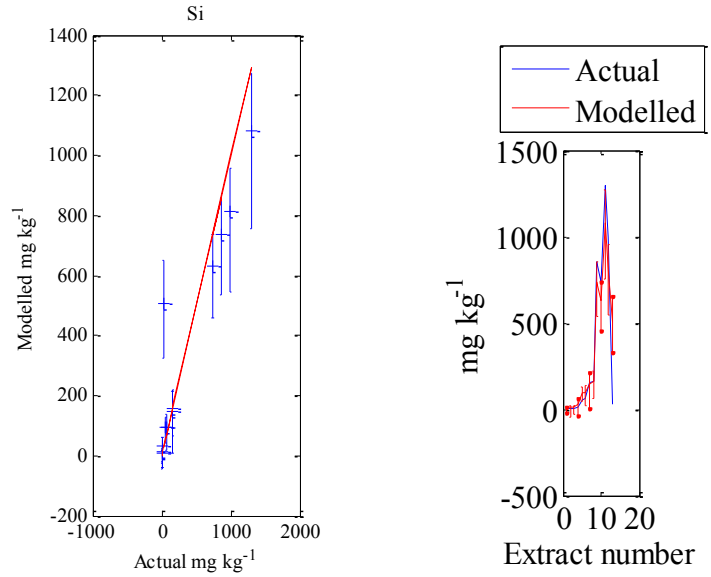
Si
Modelled mg kg-1
Actual mg kg-1
Actual
Modelled
mg kg-1
Extract number

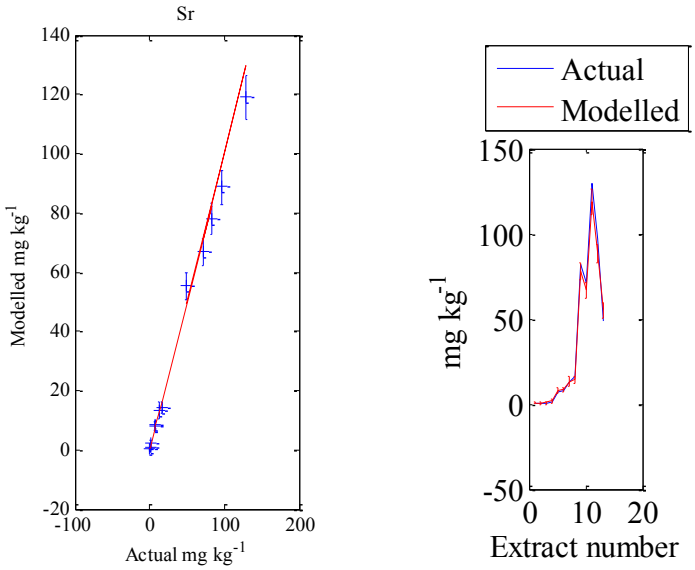
Sr
Modelled mg kg-1
Actual mg kg-1
Actual
Modelled
mg kg-1
Extract number

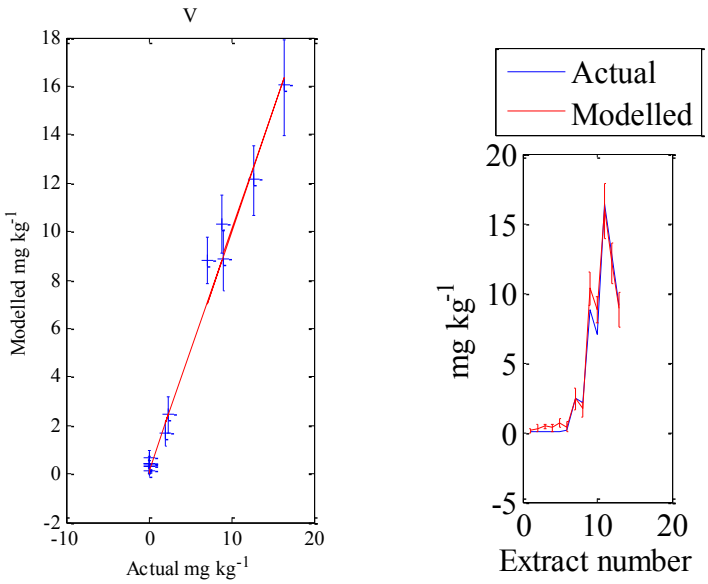
V
Modelled mg kg-1
Actual mg kg-1
Actual
Modelled
mg kg-1
Extract number

Appendix 2

Lattice plots showing the changes in CISED extraction profiles over wetting and drying events.

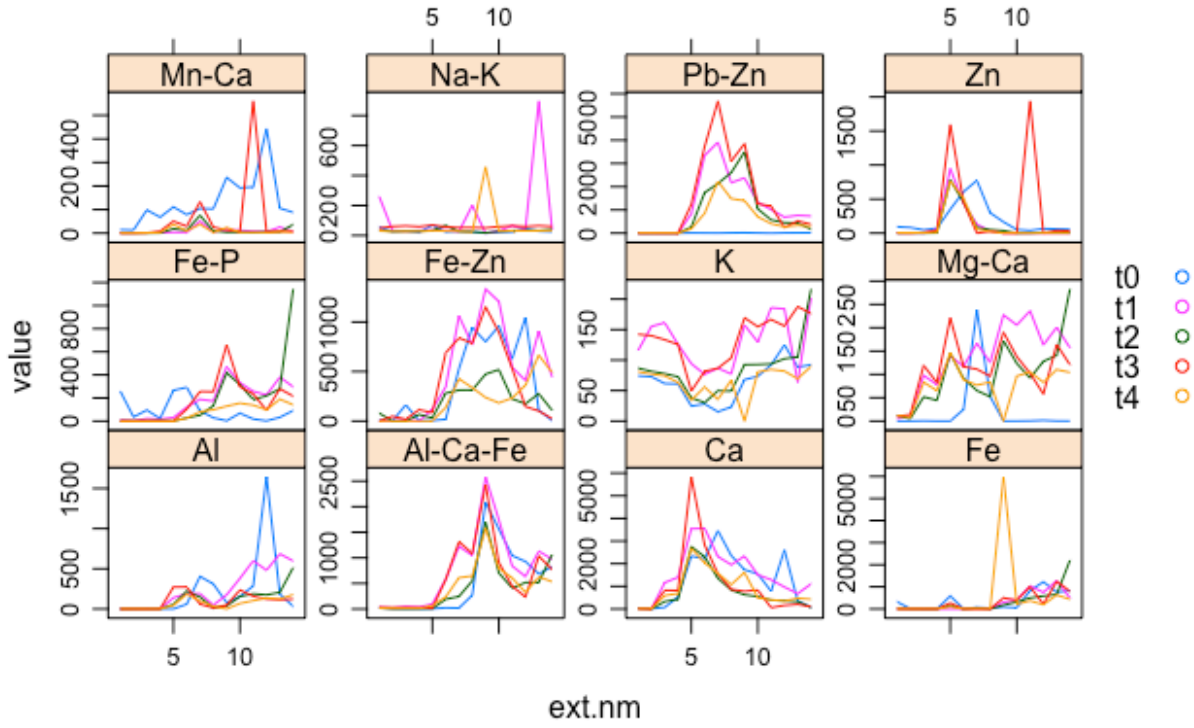

Figure A2.1 Soil 2

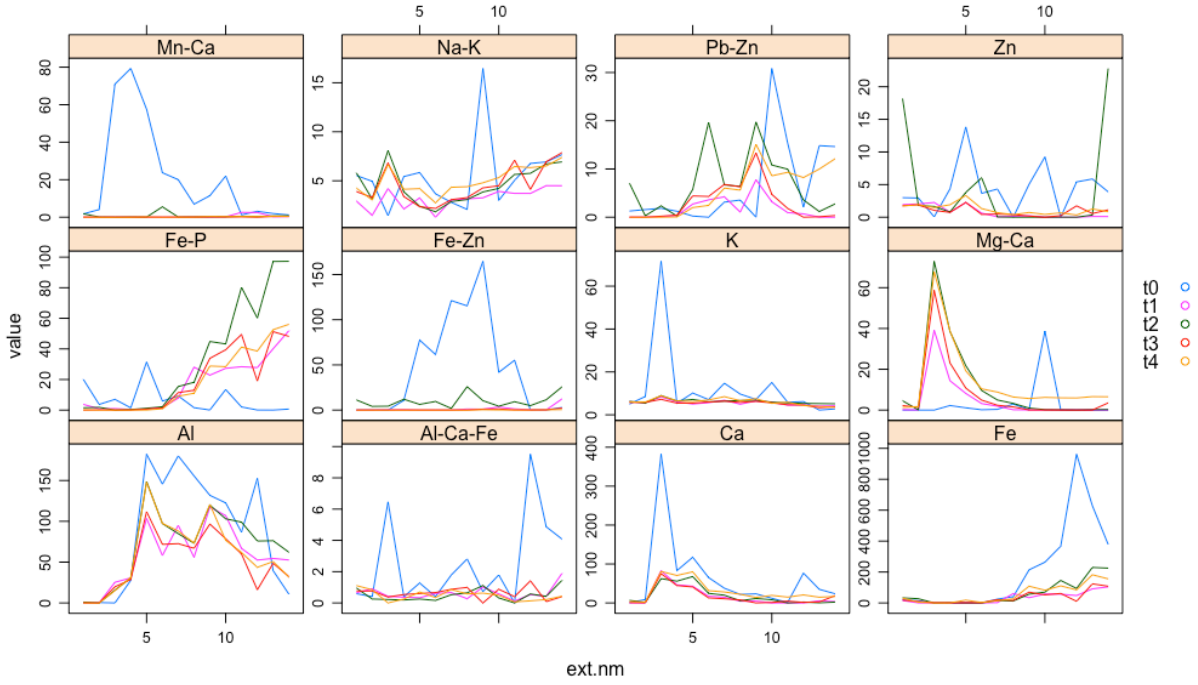

Figure A2.2: Soil 3

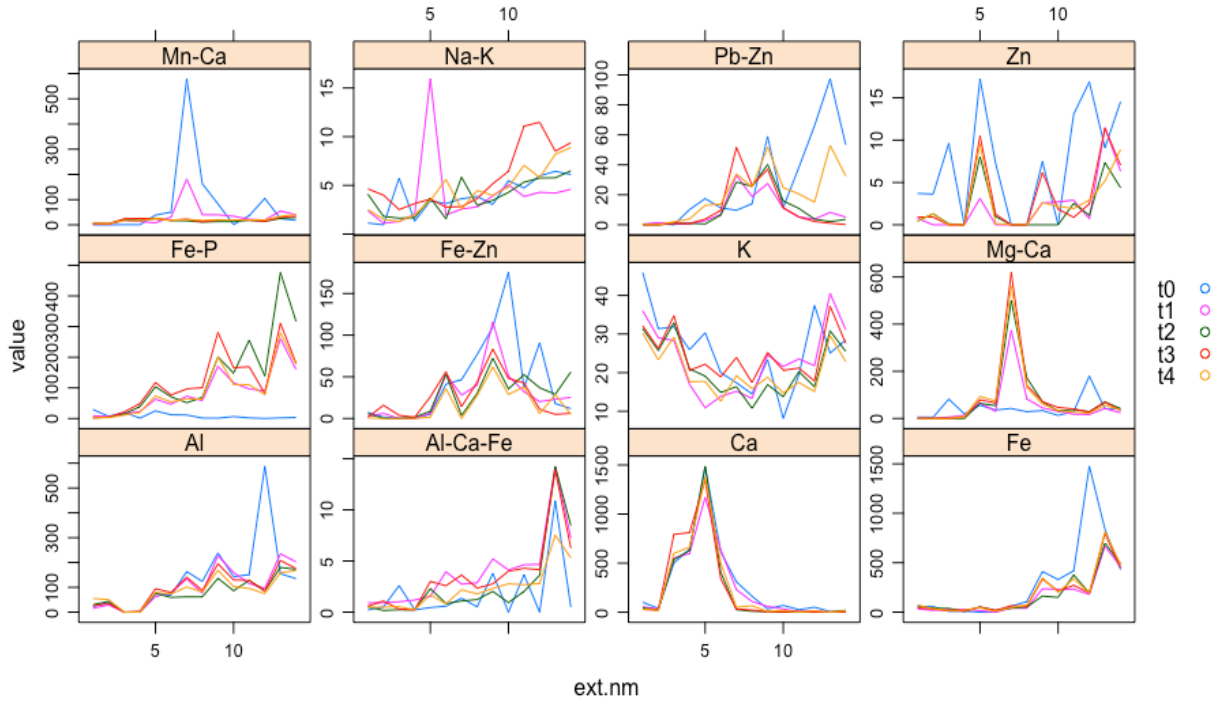

Figure A2.3: Soil 4

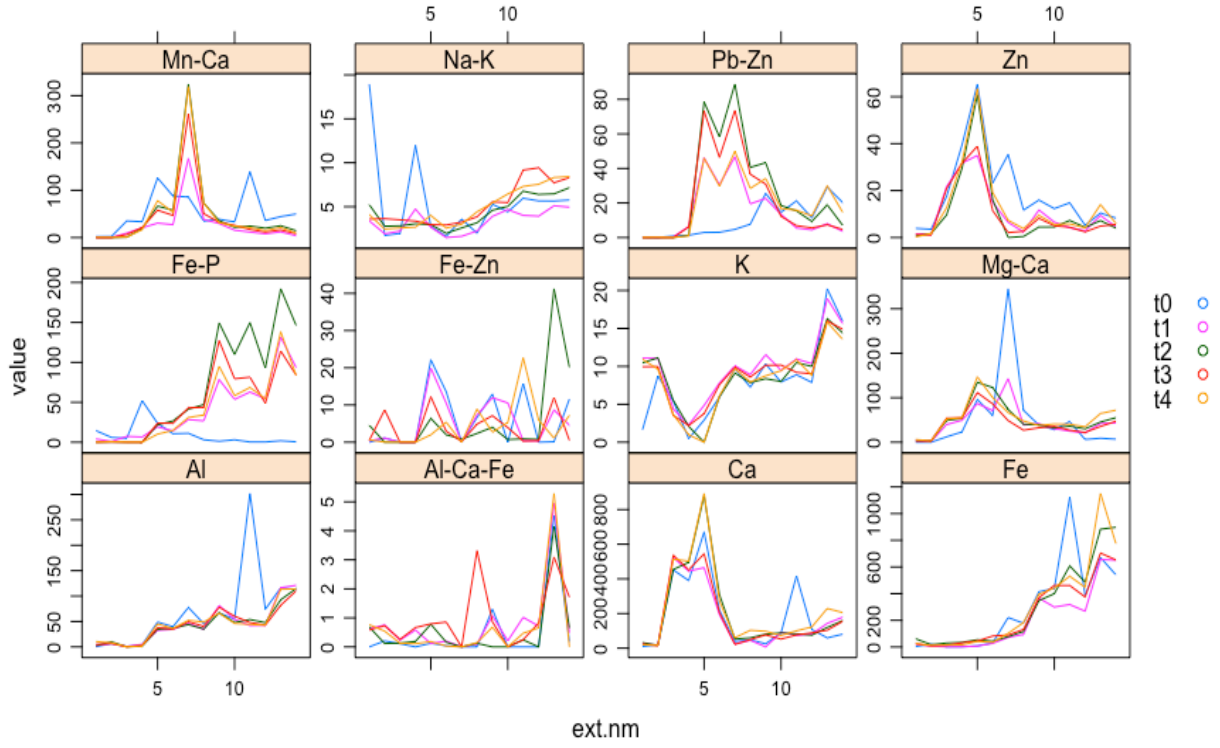

Figure A2.4: Soil 5

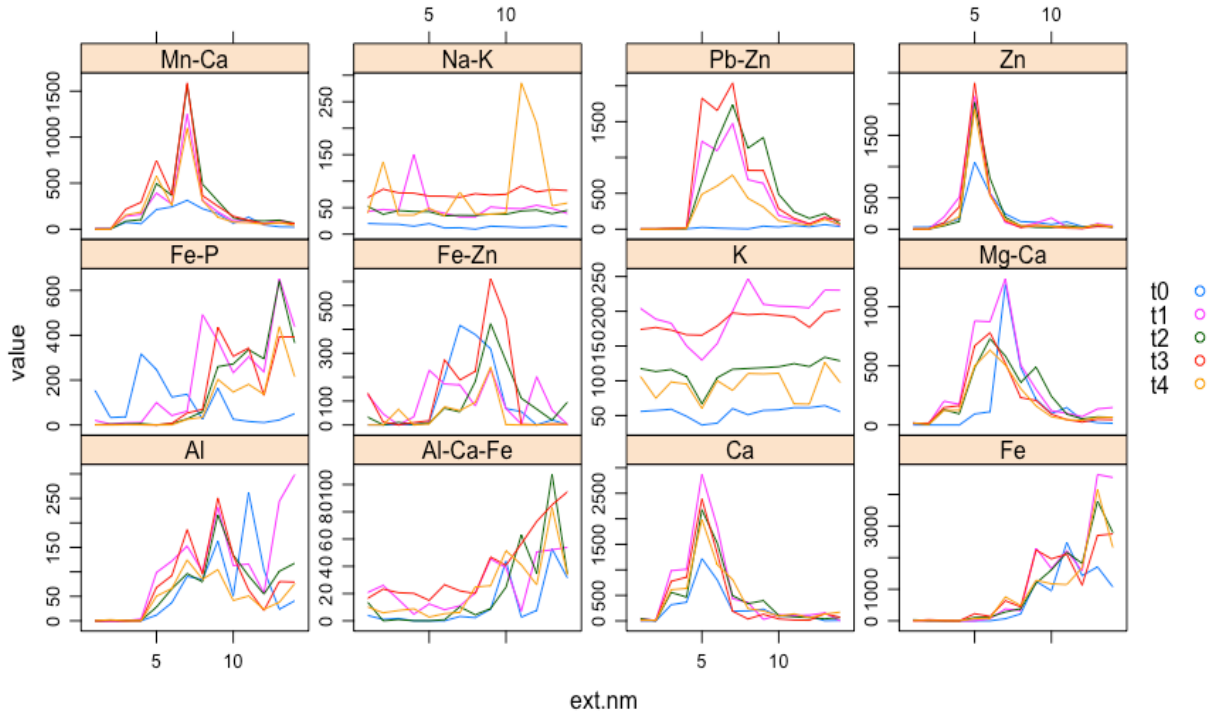

Figure A2.5: Soil 6

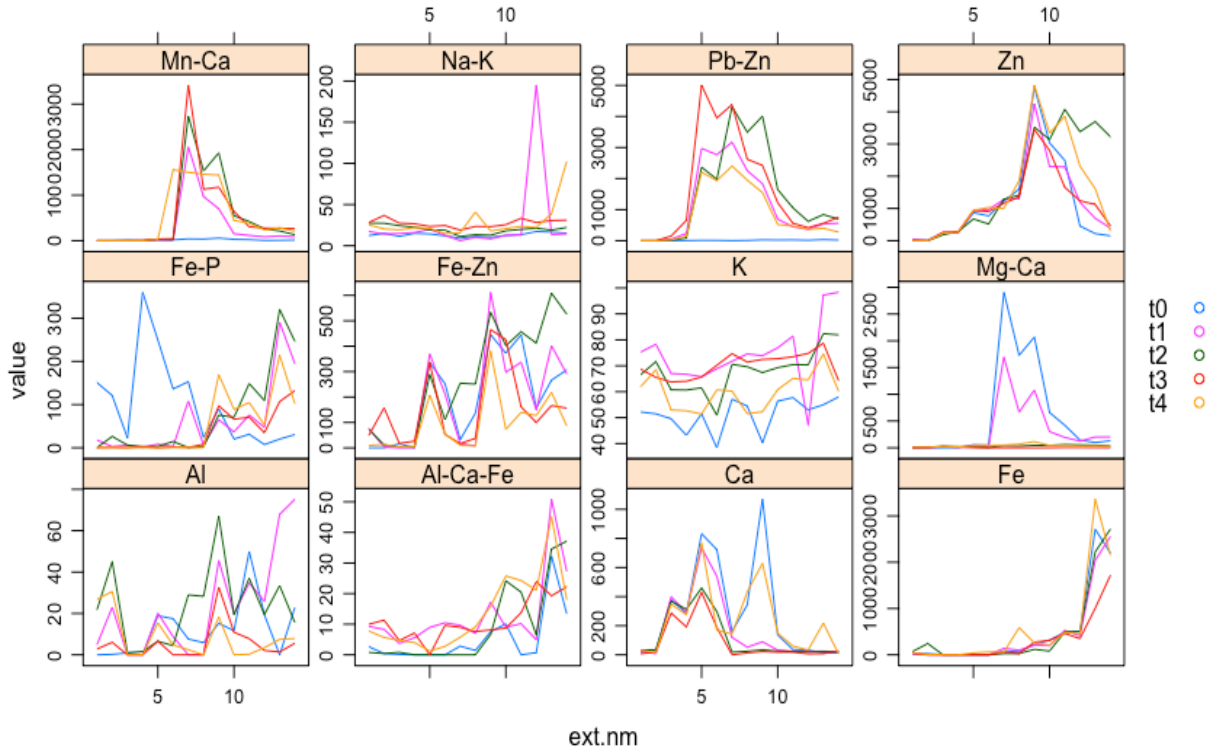

Figure A2.6: Soil 7

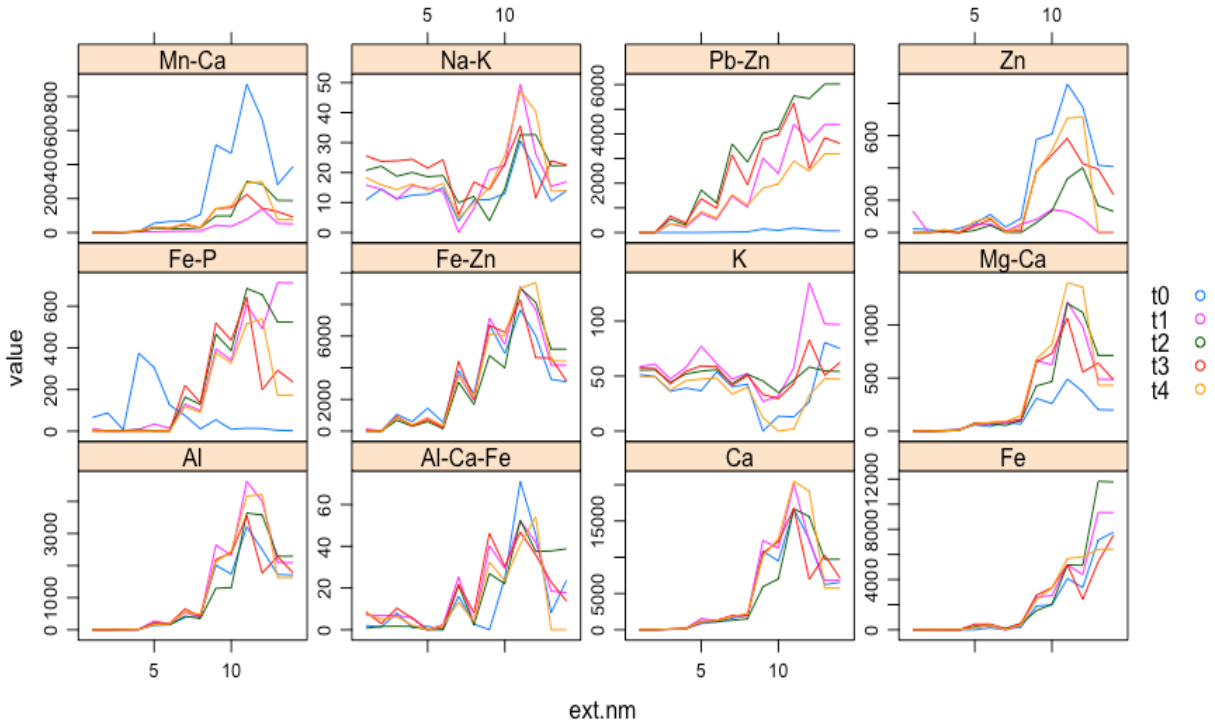

Figure A2.7: Soil 8

Table A2.1 Element concentrations of Tyne river water

Analyte	Concentration (μg L^{-1})
Al	103
As	0.50
Ca	28000
Cd	0.14
Cu	0.95
Fe	1.02
Mn	1.03
Pb	7.00
Zn	1.10
DOC	10100

Table A2.2 Pseudototal concentrations of major and trace elements for the 48 Tyne catchment soils

Al	As	Ca	Cd	Co	Cr	Cu	Fe	K	Li	Mn	Na	Ni	P	Pb	S	Si	V	Zn
7494	3.56	6159	1.84	3.43	14.09	20.00	9521	825	82.0	360	67.4	1.98	1270	249	963	0.09	18.1	277
6485	6.06	1941	2.82	8.94	15.39	15.69	23234	430	165	1237	73.1	3.54	766	259	434	0.61	20.0	218
8390	12.8	9321	7.11	9.98	13.84	34.01	20216	1297	158	1111	85.0	5.34	668	1369	861	5.12	21.5	1711
7328	9.97	6837	6.69	8.20	12.13	27.42	17452	688	131	939	60.4	5.53	638	888	715	4.40	16.9	1404
6010	8.08	8346	4.94	8.69	10.32	30.31	17350	828	130	895	76.4	6.35	254	749	667	3.97	11.9	1214
9443	8.54	4491	2.31	10.4	18.51	38.79	20385	663	164	1070	89.1	6.79	1084	102	762	0.16	30.0	144
7819	13.8	9414	13.1	9.85	12.40	53.61	19571	1225	150	1213	59.8	5.95	332	1547	1133	8.81	14.8	3558
8442	7.04	10595	5.31	9.05	14.12	30.17	18791	1083	146	861	74.7	5.77	524	768	873	7.07	19.8	1261
11130	6.76	4106	2.59	7.86	19.84	34.51	20182	640	156	387	67.9	4.84	669	205	589	0.88	32.5	221
8121	5.35	5325	3.03	7.12	13.76	27.41	12031	663	104	362	79.9	8.22	368	446	580	1.02	19.0	656
5348	5.36	6950	3.72	7.72	9.59	16.35	17011	661	127	693	57.9	4.72	254	440	722	5.41	11.7	785
4179	3.24	7292	2.57	7.21	9.04	15.25	14386	561	105	507	82.3	5.03	270	231	1290	1.11	10.2	427
6613	6.00	7952	4.74	9.47	11.58	22.05	16931	860	134	906	69.1	6.71	389	565	998	3.61	13.6	1020
6305	4.53	6084	4.09	8.16	11.24	20.03	16326	849	121	697	63.7	5.83	394	634	631	3.03	13.9	810
6890	4.81	4115	1.88	7.79	12.59	28.58	14964	533	110	552	125	4.75	569	129	572	0.10	19.7	124
7087	5.20	6211	4.68	10.4	13.37	20.68	18554	852	141	917	50.7	8.02	389	488	853	2.25	15.5	908
3771	2.66	4267	2.16	5.79	8.35	13.5	12986	464	88.4	519	66.3	4.39	309	176	510	0.36	9.75	306
2061	2.79	2666	2.00	5.33	5.96	11.08	2629	178	29.4	620	46.2	4.00	40.1	1986	508	58.2	1.82	563
3601	2.78	8932	23.4	14.2	4.50	37.8	2368	264	38.6	1756	66.7	18.1	9.57	1956	987	34.7	2.18	7281
3821	3.01	2268	2.87	6.67	5.94	13.31	3210	345	43.7	704	89.9	9.64	84.4	1003	323	105	2.55	718

3940	2.83	6198	2.76	7.21	4.58	11.2	2594	298	37.0	770	59.1	10.6	26.3	511	454	92.7	2.45	980
3620	0.60	2575	0.87	0.25	6.10	6.4	2776	313	31.7	553	56.5	5.65	79.4	104	282	134	2.77	159
3855	3.01	2505	1.02	6.02	8.09	12.4	2549	371	32.3	736	72.3	8.19	53.9	167	426	79.3	3.12	280
3609	2.53	4399	0.58	6.14	5.32	11.2	2482	432	37.1	555	62.2	8.10	88.4	85.4	310	60.0	3.41	64.2